Merged with A.R.L.I.S. ANCHORAGE, ALASKA Est. 1997
ALASKA RESOURCES LIBRARY
U.S. DEPT. OF INTERIOR
BLM - ALASKA RESOURCES LIBRARY
3 0455 00000442 4

Environmental Assessment of the Alaskan Continental Shelf

Annual Reports of Principal Investigators for the year ending March 1981

Volume VI: Transport

U.S. DEPARTMENT OF COMMERCE
National Oceanic & Atmospheric Administration
Office of Marine Pollution Assessment

U.S. DEPARTMENT OF INTERIOR
Bureau of Land Management

Annual Reports of Principal Investigators

1981

FEB 14 1983
ALASKA RESOURCES LIBRARY
U.S. DEPT. OF INTERIOR
Merged with
A.R.L.I.S.
ANCHORAGE, ALASKA
Est. 1997

GC
85.2
.A4
E57
1981
V.6

Environmental Assessment of the Alaskan Continental Shelf

Annual Reports of Principal Investigators for the year ending March 1981

Volume VI: Transport

ARLIS
Alaska Resources
Library & Information Services
Anchorage, Alaska

U.S. DEPARTMENT OF COMMERCE
National Oceanic & Atmospheric Administration
Office of Marine Pollution Assessment

U.S. DEPARTMENT OF INTERIOR
Bureau of Land Management

The facts, conclusions and issues appearing in these reports are based on interim results of an Alaskan environmental studies program managed by the Outer Continental Shelf Environmental Assessment Program (OCSEAP) of the National Oceanic and Atmospheric Administration (NOAA), U.S. Department of Commerce, and primarily funded by the Bureau of Land Management (BLM), U.S. Department of Interior, through interagency agreement.

DISCLAIMER

Mention of a commercial company or product does not constitute an endorsement by National Oceanic and Atmospheric Administration. Use for publicity or advertising purposes of information from this publication concerning proprietary products or the tests of such products is not authorized.

Volume 6

Transport

Annual Report
April 80 - May 81
Research Unit 567

THE TRANSPORT AND BEHAVIOR OF OIL SPILLED IN AND UNDER SEA ICE

R. S. Pritchard
M. D. Coon

Flow Research Company
A Division of Flow Industries, Inc.
21414 - 68th Avenue South
Kent, Washington 98031
(206) 872-8500

May 15, 1981

Table of Contents

I. Summary of Objectives, Conclusions and Implications

Research conducted during FY80 was directed towards improving our understanding of the fate of crude oil spilled as a result of petroleum development in the coastal waters off the north coast of Alaska. A considerable literature exists on the climatology, meteorology, oceanography and ice character of the Prudhoe Bay lease area. Work has been completed by RU562 on the potential for oil pooling under sea ice and by RU568 on under-ice transport of oil by currents. A major objective of our work this year was to synthesize this information into a meaningful set of oil spill scenarios for the Joint Lease Sale area at Prudhoe Bay and also for the Sale 71 area of Harrison Bay. Results indicate that an oil spill under the ice from November through April would become incorporated rapidly into the ice. Subsequent transport of the ice then determines the point at which oil is released, essentially unweathered, during spring breakup. Ice inside the barrier islands remains in place through the winter so the oil will be released to the water in essentially the same spot in spring. This stable concentration of oil may aid in cleanup operations.

Ice outside the barrier islands can be transported long distances during a single winter. To investigate the possibility that oiled ice from the Prudhoe Bay lease area might enter the Chukchi Sea and travel south through the Bering Straits, the ice dynamics model developed during AIDJEX was applied to the Chukchi. Under conditions of low ice strength it was found that the ice could travel over 400 km in 3 months implying considerable motion in the Chukchi though not to the extent of transporting ice from Barrow through the Bering Strait.

Very little is known about the behavior of oil after its release from the ice. A preliminary study has been carried out to determine the interaction of oil with low to medium concentrations of ice. Transport of oil appears to be controlled by herding of oil by ice floes with the result that the ice drift controls oil slick drift. Dispersion of the oil is controlled by turbulence in ice motions.

II. Introduction

A. General Nature and Scope of Study

This study synthesizes work on sea ice dynamics with available information on the behavior of oil spills to provide a basis for predicting the behavior of oil spills in the Arctic. Details of the interaction of oil from a blowout with an ice canopy are evaluated for a variety of ice conditions varying with geography and season. Effects of ice on dispersion, weathering and transport are considered. Ice transport is modeled numerically using a sea ice dynamics model. A field program was initiated to observe ice motions for model verification.

B. Specific Objectives

A study of ice motion in the Chukchi Sea using the ice dynamics model was made to determine the conditions under which ice breakout from the Chukchi to the Bering Sea may occur. The results of this work are given in FRC Report No. 168 which is given as an appendix to this report.

Another objective was to develop a set of twelve representative oil spill scenarios for the Prudhoe Bay lease area. The time, magnitude and location of the spills were selected by OCSEAP. The scenarios were to describe the fate and behavior on an oil spill under ice from initial release through to the release of oil into open sea water. As a prerequisite to these scenarios a compilation of the relevant meteorological, oceanographical, ice dynamic and oil property data was required. This information is given in Flow Research Report No. 175. It serves as a reference for the twelve Prudhoe Bay oil spill scenarios given in Flow Research Report No. 176. Both reports are included here as appendices.

Flow Research Report No. 189 describes the fate of oil released under the ice in the Harrison Bay offshore area. The fate of oil released onto the water surface and its interaction with low to medium concentrations of sea ice is not well known. A third objective was thus to develop a preliminary guide to the mechanisms which affect the interactions of surface oil slicks with drifting ice.

The last objective for RU 567 was to initiate field studies of ice motions in Norton Sound. Seven tracking buoys were deployed in Norton Sound over the course of the 1980 winter. The trajectories of the buoys will be analysed with the object being to verify an ice dynamics model in this area.

C. Relevance to Problems of Petroleum Development

Large portions of the Alaskan continental shelf are being considered for petroleum and gas development. An oil spill in these waters could have drastic consequences for a number of wildlife species. A knowledge of the disperson and transport of oil spilled in Alaskan coastal waters can be used to develop clean-up plans and to protect sensitive wildlife areas. Slick behavior studies can also be used to evalute the likelihood of climatic effects. Ice motions present a hazard to structures associated with offshore development. A combination of field and numerical ice dynamics studies may be used to identify hazardous areas and to forecast ice conditions for drilling operations.

III. Current State of Knowledge

The ice dynamics of the Beaufort Sea has been well characterized by the results of AIDJEX and subsequent modeling efforts. Ice outside the stamukhi zone can travel from Prudhoe Bay to Barrow in a few months. Ice within the Barrier Island lagoons is stable. Studies by RU 562 have determined the potential for oil pooling under an ice canopy. RU 568 has studied the conditions necessary for currents to transport oil under ice. Essentially these studies imply that oil will pool under the ice in layers 1 cm to 10 cm thick depending on the small scale surface roughness. Currents of 20 cm/s or more are required to cause appreciable oil pool motions. A considerable literature exists on the oceanography and meteorology of the coastal Beaufort Sea and the Bering Sea while the Chukchi Sea is still relatively unknown. Detailed ice motion studies have been restricted to the Beaufort Sea. Ocean currents cause a large part of the mean monthly ice transport while winds cause considerable seasonal variation as well as daily variability in the motion.

IV. Study Area

The oil-ice study area includes the Joint Lease Sale area at Prudhoe Bay and the proposed Sale 71 lease area to the west near Harrison Bay. The Chukchi Sea is modeled in ice breakout studies and ice motions were observed in a field study in Norton Sound.

V. Sources Methods and Rationale of Data Collection

The field study in Norton Sound was made using ADAP buoys deployed on the ice by helicopter on three occasions. The initial deployment consisted of three buoys placed along the length of Norton Sound in late January. As the ice drifted out of Norton Sound, to be replaced by new ice growth, additional buoys were deployed in locations providing the best coverage of ice motions. Data buoy locations are available every 3-6 hours.

VI. Results

The numerical study of Chukchi Sea ice dynamics (FRC 168) has successfully modeled the ice motions during breakout. Motion is concentrated in a band about 150 km wide off the northwest coast of Alaska from Cape Lisbourne to Pt. Barrow. Breakup is initiated by strong current reversals to the south which carry the ice through the Bering Straits. Ice strength is important in the Chukchi as a structural arch is developed during southward motion. During the 1976-1977 winter season modeled motions were not large enough to carry ice from Barrow through the Bering Strait.

The ice-oil study (FRC 175) shows that any oil spilled during the winter season will be released to the water during spring breakup. The oil spilled will be trapped by small scale under ice relief in relatively small areas and become encapsulated in the ice in a very short time. Outside the barrier islands large amounts of ice are incorporated into ridges implying that oil spilled near the stamukhi zone will end up in a ridge.

The scenarios presented in FRC 176 for the the joint lease sale area near Prudhoe Bay are very similar to the predicted behavior in the sale 71 lease area near Harrison Bay (FRC 189). In this area shoals offshore act to ground ridge systems which then protect the nearshore ice just as the Barrier Island protect Steffanson sound. Currents in both areas are quite small and should not transport oil under the ice. Early season deformation can be significant in the sheltered areas but the ice becomes strong enough by December to become essentially fast.

Preliminary results indicate that low to medium concentrations of ice influence the transport and diffusion of oil slicks by herding the oil. At high enough ice concentrations the oil essentially moves with the ice. Under these conditions dispersion of the oil will be controlled by diffusion of points on the ice.

Preliminary results from the Norton Sound buoy study indicate continuous motion of ice out of Norton Sound to the west. Ice motion in the northern Bearing Sea is generally southward but the region north of Norton Sound tends to have a generally northward motion. Reversals of ice motion are significant and are apparently correlated to storms.

VII. Discussion and Conclusions

Oil spilled beneath the fast ice in either lease area will be limited in extent and will not move far during the winter. Drilling regulations stipulating containment berms to be constructed around each drilling platform should prove an effective means of further enhancing the containment of even a large spill. Regulations limiting the drilling season to the end of March allow 2 months to recover spilled oil and drill relief wells further minimizing the danger of an open water spill at breakup. Once oil is released into the water cleanup efforts will become very difficult.

Oil spilled outside the fast ice zone will in all likelihood be incorporated into ridges and possibly transported large distances. The release of oil from ridges is an important process which is likely to be very different from the release by flat ice.

Oiled ice could reach Barrow but it is unlikely to travel through the Bering straits. Oiled ice from future lease areas in the Chukchi, however, might well travel into the Bering Sea because the release area is much closer to the Bering Strait.

VIII. Needs for Further Study

Several questions have been raised by the results of these studies. Oil spilled outside the barrier islands becomes incorporated into ridges. The location of the oil in the ridges and the means by which the oil is released are important unknowns since these factors will control the location, time and amount of oil released.

The dispersion of oil in low to medium concentration ice will be controlled by horizontal diffusion of the ice. Turbulent diffusion coefficients, for sea ice would provide useful estimates of the dispersion of an oil spill during spring breakup.

The performance of the ice dynamics model in the Chukchi Sea has not been validated as it has in the Beaufort Sea. Chukchi Sea ice is different from Beaufort Sea ice in that it is mostly first year growth. A simultaneous data set including wind currents and ice conditions is needed to drive a model calculation for comparison with a set of data buoy trajectories.

The sea ice dynamics model for the Chukchi should be improved to account for the weakening effect of lead formation off the Alaskan coast. The present model does not allow weakening and probably underestimates the possible ice motions.

The buoy motions obtained for Norton Sound and the Northern Bering Sea should be used to validate the Rand Ocean Model developed by RU 435. This would require some measure of the driving forces for the model. An evaluation of the buoy motions should be made to determine effects of long term currents, storm events and tidal motions.

IX. Summary of Fourth Quarter Operations

A. Field Operations

(1) 3 trips to Norton Sound

(a) 8 Jan - 20 Jan, buoys 3600, 3601 and 3602

(b) 11 Feb - 19 Feb, buoys 3603 and 3605

(c) 13 March - 15 March, buoys 3604 and 3606

(2) Personnel Involved

Don Thomas - research scientist, Flow Research Company

Jack Kollé - research scientist, Flow Research Company

(3) Methods

Buoys were assembled and tested at the airport in Nome. Deployment was by helicopter.

(4) Data Collected and Analyzed

Buoy trajectories are being collected and edited at Flow for presentation to the OCSEAP data bank. Only visual analysis is expected during this project.

JK/184R

Flow Research Report No. 168

Ice Motion in the Chukchi Sea

By

R. W. Reimer
J. C. Schedvin
and
R. S. Pritchard

September 1980

Flow Research Company
A Division of Flow Industries, Inc.
21414 - 68th Avenue South
Kent, Washington 98031
(206) 872-8500

Flow Research Report No. 168
September 1980

Acknowledgement

This study was funded by the Bureau of Land Management through interagency agreement with the National Oceanic and Atmospheric Administration as part of the Outer Continental Shelf Environmental Assessment Program.

Flow Research Report No. 168
September 1980

Table of Contents

List of Figures

List of Figures (Cont.)

1. Introduction

As part of the concern over oil spill hazards in the offshore Prudhoe Bay lease areas, consideration must be given to the possibility of spilled oil being transported through the Bering Strait. Even though Prudhoe Bay and the Bering Strait are separated by over a thousand kilometers, it is possible to envision a sequence of events which could lead to oiled pack ice passing through the Strait and into the Bering Sea. A possible scenario might have oiled ice from Prudhoe Bay incorporated in a ridge during the winter. Then, during the following summer, easterly winds along the north Alaskan coast could blow the oiled ridge to Pt. Barrow, where it might become grounded. The following winter, a year after the spill, large-scale motion in the Chukchi Sea could transport the ice all the way through the Strait. This paper is concerned with the likelihood of such large-scale motion in the Chukchi Sea.

Southward movement of ice through the Bering Strait is impeded during the winter by the formation of an arch across the opening between the eastern and western land masses. Analysis of the failure of arches has received considerable attention in the mechanics literature, particularly in the soils area where similar problems arise in the design of hoppers and bins. In the case of a soil or other granular media in a hopper, the loads causing failure of an arch across a free surface are most frequently the weight of the material. However, there may also be tractions acting on the top surface of the material stored in a bin. Some combination of these loads may collapse the arch across the hopper opening and thereby make flow through the opening possible. It is along these lines that we develop a sea ice model for transport of Chukchi Sea ice through the Bering Strait.

After studying the known oceanograpy of the Bering Strait, Reimer et al. (1979) and Pritchard and Reimer (1979) concluded that ocean currents, driven by atmospheric circulation patterns, are the loads which at times fail the arch across the Bering Strait. Whether or not the failure of the arch across the Strait permits flow as far north as Pt. Barrow is the central question of the present work. The Chukchi Sea is a good approximation to a two-dimensional hopper, with the exception of Pt. Hope peninsula which protrudes from the east side of the "hopper." This feature has not been included in any theoretical models developed so far.

In order to understand how flow of ice through the Strait may be impeded, it is necessary to understand the arching process. In general terms, arching is the condition which results when the ice pack transmits applied loads to the boundaries. A large compressive stress along a curved line (an arch) allows the applied load to be balanced even though an opening exists in the boundary. This allows a stress-free surface (called a free surface) to develop at the arch. Generally, the ability of the material to transmit loads to its boundaries is influenced by two factors: (1) the geometry of the boundaries and (2) the uniaxial compressive strength of the ice. The uniaxial compressive strength is the amount of stress the ice can sustain without support in the direction perpendicular to the applied load. This quantity is critical to the maintenance of the free surface of the arch because a state of uniaxial compression must exist there.

The problem that this work addresses specifically is: given that oiled ice is near Pt. Barrow, what is the likelihood of its being transported southward across the Chukchi Sea and through the Bering Strait? This question is not answered with certainty because of limitations in our knowledge of ice behavior and ocean currents in the Chukchi Sea. We attempt to select conditions that tend to maximize the southward flow of ice with the intent of proving that even under these extreme conditions, oiled ice cannot be transported through the Bering Strait. As a result, we find that ice would not be transported through the Bering Strait even under these extreme conditions (using ocean current data from the one year for which they are available), but there is not enough safety margin to feel confident that it could not ever happen.

The approach in this work is to simulate ice behavior using a mathematical model driven by winds and ocean currents. This allows a range of inputs to be introduced to find a range of motions. It is necessary to consider the possible ice conditions (ranging from high to low strength) and different winds and currents and how each affects the ice behavior. From this study, we have learned much about the processes that control large-scale ice motion in the Chukchi Sea. This study represents the first substantial research effort aimed at simulating Chukchi Sea ice motions on length scales on the order of tens of kilometers with daily time resolution. This knowledge compliments past studies and provides guidance for directing future research efforts.

Southward ice motion in the Chukchi Sea is impeded in the winter by an ice arch across the Bering Strait. Breakout occurs as a failure of this arch, and this process is one of the critical events leading to large-scale southward ice motion in the Chukchi Sea. Several theoretical models of the behavior of such an arch already exist. These define the applied loads in relation to an ice strength parameter at which breakout begins. One of the earliest of these models is an adaptation of soil mechanics results (Sodhi, 1977). More recently, Pritchard and Reimer (1979) modeled arching of sea ice specifically in the Bering Strait. In this latter work it is concluded that reversals of the generally northward flow of ocean currents through the Strait cause breakout.

What is most lacking in the previous investigations of this phenomenon is a data set with which to validate the models. The recent ocean current data published by Coachman and Aagaard (1980) provide a new incentive to re-examine the arching problem in the Bering Strait. This set of data makes it possible, for the first time, to model all the forces on the ice cover in the Chukchi Sea. However, even with a good ocean current data set, model verification is not possible because concurrent ice motion data are not available for long time periods.

We consider pack ice to be an elastic-plastic material, a continuum on the scale of tens of kilometers. Forces on the ice occur as a result of divergence of this interval ice stress, of frictional drag on its bottom surface by ocean currents and across its top surface by winds, as well as from sea-surface tilt and Coriolis acceleration. In addition, traction exerted by the ice pack bordering the region of interest must be taken into account. The model used is essentially the same as that developed by AIDJEX and described by Coon et al. (1974, 1978). The modifications required to adapt the AIDJEX model for use in the Chukchi Sea are described below.

In order to determine the largest southward ice motion likely to occur in the Chukchi Sea, it is necessary to consider extremes in the driving forces. This is an uncertain prospect since only one winter's ocean current data exists, and since it is not possible to determine ice conditions accurately at a given time. Our remedy for this will be to construct a worst case by considering extremes in both the wind field and the boundary traction exerted by the Arctic ice pack and to consider response for a range of ice conditions. Hence, the model calculation will not be run in real time in the sense of representing all conditions as they actually occurred on a particular day. Instead, we shall have defined an extreme condition for the winter of 1976-77.

The extent of ice motion in the Chukchi Sea is not known at this time. Figure 1 shows an isolated incident, which may or may not be typical of ice motion in the Chukchi Sea. During a 10-day sequence in January 1976 (one year before the time period being studied), a RAMS buoy drifted with the ice pack a distance of over 400 km. The buoy was left in a position where subsequent ice motion could have taken it through the Bering Strait. For the winter of 1976-77, we simulate ice motions on the order of the average daily displacement (42 km/day) but not nearly as large as the 130 km/day maximum.

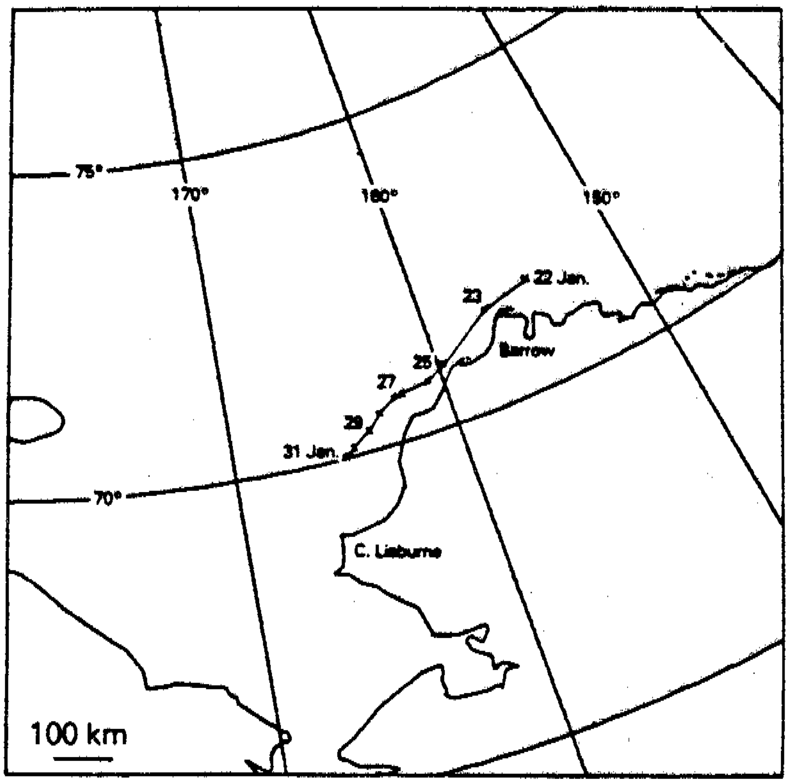

Figure 1. The Trajectory of RAMS Buoy R534 During the Breakout of January 1976. The Maximum Daily Displacement Is 130 km. Average Daily Displacement for the 10-Day Period is 42 km. From Thorndike and Cheung (1977).

2. Sea Ice Model

The mathematical model of ice dynamics incorporates a momentum equation that accounts for air and water stresses, Coriolis force, sea-surface tilt, and internal ice stress divergence. The model also requires a constitutive law relating the internal ice stress to deformations. A quasi-steady calculation is done in which ice strength is a constant and no ice redistribution or thermal growth is taken into account. The strength is varied as a parameter in different simulations but it does not change during a simulation if open water is created by deformation.

2.1 Momentum Balance

In the plane of motion of the sea ice, the momentum balance is expressed as

$$m\dot{\underset{\sim}{v}} = \underset{\sim}{\tau}_a + \underset{\sim}{\tau}_w - mf\,\underset{\sim}{k} \times \underset{\sim}{v} - mg\nabla H + \nabla\cdot\underset{\sim}{\sigma} \qquad (1)$$

where

m	is mass per unit area of ice
$\underset{\sim}{v}$	is ice velocity in the horizontal plane
$\dot{\underset{\sim}{v}}$	is material time rate of change of $\underset{\sim}{v}$
$\underset{\sim}{\tau}_a$	is traction exerted by atmosphere on upper surface of ice
$\underset{\sim}{\tau}_w$	is traction exerted by ocean on lower surface of ice
f	is the Coriolis parameter ($f = 2\Omega \sin \lambda$)
Ω	is the earth's rotation rate
λ	is latitude
g	is acceleration due to gravity
H	is sea-surface height
$\underset{\sim}{k}$	is the unit vector in the vertical direction
$\underset{\sim}{\sigma}$	is Cauchy stress resultant in excess of hydrostatic equilibrium (two-dimensional).

The horizontal position vector $\underset{\sim}{x}$ and the vertical unit vector $\underset{\sim}{k}$ are expressed in a right-handed Cartesian coordinate system. Velocity is the material rate of change of position, $\dot{\underset{\sim}{x}} = \underset{\sim}{v}$. The inertial part of the acceleration term $m\dot{\underset{\sim}{v}}$ is neglected in this quasi-steady case.

Air stress is calculated independently of the ice motion because the velocity of the air is two orders of magnitude larger than the velocity of the ice. The air stress $\underset{\sim}{\tau}_a$ is given as

$$\underset{\sim}{\tau}_a = \rho_a c_a \ |\underset{\sim}{U}_g| \ \underset{\sim}{B}_a \underset{\sim}{U}_g \ , \qquad \underset{\sim}{B}_a = \begin{pmatrix} \cos\alpha & -\sin\alpha \\ \sin\alpha & \cos\alpha \end{pmatrix} \tag{2}$$

where ρ_a is air density and c_a is the drag coefficient. The air stress is turned at an angle α to the applied geostrophic wind $\underset{\sim}{U}_g$. We assume a spatially constant air stress field in this calculation and use $\rho_a c_a = 1.1 \text{ kg/m}^3$ and $\alpha = 29^\circ$.

The effect of the oceanic boundary layer on ice motion has also been modeled as a quadratic relation between the surface traction $\underset{\sim}{\tau}_w$ exerted on the lower surface of the ice and the ice velocity relative to the geostrophic currents $\underset{\sim}{v}_g$. The traction is applied at an angle β to the relative velocity

$$\underset{\sim}{\tau}_w = \rho_w c_w \ |\underset{\sim}{v} - \underset{\sim}{v}_g| \ \underset{\sim}{B}_w(\underset{\sim}{v} - \underset{\sim}{v}_g) \ , \qquad \underset{\sim}{B}_w = \begin{pmatrix} -\cos\beta & \sin\beta \\ -\sin\beta & -\cos\beta \end{pmatrix} \tag{3}$$

where ρ_w is water density and c_w is the drag coefficient. Geostrophic currents are considered to be steady, so time variations do not appear. The values $\rho_w c_w = 8 \times 10^3 \text{ kg/m}^3$ and $\beta = 20^\circ$ are used.

The Coriolis force exerted on sea ice depends on the ice velocity, the latitude, and the mass of the sea ice. The mass of the sea ice is determined from the ice thickness which is taken as 2 m.

The sea-surface tilt term in the momentum balance arises from a varying sea-surface height which by simple force balance is seen to determine the geostrophic flow in a homogeneous ocean and is assumed independent of time. In the model the relationship $mg\nabla H = -mf \ \underset{\sim}{k} \times \underset{\sim}{v}_g$ is used.

The last term of the momentum balance is the divergence of internal ice stress. In the absence of internal ice stress, the momentum balance equations along with the air and water stress models are just sufficient to determine the two components of the ice velocity at each point. This free drift condition occurs at times in the Arctic, but is not likely in the Chukchi Sea during the winter when the confining shorelines of Alaska and Siberia prevent ice motions. Hence, we expect the stress divergence to be important, and the momentum balance cannot be evaluated at a point independently of the constitutive law.

2.2 Constitutive Law

The elastic-plastic model to be described has three separate elements that are required to specify completely the internal ice stress for a given deformation history. These are:

(1) yield surface
(2) flow rule
(3) elastic response

It is assumed that no plastic hardening occurs since a constant strength is assumed for each simulation. These elements are now discussed.

The stress state $\underset{\sim}{\sigma}$ in any plastic model is constrained to lie within a function called the yield surface. For an isotropic model this function depends only on the stress invariants and not on the principal direction. We write the constraint as

$$\phi(\sigma_I, \sigma_{II}) \leq 0 \tag{4}$$

where $\sigma_I = \frac{1}{2}\,\mathrm{tr}\,\underset{\sim}{\sigma}$ (negative pressure), $\sigma_{II} = (\frac{1}{2}\,\mathrm{tr}\,\underset{\sim}{\sigma}'\underset{\sim}{\sigma}')^{\frac{1}{2}}$ (maximum shear), and $\underset{\sim}{\sigma}' = \underset{\sim}{\sigma} - \sigma_I \underset{\sim}{1}$. The yield constraint may depend on other state parameters. In particular, the isotropic compressive strength p^* appears in the argument list.

The yield surface chosen for sea ice is shown in Figure 2. The stress invariants are constrained to be within the triangle for a given value of strength p^* . Along the straight line portion of $\phi = 0$ passing through the origin, the stress state is that of uniaxial compression. That is, one principal stress component is zero while the other is a negative value. Simulations of sea ice dynamics in the central Beaufort Sea show that it is important to use this "tensile cutoff" line to define part of the yield surface. It describes the randomly oriented leads and cracks present that require no force to open them. The other straight line used to complete the yield surface is chosen for simplicity. It reduces the shear strength by a factor of 2 compared to the triangular yield surface which has the largest possible shear strength compatible with tensile cutoff and a compressive strength of p^*. The reasons for prefering this yield curve has been presented by Pritchard (1977).

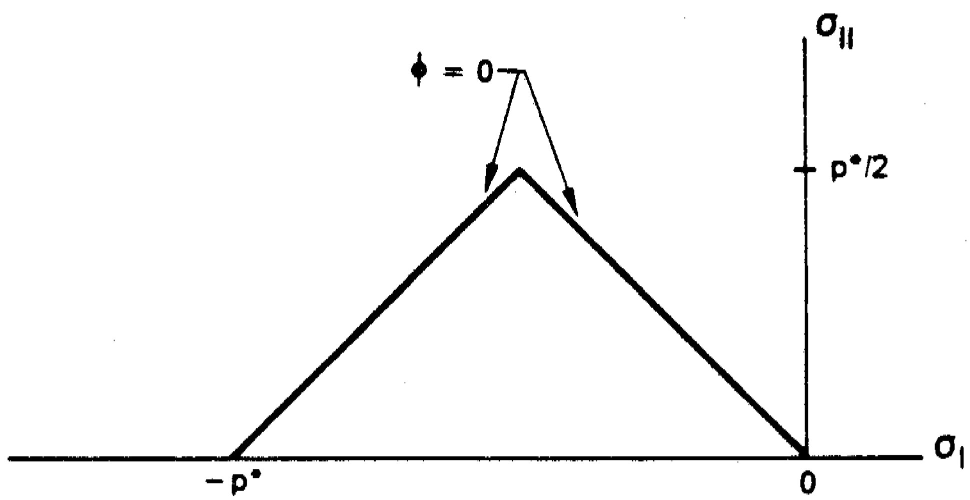

Figure 2. **Sea Ice Yield Surface. The Axes Are Stress Invariants: $\sigma_I = 1/2 \text{ tr } \sigma$ and $\sigma_{II} = (1/2 \text{ tr } \sigma' \sigma')^{1/2}$ where $\sigma' = \sigma - \sigma_I 1$ Is the Deviatoric Stress. The Diamond-Shaped Surface Is Visualized by Rotating the Curve Around the Abscissa, which Represents Independence of the Direction of the Principal Stress.**

When the stress state in the ice lies inside the yield surface, then the stress $\underset{\sim}{\sigma}$ is an isotropic function of the elastic strain $\underset{\sim}{e}$:

$$\underset{\sim}{\sigma} = (M_1 - M_2)\, \underset{\sim}{1}\, \mathrm{tr}\, \underset{\sim}{e} + 2M_2 \underset{\sim}{e} \tag{5}$$

where M_1 and M_2 are elastic moduli that have been given the values $M_1 = 10^7$ N/m and $M_2 = 0.5 \times 10^7$ N/m . The elastic strain satisfies the kinematic relation

$$\dot{\underset{\sim}{e}} - \underset{\sim}{W}\underset{\sim}{e} + \underset{\sim}{e}\underset{\sim}{W} = \underset{\sim}{D} - \underset{\sim}{D}_p \tag{6}$$

where the stretching $\underset{\sim}{D} = \frac{1}{2}(\underset{\sim}{L} + \underset{\sim}{L}^T)$, the spin $\underset{\sim}{W} = \frac{1}{2}(\underset{\sim}{L} - \underset{\sim}{L}^T)$, and the velocity gradient $\underset{\sim}{L} = \mathrm{grad}\, \underset{\sim}{v}$.

When the stress state is on the yield surface $\phi = 0$, plastic stretching occurs. As plastic flow occurs, the stress is constrained to the loading surface by the occurrence of plastic stretching $\underset{\sim}{D}_p$. The associated flow rule

$$\underset{\sim}{D}_p = \lambda \frac{\partial \phi}{\partial \sigma} , \qquad \lambda > 0 \tag{7}$$

requires that plastic stretching be orthogonal to the loading function at the instantaneous stress state.

The model equations are integrated using the finite difference scheme in Pritchard and Colony (1976). The discretization of the Chukchi Sea into a finite difference grid is shown in Figure 3. The cell size in the Bering Strait is about 15 km. The boundary conditions are a stress-free surface at the Strait, a traction across the north boundary which may be varied as a parameter, and a zero-velocity condition for all nodes lying on the coastlines. The Diomede Islands have not been included in the boundary. An initial attempt was made to include them by putting in a zero-velocity boundary condition in the center node in the Strait. However, calculations with this condition showed far too much influence due to the islands because of the coarseness of the grid. We believe that our decision to leave out the islands

ALASKA RESOURCES LIBRARY
U.S. DEPT. OF INTERIOR

introduces an error which does not affect our goal of obtaining a worst case for southward ice motion. This is because removal of the islands removes an impediment of southward flow.

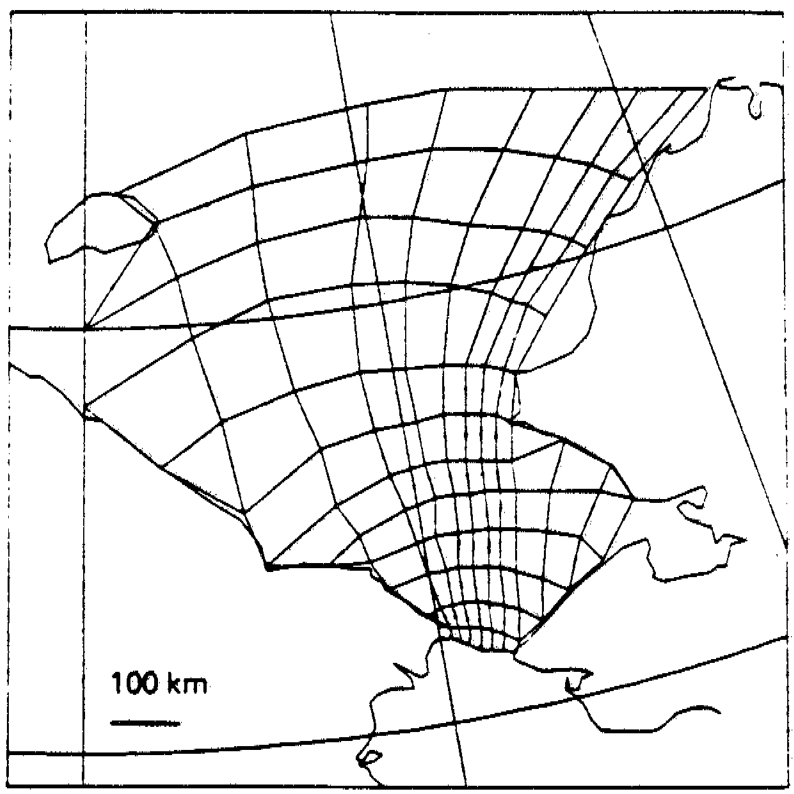

Figure 3. The Discretization of the Chukchi Sea into a Finite Difference Grid. The Cell Width in the Strait Is 15 km.

3. Ocean Current Model

The southern Chukchi Sea, for which the ocean currents are to be modeled, is a broad (200 to 300 km), shallow (approximately 50 m) basin which narrows, somewhat like a funnel, to the south where the Bering Strait connects it to the northern Bering Sea (see Figure 4). The central Chukchi Sea has depth variations of only 10 to 15 m, so major depth variations are confined almost entirely to regions close to the Alaskan and Siberian coasts. A number of topographic features define the northern edge of the area of interest. From west to east they are Long Strait, Wrangel Island, Herald Canyon, Herald Shoal (20 to 30 m), and Barrow Canyon.

A study was made of available oceanographic current data in the North Bering Sea, Bering Strait, Chukchi Sea, and Barrow Canyon regions. Much of the available data on currents and water mass movement has been collected and summarized by Coachman et al. (1975). More recent data from current meter moorings during 1976-77 are discussed in Tripp et al. (1978) and Coachman and Aagaard (1980). Most of the oceanographic data prior to 1975 were obtained during the summer or early fall. Long series of measurements are not available and, therefore, little work has been done to unravel the dynamics of the ocean currents. Coachman and Aagaard (1980) have begun to examine the dynamics with an 8-month current meter record, from September 1976 through April 1977 which includes a period from November through March when the Chukchi Sea was ice covered. While significant correlations between the current measurements and atmospheric pressure gradients are found, it is not yet possible to predict the ocean currents in detail from atmospheric forcing alone. For this reason, the typical current pattern has been deduced from the 1976-77 measurements in conjunction with the pre-1975 data.

Current meter data and water mass tracing from hydrographic sections indicate that during the summer there is a general northward flow through the Bering Strait. This flow divides in two, part passing to the east and part to the west of Herald Shoal. A southward moving current, the Siberian coastal water, is often observed in Long Strait and along the Siberian coast. This countercurrent does not appear to

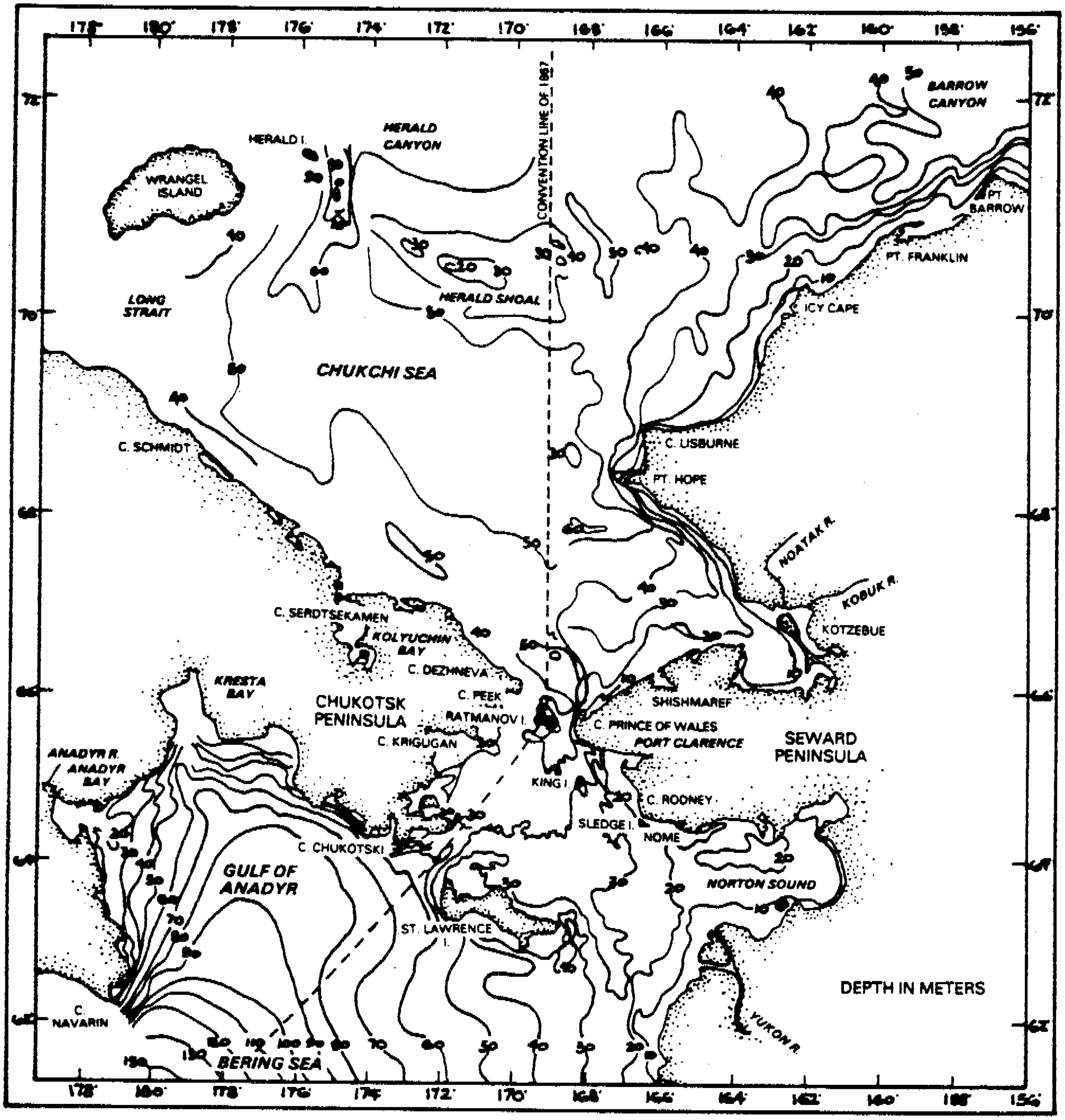

Figure 4. Chukchi Sea, Bering Strait, and Northern Bering Sea (from Coachman, Aagaard, and Tripp, 1975).

penetrate as far south as the Bering Strait but rather turns into or is mixed with the interior northward flow in the Chukchi Sea. The currents are observed to be strongly steered by the bottom topography such that the water transport between isobath contours is approximately conserved. In the summer, the water column is stratified and baroclinic currents are observed superimposed on the mean northward barotropic flow.

More recent current meter data indicate that the mean flow has some different characteristics in the winter, although the general pattern is thought to be similar. The current meter data from the winter of 1976-77 indicate that the mean flow was still northward but was significantly reduced in magnitude (from 1.5 to 2 x 10^6 m^3/s in the summer to 0.3 to 0.5 x 10^6 m^3/s in the winter). The flow also appeared to be more variable in the winter and periods of current reversal, sometimes with very strong southward flow as great as 5 x 10^6 m^3/s, were found to occur. This change from summer conditions appears to be due to changes in the prevailing atmospheric circulation and also the influence of the ice cover on the atmosphere-ocean coupling.

The correlations between Bering Strait transport and the atmospheric pressure field found by Coachman and Aagaard (1980) indicate that strong southward flow may be caused by a lowering of the sea level in the northern Bering Sea. This sea level change is caused by southward water transport under the combined effects of wind stress and atmospheric pressure. The variable ocean transports are fairly well correlated with atmospheric pressure gradients, and most of the energy in the measured currents was observed at time scales of 3 to 10 days, which is in agreement with the typical time scales of atmospheric systems moving over the area. Strong northerly winds can be particularly effective, as the ice cover in the Bering Sea is free to move to the south and thus the air stress is almost entirely transmitted to the water. On the other hand, northward ice movement in the Bering Sea is limited. This may help to explain why wintertime southward transport events seem to be more intense than northward transport.

Another feature observed in the current meter data is that during the winter the flow in the western Chukchi Sea is relatively unenergetic.

Variability seems to be reduced from the summer, the majority of the energy in the currents is for periods of 5 to 30 days, and the flow is generally toward the northwest in a broad, slow current. In contrast, the flow in the eastern Chukchi Sea, along the Alaskan coast, is highly variable. The kinetic energy of the eastern currents is concentrated at periods of 3 to 7 days and the energy density is about 5 times greater than that of the western currents.

For the ocean current model, it is assumed that the general current patterns and strong topographic steering observed in the summer and early fall data would also be found in the late fall and winter. During the winter, measurements in the Chukchi Sea have indicated that the water column is fairly homogeneous and the currents are nearly barotropic, which would further support the dominance by topographic steering. If, for example, one considers the potential vorticity $(\zeta + f)/\overline{H}$ it is possible to estimate the maximum deviations of the currents from an isobath; here, ζ is the vertical vorticity of the water relative to the rotating earth, f the local Coriolis parameter, and $\overline{H}$ the water depth (Stern, 1975). If potential vorticity is conserved, then $(\zeta + f)/\overline{H}$ must be constant. The variation in f over the region of interest is about 5 percent, while curvature of the isobaths along the Alaskan coast implies variations in ζ of 10 to 20 percent if the current follows the isobaths. For an average depth of 40 m, this implies the maximum depth variation of a current path would be $\pm$ 10 m. Typical variations would be much less in the central Chukchi with the maximum only approached near the coasts where isobath curvature is greater. But the lateral depth gradients are also greater near the coast, and thus the currents are still effectively constrained to follow the isobath contours. For the present model, variations of 10 m or less in the current depth would not significantly effect the current strengths or locations.

The ocean current model is generated by dividing the Chukchi Sea into a number of generally north-south trending regions (see Figure 5). These regions extend from the Bering Strait to an arc passing from Wrangel Island to Point Barrow. The boundaries of the regions are

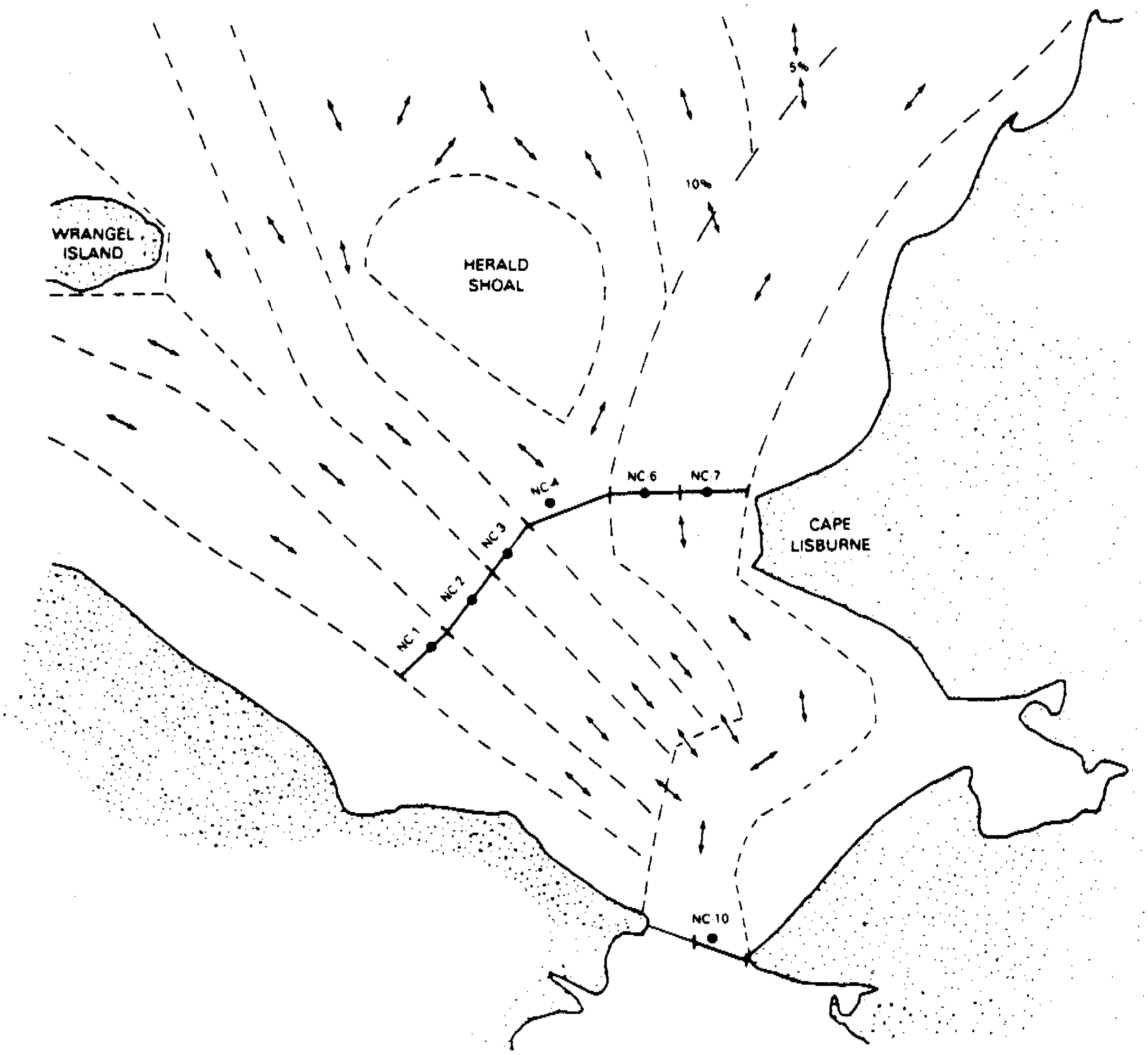

Figure 5. Current Meter Locations, Transport Sections, and Current Path Regions.

determined by the location of current meters in a section extending westward from Cape Lisburne and the bottom topography and general summer-fall current pattern. Figure 5 also shows the location of the current meters in the Cape Lisburne section, NC-1 through NC-7, as well as a current meter in the Bering Strait, NC-10. Each of the regions except the western most one contains one or more of the current meter stations. The north-south water transport in each region is determined by multiplying the cross-sectional area of the region along the current meter section times the perpendicular velocity component measured by the current meter. A similar calculation is made for NC-10 in the Bering Strait; however, the cross-sectional area used corresponds to the eastern half of the strait between Cape Prince of Wales and Big Diomede Island. Measurements have indicated that the flow through the Bering Strait is not, in general, uniform from east to west and it is desired to keep this freedom in the current model. This is implemented by assuming that the transport through the western half of the Bering Strait equals the difference between the transport through the Cape Lisburne section and the transport through the eastern half of the Strait.

Because the boundaries of the above-described regions are chosen to follow the expected current paths, the northward or southward transport in each region is constant. In this discussion, northward and southward in the Chukchi Sea are taken to mean flow away from and toward the Bering Strait, respectively. Therefore, with the transports in any region determined from the current meter sections, it is possible to calculate the water velocity at other points in the Chukchi Sea. A local current vector is calculated by assuming the direction of the current to be parallel to the region boundaries, and the current magnitude is taken to be the local transport, appropriate to the region, divided by the local cross-sectional area of the region. For points located near the boundary of two regions, an intermediate current vector is found by interpolation.

By using the above model, the current meter data are extrapolated to give currents over the Chukchi Sea. It is assumed that the current meter readings are representative of the mean currents within their section. This appears reasonable as adjacent current meters are found to be highly correlated by Coachman and Aagaard (1980) and the vertical velocity variations are believed to be less than 10 percent in the winter.

The current meter data are smoothed over a 25-hour period (to remove tidal contributions) and a new time series is produced by selecting consecutive midday values. These are used to calculate the transports and then to extrapolate values for the entire current field. This technique gives an instantaneous, coherent current field change which does not include phase differences in the current response from one part of the Chukchi to another, unless these changes are already included in the current meter measurements. For the southward flow events, Coachman and Aagaard (1980) found that from Cape Lisburne to south of the Bering Strait, the sea level changes and transport are nearly in phase on time scales of a day. Thus, for the periods of greatest interest to the present study, it is felt that no serious error is introduced into the current pattern.

One further point to consider is that the current meters and Cape Lisburne transport sections do not extend all the way to the Siberian coast. It is not believed that this causes any significant error in the total transport through the Bering Strait or in the current field. First, the currents in the western Chukchi Sea are on the average much weaker than those along the Alaskan coast. Second, the end of the NC-1 current meter section is chosen to correspond to the typical extent of influence of the Siberian coastal water (see Coachman and Aagaard, 1980). This water rarely, if ever, reaches the Bering Strait. Presumably, it turns and returns northward either along the coast or after mixing with the interior Chukchi Sea flow. This implies that the transport through the Cape Lisburne section might be biased toward northward flow if it includes some of the returning Siberian coastal water. But from the mean velocities in this region, the total additional transport is not likely to be more than 0.2 to 0.3 x 10^6 m^3/s while maximum southward transport is 5 x 10^6 m^3/s and typical southward flow is 1 to 2 x 10^6 m^3/s. Thus, the maximum errors in Bering Strait transports and velocities from this source are of the order of 10 to 20 percent.

The current field constructed in this way for 4 February 1977 is shown in Figure 6. This date is chosen because it corresponds to the largest observed southward current event during the 1976-77 experiment when the Chukchi Sea is ice covered. Southward current speeds reached values of about 0.5 m/s.

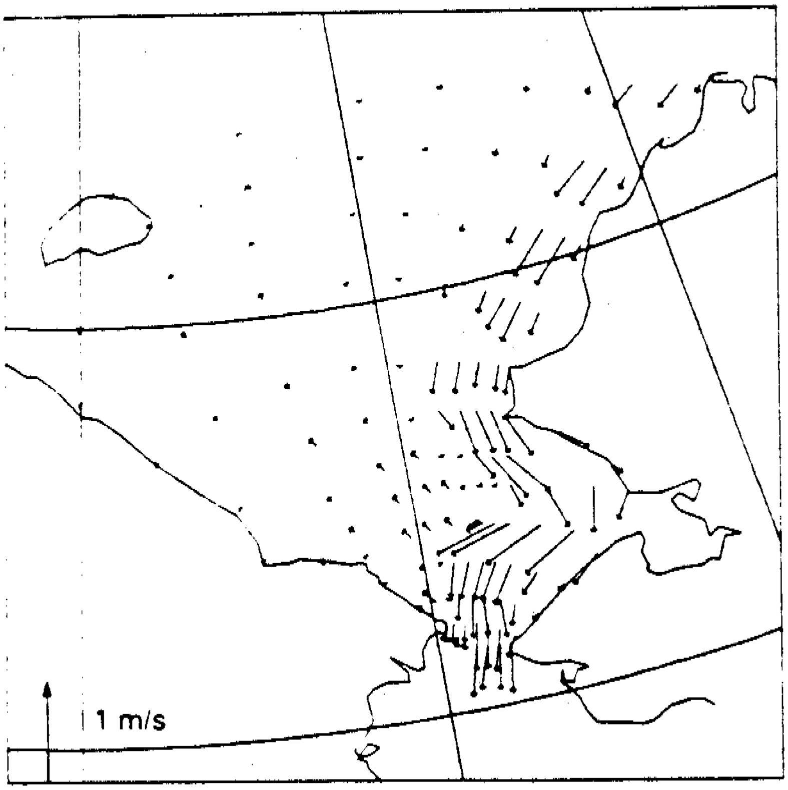

Figure 6. Current Field Constructed from Buoy Data on 5 February 1977. The Scale Arrow Represents a Velocity of 1 m/s.

4. Wind Field Model

The purpose of the wind field model is to represent an extreme of possible conditions, not to simulate the wind conditions as they exist on a particular day over the Chukchi Sea. This is motivated by our worst case approach, where we look at the conditions leading to the largest possible southward ice transport. To this end, we have taken a 20 m/s (40-knot) wind, distributed uniformly over the Chukchi, and varied its direction as a parameter. This applies a stress on the ice cover of 0.5 Pa , a value that is extremely large for the air stress but small in comparison to the loads resulting from ocean currents. The wind directions are chosen so that the resulting air stress is along the Alaskan coast between Pt. Barrow and Cape Lisburne in one case and offshore in the other. These are shown in Figures 7a and b, respectively.

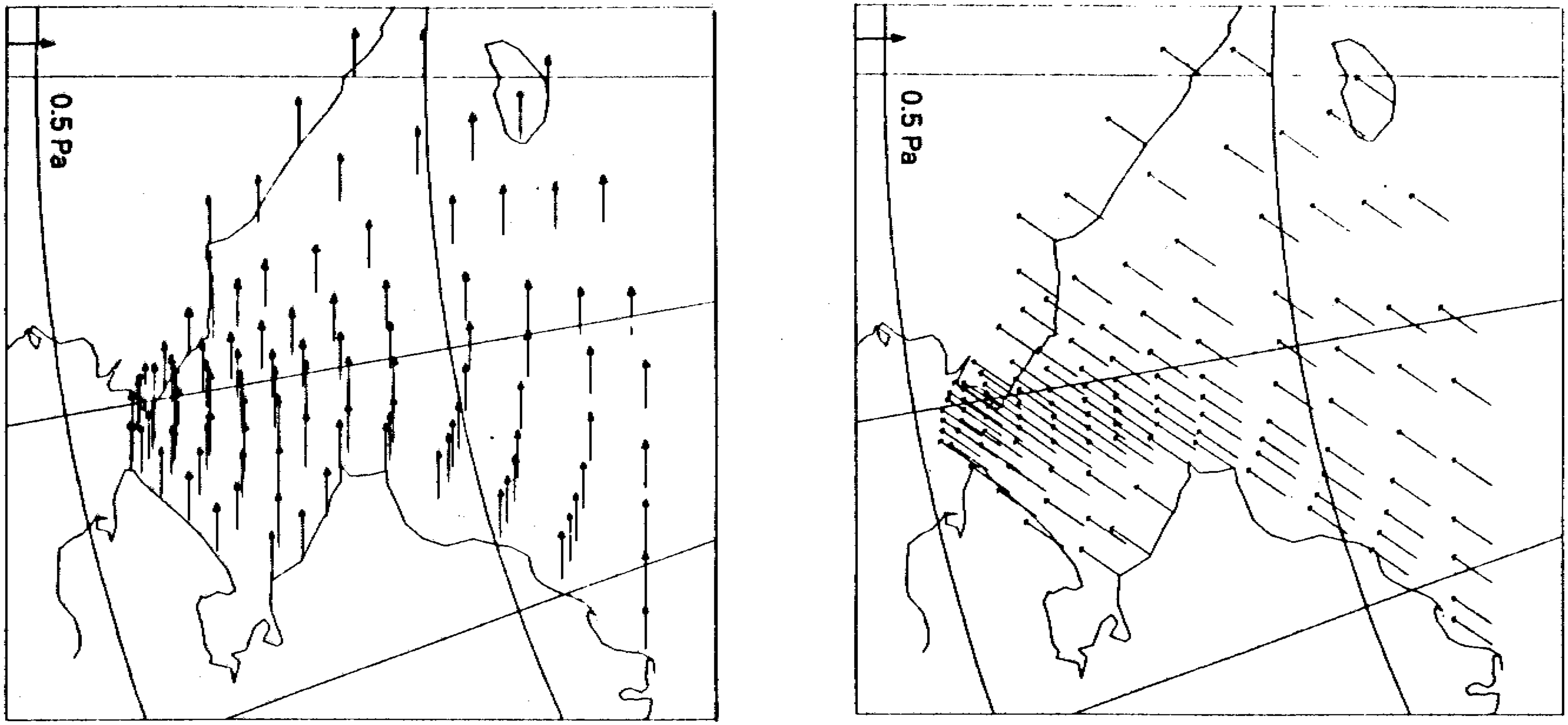

(b) Offshore Wind

(a) Alongshore Wind

Figure 7. Air Stress Fields Corresponding to a 20 m/s (40-Knot) Wind in the Two Orientations Tested.

5. Scaling of Model Equations

A nondimensional form of the mathematical model is introduced to allow the widest applicability of results of a minimum set of numerical calculations. After obtaining solutions of the nondimensional ice velocity as a function of nondimensional driving forces, actual ice velocity is determined for a range of reference velocities. This procedure minimizes the cost of numerical calculations, while at the same time it increases our understanding of the ice behavior by minimizing the number of parameters that can affect solutions.

Due to the limited ocean current data available, we scale the output of our calculations with the magnitude of the current velocity $\underset{\sim}{v}_g$. This technique allows us to predict the ice velocity as a function of current velocity for a range of other parameters. To carry out this velocity scaling, it is necessary to nondimensionalize the momentum balance equation. For a nondimensionalization of the complete model, the reader is referred to Pritchard and Thomas (1980). A portion of the derivation is repeated here because different values of the reference velocity are used. As a result, the dimensionless governing equations are slightly different.

We introduce nondimensional variables related to physical variables by reference values as follows:

$$\underset{\sim}{\tau} = \tau_R \bar{\underset{\sim}{\tau}} \qquad \underset{\sim}{v} = v_R \bar{\underset{\sim}{v}} \qquad \underset{\sim}{x} = x_R \bar{\underset{\sim}{x}} \qquad \underset{\sim}{\sigma} = \sigma_R \bar{\underset{\sim}{\sigma}} \tag{8}$$

where $\underset{\sim}{\tau}$ can represent air stress $\underset{\sim}{\tau}_a$ or water stress $\underset{\sim}{\tau}_w$, and $\underset{\sim}{v}$ can represent either ice velocity $\underset{\sim}{v}$, wind $\underset{\sim}{U}$, or ocean current $\underset{\sim}{v}_g$. The reference values are selected as

$$\begin{aligned} v_R &= v_g \\ \tau_R &= \rho_w c_w v_g^2 \\ \sigma_R &= p^* \end{aligned} \tag{9}$$

and $x_R = 85$ km , the width of the Bering Strait. The scalar v_g is selected as an appropriate speed from the ocean current field $\underset{\sim}{v}_g(\underset{\sim}{x})$

shown in Figure 6. For convenience we choose $v_g = 1$ m/s , an appropriate value that also allows us to interpret the ocean current field shown in Figure 6 as the nondimensional ocean current field $\bar{\underset{\sim}{v}}_g(\bar{\underset{\sim}{x}})$ without any further scaling. We shall perform all numerical simulations using the value of unity for v_g , and then determine the effect of longer or smaller ocean currents by varying this reference speed.

Substituting Equations (8) and (9) into the quasi-steady momentum balance provides the appropriate dimensionless momentum balance equation:

$$\bar{\underset{\sim}{\tau}}_a + \bar{\underset{\sim}{\tau}}_w + N_c \underset{\sim}{k} \times (\bar{\underset{\sim}{v}} - \bar{\underset{\sim}{v}}_g) + N_\sigma \bar{\nabla} \cdot \bar{\underset{\sim}{\sigma}} = 0 \quad , \tag{10}$$

where dimensionless air and water stress are given by

$$\bar{\underset{\sim}{\tau}}_a = N_a \, |\bar{\underset{\sim}{U}}| \, \underset{\sim}{B}_a \bar{\underset{\sim}{U}} \tag{11}$$

$$\bar{\underset{\sim}{\tau}}_w = |\bar{\underset{\sim}{v}} - \bar{\underset{\sim}{v}}_g| \, \underset{\sim}{B}_w (\bar{\underset{\sim}{v}} - \bar{\underset{\sim}{v}}_g) \ . \tag{12}$$

The dimensionless groups appearing as coefficients are given by

$$N_a = \frac{\rho_a c_a}{\rho_w c_w} \tag{13}$$

$$N_c = \frac{mf}{\rho_w c_w v_g} \tag{14}$$

$$N_\sigma = \frac{p^*}{\rho_w c_w v_g^2 \, x_R} \ . \tag{15}$$

The normalized wind $N_a^{1/2} \bar{\underset{\sim}{U}}(\bar{\underset{\sim}{x}})$ and the ocean current field $\bar{\underset{\sim}{v}}_g(\bar{\underset{\sim}{x}})$ each vary in space for each selected time (or input condition). Since v_g is arbitrary, the magnitude of the ocean current field no longer remains an independent parameter defining driving force. The ocean current field variations include only direction and spatial variations.

Other equations required to complete specification of the dimensionless model are unchanged from Pritchard and Thomas (1980). The reference values used in this work are chosen in part so that each dimensionless force in the momentum balance, Equation (10), is on the order of unity. Therefore, the relative importance of each force may be determined from the magnitude of the dimensionless group multiplying it, e.g., N_a , N_c , or N_σ . We must be cautious, however, when considering the stress divergence because the plastic behavior can concentrate stress gradients independently of the geometry of the outer boundary. In fact, we expect stress divergence to have a length scale closer to the minimum cell size of Figure 3, say 15 km. In this case $\overline{\nabla}\cdot\overline{\sigma}$ is more like 5 than unity. While not of paramount importance, this difference is enough to alter the relative size of the Coriolis and stress divergence forces.

The solution for the velocity field may be formally written as a function $\overline{\underset{\sim}{F}}$ of all driving forces and dimensionless parameters. We have

$$\overline{\underset{\sim}{v}} = \overline{\underset{\sim}{F}}\,(\overline{\underset{\sim}{x}}\ ,\ \overline{\underset{\sim}{v}}_g\ ,\ N_a^{\frac{1}{2}}\overline{\underset{\sim}{U}}\ ,\ N_c\ ,\ N_\sigma\ ,\ \alpha\ ,\ \beta) \quad , \tag{16}$$

where the entire field of $\overline{\underset{\sim}{v}}_g$ can in general affect the response at the location $\overline{\underset{\sim}{x}}$. It should be noted that nonzero boundary tractions along the northern boundary can also be included in the parameter list. For the study of southward Chukchi Sea ice motion, several of these variables can be neglected. The turning angles α and β in the planetary boundary layer and the oceanic mixed layer are held constant throughout the study. Also, we assume that the Coriolis force is less important than the stress divergence, and variations in Coriolis force can be ignored. To estimate the effect of this assumption, consider

$$\frac{N_c}{N_\sigma} = \frac{m f x_R v_g}{p^*} \quad . \tag{17}$$

For the chosen reference values, Equation (9), and a strength $p^* = 10^5$ N/m , we find that $N_c/N_\sigma = 0.24$. Since $\overline{\nabla}\cdot\overline{\underset{\sim}{\sigma}}$ is thought to be about 5 times as large as $\underset{\sim}{k} \times (\overline{\underset{\sim}{v}} - \overline{\underset{\sim}{v}}_g)$, the assumption is justified for this case.

The nondimensionalization of the model allows solutions to be obtained far more economically and also helps provide understanding of the ice behavior. It is seen clearly that strength p^* and length scale x_R affect N_σ as the square of v_g and inverse square of v_g , respectively. Thus, as length scale is reduced, equal ice stress divergence effects are observed at scaled-down strength. Also, comparable increases in strength p^* and ocean current square v_g^2 cause comparable increases in normalized ice velocity, while actual ice velocity is further scaled by v_g . These results have allowed us to simulate $\bar{\underset{\sim}{v}}$ as a function of both v_g and p^* . As will be seen, this allows us to build up a trajectory of ice motions from a history of values of ocean currents (given by v_g), and this trajectory can then be presented for different, fixed strengths p^* .

6. Results

Numerical simulations have been performed to determine the effect on Chukchi Sea ice motion of ocean currents, wind, ice strength, and loads from the Beaufort Sea ice pack. The results of this parameter study could be presented in terms of the nondimensional velocity $\underset{\sim}{v}/v_g$ and stress $\underset{\sim}{\sigma}/p^*$ derived in an earlier section of this report (Section 5). This presentation allows us to collapse the parameter list to the strength parameter N_σ (Equation (15)), the wind $\overline{N_a^{\frac{1}{2}}}\underset{\sim}{U}$, and the boundary traction at the northern boundary from the Beaufort Sea pack. The separate effects due to variations in strength and ocean current magnitude are then inferred by considering the values that define the nondimensional groups that have been discussed previously. We choose, however, to present results of physical velocity $\underset{\sim}{v}$ and stress $\underset{\sim}{\sigma}$ variables because each of these is somewhat simpler to interpret. Because of our simple reference values, it is convenient to present either result.

In the results that follow, each of the three parameters is varied independently. Variations in the strength coefficient N_σ are accomplished by varying ice strength p^* while holding other parameters constant.

6.1 Ice Strength Effects

Three model simulations are presented to learn the effects of ice strength on ice motions. For these calculations, wind stress is assumed zero, ocean current is as given in Figure 6, and strength p^* takes the values 10^6, 10^5, and 10^4 N/m . In addition, free drift (where $p^* = 0$) is known to satisfy $\underset{\sim}{U} = \underset{\sim}{v}_g$. Free-drift ice velocity is given by $\underset{\sim}{v}_g$ in Figure 6 for this case where air stress is zero. These values span the range of extreme values of interest in the Beaufort Sea and it is expected that they are also appropriate for the Chukchi Sea.

At the highest strength, $p^* = 10^6$ N/m , the entire ice cover on the Chukchi Sea remains elastic. That is, at no location does plastic failure occur. This stress field is presented in Figure 8. The scale arrow in the lower left corner represents a compressive principal stress component of magnitude equal to 10^6 N/m . As a result of the absense of plastic failure, there is no ice motion. There would be no motion at higher strengths either. At somewhat lower values of strength, localized failure will occur. This localized failure will likely occur first at the Bering Strait and then spread as strength is reduced. The maximum strength at which some ice motion occurs everywhere along the Alaskan coast has not been determined exactly, but it must be some value less that 10^6 N/m for fixed values of the other parameters.

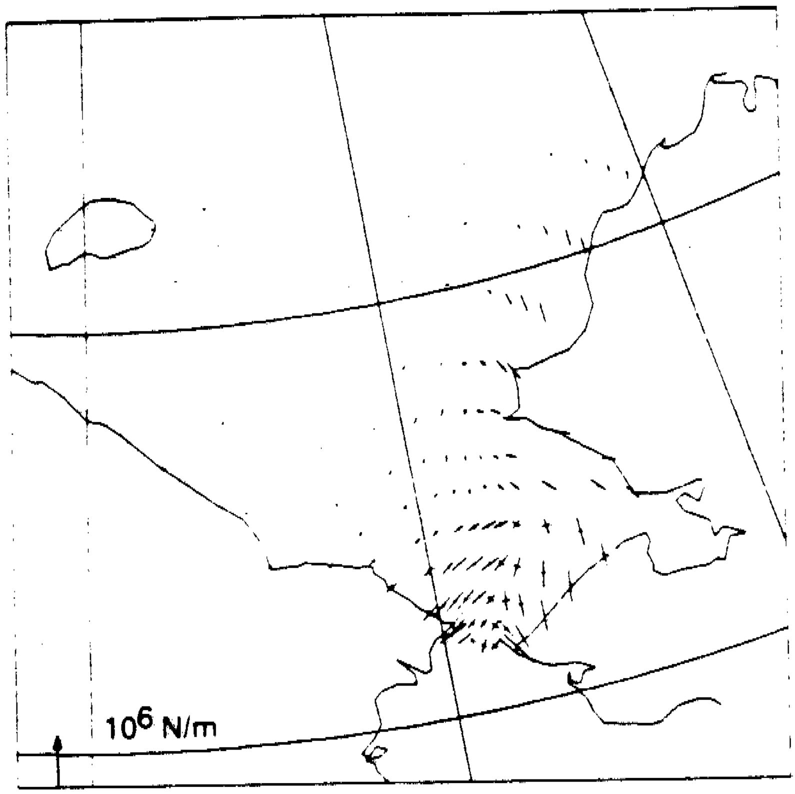

Figure 8. **Stress Field with no Applied Boundary Traction or Wind and an Ice Strength of 10^6 N/m. The Ice Velocity Is Zero Everywhere in this Case.**

The stress field in Hope Basin (Figure 8) is typical for a region in which an arch has formed. The large compressive principal stress is transmitted generally from the Alaskan coast to the Siberian coast. The nearly zero principal stress along the free surface can also be observed.

At a strength of 10^5 N/m , flow occurs. The velocity and stress fields are shown in Figure 9. The velocity scale arrow in Figure 9a represents a velocity of 1 m/s, and the stress scale arrow in Figure 9b

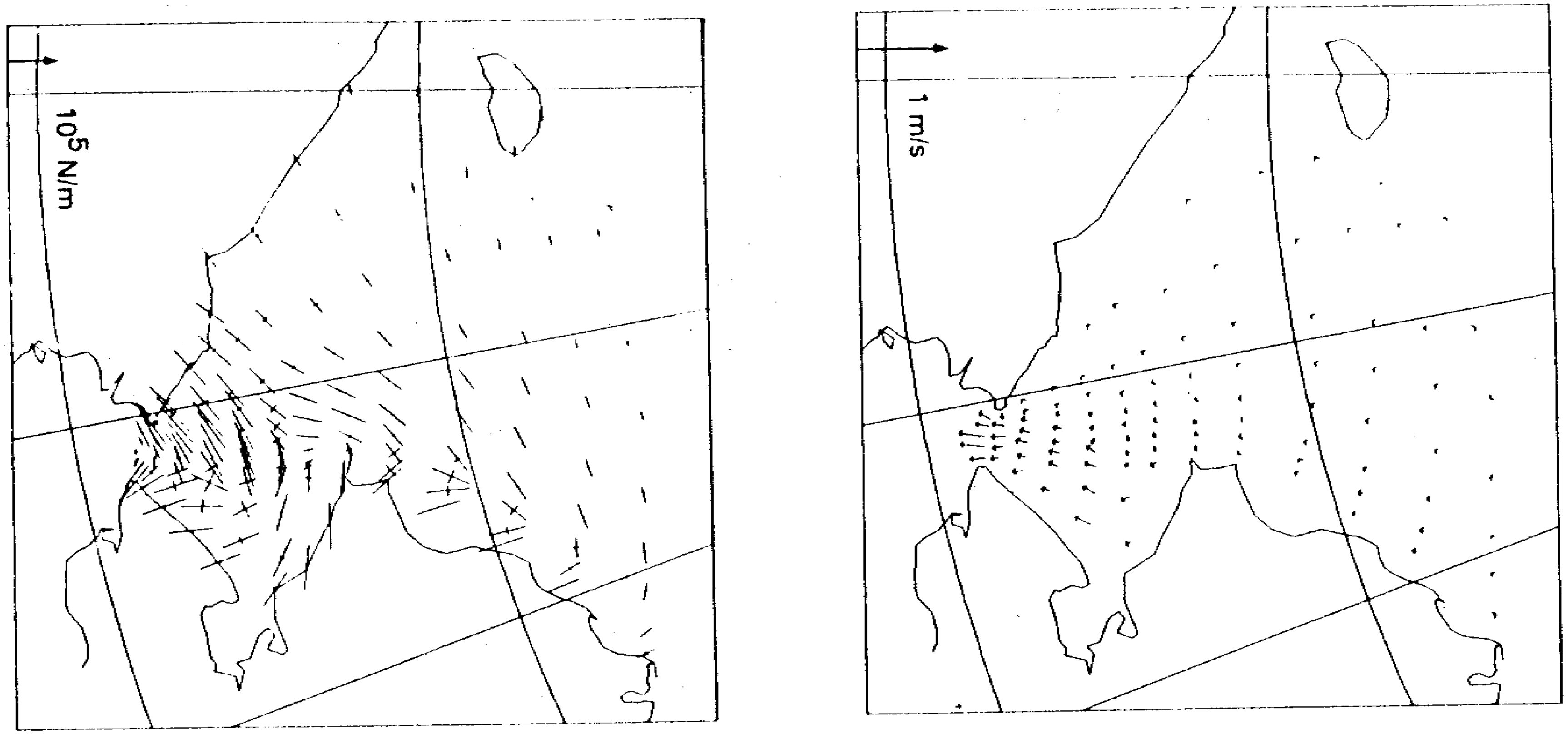

(b) Stress Field

(a) Velocity Field

Figure 9. Velocity and Stress Fields with No Applied Boundary Tractions or Wind Stress and an Ice Strength of 10^5 N/m.

is again representative of a compressive principal stress of magnitude p^* ($\equiv 10^5$ N/m for this calculation). At this strength, there is very little motion north of Cape Lisburne. A nominal value of 0.13 m/s is established. This value is used in the synthesis of results.

The stress pattern in Hope Basin is again rather typical for supporting the arch across the Bering Strait. Thus, even though the arch has collapsed, allowing southward ice motion, the stress field is relatively unchanged. An even more interesting result is observed to the north and west of Hope Basin, however. Large compressive stress is observed along the line from Pt. Barrow past Cape Lisburne all the way to the Siberian coast. This stress component restrains ice motion north of Cape Lisburne even when the arch across the Bering Strait has collapsed allowing ice in Hope Basin to move southward. This result was unanticipated and it is a very important effect on the motion of oiled ice in the northern Chukchi Sea. This effect is to impede southward motion.

Similar results are presented in Figure 10 for a yield strength of 10^4 N/m . The velocity scale is again represented by the scale arrow indicating a magnitude of 1 m/s and the stress scale arrow representing p^* ($\equiv 10^4$ N/m for this calculation). Ice motion is larger in the northern Chukchi. A typical value of 0.73 m/s is used for synthesis. The ice follows the general direction of the ocean current.

An important point concerning the presence of the Pt. Hope peninsula can be made at this time. Recalling the model description of water drag, Equation (3), the result of integrating through the oceanic boundary layer was a turning angle of 20^o between the water velocity and the water drag vector, measured counterclockwise from the water velocity vector. Careful comparison of Figures 9a and 10a with Figure 6 shows this to be the case. As a result, the ocean currents tend to drive the ice slightly toward shore, and the Pt. Hope peninsula apparently offers a significant impediment to the ice motion. Further discussion of the velocity field is presented in the next section (Section 7).

In order to test the hypothesis that currents are primarily responsible for southward ice transport, a study has been made of the effect boundary tractions and winds have on the ice velocity. These results

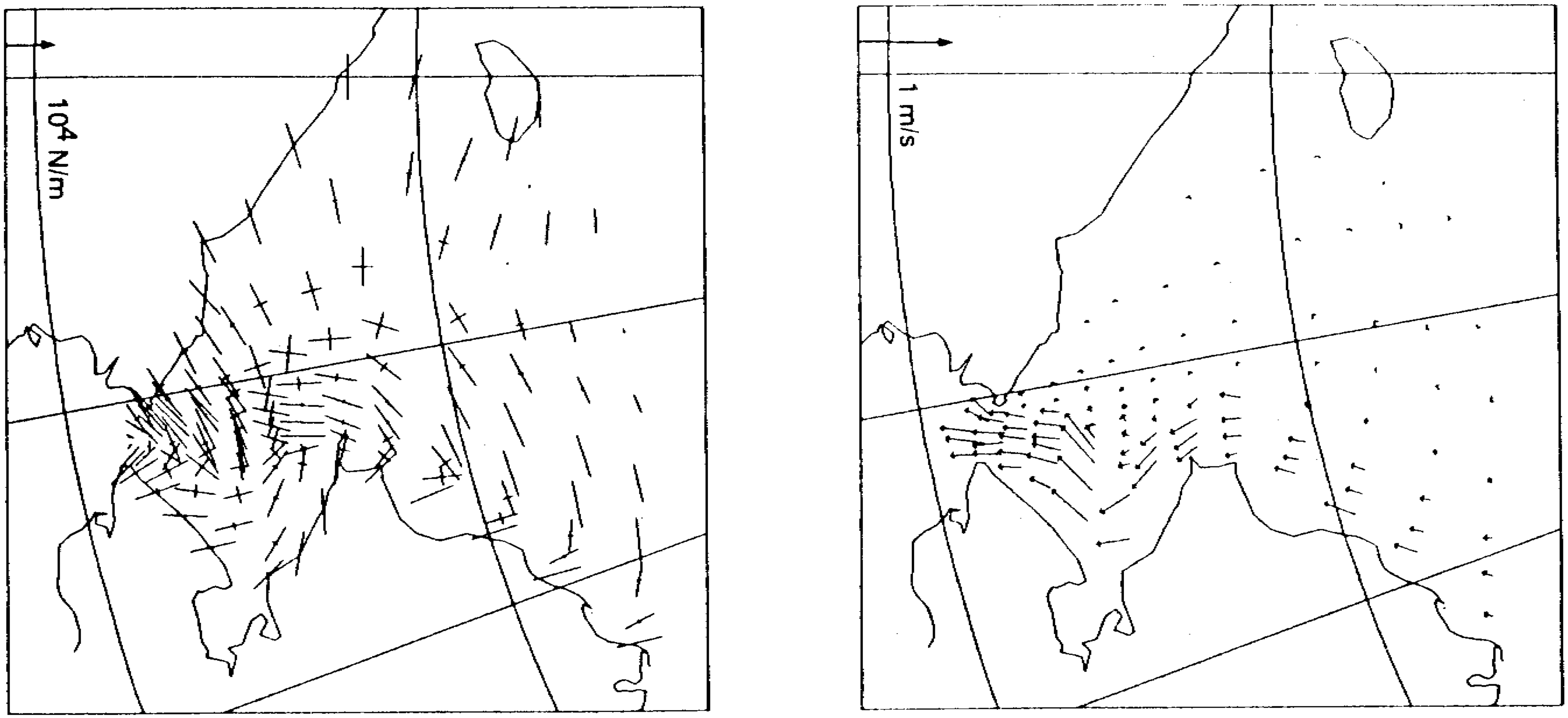

(b) Stress Field

(a) Velocity Field

Figure 10. Velocity and Stress Fields Resulting from Ocean Currents with No Applied Boundary Traction or Wind Stress and an Ice Strength of 10^4 N/m.

are presented in the following two subsections. Again, it should be emphasized that the primary concern is whether the ice north of Cape Lisburne and south of Pt. Barrow can attain an appreciable velocity. If large ice motions can occur frequently in this region, then the likelihood of transporting oiled ice from the Alaskan north slope into the Bering Sea is large. On the other hand, if the ice motion between Pt. Barrow and Cape Lisburne is always small, then it is unlikely that oiled ice can be transported into the Bering Sea.

6.2 Pack Ice Loads

Figure 11 shows the velocity and stress fields in terms of principal stresses resulting from the application of a downward traction across the top of the grid. This calculation models the effect of the Beaufort Sea ice pack on the Chukchi Sea ice. It is not known what the magnitude of such a traction would be but it cannot exceed the strength p^* ($\equiv 10^5$ N/m for this calculation). At this level, plastic failure would occur and limit the stress state in the northern Chukchi. Hence, in nondimensional variables, this result is independent of the ice strength. The basic current field shown in Figure 6 is applied and the wind stress is zero.

This ice velocity (Figure (11a)) is increased slightly by the boundary traction, but the increase is small (compare with Figure 9a). The stress field (Figure 11b) clearly shows that the load across the top is taken up by the Siberian coast, without producing a significant velocity along the Alaskan coast. The Pt. Hope peninsula essentially protects the Strait from the Arctic ice pack when the applied load is southward. The possibility of a load occurring in a southeasterly direction is not thought to be likely, since Beaufort Sea ice motion is westward at the Chukchi Sea's northern boundary. The ice velocity field is changed little by this load.

6.3 Wind Loads

Figure 12 shows the velocity and stress fields resulting from a uniform wind stress applied parallel to the shore between Pt. Barrow and Cape Lisburne (see Figure 7a). The magnitude of the wind stress is 0.5 Pa corresponding to a 20 m/s wind. The ocean currents shown in Figure 6 are acting concurrently. Ice strength is 10^5 N/m and no boundary

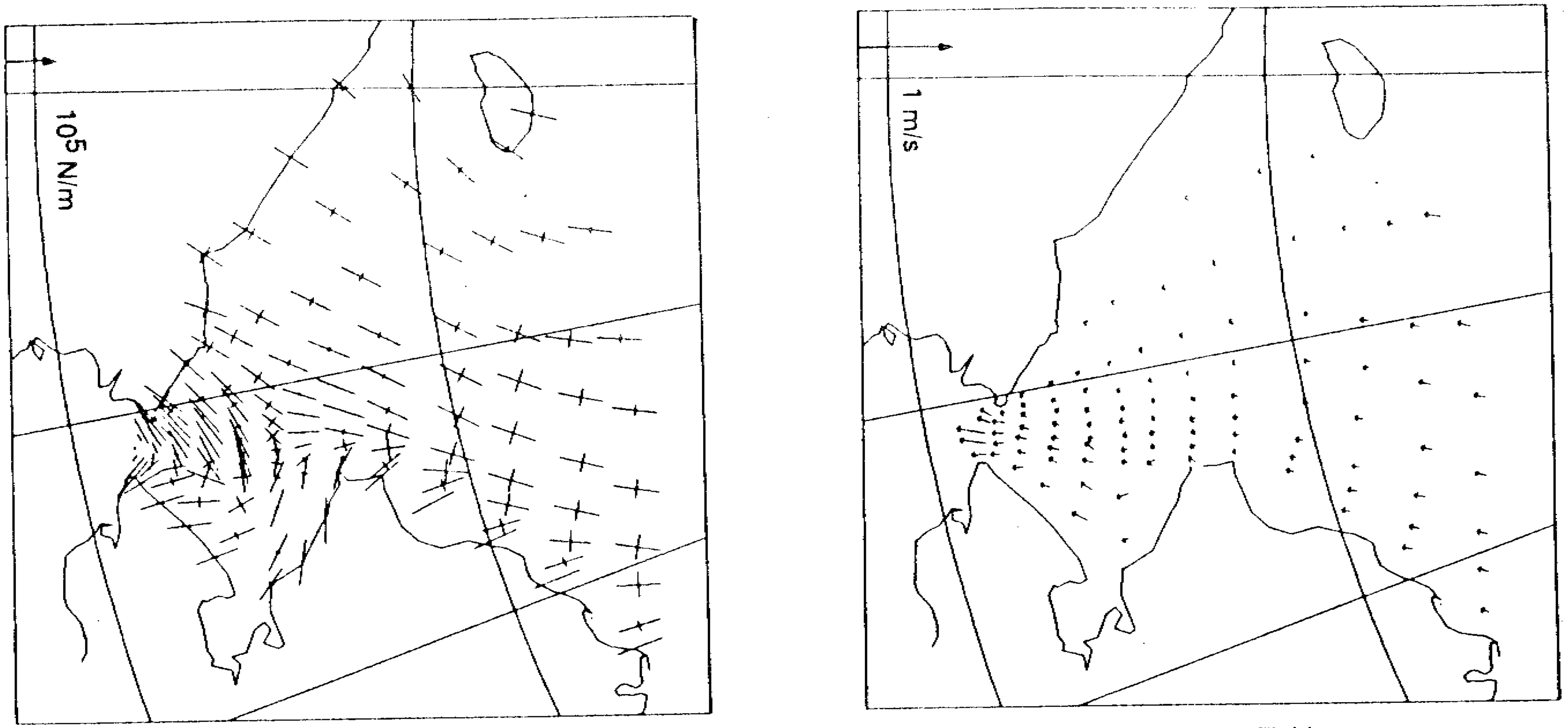

(b) Stress Field

(a) Velocity Field

Figure 11. Velocity and Stress Fields Resulting from a Traction Applied Straight Downward. Currents but Not Winds, are Present, and the Ice Strength Is 10^5 N/m.

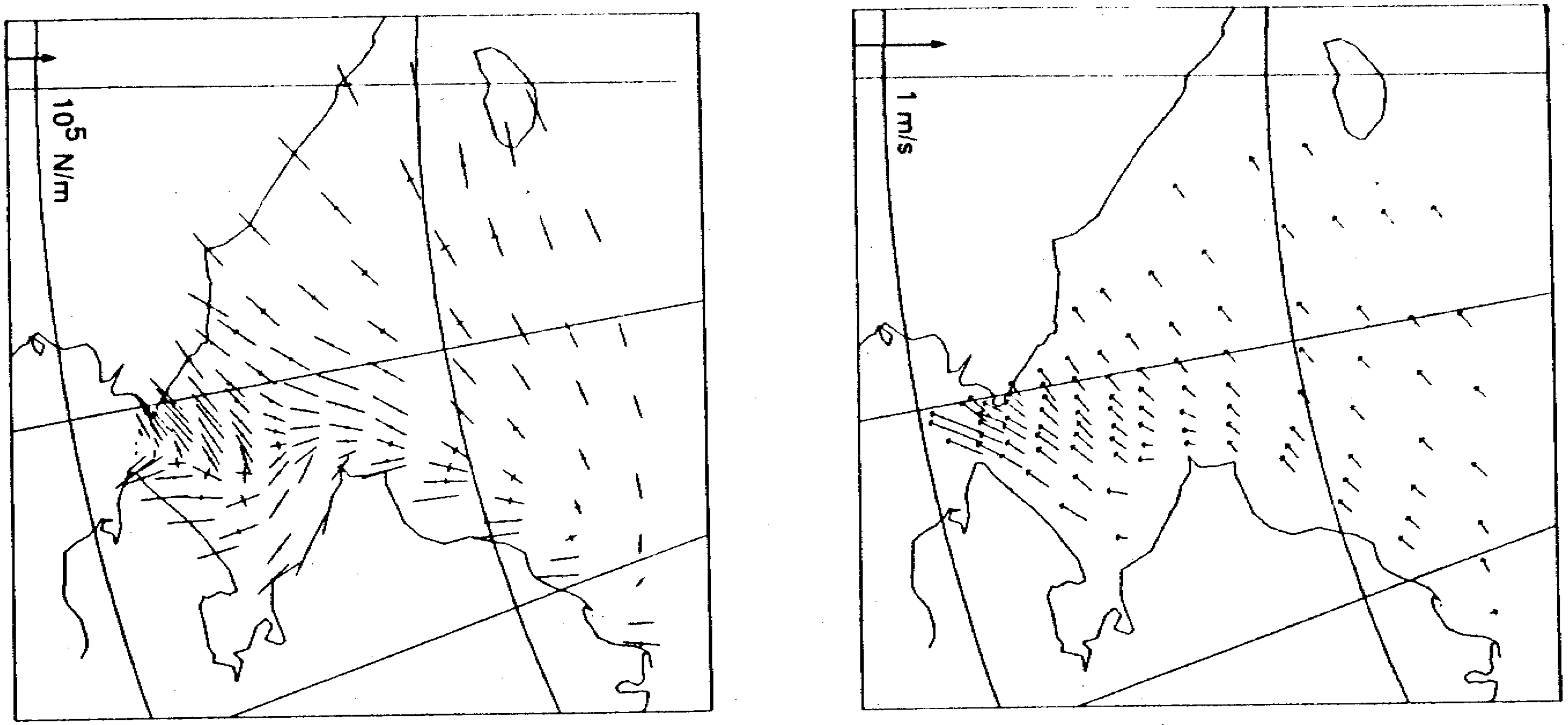

(b) Stress Field

(a) Velocity Field

Figure 12. **Velocity and Stress Fields Resulting from an Alongshore Wind Stress, Ocean Currents, and an Ice Strength of 10^5 N/m.**

traction is applied. It is again apparent that the Siberian coast takes up the loads applied to ice north of Cape Lisburne. The resulting ice velocity along the Alaskan coast between Pt. Barrow and Cape Lisburne is on the order of 20 km/day. Although this is a large contribution to the motion, the frequency of occurrence of such large winds, is low. Therefore, this is unlikely to account for a significant amount of southward ice transport.

An attempt was made to rotate the total force vector away from the coastline by applying an appropriate air stress. This is the motivation for choosing the stress field in Figure 7b. The resulting velocity and stress fields are shown in Figure 13. The southward ice motion is not enhanced, although ice moves offshore of the coast of Alaska. The stress field is not changed appreciably.

For both the pack ice loads and the southward air stress, the loads were chosen with the intent of maximizing ice velocity along the Alaskan coast. In both cases, the result was that the Siberian coast continues to take up most of the load. An arch is being formed roughly between the Siberian coast and Cape Lisburne. The large value of compressive stress apparently will remain as long as ice strength remains high. Therefore, we observe that ice strength must be reduced by creation of open water during shearing and dilating along the coast of Alaska if larger ice motion is to occur at these applied loads.

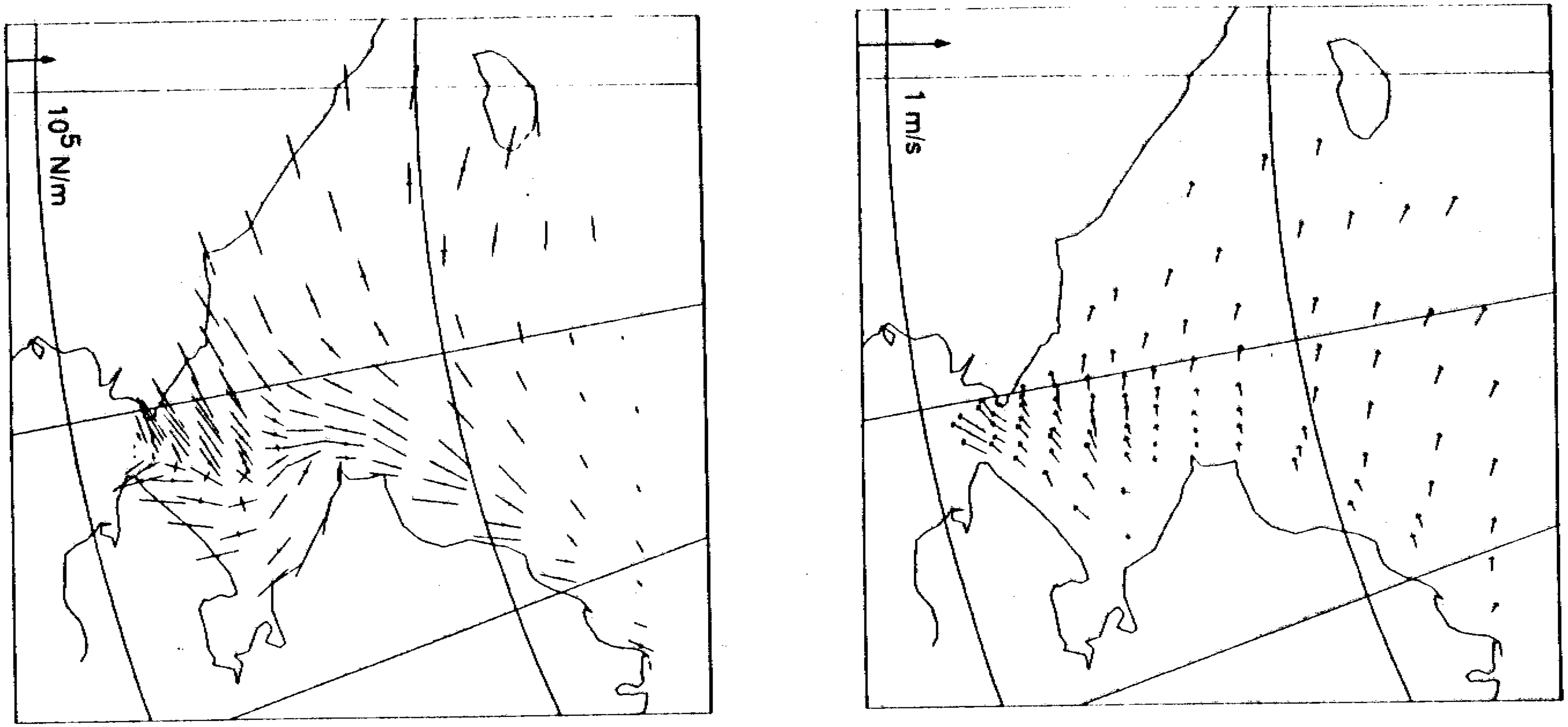

(b) Stress Field

(a) Velocity Field

Figure 13. Velocity and Stress Fields Resulting from an Offshore Wind Stress, Ocean Currents, and an Ice Strength of 10^5 N/m.

7. Ice Transport

We use the results of nondimensionalization of the model equations in Section 3 to determine the ice velocity as a function of ocean current magnitude (equal to the reference velocity). The reference velocity has been chosen to be unity for the calculated cases. It can be changed arbitrarily if its effect on N_σ is included properly. If the ocean current field depends only on this magnitude, then a wide range of ocean current conditions are described by varying v_g and using the normalized equations.

The ice velocity at any location $\underset{\sim}{x}$ satisfies Equation (16). If we suppress all parameters that are either unimportant or are not varied, then the ice velocity at a fixed location is

$$\underset{\sim}{\bar{v}} = \underset{\sim}{\bar{F}}(N_\sigma) \tag{18}$$

where no air stress or boundary traction is applied. The speed at this location can be found from the magnitude of $\underset{\sim}{\bar{F}}$. If nondimensional variables are replaced by their physical counterparts using Equations (8) and (15), we find that ice velocity $\underset{\sim}{v}$ satisfies

$$\underset{\sim}{v} = v_g\, \underset{\sim}{\bar{F}}\left(\frac{p^*}{\rho_w c_w v_g^{\,2} x_R}\right). \tag{19}$$

There are four values of $\underset{\sim}{\bar{F}}$ available if we assume wind stress and boundary loads are zero. Three calculations were presented in Section 6 with p^* varied as a parameter. The resulting values of v/v_g are plotted in Figure 14. The fourth value comes from our knowledge of the fact that at zero (or negligible) ice strength, $v/v_g = 1$. There is some uncertainty in the results for large values of N_σ because we have not determined the minimum strength at which ice motion begins. However, since even large errors in the abscissa lead to small errors in ice speed, this uncertainty is not important.

In order to obtain ice speed v as a function of p^* we pick two values of p^* (10^4 and 10^5 N/m), calculate N_σ for a range of v_g , pick values of v/v_g from the curve in Figure 14 and multiply by the

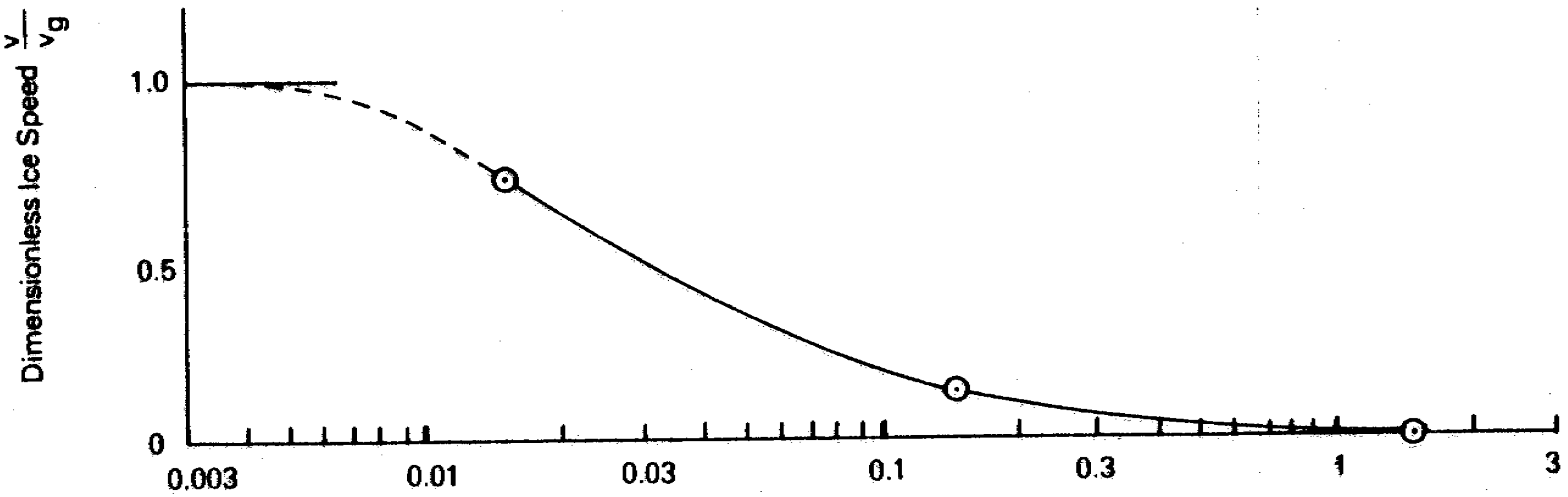

Dimensionless Strength $N_\sigma = \dfrac{p^*}{\varrho_w c_w v_g^2 x_R}$

Figure 14. Values of Four Dimensionless Velocities, Obtained from Model Calculations, and the Limiting Case of Free Drift as a Function of Dimensionless Strength.

appropriate v_g to calculate v. These results are shown in Figure 15. Note that for $p^* = 10^5$ N/m , there is an ocean current threshold of about 0.10 m/s below which the ice does not move. The threshold for this smaller p^* is not noticeable on this scale.

We now make a calculation which allows us to predict the history of ice movement through the course of the winter of 1976-77. Given v as a function of v_g for each value of p^* in Figure 15 and given the time history of v_g for the winter of 1976-77 from Coachman and Aagaard (1980) (shown as the upper curve in Figure 16 since $v = v_g$ for free-drift with no northward motion), we can calculate a time history of ice speed v for the length of the data record. This is done for two values of p^* in Figure 16. The time histories of current speeds shown in Figure 16 is taken from a meter located approximately 50 km west of Cape Lisburne. No northward motions are permitted. This is consistent with our intent of finding upper limits of southward ice motions.

The final objective of these calculations is obtained by integrating the ice velocity histories in Figure 16 to obtain ice trajectories through the course of the winter. To simplify this calculation, we assume that current speed does not vary along the Alaskan coast between Pt. Barrow and Cape Lisburne. Figure 17 shows the distance traveled by pack ice orginating at Pt. Barrow on 1 December 1976 for two values of ice strength. This distance represents the case where wind and boundary traction are zero so that only the ocean current and ice stress affect the ice trajectory. For comparison, a free drift trajectory is also shown in Figure 17. It is seen that major differences occur as strength is varied between free drift, 10^4, and 10^5 N/m. In the case of free drift, late-winter drift during 1976-77 carries ice from Pt. Barrow nearly to the Bering Strait. On the other hand, when $p^* = 10^5$ N/m , there is only about 100 km of motion. At the intermediate strength, the ice drifts about 400 km to a point midway between Point Lay and Cape Lisburne.

Since these results show a strong dependency on strength, and since we are unable to prove that it is impossible for oiled ice to be transported through the Bering Strait, we recognize that an even more thorough

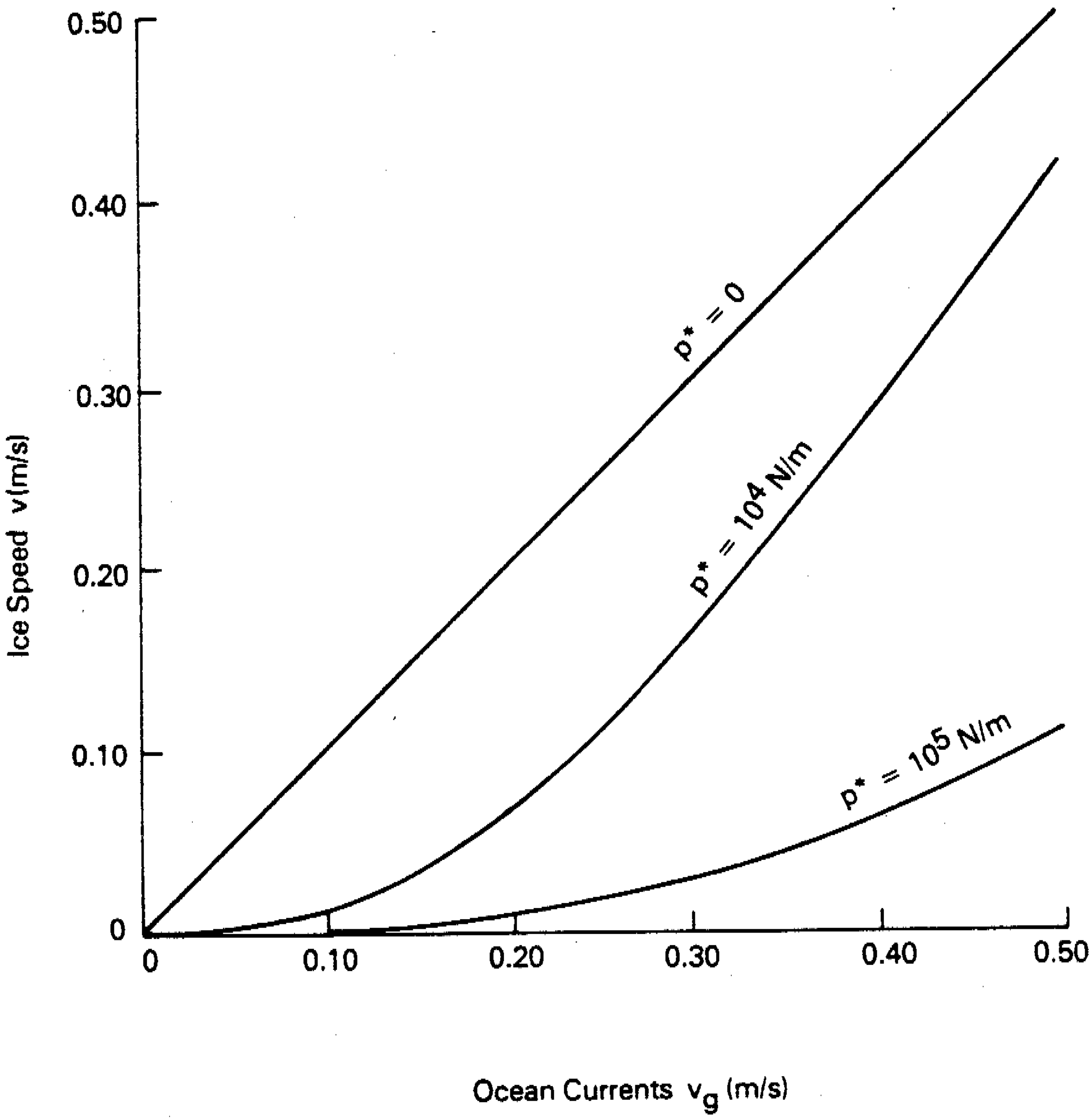

Figure 15. **Ice Velocity as a Function of Ocean Current at Constant p*, Obtained from Figure 14 by Interpolating Between Data Points and Introducing Appropriate Reference Variables.**

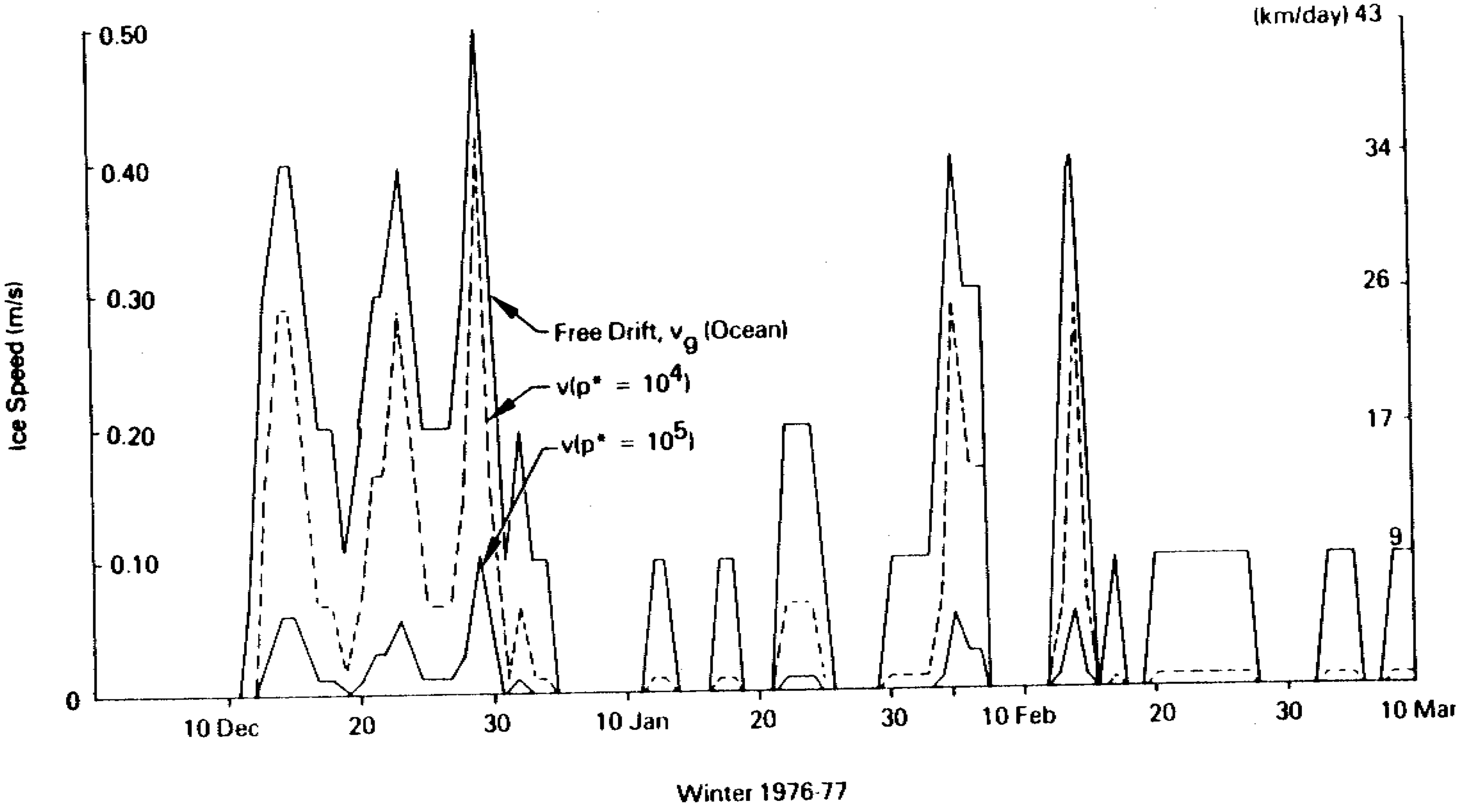

Figure 16. Ice Motion and Ocean Current History. Ocean Current Magnitude of Southward Flow Is Shown in Upper Curve. It Represents Free Drift Ice Speed. The Lower Curves are Ice Speeds Obtained by Scaling the Water Velocity by a Factor Obtained from Figure 15 for Each of the Strengths Indicated.

analysis is required in future work. It would be erroneous to think that a better knowledge of ice strength is all that is required to improve our understanding of the Chukchi Sea ice behavior, however. Instead it is necessary to consider the feedback effect of deformation of the ice on its strength. Thus, the perfectly plastic simulations presented in this work must be replaced by hardening/softening plastic simulations. Since substantial fractions of open water and thin ice can be created during deformation of the ice, the effect on strength is likely to be important.

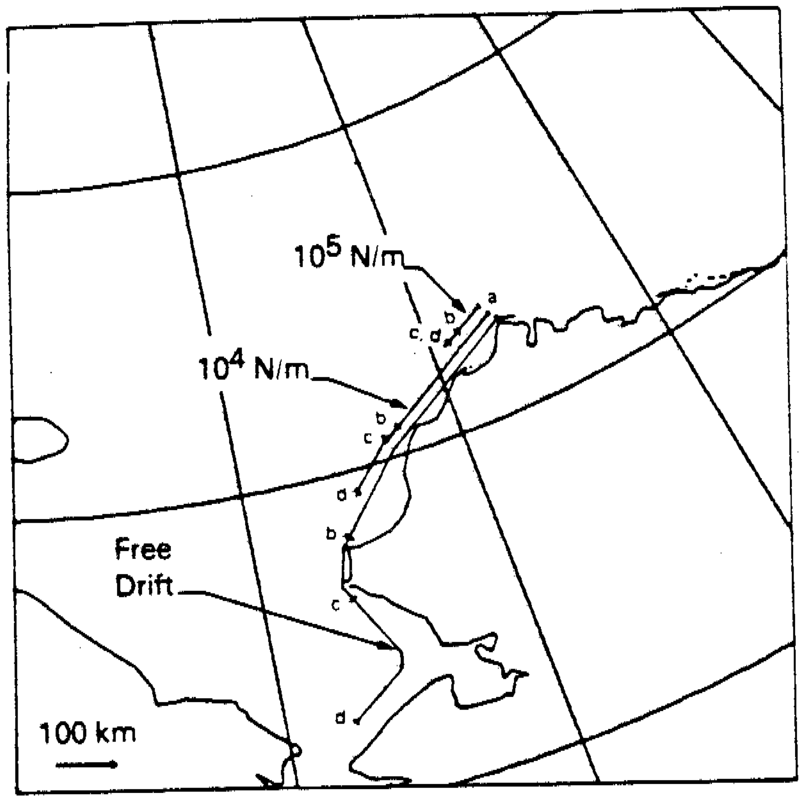

Figure 17. Trajectories Obtained for Free Drift, Strong Ice ($p^* = 10^5$ N/m), and Weak Ice ($p^* = 10^4$ N/m) by Integrating the Velocity Histories in Figure 16. The Symbols a, b, c, and d Represent Locations During Winter 1976-77 on 1 December, 1 January, 1 February, and 1 March, Respectively.

8. Conclusion

A numerical simulation of southward ice motion in the Chukchi Sea has been conducted, where wind stress and ice strength are parameters and actual ocean current data are used to compute the water stress. The sea ice model is one developed during AIDJEX with the ice redistribution capability removed. In addition, stress boundary conditions are introduced to describe the behavior of a free ice edge instead of the velocity boundary conditions normally used by the AIDJEX numerical model.

The ocean current field is extrapolated over the Chukchi Sea from data observed at seven current meters in the central Chukchi Sea during 1976-77. During the time period studied in this simulation, southward current velocities reached values of 0.5 m/s. The magnitude of the wind stress was not varied in this study, but the effect of two orientations of a 20 m/s (40-knot) wind on southward ice motion is determined. Ice strengths taking values of 10^4, 10^5 and 10^6 N/m are considered. A free drift simulation (zero strength) is also presented. A large dependence on ice strength is found. For free drift, ice is transported from Pt. Barrow to within 100 km of the Bering Strait between 1 December 1976 and 1 March 1977. No motion occurs when strength is 10^6 N/m. For a strength of 10^5 N/m, only 100 km of motion is simulated. When the strength is 10^4 N/m, ice is transported from Pt. Barrow nearly to Cape Lisburne.

Due to the coarseness of the grid used in the numerical calculations, we do not believe that ice motion in Hope Basin and through the Strait is adequately modeled. The effect of not accounting for the presence of the Diomede Islands is to predict an ice velocity in Hope Basin and the Bering Strait which is too large. The primary concern of this work, however, is to determine the magnitude of motions along the Alaskan coast between Pt. Barrow and Cape Lisburne, and an acceptable and conservative estimate of this velocity is found.

We found that ice velocities, resulting from observed ocean currents with zero wind stress and boundary traction could reach 0.3 m/s in the Hope Basin. At the same time, no appreciable ice motion occurs along the Alaskan coast north of Cape Lisburne. This motion is limited because the Siberian coast appears to apply a large compressive load, leaving an arch between Cape Lisburne and the Siberian coast. We also conclude that the Cape Lisburne peninsula protects the Strait from all southward-acting forces except ocean currents. Ocean currents are excepted because the influence of bottom topography brings the currents around this peninsula.

Using the results of several calculations in which ocean currents are applied, but wind stress and boundary tractions are assumed zero, together with the result of scaling the model equations, ice velocity is obtained as a function of ocean current velocity for several values of the ice strength. This result is used to compute an ice velocity time history for the winter of 1976-77. When this history is integrated, an estimate is obtained of the displacement of pack ice originating at Pt. Barrow during the course of one winter. It is found that ice can be transported only 100 km southward by ocean currents if the ice strength is 10^5 N/m or greater but almost all the way to the Bering Strait if the ice strength is zero. This synthesis prohibits northward ice motions in an attempt to estimate conservatively whether or not oiled ice can be transported through the Bering Strait.

When comparing our simulated ice motions, we conclude that large southward transports, such as the one recorded by RAMS buoy R534, are possible only when the ice along the Alaskan coast is very weak or when ocean currents are much larger than observed during 1976-77. As a result, we believe that large-scale motions are the result of at least two processes. Deformation must weaken the ice along the coast by the formation of open water and the ocean current must reverse its northward direction and persist in a high (0.4 to 0.5 m/s) southward flow. This concept of breakout is more complex than envisioned at the outset of this project. It requires that a hardening/softening plastic model of sea ice be used to account for open water created during deformations. Such simulations should use a history of observed atmospheric and oceanographic data driving the ice pack along the Alaskan coast because the sequence of winds and currents controls the ice strength and its response.

References

Coachman, L. K., and Aagaard, K. (1980) "Re-Evaluation of Water Transports in the Vicinity of Bering Strait," Oceanography of the Bering Sea Shelf, ed. D. W. Hood, in Press.

Coachman, L. K., Aagaard, K., and Tripp, R. B. (1975) Bering Strait, The Regional Physical Oceanography, Univeristy of Washington Press, Seattle, WA.

Coon, M. D., Maykut, G. A., Pritchard, R. S., Rothrock, D. A., and Thorndike, A. S. (1974) "Modeling the Pack Ice as an Elastic-Plastic Material," AIDJEX Bulletin 24, University of Washington, Seattle, WA, pp. 1-107.

Coon, M. D., Pritchard, R. S., and Leavitt, E. (1978) Final Report on AIDJEX Modeling Grant to the National Science Foundation.

Pritchard, R. S. (1977) "The Effect of Strength on Simulations of Sea Ice Dynamics," POAC77, ed. D. B. Muggeridge, Memorial University of Newfoundland, St. John's, Newfoundland, pp. 494-505.

Pritchard, R. S., and Colony, R. (1976) "A Difference Scheme for the AIDJEX Sea Ice Model," Numerical Methods in Geomechanics, Vol. II, ed. C. S. Desai, American Society of Civil Engineers, New York, NY, pp. 1194-1209.

Pritchard, R. S., and Reimer, R. W. (1979) "Ice Flow Through Straits," POAC '79, Vol. 3, Trondheim, Norway, pp. 61-74.

Pritchard, R. S., and Thomas, D. (1980) "The Range of Influence of Boundary Parameters in the AIDJEX Model," Sea Ice Processes and Models, ed. R. S. Pritchard, University of Washington Press, Seattle, WA, pp. 113-123.

Reimer, R. W., Pritchard, R. S., and Coon, M. D. (1979) Beaufort and Chukchi Sea Ice Motion, Part 2 - Onset of Large Scale Chukchi Sea Ice Breakout, Flow Research Report No. 133, Flow Research Co., Kent, WA.

Sodhi, D. S. (1977) "Ice Arching and the Drift of Pack Ice through Restricted Channels," CRREL Report 77-18, Cold Regions Research and Engineering Laboratory, NH, pp. 1-11.

Stern, M. E. (1975) Ocean Circulation Physics, Academic Press, New York.

Thorndike, A. S., and Cheung, J. Y. (1977) "AIDJEX Measurement of Sea Ice Motion, 11 April 1975 to 14 May 1976," AIDJEX Bulletin 35, University of Washington, Seattle, WA, pp. 1-149.

Tripp, R. B., Coachman, L. K., Aagaard, K., and Schumacher, J. D. (1978) "Low Frequency Components of Flow in the Bering Strait System," Paper 0-4 AGU, December 1978.

Flow Research Report No. 175

Behavior of Oil Spills Under Sea Ice - Prudhoe Bay

By

D. R. Thomas

December 1980

Flow Research Company
A Division of Flow Industries, Inc.
21414-68th Avenue South
Kent, Washington 98031
(206) 872-8500

Acknowledgement

This study was supported by the Bureau of Land Management through interagency agreement with the National Oceanic and Atmospheric Administration, under which a multiyear program responding to needs of petroleum development of the Alaskan Continental Shelf is managed by the Outer Continental Shelf Environmental Assessment (OCSEAP) Office.

Flow Research Report No. 175
December 1980

Table of Contents

Table of Contents (Cont.)

List of Figures

List of Figures (Cont.)

1. Introduction

During the next few years there will be many exploratory and possibly production oil wells drilled on the northern continental shelf of Alaska. Worldwide, about one in 3000 offshore wells drilled experiences some kind of blowout. Many of these are relatively harmless in terms of environmental damage. It has been estimated that the chance of a "serious" blowout incident is less than one in 100,000 wells drilled. These odds vary of course with the definition (and definer) of "serious." Irrespective of the exact probability, the odds are greater than zero, and when a serious blowout such as Santa Barbara or IXTOC 1 occurs, the consequences are also serious.

In the near future, drilling in U.S. waters in the Beaufort Sea will proceed from natural or artificial (ice or gravel) islands in relatively shallow waters. While this procedure will reduce the probability of blowouts and possibly the environmental effects by providing a stable base for control efforts and spill containment, it is possible for a blowout to occur away from the drill hole. The 1969 blowout in Santa Barbara Channel occurred through faults and cracks in the rock as far as ~0.25 km from the drill site. Thus, it is certainly conceivable that a blowout could occur underwater away from an island drill platform.

Present regulations require that any offshore drilling in the Beaufort Sea be done in the period from November through March. The entire sea surface is covered by a floating ice sheet during that time, except for the occasional brief appearance of leads of open water. Thus, sea ice will have an important bearing on the fate of oil spilled by a blowout in the Beaufort Sea.

There has been little practical experience with oil spills in ice-covered waters. Several accidental surface spills have occurred in ice covered waters in subarctic regions, for example the Buzzards Bay, Massachusetts, spill in 1977 (Ruby et al., 1977). These spills have not been in arctic-type ice which will generally be thicker, more continuous, and increasing in thickness throughout the winter. The Canadian government sponsored an oil spill experiment at Balaena Bay, N.W.T., during the winter of 1974-75, as part of the Beaufort Sea Project. That experiment is probably the single most important source of information concerning the interaction of crude oil and sea ice. For practical reasons, logistic and environmental, there were aspects of oil-ice interactions not investigated in the Balaena Bay experimental spills. These include, among others, a moving ice cover, deformation of oiled ice, large ocean currents, and the process of spring breakup when large quantities of oil are present and not being cleaned up.

Research efforts have continued since completion of the Beaufort Sea Project. The Outer Continental Shelf Environmental Assessment Program (OCSEAP) has sponsored a great deal of ecological background research in Alaskan waters, as well as research in specific oil-ice interactions (e.g., the effect of currents on oil under ice, the migration of oil through brine channels) or site-specific descriptions of the ice cover (e.g., ice motions, ice morphology). The objective of the OCSEAP Alaskan program is to insure protection of the environment during the search for and development of petroleum resources. One aspect of this endeavor is to attempt to predict the consequences of a "serious" polluting incident, such as a large oil well blowout. These predictions are an extremely important part of decision making, whether or not they are formally elucidated.

Of course, the prediction of a complex chain of events such as would follow an oil well blowout is impossible in a deterministic sense. Probabilistic predictions based upon historical data and previous experience are the only realistic results attainable. For some purposes, and at a time when data needed for predictions are lacking, it is preferable to make the worst conceivable case predictions.

As part of the process of predicting the effects of an oil well blowout, it is necessary to describe where an oil spill from a blowout would end up and when it would get there. The oil can be evaporated, dispersed into the water column, frozen into the ice and blown out to sea, moved from one location to another by currents, etc. In each case, the effects upon the environment and biological activity would be different.

The purpose of this report is to summarize relevant knowledge about Arctic sea ice and oil-ice interactions in order to provide the background information for creating oil spill scenarios. The variables and processes important in oil spills associated with sea ice are identified, as are important information gaps. This report is limited to the geographical area of the December 1979 joint state/federal lease sale near Prudhoe Bay. Generally, we restrict this report to factors which can be expected to play a major role in the sequence of events following an under-ice blowout in the lease sale region.

We begin by discussing in Section 2 the geography, climate, and oceanography of the lease sale area. The relevant factors which are discussed include the locations of the barrier islands which determine the development of ice zones, the winds which can move and deform the ice, the air temperature upon which ice freezeup, ice growth, and ice breakup depends, and ocean currents which may affect the direction and extent of oil spreading.

In Section 3 we review the characteristics of the sea ice in the lease sale area. The area is divided into zones (fast ice zone, stamukhi zone, and pack ice zone) based upon the morphological traits of the ice. The chronological development of each zone is followed. The ice characteristics which are important in connection with under-ice oil spills are ice freezeup, ice growth and decay, motion and deformation of the ice cover, and variations in ice draft and bottom topography.

In Section 4 we look at those crude oil properties which might affect oil-ice interactions. These include oil density, viscosity, pour point, surface tension, and equilibrium thickness. The oil temperature and volume of gas released during a blowout are also important parameters.

Section 5 deals with the interaction of oil from an under-ice blowout and the ice cover. The sequence of events following a blowout is divided into five distinct phases which can be considered independently. These phases are: (1) the initial phase which includes the blowout and rise of oil and gas to the surface and the immediate effect on the ice due to large volumes of hot oil and buoyant gases, (2) the spreading phase where oil buoyancy, trapped gases, ice motion, ice roughness, and ocean currents act in combination to spread or restrict the spread of oil beneath the ice, (3) the incorporation phase which includes the freezing of ice beneath layers of oil under the ice cover and building ridges of ice containing frozen-in oil, (4) the transportation phase which covers the typical motions of the ice, whether oiled or not, and (5) the release phase which begins with some of the frozen-in oil rising to the ice surface through brine drainage channels in the spring, continues with the ice melting down to the level of the incorporated oil, and ends when the ice has completely melted leaving an open-water oil slick.

In Section 6 we briefly discuss the ultimate fate of an Arctic oil spill. Although the release of oil from the ice into open water may be similar to a spill in open water, the ice does have effects on the spill which can still be important later during the open-water season.

And finally, in Section 7 we look at some of the effects an ice cover might have on oil spill cleanup strategies and techniques. Although oil spill cleanup is not a major topic of this report, completeness requires mention of the major effects an ice cover might have on cleanup.

In Section 8 we review the major aspects of oil-ice interactions and point out some important areas which require further work or additional data.

A glossary of terms related to sea ice is also included.

2. Geography, Climate, and Oceanography

2.1 Geography

The Beaufort Sea joint state/federal lease sale of December 1979 is located on the inner continental shelf off the north central coast of Alaska. The lease area extends from Flaxman Island in the east to Stump Island in the west and includes the Prudhoe Bay area. The seaward boundary follows approximately the 20-m isobath.

A chain of barrier islands and shoals lies just inshore of the 10-m isobath with about half the lease area lying between the islands and the shore. The area inshore of the islands and shoals is shallow (less than 8 m deep), protected from large wind forces (the maximum fetch along shore is about 100 km and only 20 km or less normal to the shore), and isolated from the pack ice. As a result, this area is ice free each summer with new ice growing in place each fall. Ice island fragments and large multiyear ridges cannot intrude because of the shallow waters. Because of the small fetch, ice motion and deformation is relatively small in the fall and ceases altogether once the ice has grown past about 0.5 m in thickness.

Outside the barrier islands, the shelf slope is fairly uniform and steep to the boundary of the lease area. During the summer, this area may or may not be ice free depending upon the winds and resulting pack ice motions. During the winter, large shearing or compressive forces are dissipated in this area when the pack ice is in motion relative to the ice fixed to the islands. Many of the resulting ridges become grounded, moving the zone of relative motion, the shear zone, further offshore.

Several rivers drain into the lease area. In the spring, river runoff increases by orders of magnitude, causing early ice melting and breakup near the river mouths. Large quantities of suspended particulate matter are discharged at this time.

2.2 Climate

Winds and air temperature are of crucial importance to the nearshore ice morphology in the Beaufort Sea. In the fall, development of the fast ice cover, ice motion and deformation, and location of the pack ice edge all depend upon atmospheric conditions. Throughout the winter, pack ice motions, and thus the development of the stamukhi zone, depend upon the wind. Melting and breakup of the fast ice in the spring is largely controlled by the number of accumulated thawing-degree days (TDD). During the open-water season, the nearshore currents are essentially wind driven.

2.2.1 Winds

The most complete source of surface wind data for the north coast of Alaska is the Climatic Atlas of the Outer Continental Shelf Waters and Coastal Regions of Alaska, Vol. III, Chukchi-Beaufort Sea (Brower et al., 1977).

In Figures 2.1, 2.2, and 2.3, we have summarized the wind data from the Climatic Atlas for Oliktok, Alaska, the station nearest the December 1979 lease area. Figure 2.1 shows the monthly cumulative distribution of wind speeds; the speeds are given in knots (one knot = 0.515 m/s). Figure 2.2 shows the monthly cumulative distribution of wind directions by octant. Since larger winds are more important in terms of ice motion and deformation, we show in Figure 2.3 the monthly cumulative distribution of direction for winds greater than 11 knots (6 m/s) in magnitude.

Winds for the offshore region of the Beaufort Sea may be computed from sea level pressure maps available from the National Center for Atmospheric Research for historical data (Jenne, 1975) or the National Weather Service analysis for current data. The accuracy of this data has been discussed by Leavitt (1979), and the resulting wind-driven ice drift has been presented by Thomas and Pritchard (1979).

2.2.2 Temperature

Atmospheric temperature statistics for the central Beaufort Sea coast are given in Figure 2.4. The data were taken from the Climatic Atlas (Brower et al., 1977) for the Lonely and Oliktok stations. Monthly median temperatures as well as the 5th and 95th percentiles are presented.

The temperature statistics may be compared with the dates of fast ice freezeup and breakup given by Barry (1979). The median air temperature is below $-1.8^{\circ}C$, the freezing point of sea water, from about 21 September on. Barry found that new ice forms in the fast ice zone about 3 October. The 2-week difference is presumably the time it takes

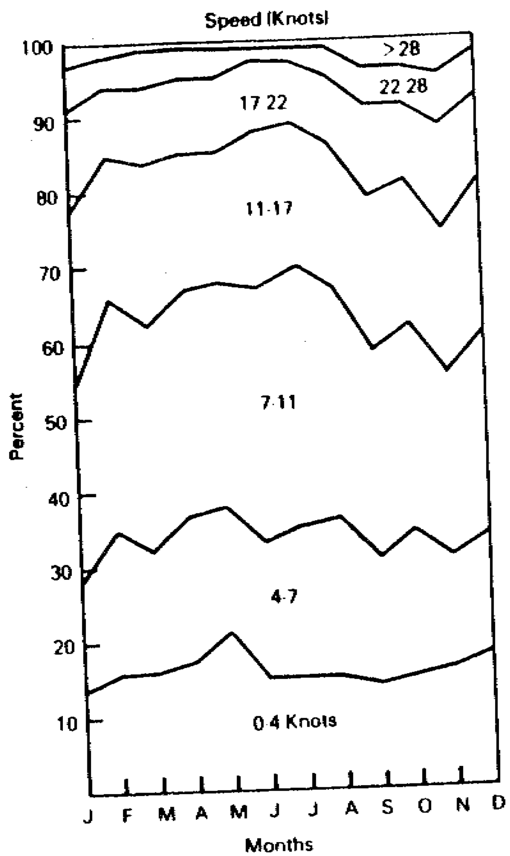

Figure 2.1. Cumulative Monthly Wind Speeds at Oliktok, Alaska. Wind speed intervals are given in knots (1 knot = 0.515 m/s). Data were taken from the Climatic Atlas (Brower et al., 1977).

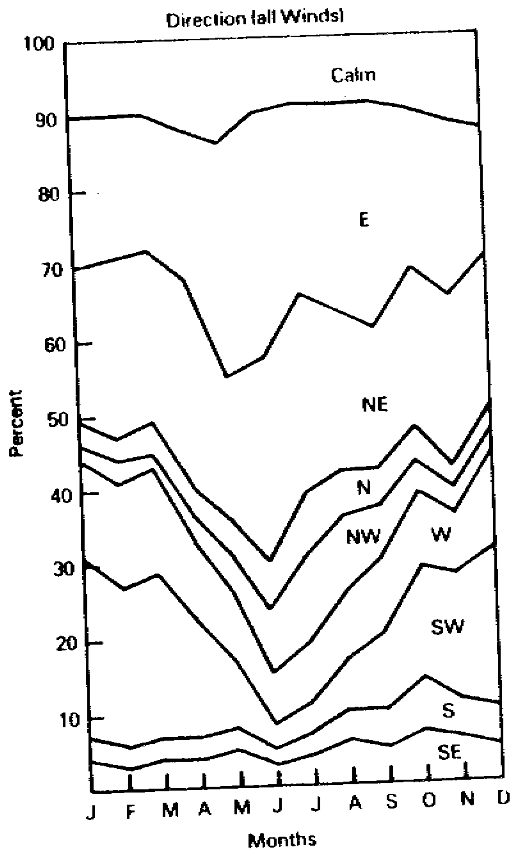

Figure 2.2. Cumulative Monthly Wind Directions at Oliktok, Alaska. Wind directions are given by octant. Data were taken from Climatic Atlas (Brower et al., 1977).

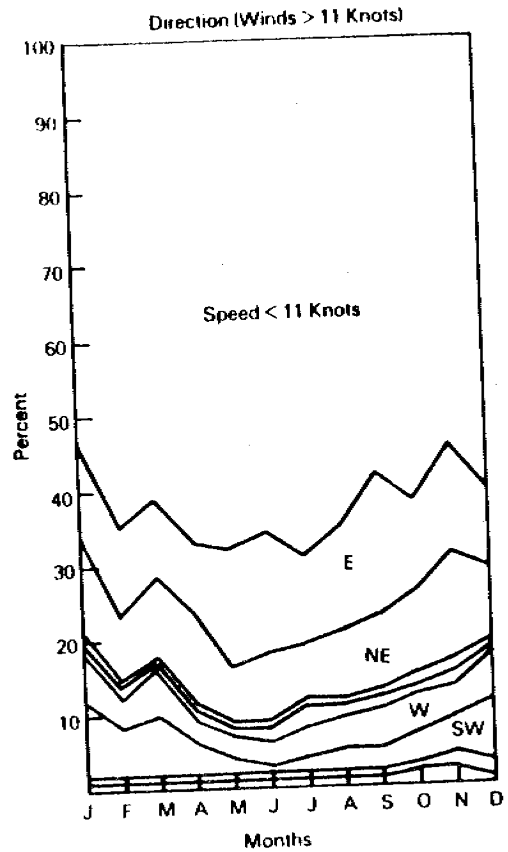

Figure 2.3. Cumulative Monthly Wind Directions for Wind Speeds Greater than 11 Knots (5.7 m/s) at Oliktok, Alaska. Wind directions are given by octant. Data were taken from the Climatic Atlas (Brower et al., 1977).

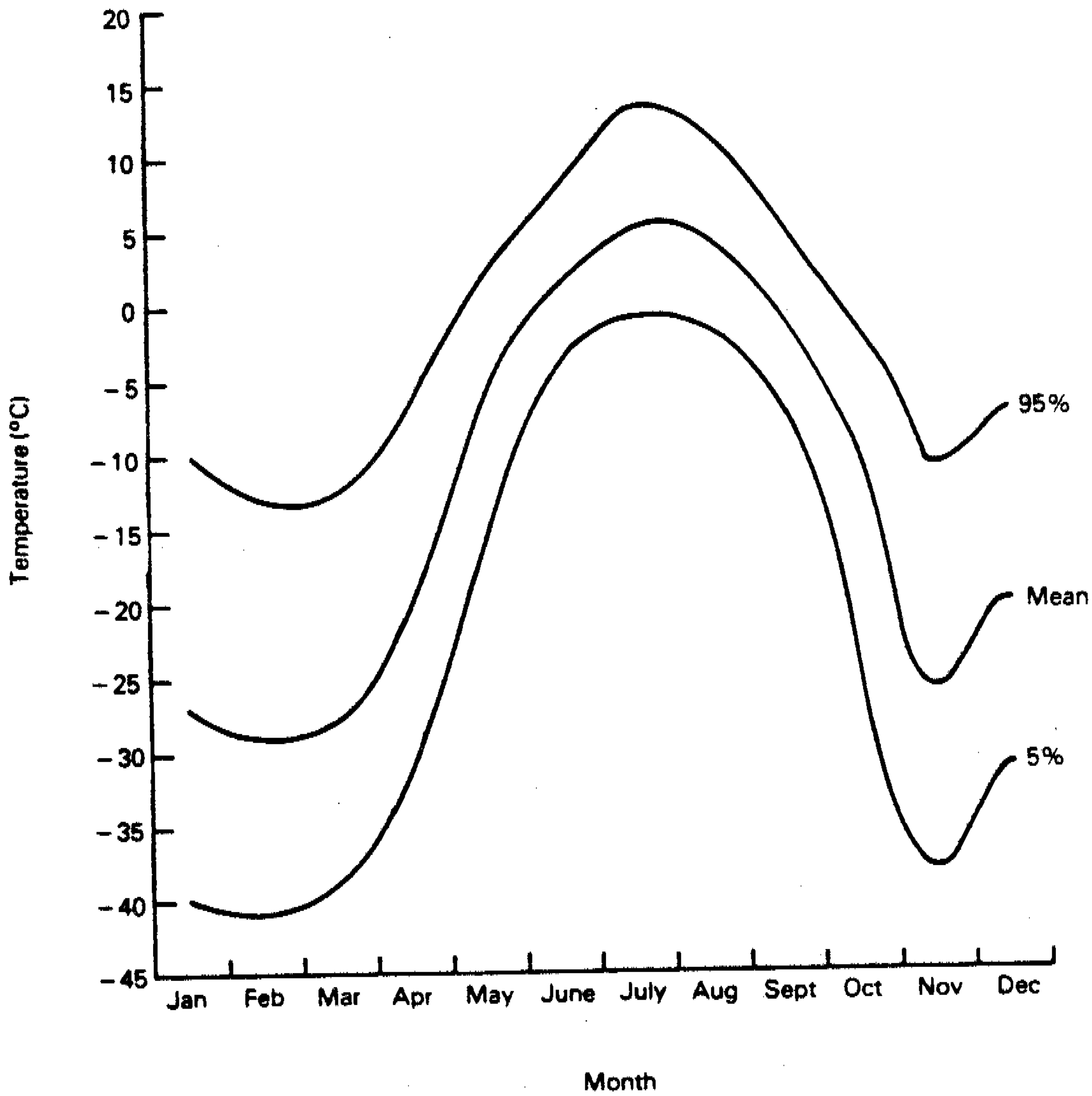

Figure 2.4. **Monthly Air Temperature Statistics for Oliktok, Alaska. The mean, 5th percentile, and 95th percentile are plotted at mid-month and connected by a freehand curve. Data were taken from the Climatic Atlas (Brower et al., 1977).**

for the shallow, well-mixed waters near shore to be cooled to near $-1.8^{\circ}C$. There is also a ± 10 day uncertainty in the dates given by Barry.

Barry (1979) also reports the first melt pools forming on the fast ice about 10 June and the fast ice mostly melted by 1 August. Bilello (1980) found a roughly one-to-one correspondence between accumulated TDD above $0^{\circ}C$ and the decrease in ice thickness in centimeters for several Canadian and Alaskan stations. From the median temperature curve, we see positive temperatures beginning about 10 June. By 1 August, there are roughly 135 accumulated TDD. Since the average ice thickness is assumed to be about 160 cm, the agreement is reasonably good. The difference is probably due to lateral melting of the ice once open water begins to appear (about the end of June).

2.3 Oceanography

The nearshore continental shelf off the north coast of Alaska is characterized by barrier island lagoon systems. Shallow sand and gravel bars and islands form a barrier 10 to 20 km offshore. The lagoons landward of these islands are quite shallow, in many areas less than 2 m deep and in general less than 10 m deep. The continental shelf break occurs just seaward of the barrier with a bathymetric gradient of -1 m/km. The entire Prudhoe Bay lease area lies landward of the 30-m isobath. Oil well drilling will occur either from barrier islands or from platforms and artificial islands within the lagoon system. Blowouts during exploratory drilling may occur just seaward of the islands, when directional drilling techniques are used, or within the lagoon system.

Within the lagoons, currents are controlled by the bottom topography, since the water is no deeper than a typical oceanic boundary layer. Thus, in summer, currents are wind driven following the bottom topography and dampening quickly when the wind stops (Mungall and Whitaker, 1979). Even a small amount of grease ice effectively prevents the transfer of momentum from surface winds to the sea. From October through June, then, under-ice currents are driven by some other source in the fast ice zone. On the average, the ice freezes to a thickness of 2 m during the winter and will freeze fast to the bottom if shallow enough. In very shallow areas, there is no water and no current at all. Where the ice freezes close to the bottom, the remaining water becomes extremely saline due to brine exclusion. This cold, dense water will flow offshore to be replaced by thermohaline circulation.

Tidal amplitudes are small along the north coast ranging from 0.05 to 0.2 m. In summer, the associated currents are also small, less than 0.01 m/s, except for tidal inlets to the lagoon system. In winter, the ice may act to intensify tidal currents by limiting the cross section available for water to flow through (Barnes et al., 1979). This effect may be especially strong at lagoon inlets. Net transport over periods greater than 12 hours, however, will be zero. The ice cover may also intensify currents due to storm surges and those associated with flooding of the ice in the spring when the rivers thaw.

Several investigators have made current measurements beneath the ice within or near the lease area. These measurements have been compiled and are shown in Figure 2.5. Time-series measurements are shown as current roses. Most of the measurements are instantaneous, single-current vectors.

Aagaard (1980) has reported time series of Lagrangian current measurements taken in April 1976 north of Narwhal Island, outside the lagoon system on the inner shelf. Two current meters were located at 10 m below the surface in 25- and 35-m-deep water. He recorded currents of 0.05 m/s or less with variable direction.

Kovacs and Morey (1978) gives four current measurements in the outer shelf area just north of Narwhal Island in May 1976. One is in water 22 m deep; the others are in 10- to 15-m-deep water. The maximum current was 0.06 m/s and the average was 0.04 m/s at 0.1 m below the ice. Similar measurements by Weeks and Gow (1980), taken 0.2 m below the ice at four stations in 10 to 15 m of water just outside the barrier islands along the entire length of the lease area, give an average of 0.025 m/s. In Kovac and Morey's data and Weeks and Gow's data, current components are either onshore or parallel to isobaths. Stronger currents were measured at a 10-m depth by Aagaard (1980); these were consistent with the weak, near-surface (0.2 m deep) currents observed by Kovacs and Morey, and Weeks and Gow, showing that the ice constrains the currents at the surface.

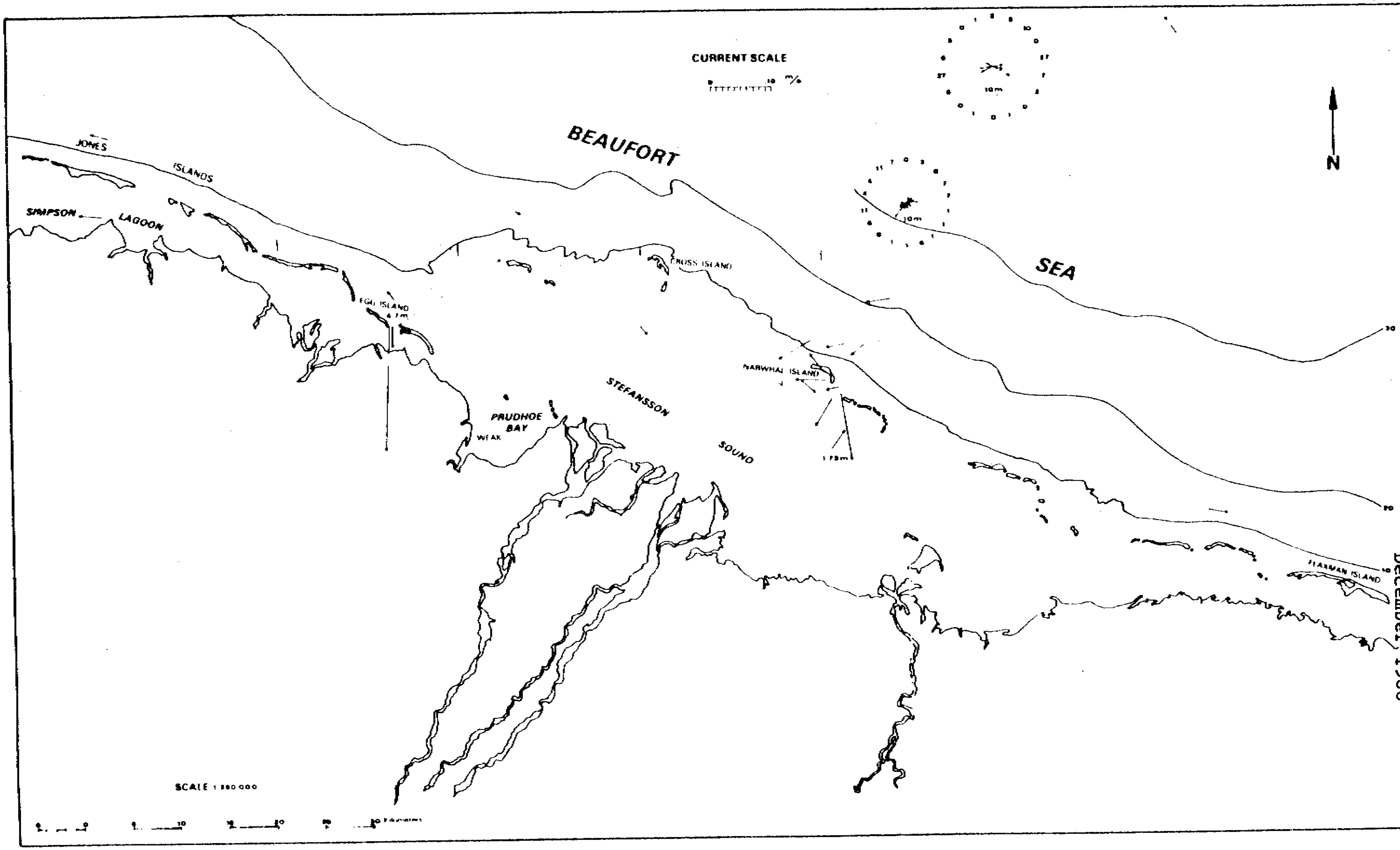

Figure 2.5. Summary of Wintertime Under-Ice Current Measurements Throughout the 1979 Joint State/Federal Lease Sale Area. Time series of current measurements are shown as current roses. Instantaneous measurements are shown as single vectors. Depth values near the vectors indicate the depth below the surface at which measurements were made. No depth values given means the current was measured just beneath the ice.

Inlet channel currents were measured by Matthews (1980) in 1977-78. One current meter was placed 4.7 m deep in the lagoon inlet channel to the east of Egg Island in 5-m-deep water. Currents of 0.02 to 0.05 m/s were recorded through the first part of June 1977 until the ice was flooded by the Kuparuk River. At that time, currents rose to 0.2 m/s out of the lagoon and the salinity dropped dramatically. Current measurements made in May 1972 by Barnes et al. (1977) show tidal components of up to 0.2 m/s through the Egg Island channel with a much lower mean flow. A single measurement by Kovacs and Morey (1978) in the channel between Narwhal and Jeanette Islands shows a current of 0.11 m/s in May 1976 at 0.1 m under the ice.

A number of measurements have been made within the lagoon system. Just south of Narwhal Island under 0.1 m of ice, Kovacs and Morey (1978) made current measurements at five locations in shallow water. The currents averaged 0.04 m/s in May 1976. Weeks and Gow (1980) gives three measurements within the lagoon system averaging 0.02 m/s at 0.2 m under the ice in April 1978. Barnes et al. (1977) measured a current in shallow water north of the Egg Island Channel in spring 1972 of less than 0.02 m/s. They also mention that currents measured within Prudhoe Bay in 4-m-deep water are "weak." Matthews (1980) has made continuous time-series measurements of currents at a site south of Narwhal Island in the middle of Stefansson Sound. Currents were measured at 1 and 2 m above the bottom in 5.6-m-deep water. Average currents were less than 0.01 m/s, but extremes of up to 0.11 m/s were measured at both meters. The currents were uniformly offshore. For continuity, Matthews argues that a return current of up to 0.2 m/s onshore must flow near the surface. No strong surface flows have been observed, but current data is sparse in this region, especially during fall freezeup when thermohaline circulations will be most pronounced.

In summary, it appears that near-surface currents in the offshore continental shelf waters should not exceed 0.1 m/s, though currents at greater depths may be higher. Within the lagoon system, currents are extremely weak, averaging less than 0.01 m/s. Currents of 0.025 m/s are not uncommon, however, and 0.1 m/s currents have been observed, though less than 1 percent of the time. Currents in the inlets to the lagoon under the ice may be considerably higher. A tidal component of up to 0.2 m/s may be common, but this provides no net transport. Currents of 0.2 m/s have are been also seen during flooding of the ice in June. Currents under the ice within the lease area are usually extremely weak, less than 0.05 m/s, with a net transport greater than 0.1 m/s occurring only during the June floods. Other mechanisms for producing large currents, such as storm surges, have not been observed during long time-series current measurements.

3. The Ice Environment

The sea ice in the lease areas off the north coast of Alaska cannot be described in any simple way. The character of the ice cover changes with time during the year, varies with location, is subject to drastic episodic events, and can differ markedly from year to year. Ice thickness near shore, for example, varies from zero (open water) in the summer to about 2 m for first-year ice in the spring. Multiyear ice reaches an equilibrium thickness of about 3 m, and deformed ice may reach thicknesses of 20 to 40 m. Bottom roughness also varies greatly, from smooth, thin ice with only millimeter-scale roughness features to the many meters of relief beneath ridges and rubble fields.

To simplify the problem somewhat, we have divided the ice off the north coast of Alaska into geographic zones based upon large-scale dynamic processes and the resulting ice morphology. These zones are the fast ice zone, the stamukhi zone, and the pack ice zone. Others have generally separated the Arctic into a pack ice zone and a seasonal ice zone and then divided the seasonal zone into the fast ice, etc. This division is useful when open water is being considered, but when the dynamics of ice motion is of interest, it is more useful to consider the ice cover in terms of the fast ice zone, the stamukhi zone, and the pack ice zone.

The fast ice zone is the nearshore area protected by barrier islands and grounded ridge systems. This zone is usually ice free during the summer with new ice forming in place during the fall. The fast ice is relatively smooth and undeformed.

Seaward of the fast ice zone is the stamukhi zone. This is a region of heavily deformed seasonal ice which forms throughout the winter in essentially the same area each year. The stamukhi zone is the past and present location of the shear zone, which is a region several hundred meters wide which marks the active boundary between the moving pack and the stationary fast ice. The location of the shear zone is determined by the geographical configuration of the coastline. Coastal promontories and barrier islands offer protection from the moving pack, which has an average motion to the west along the north Alaskan coast. Large shear ridges form along the outer edge of protected fast ice. Some of these ridges become grounded and thus act like artificial barrier islands or coastal promontories. The shear zone must then occur seaward of these grounded ridges. As winter progresses, more ridges form and become grounded, moving the shear zone seaward and extending the region of deformed ice. This region of deformed ice, which was first called the stamukhi zone by Reimnitz et al. (1977a), may extend in a band 20 to 50 km wide along the coast. As ridges become grounded, large areas may become protected from incursions of pack ice so that smooth undeformed regions of fast ice may form inside the stamukhi zone. The stamukhi zone is sometimes considered part of the fast ice zone since grounded ridges immobilize it, but we consider it a separate zone due to the character of the ice relief and the processes which create the zone.

Outside the stamukhi zone is what we consider the pack ice zone. The pack ice zone can be further divided into a seasonal ice zone and a permanent pack or central Arctic zone. The seasonal zone begins seaward of the stamukhi zone and includes the region which was largely ice free during the most recent summer season. Although the lease areas will not extend beyond the seasonal zone, in some years the central Arctic pack is driven close to shore so that the following ice season the seasonal ice zone has the characteristics of the permanent pack; therefore, both types of pack ice must be considered. In general, the pack ice zone is characterized by large motions and the formation of leads and ridges between floes.

The three geographic ice zones, fast ice, stamukhi, and pack ice, are described fully in the following sections. The general characteristics of the ice in each zone, including seasonal variations, thickness distribution, deformations, ridging, and bottom roughness, are discussed. A discussion of the open-water season which is to some extent applicable to all three zones is presented first.

3.1 Open-Water Season

Normally, the southern Beaufort Sea is ice free for about 2.5 months of the year, from late July to early October. The seaward extent of open water along the Prudhoe Bay sector of the coast varies throughout the course of the season. In situ melting varies little from year to year in the nearshore region. The ice begins melting in mid-June, primarily near river mouths. By the end of July, the fast ice is essentially gone.

The extent of open water from this time on depends upon the southern edge of the polar pack. The position of the pack ice edge can change due to episodic events such as storms and can also vary from year to year due to long-term flow patterns in the atmosphere. Stringer (1978) examined Landsat images and produced open-water maps for the years 1974 to 1977. In early August (the latest date given on the maps), open water extended from 10 to 30 km offshore in the Prudhoe Bay sector. The greatest year-to-year variation occurred to the west at the Colville River. Barry (1978) also looked at Landsat images for the Prudhoe Bay sector. He reports open water over 100 km offshore for late August 1973, 60 to 70 km offshore for August 1974, 5 to 25 km offshore for early August 1975, 25 to 50 km offshore for September 1975, 5 to 25 km offshore for mid-August 1976, and 20 km offshore for early September 1976. A survey of historical data (Hunt and Naske, 1979) confirms this wide range of open-water extent. To summarize the available data, open water begins to form usually in late June. By mid-August or September the open water will usually extend a few tens of kilometers offshore, but large variations in the open water extent are possible.

Rogers (1978) has examined temperature data from 1921 and meteorological data from 1940 to the present. He has found correlations between air temperature, sea level pressure (SLP) distribution, and surface wind direction with northward pack ice retreat at Pt. Barrow. The trends in SLP and accumulated thawing-degree days (TDD) indicate a decline in favorable nearshore ice conditions. Due to topological effects, the open-water extent in the Prudhoe Bay sector does not correspond directly with that at Pt. Barrow, but the basic trend is the same. Ice edge statistics from the Climatic Atlas for the Chukchi-Beaufort Seas (Brower et al., 1977) indicate that the extreme distance from the coast near Prudhoe Bay to the ice edge (defined as an ice concentration of one-eighth or more) can be more than 400 km (late September). The mean distance taken from the atlas also peaks in September at about 100 km from shore.

In Figure 3.1 we present a plot of the mean and extreme distance from the shore near Prudhoe Bay to the ice edge. The data were taken from the Climatic Atlas which in turn used aerial, ship, and satellite

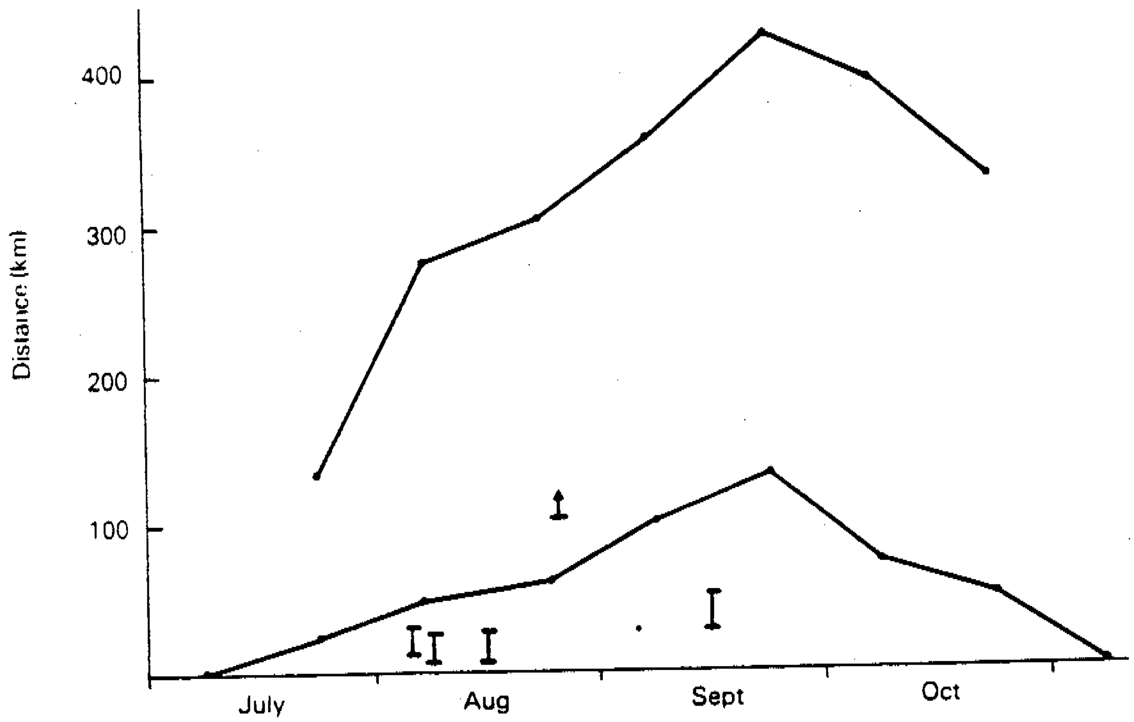

Figure 3.1. Monthly Mean and Extreme Distance from Shore near Prudhoe Bay to the Ice Edge. Monthly mean minimum distance is zero for all months. Data were taken from the Climatic Atlas (Brower et al., 1977). Also shown are limits of observed open-water extent as measured from landsat images by Barry (1978) and Stringer (1978).

observations of the ice edge for the years 1954 to 1970. Numbers were estimated to the nearest 10 km from the maps at longitudes between $147^{o}30'$ and 150^{o} west. Note that the extreme minimum extent of open water is zero. Superimposed on the plot are the ranges of observed open-water extent as measured from Landsat images by Barry (1978) and Stringer (1978).

While the extreme minimum extent of open water is zero, this does not mean that the fast ice does not melt and break up. Rogers (1978), in correlating accumulated TDD with fast ice breakup, records only 2 years between 1921 and 1976 when less than 250 TDD were accumulated. Some melting and breakup probably occurred during those 2 years. The most frequent cause of scant open water along the coast is incursions of wind-driven pack ice.

Along the Prudhoe Bay sector of the coast, zero open water in Figure 3.1 refers to the area seaward of the barrier islands. It is highly improbable that the fast ice inside the islands or remnants of grounded ridge systems would persist through the summer. Except for isolated floes, the pack ice will remain outside the islands and grounded ridges.

In summary, the fast ice begins to melt in mid-June, and from late July to early October, the fast ice zone is generally ice free. The mean open-water extent outside the barrier islands is 100 km offshore in September, and the extreme distance can be more than 400 km. Large variations in the open-water extent are caused by incursions of wind-driven pack ice.

3.2 Fast Ice Zone

The fast ice zone is the area near shore that is usually ice free during the summer with new ice forming in place during the fall. The ice is relatively smooth, remaining motionless and protected from large deformations by barrier islands and grounded ridge systems.

3.2.1 Freezeup

Sometime in late September to mid-October new ice begins to grow in the fast ice zone. Sea ice can begin to grow in one of three different forms: columnar, frazil, or slush ice (Weeks, 1976; Martin, 1977). Columnar ice grows in still sea water. This ice is relatively smooth on the bottom, but the lower 10 to 40 mm consist of a porous and fragil skeletal layer. Frazil ice grows when a wind blows across sea water that is at its freezing point. Wind-generated waves stir and slightly supercool the water column so that ice crystals form below the surface. Upon reaching the surface they form a porous mass with a random crystal structure. The wind tends to pile this ice up creating thickness variations of several centimeters. When snow accompanies the wind, the third kind of ice, slush ice, forms. The snow is mixed with the sea water and is probably accompanied by frazil ice formation. Once a layer of ice solid enough to protect the sea from direct stirring by the wind has formed, columnar ice growth begins. As sea ice grows downward, the ice crystals form a series of plates of pure ice with layers of extruded brine between. As growth continues, bridging occurs laterally between the plates, trapping series of elongated brine pockets. As the ice season progresses, some of these brine pockets drain or become interconnected vertically and horizontally. It is not until about late April or May when air and ice temperatures warm up toward freezing that brine drainage results in top-to-bottom opening and enlarging of the drainage channels. The horizontal spacing of these open channels is about 0.1 m (Martin, 1977).

Barry (1978, 1979) studied satellite images for 5 years and arrived at the average date of new ice formation of 3 October, ± 7 to 10 days. The new ice begins to form first in the shallow waters near shore where salinity is lower and where the water can cool faster. By mid-October, the ice cover has usually become continuous (Barry, 1978, 1979), weather conditions permitting. This thin ice in unprotected areas is free to move when driven by modest winds and can easily be deformed.

3.2.2 Deformation

In regions sheltered by the barrier islands or grounded pressure ridge systems remaining from previous seasons, it is possible for the fast ice to grow in place with little or no surface relief, depending upon the winds (and waves) during freezeup. It is almost certain, though, that some deformation will occur in this thin ice. The deformation may occur as pancake floes, rafting, or small pressure ridges. Most of the deformation will create relief of only a few centimeters.

The amount of deformation that occurs is dependent on the strength of the ice and the wind stress. An estimate of the isotropic compressive strength of a uniform sheet of thin ice (less than about 0.5 m thick) may be made based upon the ice model developed by AIDJEX. Using the AIDJEX model formulation, Rothrock (1979) estimated the compressive strength (p^*) of ice of uniform thickness to be $0.17\ h^2 \times 10^5$ N/m where h is the ice thickness in meters. Pritchard (to appear, 1981), using different values of some of the parameters, calculates ice strength to be 2 or 3 times larger than that. Parmerter (1974) has modeled the rafting of thin ice. Using nominal values of ice properties and rafting as the deformation mode, Parmerter's results yield a strength about one-half that based upon the ridging model. Parmerter also calculated that the switch from rafting to ridging occurs when the ice is about 0.17 m in thickness.

Assuming that a strength of $0.17\ h^2 \times 10^5$ N/m is of the right order of magnitude for thin sea ice, what kinds of winds will cause deformation? The stress generated by a wind will depend upon the speed of the wind, the fetch of the wind, and the drag coefficient. The wind stress times the fetch, or the force that must be resisted by the strength of the ice, p^*, may be written as

$$\tau^* = \ell \rho_a C_a U^2 \quad , \tag{3.1}$$

where ℓ is the fetch, ρ_a is the air density, C_a is the atmospheric drag coefficient, and U is the wind speed. Using nominal values of $\rho_a = 1.4\ \mathrm{kg/m^3}$ and $C_a = 9 \times 10^{-4}$ (Thomas and Pritchard, 1979), $\tau^* = 1.26\ \ell U^2 \times 10^{-3}$ N/m . Ice motion and deformation will occur whenever $\tau^* > p^*$, or when $\ell U^2 > 1.3\ h^2 \times 10^7\ \mathrm{m^3/s^2}$.

In Figure 3.2 we show the critical values of wind speed, U, as a function of ice thickness, h, for several values of fetch, ℓ. The information in Figure 3.2 is not intended to be used as an accurate predictor of when ice deformation occurs. It does illustrate, however, that for reasonable values of material properties, modest winds can produce deformation in very thin ice.

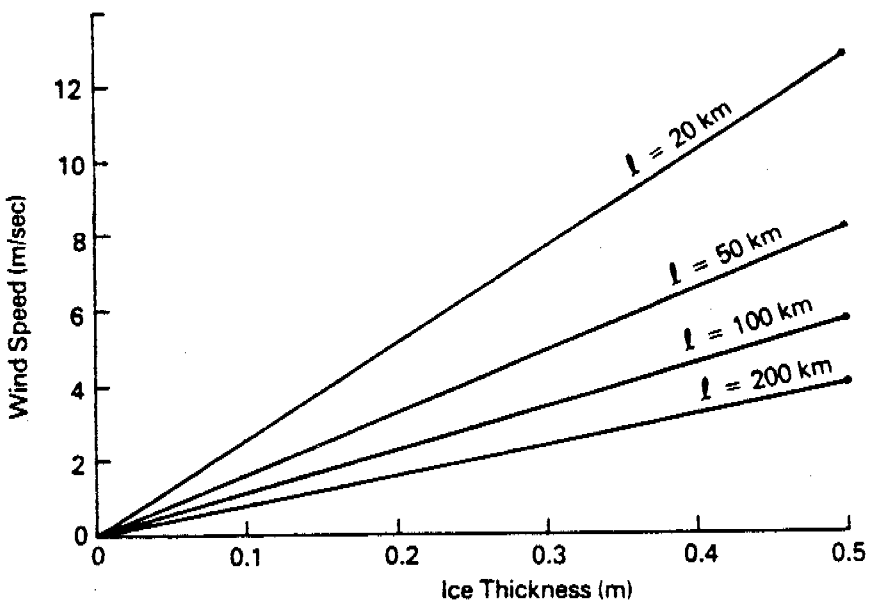

Figure 3.2. **Wind Speed Needed to Cause Deformation in a Uniform Ice Sheet, as a Function of Ice Thickness and Wind Fetch.**

As the ice becomes thicker during the winter, it becomes strong enough to withstand the normal range of wind stress. Assuming that this region is protected from incursions of pack ice by barrier islands or grounded ridges, no significant deformation occurs. Measurements of motion in the fast ice zone during April and May 1976 and 1977 (Tucker et al., 1980) and from December 1976 through May 1977 (Agerton and Kreider, 1979) showed displacements of at most a few meters; these have been attributed to thermal expansion. Tidal cracks also form at the junction of floating ice and ice grounded in water depths less than the ice thickness. About 10 to 75 percent of the fast ice zone lies between the shore and the 2-m water depth (about the maximum thickness for first-year ice). Therefore, a majority of the ice in this zone will become grounded during the winter.

Storm surges may also occur during the ice season. Mid-winter surges with heights of up to 1.5 m have been reported (Henry and Heaps, 1976). Negative surges of 1.0 m have also occurred (Aagaard, 1978). These events would tend to fracture the ice cover but not to cause any significant deformation.

3.2.3 Ice Thickness

Measurements of the fast ice thickness have been made at several locations along the southern Beaufort Sea coast. Schell (1974) presents a composite of ice thickness data taken during the years 1970 to 1973 at Harrison Bay-Simpson Lagoon and at Elson Lagoon-Dease Inlet. New ice was observed to form around the first of October and to grow in thickness almost linearly through the next February. Growth rates were about 10 mm/day, decreasing somewhat during March and April and leveling off during May. The maximum mean thickness was about 1.8 m with a range of 1.45 to 2.25 m. Schell's data is reproduced in Figure 3.3.

NORCOR (1975) presents the results of ice thickness measurements at Balaena Bay and Cape Parry during the 1974-75 season. While these locations are about a thousand kilometers east of the Prudhoe Bay area, the latitude is about the same. A maximum mean thickness of 1.55 m was observed during May with a range of 1.35 to 1.75 m (approximately 24 percent of the mean). Data for Cape Parry only for the years 1970 to

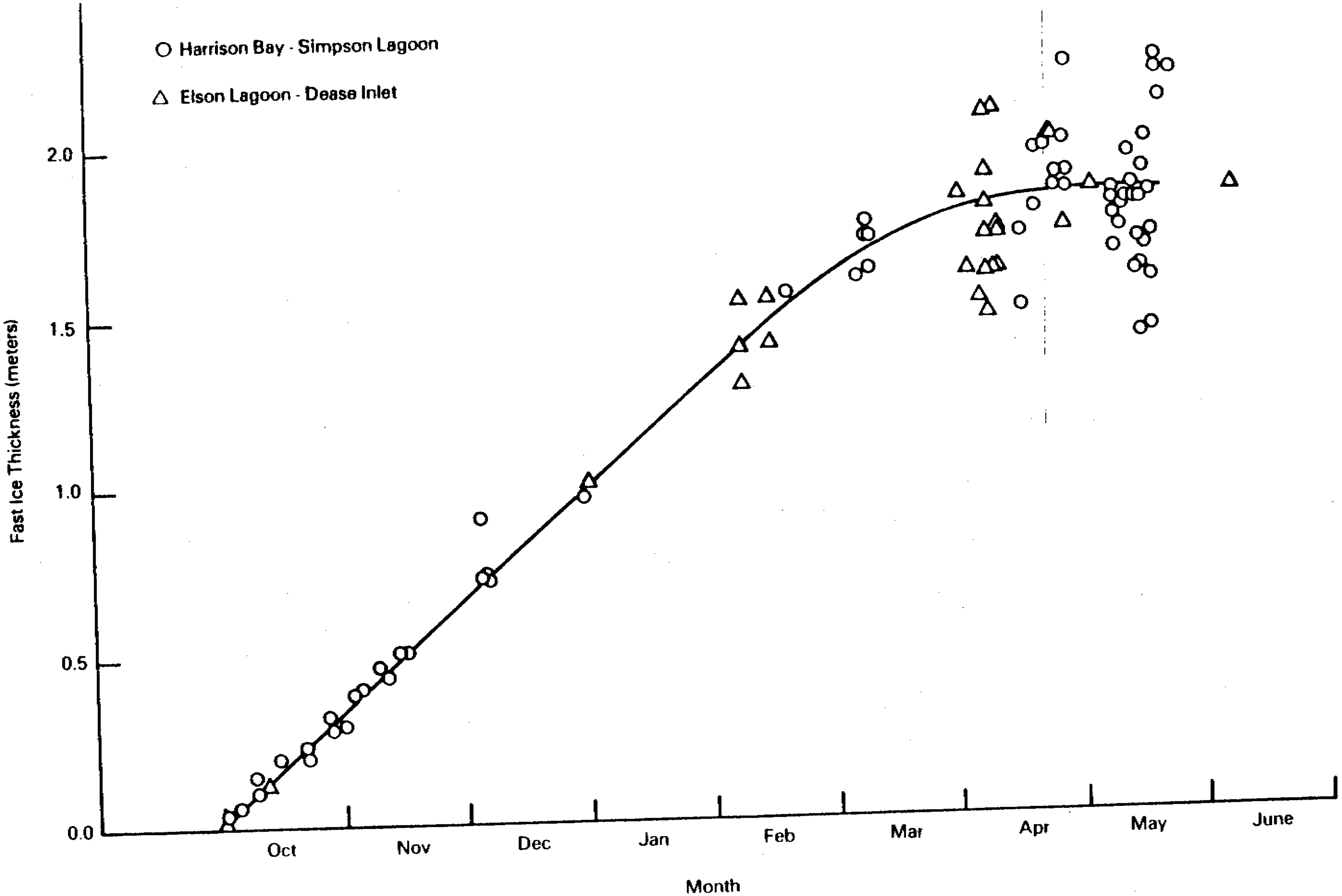

Figure 3.3. Fast Ice Thickness Data, North Coast of Alaska, 1970-73. (Figure 5 from Schell, 1974.)

1975 showed a median ice thickness in May of about 1.70 m with a range of 1.45 to 2.00 m (approximately 32 percent of the median).

Kovacs (1979) reports ice thickness measurements made in May 1978. At a site near Tigvariak Island, the mean thickness was about 1.56 m. This site had a heavy snow cover and could be expected to have thinner ice than areas with less snow. Kovacs (1977) reports average ice thickness measurements of 1.87 m near Prudhoe Bay in April 1976. The range of measurements was 1.70 to 2.01 m (approximately 17 percent of the mean).

Barnes et al. (1979) report on ice thickness measurements at three sites in Prudhoe Bay-Stefansson Sound taken in May 1978. Means at the three sites ranged from 1.34 to 1.57 m with ranges of 14 to 31 percent of the mean. Correlations between snow depth and ice thickness ranged from -0.5 to -0.7. Obviously, the thickness to which fast ice grows depends upon location, year, and snow cover. The actual mean thickness is not too important since the primary effect of thickness will be the time it takes for the ice to melt and break up in the spring.

Bilello (1980) looked at decay patterns of fast ice, primarily in the Canadian Archipelago. From a maximum thickness in May (1.55 to 2.30 m), the ice generally melts to zero thickness during the first 3 weeks of July. Decay at Kotzebue, the only Alaskan station studied, occurred in the later part of June. These dates correspond roughly with the date of 1 August given by Barry (1979). All these miscellaneous data are shown in Figure 3.4.

From the data described above it should be possible to give the range of mean ice thickness throughout the year in the fast ice zone. First, freezeup takes place about the first of October but probably varies a week or so in either direction. Growth rates are approximately linear at about 10 mm/day through the end of February. Maximum ice thickness is reached about mid-May with melting starting around the first of June. By August, again plus or minus 1 week, most of the ice will have melted. The average ice thickness in May may vary between 1.35 and 1.85 m, depending upon location and weather (temperature and snowfall) that season. Figure 3.5 shows this range of mean ice thicknesses.

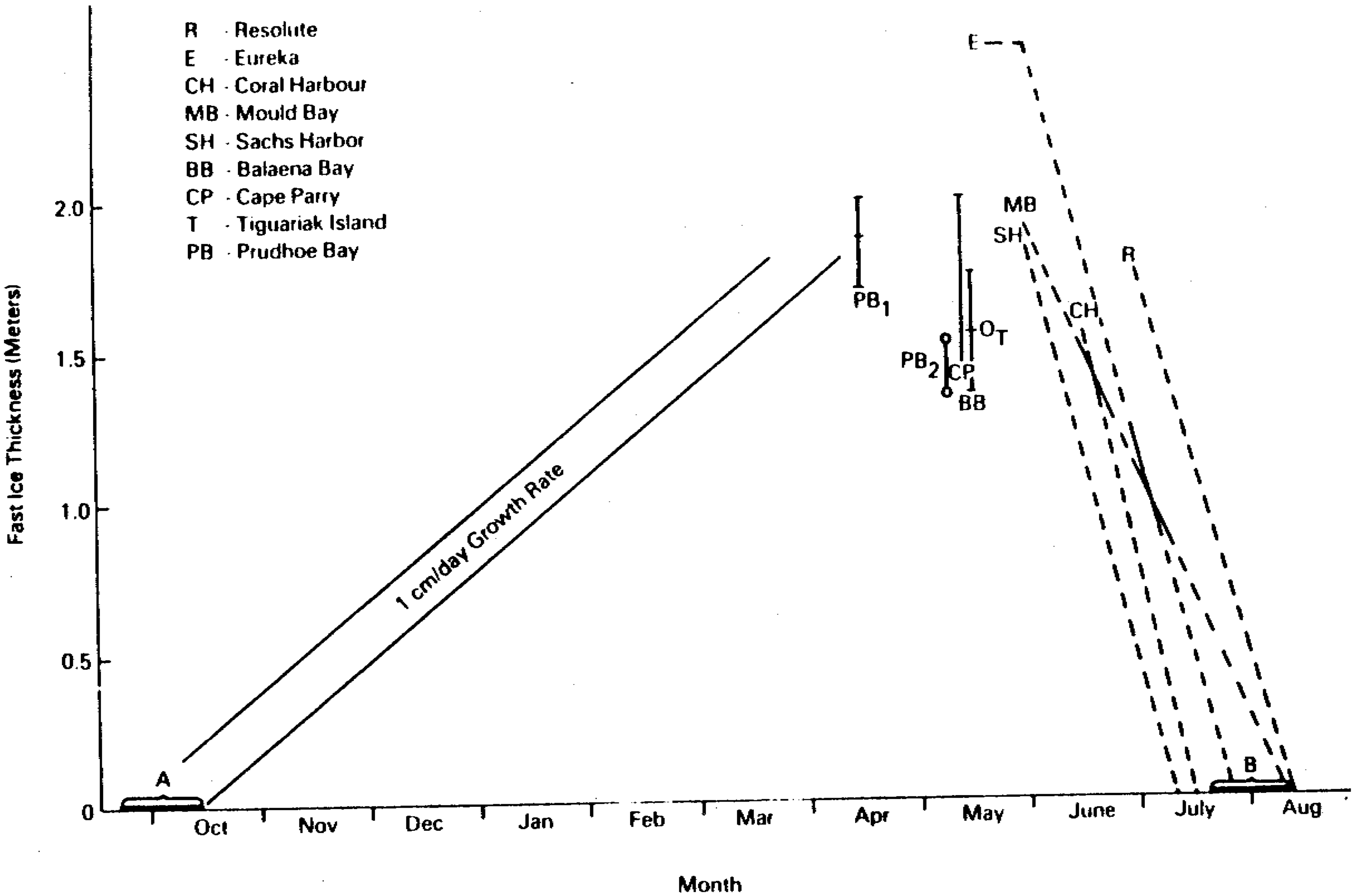

Figure 3.4. **Composite Data for Arctic Fast Ice Growth, Decay, and Thickness Range. Intervals A and B indicate the approximate dates of freezeup and ice-free water in the fast ice zone along the north coast of Alaska. Solid lines represent ice growth of 1 cm/day beginning early and late in interval A. Dashed lines are typical fast ice decay rates at various Arctic stations (Bilello, 1980). Vertical bars are ranges of fast ice thickness measurements (NORCOR, 1975; Kovacs, 1977 and 1979; Barnes et al., 1979).**

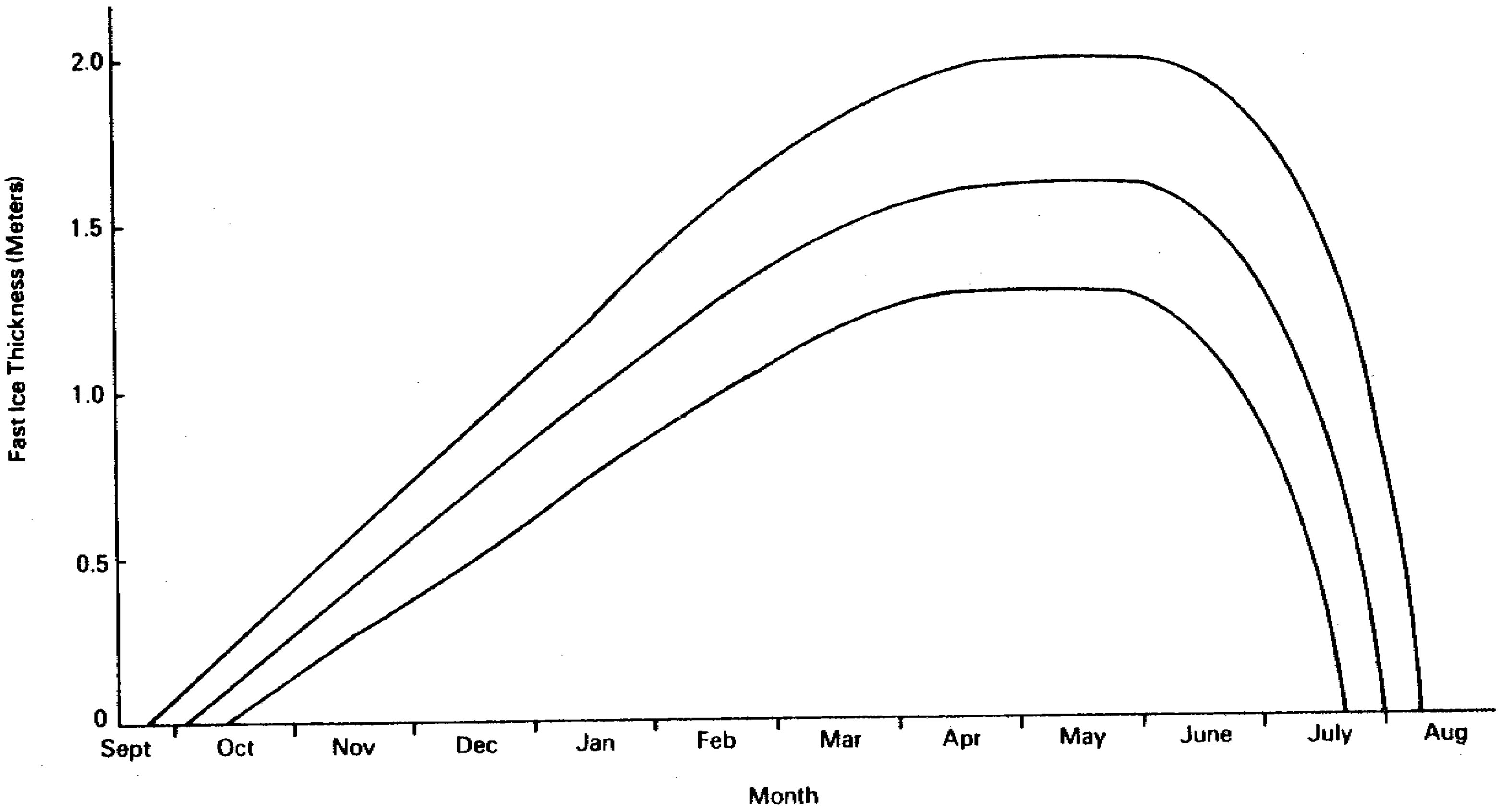

Figure 3.5. **Typical Fast Ice Mean Thickness and Approximate Range of Mean Thicknesses Throughout the Year for the North Coast of Alaska. These curves are derived from the data presented in Figures 3.3 and 3.4.**

3.2.4 Bottom Roughness

The bottom roughness is a primary factor when oil containment is being considered, since oil released beneath the ice would immediately fill any under-ice voids. Bottom roughness is measured in terms of the variations of ice draft over a given area. The reports discussed in the previous section give ranges of ice thicknesses from 14 to 44 percent of the mean. Since these are thickness variations, the variations in draft must be somewhat less. Using the data presented in Barnes et al. (1979) for the Prudhoe Bay area in May, the variations in draft amount to 26, 32, and 40 cm for three sites, corresponding to 24, 17, and 26 percent of the mean ice thickness. NORCOR (1975) found the fast ice in Balaena Bay to have a maximum variation in thickness of 20 percent the ice thickness for ice greater than 0.5-m thick. This thickness variation is related to variations in snow cover on top of the ice (Barnes et al., 1979; Kovacs, 1979).

For new ice less than 0.5 m in thickness, other mechanisms act to cause bottom roughness, as discussed in Section 3.2.1, Freezeup. Thickness variations of thin ice have not been reported in the literature. For ice of 0.5 m and thicker, NORCOR (1975) reports that in addition to the large-scale roughness due to variation in the snow cover, a small-scale roughness with relief of a few centimeters and spacings of 0.1 m was present under the ice. This scale of variation was attributed to random variations in the ice growth. It seems reasonable to suppose that these random variations in thickness occur under very thin ice.

3.2.5 Ice Decay and Breakup

In late May or early June, the decay of the fast ice in the Beaufort Sea begins. The first stage of the decay is the flooding of nearshore ice by the increasing river flow. Areas of several hundred square kilometers may be flooded in early June (Barry, 1979). The first openings in the fast ice zone appear near the river mouths. These shore polynyas spread laterally and seaward from mid-June through early July. Meanwhile, the ice sheet itself is melting from the surface. The first melt pools form on the ice surface about 10 June (Barry, 1979). By the end of June, the fast ice has thinned and weakened enough that wind and water stresses can cause movement and openings. The first ice motions are often toward the shore polynyas. Early in July, some of the surface melt-water ponds drain through cracks and thaw holes.

Seaward of the smooth fast ice zone, the stamukhi zone remains mostly fast during this time due to grounded ridges. Therefore, the extent of nearshore ice motion is limited by the stamukhi zone as well as by the barrier islands. The melting fast ice will almost certainly drift about a great deal within the limited area available. During the months of June and July, approximately 60 percent of the winds blow from the east or northeast. The ice drift is therefore mostly toward the west.

The nearshore area is usually ice free or nearly so by the first of August. The actual date by which an area is ice free will vary greatly due to the ice thickness, the temperature, and the movement of loose ice from one area to another by wind. The melting rate of the ice is almost linearly related to accumulated thawing-degree days, one centimeter of ice being melted for each TDD (Bilello, 1980).

3.3 Stamukhi Zone

Following Reimnitz et al. (1977a, 1977b) we use the term "stamukhi zone" for the recurring band of grounded ridges lying seaward of the fast ice zone. Since new ridges are being built and becoming grounded throughout the ice season, the dimension of the stamukhi zone is expanded with each ridge which becomes grounded. At times, we use the term "stamukhi zone" to mean the entire region where grounded ridges normally occur. Context will determine which of these meanings is implied.

3.3.1 Freezeup

Early in the fall during freezeup, the stamukhi zone is covered by thin new ice. Remnants of the previous winter's grounded ridge systems are likely to have survived in place, but the density of these ridges will be low. Some multiyear floes are also likely to be incorporated in the ice cover forming in this zone (Campbell et al., 1976), depending upon the position of the pack ice at the time of freezeup. The amount of multiyear ice in the entire seasonal ice zone can range from near 0 to near 100 percent. The stamukhi zone, being relatively close to shore, probably would have low concentrations of multiyear ice.

While the ice is mostly thin during the fall in this area, deformation occurs easily with only moderate winds or pack ice pressure. During the early part of the ice season, this area will develop much as the fast ice zone does. A greater amount of deformation will probably occur than in the fast ice zone since the barrier islands act to protect the fast ice zone from incursions by the pack ice and to some extent limit the effective fetch of the wind.

3.3.2 Deformation

By late November, the new ice has grown to a thickness (0.5 m or more) that can resist wind stresses generated within this area. The pack ice offshore can still be moved by wind of a sufficient magnitude acting over a much larger fetch. The motion of the pack ice off the north coast of Alaska is generally westward. When a component of onshore stress exists in the pack, along with an alongshore motion, a line of slippage occurs between the moving pack and the stationary fast ice. The location of this line of slippage depends upon the configuration of the coastline, coastal promontories tending to protect areas downstream (to the west). The barrier islands and surviving grounded ice features act as extensions of the coast. Shear ridges develop along this line of slippage. The actual shear ridge building seems to occur in a zone only a few hundred meters wide (Reimnitz et al., 1977a, 1977b) which is called the active shear zone.

As shear ridges are being built, some become grounded. This grounding initially occurs between the 10- and 20-m isobaths, depending upon the shape of the coast and the size of the ridges being built. When a ridge becomes grounded, it stabilizes the shoreward ice, so the active shear zone must move seaward. As the shear zone is continually moved seaward during the course of the winter, an ever-widening zone of deformed ice and grounded ridges is left behind. By late winter, this deformed ice zone, the stamukhi zone, can be 20 km or more wide in the region of Prudhoe Bay.

The stamukhi zone shoreward of the active shear zone exhibits little significant motion throughout the winter. Tucker et al. (1980) and Weeks et al. (1977) report measured motions in the fast ice of only a few meters which they attribute to thermal expansion of the ice. In the stamukhi zone, motions were larger but still on the order of hundreds of meters during the months of April and May. The stations furthest seaward were in pack ice with motions slightly over 1 km observed during April and May 1977 and motions of about 7 km during April and May 1976. These motions were predominately offshore/onshore with little shearing taking place. The ice generally returned to near its original position after moving offshore then onshore, which implies that leads must have opened and closed. Thin ice forming in these newly opened leads must have been deformed into pressure ridges. Thus, even during times when the pack ice is relatively motionless and the shear zone inactive, deformation still occurs seaward of grounded ridge systems.

3.3.3 Extent of Stamukhi Zone

The extent of the stamukhi zone varies with the time of year and geographical position. There is annual variation also, although the larger grounded ridge systems tend to occur in the same places each year (Stringer, 1978; Barry, 1979). In early winter, ridges become grounded in water 8 to 15 m deep, but by late winter they may become grounded in waters 20 m or more deep. Off Cross Island, the stamukhi zone is well defined and is about 20 km wide at the end of winter. Figure 3.6 (from Reimnitz et al., 1977a) gives a general picture of the stamukhi zone from Harrison Bay to Prudhoe Bay. The heavy black arrows represent pack ice motion.

3.3.4 Amount of Deformed Ice

Estimating the amount of deformed ice in the stamukhi zone is extremely difficult. From observations and photographs, one knows that in places 100 percent of the ice cover consists of highly deformed ice, but areas of flat, undeformed ice may also exist. Typical values are difficult to estimate for several reasons. One reason is that new ridges are being built throughout the winter. Other reasons are the spatial variability and yearly variations in ridge density.

Tucker et al. (1979) have reported on ridge densities over the continental shelves of the Beaufort and Chukchi Seas. Laser profilometer data were collected during February, April, and December 1976 and March 1978 at several locations along the coast including Cross Island. Ridge densities were averaged over 20-km segments of the track perpendicular to the shore. A ridge was defined as ice more than 0.9 m higher than the surrounding ice.

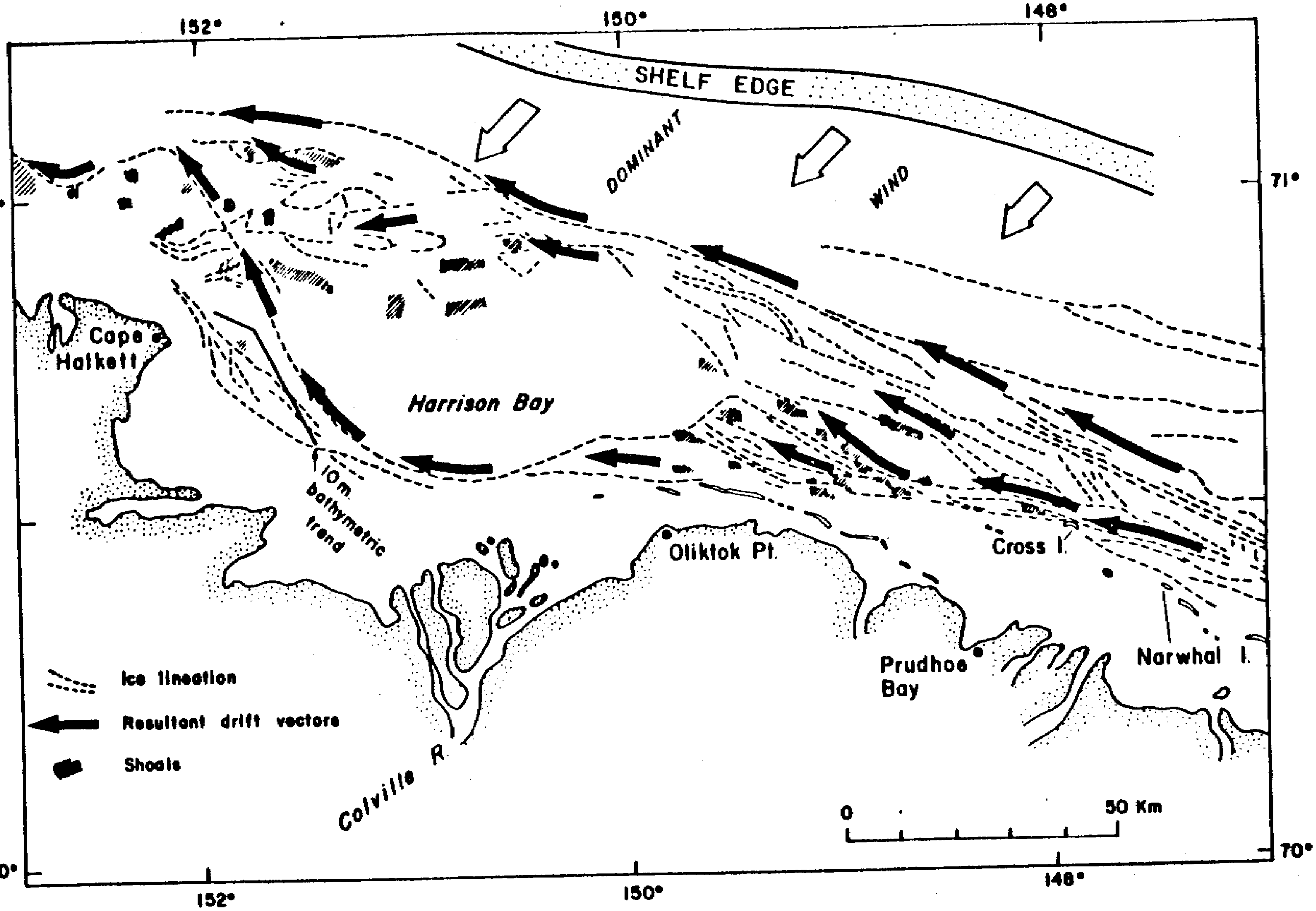

Figure 3.6. Generalized View of the Stamukhi Zone between Harrison Bay and Prudhoe Bay. (Figure 10 from Reimnitz et al., 1977a.) Predominant pack ice motions and winds are indicated. Major linear ice features (ridges and linear hummock fields) were traced from Landsat images.

The data for the Cross Island track is given in Figure 3.7. Note that three different ice seasons are represented in Figure 3.7: the winters of 1975-76, 1976-77, and 1977-78. Due to probable annual variations in ice motion and ridge building, we can assume that Figure 3.7 does not give a progression of ridge densities from December through April. In general, the density of ridges is greatest in the first or second 20-km segment out from Cross Island, then decreases over the next 40 to 80 km. The pack ice in the central Beaufort Sea had a ridge density of about 2.5 ridges per kilometer in February 1976 (represented by the AIDJEX data point in Figure 3.7). The largest ridge density shown in Figure 3.7 is the 12 ridges per kilometer in March 1978 for the 20-km segment just north of Cross Island.

From the motions observed in this region by Weeks et al. (1977), it is likely that many of the ridges built in the stamukhi zone are pressure ridges rather than shear ridges. During a storm with offshore winds, the pack ice will move offshore, opening leads between the fast ice and the pack. Leads are also opened in the pack due to differences in motion throughout the pack, but the largest difference in motion usually occurs between the stationary fast ice and the pack. During most of the year, thin ice begins to form immediately on these open leads. Then, when onshore winds blow, the pack closes up the leads and, with or without a shearing type of motion, one or more new ridges are built.

During the early months of 1976, an AIDJEX buoy was located about 30 km offshore of Cross Island (Thorndike and Cheung, 1977). From 1 January to 21 April 1976, the net motion of this buoy was only 9.6 km. The net onshore motion was 6 km. The radial position error of this type of buoy is about 2 km. Thus, the onshore motion of this buoy was between 2 and 10 km during the first 3-2/3 months of 1976. This onshore motion must have created some new ridges between the buoy and the shore. If any thin ice existed in the 30 km offshore from Cross Island during that period, it would have been the first ice ridged. Since the net motion was onshore, thicker ice must also have been built into ridges. As a rough estimate, assume that the ridges produced by the 2- to 10-km onshore motion were built from ice 0.5 m thick. Then, between 4,000 and

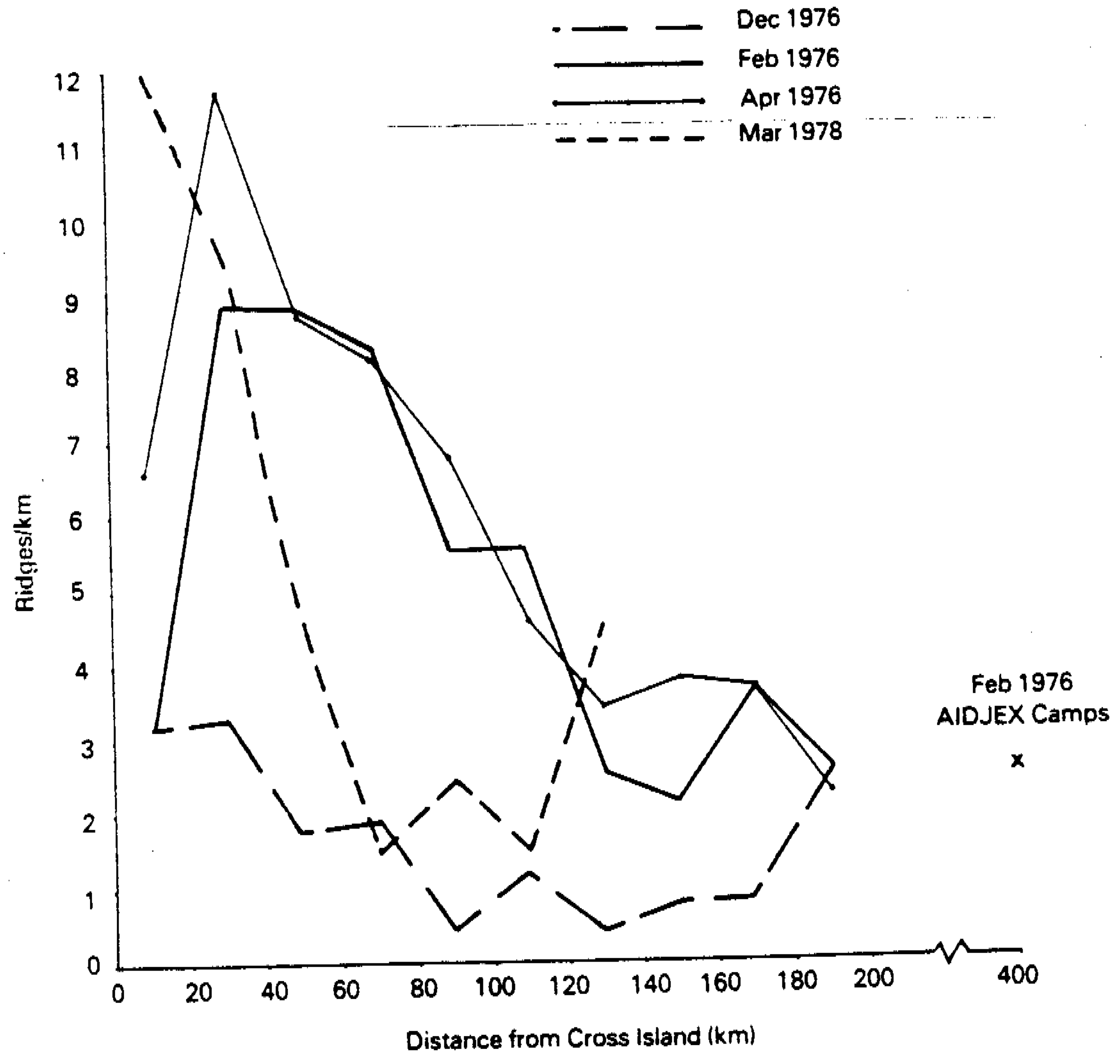

Figure 3.7. Ridge Densities Offshore from Cross Island. Values are averages for 20 km segments of laser profiles extending north of the island. Data taken from Tucker et al., (1979).

20,000 m^3 of ice (all volumes are for 1-m widths in the east-west direction) was built into ridges between the buoy and Cross Island during the 3-2/3 months. This equals a monthly rate of 1090 to 5455 m^3/month of deformed ice produced.

To determine the volume of ice built into a ridge, we must define a ridge size and shape. Many pressure ridges have a roughly triangular profile above and below the ice surface. We assume this to be the typical shape of ridges built in the stamukhi zone from first-year ice. The average slope of the above-water sail of first-year pressure ridges is 24^o, and the slope of the subsurface ridge keel is 33^o (Weeks et al., 1971). The depth of the keel is about 4 times the sail height (Kovacs, 1974). The area of the above-water portion of a ridge profile is $H^2/\tan(24^o)$, where H is the height of the sail. The submerged portion of the ridge has an area of $16\ H^2/\tan(33^o)$. Thus, the area of a typical ridge profile is roughly 27 H^2. The average height of ridge sails in the stamukhi zone is about 1.5 m (Tucker et al., 1979). If 10 percent of a ridge volume consist of voids between irregularly shaped ice blocks, (Rigby and Hanson, 1976), then the area of ice in a typical ridge profile is about 54 m^2.

3.4 Pack Ice Zone

The pack ice zone is considered to be the area seaward of the maximum extent of deformed ice in the stamukhi zone. The ice in this area is generally more free to move and deform under wind and current stresses. It is this motion or possible motion that distinguishes this zone from the others in the context of oil spill pollution pathways.

The pack ice zone can be further divided into a seasonal or off-shore zone and a permanent pack or central Arctic zone. The seasonal pack ice zone is considered to begin seaward of the active shear zone and includes only the ice that is free to move as pack ice. The lease areas offshore of Prudhoe Bay do not extend beyond the seasonal pack ice zone. The permanent pack or central Arctic zone is seaward of the seasonal zone and is covered with pack ice year round.

A problem arises in that some seasons the central Arctic pack is driven close to shore during the summer so that the following ice season the ice in the seasonal ice zone has the characteristics of the permanent pack. We must therefore examine the characteristics of both types of pack. Normally, the ice in the seasonal zone is mostly first-year ice while the Arctic pack has a high proportion of ice that has survived at least one melt season. Multiyear ice is generally thicker, less saline, and less porous than first-year ice.

3.4.1 Ice Thickness

Thorndike et al. (1975) modeled 2 years of ice thickness distribution for the central Arctic zone, using a measured initial thickness distribution (Swithinbank, 1972) and strain rates derived from drifting stations. The modeled climatological mean thickness for central Arctic pack ice varied from 2.8 to 3.2 m in late summer/early fall to about 3.8 to 4.2 m for winter/spring. Using the same model, and starting with open water in August, a maximum thickness of 1.7+ m is reached in April/May.

Wadhams and Horne (1978) present the results of submarine sonar ice profiles in the central Beaufort Sea during April 1976. Mean drafts over 50-km sections ranged from 2 to 3.8 m, with an overall mean of 3.07 m. The most probable draft (mode) for level ice was 2.7 to 2.8 m. The overall mean thickness was thus about 3.45 m, and the level ice mode thickness was about 3.1 m.

Taking into account measurement errors, seasonal variations in growth rates, and concentrations of multiyear ice it is reasonable to accept the convention that first-year ice grows to a thickness of about 2 m in the pack ice zone while multiyear ice will average about 3 m (level ice only) (Weeks, 1976).

3.4.2 Ice Type and Concentration

Ramseier et al. (1975) compiled maps of first-year and multiyear ice concentrations over the Beaufort Sea for the years 1972 to 1975. The maps were compiled from NIMBUS 5 satellite passive microwave imagery. Early in September, the seasonal pack ice zone (out to about 200 km from shore) contains 50 to 100 percent open water, and the central Beaufort Sea (permanent pack ice zone) contains 0 to 25 percent open water. Early in October, more year-to-year variation is evident. In 1974, no open water existed for about 100 km offshore, with 0 to 25 percent open

100 km offshore, with 0 to 25 percent open water in the central Beaufort Sea. In 1975, the seasonal pack ice zone still contained 25 to 100 percent open water out to about 200 km from shore.

By December, open water has been frozen into first-year ice. In December 1972 and 1973, 45 to 65 percent of the ice within approximately 200 km of shore was first-year ice, the remainder being multiyear ice. The central Beaufort Sea contained 0 to 45 percent first-year ice. In 1979, the central Beaufort Sea only had 0 to 15 percent first-year ice while the seasonal ice zone had 0 to 45 percent first-year ice. Large-scale ice motions during the summer and fall obviously have a significant effect on the amount of multiyear ice in the seasonal pack ice zone.

Typically, the seasonal pack ice zone seems to contain about half first-year and half multiyear ice. The central Beaufort Sea seems to have from over half to 100 percent multiyear ice. Weeks (1976) gives a summary of ice types identified by U. S. Navy Birdseye ice reconnaissance flights. The seasonal ice zone contained 46 percent multiyear ice and 53 percent first-year ice (with approximately 1 percent open water). The central Arctic Basin contained 81 percent multiyear ice, 18 percent first-year ice, and approximately 1 percent open water. These were wintertime mean values.

The amount of open water in the winter pack ice was given by Weeks (1976) as about 1 percent. Wadhams and Horne (1978) report the amount of thin ice (0 to 0.5 m draft) observed by the U.S.S. GURNARD in April 1976 to be 0.9 percent overall, varying from 0.2 to 3.5 percent over different sections of the Beaufort Sea. For ice with draft less than 1 m, the overall mean was 3.4 percent. This thin ice is distributed in refrozen leads and polynyas. Narrow leads less than 50 m in width were found to occur at the spacing of 4.6 per kilometer. Leads from 50 to 500 km in width were spaced at about 0.1 per kilometer. A great deal of variation was observed to exist along the submarine track, but the variation did not seem to be related to position offshore. Thus, one need only travel a little over 200 m on the average across ice 2- or 3-m thick before finding some ice only 1-m or less thick. No mean lead width is given by Wadhams and Horne, but it is probably closer to zero than 50 m since the frequency of leads decreases sharply with width. Information on the length of leads is also lacking. Hibler and Ackley (1974b) found the majority of ridges to be less than about 1 km in length. Since ridges are built from thin ice in refrozen leads, the majority of leads are probably less than 1 km in length. For very narrow leads, the effective length is probably much less than 1 km since irregularities along lead boundaries will tend to touch first as the ice floes open up then shift about.

Weeks et al. (1977) examined side-looking airborne radar (SLAR) images taken on flights north of Alaska in late September 1975. New ice had begun to form between the multiyear floes in the seasonal ice zone. They found the majority of these floes to be roughly circular in shape and between 100 and 700 m in diameter with floe size being distributed approximately as a negative exponential. Figure 3.8, reproduced from Weeks et al. (1977), shows the floe size distribution.

In the fall and early winter then, the ice cover in the seasonal pack ice zone will consist of about 50 percent multiyear floes from 100 to 200 m in diameter and 50 percent much thinner ice between the old floes. Later in the winter and in the spring, the difference in draft between multiyear and first-year ice will be much less. New leads, and thus new areas of thin ice, will be continually created during the winter. At any time, about 1 percent of the area within the pack is open water or very thin ice. Much of this thin ice existing after freezeup or created during the winter ultimately gets broken up and piled into rubble fields and pressure ridges.

3.4.3 Ridges

Measurements of the number of ridges in the pack ice zone show considerable regional and temporal variation. Therefore, it is only possible to make a rough approximation of the number of ridges in the seasonal and permanent pack zones during various times of the year.

Weeks et al. (1980) report a ridge density of 6.63 per kilometer for the region 50 to 100 km offshore of Barter Island (laser profile, February 1976). Wadhams and Horne (1978) report a keel density of 14.77 per kilometer for the region approximately 60 to 110 km offshore of Barter Island (U.S.S. GURNARD sonar profile, April 1976). If each

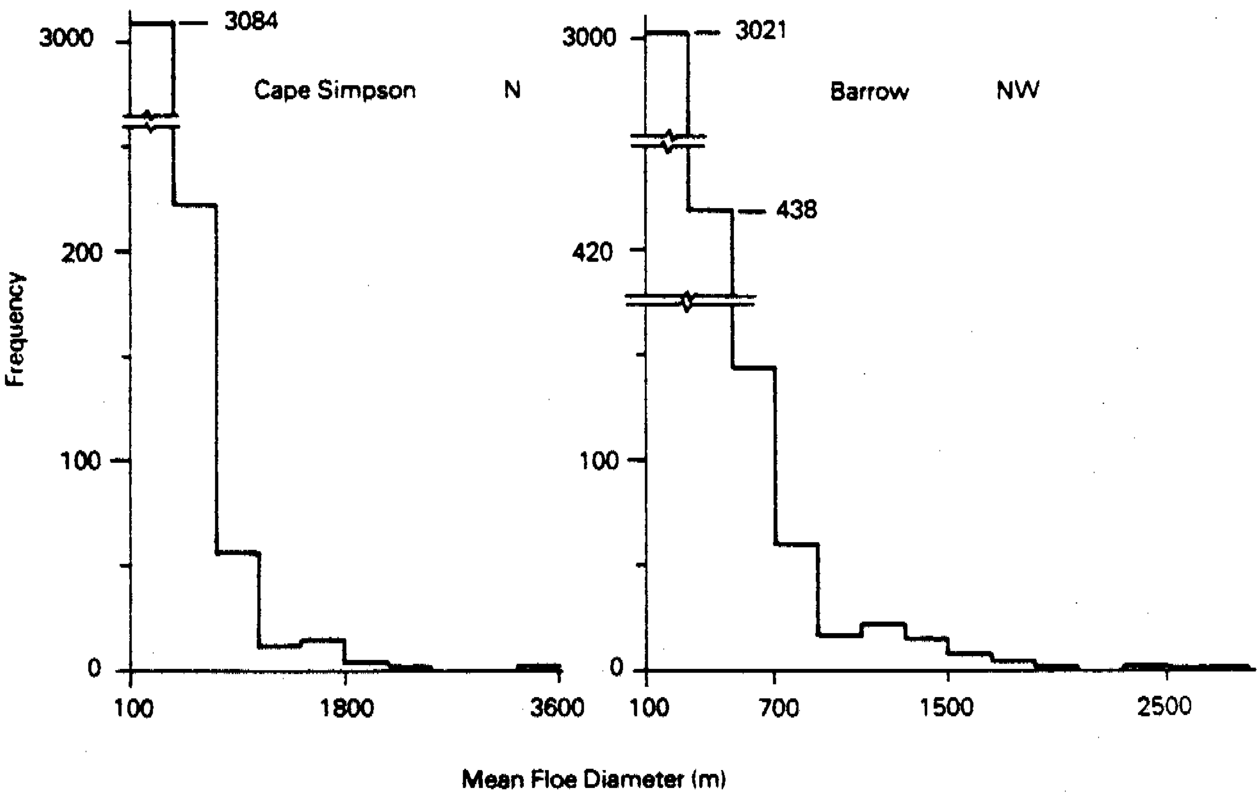

Figure 3.8. Histograms of Floe Size Distribution for Two Areas in the Beaufort Sea During September 1975. (Figure 7 from Weeks et al., 1980.)

ridge observed above the ice surface is associated with a keel beneath the surface, why is there such a large difference between the number of surface ridges in February and the number of keels just 2 months later? There are probably several reasons for this. First, it is likely that the definitions of ridges and keels did not include the same ice structures. Second, there may have been more ridges built during those 2 months. While AIDJEX buoys in the area at that time showed only small net motions, there was considerable back-and-forth motion occurring (Thorndike and Cheung, 1977; Tucker et al., 1980) which probably caused more ridges to be built. And third, there might be some variation due to the exact area sampled.

In the next two 50-km sections offshore of Barter Island, Wadhams and Horne (1978) reports keel densities of 10.28 and 8.11 keels per kilometer while Weeks et al. (1980) report 4.27 and 3.79 ridges per kilometer. The ridge densities between 50 and 100 km offshore varied from 2.82 per kilometer at Barrow to 7.56 per kilometer at Cross Island (Weeks et al., 1980). It seems reasonable to accept the submarine count of about 14.77 keels (ridges) per kilometer as typical in the seasonal pack ice zone. Weeks (1976) gives confirmation of the higher number in giving summaries of U.S. Navy Birdseye ridge data of 16 to 22 ridges per kilometer off the north coast of Alaska during the summer.

For the central Beaufort Sea area, Wadhams and Horne (1978) reports an average keel density of 6.71 per kilometer. If the ice in this area is assumed to be mostly multiyear ice, we can estimate the ridge/keel density at freezeup in the seasonal pack ice zone. Right at freezeup, before thin ice has had a chance to become deformed, the ridge/keel density will be 6.71 times the concentration of multiyear ice. Assuming a 50 percent multiyear ice cover at the time of freezeup (October), the ridge/keel density would be 3.35 per kilometer. Then, 14.77 minus 3.35 or 11.42 new ridges/keels per kilometer must be built by the next April. This amounts to an average rate of 1.27 ridges per kilometer per month during the fall and winter. The rate is probably much higher during the fall when more thin ice is present. Furthermore, there is probably such a region-to-region and year-to-year variation in ridging intensity that all the above numbers can be considered as no more than very rough approximations. Wadhams (1975) reports many fewer ridges in April 1975 from the Mackenzie Delta to the central Beaufort Sea. Nearshore ridge counts were only 1 or 2 per kilometer while in the central Beaufort Sea the density was 2 to 3 ridges per kilometer. Some ridge/keel density measurements for the area near Cross Island are given in Figure 3.7.

3.4.4 Ice Motion

The variations in speed of the nearshore pack ice have not been adequately reported. Thorndike and Colony (1980) have described the ice motion of a station in the central Beaufort Sea, and Tucker et al. (1980) have described the motion of nearshore pack ice, but for only a short period of time. Examination of these two sources shows that there is a seasonal difference in ice motion (less motion during winter and spring) and that pack ice motion probably decreases toward the pack ice edge (at least during winter).

In Figure 3.9 we show a histogram of the speed of one of the AIDJEX data buoys during the winter of 1975-76. This buoy (number R61) was located approximately 50 to 60 km offshore near Prudhoe Bay. During January to mid-May, the monthly histograms appeared very similar, so the data were combined into a winter ice speed histogram. During that winter, at least, the pack ice nearest shore was most likely to be moving at speeds between 0 and 1 m/min (1.67 cm/s). The mean speed was about 2 m/min.

Lacking enough data to see the seasonal variations of nearshore pack ice motion, we also looked at the motion of two manned camps in the central Beaufort Sea. Figure 3.10 shows histograms of ice speeds for these two camps throughout the year. Monthly histograms were made first and then the similar consecutive months were lumped together. During the summer months, July through September, the ice is almost constantly in motion. During freezeup in October, the pack is still in constant motion but at somewhat slower speeds than in the summer. The fall-early winter (November through January) speeds have decreased sharply with about half being less than 2 m/min. The winter months (February through April) look much like the nearshore motion with over half the speeds being less than 1 m/min. During May and June, speeds begin to increase again as new ice growth stops and the pack begins to loosen up.

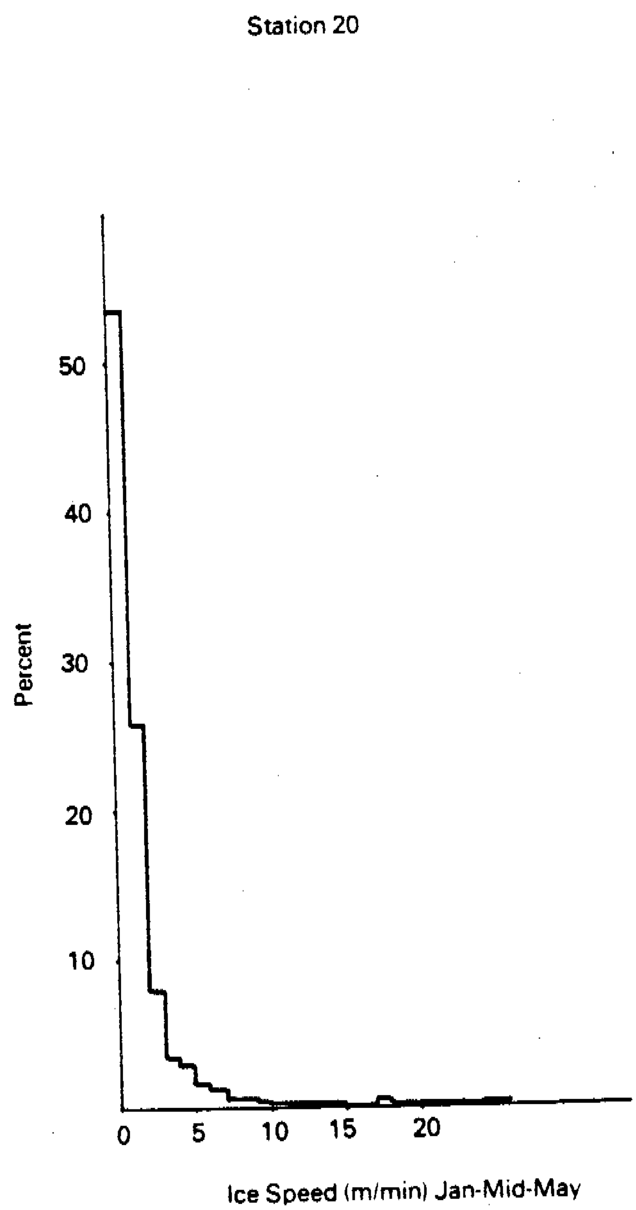

Figure 3.9. Histograms of Ice Speed as Determined from the Motion of a Satellite-Tracked Buoy Located about 40 km North of Flaxman Island. Data taken from Thorndike and Cheung (1977) for AIDJEX Station 20 from January 1976 through mid-May 1976.

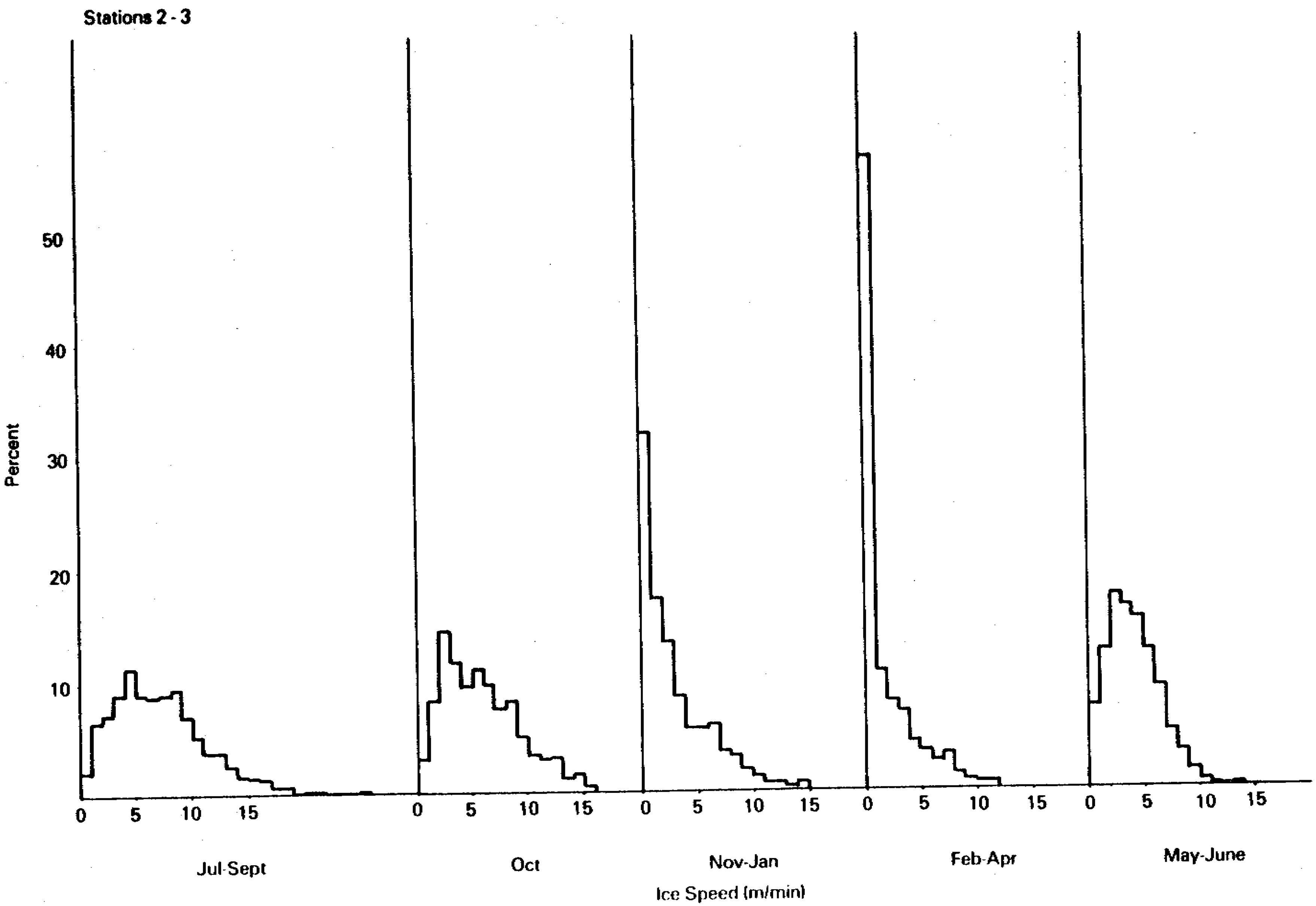

Figure 3.10. Histograms of Ice Speed for Two Manned Camps in the Central Beaufort Sea During 1975 and 1976. Months with similiar distributions of ice speeds are pooled. Data taken from Thorndike and Cheung (1977) for AIDJEX Stations 2 and 3 from April 1975 through May 1976.

4. Properties of Crude Oils

Until oil is actually found in the continental shelf area north of Alaska, we will not know the properties of that oil. Even after oil is discovered, its properties may vary at different locations or depths. Fortunately, most of the properties of crude oil will not vary to such an extent that unexpected or radical behavior will occur. Furthermore, many of the interactions of crude oil and sea ice can be expressed as functions of oil characteristics. Although there is little reason to expect offshore oil discoveries to completely resemble the Prudhoe Bay field, we will often use the properties of a Prudhoe Bay crude as typical values. After all, the regions are close geographically, and Prudhoe Bay crudes are fairly typical. Examples are sometimes given with reference to Norman Wells or Swan Hills crudes as these were used in the Beaufort Sea Project's experimental oil spills at Balaena Bay, N.W.T., and they represent a range of crude oils.

One important property of crude oil in relation to an Arctic oil spill is pour point. Generally, a crude oil's pour point will be below the ambient water temperature; but, during the winter, air temperatures can be much lower than a typical crude's pour point. For oil on top of the ice during winter, a relatively high pour point will inhibit spreading and evaporation (due to less surface area).

Other important oil properties are density, viscosity, surface tension, and contact angle of the oil-ice-water contact. These properties will determine such things as the spreading rate of oil on water or under ice, the equilibrium slick thickness, and the migration rates up through brine drainage channels. Typical values of some of these properties for Prudhoe Bay, Norman Wells, and Swan Hills crudes are given in Table 4.1. While it is not possible to predict each property of the oil, we can be fairly confident of the range of possible values. More often than not, the variability of a property within a typical range will not have a significant effect on the prediction of oil-ice interactions.

Some characteristics of the oil reservoir, the individual well, and the environment will also influence the nature of the blowout and resulting oil spill. The flow rate of the oil during the blowout and the duration of the blowout can vary widely from a few barrels per day for a few days to several thousands of barrels per day for many days or months. The temperature of the reservoir will be depth dependent (2 to 3°C per 100-m depth). Oil found at a depth of 3000 meters would be at a temperature between 60 and 90°C. In the event of a large blowout, the heat contained in the oil could melt a significant amount of ice directly over the blowout.

The amount of gas released with the oil during a blowout can also be important in ice-covered waters. If it is not immediately vented, the gas can have a large effect on the spread of the oil slick by filling voids in the ice which would otherwise be filled by oil. The ratio of gas to oil of 150 has been typically used in the literature. This ratio is dependent largely upon the depth of the reservoir, and the ratio of 150 corresponds roughly to a depth of 3000 meters.

The composition and physical properties of the crude oil, as well as environmental conditions, will determine the ultimate fate of an oil spill in a marine environment. Mechanisms which play an important role in this fate are spreading, transport, evaporation, dissolution, dispersion (oil in water emulsions), emulsification (water in oil emulsions), sedimentation, biodegradation, and autooxidation. The presence of an ice canopy greatly affects all these mechanisms.

The bulk of this report concerns the spreading and transport of oil under or in sea ice. During the initial blowout, there is likely to be some dissolution, dispersion, and emulsification of the crude oil because of the violent turbulence of the blowout plume. If open water exists over the blowout site, some evaporation will also occur. The amount of hydrocarbons entering the water column or evaporated at this time will probably not be significant in terms of volume of oil but may or may not be critical to sensitive organisms. Sedimentation could also occur at this time if the spilled oil comes into contact with silt-laden slush ice which is often found off the Alaskan coast. Autooxidation and biodegradation happen so slowly, especially in cold Arctic waters, that they need not be considered except in the very long term.

During the Arctic winter and in the absence of large currents, oil released under sea ice will quickly become encapsulated in the ice. Once this occurs, the oil is protected from all forms of weathering until the oil is released from the ice in the spring. At that time, the weathering processes begin anew and become an important factor in the spill's fate.

Table 4.1. Typical Crude Oil Properties

Crude Source	Density (kg/m^3)	Viscosity (Pa•s)	Pour Point (°C)	Surface Tension (N/m)	Contact Angle (°)	Equilibrium Thickness (mm)
Prudhoe Bay	mean: 890 range: 870–910	0.019 (at 0°C) 0.175 (at -2°C) 1.000 (at -8°C)	-9.5	-	-	-
Norman Wells	845 (at 0°C) 855 (at -10°C)	0.012 (at 0°C) 0.018 (at -15°C)	-45	0.033	20	12
Swan Hills	837 (at 0°C) 845 (at -10°C)	0.034 (at 0°C) 0.045 (at -15°C)	-4	0.031	42	8.6

5. The Interaction of Oil and Sea Ice

If an underwater blowout occurs releasing large quantities of crude oil and gas into the water beneath the Arctic ice cover, one can expect a different chain of events than from an open-water blowout. No such under-ice blowout has occurred yet, but from experimental work (NORCOR, 1975; Martin, 1977; Topham, 1975; Cox et al., 1980) and from observations made at accidental surface spill sites in icy waters (Ruby et al., 1977; Deslauriers, 1979), one can predict the course of events for an under-ice blowout with reasonable confidence.

For convenience, we have divided the interactions between crude oil and sea ice into five distinct phases. These are:

(1) The initial phase which includes the blowout and subsequent rise to the surface of the oil and its initial interaction with the ice cover, such as melting or breaking of the ice.

(2) The spreading phase where the oil spreads laterally beneath the ice by means of water currents or buoyancy.

(3) The incorporation phase which includes freezing of the oil lens into the ice cover, soaking into the skeletal layer beneath the ice or into the snow layer on top of the ice, and building of deformed ice features made of oiled ice.

(4) The transportation phase which is mainly applicable to the pack ice or to breakup in the other zones.

(5) The release phase where the oil is released from the ice back into the atmosphere and water column.

These five major phases will occur, or at least begin to occur, sequentially. In the event of a large blowout lasting more than a few days, considerable overlap will occur between phases. Depending upon the circumstances, some parts of the five phases may not happen or will be inconsequential. For example, if the blowout occurs during the summer, very little oil will be incorporated into the ice.

In the rest of this section (Section 5), the five major phases of interaction between crude oil and sea ice are discussed separately.

5.1 Initial Phase

The initial phase includes the blowout and the immediate impact of the oil and gas as it rises to the surface and interacts with the ice cover. The major events are the formation of a plume and wave ring, cracking of ice caused by gas bubbles, melting of ice due to the heat content of the oil, and the formation of pools of oil on the surface.

5.1.1 The Underwater Plume

The blowout is assumed to consist of the continuous release over a minimum of several days of large quantities of crude oil and many times that amount of gases. Topham (1975) reports the results of experimental releases of oil and compressed air underwater. The experiments were simulations of small well blowouts in open-water conditions. The presence of an ice cover over the blowout site is not thought to have a significant effect on the experimental results.

As gas is released underwater, it breaks up into small bubbles and rises to the surface. Oil accompanying the gas and part of the surrounding water is carried along, forming an underwater plume. This plume is initially conical in shape but becomes nearly cylindrical with height above the release point. The height at which the plume becomes cylindrical, and thus the diameter of the plume, is thought to be a function of the gas release rate. The centerline velocities of experimental plumes did not vary significantly with the depth or air flow rate for the range of experimental values (flow rates of 3.6 to 40 m^3/min at depths of 33 to 60 m, Topham, 1975).

As the plume reaches the water surface, the vertical transport changes to a radial current flowing outward. A concentric wave ring is produced at some distance from the plume marking the location of a reversal in radial surface currents. A downward current is found here, extending to a depth of about 10 m. The presence of this wave ring, and the reversal of surface currents, is important since the wave ring will act to contain some of the oil released near the blowout site. Small droplets of oil or oil-and-water emulsions will likely be swept downward at the wave ring. The majority of oil from the blowout will rise to the surface in drops of 1-mm mean diameter, but 1 or 2 percent will be in fine droplets of approximately 0.05 mm in diameter (Topham, 1975). Drops of this size have a natural rise rate of about 0.5 mm/s. Subsurface currents could carry the very small droplets many kilometers downstream during their slow rise to the surface. Dissolution is generally not considered to be important in the Arctic (NORCOR, 1975). The formation of emulsions and their fate in Arctic waters is an unknown quantity at this time.

Topham (1975) also gives the following empirical formula for determining the radius of the wave ring:

$$R = 0.39\ Z \left(\frac{V_f \times 10.36}{Z + 10.36}\right)^{1/3}, \tag{5.1}$$

where Z is the water depth in meters and V_f is the volume flow rate of gas in m^3/min. The formula gives reasonable results for the test conditions of depths from 33 to 60 m and flow rates of 3.6 to 40 m^3/min. For a large blowout in the shallow waters near shore the formula may not be as reliable but should still give a reasonable first approximation. In Figure 5.1 we give the computed radius of the wave ring as a function of the gas flow rate and water depth at 10- to 30- m depths.

The wave ring is particularly important in fast ice areas since most of the action of the blowout is concentrated under one small area of ice. In the moving pack, it is considerably less important.

5.1.2 Gas Under the Ice

The first interaction between the blowout and the ice cover is the collection of gas beneath the ice if no holes or cracks exist directly over the blowout. Assuming the ratio of gas to oil at the surface to be 150 to 1, then gas will be released at rates like 33 m^3/min in the case of a small blowout (2000 bbls/day of oil) or 828 m^3/min in the case of an extreme event (50,000 bbls/day of oil). Within minutes, large pockets of gas will have accumulated beneath the ice.

Topham (1977) studied the problem of a submerged gas bubble bending and breaking an ice sheet. For thin ice, there is little doubt that a gas bubble a few centimeters in thickness and a few meters in radius will crack the ice. For thicker ice, up to 2 m thick, the situation is not so clear. In rough ice where large, thick pockets of gas can

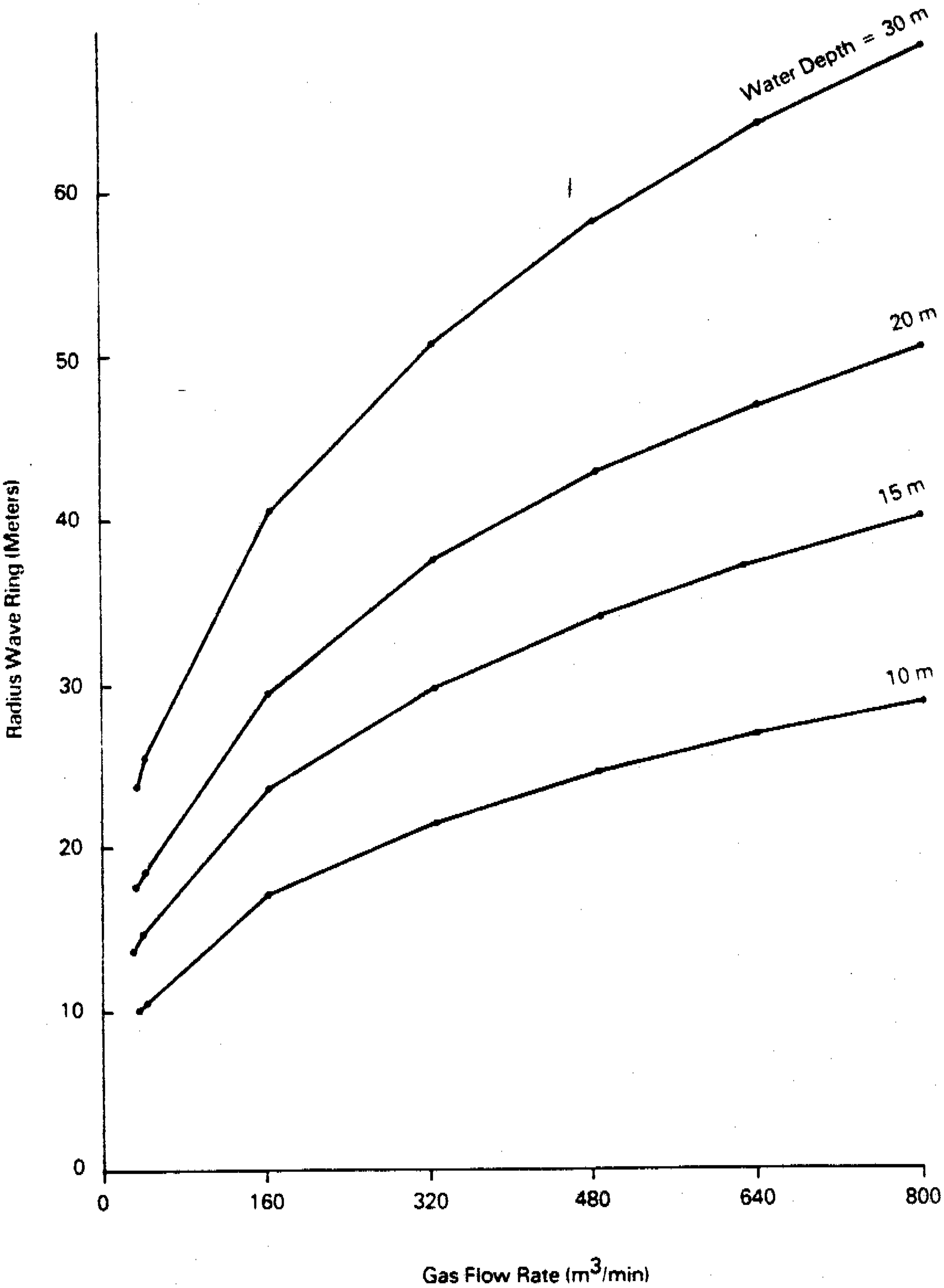

Figure 5.1. Radius of Wave Ring as Function of Water Depth and Gas Flow Rate.

collect, the radius needed to crack the ice is a few tens of meters. In smoother ice where the gas will collect only to a few centimeters in thickness, the critical radius can extend from a few hundreds of meters to several kilometers. (The radius is very sensitive to changes in bubble thickness at small thicknesses.)

We believe that the gas will break the ice cover in the fast ice areas nevertheless. For one thing, natural weaknesses exist in the ice in the form of thermal cracks which probably occur every few hundred meters (Evans and Untersteiner, 1971). At the most, gas will spread a few hundreds of meters under the ice before cracking the ice or coming to a natural crack. Once a crack is formed (or if one already exists) near the blowout site, the ice over the blowout is likely to be further fractured and broken up by the turbulence or by sinking into the low-density gas-in-water mixture near the center of the plume.

Under a moving ice canopy, the ice may or may not be broken up as it passes over the gas plume. If the ice is moving at the rate of 1 km/day this amounts to an average of about 42 m/hr. Gas flow rates of 40 to 800 m^3/min will deposit from 2400 to 48,000 m^3 of gas under the ice in 1 hour. If this gas collects to an average depth of 0.1 m, the under-ice bubble will cover an area of 24,000 to 480,000 m^2 in 1 hour. For first-year ice, the motion experienced during that hour is probably of no significance; the ice will be broken up much as stationary ice would be. If the ice is moving at several kilometers per day over a small blowout, however, it is possible that breakage will not occur.

It has been the opinion of some investigators (Logan et al., 1975; Milne and Herlinveaux, n.d.) that large multiyear floes will not be broken up as they move across an underwater gas plume. Topham's work (1977) seems to support this view, although it is possible to imagine situations where a multiyear floe could be broken by gas pressure underneath. Suppose a large multiyear floe were stationary over a blowout and a system of deep, consolidated, multiyear ridge keels completely surrounded the blowout. Unless thermal cracks were present and extended through the ice, a very deep, large pocket of gas could collect and possibly crack the ice. For moving multiyear floes, though, it is unlikely that gas can collect to a depth that will cause the ice to fail. Thermal cracks themselves provide an alternate path for releasing the gas though. In Section 5.2.3, we discuss the effects of thermal cracks.

5.1.3 Thermal Effects

A possible contributory factor in breaking a stationary or slowly moving sheet of first-year ice is the heat content of the oil. When hot oil escapes from the blowout outlet it breaks up into small droplets (0.5 to 1.0 mm in diameter). Most or all of the surplus heat of the oil would be transferred to the water column which in turn is carried to the underside of the ice by the gas-induced plume. Some of the heat from the warmed water will then go into melting the ice, with the greatest part of the melting occurring in the area enclosed by the wave ring.

Ashton (1974) considered the use of air bubble-induced plumes to melt ice where the only source of heat was the water column. In shallow waters of the Arctic, this source of heat will be small during most of the ice season, but it can enhance the melting.

The specific heat of sea ice is about 2010 J/(kg•K) and that of a typical crude oil is 1717 J/(kg•K). The heat of fusion of water (fresh) is about 334,107 J/kg. If the ice sheet has an average temperature of $-10^{o}C$, it will require $10^{o}C \times 2010$ J/(kg•K) + 334,107 J/kg or 354,207 J/kg to warm and melt the ice. Crude oil provides 1717 J/kg of heat for each degree of temperature above freezing. To warm and melt each kilogram of sea ice at $-10^{o}C$, about 206 kg•K of crude oil is required. Since the densities of ice and crude oil are about the same, each volume of oil will melt roughly 1/200th that volume of ice for each degree of temperature above freezing of the oil.

Consider the case of a very large blowout of 40,000 bbls/day (6360 m^3/day). In water depths of 10 m, we see from Figure 5.1 that the wave ring is about 30 m in radius or 2827 m^2 in area. Each day, for each degree of temperature of the oil, 1/200th of 6360 m^3 or approximately 318 m^3 of ice will be melted, and if melting is spread evenly over the area of the wave ring, an 0.11 m thickness of ice per day per degree would be melted. If the oil were at a temperature of $100^{o}C$, then over 11 m of ice could be melted each day over the blowout site. This figure is probably much too high, since the heat from the oil would be spread over a much larger area by existing currents and by circulation induced by the plume. Thus a much larger volume of water would be warmed slightly, with possibly only a decrease in ice growth rates over a large area accompanying the heat release. Still, one would expect the ice directly over the blowout to receive a higher proportion of the heat from the oil. If the ice becomes broken up due to the gas plume, some heat will escape directly to the atmosphere, but more ice is likely to be melted since more ice surface will be exposed to the warm oil and water.

Further speculation on the amount of ice melted by the hot oil is probably pointless at this time. The most important point is that in stationary ice or very slowly moving first-year ice, melting will tend to weaken ice over the blowout, making it more probable that gas bubbles trapped beneath the ice will fracture it and escape. For very large blowouts, a significant amount of ice may be melted, leaving a pool of open water directly over the blowout. Large amounts of oil could collect in this open-water pool.

5.1.4 Oil on the Ice Surface

The density of sea water, ρ_w, is about 1020 kg/m^3 and the density of sea ice, ρ_i, is about 910 kg/m^3. Densities of fresh crude oils, ρ_o, may range from about 800 to 900 kg/m^3. The freeboard of sea ice will average $\bar{h}\,(\rho_w - \rho_i)/\rho_i$ (about 0.121 times the average ice thickness, $\bar{h}$). The equivalent freeboard for crude oil will range from 0.133 to 0.275 times the oil thickness. Thus, if one tries to fill a hole through the ice with crude oil, the oil will overflow the top of the hole before it is filled to the bottom. During much of the ice season, the atmospheric temperature is so low that crude oil exposed to the atmosphere behaves more like a solid than a liquid. It is therefore unlikely that great pools of oil will flood the upper ice surface through holes and cracks. Even during the spring, when the atmosphere is at a temperature above the oil's pour point, the snow cover, snow drifts, and natural roughness of the ice surface will tend to limit the spread of oil on the surface.

One must also remember that during the winter in the Arctic, open water is extremely rare. Motion of the pack is continually producing small amounts of open water, but the heat exchange is so rapid from water to air that in a matter of hours a few centimeters of ice has formed. In the fast ice zone, the only naturally occurring holes where oil might escape to the surface would be thermal cracks which extend through the ice. Other holes through the fast ice will include the one probably produced by the blowout and any man-made holes or slots.

5.2 Spreading Phase

Once oil gets underneath an ice sheet, several factors will control the concentration and areal extent of the oil spread. The bottom roughness of the ice, the presence of gas under the ice, the magnitude and direction of ocean currents, and movement of the ice cover are the primary factors affecting the spread of the oil. Of secondary importance are the oil properties such as density, surface tension, equilibrium thickness, and viscosity. The effect of these latter properties are fairly well understood (NORCOR, 1975; Cox et al., 1980; Rosenegger, 1975) and, while important to understanding the basic mechanisms of oil-water-ice interactions, will not have as profound an effect on the extent of oil coverage as the grosser, more variable factors such as bottom roughness or ocean currents.

5.2.1 Bottom Roughness and Oil Containment

The bottom roughness of the ice will vary significantly between the three morphological zones, as discussed in Section 3. The fast ice zone will have roughness determined chiefly by spatial variations in snow cover causing differences in ice growth rates. The stamukhi zone will be dominated by deep ridge keels. In the pack ice zone, both the above types of roughness are present along with frequent refrozen leads and a high percentage of multiyear floes which have exaggerated underside relief. In addition, all ice growing in sea water has a microscale relief due to the columnar nature of new ice growth and to random variations in growth.

If oil alone is released under sea ice, or if any accompanying gas is vented, the oil begins filling under-ice voids near the blowout. As a void fills downward with oil, the oil eventually reaches a depth where it can begin escaping over neighboring summits of ice or through "passes" to the next void. If the ice itself is moving over the site of the blowout, the voids may not be completely filled and only that ice passing directly over the blowout plume will collect oil.

If new ice forms in calm conditions, the ice will have an essentially flat, smooth surface underneath. Oil will spread underneath this ice to some equilibrium thickness depending upon a balance between surface tension and buoyancy forces. Cox et al., (1980) report test results for oil of various densities. The equilibrium slick thickness ranged from 5.2 to 11.5 mm for oils with densities in the range of crude oils.

For a constant surface tension, a good approximation of slick thickness can be made using the empirical relationship (Cox et al., 1980)

$$\delta = -8.50\left(\rho_w - \rho_o\right) + 1.67 , \tag{5.2}$$

where δ is the slick thickness in centimeters and $(\rho_w - \rho_o)$ is the density difference between oil and water. The minimum stable drop thickness for crude oil under ice has generally been reported to be about 8 mm (Lewis, 1976). Using this value, we see that 8000 m^3 (50,318 bbls) of oil will spread under each square kilometer of smooth ice. This is the minimum volume of oil that can spread under 1 km^2 of ice in the absence of currents. Generally, sea ice, even smooth new ice, will not be perfectly smooth so that each square kilometer will actually hold more oil than that.

As the ice season progresses, a snow cover accumulates on the ice. Maximum snowfall occurs in October and November, so the new ice very quickly acquires this snow cover. Winds are frequent in the Arctic, and in most areas the snow will collect in parallel drifts, perpendicular to the prevailing wind direction. Barnes et al. (1979) found these snow drifts to be fairly stable throughout the ice season. These snow drifts, being mostly dead air space, insulate the ice from the low atmospheric temperatures, causing reduced ice growth beneath. The underside of the ice takes on an undulating appearance and as ice continues to grow throughout the winter, these undulations become more pronounced. Thus, oil containment capacity increases through the winter.

NORCOR (1975), reporting on the Balaena Bay experiment, found ice thicker than about 0.5 m to have a thickness variation of about 20 percent the mean ice thickness. Not all of this variation will be available for oil containment. Because of natural variations in the snow cover and drift patterns, voids under the ice will tend to be interconnected by passes. These passes may be at any depth within the range of ice drafts but presumably the most likely depth will be the mean ice draft.

A simple model of the oil containment volume of smooth first-year ice can be formulated based upon the above and the assumption that ice relief is sinusoidal in character perpendicular to the snow drifts with each trough connected to adjacent ones by passes at the mean ice draft. The volume contained in a 1-m length of a typical trough is

$$V = \frac{r}{2} \int_{0}^{\ell/2} \sin\left(\frac{2\pi}{\ell} x\right) dx = \frac{\ell r}{2\pi} \quad , \qquad (5.3)$$

where r is the peak-to-trough roughness amplitude and ℓ is the average spacing of the troughs. A typical value of ℓ is about 10 m. For an area of 1 km^2, the total containment volume is $(r/2\pi)\ 10^6\ m^3$. Using a value for roughness of $0.2\ \bar{h}$ (20 percent the average ice thickness, $\bar{h}$), we have plotted oil containment versus ice thickness in Figure 5.2. Below ice thicknesses of 0.25 m, we assume oil spreads to about the equilibrium thickness (8 mm).

Kovacs (1977, 1979, 1980) has mapped the underside relief of the fast ice at various places and times using an impulse radar system which "sees" the ice-water interface. From contour maps of the ice bottom, he has measured the volume of the voids which lie above the mean ice draft. These data points are plotted in Figure 5.2 as the numbered points. Point 1 is from data collected in May 1978 off the northwest side of Tigvariak Island (Kovacs, 1979). The mean ice thickness was 1.56 m. The area is representative of high snow-accumulation areas having an average snow depth of 0.33 m (s.d. = 0.07 m). Point 2 was profiled in April 1976 at a site south of Narwhal Island (Kovacs, 1977). The average ice thickness was 1.91 m and the snow cover was reported as "less snow than the Tigvariak Island site" (Kovacs, 1979). Point 3 was profiled during the spring of 1979 near Prudhoe Bay (Kovacs, 1980). The mean ice thickness was 1.89 m and a containment volume of 60,000 m^3/km^2 was measured. This area had undergone deformation during fall freezeup, which probably explains the large subsurface relief compared to the other sites.

The sinusoidal model seems to give a reasonable approximation to maximum containment volumes for thicker first-year sea ice. The scatter of data points about the plot in Figure 5.2 gives an indication of the variability due to variations in snow cover. The range of variability in containment volume is estimated to be about 50 percent of the calculated value.

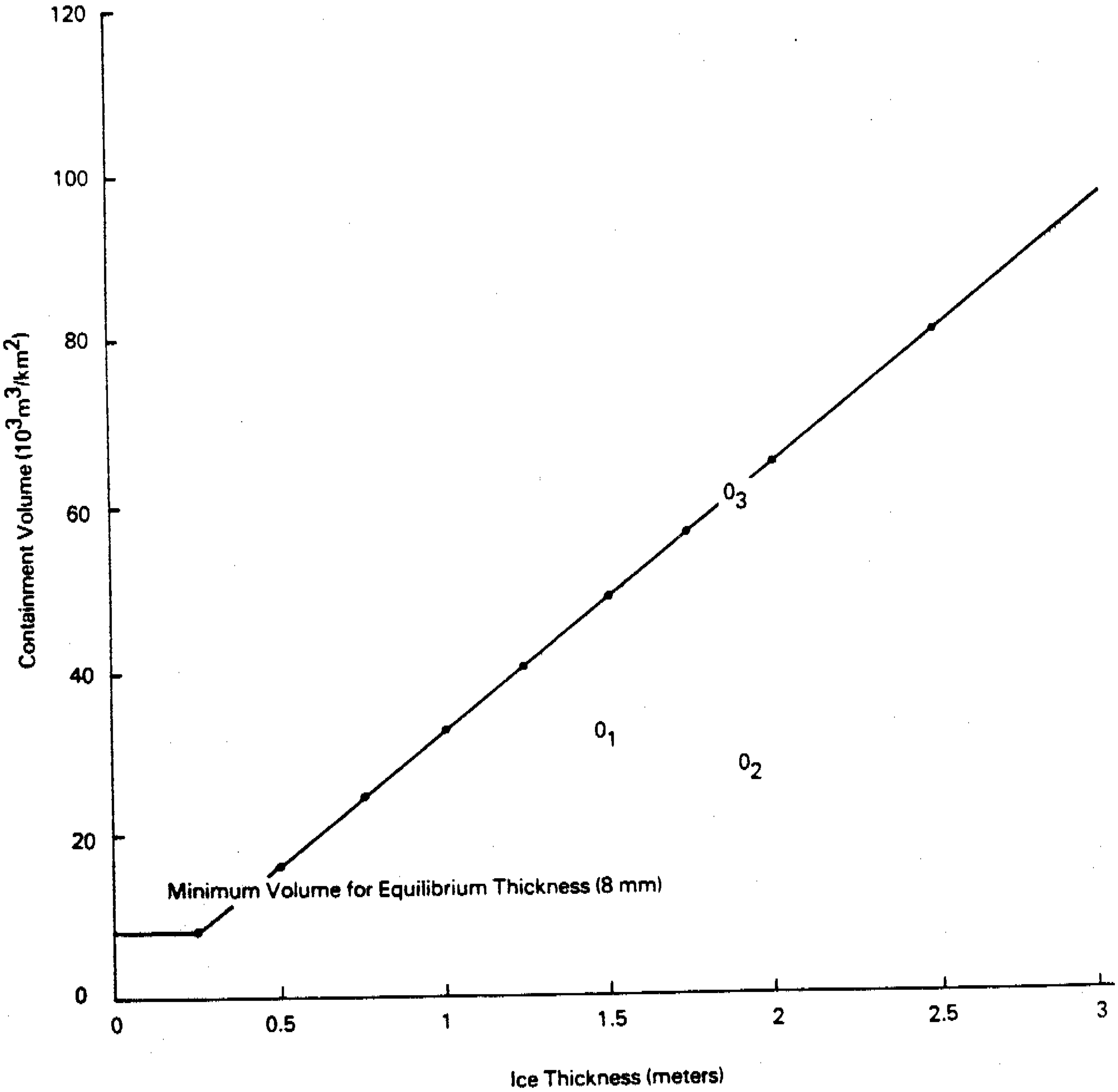

Figure 5.2. **Oil Containment Volume Versus Ice Thickness. Points 0_1, 0_2, and 0_3 are observed values (Kovacs, 1978, 1979, 1980). The line represents containment volume computed using a sine model of ice roughness.**

If deformation occurs in the inner fast ice zone, it will take place in the fall when the ice is thin. Most of this deformation is minor in character - raised rims on edges of individual floes, rafting, and a few small ridges or rubble fields. The relief will generally be only a few centimeters deep, which will tend to increase the oil containment capacity. As the ice grows thicker and stronger, new deformation ceases and the existing deformed features below the ice tend to be leveled out, by differential ice growth between thicker and thinner ice, and to be obscured by the relief due to an accumulating snow cover.

Kovacs and Weeks (1979) did observe some major deformations occurring inside the barrier islands. A severe storm in early November 1978 with winds at 55 to 65 km/hr (30 to 35 knots) gusting to 110 km/hr (60 knots) broke up the fast ice, producing ice motions greater than 1 km and building ridges up to 4 m high. Three previous years' observations had not seen such events, but obviously they must be considered. In terms of the spreading of oil under the ice, the increased roughness created by the deformation should limit the spread by creating more voids for the collection of oil. If frequent enough and intersecting, the ridges would limit the directions which oil could spread or possibly trap deeper pools of oil.

Outside the inner fast ice zone, in the stamukhi zone, deformational events continue to occur throughout the winter creating a bottomside relief many meters deep. If we assume that there are 12 ridges per kilometer in the stamukhi zone (Section 3.3.4) and the average ridge keel width is 20 m, based upon the typical ridge described in Section 3.4.4, then the average extent of undeformed ice between ridges is 63 m. This is in the direction perpendicular to the coastline since the ridges tend to parallel the coast. Parallel to the general ridge direction the extent of undeformed ice between ridges will be greater but usually not much greater. Since the best we can hope to do in this type of ice terrain is to make an order-of-magnitude estimation of oil containment potential, let us assume that the average under-ice void between ridges is roughly a square 63 m on a side.

Ridges in the stamukhi zone are often large enough to become grounded in waters 25 m or more deep; however, most of the ridges are probably not that deep. Wadhams and Horne (1978) report the mean depth of ridge keels in the region about 100 km offshore to be 8.57 m. There will, of course, be variations in depth along any one ridge. Rigby and Hanson (1976) profiled a section of a pressure ridge in the central Beaufort Sea and found the depth to vary from about 7 to 10 m. Hibler and Ackley (1974a) profiled several kilometers of pressure ridge sails in the Beaufort Sea. The range of sail height variations was generally equal to or greater than the mean ridge height. A conservative approach (in terms of oil containment) is to assume that keel depths are just as variable as sail heights. Then, an 8-m-deep keel will be assumed to vary from 4 to 12 m. Thus, in the stamukhi zone, we have the potential of forming pools of oil 15,876 m^3 or larger in volume.

Whether the oil can actually collect in pools that deep is another matter. The only direct evidence we have of the interaction of oil and ridges occurred in Buzzards Bay, Massachusetts, in 1977. Deslauriers (1979) observed that the spilled oil tended to be trapped between the ice blocks making up the ridges with some oil appearing on the surface. These observations may not be applicable to large Arctic pressure and shear ridges which can be several tens of meters in width with a lower probability of interconnecting voids extending through the ridges at shallow depths. This is even more unlikely as the ridges age and some of the interior voids freeze.

If oil collects in deep pools surrounded by ridge keels, there is an increased probability of it reaching the ice surface either through naturally occurring thermal cracks, through the loose blocks of an unconsolidated ridge, or through holes and cracks produced by the gas from the blowout. The oil, being less dense than ice and assuming a pour point less than the freezing temperature of sea water, could possibly pool as deep as 1 m on the top surface of the ice. Then the height and compactness of the surrounding ridge sails would be important in containing the oil.

If no cracks or voids exist in the ice and the gas pressure does not itself break the ice, then large volumes of gas could be trapped by the ridges in the stamukhi zone. This is at worst a local problem since it is unlikely that areas large enough to be significant will be impermeable to gas.

In actuality, the probability of a blowout in the stamukhi zone following the general scenario outlined above must be fairly low. Enough different types of events can occur that using mean values can suggest an unrealistic outcome to an oil spill scenario. For example, the blowout could occur in a part of the stamukhi zone which has been left untouched by ridging events. Then a blowout would proceed as if it were under smooth ice in the inner fast ice zone. Often, in the stamukhi zone, large ridge or hummock fields with overlapping keels form. Most of the oil released in such an area would probably end up in amongst the ice rubble forming the keels if the deformation occurred during the same season. Under multiyear grounded ridge systems or hummock fields, the keels will be more consolidated and pools of oil and gas may collect.

Further out, in the pack ice zone, the variety of under-ice relief increases. Not only are there first-year ice floes and pressure ridges, but variable amounts of multiyear ice and refrozen leads also exist.

Underneath multiyear ice, vast quantities of oil or gas may be contained. Kovacs (1977) profiled the bottom of a multiyear floe and estimated that 293,000 m^3/km^2 of space existed above the mean draft of 4.31 m. This is an order of magnitude greater than the volume under first-year ice at the end of the ice season. Other investigators (Ackley et al., 1974) also report greater relief under multiyear ice than under first-year ice. Theoretical studies indicate that Arctic ice approaches an equilibrium thickness after several years of thermodynamic growth and ablation (Maykut and Untersteiner, 1971). Evidently, enough factors vary on small spatial scales to provide the considerable relief observed. Old ablated ridges, refrozen leads and melt ponds, and snow drifts might all contribute to the greater relief of multiyear ice.

Refrozen leads will also hold large amounts of oil or gas. The ice in a lead is relatively thin and smooth, while the ice of the original floe will have a draft up to 3 m deeper than the ice in the lead. A large lead may be several kilometers wide and many kilometers long, in which case the lead would limit the direction of spreading of the oil but not the area covered. A large flaw lead does often form all along the Alaskan coast along the southern boundary of the moving pack.

However, most leads will be quite narrow, less than 50 m wide (Wadhams and Horne, 1978). Since leads do not form as perfectly straight lines but rather follow the meandering floe boundaries or recent thermal cracks, there will generally be many points of contact along the lead. Thus, if oil or gas does come up beneath a refrozen lead or flows into it from the surrounding ice, it will usually be collected in an elongated pool rather than spreading indefinitely along the lead. If a refrozen lead does exist, then there is a high probability of the oiled ice in the lead being built into a ridge. We discuss this possibility in Section 5.3.3.

There is also some probability of oil from a blowout coming up in open water in a newly opened lead. Throughout most of the ice season in the Beaufort Sea this probability must be fairly low. New ice begins to form immediately, and within 1 day a solid ice cover will exist in new leads. Oil beneath thin ice in leads will have a higher probability of appearing on the surface than oil beneath thicker ice will have. The ice motion which produces leads will also open leads wider or close leads by rafting or ridging the thin ice. Gas collecting under a lead can also break the ice. As we observed previously, the spreading of oil on the surface would probably not be significant due to the low temperatures and snow cover.

5.2.2 Effect of Currents

Outside of buoyancy spreading or a moving ice cover over a blowout, the only other significant contribution to the spread of oil beneath sea ice is ocean currents. Until the oil is completely encapsulated by new ice growth, currents of sufficient magnitude can move the oil laterally beneath the ice until an insurmountable obstruction is reached or the currents cease.

NORCOR (1975) performed some oil spill experiments near Cape Parry in March 1975 in the presence of currents about 0.1 m/s in magnitude. In one test, the ice appeared to be perfectly flat with roughness variations of 2 to 3 mm. Oil discharged under this ice spread predominately downstream to a thickness of about 6 mm. After all the oil had been discharged, movement of the oil lens appeared to stop.

A second test was performed nearby in the same current regime but in ice with more underside relief. Troughs of up to 0.5 m in depth were present, as well as a small ridge keel downstream from the test site. Again the oil spread downstream until one of the depressions was reached. At that point, the oil collected in a stationary pool averaging about 0.1 m in depth.

Evidently, currents of only 0.1 m/s may influence the direction of the spread of crude oil under ice but will not greatly affect the amount of spreading.

More recently, ARCTEC has been able to quantify the relationship between current speed, bottom roughness, and the movement of oil under ice (Cox et al., 1980). From flume experiments, ARCTEC determined that for smooth ice or ice with roughness less than about the equilibrium slick thickness, there is a threshold water velocity below which the oil does not move. For smooth ice, the threshold velocity was about 0.035 m/s; for roughness scales of 1 mm, the threshold was 0.1 to 0.16 m/s (depending upon oil density); and for 10 mm roughness, the threshold velocity was 0.2 to 0.24 m/s. For currents above the threshold velocity, the oil moved at some fraction of the current speed.

For bottom roughness elements with depths several times the slick equilibrium thickness, a boom-type containment/failure behavior was observed. The oil collected upstream of the obstruction to some equilibrium volume, after which additional oil flowed beneath the obstruction. The size and shape of the obstruction had little effect on oil containment. Thus, even mild slopes act as barriers to oil movement.

As the water velocity increases beneath the ice, a Kelvin-Helmholtz instability eventually occurs, in which case the entire slick is flushed from behind the obstruction. Figure 5.3, reproduced from Cox et al. (1980), shows the relationship between the flushing velocity and the water-oil density difference. For the range of oil densities tested, the failure velocities ranged from about 0.14 to 0.22 m/s.

5.2.3 Effect of Ice Motion

The motion, if any, of the ice cover over a blowout is another mechanism by which oil can be spread beneath the ice. If the ice motion is large enough, the containment potential of the ice may not be realized

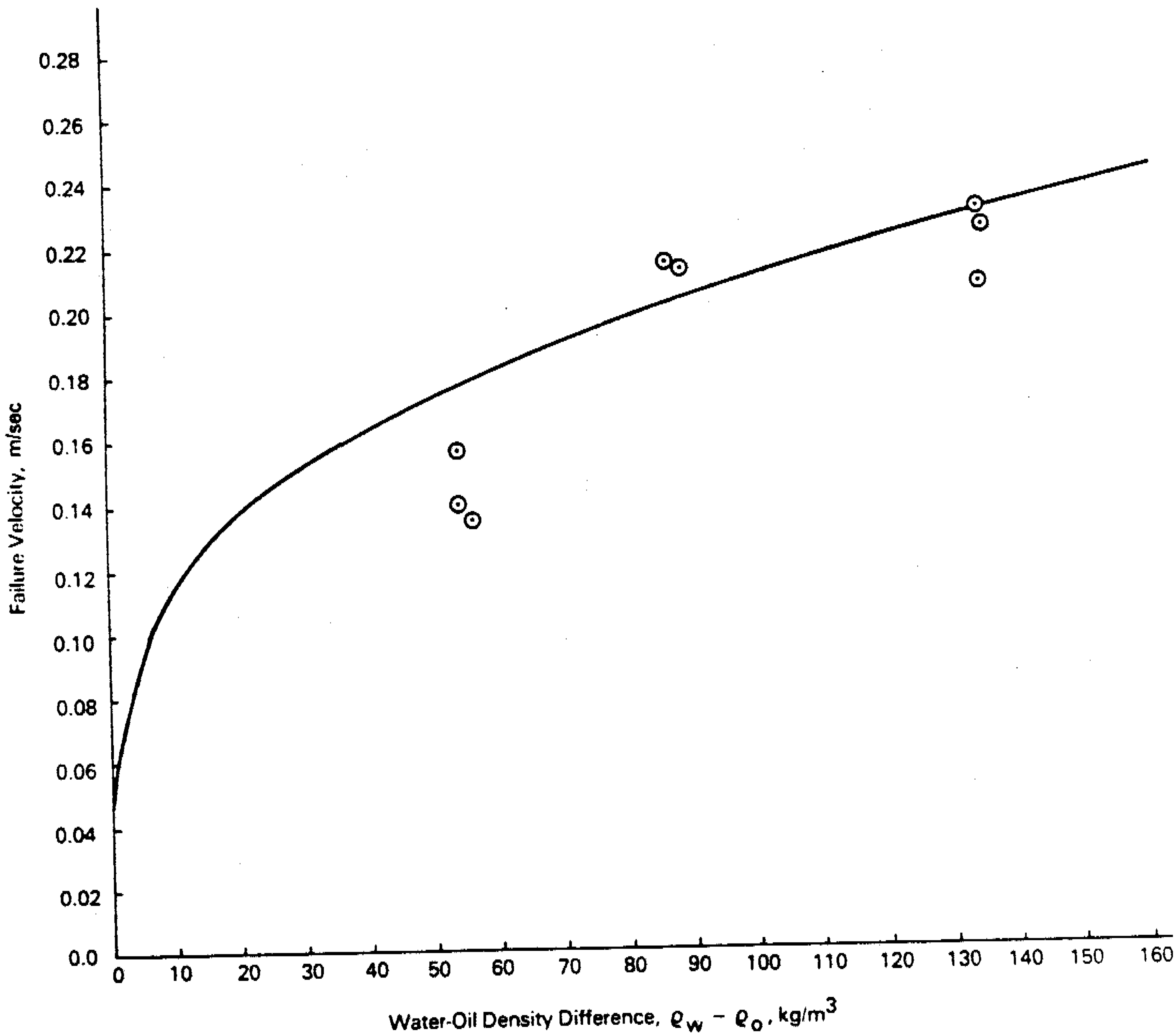

Figure 5.3. Relationship Between Failure Velocity and Water-Oil Density Difference for Containment of Oil Upstream of an Obstruction. (Figure 6.11 from Cox et al., 1980.) Results are applicable to shallow water only. Circled points are observations from flume tests.

and a greater area of ice may be contaminated with oil. For high ice velocities, the gases from a blowout may not be concentrated enough to break thicker ice. Some of the gas will escape through natural cracks in the ice, but the remainder will further increase the area over which oil will spread.

Motion of the ice in the fast ice zone is largely confined to the fall just after freezeup or after breakup in the spring. During the majority of the ice season, motion of the fast ice can be measured in meters (Tucker et al., 1980). Kovacs and Weeks (1979) have observed that motions of kilometers in magnitude can occur in the fast ice soon after freezeup while the ice is thin and weak. Motions of this magnitude are due to severe storms which are not uncommon in the fall. The frequency of occurrence of such motions and the amount of motion have not been documented otherwise.

We should be able to at least approximate the probability of significant ice motion in the fall in the fast ice zone during the duration of a blowout. First, we observe that when new ice is forming, typically in early October, any wind other than a gentle breeze will probably move the ice about. Conversely, by late November the ice has grown to 0.5 to 0.60 m in thickness and, with the limited fetch available, only an extraordinarily strong wind can produce significant motions.

During the early ice season the fast ice grows at about 0.01 m/day. In Figure 5.4(a) we show the average fast ice thickness for the months of October and November. We know that for a given fetch, the wind speed needed to cause a thin, continuous sheet of ice to fail and start moving is linearly related to the ice thickness (see Figure 3.2). Furthermore, Kovacs and Weeks (1979) have reported large ice motions (greater than 1 km) in the fast ice zone when winds of 55 to 65 km/hr (30 to 35 knots) blew in early November. Lesser winds might possibly have caused the ice to move, but for now this is the best estimate. In Figure 5.4(b) we show an estimate of the wind speed needed to move a continuous ice cover as a function of ice thickness (see Section 3.2.2).

The probability of a wind greater than a given magnitude occurring is shown in Figure 5.4(c). The data were taken from the Climatic Atlas (Brower et al., 1977) for Oliktok. Data for the months of October and November were combined since the wind statistics were similar for those

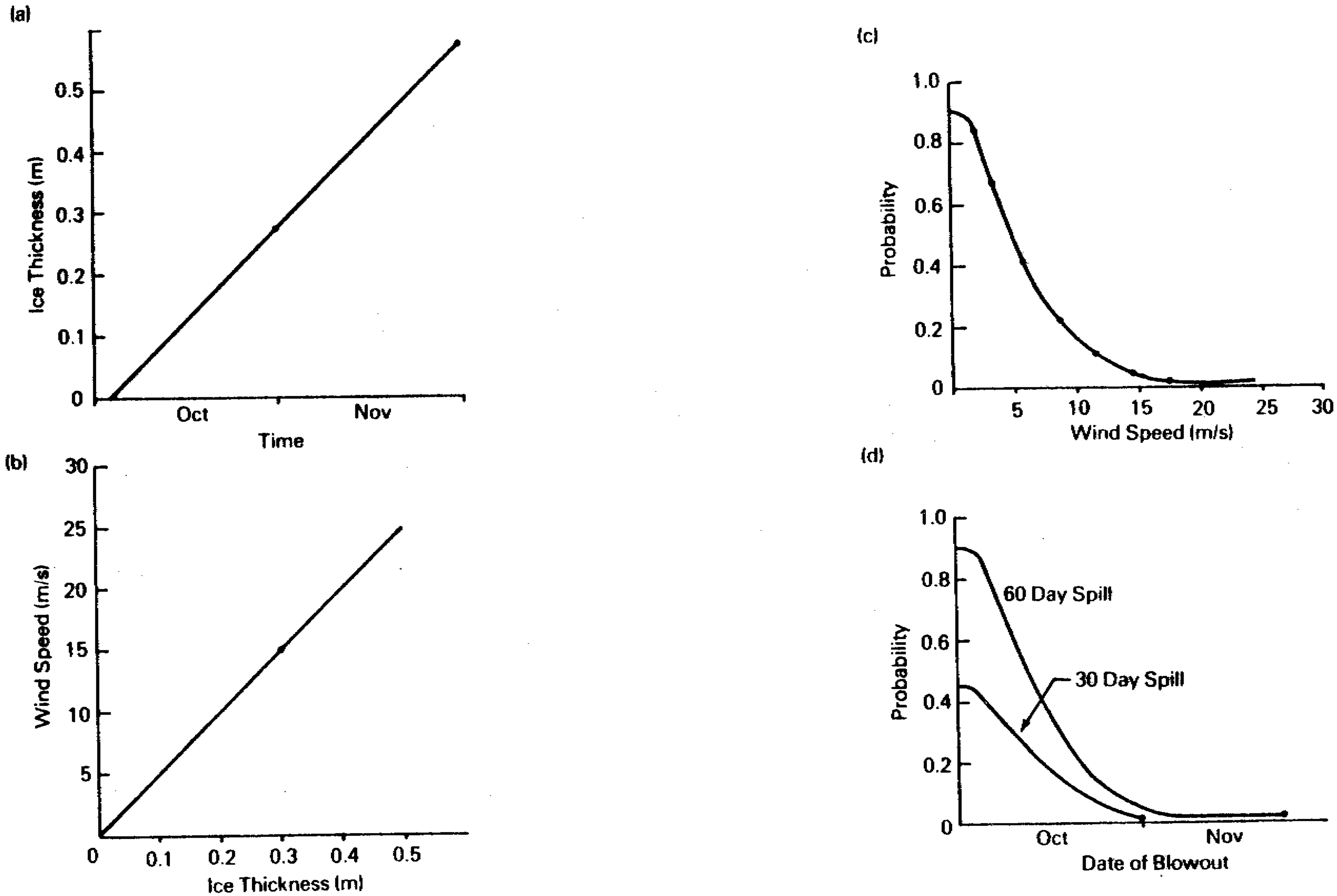

Figure 5.4. Estimating the Probability of Ice Deformation Occurring in the Fast Ice Zone During the Course of an Oil Spill Which Begins During October or November. (a) Ice thickness as a function of time during October and November. (b) Estimate of the wind speed needed to deform ice. (c) Probability of winds of different magnitudes occurring during October and November. (d) Resulting probability of ice deformation occurring during the course of a spill as a function of data and duration of spill. Spills lasting 30 or 60 days are illustrated. Other durations may be linearly interpolated.

months. These data ignore the important aspect of the duration of winds. Since steady winds are more likely to cause ice motion than gusts, the probabilities shown in Figure 5.4(c) might be somewhat high. Also, the probabilities are for a wind occurring some time during the 2-month period. Any period shorter than 2 months would have a smaller probability of any wind speed occurring. In Figure 5.4(d) we show a rough and qualitative estimate of these probabilities of winds of any magnitude occurring during intervals of different lengths. From this plot one can estimate the likelihood of a spill happening during October or November when winds are blowing strongly enough to move the ice. Thus, a spill in the fast ice zone lasting at least 60 days, starting in early October, has about a 90 percent probability of being affected by significant ice motion sometime during the course of the spill. But a 5-day spill starting in early November has a very small chance of occurring under moving ice.

A blowout in the pack ice zone has a much higher probability of occurring under a moving ice cover. The area of ice under which oil spreads will depend upon many factors: the velocity of the ice, the discharge rate of oil and gas from the blowout, the amount of gas which can escape, the diameter of the blowout plume, the roughness of and amounts of different ice types and thicknesses, and the duration of the blowout. While it is impossible to describe exactly what will happen for a specific blowout under pack ice, it is possible to estimate roughly the area of moving ice which would collect oil in a typical blowout situation. This could vary significantly from the case of a blowout under stationary ice.

First, we assume that the width of the oiled ice after passing over the blowout will be at least the surface diameter of the wave ring over the blowout and that the oil (and gas) will not pool under moving ice any deeper than it would under stationary ice.

The expected flow rate of gas involved in a Beaufort Sea blowout is about 150 times the flow rate of the oil. The total flow rate of oil and gas from the blowout will be effectively reduced by the amount of gas that is immediately vented. The escape rate of the gas will depend upon the ice type and thickness, the speed of the ice cover, and the amount of gas released. If the amount of gas released is very small, or if the ice is moving so fast that only a small volume of gas collects under any portion of the ice, the buoyancy forces may not be adequate to cause breakage. Thicker ice requires greater volumes of gas before failure than thin ice does. Very thick ice may not be broken by any amount of gas trapped beneath it. Some gas will always escape through natural cracks in the ice. The cracks, caused by thermal contraction of the ice, will be spaced at roughly equal distances, and the spacing will depend upon temperature changes, ice thickness, and properties of the ice. Crack spacing and direction will be somewhat haphazard, but it is not unreasonable to assume that the cracks form a roughly orthogonal grid breaking the ice sheet into discrete floes.

If the volume of oil and gas released while an unbroken ice floe is passing overhead is greater than the amount the ice floe can contain in voids or an equilibrium film, the remainder must escape through the bounding cracks or pass underneath the cracks to the next section of ice. It seems likely that any gas coming upon a crack in the ice will escape to the atmosphere. Some oil will possibly flow out upon the ice surface, some will fill up the crack itself, and some oil will probably spread beyond the crack. The maximum width of oiled ice after passing over a blowout is roughly the spacing between cracks (ignoring oil which leaks beyond the cracks).

The width of the swath of oiled ice, W_o , is thus bounded by the blowout plume diameter, W_b , and the spacing between cracks in the ice, W_c :

$$W_b \leq W_o \leq W_c \quad . \tag{5.4}$$

Between these limits, the swath width depends upon the oil flow rate, Q , the gas flow rate, $150\ Q$, the ice speed, S , and the average thickness of oil and gas which can be contained beneath the ice, T . This width is merely the volume of oil and gas released per unit time divided by the thickness of the oil and gas layer and the distance traveled per unit time:

$$W_o = \frac{151\ Q}{TS} \quad . \tag{5.5}$$

At some low ice speed, the swath width, W_o , is exactly equal to the crack spacing, W_c . That speed is $151\ Q/TW_c$. At speeds lower than this, the swath width remains constant at W_c . As ice speed is increased, the swath width, W_o , will decrease until it is exactly equal to the blowout plume diameter, W_b . That occurs when the ice speed is $151\ Q/TW_b$. At even higher speeds, the swath width remains constant at W_b but the voids beneath the ice are not filled to capacity.

The length L_o , of the swath of oiled ice will merely be

$$L_o = SM \quad , \tag{5.6}$$

where M is the duration of the blowout and S is the ice speed as before. For very low ice speeds or blowouts of short duration, the swath length will be just one floe length, W_c . This occurs when ice speed is less than or equal to W_c/M .

In Figure 5.5 we summarize the relationship between ice speed and the width, length, and area of the swath of oiled ice that results from a moving ice cover passing over a blowout. The blowout is assumed to release oil at the rate of Q m^3/min and gas at the rate 150 Q m^3/min for a period of M minutes. The blowout plume (wave ring) is W_b meters in diameter. The ice has cracks every W_c meters and has voids underneath that will hold gas and oil to an average depth of T meters . For ice speeds less than W_c/M m/min , the swath length is equal to the crack spacing, W_c . For speeds greater than W_c/M m/min , the swath length increases linearly with ice speed. The swath width is constant and equal to the crack spacing, W_c , for ice speeds less than 151 Q/W_c m/min, constant and equal to the plume width, W_b , for ice speeds greater than 151 Q/W_bT m/min, and inversely related to ice speed for intermediate speeds.

The average thickness of the oil-and-gas layer beneath the ice will be T , except when the ice is moving so fast that voids in the ice passing directly over the blowout plume are not completely filled. Not all this thickness, T , will be oil. If gas spreads beneath the ice, filling or partly filling the under-ice voids, oil cannot fill the voids. Experimental work by Topham (1979) suggests that oil will collect on the perimeter of gas bubbles.

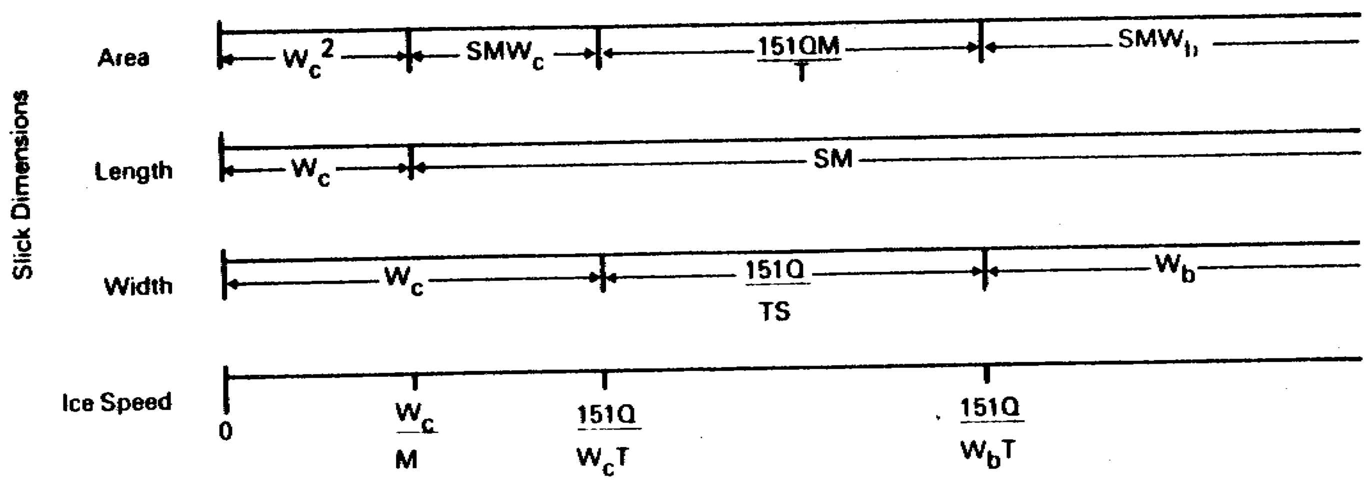

Figure 5.5. Dimensions of an Under-Ice Oil Slick Resulting from a Blowout Under a Moving Ice Cover. Dimensions of the slick depend upon ice speed S, blowout duration M, average containment depth of oil under the ice T, flow rate of the oil Q, diameter of the blowout wave ring W_b, and average crack spacing W_c. Gas flow from the blowout is assumed to be 150 times the flow of oil.

The oil slick dimensions given above and in Figure 5.5 apply only to a steady-state situation where one type and thickness of ice is passing over a steady blowout at a constant velocity. In the real world, different ice types will be passing over the blowout at speeds and directions which vary during the course of the blowout.

5.2.4 Effect of Ice Growth

During the fall and winter, the first-year ice over the inner continental shelf is increasing in thickness by about 10 mm/day. For a blowout lasting several days under a smooth, stationary ice cover, and in the absence of large currents, this ice growth may be significant in limiting the spread of the oil. When an area of ice contains a layer or pools of oil, the ice does not immediately begin growing beneath the oil. In the region near the blowout site, the heat from the warm oil or from bottom water circulated by the blowout plume will tend to reduce the ice growth or actually melt some of the ice. Meanwhile, unoiled ice outside this region will continue growing, increasing the oil containment potential of the ice near the blowout.

5.3 Incorporation Phase

How oil becomes incorporated into the ice cover will vary with the ice morphology and the season. In the fast ice zone in the fall, thin new ice as well as slush ice and broken-up ice pieces will exist. Later in the winter, there is relatively smooth first-year ice, with little open water or broken-up ice. Late in the spring, there will be more open water and individual ice floes. In the stamukhi zone, in addition to the above conditions, oil will come in contact with ridges, and oiled ice may be built into ridges. In the pack ice, all of the above conditions plus multiyear ice will exist. Thus, we must consider the possibilities of oil rising to the surface through leads and cracks when the ice cover has not yet formed, oil being trapped beneath a solid ice cover, and oil encountering or being built into ridges.

5.3.1 Oil On the Ice Surface or In Open Water

When new ice begins to form in the fall, it forms as a highly porous layer of ice crystals. Oil spilled beneath this ice will rise to the surface. Within a few days, the ice will have solidified beneath the oil, trapping it on the surface. Snow will probably cover most of the oil through the remainder of the ice season.

For the most part, oil trapped on the ice surface will differ little from oil trapped below thin ice. Two possibly important differences can be noted. First is the presence of suspended sediments in the water during the fall freezeup period. Barnes and Fox (1979) documented the presence of sediment-laden ice within the fast ice zone. Sediment concentrations ranged from 0.003 to 2 kg/m^3 of ice with considerable variation in regional distribution. A considerable yearly variation in the amount of "dirty ice" was also observed. The effect of sediment particles on crude oil is largely unknown. Eventually, as the ice melts, there will be hydrocarbon-coated particles sinking to the bottom. Second, the oil on the ice surface, even when covered by snow, is subject to evaporation. The evaporation rate varies considerably depending upon the constituent hydrocarbon fractions of the crude oil, temperature, and exposure to the atmosphere. Both low temperatures and snow cover will tend to decrease evaporation rates by an unknown amount. NORCOR (1975) measured evaporation rates as high as 25 percent within 1 month. This was for a Norman Wells crude on the surface during the winter with a few centimeters of snow cover. Rates decreased sharply after the first months, but 30 percent or more of the oil may have evaporated by spring. This amount of weathering could cause difficulty in burning the oil the following spring.

Oil which surfaces in newly opened leads or in the broken ice directly over a blowout will also have new ice growing beneath and will be subject to weathering throughout the remainder of the winter. Another route by which oil can appear on the ice surface during the winter months is through thermal cracks. Oil, being less dense than sea ice, will tend to overflow the tops of cracks rather than the bottoms. Cold temperatures and an absorbent snow cover will limit the spread of the oil to a distance of a meter or so (NORCOR, 1975). This is not likely to be a significant source of surfaced oil during the Arctic winter.

5.3.2 Oil Under Level Ice

Most of the oil from a winter blowout will end up underneath the ice canopy. Gas trapped under the ice will probably escape within a day or so. Observations made by divers beneath first-year ice confirm this (Reimnitz and Dunton, 1979).

The majority of the oil will thus end up as films, drops, or pools beneath the sea ice. In the absence of strong ocean currents, the oil becomes encapsulated by new ice growth. NORCOR (1975) observed the time needed to form an ice sheet below an oil lens to be a function of the thermal gradient in the ice and the thickness of the oil. In the fall, when the ice and oil slick is thin, a layer of new ice will completely form beneath the oil within 5 days. During the winter, that time increases to 7 days and in the spring to 10 days. Ice growth beneath large, deep pools of oil has not been studied.

Martin (1977) observed no traces of oil in the ice which forms beneath an oil lens. The skeletal layer in the ice above an oil lens does appear to become heavily oiled for 0.04 to 0.06 m into the ice, but has been found to contain less than 4 percent (volume) of oil (Martin, 1977; NORCOR, 1975). This is equivalent to an oil film about 2 mm in depth, or about 25 percent of the equilibrium thickness of oil under thin, smooth ice.

A layer of oil beneath sea ice tends to raise the salinity of the ice above the oil and lower the salinity of the new ice directly below the oil (NORCOR, 1975). The oil layer may trap rejected brine in the ice above, or, by insulating the ice from the sea water, lower the ice temperature above the oil lens. This insulating effect also causes slow initial ice growth below the oil which results in a lower-salinity ice. The high-salinity ice directly above the oil will likely accelerate the migration of oil into brine channels when the ice begins to warm. The effect of included oil on the growth of the ice sheet appears to be minimal beyond the first few days (NORCOR, 1975).

The incorporation of oil into multiyear ice has not been studied at the present time. Presumably it will occur much as it does in first-year ice. Growth rates are lower under thick multiyear ice than under thinner first-year ice, but it has been postulated that a thick oil lens, as would collect under multiyear ice, will actually enhance ice growth due to convective heat transfer through the oil.

5.3.3 Oil Incorporated in Deformed Ice

One possible fate of oil spilled under sea ice is to be incorporated into a newly built pressure or shear ridge. Some of the oil may remain in these ridges in an unweathered state through several melt seasons.

The oiled ridges can travel great distances releasing the oil along their paths. This in fact may be advantageous since the oil would be released slowly over a greater area. The removal of the oil from the sensitive coastal regions and the release of it in lower concentrations elsewhere could be desirable. Thus, it is important to know the probability of oiled ice becoming incorporated into a ridge and the amount of oil that could be incorporated.

5.3.3.1 Fast Ice Zone

The building of large ridges does not generally occur in what we have defined as the fast ice zone. This is because of the barrier islands along this part of the coast, which, along with grounded ridge systems, serve to protect the fast ice zone from being affected by the pack ice. Exceptions certainly occur, especially in the Harrison Bay or Camden Bay regions during early freezeup before protecting ridges become grounded. For most of the coastline along the 1979 lease sale area, we believe that oiled ice in the fast ice zone has essentially zero chance of being incorporated into a large ridge.

There is some chance of oil-contaminated ice in the fall being involved in minor deformation, but we do not consider this minor deformation in newly formed fast ice to be significant for the following reason. Minor deformation, mostly rafting, will occur in the fall when the ice is thin. At the most, rafting will halve the area of oiled ice (and double the average oil concentration under the ice). This is probably within the range of accuracy of present oil-spreading models. Furthermore, the effect of that deformation will be hardly noticeable at breakup in the spring. At that time, due to ice growth through the winter, rafted and undeformed ice will be approximately the same thickness. It will all break up and release oil at about the same time.

5.3.3.2 Stamukhi Zone

Outside the fast ice zone and the barrier islands lies the stamukhi zone. This zone comprises the past, present, and future position of the active shear zone which is the line of slippage between the moving pack ice and the stationary fast ice. All observations indicate that this zone is the most heavily ridged area in the southern Beaufort Sea with ridge densities as high as 12 ridges per kilometer (Tucker et al. 1979). A great part of the ridge building occurs in the fall when storms are most intense, but ridge building continues throughout the ice season.

If a blowout occurs in the stamukhi zone and a large area of ice becomes contaminated with oil, we would like to know the amount of oil which gets incorporated into new ridges built between the time of the spill and the end of the ice season. This will obviously depend upon the number of ridges built in the area of the spill and the amount of ice deformed into each ridge. We will develop a simple model of the percentage of the ice cover which is deformed into ridges throughout the ice season and then, using typical values of parameters, estimate the percentage of an oil spill which would be incorporated into ridges.

First, we formally define the stamukhi zone as the region of ice lying offshore of the barrier islands or the smooth, motionless fast ice zone and extending just far enough seaward to include all the ice which undergoes large amounts of deformation during the ice season. At the end of the ice season, the stamukhi zone is easiest to define since it is just that region with a greater density of ridges than the pack ice has. At the start of the ice season, the stamukhi zone may be covered with flat, undeformed ice.

To simplify the problem, we make the following assumptions: (1) Ridges form parallel to shore and are of infinite length, allowing us to consider the problem as one-dimensional. (2) The distribution of ridges is uniform throughout the stamukhi zone. (3) Strains are uniform throughout the stamukhi zone. (4) All areas of the stamukhi zone are equally likely to be ridged. (5) All ridges are the same size and shape. (6) Only ice of one constant thickness is built into ridges and some ice of that thickness is always present throughout the stamukhi zone.

Since the stamukhi zone is assumed to develop uniformly, we can look at the history of some unit length of ice (measured at the end of the ice season). Let the length of this section of ice be

$$L = L(t) \quad , \tag{5.7}$$

with the final length at the end of the ice season being 1 km. The number of ridges which intersect this element of ice is

$$N = N(t) \ . \tag{5.8}$$

Then, the density of ridges within this element at any time is

$$D = D(t) = \frac{N(t)}{L(t)} \ . \tag{5.9}$$

The cross-sectional area of a ridge, A, is assumed to be constant. This area is

$$A = \ell h \quad , \tag{5.10}$$

where ℓ is the length of flat ice of thickness h which has been crushed to build a ridge. For now, we assume that A is 54 m^2 (see Section 3.3.4) and that all ice built into ridges is 0.2 m thick; then, ℓ is 270 m.

Ridges are built only when the ice closes up (i.e., when $L(t)$ is decreasing). During the periods when the ice is closing, we can write

$$\dot{L} = -\ell\dot{N} \quad , \tag{5.11}$$

where $\dot{L}$ is the rate of ice convergence, $\dot{N}$ is the rate at which new ridges are being built in the region of dimension L, and ℓ is the extent of flat ice which is built into each ridge.

Suppose that at some time, T, a large oil spill occurs beneath the ice and the entire element we are considering becomes contaminated with oil. We would like to calculate the fraction of oil that is built into ridges between the time of the spill, $t = T$, and the end of the ice season, $t = F$. If the ice always converges and never opens new leads, this fraction is merely the proportion of ice in the element at time T which becomes built into ridges by time F. During periods when the ice opens ($L(t)$ increases), no new ridges are built, so the fraction of oiled ice in ridges does not change. A period of opening followed by a period of closing and new ridge building will reduce the rate at which oiled ice is built into ridges since there will then be more unoiled ice available for ridge building. We will assume that opening does not take place in significant amounts, so that $\dot{L} \leq 0$ always.

The rate at which oiled ice is built into ridges, when all the ice at time T is contaminated with oil, is

$$\dot{P}(T, t) = -\frac{\dot{L}}{L(T)} \quad . \tag{5.12}$$

where P is the percent of oiled ice built into ridges.
The total amount of oiled ice which is built into ridges between time T and time F (the end of the ice season when ridge building ceases) is

$$P(T, F) = -\frac{1}{L(T)} \int_T^F \dot{L}\, dt \quad . \tag{5.13}$$

Generally, we do not know the value of $L(t)$ other than at time F, when we have chosen L to be 1 km:

$$L(F) = 1 \text{ km} \quad . \tag{5.14}$$

We do have some data on ridge density, D, though (see Tucker et al., 1979). If we substitute Equation (5.11) into Equation (5.13) and perform the integration, we get

$$P(T, F) = \frac{\ell\left[N(F) - N(T)\right]}{L(T)} \quad . \tag{5.15}$$

Then Equations (5.9), (5.14), and (5.15) can be solved to get the formula

$$P(T, F) = \frac{\ell\left[D(F) - D(T)\right]}{1 + \ell\, D(F)} \quad . \tag{5.16}$$

In Table 5.1 we present an example. The ice season is presumed to last from October through June. The ice starts out without any ridges and develops one additional ridge per kilometer each month. These ridge densities are near the values measured by Tucker et al. (1979), which are reproduced in Section 3.3.4. Two different ice thicknesses are used (0.2 and 0.5 m) which result in different lengths of ice deformed in a ridge (0.27 km and 0.11 km, respectively) and different fractions of the oiled ice which could be expected to be built into ridges. For example, a spill which occurs in February will have about 31 percent of the oil incorporated into ridges by the end of June if the thickness of the ice being built into ridges is 0.2 m, or about 22 percent if the ice thickness is 0.5 m.

Equation (5.16) can be used to calculate the fraction of oiled ice built into ridges during any period. Using T = January, F = April, and h = 0.2 m, P is 28 percent. An AIDJEX buoy which was located about 30 km offshore from Cross Island in January 1976 moved about 6 $\pm$ 4 km toward shore between January and April. Therefore, about 20 $\pm$ 13 percent of the original 30 km of ice between the buoy and Cross Island must have been built into ridges. We see that the model does give realistic results. Therefore, it is evident that significant amounts of any oil spilled in the stamukhi zone might end up in ridges built subsequent to the spill. Whether that oil remains in the ridges long is not known.

5.3.3.3 Pack Ice Zone

Proceeding from the stamuhki zone out to the pack ice zone, we can make a rough estimate of the probability of oiled ice being built into a ridge.

First, we note that if the oil comes up under a large multiyear flow, there is only a small chance of it later becoming part of a ridge. Most of the ice involved in ridging has been observed to be young ice, thinner than about 0.5 m (R. M. Koerner, personal communication, in Weeks et al., 1971). It is possible that when a lead opens across a multiyear floe, oil trapped in the ice nearby could drain into the open lead and later be incorporated into a ridge if the lead closes up. This possibility may be discounted as it would have little effect on the percentage of a large spill involved in ridging. So the main concern is the amount of thin ice available for ridging at any time.

Table 5.1. Proportion of Oiled Ice Built into Ridges for Spills Occurring at Nine Times During the Ice Season and for Two Possible Ice Thicknesses.

Month	Ridge Density, D	$h = 0.2$ m P $\ell = 0.270$ km	$h = 0.5$ m P $\ell = 0.108$ km
October	1	0.63	0.44
November	2	0.55	0.38
December	3	0.47	0.33
January	4	0.39	0.27
February	5	0.31	0.22
March	6	0.24	0.16
April	7	0.16	0.11
May	8	0.08	0.05
June	9	0.0	0.0

Kovacs and Mellor (1974) state that there is 1 to 5 percent open water in the seasonal pack ice zone. Wadhams and Horne (1978) report from 0.1 to 3.5 percent thin ice (less than 0.5 m) with a mean value of 0.9 percent. These percentages certainly vary with time of year, especially in the fall when one-half or more of the ice in the seasonal pack zone is thin ice. There is probably a variation with distance from shore, too. Ramseier et al. (1975) report more multiyear floes and larger floe sizes as one goes northward from the coast. Wadhams and Horne (1978) found higher ridge densities in the southern pack ice compared to the central Beaufort Sea. They also note that leads covered with thin ice are frequent, with an average spacing of just over 200 m, and are generally less than 50 m in width.

If we use the largest value of 5 percent open water and thin ice as the measure of ice available for ridging and assume that this thin ice is distributed in frequent leads, we have a narrow range of probabilities of oiled ice being built into a ridge; from 0 to 5 percent. For a large spill or a blowout that lasts for days or months where pack ice motion could be expected, then we actually have an estimate of the percentage of oil that would be trapped in ridges.

Again, we must note that in the fall a much larger percentage of the seasonal pack ice zone is covered by thin ice. While not all of that thin ice will be involved in ridging, the percentage will certainly be larger than later in the winter.

5.4 Transportation Phase

Estimating the possible motion of oiled ice in the vicinity of the offshore lease area near Prudhoe Bay is extremely difficult. This is due simply to the lack of data. Only a few buoy observations made by AIDJEX during the winter and spring of 1976 (Thorndike and Cheung, 1977) and some radar ranging by Tucker et al. (1980) during 1976 and 1977 in and near the fast ice exist in the public domain. This data is insufficient for making reliable predictions of future ice motions. It might be thought that the history of ice motions could be modeled using historical winds and an ice model and that statistics could be formulated from these model results. Historical wind fields for the area do exist

(Jenne, 1975), although their accuracy might be questioned due to a lack of reporting stations north of the Alaskan coast. The problem is that ice motions are strongly dependent on the strength of the ice sheet (ice thickness and compactness), and data on ice strength is probably more rare than motion data.

Fortunately, the task is not completely without solution. While the means and variation of ice motion may be impossible to compute at this time, the range of possible motions can be computed by using the data from observed and historical motions. In the following, we describe the possible motion of sea ice, or oiled ice, in the three morphological zones.

5.4.1 Fast Ice Zone

First, we observe that the term "fast ice" is itself indicative of the motion or lack of motion of the ice near shore (fast here meaning fixed, not swift). This ice has been observed longest by mankind and, from all reports, it truly is motionless throughout most of the ice season. (See Shapiro and Metzner, 1979, for narratives of North Slope Borough residents concerning ice conditions from about 1930 to recent times.) Measurements of fast ice motion (Tucker et al., 1980) confirm the wintertime rigidity of the fast ice within the barrier islands or grounded ridge systems. Early in the winter (October and November), strong winds are able to move this nearshore ice. Large amounts of motion are probably not common, but one case has been reported in the literature (Kovacs and Weeks, 1979) where motions of a few kilometers were observed near shore in early November as the result of high winds. By December, the fast ice is thick enough to resist typical storms and it will remain so until breakup in June or July.

Rivers begin flooding the nearshore fast ice in late May or early June. Shore polynyas form and spread from mid-June through early July. The ice sheet is meanwhile becoming thinner and rotten. Sometime during July, the ice becomes weak enough that winds will cause it to move about. At first the most likely direction of motion is towards the shore polynyas, as the ice is weakest in that direction. Soon, though, enough open water exists that the ice can move in any direction. The predominance of winds during the summer are from the east or northeast, so typically the ice will be driven westward and along shore.

5.4.2 Stamukhi Zone

Grounded ridges along the outer boundary of the fast ice, in the stamukhi zone, will sometimes remain stranded throughout the summer. If they are not securely grounded, they too will be driven by the winds and currents. If the ridged ice is driven out to sea into the pack, the ridges may last for several years and travel great distances to the west and north. Or the ridges, once afloat, may be driven onshore further to the west.

5.4.3 Pack Ice Zone

The pack ice motion has a long-term westward trend. Over periods of a few days, the motion may be to the east, but eventually the westward trend dominates. During the winter there are often periods of days or weeks when no significant pack ice motion occurs. This happens when the pack is very consolidated and the winds are small or have blown from the north or west for long periods. On the other hand, for most of the summer and occasionally during the winter when the pack is unconsolidated, the ice has little or no internal resistance to the wind and water forces and moves about freely. This condition, known as free drift, represents the maximum extreme of possible ice motion. In between these extremes of no motion and free drift, ice motion will depend upon the atmospheric and oceanic driving forces, the sea surface tilt, the Coriolis effect, and internal stresses transmitted through the ice. This last term is the difficult one to model for long periods of time since small errors in velocity will affect the distribution of ice and thus the ice strength which in turn affects future velocities.

Thomas and Pritchard (1979) bypassed this difficulty by computing the extremes of possible pack ice motion. Wind data for the past 25 years were used to compute monthly free drift ice trajectories. Monthly means and variations were then computed. During the summer when the pack is usually open, these monthly average trajectories represent the most likely ice motions. During the winter when the ice is usually not in a free drift condition, the results represent a most likely maximum motion. Note that while an individual monthly trajectory during a light ice year may be longer than the maximum represented by mean free drift, it usually will not be.

The mean motion, or limit to motion depending upon the season, is generally to the northwest near Prudhoe Bay, at between 0.67 and 3.67 km/day. Ocean currents were not included when free drift trajectories were computed. Near the shore around Prudhoe Bay, the currents are generally small and variable to the east or west. Further offshore around the shelf break, currents are larger but they still reverse directions. Beyond the shelf, the southern edge of the Beaufort Gyre circulation contributes to the westward motion. During the winter, observed motions (Thomas and Pritchard, 1979) were generally to the west near Prudhoe Bay, although in February 1976 the motions were consistently to the east. Observed monthly motions throughout the Beaufort Sea were generally less than or equal to the mean free drift maximum.

Daily ice motions are more variable than monthly motions. While the westward trend persists from month to month over many years, daily motions exhibit a great deal of meandering and back-and-forth motion in all directions. Average daily ice speeds are therefore higher than average monthly ice speeds.

5.5 Release Phase

Oil spilled in the winter beneath the sea ice is not seen to be an immediate threat to the environment. This is due to the ice itself, which contains the spill in a relatively small area away from land and insulates the oil from interaction with the ocean and atmosphere. Eventually, the oil is released from the ice and begins to interact with and become a danger to its environs.

For first-year sea ice, this release is well understood and has been documented by NORCOR (1975) and Martin (1977). The oil trapped in first-year ice may be released by two major routes: by rising to the ice surface through brine drainage channels or by having the ice melt completely. Oil released from newly opened cracks or leads through the oiled ice areas will not be in significant amounts. The release of oil from beneath multiyear ice has not been studied but it is expected to occur much more slowly, if at all, than from beneath first-year ice.

5.5.1 Brine Drainage Channels

In late February or early March, the mean temperature begins to rise in the southern Beaufort Sea area. As the ice begins to warm up, brine trapped between the columnar ice crystals begins to drain. Oil trapped beneath the ice will probably accelerate this brine drainage by raising the ice salinity directly over the oil. Martin (1977) observed that oil released beneath the ice during the winter migrated 0.16 m upward through brine channels by 22 February. Once the air and ice temperature approach the freezing point, the brine channels will have extended through the ice. This may occur in late April or May. Once the channels are extended to the surface and are of sufficient diameter, oil will begin appearing on the ice surface. Oil released under ice with top-to-bottom brine channels also begins to appear on the surface within an hour (NORCOR, 1975).

The rate at which oil flows up through the brine channels will depend upon the character of the ice, the temperature, and the properties of the oil. Flow rates must be fairly low, since it has been observed that not all the oil is released until the ice has melted down to the initial level of the oil lens (NORCOR, 1975). An upper bound can easily be set, though. Oil has been observed to take about 1 hour to migrate up through about 2 m of ice with open brine channels. The brine channels were about 4 mm in diameter, so each brine channel had a maximum volume flow of $8 \pi \times 10^{-6}$ m^3/hr. The brine channels were spaced from 0.2 to 0.3 m apart. Each square meter of ice contains about 16 brine channels, then, and the flow rate per square meter area is about 0.0004 $m^3/hr/m^2$. This is equivalent to an oil film 0.4-mm thick being released each hour. The actual flow rate must be smaller than this.

Cox et al., (1980) have presented a theoretical treatment of oil released from sea ice through brine channels. We summarize some results from their work here for purposes of comparison with observed results from the 1974-75 Balaena Bay experiment (NORCOR, 1975). The results are given in the original cgs units.

The brine channel diameter can be computed as

$$d = K \left(\frac{T}{NL^2} \right)^{\frac{1}{2}} , \tag{5.17}$$

where d = channel diameter (cm)

T = thawing-degree days ($^{o}C \cdot$time)

N = number of channels per square centimeter

L = ice thickness (cm)

K = constant [2.13 $cm^2/(^{o}C \cdot day)^{1/2}$] .

Oil begins to flow through brine channels when

$$d' = \frac{4\sigma}{\delta} \frac{\cos \alpha}{(\rho_w - \rho_o)g} \quad , \tag{5.18}$$

where d' = channel diameter at inception of flow (cm)

σ = net surface tension for oil, water, and ice (dyne/cm)

α = contact angle of oil and ice (deg)

δ = thickness of oil lens (cm)

$(\rho_w - \rho_o)$ = difference in oil and water densities (gm/cm^3)

g = gravitational acceleration (cm/s^2).

Once $d \geq d'$, oil flows up the channel at the rate

$$\overline{u} = \frac{\rho_w - \rho_o \quad g\delta d^2}{32\ L\mu_o} \quad , \tag{5.19}$$

where the additional parameter, μ_o , is the oil viscosity.

From NORCOR (1975) we take some typical values of parameters to be:

N = 0.0016 channels/cm^2 (25-cm spacing between channels)

L = 150 cm (ice thickness above oil which first surfaced)

δ = 3.0 cm (average oil thickness over test area)

μ_o = 34 cP (density of unweathered Swan Hills crude at $0^{o}C$)

ρ_o = 0.840 gm/cm^3.

The other parameters are:

g = 980 cm/s^2

ρ_w = 1.030 gm/cm^3

α = 30^{o}

σ = 30 dyne/cm.

Then, from Equation (5.18), we can compute the minimum brine channel diameter for oil flow as $d' = 0.19$ cm. This is probably an upper limit since only the buoyancy of the oil is considered. If ice has formed beneath the oil lens, an additional pressure due to ice buoyancy may be present.

The time it takes for the brine channels to melt open to this diameter may be computed from Equation (5.17) as $T = 0.3$ thawing-degree days. From temperature profiles of the ice (NORCOR, 1975), we see that the ice surface on 4 May was at $-4^{\circ}C$ and on 11 May at $-1^{\circ}C$. The average air temperature had been above $-2^{\circ}C$ between 3 May and 11 May. Mean brine channel diameters in early May were about 0.4 cm. We see that d', the inception-of-flow diameter, is a factor of 2 too small. Using a value of $d = 0.4$ cm, T is found to be little more than one thawing-degree day. Thus, brine channels open up enough to allow oil flow soon after the ice surface warms to the melting point. Surfaced oil at Balaena Bay was first reported on 9 May (NORCOR, 1975).

Assuming a brine channel diameter of 0.4 cm, the oil velocity up through the ice is $\overline{u} = 0.00055$ cm/s. Each channel will thus drain 0.00007 cm^3/s of oil. If there are 0.0016 channels per square centimeter and a 3-cm depth of oil beneath the brine channel, it will take 3×10^7 s or over 300 days to completely drain the oil. By assuming the brine channel diameter to be 1 cm, this time can be reduced to about 50 days, a more reasonable time. For practical purposes, though, the experience gained from the Canadian Beaufort Sea Project is more useful in predicting the release of oil from first-year fast ice.

Oil which surfaces through brine channels will primarily be found floating on the surfaces of melt pools. If melt pools do not exist when the oil surfaces, they will soon form due to the lowering of the surface albedo. Snow seems to form an effective barrier to the spread of the oil, but wind and waves will splash oil onto surrounding snow causing the pools to grow in size. Oil-in-water emulsions were observed to form in the melt pools when winds were over about 25 km/hr. As much as 50 percent of the oil in a melt pool could be in the form of emulsions, but generally the emulsions would break down within a day after the winds have died down (NORCOR, 1975).

The rates at which oil will be evaporated, emulsified, or dissolved will be considerably lower in the case of an Arctic oil spill than in lower latitudes. Not only does the ice serve to protect the oil during the winter, but in the spring the oil is released over periods of weeks. The ice also acts to moderate the wind effects, so smaller waves and less mixing occur in melt pools and open leads. The lower temperatures also increase the stability of the oil. In general, the only process which will have a significant effect on the quantity of oil during the spring release period is evaporation.

NORCOR (1975) estimated that some test sites of the Balaena Bay experiment had more than 50 percent of the oil evaporated by late June. Using the data reported by NORCOR, we have attempted to describe the release and evaporation of crude oil in the first-year fast ice zone during the spring. In Figure 5.6 we show two possible release rates of the oil trapped in the ice. Point A, on 9 May, indicates when the first sign of surfacing oil was seen. Point D indicates when the oiled areas were ice free so that no oil could still be trapped within the ice. Assuming a linear release rate during this 7.5 week period, line AD shows a possible slow release of the oil.

After the first oil surfaced on 9 May, a period of cold temperatures and snowfall occurred, and no new oil was reported on the surface until 24 May (point A'). By 16 June (point D'), it was reported that "the flow of oil from the ice had almost completely stopped," since the ice had melted down to the trapped oil lens in most cases. We take the line A'D' to represent a possible fast release of the oil. Points B and C represent estimates of the percentage of oil evaporated and burned by 7 June and 17 June, respectively. The lines showing the percentage of oil surfaced must lie on or above points B and C.

Figure 5.7 shows the evaporation rates for a light or medium crude computed by the method of Nadeau and Mackay (1978). Rates for three oil temperatures, 0, 5, and 15°C, are shown. The mean air temperatures for May and June are -5 and 1°C, respectively (Figure 2.4). NORCOR (1975) measured the temperature of oil layers on the ice or in melt pools and found them to be as much as 10°C and averaging 7°C higher than the ambient air temperature.

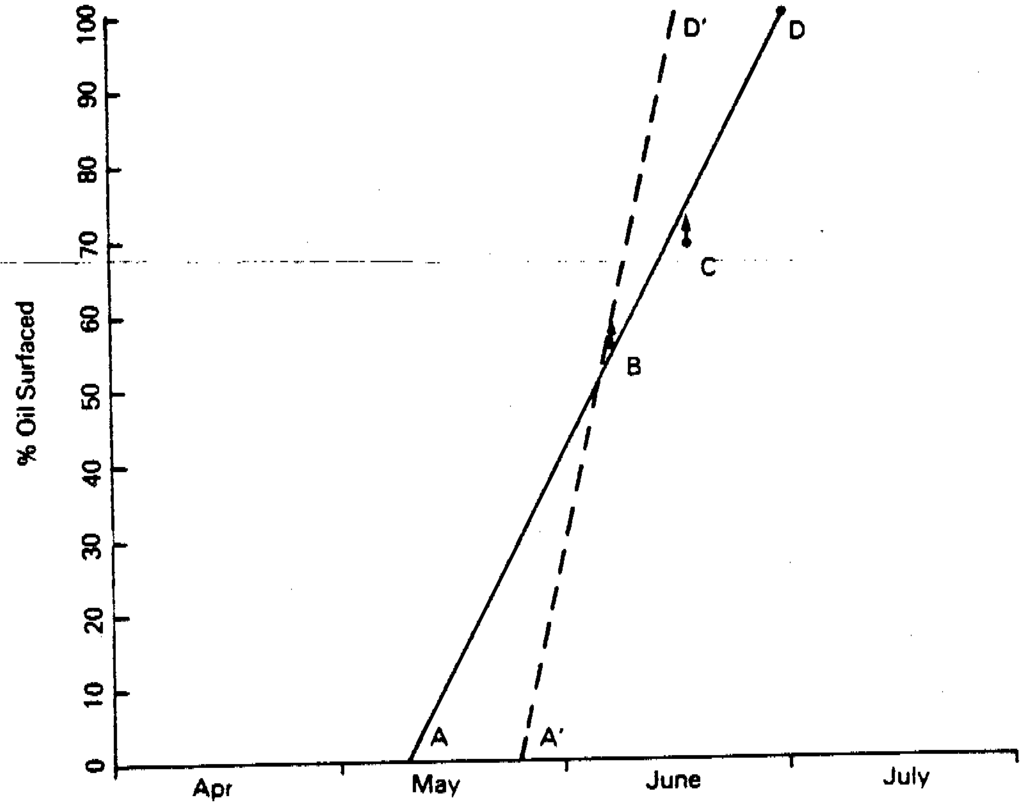

Figure 5.6. Two Possible Release Rates of Oil Frozen into Sea Ice During the Experimental Oil Spills at Balaena Bay (NORCOR, 1975). Point A, on 9 May, indicates when the first oil appeared on the ice surface. Point D, the end of June, indicates when all the ice in the experimental area had melted. Thus line AD is the slowest rate at which oil could have been released. Point A', 24 24 May indicates when oil resumed flowing after a spell of cold weather, and Point D' indicates when the flow of oil was observed to stop. Line A'D' then is the fastest rate at which oil could have been released. Points B and C represent estimates of the percentage of oil which had evaporated or been cleaned up on 7 June and 17 June, respectively. At least the indicated percentages of oil must have been released from the ice by those dates.

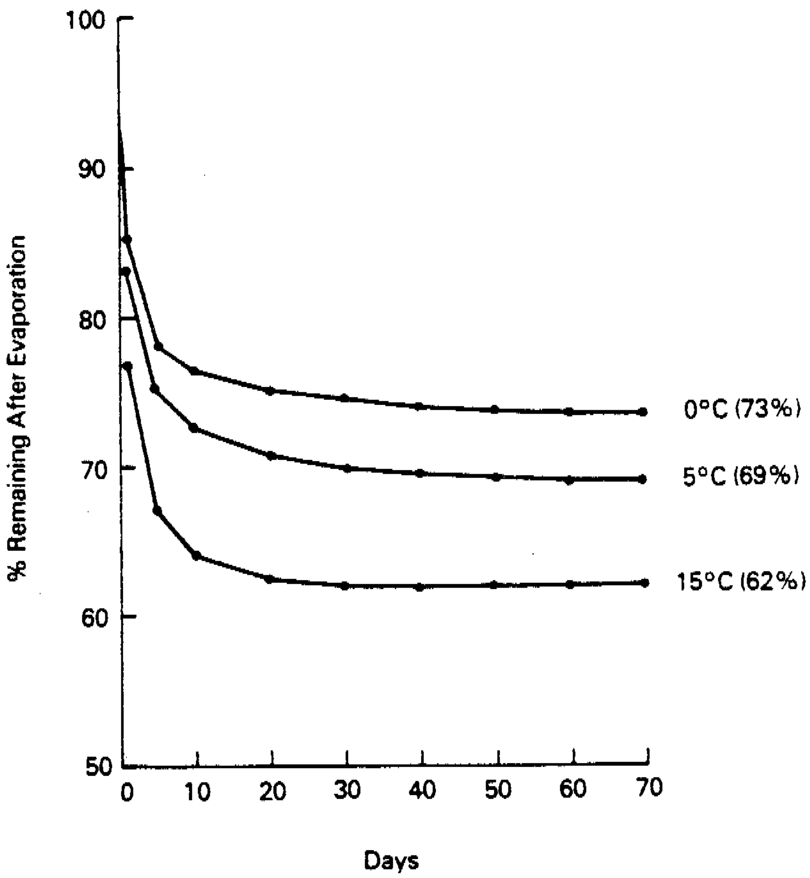

Figure 5.7. **Evaporation Curves of Crude Oil at Temperatures of 0, 5, and 15°C. The percent of oil remaining as a function of time and temperature is given (computed by the method of Nadeau and Mackay (1978)).**

In Figures 5.8 and 5.9 we have applied the extremes of evaporation rates (for 0 and 15°C) to the surfaced oil for each of the two release rates in Figure 5.6. The abscissa corresponds to the time of year, while the ordinate gives the percentage of oil. The percentage of oil still trapped in the ice, the percentage evaporated, and the percentage remaining on the ice or water surface are given.

5.5.2 Surface Melting

Most of the undeformed first-year ice near shore will melt during the summer months. Thus, any oil which does not reach the ice surface through open brine drainage channels will be released when the ice melts down to the oil layer. Typically, the nearshore area first begins to open and break up around the end of June and is mostly ice free by the end of July (Barry, 1979). Oil on the ice surface (via brine channels) will accelerate ice melting and breakup by lowering the albedo. NORCOR (1975) estimated that ice contaminated by oil would break up about 2 weeks earlier than unoiled ice.

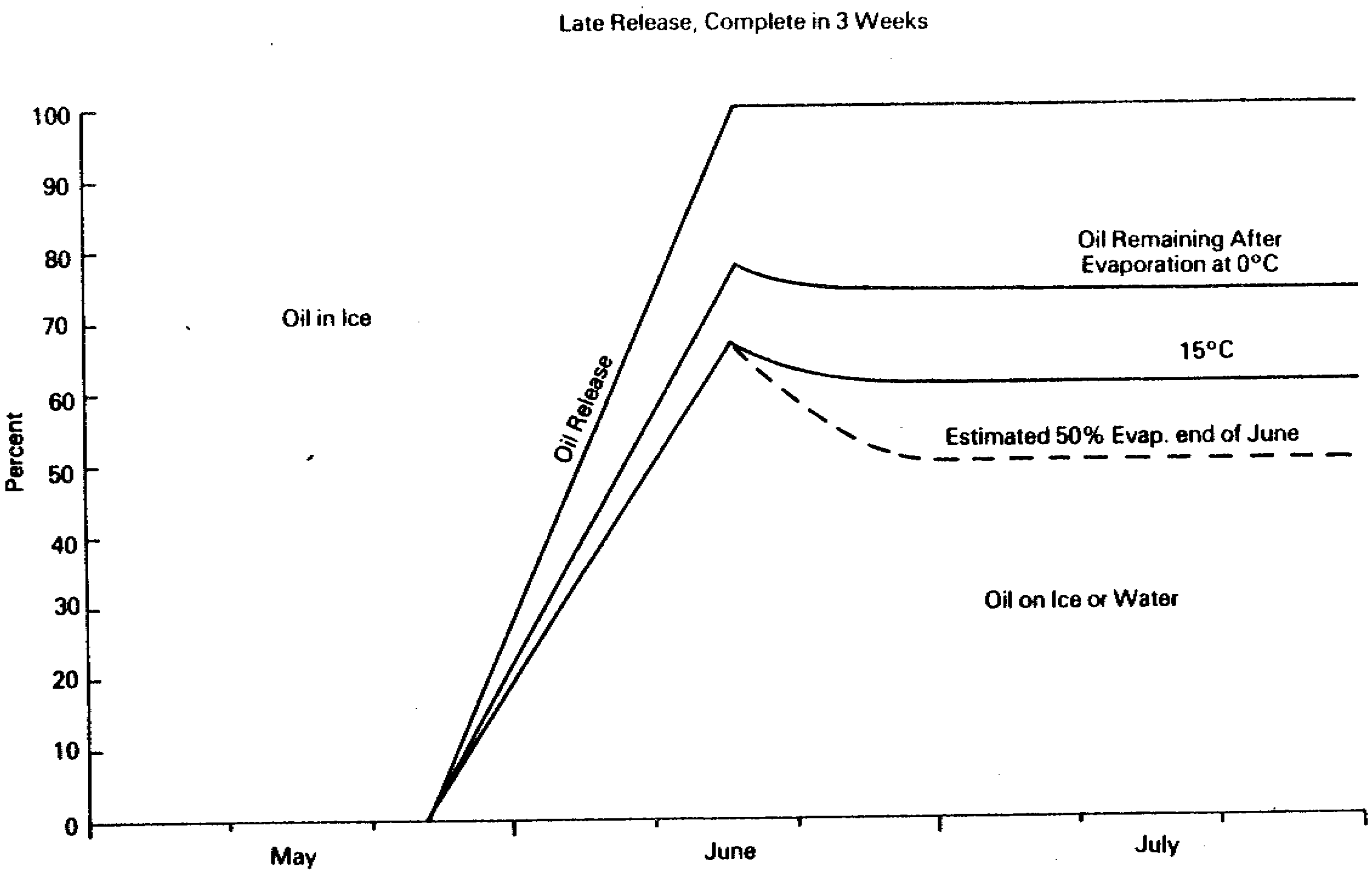

Figure 5.8. **Combined Oil Release (Fast) and Evaporation Curves. The upper curve gives the amount of oil released from the sea ice; lower curves give the amount of oil remaining on the surface after evaporation of the released oil. Evaporation at temperatures of 0 and 15°C are given, as well as the observed estimate of 50% evaporation.**

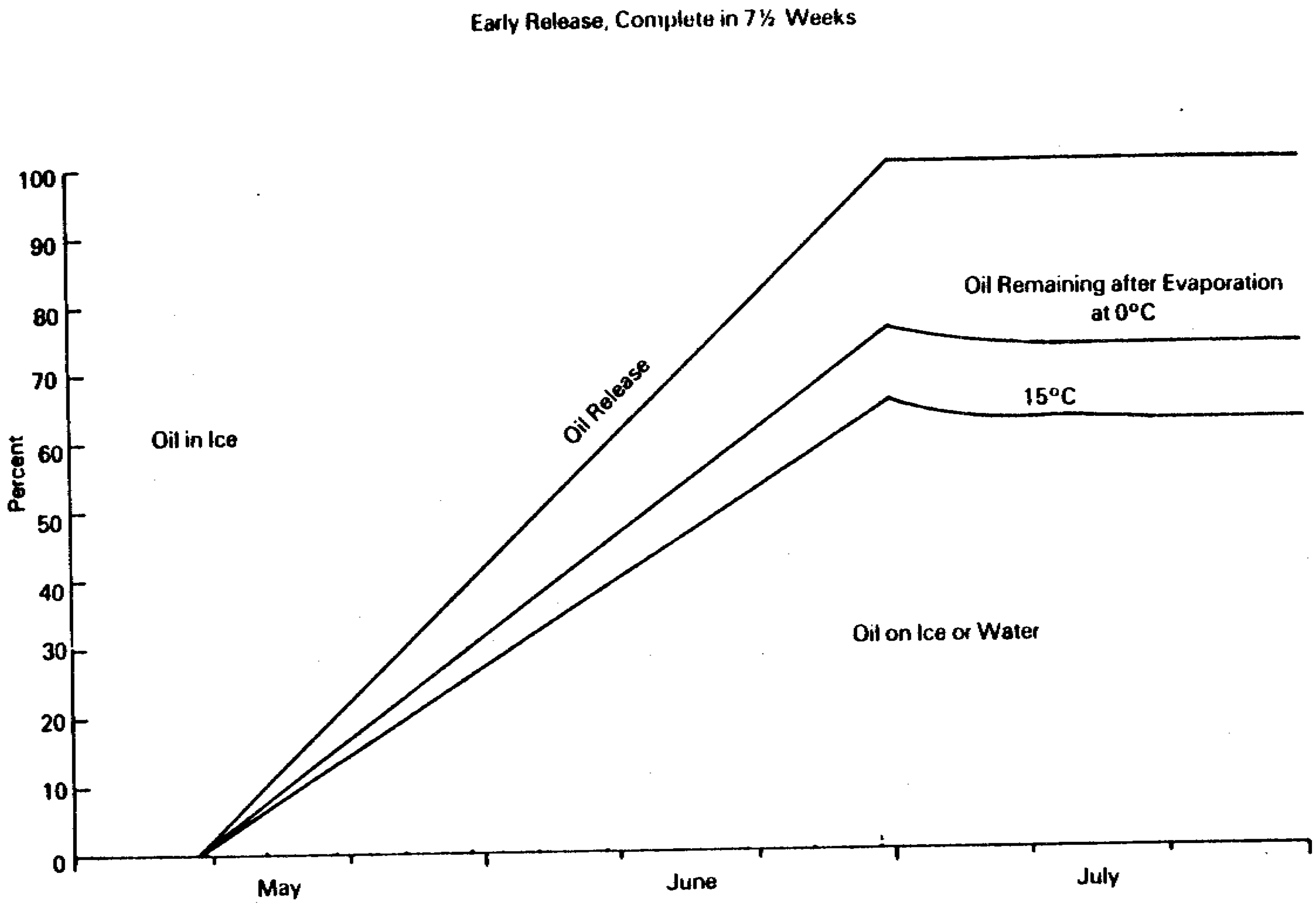

Figure 5.9. **Combined Oil Release (Slow) and Evaporation Curves. The upper curve gives the amount of oil released from the sea ice; lower curves give the amounts of oil remaining on the surface after evaporation at temperatures of 0 and 15°C.**

6. Fate of Oil

We have seen that the vast majority of oil spilled in the Beaufort Sea during the ice season would be held in abeyance by the ice until spring, then the oil begins to appear on the ice surface. The surfaced oil begins to weather and to cause accelerated melting of the ice. Typically, the ice in the contaminated area will all have melted by mid-July, at which time about 50 percent of the oil will have evaporated (assuming no cleanup takes place). Emulsification, dispersion, and dissolution of the oil on the open-water surface will also occur. Silt from the now flowing rivers may also cause some oil to be sedimented.

Until all the ice has melted, the rates at which these natural processes degrade and disperse the oil will be low. The release of the oil over a period of time, the reduced surface area because of confinement by the ice, and small fetches for wind energy input all contribute to the low rates. The amounts of oil removed by these processes will be insignificant but may have a critical effect on the ecology of the area.

Once the area becomes free of ice, the situation becomes nearly that of an open-water spill. The major difference is the evaporative losses of the oil by this time. As a result, other dissipative processes remain low.

Because of the prevailing winds in the southern Beaufort Sea, the open-water slicks are most likely to be driven onshore to the west or southwest. Since these slicks are partly weathered, they will tend to be more concentrated than a recent spill from a blowout. Southerly or easterly winds will drive the slicks offshore, breaking them up and spreading them over a larger area. Eventually the winds will reverse, then an even larger stretch of coast is in danger of contamination.

Ultimately, oil deposited upon beaches will probably be the second largest (after evaporation) sink for hydrocarbons. Sedimentation to the sea bottom will also be important. Over much longer time periods, oxidation and biodegradation will dispose of small percentages of the oil.

7. The Effects of Ice on Cleanup

It is not the purpose of this report to propose or evaluate methods of oil spill cleanup in Arctic waters. It is worthwhile, though, to review the characteristics of the ice cover and oil-ice interactions which will affect cleanup activities.

Several important distinctions in cleanup strategies can be made. These are: (1) open-water versus ice cleanup, (2) large spills versus small ones, (3) collecting the oil versus chemically or physically altering and redistributing the hydrocarbon constituents, and (4) cleanup in the fast ice zone versus cleanup in the moving pack. Some of these distinctions can be made in nonarctic regions, but the presence of sea ice causes special problems. Further distinctions could be made, but in this study we are only concerned with spills occurring from a blowout under the ice during the November to March drilling season. Cleanup of surface spills or summertime spills would differ somewhat.

How does the ice affect the cleanup of oil from the water surface in the spring? A wintertime spill will remain isolated in the ice until the spring. It then begins to surface in low concentrations over the area containing oil. The oil will not be completely released from the ice until the ice has melted. Meanwhile, the surfaced oil will weather, becoming denser and more viscous and possibly forming water-in-oil emulsions. As the oiled ice melts and the surrounding ice breaks up, the result will be broken ice floes with weathered oil floating between the floes. These floes themselves will be contaminated with oil. Booms to contain the floating oil slick will probably not be practicable until the area is mostly clear of ice, which may be too late to prevent shoreline contamination. The ice floes will also prevent any massive effort to remove the oil from the water surface. Since the oil is more viscous than when first released, and due to the confining effect of ice floes, slick thickness may be as great as 0.01 m. This may at times allow effective cleanup by small surface skimmers, but weather and ice conditions could easily prevent this kind of operation. As a secondary method for cleaning up remnants of a large spill, surface collection should be considered.

Another method of cleaning up the relatively concentrated, weathered oil slick which appears after the ice melts is the application of chemical dispersants by aircraft. However, the thickness of the slick, low temperatures, and low wave energy for mixing would probably all reduce the effectiveness of dispersants. Whether it is desirable to introduce large quantities of hydrocarbons and chemical dispersants into the shallow shelf waters is a matter we cannot judge.

Cleaning the oil from the ice before the ice melts and breaks up is another possibility. One could either remove the oil from beneath the ice or wait until the oil reaches the ice surface. Both methods present difficulties. Removing the oil from beneath the ice requires drilling through the ice. One must know not only where the oil is but where the oil pools are deepest, in order to collect the most oil. This is a remote sensing problem and will likely be solved, but even then, this method only seems practicable for small spills. The number of holes to be drilled in the case of a large spill would be prodigious, not to mention all the surveying, collection facilities, transportation, etc., involved, all in the dark, cold Arctic winter. If the oil were trapped in a small number of very large pools, which is unlikely, this method would be the most reasonable way of cleaning up large spills. This method is probably more applicable in the fast ice zone than in the pack ice for purely logistic reasons.

Burning the oil as it surfaces is much less labor intensive and has been used in cleaning up experimental spills (NORCOR, 1975). It is doubtful if burning would be as effective or practicable in the case of very large spills, where thousands of separate melt pools containing oil must be burned, each several times. Not all the oil is consumed by burning, either, with 10 to 60 percent remaining after each burn. For a complete cleanup, the residuals from burning must be picked up by hand. Much of the oil that will burn in open flames would eventually have evaporated anyway. For a spill in the moving pack, burning the surfaced oil in the spring may be the only way of disposing of significant quantities of oil. Burning the oil in a hole directly over the blowout is another possibility. This could be especially useful in pack ice, as long as ice motions are not large. Maintaining an open hole and a flame would be difficult when ice motions are large. Gas from the blowout will also make operations near the blowout dangerous.

To summarize our views, we offer the following cleanup scenarios, one each for the pack ice, the smooth fast ice, and the stamukhi zones.

Pack Ice Zone: Oil from a blowout under stationary or slowly moving pack ice might be partially collected from the blowout site if the blowout occurs near an island or other facility which could pump and store the oil. Burning of oil and gas during the blowout could also be partially useful if recovery is impracticable. If the pack ice is moving more than a few hundred meters per day, recovery would probably be impossible and even burning would be difficult. In this case, it would probably be most important to ensure gas release over or near the blowout in order to reduce oil spread under the ice. Markers and beacons could be placed to help locate the oiled ice later. Nothing else could be done until spring when the oil begins to surface. Burning of oiled melt pools, probably by air-dropped incendiary devices, could then be used to dispose of some of the oil. Most of the oil and the residue from burning would still be on the ice surface or in newly opened leads. Dispersants could be used as soon as oil appears in open-water leads and polynyas. As summer proceeds and the lighter, more toxic components evaporate, seeding with petroleumlytic microbes and fertilization could enhance biodegradation. Since the long ice season effectively halts all natural processes acting to degrade and disperse the spill, summertime activities would be important for reducing the chances of harm in future years. The environmental contamination would probably persist for several years in any case, especially since oiled ridges may be capable of retaining some oil through the summer.

Fast Ice Zone: A blowout and oil spill in this region could potentially be the most harmful, but effective cleanup may be possible. The ice is fast and will not move between November or December and the following June, currents are low so the oil will not be moved about under the ice, and the ice provides a stable work platform. Nevertheless, a large spill could cover several square kilometers. The spill area could be reduced considerably by early ice season preventive measures. These measures could be as simple as cleaning the snow from narrow strips about possible blowout sites to promote faster ice growth and more under-ice containment potential. Other methods of increasing oil containment under the ice can be postulated (skirts frozen into the ice, air-bubble systems to reduce ice growth), but it is obvious that none of these methods are foolproof until after the ice has become thick and strong enough not to be moved about by winds. Another requirement is that the ice be safe for surface travel.

The blowout itself will likely create an area of open water in the fast ice overhead. Gases will escape through this opening and probably a great deal of oil will be trapped on the water surface and contained by the surrounding ice. This area of open water could be enlarged by blasting. If storage facilities are available, oil could be pumped directly from the pool during the blowout. For very large blowouts, the hole in the ice over the blowout will likely not be able to contain all the oil released. In that case, a great deal of oil must be removed from the hole very quickly to prevent the oil from overflowing onto or under the ice.

Oil from a large blowout which has been allowed to spread beneath the ice, especially early in the ice season when bottomside relief is smallest, will be very difficult to collect during the winter. The oil can cover a large area and will collect in many small pools beneath the ice. At the moment, no proven technology exists for locating these pools except by trial and error drilling. Other possibilities are being developed, but they too will probably be labor intensive when looking for small pools. Even when the oil is found, it would be impossible to extract 100 percent of the oil from the ice. After new ice growth has completely encapsulated the oil lens, it will be even more difficult to remove oil from beneath the ice. In practice, oil which has been allowed to spread beneath the shore-fast ice with only natural roughness present will need to be left until spring.

When oil begins to appear on the ice surface in the spring, concentrations will still be so low that removing the oil will be impracticable.

Burning the oil at this time would be much simpler logistically. For small spills or remnants of large spills, a significant proportion might be disposed of by burning. However, it is unlikely that all the oil could be burned before breakup of the fast ice. Small-scale open-water methods could be used after breakup.

We feel the key to successful cleanup of large spills in the fast ice is by artificially creating more oil containment in or under the ice before or during the blowout. If most of the spill can be contained in a few large concentrations then later removed, burning and conventional open-water cleanup methods would be practicable for disposing of the remnant.

Stamukhi Zone: Oil spill cleanup in this region may or may not be possible depending upon many factors. A large amount of ridge building takes place, but a grounded ridge can extend the fast ice boundary seaward. The greater bottomside ice relief will tend to concentrate the oil in the region inside grounded ridge systems, but outside, oiled ice may be built into ridges. Oil in ridges may be impossible to clean up, since ridges may be able to hold oil for several years. This could be advantageous since the oil would be released slowly over many summers and over a large area as the ridges drift with the pack, thus reducing the level of contamination at any one place and time.

Oil trapped in deep pools behind ridge keels would likely be recoverable but would require great effort. The distance from shore and the difficulty of surface travel would be obstacles to cleanup but probably not insurmountable. Springtime burning of oil would also be hindered by the topography.

As in the smooth fast ice zone, the most successful cleanup would involve concentrating oil in a smaller area. Since planned relief may be more difficult to implement in the stamukhi zone, one could only hope that ridges are located to provide this concentration. If the oil is not contained by natural features or cannot be collected directly from the blowout site, springtime burning of surfaced oil must be attempted. For small amounts of oil this can be effective, but for very large spills the majority of oil will remain. After cleanup and evaporation of surfaced oil, probably 40 to 50 percent of a large spill will remain in ridges, on unmelted ice floes, or on the water surface. If the pack retreats northward for the summer, conventional open-water cleanup methods might remove a little more (0 to 10 percent) of the oil. Dispersants could be used at this time too. If the pack remains near shore through the summer, cleanup will have to be concentrated on the beaches and open-water lagoons behind the barrier islands, probably along great stretches of the Alaskan coast. Release of oil from the ice is likely to occur in subsequent summers making cleanup a long-term, wide-area project.

8. Discussion

The events following an under-ice blowout may usefully be divided into five more or less independent and sequential phases. The phases are: (1) the initial phase, (2) the spreading phase, (3) the incorporation phase, (4) the transportation phase, and (5) the release phase. Depending upon the season, location, and duration of the blowout, several of these phases may occur simultaneously or may not occur at all, but generally a particle of oil can be followed through each phase in turn.

The initial phase of an under-ice blowout consists of the release of oil and gas from the sea floor, the rise of the oil and gas to the surface, and the initial interaction of the oil and gas with the existing ice cover. The buoyant gas and oil entrain large amounts of water while rising to the surface. This plume and the resulting surface wave ring are only marginally important to the eventual fate of the oil. The turbulence at the surface may play some part in breaking up the ice over the blowout, especially when the ice cover is moving. A much more important factor, though, is the buoyancy of the gas from the blowout. Under a stationary ice cover, this gas is almost certain to cause breakage of the ice which allows the gas to escape to the atmosphere. Under a moving ice cover, especially for thicker multiyear ice, it is not certain that the gas trapped beneath the ice will cause the ice to break. Large amounts of gas trapped beneath the ice can have a significant effect on the spread of oil under the ice. It is believed, though, that only a limited quantity of gas can be trapped under sea ice due to the presence of naturally occurring thermal cracks in the ice. These cracks provide escape routes for the gas or at least weaken the ice so that trapped gases can break the ice and then escape. From theoretical studies and casual observations, these thermal cracks in the ice occur frequently enough that only a small percentage of any gas from a blowout will be trapped under the ice. Because of the possible importance of cracks to the escape of gas, especially for thicker multiyear ice, quantitative data on the development and spacing of thermal cracks in the different ice zones at different times of the year is desirable.

During the initial phase of a blowout under stationary ice, the heat of the oil and possibly heat from bottom water circulated by the blowout plume can also be instrumental in producing an ice-free area directly over the blowout. A large quantity of oil will replace the melted ice, although this may be a fairly small percentage of the total oil released. This melt hole could, however, act as a reservoir from which oil could be pumped.

It is unlikely that much oil will be deposited on the ice surface during a winter blowout. The oil will tend to overflow onto the ice wherever an opening occurs, but low air temperatures and snow on top of the ice will act to restrict the horizontal spread.

A spreading phase follows the initial phase of the blowout. This phase considers the relative motion and concentration of oil beneath the ice layer. Factors which are particularly important during the spreading phase are the bottom roughness of the ice, ocean currents, existing ridge keels, motion of the ice cover, and increasing ice thickness. The roughness of the underside of the ice generally provides an upper limit to the size of the under-ice oil slick, except under very smooth, new ice. For very smooth ice, the size of the slick is determined by the equilibrium thickness of oil under ice, which is many orders of magnitude greater than slick thickness on open water.

For blowouts lasting more than a few days, the spread of oil beneath the ice may be significantly restricted by the increasing thickness of the ice outside the immediate blowout vicinity. For very large blowouts, and in the absence of ice motions or large under-ice currents, this mechanism would tend to collect the oil in a single, relatively small but deep pool. The implications for cleanup are obvious. Further thought and work should be devoted to this topic.

Under-ice currents can be a major factor in the spread and transport of oil spilled under sea ice. In the 1979 lease sale area near Prudhoe Bay, however, currents are generally too small during the ice season to affect oil spread. Tidal channels between barrier islands (and possibly grounded ridges) are an exception but probably not significant in terms of area since the tidal currents are oscillatory.

Ridge keels also can affect the direction of oil spreading. In the stamukhi zone, ridges may be frequent enough to control the size of the under-ice slick.

Motion of the ice cover may also control the size of the slick. While much of the gas is likely to escape through existing cracks in the ice, the ice motion may allow some gas to be trapped. The amount of gas that can be trapped depends upon ice speed and thermal crack spacing. Because of the importance of gas release, especially in thicker, moving pack ice, the existence and spacing of cracks in the ice should be confirmed by field studies.

An incorporation phase will follow the spreading phase. Oil spilled under sea ice during the winter will generally become encapsulated within the ice. This oil is protected from weathering processes until the ice begins to warm in the spring, releasing the oil. This is probably the most important aspect of under-ice oil spills in the Arctic. It means that spills which occur from sometime in October through the following May will in effect occur at the beginning of the ice breakup period in the late spring. Oil is thus released into a limited amount of open water at a time critical to all levels of biological activity. This delay, however, does allow time for cleanup efforts between the actual and effective release of the oil.

Oil spilled outside the grounded ridges which delineate the protected fast ice zone has an indeterminate but relatively high chance of being incorporated into a ridge. Due to ice motions relative to a fixed boundary, a large amount of ridge building occurs in this area during periods of pack ice motion. We have shown that significant percentages of large oil spills occurring in this area at certain times of the year will be incorporated into ridges. This conclusion was made on the basis of a limited amount of data concerning ridge counts. Data on ridge densities need to be collected throughout the ice season in order to accurately describe the development of the stamukhi zone and predict the amount of oil from spills occurring at different times that will be incorporated into ridges. Data over many ice seasons are necessary in order to assess the uncertainty of predictions.

The whole problem of oil after it is incorporated in ridges is largely conjectural at this time. The amount of oil which can be held inside a ridge and how long it will remain in the ridge are important questions when considering the possibility of a blowout in the stamukhi zone. No data exists concerning the interaction of crude oil and pressure or shear ridges in Arctic sea ice. Field or laboratory experiments will be necessary in order to begin answering these questions.

During the transportation phase, oil which is trapped by bottom roughness or which is frozen into the ice is moved about with the ice cover. In the fast ice zone, transport does not occur except early in the ice season when the ice is thin and weak or late in the ice season as the ice breaks up and begins to move. Even during those times, the amount of ice motion is small, less than a few kilometers.

It is in the pack ice zone that significant transportation of the oil by the ice takes place. The pack moves generally to the west with much short-term meandering. It is likely that some of the oil will be spread over a large area in low concentrations. Differential motions of individual floes within the pack after the blowout will tend to further separate oiled areas of ice.

In the spring, all the oil except possibly that trapped within ridges will begin to be released from the ice. This release phase takes place by two routes: surfacing of the oil through brine drainage channels and melting of the ice cover. By mid to late July, most of the oil-contaminated ice will have melted, leaving partially weathered oil on the water surface. Open-water areas and shorelines to the west, possibly as far as the Chukchi Sea, may be contaminated with oil during the summer. During the period when the oil is being released and the ice is melting and breaking up, the motion of the oil already released on the water is largely unknown. The concentration of the ice cover and the motion of the ice undoubtedly influence the motion of the oil, but further work is needed to determine the extent of the influence.

Cleanup of any large under-ice oil spill will be extremely difficult in the spring. This is because oil will surface slowly in many separate melt pools over a large area for a long period of time. As soon as the oil surfaces, it begins to weather, making it difficult to burn. The continuous release and weathering of the oil makes it necessary to burn each melt pool containing surfaced oil several times. The surfaced oil also accelerates the deterioration of the ice cover, decreasing the time interval when the ice is safe for surface work. A spill covering several square kilometers will surface in many thousands of separate pools. In the pack ice, these pools are likely to be separated and spread over many kilometers. Even in the fast ice, the logistics of burning or cleaning up many thousands of pools of oil will become prohibitive.

Cleaning the oil from the water surface as the ice melts will also be difficult. Conventional open-water cleanup methods will be difficult to use until the ice concentration is low, which may be too late for preventing widespread dispersion of the oil. For small spills or remnants of large spills, both burning and open-water cleanup methods could be practical.

A much safer cleanup strategy would involve pumping the oil from beneath the ice during the winter or early spring. Logistically, this would be extremely difficult, unless the oil was pooled in large concentrations beneath the ice. This is unlikely to occur naturally, except perhaps in the fast ice zone where ice growth can outpace oil accumulation or in heavily ridged areas of the stamukhi zone. However, in the fast ice zone, an effective preventive measure would be to create under-ice reservoirs by artificially redistributing snow in areas where blowouts might occur. In the pack ice, this procedure would be impractical due to ice motions.

The OCSEAP and other studies of Arctic sea ice or oil-ice interactions referenced in this work have provided much insight into the probable course of events following a large under-ice oil spill. In this work we have synthesized the relevant material from previous studies in order to produce a background document to aid in the writing of Arctic oil spill scenarios. It must be realized, though, that some of this present work is conjectural. Hopefully, many of these conjectures will forever remain conjectures, since experience with actual spills will be necessary to remove all uncertainty. However, in many cases, additional field or laboratory studies will resolve uncertainties associated with the predicted course of events following an under-ice oil spill.

One major purpose of this work is to identify factors which will or might be important to the fate of an oil spill under Arctic sea ice. We have examined the probable effects of such factors, and the effects of variations in these factors. When the behavior of an oil spill is very sensitive to some environmental factor or characteristic of the ice, then it is important to take that factor into account during contingency planning. This sensitivity also identifies areas where further research would be useful.

References

Aagaard, K., and contributors (1978) "Physical Oceanography and Meteorology," Environmental Assessment of the Alaskan Continental Shelf, Interim Synthesis: Beaufort/Chukchi, NOAA/OSCEAP, Boulder, Colorado, pp. 56-100.

Aagaard, K. (1980) "Current Measurements in Possible Dispersal Regions of the Beaufort Sea," To appear in: Environmental Assessment of the Alaskan Continental Shelf, Annual Reports, NOAA/OSCEAP, Boulder, Colorado.

Ackley, S. F., W. D. Hibler III, F. K. Kugzruk, A. Kovacs, and W. F. Weeks (1974) "Thickness and Roughness Variations of Arctic Multi-Year Sea Ice," University of Washington, Seattle, AIDJEX Bulletin No. 25, pp. 75-96.

Agerton, D. J., and J. R. Kreider (1979) "Correlation of Storms and Major Ice Movements in the Nearshore Alaskan Beaufort Sea," Proceedings Port and Ocean Engineering Under Arctic Conditions, Trondheim, Norway, Vol. 1., pp. 177-190.

Ashton, G. D. (1974) Air Bubble Systems to Suppress Ice, CRREL Special Report 210, Hanover, New Hampshire.

Barnes, P., and D. Fox (1979) "Sediment-Laden First-Year Ice, Central Beaufort Coast, Alaska," Environmental Assessment of the Alaskan Continental Shelf, Annual Reports, NOAA/OSCEAP, Boulder, Colorado. Vol. IX, Hazards, pp. 231-243.

Barnes, P. W., E. Reimnitz, and G. Smith (1977) Some Coastal Oceanographic Observations Beaufort Sea, Alaska, U. S. Geol. Survey Open-File Report 77-477, Menlo Park, California.

Barnes, P., E. Reimnitz, L. Toimil, and H. Hill (1979) Fast Ice Thickness and Snow Depth in Relation to Oil Entrapment Potential, Prudhoe Bay, Alaska, U.S. Geol. Survey Open-File Report 79-539, Menlo Park, California.

Barry, R. G. (1978) "Study of Climatic Effects on Fast Ice Extent and Its Seasonal Decay Along the Beaufort-Chukchi Coasts," Environmental Assessment of the Alaskan Continental Shelf, Annual Reports, NOAA/OSCEAP, Boulder, Colorado. Vol. IX. Transport, pp. 604-719.

Barry, R. G. (1979) "Study of Climatic Effects on Fast Ice Extent and its Seasonal Decay Along the Beaufort-Chukchi Coasts," Environmental Assessment of the Alaskan Continental Shelf, Final Reports, NOAA/OCSEAP, Boulder, Colorado. Vol. 2. Physical Science Studies, pp. 272-375.

Bilello, M. A. (1980) "Decay Patterns of Fast Sea Ice in Canada and Alaska," Sea Ice Processes and Models, Ed. R. S. Pritchard, University of Washington Press, Seattle, Washington, pp. 313-326.

Brower, W. A., H. F. Diaz, A. S. Prechtel, H. W. Searby, and J. L. Wise (1977) Climatic Atlas of the Outer Continental Shelf Waters and Coastal Regions of Alaska, Vol. III, Chukchi-Beaufort Sea. Arctic Environmental Information and Data Center, U. of Alaska, Anchorage, Alaska.

Campbell, W. J., P. Gloerson, W. J. Webster, T. T. Wilheit, and R. O. Ramseier (1976) "Beaufort Sea Ice Zones as Delineated by Microwave Imagery," J. Geophys. Res., Vol. 81, No. 6, pp. 1103-1110.

Cox, J. C., L. A. Schultz, R. P. Johnson, and R. A. Shelsby (1980) "The Transport and Behavior of Oil Spilled In and Under Sea Ice," To appear in: Environmental Assessment of the Alaskan Continental Shelf, Final Reports, NOAA/OCSEAP, Boulder, Colorado.

Deslauriers, P. C. (1979) "The Bouchard No. 65 Oil Spill in the Ice-Covered Waters of Buzzards Bay," J. Petroleum Technology, Vol. XXXI, September, pp. 1092-1100.

Evans, R. J., and N. Untersteiner (1971) "Thermal Cracks in Floating Ice Sheets," J. Geophys. Res., Vol. 76, No. 3, January, pp. 694-703.

Henry, R. F., and N. S. Heaps (1976) "Surges in the Southern Beaufort Sea," J. Fish. Res. Board Canada, Vol. 33, No. 10, pp. 2362-2376.

Hibler, W. D. III, and S. F. Ackley (1974a) "Height Variations Along Sea Ice Pressure Ridges and the Probability of Finding 'Holes' for Vehicle Crossings," AIDJEX Bulletin No. 25, University of Washington, Seattle, pp. 97-106.

Hibler, W. D. III, and S. F. Ackley (1974b) "A Sea Ice Terrain Model and Its Application to Surface Vehicle Trafficability," AIDJEX Bulletin No. 25, University of Washington, Seattle. pp. 107-126.

Hunt, W. R., and G. M. Naske (1979) "A Baseline Study of Historic Ice Conditions in the Beaufort Sea, Chukchi Sea and Bering Strait," Environmental Assessment of the Alaskan Continental Shelf, Final Reports, NOAA/OCSEAP, Boulder, Colorado. Vol. 1. Physical Science Series, pp. 122-534.

Jenne, R. L. (1975) Data Sets for Meteorological Research, National Center for Atmospheric Research Technical Note NCAR-TN/IA-III, Boulder, Colorado.

Kovacs, A. (1977) "Sea Ice Thickness Profiling and Under-Ice Oil Entrapment," Proceedings 1977 Offshore Technology Conference, Houston, Texas. Vol. III, pp. 547-554.

Kovacs, A. (1979) "Oil Pooling Under Sea Ice," Environmental Assessment of the Alaskan Continental Shelf, Annual Reports, Vol. VIII, Transport, pp. 310-353.

Kovacs, A. (1980) "Oil Pooling Under Sea Ice," To Appear in: Environmental Assessment of the Alaskan Continental Shelf, Annual Reports, NOAA/OCSEAP, Boulder, Colorado.

Kovacs, A., and M. Mellor (1974) "Sea Ice Morphology and Ice as a Geologic Agent in the Southern Beaufort Sea," The Coast and Shelf of the Beaufort Sea, Eds. C. Reed and E. Slater, Arctic Institute of North America, Arlington, Virginia, pp. 113-162.

Kovacs, A., and R. M. Morey (1978) "Radar Anisotropy of Sea Ice Due to Preferred Azimuthal Orientation of the Horizontal C Axes of Ice Crystals," J. Geophys. Res., Vol. 83, No. C12, pp. 6037-6046.

Kovacs, A., and W. F. Weeks (1979) "Dynamics of Near-Shore Ice," Environmental Assessment of the Alaskan Continental Shelf, Annual Reports, NOAA/OCSEAP, Boulder, Colorado. Vol. VII, Transport, pp. 181-207.

Leavitt, E. (1979) "Comparison between Geostrophic Winds Derived from the Standard Pressure Measurement Network and the AIDJEX Network," Environmental Assessment of the Alaskan Continental Shelf, Annual Reports, NOAA/OCSEAP, Boulder, Colorado. Vol. VIII. Transport, pp. 46-56.

Lewis, E. L. (1976) Oil in Sea Ice, Pacific Marine Science Report 76-12, Institute of Ocean Sciences, Patricia Bay, Victoria, B.C.

Logan, W. J., D. E. Thornton, and S. L. Ross (1975) Oil Spill Counter-Measures for the Beaufort Sea, Appendix, Beaufort Sea Technical Report No. 31b, Beaufort Sea Project, Dept. of the Environment, Victoria, B. C.

Martin, S. (1977) The Seasonal Variation of Oil Entrainment in First Year Sea Ice: A Comparison of NORCOR/OCS Observations, Dept. of Oceanography, Spec. Report #71, University of Washington, March.

Matthews, J. B. (1980) "Observations of Surface and Bottom Drifter Movements in the Beaufort Sea Near Prudhoe Bay, Alaska," Submitted to J. Geophys. Res.

Maykut, G. A., and N. Untersteiner (1971) "Some Results from a Time Dependent Thermodynamic Model of Sea Ice," J. Geophys. Res., Vol. 76, No. 6, pp. 1550-1575.

Milne, A. R., and R. H. Herlinveaux (n.d.) Crude Oil in Cold Water, Ed. R. J. Childerhose, Beaufort Sea Project, Institute of Ocean Sciences, Sidney, B.C.

Mountain, D. G., L. K. Coachman, and K. Aagaard (1976) "On the Flow Through Barrow Canyon," J. Phys. Oceanography, Vol. 6, pp. 461-470.

Mungall, J., and R. Whitaker (1979) "Oceanographic Processes in a Beaufort Sea Barrier Island-Lagoon System: Numerical Modeling and Current Measurements," Environmental Assessment of the Alaskan Continental Shelf, Annual Reports, NOAA/OCSEAP, Boulder, Colorado, Vol. VIII. Transport, pp. 182-287.

Nadeau, J. S., and D. Mackay (1978) "Evaporation Rates of Complex Hydrocarbon Mixtures Under Environmental Conditions," Spill Technology Newsletter, Vol. 3 No. 2, March-April.

NORCOR Engineering and Research, Ltd. (1975) The Interaction of Crude Oil with Arctic Sea Ice, Beaufort Sea Technical Report #27, Beaufort Sea Project, Dept. of the Environment, Victoria, B.C.

Parmerter, R. (1974) "A Mechanical Model of Rafting," AIDJEX Bulletin No. 23, University of Washington, Seattle, pp. 97-116.

Pritchard, R. S. (1981) "Mechanical Behavior of Pack Ice," To appear in Mechanical Behaviour of Structural Media, Ed. A. P. S. Selvadurai, Elsevier, Amsterdam.

Ramseier, R. O., M. R. Vant, L. D. Arsenault, L. Gray, R. B. Gray, and W. J. Chudobiak (1975) Distribution of Sea Ice Thickness in the Beaufort Sea, Beaufort Sea Technical Report No. 30, Beaufort Sea Project, Dept. of the Environment, Victoria, B.C.

Reimnitz, E., L. J. Toimil, and P. Barnes (1977a) "Arctic Continental Shelf Processes and Morphology Related to Sea Ice Zonation, Beaufort Sea, Alaska," AIDJEX Bulletin No. 36, University of Washington, Seattle, pp. 15-64.

Reimnitz, E., L. J. Toimil and P. W. Barnes (1977b) "Stamuhhi Zone Processes: Implications for Developing the Arctic Offshore," Proceedings 1977 Offshore Technology Conference, Houston, Texas. Vol. III, pp. 513-518.

Reimnitz, E. and K. Dunton (1979) "Diving Observations on the Soft Ice Layer Under the Fast Ice at DS11 in the Stefansson Sound Boulder Patch," Environmental Assessment of the Alaskan Continental Shelf, Annual Reports, NOAA/OCSEAP, Boulder, Colorado, Vol. IX. Hazards. pp. 210-230.

Rigby, F. A. and A. Hanson (1976) "Evolution of a Large Arctic Pressure Ridge," AIDJEX Bulletin No. 34, December, University of Washington, Seattle, pp. 43-72.

Rogers, J. C. (1978) "Meteorological Factors Affecting Interannual Variability of Summertime Ice Extent in the Beaufort Sea," Monthly Weather Review, Vol. 106, No. 6, June.

Rosenegger, L. W. (1975) Movement of Oil Under Sea Ice, Beaufort Sea Technical Report No. 28, Beaufort Sea Project, Dept. of the Environment Victoria, B.C.

Rothrock, D. A. (1979) "Modeling Sea-Ice Features and Processes," J. of Glaciology, Vol. 24, No. 90, pp. 359-375.

Ruby, C. H., L. G. Ward, I. A. Fischer, and P. J. Brown (1977) "Buzzards Bay Oil Spill-An Arctic Analogue." Proceedings Fourth International Conference on Port and Ocean Engineering Under Arctic Conditions, St. John's, Newfoundland, pp. 844-855.

Schell, D. M. (1974) "Seasonal Variations in the Nutrient Chemistry and Conservative Constituents in Coastal Alaskan Beaufort Sea Waters," Environmental Studies of an Arctic Estuarine System, Institute of Marine Science, University of Alaska, Fairbanks.

Shapiro, L. H., and R. C. Metzner (1979) "Historical References to Ice Conditions Along the Beaufort Sea Coast of Alaska," Environmental Assessment of the Alaskan Continental Shelf, Annual Reports, NOAA/OCSEAP, Boulder, Colorado. Vol. IX. Hazards, pp. 632-682.

Stringer, W. J. (1978) Morphology of Beaufort, Chukchi and Bering Seas Nearshore Ice Conditions by Means of Satellite and Aerial Remote Sensing, Geophysical Institute, U. of Alaska, Fairbanks.

Swithinbank, C. (1972) "Arctic Pack Ice from Below," Sea Ice: Proceedings of an International Conference, Reykjavic, Iceland, Ed. T. Karlsson, National Research Council, Reykjavic, pp. 246-254.

Thomas, D. R., and R. S. Pritchard (1979) "Beaufort and Chukchi Sea Ice Motion; Part I. Pack Ice Trajectories," Environmental Assessment of the Alaskan Continental Shelf, Annual Reports, NOAA/OCSEAP, Boulder, Colorado. Vol. VIII, Transport, pp. 361-469.

Thorndike, A. S., and J. Y. Cheung (1977) "AIDJEX Measurements of Sea Ice Motion, 11 Apr 1975 to 14 May 1976," AIDJEX Bulletin No. 35, January, University of Washington, Seattle.

Thorndike, A. S., and R. Colony (1980) "Large-scale Ice Motion in the Beaufort Sea during AIDJEX, April 1975-April 1976," Sea Ice Processes and Models, Ed. R. S. Pritchard, University of Washington Press, Seattle, Washington, pp. 249-260.

Thorndike, A. S., D. A. Rothrock, G. A. Maykut, and R. Colony (1975) "The Thickness Distribution of Sea Ice," J. Geophys. Res., Vol. 80, No. 33, November, pp. 4501-4513.

Topham, D. R. (1975) Hydrodynamics of an Oil Well Blowout, Beaufort Sea Technical Report No. 33, Beaufort Sea Project, Dept. of the Environment, Victoria, B.C.

Topham, D. R. (1977) "The Deflection of an Ice Sheet by a Submerged Gas Source," J. Appl. Mech., June, pp. 279-284.

Topham, D. R. (1979) "The Disposition of Gas/Oil Mixtures Trapped Under Ice," Oil, Ice and Gas, Proceedings of a Workshop held in Toroonto, Canada, October 10 and 11, 1979, pp. 55-73.

Tucker, W. B., W. F. Weeks, and M. Frank (1979) Sea Ice Ridging Over the Alaskan Continental Shelf, CRREL Report 79-8, Hanover, New Hampshire.

Tucker, W. B., W. F. Weeks, A. Kovacs, and A. J. Gow (1980) "Nearshore Ice Motion at Prudhoe Bay, Alaska," Sea Ice Processes and Models, Ed. R. S. Pritchard, University of Washington Press, Seattle, Washington, pp. 261-272.

Wadhams, P. (1975) Sea Ice Morphology in the Beaufort Sea, Beaufort Sea Technical Report No. 36, Beaufort Sea Project, Dept. of the Environment, Victoria, B.C.

Wadhams, P. and R. Horne (1978) An Analysis of Ice Profiles Obtained by Submarine Sonar in the AIDJEX Area of the Beaufort Sea, Scott Polar Research Institute Technical Report 78-1, Cambridge.

Weeks, W. (1976) "Sea Ice Conditions in the Arctic," AIDJEX Bulletin No. 34, University of Washington, Seattle, pp. 173-206.

Weeks, W. F. and D. L. Anderson (1958) "An Experimental Study of Strength of Young Sea Ice," Trans. of the Amer. Geophys. Union, Vol. 39 No. 4, pp. 641-647.

Weeks, W. F., and A. J. Gow (1980) "Crystal Alignment in the Fast Ice of Arctic, Alaska," J. Geophys. Res., Vol. 85, No. C2, pp. 1137-1146.

Weeks, W. F., A. Kovacs, and W. D. Hibler III (1971) "Pressure Ridge Characteristics in the Arctic Coastal Environment," Proceedings 1st International Conference on Port and Ocean Engineering under Arctic Conditions, Trondheim, Norway, Vol. I, pp. 152-183.

Weeks, W. F., A. Kovacs, S. J. Mock, W. B. Tucker, W. D. Hibler III, and A. J. Gow (1977) "Studies of the Movement of Coastal Sea Ice Near Prudhoe Bay, Alaska, U.S.A.," J. Glaciology, Vol. 19, No. 81, pp. 533-546.

Weeks, W. F., W. B. Tucker III, M. Frank, and S. Fungcharoen (1980) "Characterization of the Surface Roughness and Floe Geometry of Sea Ice Over the Continental Shelves of the Beaufort and Chukchi Seas," Sea Ice Processes and Models, Ed. R. S. Pritchard, University of Washington Press, Seattle, Washington, pp. 300-312.

World Meteorological Organization (1970) WMO Sea-Ice Nomenclature: Terminology Codes and Illustrated Glossary, WMO Publication No. 259. Tech. Pub. No. 145, Geneva.

Glossary of Ice Terminology

An alphabetical list of the ice terminology used in this report is given below. Many of the terms are taken from Weeks (1976), who in turn took many definitions from the WMO/OMM/BMO No. 259, published in 1970 by the World Meteorological Organization. Definitions marked with an asterisk are added or modified by Weeks (1976). Definitions marked with two asterisks are added or modified significantly by ourselves.

BOTTOM-FAST ICE **

Fast ice grown in place in shallow waters which becomes grounded when the ice draft equals the water depth.

BRASH ICE

Accumulation of floating ice made up of fragments not more than 2 m across.

BREAKUP *

A general expression applied to the formation of a large number of fractures through a compact ice cover, followed by a rapid diverging motion of the separate fragments.

COLUMNAR ICE **

Ice grown in undisturbed water where the ice forms long columnar crystals with a horizontal c-axis. When ice grows in still, open water, the top 10 to 20 mm consists of very small, randomly oriented crystals. Below this, columnar growth occurs.

COMPACTNESS *

The ratio of the area of the sea surface actually covered by ice to the total area of the sea surface under consideration. Therefore, a compactness of 0 corresponds to ice-free conditions and a compactness of 1, to compact pack ice (cf. concentration).

CONCENTRATION

The ratio in tenths of the sea surface actually covered by ice to the total area of sea surface, both ice covered and ice free, at a specific location or over a defined area (cf. ice cover). May be expressed in the following terms:

Compact pack - concentration 10/10, no water visible.

Consolidated pack ice - concentration 10/10, foes frozen together.

Very close pack ice - concentration 9/10 to less than 10/10.

Close pack ice - concentration 7/10 to 8/10, floes mostly in contact.

Open pack ice - concentration 4/10 to 6/10, many leads and polynyas, floes generally not in contact.

Very open pack ice - concentration 1/10 to 3/10.

CONVERGENCE *

Used to describe the condition where div $\underset{\sim}{v}_i$ is negative (cf. divergence)

CONVERGING *

Ice fields and floes are said to be converging when they are subjected to a convergent motion that increases the concentration and compactness of the ice or increases the stresses in the ice.

CRACK

Any fracture which has not yet parted.

DEFORMED ICE

A general term for ice which has been squeezed together and in places forced upward (and downward). Forms of deformation include rafting, ridging, and hummocking.

DIVERGENCE *

Formally defined as div $\underset{\sim}{v}_i = \frac{\partial v_x}{\partial x} + \frac{\partial v_y}{\partial y}$ where $\underset{\sim}{v}_i$ is the ice drift velocity. The divergence can be considered as the change in area per unit area at a given point. The word is also used to indicate a generally diverging motion in the ice.

DIVERGING

Ice fields or floes are said to be diverging when they are subjected to a divergent or dispersive motion, thus reducing the ice compactness and concentration or relieving stresses in the ice (cf. converging).

DRAFT *

The distance, measured normal to the sea surface, between the lower surface of the ice and the water level.

FAST ICE (1) *

Sea ice of any origin which remains fast (attached with little horizontal motion) along a coast or to some other fixed object.

FAST ICE (2) **

Smooth, fast ice which is grown in place and protected from pack ice incursions by barrier islands or the stamukhi zone.

FINGER RAFTING

Type of rafting whereby interlocking thrusts are formed, each floe thrusting "fingers" alternately over and under the other. Common in nilas and grey ice.

FIRST-YEAR ICE

Sea ice of not more than one winter's growth.

FLAW LEAD

A lead between pack ice and fast ice.

FLOATING FAST ICE **

Fast ice which does not extend to the sea floor.

FLOE

Any relatively flat piece of sea ice 20 m or more across (cf. ice cake). Floes are subdivided according to horizontal extent:
Giant floe - more than 10 km across.
Vast floe - 2 to 10 km across.
Big floe - 500 to 2000 m across.
Medium floe - 100 to 500 m across.
Small floe - 20 to 100 m across.

FLOEBERG

A massive piece of sea ice composed of a hummock, a group of hummocks, or a rubble field, frozen together and separated from any surrounding ice. It may have a freeboard of up to 5 m.

FLOODED ICE

Sea ice which has been flooded by melt water or river water and is heavily loaded with water and wet snow.

FRACTURE

Any break or rupture through very close, compact or consolidated pack ice (see concentration), fast ice, or a single floe resulting from deformation processes (cf. lead). Fractures may contain brash ice and be covered with nilas or young ice. The length may be a few meters or many kilometers.

FRAZIL ICE

Fine spicules or plates of ice, suspended in water.

FREE DRIFT **

Ice motion produced by only the wind and water stress and Coriolis acceleration. The ice must be in a low enough concentration or thin enough that it will not transmit stresses internally.

FREEBOARD *

The distance, measured normal to the sea surface, between the upper surface of the ice and the water level.

FREEZEUP **

The formation of a continuous ice cover over the seasonal ice zone. Freezeup starts with the first formation of new ice and ends when the ice cover is complete.

GREASE ICE

A stage of freezing, later than that of frazil ice, in which the crystals have coagulated to form a soupy layer on the surface. Grease ice reflects little light, giving the sea a matte appearance.

GREY ICE

Young ice 10-15 cm thick. Less elastic than nilas and breaks on swell. Usually rafts under pressure.

GREY-WHITE ICE

Young ice 15-30 cm thick. Under pressure more likely to ridge than to raft.

GROUNDED ICE *

Floating ice (e.g., ridge, hummock, ice island) which is aground (stranded) in shoal water.

HUMMOCK

A hillock of broken ice which has been forced upward by pressure. May be fresh or weathered.

HUMMOCK FIELD *

An area of sea ice that essentially has all been deformed into a series of hummocks (cf. rubble field).

ICE CAKE

Any relatively flat piece of sea ice less than 20 m across (cf. floe).

ICE CANOPY **

Sea ice from the point of view of the submariner.

ICE COVER

The ratio of an area of ice of any concentration to the total area of sea surface within some large geographic locale; this locale may be global, hemispheric, or prescribed by a specific oceanographic entity, such as Baffin Bay or the Barents Sea.

ICE DRIFT **

Ice motion produced by wind stress, ocean current stress, Coriolis force and internal ice stress.

ICE EDGE

The demarcation at any given time between the open sea and sea ice of any kind, whether fast or drifting.

ICE FREE

No sea ice present (see also open water).

ICE ISLAND

A large piece of floating ice, with a freeboard of approximately 5 m, which has broken away from an Arctic ice shelf. Ice islands usually have a thickness of 30 to 50 m, an area of from a few thousand square meters to several hundred square kilometers, and a regularly undulating upper surface.

KEEL *

The underside of a ridge that projects downward below the lower surface of the surrounding sea ice.

LEAD *

Any fracture or passage through sea ice that is generally too wide to jump across. A lead may contain open water (open lead) or be ice covered (frozen lead).

LEVEL ICE

Sea ice which has been unaffected by deformation.

MELT POND **

An accumulation of meltwater on the surface of sea ice.

MULTIYEAR ICE **

Old ice which has survived at least one summer's melt. The ice is almost salt-free and is 3 m or more in thickness. Sometimes a further division into second-year and multiyear ice is made.

NEW ICE **

A general term for recently formed ice.

NILAS

A thin elastic crust of ice up to 10 cm thick, with a matte surface. Bends easily under pressure, thrusting in a pattern of interlocking "fingers" (finger rafting). Dark nilas, up to 5 cm thick is very dark in color; light nilas, 5-10 cm thick, is rather lighter in color.

OLD ICE

Sea ice which has survived at least one summer's melt. Most topographic features are smoother than on first-year ice.

OPEN WATER

A large area of freely navigable water in which sea ice is present in less than 1/10 concentration (see also ice free).

PACK ICE

Any accumulation of sea ice, other than fast ice, no matter what form it takes or how it is disposed (see also concentration).

PANCAKE ICE

Predominantly circular pieces of ice from 30 cm to 3 m in diameter, and up to about 10 cm in thickness, with raised rims due to the pieces striking against one another.

POLYNYA

Any nonlinearly shaped opening enclosed in ice. Polynyas may contain brash ice or be covered with new ice, nilas, or young ice. If it is limited on one side by the coast, it is called a shore polynya; if it is limited by fast ice, it is called a flaw polynya; if it is found in the same place every year, it is called a recurring polynya.

PRESSURE RIDGE

A general expression for any elongated (in plan view) ridgelike accumulation of broken ice caused by compressive forces breaking and piling up thin ice along a refrozen lead.

RAFTING *

Process whereby one piece of ice overrides another; most obvious in new and young ice (cf. finger rafting), but common in ice of all thicknesses.

RIDGING

The process whereby ice is deformed into ridges.

ROTTEN ICE

Sea ice which has become honeycombed and which is in an advanced state of disintegration.

ROUGHNESS (or BOTTOM ROUGHNESS) **

The vertical relief on the bottomside of an ice sheet. May range in scale from millimeters (skeletal layer) to meters (ridge keels). Horizontal scales range from millimeters to kilometers. Measurements of roughness are given as the variation of ice draft over an appropriate horizontal scale.

RUBBLE FIELD *

An area of sea ice that has essentially all been deformed. Unlike hummock field, does not imply any specific form of the upper or lower surface of the deformed ice.

SAIL *

The upper portion of a ridge that projects above the upper surface of the surrounding sea ice.

SASTRUGI

Sharp, irregular, parallel ridges formed on a snow surface by wind erosion and deposition. On mobile floating ice, the ridges are parallel to the direction of the prevailing wind at the time they were formed.

SEASONAL ICE ZONE **

The nearshore area over the continental shelf that is normally ice free during part of the year, but freezes over the rest of the year. Normally, the ice cover in the seasonal ice zone is mostly first-year ice.

SECOND-YEAR ICE

Old ice which has survived only one summer's melt.

SHEARING

An area of pack ice that is subject to shearing motion when the ice motion varies significantly in the direction normal to the motion, subjecting the ice to rotatory forces. These forces may result in phenomena similar to a flaw.

SHEAR RIDGE *

A line or wall of broken ice that is formed when adjacent floes move parallel to the boundary that separates them. Shear ridges commonly are quite straight in plan view. The sail of a shear ridge also usually has one vertical or nearly vertical side.

SHEAR ZONE **

An area in which a large amount of shearing deformation has been concentrated. Specifically the active zone between fast ice and the moving pack.

SKELETAL LAYER **

The bottom 10 to 40 mm of columnar sea ice. This ice layer is very porous and fragile.

SLUSH ICE

Snow which is saturated and mixed with water on land or ice surfaces or formed as a viscous mass floating in water after a heavy snowfall.

SMOOTH FAST ICE **

Fast ice which has not undergone any significant deformation. Thin ice which is rafted or formed into pancake floes will eventually become smooth through weathering.

STAMUKHA **

A fragment of sea ice that becomes grounded in shallow water (as opposed to ice grown in place that reaches the bottom, cf. bottom-fast ice).

STAMUKHI ZONE **

A zone more or less parallel to the coast containing many grounded ice features (ridges). The ridges are built in place where the moving pack ice impinges upon fast ice. The stamukhi zone can be considered the past history of the shear zone, the region where shearing and ridge building actually takes place.

THAW HOLE *

Vertical hole in sea ice formed when a melt pond melts through to the underlying water.

TIDAL CRACK **

A crack which forms from flexure at the junction of bottom-fast ice and floating fast ice.

WEATHERING

Processes of ablation and accumulation which gradually eliminate irregularities in an ice surface.

YOUNG ICE

Ice in the transition stage between nilas and first year ice, 10-30 cm in thickness. May be subdivided into grey ice and grey-white ice.

Flow Research Report No. 176

Prudhoe Bay Oil Spill Scenarios

By

D. R. Thomas

December 1980

Flow Research Company
A Division of Flow Industries, Inc.
21414-68th Avenue South
Kent, Washington 98031
(206) 872-8500

Flow Research Report No. 176
December 1980

Acknowledgement

This study was supported by the Bureau of Land Management through interagency agreement with the National Oceanic and Atmospheric Administration, under which a multiyear program responding to needs of petroleum development of the Alaskan Continental Shelf is managed by the Outer Continental Shelf Environmental Assessment (OCSEAP) Office.

Flow Research Report No. 176
December 1980

Table of Contents

Introduction

The purpose of this report is to describe the most likely sequence of events following an offshore oil well blowout during the ice season in the Beaufort Sea. The descriptions pertain specifically to the December 1979 joint state/federal lease sale area offshore of Prudhoe Bay, Alaska. The lease area extends from Flaxman Island in the east to Stump Island in the west. The seaward edge of the lease area follows approximately the 20 m isobath which is about 25 km offshore in this area.

Twelve hypothetical blowout scenarios are described in this report. The parameters which describe these blowouts were chosen by the Outer Continental Shelf Environmental Assessment Program (OCSEAP) and are intended to cover the range of ice conditions under which blowouts might occur in the lease area. The parameters that are varied are location, time of year, and duration of the blowout.

Three blowout locations are used to cover the possible range of sea ice conditions occurring in the lease sale area. These locations are: (1) the fast ice zone - the area near shore behind the barrier islands that develops a relatively smooth ice cover which remains motionless throughout the ice season, (2) the stamukhi zone - the area seaward of the fast ice zone where highly deformed ice develops as the moving pack ice impinges upon the stationary shore-fast ice, and (3) the pack ice zone - the area outside the barrier islands that contains a mixture of thick multiyear ice and thinner first-year ice. The ice in this zone is frequently moved about by the wind and ocean currents, with leads and ridges developing because of differential ice motion.

The times specified for the hypothetical blowouts are just after freezeup in the fall when the ice cover is thin and growing and just before breakup in the spring when the ice has reached its maximum thickness. Since present regulations allow drilling only from November through March, we have chosen the dates of 1 November and 31 March for the hypothetical blowouts. These dates span the specified period, after allowing for a blowout duration of up to 90 days.

Two blowout durations and oil flow rates are specified. The first consists of the release of 40,000 barrels of oil per day for a period of 5 days. The second consists of the release of 50,000 barrels of oil per day for a period of 90 days. The flow rates specified might seem unrealistically large, but they are considered here as an upper limit. The description of events following a blowout with smaller flow rates will be similar in most respects to those described in this report but with proportionally smaller numbers where appropriate.

The combination of 3 locations, 2 times, and 2 durations gives the 12 possible blowout situations which we consider. These 12 combinations are given in Table 1. The numbers from 1 to 12 in the location columns correspond to the 12 numbered blowout scenarios presented in this report.

Table 1. Combinations of Location, Time of Year, and Duration of Blowout which Result in 12 Possible Blowout Situations.

		Location		
Season	Duration	Fast Ice	Stamukhi	Pack
Fall	5 day	1	2	3
	90 day	4	5	6
Spring	5 day	7	8	9
	90 day	10	11	12

The scenarios are initiated by assuming that a blowout corresponding to one of the 12 combinations of parameters given in Table 1 has occurred. The initial interaction of the blowout and the ice cover is described followed by descriptions of the spread of oil beneath the ice, the incorporation of the oil into the ice cover, the motion of the oiled ice, the release of the oil from the ice, and the fate of the oil after the ice has melted. For each phase of the oil and ice interaction, the most probable sequence of events is given without references and with only minimal elaboration and qualifications. In many cases, a lack of data or the range of variation of relevant variables reduce the confidence with which the most probable events can be described. In those cases we have tried to make reasonable conjectures as to what might happen.

The data used in developing these scenarios have been collected and summarized in a separate report (Thomas, 1980).* This was done to avoid repetition in the scenarios, but it also provides a more logical format for discussing background material, presenting references, analyzing probabilities and justifying conjectures. The separate report also discusses possible alternatives in the sequence of events following a blowout. The scenarios, then, can follow what we consider the most likely sequence, without evolving into a complicated branching structure.

The subject matter discussed in these scenarios is limited to the effect an ice cover will have on the spilled oil. The possible causes of a blowout and the probability of a blowout are not treated beyond assuming that the blowout occurs under an ice cover some distance away from any natural or artificial island being used as a drilling platform. The development and application of open-water oil spill spreading and trajectory models and the ultimate long-term fate of spilled oil and its deleterious effect on the environment are beyond the scope of this work. The mechanisms and strategies involved in an oil spill cleanup are also not treated in the scenarios. Our intention is to describe what will most likely happen to the oil without human intervention. Thus, results are most useful for determining the possible consequences of a spill as well as assessing the possibility of cleanup and developing cleanup strategies.

---

*Thomas, D.R., 1980. Behavior of Oil Spills Under Sea Ice - Prudhoe Bay. Flow Research Report No. 175, Flow Research Company, Kent, Washington.

Oil Spill Scenario No. 1

On 1 November, about 4 weeks after freezeup, an underwater oil well blowout is assumed to occur under the newly developed fast ice in Stefansson Sound. The hypothetical blowout releases 2 x 10^5 barrels (3.18 x 10^4 m^3) of oil over a period of 5 days.

Scene

Stefansson Sound is located inside the barrier islands within the fast ice zone. At the time of the blowout, a thin (0.2 to 0.3 m thick), continuous ice canopy extending from the shore to the barrier islands covers the sound. Winds during the freezeup period and immediately after have produced pancake floes with thick edges, and some rafting and ridging has occurred, but as the ice continues to thicken, these irregularities are smoothed out. The fast ice consists of large areas of flat ice with bottom relief of 0.01 to 0.02 m, possibly with occasional areas of greater relief where rafting or ridging has occurred.

Water depths in the vicinity of the blowout are about 6 m. Wind-driven currents died out as soon as the ice cover formed and now the under-ice currents are driven by the tides and a thermohaline circulation. The tidal component is weak (less than 0.01 or 0.02 m/s) and oscillatory. The thermohaline currents produced by cold, salty water flowing offshore along the bottom are on the average small, but extremes of up to 0.11 m/s have been observed. It is postulated that an onshore current of up to 0.2 m/s must exist just beneath the ice to replace the water flowing offshore along the bottom, but this has not been observed. In general, measured currents beneath the fast ice inside the barrier islands are small, about 0.02 to 0.03 m/s, and variable.

Water temperatures in the shallow sound are near freezing and the 90th percentile air temperature range during early November is about -35 to -6°C.

Blowout

A ruptured casing and a fault in the bedrock allow the oil and gas to escape under the solid ice canopy some distance from the well head. The reservoir is assumed to be about 3000 m deep and the crude oil similar to a Prudhoe Bay crude (density about 890 kg/m^3 and pour point about -9.5°C).

A total of 3.18×10^4 m^3 of crude oil escapes over a period of 5 days before control efforts successfully stop the flow. An estimated 4.8×10^6 m^3 of gas is also released. Flow rates during the 5-day blowout average 4.4 m^3/min of oil and 670 m^3/min of gas.

During the blowout, a plume of oil, gas bubbles, and entrained water rises to the surface. Gas trapped under the thin ice immediately breaks up the ice over the plume, allowing all the gas released during the blowout to escape to the atmosphere.

The vertical currents in the plume flow radially outward at the surface then downward at some distance from the plume to complete a closed circulation system. The downward-flowing currents entrain some water from outside the circulation system and a weak, inward-flowing surface current is developed outside the plume region to replace this entrained water. A wave ring forms where the outward- and inward-flowing surface currents meet. For a 6-m water depth and a gas flow rate of 670 m^3/min, the diameter of this wave ring is calculated to be about 35 m.

The crude oil, at a temperature between 60 and 90°C contains enough heat to melt between 9.5×10^3 and 1.4×10^4 m^3 of sea ice. Since surface currents outside the wave ring tend to flow inward toward the blowout, the oil and heat will tend to concentrate inside the wave ring. Some warm oil or heated water will escape the circulation system inside the wave ring, possibly melting the ice cover thinner or reducing the ice growth rate. The bottom water entrained in the plume is likely to be so cold in these shallow areas that it contributes little to ice melting.

Approximately 200 m^3 of ice lies within the wave ring. This is the minimum amount of ice that will be melted during the course of the blowout. As the ice melts, it is replaced by crude oil which has about the same density as sea ice. This volume of oil is only about 0.6 percent of the total released during the blowout.

In general, the oil undergoes very little physical or chemical change during the blowout. Evaporation is unimportant because so little oil is exposed to the atmosphere. Outside the blowout plume there is no mixing energy to form emulsions. Dissolution and sedimentation occur, but probably in very insignificant amounts.

Spread of Oil Beneath the Ice

Other than the small amount of oil in the central melt hole, most of the oil will spread beneath the ice. Very little oil will flow onto the top surface of the ice through cracks in the ice or the melt hole. In sea water with a density of 1020 kg/m^3 a layer of oil with a density of 890 kg/m^3 will have only 9 mm more freeboard than a 0.3-m-thick ice sheet with a density of 910 kg/m^3 when the oil draft is equal to the ice draft. Air temperatures below the oil's pour point, ice roughness, and snow on the ice will all tend to prevent the oil from spreading onto the ice surface, thus increasing the thickness of the oil pool enough that oil will begin flowing beneath the ice.

Beneath a perfectly smooth sheet of ice, the oil will spread until an equilibrium thickness of about 8 mm is reached everywhere. Neglecting oil on the ice surface or in the central melt hole, 3.18×10^4 m^3 of oil will cover an area of 4 km^2 (a circle of radius 1.13 km). This should be considered an upper limit to the size of the under-ice oil slick. In reality, the oil will cover less area than this for two reasons. First, even new, thin fast ice will contain a small amount of bottom relief in an area of 4 km^2. This relief will cause oil to pool deeper than 8 mm until it can flow beneath or around the obstruction. Second, and even more important, though, is the growth of new ice. Over the 5-day blowout, the ice sheet outside the oil slick will thicken by about 0.01 m per day. As the oil spreads beneath the ice near the blowout site, the ice outside that area grows thicker, providing more containment volume near the blowout. Assuming the first day's oil flow (6.4×10^3 m^3) fills an area of 0.8 km^2 to a depth of 8 mm, 0.01 m of ice growth outside the oiled area allows the second day's oil flow to fill the same area to a greater depth, and so on for 5 days. Thus, the final under-ice oil slick can cover an area as small as 0.8 km^2.

The currents in the nearshore area are generally too small to affect the size of the oil-contaminated area. Occasional brief currents of up to 0.2 m/s may occur. Currents of this magnitude will move an oil slick under smooth ice but not under natural sea ice with 0.01 or 0.02 m of relief and a skeletal layer of growing ice crystals. The primary effect of currents will be to control the direction of the oil spread, not the extent of the spread.

Incorporation of Oil Into the Ice

Approximately 5 days after oil ceases to flow, new ice growth will have completely encapsulated all the oil which spread beneath the ice. A small amount of oil (equivalent to a film about 2 mm thick) will soak into the 0.04 to 0.06 m skeletal layer above the oil. The new ice growing beneath the oil layer will contain no oil.

Ice also forms beneath the oil pool in the central melt hole. By May, when ice growth stops, about 1.4 m of ice will have grown beneath the oil.

Any oil on the ice surface will be covered by snow. The oil, being totally isolated from the water and air, will experience no weathering throughout the winter.

Transport of Oiled Ice

A major storm before about mid-November can break up the fast ice behind the barrier islands. The fetch of winds in Stefansson Sound can be up to about 50 km. A wind of 8 m/s (16 knots) acting over a fetch of 50 km is required to fail 0.5-m-thick ice. In November, winds greater than 8 m/s (16 knots) blow only about 27 percent of the time. Larger winds are less likely and winds from some directions will have a shorter fetch. The ice cover will grow thicker and stronger daily. Therefore, the fast ice will most likely remain motionless and undeformed after mid-November.

Storms have been observed on occasion to move and deform the fast ice during November. Even in the event of such a storm, the relatively small area of oil-contaminated ice is unlikely to be heavily ridged or to be moved more than a few kilometers.

Release of Oil From the Ice

In late February or early March, as the air temperature begins to rise, brine trapped between the columnar ice crystals will begin to drain. By late April or early May, the brine channels will have become large enough that oil will begin to appear on the ice surface. Periods of cold weather will stop the oil flow temporarily, but by late May pools of oil will be collecting on the ice surface. Because of the lowered albedo of the oiled ice, melting of the ice surface also begins in late May.

The oil, being close to the ice surface, will have completely surfaced in early June. The presence of oil on the ice surface will accelerate the local ice breakup by about 2 weeks. Thus, by mid-June, the oil-contaminated ice will have broken up enough that it can be moved by the wind. About the same time, rivers will begin flowing again, flooding the ice about the river mouths. By mid-June, shore polynyas have been melted by the flowing rivers. The most likely ice motion will be toward the shore and the area of open water.

By early to mid-July, all the ice which is contaminated by oil will have melted. In 2 or 3 more weeks, all the uncontaminated ice will have melted leaving the oil slick on the water surface.

Fate of the Oil

As soon as oil begins to appear on the ice surface in May, weathering processes will begin. By the end of June, approximately 50 percent of the oil will have evaporated. Some water-in-oil emulsions will form where oil is floating on surface melt pools exposed to agitation by the winds. Other weathering processes will take place as the oil is released from the ice, but only insignificant amounts of oil will be involved. The low temperatures, the reduced wind action due to the remaining ice cover, and the thick, viscous oil layer on the water surface will act to inhibit dissolution, bacterial degradation, and dispersion. The silt carried out by the flowing rivers may increase the rate of sedimentation, though.

The pack ice does not generally retreat until sometime after early July. Grounded ridges seaward of the barrier islands may remain grounded until late summer, thus preventing the oil from being blown out to sea until later in the summer. By that time most of the oil will have been blown onto mainland beaches to the west or southwest due to the prevailing wind direction (from the east or northeast about 60 percent of the time during June). Of course, the probability is still high that some of the oil will be blown offshore onto island beaches or into the pack.

The above scenario assumes that no cleanup of the oil takes place. If part of the oil is cleaned up following the blowout, the major change in the scenario would be a reduction in the amount of oil involved.

Oil Spill Scenario No. 2

On 1 November, about 4 weeks after freezeup, an underwater oil well blowout is assumed to occur 5 km northeast of Narwhal Island in the stamukhi zone. The hypothetical blowout releases 2×10^5 barrels (3.18×10^4 m^3) of oil over a period of 5 days.

Scene

Narwhal Island lies about 20 km offshore of the Alaskan coast, just north of the Sagavanirktok River mouth. It is one of the barrier islands which protect the fast ice shoreward of the islands from interaction with the pack ice. Outside the islands, new first-year ice began freezing in early to mid-October. This new ice is not protected from interaction with the pack ice. The predominant easterly winds can also move and deform this ice. In early November, the ice cover over the blowout site mostly consists of rafted and rubbled thin ice (0.2- to 0.3-m thick) and a few ridges. The ridge density is about 1 to 2 ridges/km. Ice motion and deformation will continue until a ridge becomes securely grounded seaward of the blowout site. This usually occurs before January or February. The density of ridges in the area of the blowout increases by about 1 or 2 ridges/km per month so that in February there will be 5 to 10 ridges/km.

Ice motions in the stamukhi zone during the fall are generally toward the west and range from 30 to 90 km/month. Average ice speeds are about 2 m/min (~3 km/day). These motions are not continuous but occur during periods of high winds. Typically, the ice is motionless or nearly so about half the time and it averages about 6 km/day of motion about half the time. The ice motion is generally towards the west but some meandering motion or eastward motion can be expected. For the purpose of this scenario, the ice remains nearly motionless for the first 2.5 days of the blowout and then moves at speeds of 6 km/day the final 2.5 days, with a net westward motion of 4 km/day.

Water depths in the vicinity of the blowout are about 15 m. Wind-driven currents died out as soon as the ice cover formed, and now the under-ice currents are due to the tides and the mesoscale circulation. The tidal component is weak, less than 0.01 or 0.02 m/s, and oscillatory. The geostrophic component is also weak, 0.01 to 0.05 m/s, and generally toward the east or west, but with considerable variation. In general, measured currents beneath the ice just outside the barrier islands are small, about 0.02 to 0.03 m/s, and variable.

Water temperatures are near freezing and the 90th percentile air temperature range during November is about -2 to -22°C.

Blowout

A ruptured casing and a fault in the bedrock allow the oil and gas to escape under the solid ice canopy some distance from the well head. The reservoir is assumed to be about 3000 m deep and the crude oil similar to a Prudhoe Bay crude (density about 890 kg/m^3 and pour point about -9.5°C).

A total of 3.18×10^4 m^3 of crude oil escapes over a period of 5 days before control efforts successfully stop the flow. An estimated 4.8×10^6 m^3 of gas is also released. Flow rates during the 5-day blowout average 4.4 m^3/min of oil and 670 m^3/min of gas.

During the blowout, a plume of oil, gas bubbles, and entrained water rises to the surface. The vertical currents in the plume flow radially outward at the surface then downward at some distance from the plume to complete a closed circulation system. The downward-flowing currents entrain some water from outside the circulation system, and a weak, inward-flowing surface current is developed outside the plume region to replace this entrained water. A wave ring forms where the outward- and inward-flowing surface currents meet. For a 15-m water depth and a gas flow rate of 670 m^3/min, the diameter of this wave ring is calculated to be about 76 m.

Gas trapped under the thin ice immediately breaks up the ice over the plume, allowing all the gas released during the blowout to escape to the atmosphere. Ice motion during the blowout does not affect the escape of the gas. Motions of 6 km/day amount to only 4 m/min, which is slow enough to allow large quantities of gas to collect under and break up the thin ice. During the 5-day blowout, the ice moves about 15 km resulting in a 15-km-long strip of broken ice.

The crude oil, at a temperature between 60 and 90°C, contains enough heat to melt between 9.5×10^3 and 1.4×10^4 m^3 of sea ice. Since surface currents outside the wave ring tend to flow inward toward the blowout, the oil and heat will tend to concentrate inside the wave ring. However, some warm oil or heated water will escape the circulation system inside the wave ring, possibly melting the ice cover thinner or reducing the ice growth rate. The bottom water entrained in the plume is likely to be so cold in these shallow areas that it contributes little to ice melting.

For 2.5 days during the blowout, the ice remains motionless, and the approximately 10^3 m^3 of ice within the 76 m diameter wave ring is completely melted. As the ice melts, it is replaced by crude oil which has about the same density as sea ice. This volume of oil is only about 3.0 percent of the total released during the blowout. For the remaining 2.5 days during the blowout, the ice moves 15 km. As much as 4.8×10^3 to 7.2×10^3 m^3 of ice could be melted by the warm oil released during this period. Some oil will be floating on the water surface between broken up and partially melted ice blocks along the blowout track, but the amount is small, probably only a few percent of the total oil released.

In general, the oil undergoes very little physical or chemical change during the blowout. Evaporation is unimportant because so little oil is exposed to the atmosphere. Outside the blowout plume, there is no mixing energy to form emulsions. Dissolution and sedimentation occur, but probably in very insignificant amounts.

Spread of Oil Beneath the Ice

Only about 10 percent or less of the oil released ends up floating among the broken ice pieces along the blowout track and in the central melt hole. Very little oil will flow onto the top surface of the ice. A 0.3-m-thick layer of oil with a density of 890 kg/m^3 will have only about 8 mm more freeboard than a 0.3-m-thick ice sheet with a density of 910 kg/m^3 in sea water with a density of 1020 kg/m^3. Air temperatures below the oil's pour point, ice roughness, and snow on the ice will all tend to prevent the oil from spreading onto the ice surface, thus increasing the thickness of the oil pool so that oil will begin flowing beneath the ice. Approximately 50 percent of the oil (1.6×10^4 m^3) spreads in a slick in the area melted by the blowout and under the ice immediately around it during the 2.5 days when the ice does not move. The remaining 50 percent spreads beneath the ice to either side of the 15-km-long blowout track.

Beneath a perfectly smooth sheet of ice, the oil will spread until an equilibrium thickness of about 8 mm is reached everywhere. Neglecting oil on the ice surface or in the central melt hole, the 1.6×10^4 m^3 of oil released during the 2.5 days of no ice motion will cover an area of 2 km^2 (a circle with a radius of 0.8 km). This should be considered an upper limit to the size of the under-ice oil slick. In reality, the oil will cover less area than this for two reasons. First, even new, thin fast ice will contain a small amount of bottom relief in an area of 2 km^2. This relief will cause oil to pool deeper than 8 mm until it can flow beneath or around the obstruction. Second, and even more important, is the growth of new ice. Over the 2.5 days when the ice remains motionless, the ice sheet outside the oil slick will thicken by about 0.01 m/day. As the oil spreads beneath the ice near the blowout site, the ice outside that area grows thicker, providing more containment volume near the blowout. Assuming the first day's oil flow (6.4×10^3 m^3) fills an area of 0.8 km^2 to a depth of 8 mm, then 0.01 m of ice growth outside the oiled area allows the second day's oil flow to fill the same area to a greater depth, and so on for 2.5 days. Thus, the under-ice oil slick after 2.5 days may cover an area as small as 0.8 km^2.

During the 2.5 days when ice motion occurs, 1.6×10^4 m^3 of oil spreads to either side of the 15-km-long track of the blowout. Assuming a minimum oil thickness beneath the ice of 8 mm, an area of 2.0 km^2 will be oiled. This area is a strip 15 km long and 130 m wide. Ice growth will not affect the oil spread while the ice is in motion.

The currents over the inner shelf are generally too small to affect the size of the oil-contaminated area. The primary effect of currents will be to control the direction of the oil spread, not the extent of the spread.

Incorporation of Oil Into the Ice

Approximately 5 days after the oil ceases to flow, new ice growth will have completely encapsulated all the oil which spread beneath the ice. A small amount of oil (equivalent to a film about 2 mm thick) will soak into the 0.04- to 0.06-m-thick skeletal layer above the oil. The new ice growing beneath the oil layer will contain no oil. By May, when ice growth stops, about 1.4 m of ice will have grown beneath the oil.

Ice also will form beneath the oil floating on the water surface. Any oil on the ice surface will be covered by snow. The oil, being totally isolated from the water and air, will experience no weathering throughout the winter.

Some of the oiled ice will be incorporated into ridges between the time of the blowout and February, when a grounded ridge is likely to be formed which protects the oiled area from further deformation. Between November and February, about 30 percent of the ice in the area will be deformed into ridges. One of the most likely areas to be ridged is the 15-km-long strip of broken up ice extending from the blowout to the west.

Transport of Oiled Ice

The ice contaminated by oil is free to move until a ridge becomes grounded seaward of the oiled ice area. In the area 5 km north of Narwhal Island, ridges may be expected to become grounded by February. Before this happens though, the oiled ice can be moved as far as 180 km toward the west. Somewhere in this interval, it is likely that the oiled ice will become immobilized by stranded ridges.

Release of Oil From the Ice

In late February or early March, as the air temperature begins to rise, brine trapped between the columnar ice crystals will begin to drain. By late April or early May, the brine channels will have become large enough that oil will begin to appear on the ice surface. Periods of cold weather will stop the oil flow temporarily, but by late May, pools of oil will be collecting on the ice surface. Because of the lowered albedo of the oiled ice, melting of the ice surface also begins in late May.

The oil trapped in undeformed ice, being close to the ice surface, will have completely surfaced in early June. The presence of oil on the ice surface will accelerate the local ice breakup by about 2 weeks (mid-June), but grounded ridges in the area prevent any significant ice motion until mid-July.

By early to mid-July, all the undeformed ice which is contaminated by oil will have melted leaving an oil slick on the water surface. In 2 or 3 more weeks all the uncontaminated ice except for ridges will have melted.

Most of the oil trapped in ridged ice will not escape at this time. During the winter, the ridges have become consolidated masses of ice. Brine drainage and release of trapped oil will occur, but at a much slower rate than in an undeformed ice sheet. Oil which does escape from a ridge will accelerate melting of the ridge, but the ridge may still last through the summer. About 30 percent of the total oil released remains in ridges. By the end of the summer, most of the oiled ridges will be in the northern Chukchi Sea. A few securely grounded ridges may remain in place through the summer.

Fate of the Oil

As soon as oil begins to appear on the ice surface in May, weathering processes will begin. By the end of June, approximately 35 percent of the oil will have evaporated. Another 30 percent of the oil remains trapped within ridges. These ridges release oil slowly in widely scattered locations throughout the first summer and possibly through subsequent summers. This oil is in low concentrations and generally far away from the biologically productive inner shelf waters. About 35 percent of the oil remains on the water surface after the ice has melted. This oil is in several slicks scattered between Narwhal Island and Harrison Bay. Some water-in-oil emulsions will form where oil is floating on surface melt pools exposed to agitation by the winds. Other weathering processes will take place as the oil is released from the ice, but only insignificant amounts of oil will be involved. The low temperatures, the reduced wind action due to the remaining ice cover, and the thick, viscous oil layer on the water surface will act to inhibit dissolution, bacterial degradation, and dispersion.

The pack ice does not generally retreat until sometime after early July. Grounded ridges seaward of the blowout site may remain grounded until late summer, thus preventing the oil from being blown out to sea until later in the summer. Grounded ridges are not continuous along the coast though, so some oil is likely to be blown offshore into the pack ice. Most of the oil will be blown onto island or mainland beaches to the south or southwest due to the prevailing wind direction (from the east or northeast about 60 percent of the time during June).

The above scenario assumes that no cleanup of the oil takes place. If part of the oil is cleaned up following the blowout, the major change in the scenario would be a reduction in the amount of oil involved.

Oil Spill Scenario No. 3

On 1 November, about 4 weeks after freezeup, an underwater oil well blowout is assumed to occur 20 km north of Cross Island in the pack ice zone. The hypothetical blowout releases 2 x 10^5 barrels (3.18 x 10^4 m^3) of oil over a period of 5 days.

Scene

Cross Island lies about 20 km offshore of the Alaskan coast, just north of the Sagavanirktok River mouth. North of the island, new first-year ice began freezing in early to mid-October. The predominant easterly winds move and deform this ice so that by early November, the ice cover over the blowout site mostly consists of rafted and rubbled thin ice (0.2 to 0.3 m thick), and a few scattered multiyear floes. The ridge density is about 1 to 2 ridges/km. The density of ridges in the area of the blowout increases by about 1 or 2 ridges/km per month.

Ice motions during the fall are generally toward the west and range from 30 to 90 km per month. These motions are not continuous but occur during periods of high winds. Typically, the ice is motionless or nearly so about half the time and it averages about 6 km/day of motion about half the time. For the purpose of this scenario, the ice remains motionless for the first 2.5 days of the blowout and then moves at speeds of 6 km/day the final 2.5 days, with a net westward motion of 4 km/day.

Water depths in the vicinity of the blowout are about 30 m. Wind-driven currents died out as soon as the ice cover formed, and now the under-ice currents are due to the tides and the mesoscale circulation. The tidal component is weak, less than 0.01 or 0.02 m/s, and oscillatory. The geostrophic component is also weak, less than about 0.05 m/s, at depths of 10 m below the surface and generally toward the east or west, but with considerable variation. In general, measured currents just beneath the ice outside the barrier islands are small, about 0.02 to 0.03 m/s, and variable.

Water temperatures are near freezing and the 90th percentile air temperature range during early November is about -35 to -6°C.

Blowout

A ruptured casing and a fault in the bedrock allow the oil and gas to escape under the solid ice canopy some distance from the well head. The reservoir is assumed to be about 3000 m deep and the crude oil similar to a Prudhoe Bay crude (density about 890 kg/m^3 and pour point about -9.5^oC).

A total of 3.18×10^4 m^3 of crude oil escapes over a period of 5 days before control efforts successfully stop the flow. An estimated 4.8×10^6 m^3 of gas is also released. Flow rates during the 5-day blowout average 4.4 m^3/min of oil and 670 m^3/min of gas.

During the blowout, a plume of oil, gas bubbles, and entrained water rises to the surface. Gas trapped under the thin ice immediately breaks up the ice over the plume, allowing all the gas released during the blowout to escape to the atmosphere. Ice motion during the blowout does not affect the escape of the gas. Motions of 6 km/day amount to only 4 m/min, which is slow enough to allow large quantities of gas to collect under and break up the thin ice. During the 5-day blowout, the ice moves about 15 km resulting in a meandering 15-km-long strip of broken ice extending from the blowout site toward the west.

The vertical currents in the plume flow radially outward at the surface then downward at some distance from the plume to complete a closed circulation system. The downward-flowing currents entrain some water from outside the circulation system, and a weak, inward-flowing surface current is developed outside the plume region to replace this entrained water. A wave ring forms where the outward- and inward-flowing surface currents meet. For a 30-m water depth and a gas flow rate of 670 m^3/min, the diameter of this wave ring is calculated to be about 130 m.

The crude oil, at a temperature between 60 and 90^oC, contains enough heat to melt between 9.5×10^3 and 1.4×10^4 m^3 of sea ice. Since surface currents outside the wave ring tend to flow inward toward the blowout, the oil and heat will tend to concentrate inside the wave ring. However, some warm oil or heated water will escape the circulation system inside the wave ring, possibly melting the ice cover thinner or reducing the ice growth rate. The bottom water entrained in the plume is likely to be so cold in these shallow areas that it contributes little to ice melting.

For 2.5 days during the blowout, the ice remains nearly motionless, moving perhaps a few hundred meters. The warm oil released during that time contains enough heat to melt between 4.8×10^3 and 7.2×10^3 m^3 of ice. Because of heat loss to the atmosphere, the smaller quanity is probably more likely. As the ice melts, it is replaced by crude oil which has about the same density as sea ice. This volume of oil is about 15 percent of the total released during the 5-day blowout. For the remaining 2.5 days during the blowout, the ice moves 15 km and another 4.8×10^3 m^3 of ice will be melted by the warm oil released during this period. This will amount to only a few mm thickness along the track swept by the wave ring and can be ignored. For the 5-day period then, a total of about 15 percent of the oil ($\sim 4.8 \times 10^3$ m^3) is on the water surface between broken-up and partially melted ice blocks.

In general, the oil undergoes very little physical or chemical change during the blowout. Evaporation is unimportant because so little surface area is exposed to the atmosphere. Outside the blowout plume, there is no mixing energy to form emulsions. Dissolution and sedimentation occur, but probably in very insignificant amounts.

Spread of Oil Beneath the Ice

Approximately 15 percent of the oil ends up floating among the broken ice pieces along the 15 km blowout track and in the melted, broken up area formed during the stationary period. Very little oil will flow onto the top surface of the ice. A 0.3-m-thick layer of oil with a density of 890 kg/m^3 will have only about 8 mm more freeboard than a 0.3-m-thick ice sheet with a density of 910 kg/m^3 in sea water with a density of 1020 kg/m^3. Air temperatures below the oil's pour point, ice roughness, and snow on the ice will all tend to prevent the oil from spreading onto the ice surface, thus increasing the thickness of the oil pool so that oil will begin flowing beneath the ice.

Approximately 35 percent of the oil (1.3×10^4 m^3) spreads in a slick in the area under the ice immediately around the blowout during the 2.5 days when the ice does not move. The remaining 50 percent (1.6×10^4 m^3) spreads beneath the ice to either side of the 15-km-long track of broken ice during the period of ice motion.

Beneath a perfectly smooth sheet of ice, the oil will spread until an equilibrium thickness of about 8 mm is reached everywhere. Neglecting oil on the ice surface or in the central melt hole, the 1.6×10^4 m^3 of oil released during the 2.5 days of no ice motion will cover an area of 2 km^2 (a circle with a radius of 0.8 km). This should be considered an upper limit to the size of the under-ice oil slick. In reality, the oil will cover less area than this for two reasons. First, even new, thin fast ice will contain a small amount of bottom relief in an area of 2 km^2. This relief will cause oil to pool deeper than 8 mm until it can flow beneath or around the obstruction. Second, and even more important, is the growth of new ice. During the 2.5 days when the ice remains motionless, the ice sheet outside the oil slick will thicken by about 0.01 m/day. As the oil spreads beneath the ice near the blowout site, the ice outside that area grows thicker, providing more containment volume near the blowout. Assuming the first day's oil flow (6.4×10^3 m^3) fills an area of 0.8 km^2 to a depth of 8 mm, then 0.01 m of ice growth outside the oiled area allows the second day's oil flow to fill the same area to a greater depth, and so on for 2.5 days. Thus, the under-ice oil slick after 2.5 days may cover an area as small as 0.8 km^2.

During the 2.5 days when ice motion occurs, 1.6×10^4 m^3 of oil spreads to either side of the 15 km long track of the blowout. Assuming the oil spreads to an average thickness beneath the ice of 8 mm, an area of 2.0 km^2 will be oiled. This area is a strip 15 km long and 130 m wide. Ice growth will not affect the oil spread while the ice is in motion.

The currents over the inner shelf are generally too small to affect the size of the oil-contaminated area. The primary effect of currents will be to control the direction of the oil spread, not the extent of the spread.

Incorporation of Oil Into the Ice

Approximately 5 days after the oil ceases to flow, new ice growth will have completely encapsulated all the oil which spread beneath the ice. A small amount of oil (equivalent to a film about 2 mm thick) will soak into the 0.04- to 0.06-m-thick skeletal layer above the oil. The new ice growing beneath the oil layer will contain no oil.

Ice also will form beneath the oil floating on the water surface. By May, when ice growth stops, about 1.4 m of ice will have grown beneath the oil. Any oil on the ice surface will be covered by snow. The oil, being totally isolated from the water and air, will experience no weathering throughout the winter.

About 5 percent of the ice in the pack ice zone consists of thin ice in refrozen leads, which is the most likely ice to be built into ridges. During November though, all the ice in the vicinity of the blowout is thin enough to be built into ridges. Typically, about 10 percent of the ice contaminated with oil might be built into ridges. In the worst case, about 50 percent of the ice might become ridged. This would happen if all the broken up ice along the blowout track, which is weaker than the surrounding ice, were built into ridges.

Transport of Oiled Ice

During the months just after the blowout (November through January) the pack ice averages about 60 km/month of motion mostly toward the west. During the winter (February through April) motions average about half that, or 30 km/month. From May through the summer ice motions increase again with motions of more than 100 km/month possible during the summer. The direction of motion varies with a general trend toward the west.

By the end of the blowout, oil has contaminated a relatively narrow swath of ice extending about 10 km west of the blowout site. By June this oiled ice can have moved as far as 330 km further west. During the spring and summer, some of this oiled ice is almost certain to be moved into the Northern Chukchi Sea.

The oiled ice is likely to become spread over a large area during the winter. Ridges can become grounded to the west of the blowout, shifting the shear zone farther out to sea and thus immobilizing part of the oiled ice until spring or summer. In fact, the distinction between the nearshore pack ice zone and the stamukhi zone is not absolute as winter progresses, and oiled pack ice may become ridged and then grounded in shallow waters to the west.

Release of Oil From the Ice

In late February or early March, as the air temperature begins to rise, brine trapped between the columnar ice crystals will begin to drain. By late April or early May, the brine channels will have become large enough that oil will begin to appear on the ice surface. Periods of cold weather will stop the oil flow temporarily, but by late May, pools of oil will be collecting on the ice surface. Because of the lowered albedo of the oiled ice, melting of the ice surface also begins in late May.

The oil trapped in undeformed ice, being close to the ice surface, will have completely surfaced in early June. The presence of oil on the ice surface will accelerate the local ice breakup by about 2 weeks (mid-June). By early to mid-July, all the undeformed ice which is contaminated by oil will have melted leaving an oil slick on the water surface.

Most of the oil trapped in ridged ice will not escape at this time. During the winter, the ridges have become consolidated masses of ice. Brine drainage and release of trapped oil will occur, but at a much slower rate than in an undeformed ice sheet. Oil which does escape from a ridge will accelerate melting of the ridge, but the ridge may still last through the summer. About 10 percent of the total oil remains in ridges. By the end of the summer, most of the oiled ridges will be in the northern Chukchi Sea. A few securely grounded ridges may remain in place through the summer.

Fate of the Oil

As soon as oil begins to appear on the ice surface in May, weathering processes will begin. By the end of June, approximately 45 percent of the oil will have evaporated. Another 10 percent of the oil remains in ridges. These ridges release oil slowly in widely scattered locations throughout the first summer and possibly through subsequent summers. This oil is in low concentrations and generally far away from the biologically productive inner shelf waters. About 45 percent of the oil ($\sim 1.4 \times 10^4$ m^3) remains on the water surface. This oil is in several slicks scattered between Narwhal Island and Point Barrow. Some water-in-oil emulsions will form where oil is floating on surface melt pools exposed to agitation by the winds. Other weathering processes will take place as the oil is released from the ice, but only insignificant amounts of oil will be involved. The low temperatures, the reduced wind action due to the remaining ice cover, and the thick, viscous oil layer on the water surface will act to inhibit dissolution, bacterial degradation, and dispersion.

The pack ice does not generally retreat until sometime after early July. By that time, most of the oil will have been blown onto island or mainland beaches to the south or southwest due to the prevailing wind direction (from the east or northeast about 60 percent of the time during June). Of course, the probability is still high that some of the oil will be blown offshore into the permanent pack ice.

The above scenario assumes that no cleanup of the oil takes place. If part of the oil is cleaned up following the blowout, the major change in the scenario would be a reduction in the amount of oil involved.

Oil Spill Scenario No. 4

On 1 November, about 4 weeks after freezeup, an underwater oil well blowout is assumed to occur under the newly developed fast ice in Stefansson Sound. The hypothetical blowout releases 4.5 x 10^6 barrels (7.15 x 10^5 m^3) of oil over a period of 90 days.

Scene

Stefansson Sound is located inside the barrier islands within the fast ice zone. At the time of the blowout, a thin (0.2 to 0.3 m thick), continuous ice canopy extending from the shore to the barrier islands covers the sound. Winds during the freezeup period and immediately after have produced pancake floes with thick edges and some rafting and ridging has occurred, but as the ice continues to thicken, these irregularities are smoothed out. The fast ice consists of large areas of flat ice with bottom relief of 0.01 to 0.02 m, possibly with occasional areas of greater relief where rafting or ridging has occurred.

Water depths in the vicinity of the blowout are about 6 m. Wind-driven currents died out as soon as the ice cover formed and now the under-ice currents are driven by the tides and a thermohaline circulation. The tidal component is weak (less than 0.01 or 0.02 m/s) and oscillatory. The thermohaline currents produced by cold, salty water flowing offshore along the bottom are on the average small, but extremes of up to 0.11 m/s have been observed. It is postulated that an onshore current of up to 0.2 m/s must exist just beneath the ice to replace the water flowing offshore along the bottom, but this has not been observed. In general, measured currents beneath the fast ice inside the barrier islands are small, about 0.02 to 0.03 m/s, and variable.

Water temperatures in the shallow sound are near freezing and the 90th percentile air temperature range during early November is about -35 to -6°C, and about -45 to -12° by the end of January.

Blowout

A ruptured casing and a fault in the bedrock allow the oil and gas to escape under the solid ice canopy some distance from the well head. The reservoir is assumed to be about 3000 m deep and the crude oil similar to a Prudhoe Bay crude (density about 890 kg/m^3 and pour point about -9.5°C).

A total of 7.15×10^5 m^3 of crude oil escapes over a period of 90 days before control efforts successfully stop the flow. An estimated 1.07×10^8 m^3 of gas is also released. Flow rates during the 90-day blowout average 5.5 m^3/min of oil and 830 m^3/min of gas.

During the blowout, a plume of oil, gas bubbles, and entrained water rises to the surface. Gas trapped under the thin ice immediately breaks up the ice over the plume, allowing all the gas released during the blowout to escape to the atmosphere.

The vertical currents in the plume flow radially outward at the surface then downward at some distance from the plume to complete a closed circulation system. The downward-flowing currents entrain some water from outside the circulation system and a weak, inward-flowing surface current is developed outside the plume region to replace this entrained water. A wave ring forms where the outward- and inward-flowing surface currents meet. For a 6-m water depth and a gas flow rate of 830 m^3/min, the diameter of this wave ring is calculated to be about 38 m.

The crude oil, at a temperature between 60 and 90°C contains enough heat to melt between 2.1×10^5 and 3.2×10^5 m^3 of sea ice. Since surface currents outside the wave ring tend to flow inward toward the blowout, the oil and heat will tend to concentrate inside the wave ring. Some warm oil or heated water will escape the circulation system inside the wave ring, possibly melting the ice cover thinner or reducing the ice growth rate. The bottom water entrained in the plume is likely to be so cold in these shallow areas that it contributes little to ice melting.

One day's oil flow (7900 m^3) contains enough heat to melt between 2400 and 3600 m^3 of sea ice. Since the heat will be concentrated within the wave ring, the ice lying within the wave ring is melted shortly after the blowout begins. As the ice melts, it is replaced by crude oil which has about the same density as sea ice. As oil continues to be released during the 90 day blowout, much of the heat from the oil is transferred directly to the atmosphere through the hole already melted in the ice. Some heat goes into melting the ice laterally about the melt hole and some is transferred to the water column to be eventually distributed to the ice further from the blowout. The heat distributed beneath the ice will reduce or halt growth of new ice during the course of the blowout. Lateral melting of ice about the central melt hole proceeds much slower than the melting of the original hole in the ice because of the much smaller surface area exposed to the oil.

In general, the oil undergoes very little physical or chemical change during the blowout. Evaporation is unimportant because so little oil is exposed to the atmosphere. Outside the blowout plume there is no mixing energy to form emulsions. Dissolution and sedimentation occur, but probably in very insignificant amounts.

Spread of Oil Beneath the Ice

Other than the relatively small amount of oil in the central melt hole, most of the oil will spread beneath the ice. Very little oil will flow onto the top surface of the ice through cracks in the ice or the melt hole. In sea water with a density of 1020 kg/m^3 a layer of oil with a density of 890 kg/m^3 will have only 8 mm more freeboard than a 0.3 m thick ice sheet with a density of 910 kg/m^3 when the oil draft is equal to the ice draft. Air temperatures below the oil's pour point, ice roughness, and snow on the ice will all tend to prevent the oil from spreading onto the ice surface, thus increasing the thickness of the oil pool enough that oil will begin flowing beneath the ice.

Beneath a perfectly smooth sheet of ice, the oil will spread until an equilibrium thickness of about 8 mm is reached everywhere. Neglecting oil on the ice surface or in the central melt hole, 7.15×10^5 m^3 of oil will cover an area of 89 km^2 (a circle of radius 5.3 km) to a thickness of 8 mm. This should be considered an upper limit to the size of the under-ice oil slick. In reality, the oil will cover less area than this for two reasons. First, even new, thin fast ice will contain a small amount of bottom relief in an area of 89 km^2. This relief will cause oil to pool deeper than 8 mm until it can flow beneath or around the obstruction. Second, and even more important, though, is the growth of new ice. Over the 90-day blowout, the ice sheet outside the oil slick will thicken by about 0.01 m per day. By the end of January the fast ice averages 1.12 m in thickness. As the oil spreads beneath the ice near the blowout site, the ice outside that area grows thicker, providing more containment volume near the blowout. Assuming the first day's oil flow (7.9×10^3 m^3) fills an area of about 1 km^2 to a depth of 8 mm, 0.01 m of ice growth outside the oiled area allows the second day's oil flow to fill the same area to a greater depth, and so on for 90 days. As noted in the previous section, heat from the oil will aid in preventing new ice growth in this area. Thus, the final under-ice oil slick can cover an area as small as 1 km^2. The thickness of this pool of oil will be about 0.72 m. This is a lower bound to the size of the oil slick. Currents and bottom side ice roughness will tend to channel the flow of oil in the downstream direction and around obstructions. Changing current directions or increasing depth of the under ice oil pool will expose new areas to the spreading oil. New ice begins to grow beneath pools of oil under the ice 5 to 7 days after oil spread in the area ceases. For these various reasons, the oil will probably spread over an area larger than 1 km^2.

Another rough estimate to the size of the under-ice oil slick, is to assume the oil spreads in all directions (over a 90-day period) to an average depth everywhere of about 0.07 m. During the month of October, before the blowout occurs, the deformation that occurs generally takes the form of rafting. The average ice thickness of the rafted ice will be about 0.15 m. Thus over areas of several km^2 the average bottomside roughness which can trap large pools of oil is about 0.15 m. The 90-day oil spill, spread to this depth under about one half the ice covers about 10 km^2.

The currents in the nearshore area are generally too small to affect the size of the oil-contaminated area. Occasional brief currents of up to 0.2 m/s may occur. Currents of this magnitude will move an oil slick under smooth ice but not under natural sea ice with 0.01 or 0.02 m of relief and a skeletal layer of growing ice crystals. The primary effect of currents will be to control the direction of the oil spread, not the extent of the spread.

Incorporation of Oil Into the Ice

Approximately 5 to 7 days after oil ceases to flow, new ice growth will have completely encapsulated all the oil which spread beneath the ice. Due to the duration of the blowout it is likely that some areas will accumulate multiple layers of oil, separated by layers of ice. This will have no significant effect on later behavior of the oil. Very large, deep pools of oil beneath the ice may take longer to be encapsulated by ice, but this also, will have no significant effect on later behavior. A small amount of oil (equivalent to a film about 2 mm thick) will soak into the 0.04- to 0.06-m skeletal layer above the oil. The new ice growing beneath the oil layer will contain no oil.

Ice also forms beneath the oil pool in the central melt hole. Between 1 November, and May, when ice growth stops, the ice increases in thickness about 1.4 m. The ice beneath the oil will be less than 1.4 m thick, and for oil released during the end of the blowout period (late January) only about 0.5 m of ice growth can occur beneath the oil.

Any oil on the ice surface will be covered by snow. The oil, being totally isolated from the water and air, will experience no significant weathering throughout the winter.

Transport of Oiled Ice

A major storm before about mid-November can break up the fast ice behind the barrier islands. The fetch of winds in Stefansson Sound can be up to about 50 km. A wind of 8 m/s (16 knots) acting over a fetch of 50 km is required to fail 0.3-m-thick ice. In November, winds greater than 8 m/s blow only about 27 percent of the time. Larger winds are less likely and winds from some directions will have a shorter fetch. The ice cover will grow thicker and stronger daily. Therefore, the fast ice will most likely remain motionless and undeformed after mid-November.

Storms have been observed on occasion to move and deform the fast ice during early November. Even in the event of such a storm, the relatively small area of oil-contaminated ice at this stage of the blowout is unlikely to be heavily ridged or to be moved more than a few kilometers.

Release of Oil From the Ice

In late February or early March, as the air temperature begins to rise, brine trapped between the columnar ice crystals will begin to drain. By late April or early May, the brine channels will have become large enough that oil will begin to appear on the ice surface. Periods of cold weather will stop the oil flow temporarily, but by late May pools of oil will be collecting on the ice surface. Because of the lowered albedo of the oiled ice, melting of the ice surface also begins in late May.

The oil, being close to the ice surface, will have completely surfaced in early June. The presence of oil on the ice surface will accelerate the local ice breakup by about 2 weeks. Thus by mid-June, the oil-contaminated ice will have broken up enough that it can be moved by the wind. About the same time, rivers will begin flowing again, flooding the ice about the river mouths. By mid-June, shore polynyas have been melted by the flowing rivers. The most likely ice motion will be toward the shore and the area of open water.

By early to mid-July, all the ice which is contaminated by oil will have melted. In 2 or 3 more weeks all the uncontaminated ice will have melted leaving the oil slick on the water surface.

Fate of the Oil

As soon as oil begins to appear on the ice surface in May, weathering processes will begin. By the end of June, approximately 50 percent of the oil will have evaporated. Some water-in-oil emulsions will form where oil is floating on surface melt pools exposed to agitation by the winds. Other weathering processes will take place as the oil is released from the ice, but only insignificant amounts of oil will be involved. The low temperatures, the reduced wind action due to the remaining ice cover, and the thick, viscous oil layer on the water surface will act to inhibit dissolution, bacterial degradation, and dispersion. The silt carried out by the flowing rivers may increase the rate of sedimentation, though.

The pack ice does not generally retreat until sometime after early July. Grounded ridges seaward of the barrier islands may remain grounded until late summer, thus preventing the oil from being blown out to sea until later in the summer. By that time most of the oil will have been blown onto mainland beaches to the west or southwest due to the prevailing wind direction (from the east or northeast about 60 percent of the time during June). Of course, the probability is still high that some of the oil will be blown offshore onto island beaches or into the pack.

The above scenario assumes that no cleanup of the oil takes place. If part of the oil is cleaned up following the blowout, the major change in the scenario would be a reduction in the amount of oil involved.

Oil Spill Scenario No. 5

On 1 November, about 4 weeks after freezeup, an underwater oil well blowout is assumed to occur 5 km northeast of Narwhal Island in the stamukhi zone. The hypothetical blowout releases 4.5×10^6 barrels (7.15×10^5 m^3) of oil over a period of 90 days.

Scene

Narwhal Island lies about 20 km offshore of the Alaskan coast, just north of the Sagavanirktok River mouth. It is one of the barrier islands which protect the fast ice shoreward of the islands from interaction with the pack ice. Outside the islands, new first-year ice began freezing in early to mid-October. This new ice is not protected from interaction with the pack ice. The predominant easterly winds can also move and deform this ice. In early November, the ice cover over the blowout site mostly consists of rafted and rubbled thin ice (0.2- to 0.3-m thick) and a few ridges. The ridge density is about 1 to 2 ridges/km. Ice motion and deformation will continue until a ridge becomes securely grounded seaward of the blowout site. This usually occurs before January or February. The density of ridges in the area of the blowout increases by about 1 or 2 ridges/km per month so that in February there will be 5 to 10 ridges/km. The level undeformed ice increases in thickness from about 0.3 m in early November to about 1.13 m at the end of January.

Ice motions in the stamukhi zone during the fall are generally toward the west and range from 30 to 90 km/month. Average ice speeds are about 2 m/min (~3 km/day). These motions are not continuous but occur during periods of high winds. Typically, the ice is motionless or nearly so about half the time and it averages about 6 km/day of motion about half the time. The ice motion is generally towards the west but some meandering motion is to be expected as well as occasional significant motions to the east. For the purpose of this scenario, it is arbitrarily assumed that during the 90-day blowout period (November through January) each consecutive 5-day period consists of 2.5 days of no ice motion followed by 2.5 days where the total ice motion averages 6 km/day and the net westward transport averages 4 km/day. Thus, after 90 days, the original ice over the blowout ends up 180 km west of the blowout site after traveling a total of 270 km.

Water depths in the vicinity of the blowout are about 15 m. Wind-driven currents died out as soon as the ice cover formed, and now the under-ice currents are due to the tides and the mesoscale circulation. The tidal component is weak, less than 0.01 or 0.02 m/s, and oscillatory. The geostrophic component is also weak, 0.01 to 0.05 m/s, and generally toward the east or west, but with considerable variation. In general measured currents beneath the ice just outside the barrier islands are small, about 0.02 to 0.03 m/s, and variable.

Water temperatures are near freezing and the 90th percentile air temperature range during early November is about -35 to $-6^{o}C$. By the end of January, the air temperature range is about -45 to $-12^{o}C$.

Blowout

A ruptured casing and a fault in the bedrock allows the oil and gas to escape under the solid ice canopy some distance from the well head. The reservoir is assumed to be about 3000 m deep and the crude oil similar to a Prudhoe Bay crude (density about 890 kg/m^3 and pour point about $-9.5^{o}C$).

A total of 7.15×10^5 m^3 of crude oil escapes over a period of 90 days before control efforts successfully stop the flow. An estimated 1.07×10^8 m^3 of gas is also released. Flow rates during the 90-day blowout average 5.5 m^3/min of oil and 830 m^3/min of gas.

During the blowout, a plume of oil, gas bubbles, and entrained water rises to the surface. The vertical currents in the plume flow radially outward at the surface then downward at some distance from the plume to complete a closed circulation system. The downward-flowing currents entrain some water from outside the circulation system and a weak, inward-flowing surface current is developed outside the plume region to replace this entrained water. A wave ring forms where the outward- and inward-flowing surface currents meet. For a 15 m water depth and a gas flow rate of 830 m^3/min, the diameter of this wave ring is calculated to be about 82 m.

During the early part of the blowout, gas trapped under the thin ice immediately breaks up the ice over the plume, allowing all the gas to escape to the atmosphere. Ice motions of 6 km/day are slow enough not to affect ice breakage by the gas. During the later part of the blowout, thicker ice will be passing over the blowout. When the ice cover is motionless or moving very slowly, the trapped gas will still break up this thicker ice. When thick ice is passing over the blowout at higher speeds though, the gas may not consistently break up the ice. Then the gas and oil from the blowout may spread beneath the ice until the gas reaches a natural weakness in the ice cover.

The crude oil, at a temperature between 60 and 90°C contains enough heat to melt between 2.1×10^5 and 3.2×10^5 m^3 of sea ice. Since surface currents outside the wave ring tend to flow inward toward the blowout, the oil, and heat, will tend to concentrate inside the wave ring. Some warm oil or heated water will escape the circulation system inside the wave ring, possibly melting the ice cover thinner or reducing the ice growth rate. The bottom water entrained in the plume is likely to be so cold in these shallow areas that it contributes little to ice melting.

One day's oil flow (7900 m^3) contains enough heat to melt between 2400 and 3600 m^3 of sea ice, or in 0.3 m thick ice, a circular area between 100 and 120 m in diameter. Since the heat will be concentrated within the 82-m-diameter wave ring, the ice lying within the wave ring is melted first. As the ice melts, it is replaced by crude oil which has about the same density as sea ice. As oil continues to be released during periods of no ice motion, much of the heat from the oil is transferred directly to the atmosphere through the hole already melted in the ice. Some heat goes into melting the ice laterally about the melt hole and some is transferred to the water column to be eventually distributed to the ice further from the blowout. The heat distributed beneath the ice will reduce or halt growth of new ice during the course of the blowout. Lateral melting of ice about the central melt hole proceeds much slower than the melting of the original hole in the ice because of the much smaller surface area exposed to the oil.

Toward the end of the blowout in January, the ice is roughly 1.1 m in thickness. The heat contained in the oil released during 2.5 days at that time will melt a hole roughly 80 to 100 m in diameter through 1.1 m thick ice. Again, the maximum size of the melt hole will probably not be larger than the size of the wave ring with the surplus heat escaping to the atmosphere or the water column. If during each 2.5 day period when the ice remains in place over the blowout, all the ice within the 82 m diameter wave ring is melted, the amount of ice melted increases from 1600 m^3 in 2.5 days at the start of the blowout to 5800 m^3 in 2.5 days at the end of the blowout. Approximately 10 percent of the total oil released during the 90-day blowout ends up in 18 separate melt holes spaced about 10 km apart.

During the periods when the ice cover is moving over the blowout, ice melting will take place but the amount of ice melted will average from 5 to 7 mm in thickness along the track swept by the wave ring. This can be ignored in terms of oil dispersion under the ice.

In general, the oil undergoes very little physical or chemical change during the blowout. Evaporation is unimportant because so little oil is exposed to the atmosphere. Outside the blowout plume there is no mixing energy to form emulsions. Dissolution and sedimentation occur, but probably in very insignificant amounts.

<u>Spread of Oil Beneath the Ice</u>

Other than the relatively small amount of oil in the central melt hole, most of the oil will spread beneath the ice. Very little oil will flow onto the top surface of the ice through cracks in the ice or the melt hole. In sea water with a density of 1020 kg/m^3 a layer of oil with a density of 890 kg/m^3 will have only 9 mm more freeboard than a 0.3-m-thick ice sheet with a density of 910 kg/m^3 when the oil draft is equal to the ice draft. Air temperatures below the oil's pour point, ice roughness, and snow on the ice will all tend to prevent the oil from spreading onto the ice surface, thus increasing the thickness of the oil pool enough that oil will begin flowing beneath the ice.

During the first 2.5 day period when the ice remains motionless over the blowout, about 1,600 m^3 of oil replaces melted ice inside the wave ring area. The remaining 1.8 x 10^4 m^3 of oil released during that 2.5 days spreads beneath the ice about the blowout. The oil spreads over an area of about 2.25 km^2 to an average depth of 8 mm. At the end of the blowout, ice thickness has increased so that 6,000 m^3 of oil accumulates in the melt hole over a 2.5 day period and 1.4 x 10^4 m^3 of oil spreads beneath the surrounding ice. The ice roughness has also increased so that now the oil can form deep pools beneath the ice (about 0.113 m deep), but averages only 0.036 m deep over an area of about 0.39 km^2. Typically then, a 2.5 day period of no ice motion allows oil to spread beneath the ice over about 1 km^2 to an average depth of about 18 mm. During the 45 days of the blowout when the ice is motionless about 18 km^2 of ice would be contaminated with oil. This assumes that no significant amount of gas remains trapped beneath the ice. Ridges will tend to restrict the spread of oil during December and January. Ice growth also restricts oil spread when the ice is not moving.

During the periods when the ice is in motion, and assuming that all the gas escapes, about 4.9 x 10^5 m^2 of ice is swept by the wave ring each day. One days oil flow (7900 m^3) would cover that area to a depth of 0.016 m. Due to ice melt and naturally occurring ice roughness the oil will generally not spread beyond this area. For the 45 days when ice motion occurs, a total of 22 km^2 of ice is contaminated by oil. Thus, during the entire 90 day blowout, at most 40 km^2 of ice is contaminated by oil. About 10 percent of the total oil released is in the 18 melt holes produced during periods of no ice motion.

The currents over the inner shelf are generally too small to affect the size of the oil-contaminated area. The primary effect of currents will be to control the direction of the oil spread, not the extent of the spread.

Incorporation of Oil Into the Ice

Approximately 5 to 7 days after the oil ceases to flow, new ice growth will have completely encapsulated all the oil which spread beneath the ice. A small amount of oil (equivalent to a film about 2 mm thick) will soak into the 0.04- to 0.06-m-thick skeletal layer above the oil. The new ice growing beneath the oil layer will contain no oil.

Ice also will form beneath the oil floating on the water surface in the melt holes formed when the ice cover remained stationary over the blowout. By May, when ice growth stops, as much as 1.4 m of ice will have grown beneath the oil. Any oil on the ice surface will be covered by snow. The oil, being totally isolated from the water and air, will experience no weathering throughout the winter.

Some of the oiled ice will be incorporated into ridges between the time of the blowout and February, when a grounded ridge is likely to be formed which protects the oiled area from further deformation. Between November and February, about 30 percent of the ice in the area will be deformed into ridges, but since oil is released continuously over 90 days, only about 15 percent of the oiled ice will be built into ridges by the end of the blowout or soon after.

Transport of Oiled Ice

The ice contaminated by oil is free to move until a ridge becomes grounded seaward of the oiled ice area. The grounded ridge will stabilize the ice lying toward shore. In the area 5 km north of Narwhal Island, ridges may be expected to become grounded by February. Before this happens though, the oiled ice can be moved as far as 180 km toward the west. Somewhere in this interval, it is likely that the oiled ice will become immobilized by stranded ridges.

Release of Oil From the Ice

In late February or early March, as the air temperature begins to rise, brine trapped between the columnar ice crystals will begin to drain. By late April or early May, the brine channels will have become large enough that oil will begin to appear on the ice surface. Periods of cold weather will stop the oil flow temporarily, but by late May, pools of oil will be collecting on the ice surface. Because of the lowered albedo of the oiled ice, melting of the ice surface also begins in late May.

The oil trapped in undeformed ice, being close to the ice surface, will have completely surfaced in early June. The presence of oil on the ice surface will accelerate the local ice breakup by about 2 weeks (mid-June), but grounded ridges in the area prevent any significant ice motion until mid-July.

By early to mid-July, all the undeformed ice which is contaminated by oil will have melted leaving an oil slick on the water surface. In 2 or 3 more weeks all the uncontaminated ice except for ridges will have melted.

Most of the oil trapped in ridged ice will not escape at this time. During the winter, the ridges have become consolidated masses of ice. Brine drainage and release of trapped oil will occur, but at a much slower rate than in an undeformed ice sheet. Oil which does escape from a ridge will accelerate melting of the ridge, but the ridge may still last through the summer. About 15 percent of the total oil released remains in ridges. By the end of the summer, most of the oiled ridges will be in the northern Chukchi Sea. A few securely grounded ridges may remain in place through the summer.

Fate of the Oil

As soon as oil begins to appear on the ice surface in May, weathering processes will begin. By the end of June, approximately 42 percent of the oil will have evaporated. About 15 percent of the oil remains trapped within ridges. These ridges release oil slowly in widely scattered locations throughout the first summer and possibly through subsequent summers. This oil is in low concentrations and generally far away from the biologically productive inner shelf waters. About 42 percent of the oil remains on the water surface after the ice has melted. This oil is in several slicks scattered as far as 180 km west of Narwhal Island. Some water-in-oil emulsions will form where oil is floating on surface melt pools exposed to agitation by the winds. Other weathering processes will take place as the oil is released from the ice, but only insignificant amounts of oil will be involved. The low temperatures, the reduced wind action due to the remaining ice cover, and the thick, viscous oil layer on the water surface will act to inhibit dissolution, bacterial degradation, and dispersion.

The pack ice does not generally retreat until sometime after early July. Grounded ridges seaward of the blowout site may remain grounded until late summer, thus preventing the oil from being blown out to sea until later in the summer. Grounded ridges are not continuous along the coast though, so some oil is likely to be blown offshore into the pack ice. Most of the oil will have been blown onto island or mainland beaches to the south or southwest due to the prevailing wind direction (from the east or northeast about 60 percent of the time during June).

The above scenario assumes that no cleanup of the oil takes place. If part of the oil is cleaned up following the blowout, the major change in the scenario would be a reduction in the amount of oil involved.

Oil Spill Scenario No. 6

On 1 November, about 4 weeks after freezeup, an underwater oil well blowout is assumed to occur 20 km north of Cross Island in the pack ice zone. The hypothetical blowout releases 4.5×10^6 barrels (7.15×10^5 m^3) of oil over a period of 90 days.

Scene

Cross Island lies about 20 km offshore of the Alaskan coast, just north of the Sagavanirktok River mouth. North of the island, new first-year ice began freezing in early to mid-October. The predominantly easterly winds move and deform this ice so that by early November, the ice cover over the blowout site consists mostly of rafted and rubbled thin ice (0.2- to 0.3-m thick), and a few scattered multiyear floes about 3 m thick. The ridge density of the near shore pack ice is about 1 to 2 ridges/km and increases by about 1 or 2 ridges/km per month. By the end of January the ridge density will be about 5 to 10 ridges/km. The level undeformed ice increases in thickness from about 0.3 m in early November to about 1.13 m at the end of January.

Ice motions in the near shore fast ice zone during the fall are generally toward the west and range from 30 to 90 km per month. These motions are not continuous but occur during periods of high winds. Typically, the ice is motionless or nearly so about half the time and it averages about 6 km/day of motion about half the time. The ice motion is generally towards the west but some meandering motion is to be expected as well as occasional significant motions to the east. For the purpose of this scenario, it is arbitrarily assumed that during the 90-day blowout period (November through January) each consecutive 5-day period consists of 2.5 days of no ice motion followed by 2.5 days where the total ice motion averages 6 km/day and the net westward transport averages 4 km/day. Thus, after 90 days, the original ice over the blowout ends up 180 km west of the blowout site after traveling a total of 270 km.

Water depths in the vicinity of the blowout are about 30 m. Wind-driven currents died out as soon as the ice cover formed, and now the under-ice currents are due to the tides and the mesoscale circulation. The tidal component is weak, less than 0.01 or 0.02 m/s, and oscillatory. The geostrophic component is also weak, less than about 0.5 m/s, at depths of 10 m below the surface and generally toward the east or west, but with considerable variation. In general, measured currents just beneath the ice outside the barrier islands are small, about 0.02 to 0.03 m/s, and variable.

Water temperatures are near freezing and the 90th percentile air temperature range during early November is about -35 to $-6^{\circ}C$. By the end of January, the air temperature range is about -45 to $-12^{\circ}C$.

Blowout

A ruptured casing and a fault in the bedrock allows the oil and gas to escape under the solid ice canopy some distance from the well head. The reservoir is assumed to be about 3000 m deep and the crude oil similar to a Prudhoe Bay crude (density about 890 kg/m^3 and pour point about $-9.5^{\circ}C$).

A total of 7.15×10^5 m^3 of crude oil escapes over a period of 90 days before control efforts successfully stop the flow. An estimated 1.07×10^8 m^3 of gas is also released. Flow rates during the 90-day blowout average 5.5 m^3/min of oil and 830 m^3/min of gas.

During the blowout, a plume of oil, gas bubbles, and entrained water rises to the surface. During the early part of the blowout, gas trapped under the thin ice immediately breaks up the ice over the plume, allowing all the gas to escape to the atmosphere. Ice motions of 6 km/day are slow enough not to affect ice breakage by the gas. During the later part of the blowout, thicker ice will be passing over the blowout. When the ice cover is motionless or moving very slowly, the trapped gas will still breakup this thicker ice. When thick ice is passing over the blowout at higher speeds though, the gas may not consistently breakup the ice. Then the gas and oil from the blowout may spread beneath the ice until the gas reaches a natural weakness in the ice cover.

The vertical currents in the plume flow radially outward at the surface then downward at some distance from the plume to complete a closed circulation system. The downward-flowing currents entrain some water from outside the circulation system and a weak, inward-flowing surface current is developed outside the plume region to replace this entrained water. A wave ring forms where the outward- and inward-flowing surface currents meet. For a 30 m water depth and a gas flow rate of 830 m^3/min, the diameter of this wave ring is calculated to be about 140 m.

The crude oil, at a temperature between 60 and 90°C contains enough heat to melt between 2.1×10^5 and 3.2×10^5 m^3 of sea ice. Since surface currents outside the wave ring tend to flow inward toward the blowout, the oil, and heat, will tend to concentrate inside the wave ring. Some warm oil or heated water will escape the circulation system inside the wave ring, possibly melting the ice cover thinner or reducing the ice growth rate. The bottom water entrained in the plume is likely to be so cold in these shallow areas that it contributes little to ice melting.

The oil released during 2.5 days contains enough heat to melt between 6×10^3 and 9×10^3 m^3 of sea ice, or in 0.3 m thick ice, a circular area between 160 and 200 m in diameter. Since the heat will be concentrated within the wave ring, the ice lying within the wave ring is melted shortly after the blowout begins. As the ice melts, it is replaced by crude oil which has about the same density as sea ice. As oil continues to be released during periods of no ice motion, much of the heat from the oil is transferred directly to the atmosphere through the hole already melted in the ice. Some heat goes into melting the ice laterally about the melt hole and some is transferred to the water column to be eventually distributed to the ice further from the blowout. The heat distributed beneath the ice will reduce or halt growth of new ice during the course of the blowout. Lateral melting of ice about the central melt hole proceeds much slower than the melting of the original hole in the ice because of the much smaller surface area exposed to the oil.

Toward the end of the blowout in January, the first-year ice passing over the blowout is roughly 1.1 m in thickness. The heat contained in the oil released during 2.5 days at that time will not melt all the ice within the wave ring. The maximum amount of ice melted will probably not be larger than about 6×10^3 m^3, with any surplus heat escaping to the atmosphere or the water column. The amount of the first year ice melted increases from 4.6×10^3 m^3 in 2.5 days at the start of the blowout to 6,000 m^3 in 2.5 days at the end of the blowout. Approximately 13 percent of the total oil released during the 90-day blowout ends up in 18 separate melt holes spaced about 10 km apart.

During the periods when the ice cover is moving over the blowout, ice melting will take place but the amount of ice melted will average from 3 to 4 mm thickness along the track swept by the wave ring. This can be ignored in terms of oil dispersion under the ice.

In general, the oil undergoes very little physical or chemical change during the blowout. Evaporation is unimportant because so little oil is exposed to the atmosphere. Outside the blowout plume there is no mixing energy to form emulsions. Dissolution and sedimentation occur, but probably in very insignificant amounts.

Spread of Oil Beneath the Ice

Other than the relatively small amount of oil in the central melt hole, most of the oil will spread beneath the ice. Very little oil will flow onto the top surface of the ice through cracks in the ice or the melt hole. In sea water of density 1020 kg/m^3 a layer of oil of density 890 kg/m^3 will have only 9 mm more freeboard than a 0.3-m-thick ice sheet with density 910 kg/m^3 when the oil draft is equal to the ice draft. Air temperatures below the oil's pour point, ice roughness, and snow on the ice will all tend to prevent the oil from spreading onto the ice surface, thus increasing the thickness of the oil pool enough that oil will begin flowing beneath the ice.

During the first 2.5 day period when the ice remains motionless over the blowout, about 4.6×10^3 m^3 of oil replaces melted ice inside the wave ring area. The remaining 1.5×10^4 m^3 of oil released during that time spreads beneath the ice about the blowout. The oil spreads over an area of about 1.9 km^2 to an average depth of 8 mm. At the end of the blowout, ice thickness has increased so that 6×10^3 m^3 of oil accumulates in the melt hole over a 2.5 day period and 1.4×10^4 m^3 of oil spreads beneath the surrounding ice. The ice roughness has also increased so that now the oil can form pools beneath the ice about

0.11 m deep, but averages only 0.035 m deep over an area of about 0.4 km^2. Typically then, a 2.5 day period of no ice motion allows oil to spread beneath the ice over an area of about 1 km^2 to depths of 8 to 35 mm. During the 45 days of the blowout when the ice is motionless a maximum of about 18 km^2 of ice would be contaminated with oil. This assumes that no significant amount of gas remains trapped beneath the ice. Ridges will tend to restrict the spread of oil during December and January. Ice growth also restricts oil spread when the ice is not moving. Allowing for ice growth, as little as 10 km^2 would be contaminated with oil during the periods of little ice motion.

During the periods when the ice is in motion, and assuming that all the gas escapes, about 8.4×10^5 m^2 of ice is swept by the blowout wave ring each day. One days oil flow (7.9×10^3 m^3) would cover that area to a depth of 9 mm. Due to ice melt and naturally occurring ice roughness the oil will generally not spread beyond this area. When multiyear floes pass over the blowout, the width of the contaminated area will increase due to large quantities of trapped gases. As the gas spreads beneath the ice, it eventually finds a weakness and can escape. For the 45 days when ice motion occurs, a total of 38 km^2 of ice is contaminated by oil. Thus, during the entire 90-day blowout, at most about 56 km^2 of ice is contaminated by oil. About 13 percent of the total oil released is in the 18 melt holes produced during periods of no ice motion.

The currents over the inner shelf are generally too small to affect the size of the oil-contaminated area. The primary effect of currents will be to control the direction of the oil spread, not the extent of the spread.

Incorporation of Oil Into the Ice

Approximately 5 to 7 days after the oil ceases to flow, new ice growth will have completely encapsulated all the oil which spread beneath the ice. A small amount of oil (equivalent to a film about 2 mm thick) will soak into the 0.04- to 0.06-m-thick skeletal layer above the oil. The new ice growing beneath the oil layer will contain no oil.

Ice also will form beneath any oil floating on the water surface. By May, when ice growth stops, as much as 0.5 m of ice will have grown beneath the oil. Any oil on the ice surface will be covered by snow. The oil, being totally isolated from the water and air, will experience no weathering throughout the winter.

About 5 percent of the ice in the pack ice zone consists of thin ice in refrozen leads, which is the most likely ice to be built into ridges. During November, though, all the ice in the vicinity of the blowout is thin enough to be built into ridges. Typically, about 10 percent of the ice contaminated with oil might be built into ridges. In the worst case, about 50 percent of the ice might become ridged. This would happen if all the broken up ice along the blowout track, which is weaker than the surrounding ice, were built into ridges.

Transport of Oiled Ice

During the course of the blowout (November through January) the pack ice averages about 60 km/month of motion mostly toward the west. During the winter (February through April) motions average about half that, or 30 km/month. From May through the summer ice motions increase again with motions of more than 100 km/month possible during the summer. The direction of motion varies with a general trend toward the west.

By the end of the blowout, then, oil has contaminated a relatively narrow swath of ice extending as far as 180 km west of the blowout site. By May this oiled ice can have moved as far as 90 km further west. During the spring and summer, some of this oiled ice is almost certain to be moved into the northern Chukchi Sea.

The oiled ice is likely to become spread over a large area during the winter. Ridges can become grounded to the west of the blowout, shifting the shear zone farther out to sea and thus immobilizing part of the oiled ice until spring or summer. In fact, the distinction between the nearshore pack ice zone and the stamukhi zone is not absolute as winter progresses, and oiled pack ice may become ridged and then grounded in shallow waters to the west.

Release of Oil From the Ice

In late February or early March, as the air temperature begins to rise, brine trapped between the columnar ice crystals will begin to drain. By late April or early May, the brine channels will have become large enough that oil will begin to appear on the ice surface. Periods of cold weather will stop the oil flow temporarily, but by late May, pools of oil will be collecting on the ice surface. Because of the lowered albedo of the oiled ice, melting of the ice surface also begins in late May.

The oil trapped in undeformed ice, being close to the ice surface, will have completely surfaced in early June. The presence of oil on the ice surface will accelerate the local ice breakup by about 2 weeks (mid-June). By early to mid-July, all the undeformed ice which is contaminated by oil will have melted leaving an oil slick on the water surface.

Most of the oil trapped in ridged ice will not escape at this time. During the winter, the ridges have become consolidated masses of ice. Brine drainage and release of trapped oil will occur, but at a much slower rate than in an undeformed ice sheet. Oil which does escape from a ridge will accelerate melting of the ridge, but the ridge may still last through the summer. About 10 percent of the total oil released remains in ridges. By the end of the summer, most of the oiled ridges will be in the northern Chukchi Sea. A few securely grounded ridges may remain in place through the summer.

Fate of the Oil

As soon as oil begins to appear on the ice surface in May, weathering processes will begin. By the end of June, approximately 45 percent of the oil which has surfaced will have evaporated. About 10 percent of the oil remains in ridges. These ridges release oil slowly in widely scattered locations throughout the first summer and possibly through subsequent summers. This oil is in low concentrations and generally far away from the biologically productive inner shelf waters. About 45 percent of the oil ($\sim 3.2 \times 10^5$ m^3) remains on the water surface. This oil is in several slicks scattered between Narwhal Island and Point Barrow.

Some water-in-oil emulsions will form where oil is floating on surface melt pools exposed to agitation by the winds. Other weathering processes will take place as the oil is released from the ice, but only insignificant amounts of oil will be involved. The low temperatures, the reduced wind action due to the remaining ice cover, and the thick, viscous oil layer on the water surface will act to inhibit dissolution, bacterial degradation, and dispersion.

The pack ice does not generally retreat until sometime after early July. By that time, most of the oil will have been blown onto island or mainland beaches to the south or southwest due to the prevailing wind direction (from the east or northeast about 60 percent of the time during June). Of course, the probability is still high that some of the oil will be blown offshore into the permanent pack ice.

The above scenario assumes that no cleanup of the oil takes place. If part of the oil is cleaned up following the blowout, the major change in the scenario would be a reduction in the amount of oil involved.

Oil Spill Scenario No. 7

On 31 March, just at the end of the drilling season, an underwater oil well blowout is assumed to occur under the fast ice in Stefansson Sound. The hypothetical blowout releases 2×10^5 barrels (3.18×10^4 m^3) of oil over a period of 5 days.

Scene

Stefansson Sound is located inside the barrier islands within the fast ice zone. At the time of the blowout, a continuous ice canopy about 1.5 m thick extending from the shore to the barrier islands covers the sound. Winds during the freezeup period and immediately after produced much small-scale relief, such as rafted floes but, as the ice season progresses the primary under-ice relief is due to differential ice growth beneath variations in the snow cover. By the end of March, these undulations in the bottom surface of the ice provide an average containment volume of 4.8×10^4 m^3/km^2.

Water depths in the vicinity of the blowout are about 6 m. Wind-driven currents died out as soon as the ice cover formed and now the under-ice currents are driven by the tides and a thermohaline circulation. The tidal component is weak (less than 0.01 or 0.02 m/s) and oscillatory. The thermohaline currents produced by cold, salty water flowing offshore along the bottom are on the average small, but extremes of up to 0.11 m/s have been observed. It is postulated that an onshore current of up to 0.2 m/s must exist just beneath the ice to replace the water flowing offshore along the bottom, but this has not been observed. By the end of March, ice growth is slow and the thermohaline circulation much less important. In general, measured currents beneath the fast ice inside the barrier islands are small, about 0.02 to 0.03 m/s, and variable.

Water temperatures in the shallow sound are near freezing and the 90th percentile air temperature range for early April is about -36 to -11°C. By the end of June, the air temperature range is -2 to +11°C.

Blowout

A ruptured casing and a fault in the bedrock allow the oil and gas to escape under the solid ice canopy some distance from the well head. The reservoir is assumed to be about 3000 m deep and the crude oil similar to a Prudhoe Bay crude (density about 890 kg/m^3 and pour point about $-9.5^{o}C$).

A total of 3.18×10^4 m^3 of crude oil escapes over a period of 5 days before control efforts successfully stop the flow. An estimated 4.8×10^6 m^3 of gas is also released. Flow rates during the 5-day blowout average 4.4 m^3/min of oil and 670 m^3/min of gas.

During the blowout, a plume of oil, gas bubbles, and entrained water rises to the surface. Gas trapped under the ice soon breaks up the ice over the plume, allowing all the gas released during the blowout to escape to the atmosphere.

The vertical currents in the plume flow radially outward at the surface then downward at some distance from the plume to complete a closed circulation system. The downward-flowing currents entrain some water from outside the circulation system and a weak, inward-flowing surface current is developed outside the plume region to replace this entrained water. A wave ring forms where the outward- and inward-flowing surface currents meet. For a 6-m water depth and a gas flow rate of 670 m^3/min, the diameter of this wave ring is calculated to be about 35 m.

The crude oil, at a temperature between 60 and $90^{o}C$ contains enough heat to melt between 9.5×10^3 and 1.4×10^4 m^3 of sea ice. Since surface currents outside the wave ring tend to flow inward toward the blowout, the oil and heat will tend to concentrate inside the wave ring. Some warm oil or heated water will escape the circulation system inside the wave ring, possibly melting the ice cover thinner or reducing the ice growth rate. The bottom water entrained in the plume is likely to be so cold in these shallow areas that it contributes little to ice melting.

Approximately 1.4×10^3 m^3 of ice lies within the wave ring. This ice is completely melted during the course of the blowout. As the ice melts, it is replaced by crude oil which has about the same density as sea ice. This volume of oil is only about 4.4 percent of the total released during the blowout.

In general, the oil undergoes very little physical or chemical change during the blowout. Evaporation is unimportant because so little oil is exposed to the atmosphere. Outside the blowout plume there is no mixing energy to form emulsions. Dissolution and sedimentation occur, but probably in very insignificant amounts.

Spread of Oil Beneath the Ice

Other than the relatively small amount of oil in the central melt hole, most of the oil will spread beneath the ice. Very little oil will flow onto the top surface of the ice through cracks in the ice or the melt hole. A 1.5-m-thick layer of oil with a density of 890 kg/m^3 will have only about 0.04 m more freeboard than a 1.5-m-thick ice sheet with a density of 910 kg/m^3 in sea water with a density of 1020 kg/m^3. Air temperatures below the oil's pour point, ice roughness, and snow on the ice will all tend to prevent the oil from spreading onto the ice surface, thus increasing the thickness of the oil pool enough that oil will begin flowing beneath the ice.

By the end of March, the 1.5-m-thick first-year fast ice has an average roughness amplitude of about 0.3 m. Ice with this amount of roughness has the potential of containing about 4.8×10^4 m^3/km^2 of oil. Thus, 3.18×10^4 m^3 of oil from the blowout spreads to cover only 0.66 km^2 of ice, or slightly less when the oil contained in the central melt hole is taken into account. Ice growth is very slow in April, and changes in containment potential during the 5-day blowout can be neglected.

The currents in the nearshore area are generally too small to affect the size of the oil-contaminated area. Occasional brief currents of up to 0.2 m/s may occur. Currents of this magnitude will move an oil slick under smooth ice but not under natural sea ice with 0.3 m of relief and a skeletal layer of growing ice crystals. The primary effect of currents will be to control the direction of the oil spread, not the extent of the spread.

Incorporation of Oil Into the Ice

Approximately 10 days after oil ceases to flow, new ice growth will have completely encapsulated the oil which spread beneath the ice. A small amount of oil (equivalent to a film about 2 mm thick) will soak into the 0.04- to 0.06-m-thick skeletal layer above the oil. The new ice growing beneath the oil layer will contain no oil.

Ice also forms beneath the oil pool in the central melt hole. By May, when ice growth stops, only about 0.1 m of ice will have grown beneath the oil.

Any oil on the ice surface may be partially covered by blowing snow. The oil encapsulated within the ice, being totally isolated from the water and air, will experience no weathering throughout the remainder of the winter.

Transport of Oiled Ice

No significant ice motion takes place in the fast ice zone between the blowout in late March-early April and about mid-June. At that time, oil-contaminated ice will have broken up enough to be moved by the winds.

Release of Oil From the Ice

In late February or early March, as the air temperature began to rise, brine trapped between the columnar ice crystals began to drain. By late April or early May, the brine channels will have become large enough that oil will begin to appear on the ice surface. Periods of cold weather will stop the oil flow temporarily, but by late May pools of oil will be collecting on the ice surface. Because of the lowered albedo of the oiled ice, melting of the ice surface also begins in late May.

The oil, being close to the ice surface, will have completely surfaced in early June. The presence of oil on the ice surface will accelerate the local ice breakup by about 2 weeks. Thus, by mid-June, the oil-contaminated ice will have broken up enough that it can be moved by the wind. About the same time, rivers will begin flowing again, flooding the ice about the river mouths. By mid-June, shore polynyas will have been melted by the flowing rivers. The most likely ice motion will be toward the shore and the area of open water.

By early to mid-July, all the ice which is contaminated by oil will have melted. In 2 or 3 more weeks all the uncontaminated ice will have melted leaving the oil slick on the water surface.

Fate of the Oil

As soon as oil begins to appear on the ice surface in May, weathering processes will begin. By the end of June, approximately 50 percent of the oil will have evaporated. Some water-in-oil emulsions will form where oil is floating on surface melt pools exposed to agitation by the winds. Other weathering processes will take place as the oil is released from the ice, but only insignificant amounts of oil will be involved. The low temperatures, the reduced wind action due to the remaining ice cover, and the thick, viscous oil layer on the water surface will act to inhibit dissolution, bacterial degradation, and dispersion. The silt carried out by the flowing rivers may increase the rate of sedimentation, though.

The pack ice does not generally retreat until sometime after early July. Grounded ridges seaward of the barrier islands may remain grounded until late summer; thus preventing the oil from being blown out to sea at least until later in the summer. By that time most of the oil will have been blown onto mainland beaches to the west or southwest due to the prevailing wind direction (from the east or northeast about 60 percent of the time during June). Of course, the probability is still high that some of the oil will be blown offshore onto island beaches or into the pack.

The above scenario assumes that no cleanup of the oil takes place. If part of the oil is cleaned up following the blowout, the major change in the scenario would be a reduction in the amount of oil involved.

Oil Spill Scenario No. 8

On 31 March, just at the end of the drilling season, an underwater oil well blowout is assumed to occur 5 km northeast of Narwhal Island in the stamukhi zone. The hypothetical blowout releases 2 x 10^5 barrels (3.18 x 10^4 m^3) of oil over a period of 5 days.

Scene

Narwhal Island lies about 20 km offshore of the Alaskan coast, just north of the Sagavanirktok River mouth. It is one of the barrier islands which protect the fast ice shoreward of the islands from interaction with the pack ice. The ice cover outside the barrier islands has been subject to much ridge building activity during the preceeding fall and winter. By the end of March, there are approximately 6 to 12 ridges/km in the area of the blowout. Many of these ridges are grounded, so no significant ice motions occur until the following summer. The ridges generally run parallel to the shore, but intersecting ridges tend to divide the area into large irregular areas of flat ice. On the average there is from 65 to 150 m of flat ice between ridges. The flat ice is mostly first-year ice about 1.5 m thick.

Water depths in the vicinity of the blowout are about 15 m. Wind-driven currents died out as soon as the ice cover formed, and now the under-ice currents are due to the tides and the mesoscale circulation. The tidal component is weak, less than 0.01 or 0.02 m/s, and oscillatory. The geostrophic component is also weak, 0.01 to 0.05 m/s, and generally toward the east or west, but with considerable variation. In general, measured currents beneath the ice just outside the barrier islands are small, about 0.02 to 0.03 m/s, and variable.

Water temperatures are near freezing and the 90th percentile air temperature range during early April is about -36 to -11°C, warming up to -2 to +11°C by the end of June.

Blowout

A ruptured casing and a fault in the bedrock allow the oil and gas to escape under the solid ice canopy some distance from the well head. The reservoir is assumed to be about 3000 m deep and the crude oil similar to a Prudhoe Bay crude (density about 890 kg/m^3 and pour point about -9.5°C).

A total of 3.18×10^4 m^3 of crude oil escapes over a period of 5 days before control efforts successfully stop the flow. An estimated 4.8×10^6 m^3 of gas is also released. Flow rates during the 5-day blowout average 4.4 m^3/min of oil and 670 m^3/min of gas.

During the blowout, a plume of oil, gas bubbles, and entrained water rises to the surface. The vertical currents in the plume flow radially outward at the surface then downward at some distance from the plume to complete a closed circulation system. The downward-flowing currents entrain some water from outside the circulation system, and a weak, inward-flowing surface current is developed outside the plume region to replace this entrained water. A wave ring forms where the outward- and inward-flowing surface currents meet. For a 15-m water depth and a gas flow rate of 670 m^3/min, the diameter of this wave ring is calculated to be about 76 m.

The escaping gas and the turbulent blowout plume may not immediately break up the ice canopy overhead. But gas is escaping at the rate of 670 m^3/min and the surrounding ridges will be able to hold most of the gas within a few thousand square meters area. The ice will also be weakened by cracks generated by thermal contraction. Thus, within a short time a large submerged gas bubble forms, causing the ice sheet overhead to bend and break. Thereafter, the vast majority of the gas from the blowout will escape to the atmosphere. Once the escaping gas is vented to the atmosphere, the oil from the blowout will begin to collect under and between ice floes near the blowout.

The crude oil, at a temperature between 60 and 90°C, contains enough heat to melt between 9.6×10^3 and 14.4×10^3 m^3 of sea ice. In 1.5-m-thick ice, this is equivalent to a circle between 44 and 66 m in diameter. Since surface currents outside the wave ring tend to flow inward toward the blowout, the oil and heat will tend to concentrate inside the wave ring. However, some warm oil or heated water will escape the circulation system inside the wave ring, possibly melting the ice cover thinner or reducing the ice growth rate. The bottom water entrained in the plume is likely to be so cold in these shallow areas that it contributes little to ice melting. Much of the ice within the wave ring will be melted by the warm oil and an area of open water will possibly develop. This open-water area will not be large, though.

In general, the oil undergoes very little physical or chemical change during the blowout. Evaporation is unimportant because so little oil is exposed to the atmosphere. Outside the blowout plume, there is no mixing energy to form emulsions. Dissolution and sedimentation occur, but probably in very insignificant amounts.

Spread of Oil Beneath the Ice

Assuming that the oil melts a minimum of 9.6×10^3 m^3 of ice directly over the blowout, then 30 percent or more of the total oil released will be able to replace this melted ice and remain in the immediate vicinity of the blowout. Some of this oil will be on the water surface in the central melt hole or in cracks through the ice. The spread of oil onto the upper surface of the ice will depend upon the depth to which oil can pool beneath the ice. In an opening through 1.5-m-thick ice with a density of 910 kg/m^3 floating in sea water with a density of 1020 kg/m^3, floating crude oil with a density of 890 kg/m^3 will have only 45 mm more freeboard than the surrounding ice when the oil and ice have equal drafts. Air temperatures below the oil's pour point, ice roughness and snow on the ice surface will all tend to restrict the spread of oil on the upper ice surface. Significant spreading on the surface will occur only if the oil can pool to depths of several meters beneath the ice.

The keels of ridges in the area might restrict the spread of oil beneath the ice and form deep pools of oil. It is unlikely that oil will form pools deeper than about 2 m behind ridge keels before flowing through gaps in the keel to the adjacent areas of flat ice. A 2-m-deep pool of oil beneath the ice will force some oil out onto the upper ice surface, but the oil on the surface will amount to only a small percent of the total and will cover a relatively small area before being stopped by ridges or snow drifts.

About 30 percent of the oil released replaces melted ice directly over the blowout. In densely ridged areas, the remaining oil may pool between ridge keels to a depth of about 2 m. An area of about 11×10^3 m^2 would hold this oil. If the area is not so heavily ridged, the oil could pool in the naturally occurring ice roughness to an average depth everywhere of about 0.05 m. No significant amount of oil would be forced onto the ice surface. Seventy percent of the oil released will cover about 0.45 km^2 to an average depth of 0.05 m. Thus, even the maximum area of possible oil contamination is relatively small. The difference between the minimum and maximum extent of oil spread (and thus the depth of the oil layer) can be extremely significant, though, when cleanup is considered.

The currents over the inner shelf are generally too small to affect the size of the oil-contaminated area. The primary effect of currents will be to control the direction of the oil spread, not the extent of the spread.

Incorporation of Oil Into the Ice

Oil on the upper surface of the ice will be mixed with snow and possibly covered by new or blowing snow. If the oil has spread beneath flat ice, collecting in individual pools averaging 0.15 m in depth, it will be encapsulated by new ice growth below the pools. Approximately 0.1 m of new ice growth may be expected below the pools of oil before ice growth stops in May. If the oil has collected in very deep and continuous pools between confining ridge keels, ice growth may not occur beneath the oil. The oil will remain in place, though, due to the absence of ice motion or large currents.

New ridges are not likely to be built in the immediate vicinity of the blowout before spring breakup occurs. Grounded ridges will prevent ice motions except possibly in the event of a severe springtime storm.

Oil may still become incorporated into existing ridges. The ridges in the area are mostly of recent origin and are not completely consolidated. Oil will fill some of the voids in the ridge keels. The percentage of oil involved will be relatively small, but that oil may remain in the ridges through one or more melt seasons.

Transport of Oiled Ice

Until breakup occurs in June, the ice over the blowout site will remain in place. Ridges which have become grounded in waters up to 20 m deep during the winter anchor the surrounding ice cover.

Release of Oil From the Ice

In late February or early March, as the air temperature began to rise, brine trapped between the columnar ice crystals began to drain. By late April or early May, the brine channels will have become large enough that oil can travel up the channels and begin to appear on the ice surface. Periods of cold weather will stop the oil flow temporarily, but by late May, pools of oil will be collecting on the ice surface. Because of the lowered albedo of the oiled ice, melting of the ice surface also begins in late May. Oil already on the ice surface and mixed with snow may locally accelerate the appearance of oil pools and ice melting.

Since most of the oil lies beneath 1.5 m of ice, not all the oil will surface until all the level ice over the oil slick has melted. The presence of oil on the ice surface will accelerate the local ice melting and breakup by about 2 weeks (mid-June), but grounded ridges in the area prevent any significant ice motion until mid-July.

By early to mid-July, all the undeformed ice which is contaminated by oil will have melted leaving an oil slick on the water surface. In 2 or 3 more weeks, all the uncontaminated ice except for ridges will have melted.

Most of the oil trapped in ridged ice will not escape at this time. During the winter, the ridges have become consolidated masses of ice. Brine drainage and release of trapped oil will occur, but at a much slower rate than in an undeformed ice sheet. Oil which does escape from a ridge will accelerate melting of the ridge, but the ridge may still last through the summer. By the end of the summer, most of the oiled ridges will be in the northern Chukchi Sea. A few securely grounded ridges will remain in place through the summer.

Fate of the Oil

As soon as oil begins to appear on the ice surface in May, weathering processes will begin. By about mid-June, approximately 50 percent of the oil will have evaporated. Most of the remaining oil is in open-water slicks among the remaining ice floes and grounded ridges seaward of Narwhal Island. Due to the partly weathered state of the oil and the intact ice surrounding the oil-contaminated area, the oil slick, or slicks, which may cover several square kilometers of water, are still much smaller than would be a slick of unweathered oil released into open-water conditions. Some water-in-oil emulsions will form where oil is floating on surface melt pools exposed to agitation by the winds. Other weathering processes will take place as the oil is released from the ice, but only insignificant amounts of oil will be involved. The low temperatures, the reduced wind action due to the remaining ice cover, and the thick, viscous oil layer on the water surface will act to inhibit dissolution, bacterial degradation, and dispersion.

The pack ice does not generally retreat until sometime after early July. Grounded ridges seaward of the blowout site may remain grounded until late summer; thus preventing the oil from being blown out to sea until later in the summer. Grounded ridges are not continuous along the coast, though, so some of the oil is likely to be blown offshore into the pack ice. Most of the oil will be blown onto island or mainland beaches to the south or southwest due to the prevailing wind direction (from the east or northeast about 60 percent of the time during June).

The above scenario assumes that no cleanup of the oil takes place. If part of the oil is cleaned up following the blowout, the major change in the scenario would be a reduction in the amount of oil involved.

Oil Spill Scenario No. 9

On 31 March, just at the end of the drilling season, an underwater oil well blowout is assumed to occur 20 km north of Cross Island in the pack ice zone. The hypothetical blowout releases 2 x 10^5 barrels (3.18 x 10^4 m^3) of oil over a period of 5 days.

Scene

Cross Island lies about 20 km offshore of the Alaskan coast, just north of the Sagavanirktok River mouth. The ice cover north of the island has been subject to much ridge building activity during the preceding fall and winter. By the end of March there are approximately 6 to 12 ridges/km in the area of the blowout. The ridges generally run parallel to the shore but intersecting ridges tend to divide the area into large irregular areas of flat ice. On the average there is from 63 to 146 m of flat ice between ridges. The flat ice is mostly first-year ice about 1.55 m thick.

Ice motions in the near shore fast ice zone during April and afterwards are generally toward the west and range from 30 to 90 km per month. These motions are not continuous but occur during periods of high winds. Typically, the ice is motionless or nearly so about half the time and it averages about 6 km/day of motion about half the time. The ice motion is generally towards the west but some meandering motion is to be expected as well as occasional significant motions to the east. For the purpose of this scenario, it is arbitrarily assumed that the 5-day period consists of 2.5 days of no significant ice motion followed by 2.5 days where the total ice motion averages 6 km/day and the net westward transport averages 4 km/day. Thus, after 5 days, the original ice over the blowout ends up 10 km west of the blowout site after traveling a total of 15 km.

Water depths in the vicinity of the blowout are about 30 m. Wind-driven currents died out as soon as the ice cover formed, and now the under-ice currents are due to the tides and the mesoscale circulation. The tidal component is weak, less than 0.01 or 0.02 m/s, and oscillatory. The geostrophic component is also weak, 0.01 to 0.05 m/s, and generally toward the east or west, but with considerable variation. In general, measured currents beneath the ice just outside the barrier islands are small, about 0.02 to 0.03 m/s, and variable.

Water temperatures are near freezing and the 90th percentile air temperature range is about -36 to -11°C in early April, warming up to -2 to +11°C by the end of June.

Blowout

A ruptured casing and a fault in the bedrock allow the oil and gas to escape under the solid ice canopy some distance from the well head. The reservoir is assumed to be about 3000 m deep and the crude oil similar to a Prudhoe Bay crude (density about 890 kg/m^3 and pour point about -9.5°C).

A total of 3.18×10^4 m^3 of crude oil escapes over a period of 5 days before control efforts successfully stop the flow. An estimated 4.8×10^6 m^3 of gas is also released. Flow rates during the 5-day blowout average 4.4 m^3/min of oil and 670 m^3/min of gas.

During the blowout, a plume of oil, gas bubbles, and entrained water rises to the surface. The vertical currents in the plume flow radially outward at the surface then downward at some distance from the plume to complete a closed circulation system. The downward-flowing currents entrain some water from outside the circulation system, and a weak, inward-flowing surface current is developed outside the plume region to replace this entrained water. A wave ring forms where the outward- and inward-flowing surface currents meet. For a 30-m water depth and a gas flow rate of 670 m^3/min, the diameter of this wave ring is calculated to be about 130 m.

The escaping gas and the turbulent blowout plume may not immediately breakup the ice canopy overhead. When the ice is motionless and gas is escaping at the rate of 670 m^3/min, the surrounding ridges will be able to hold a great deal of gas within a few thousand square meters near the blowout. The ice may already contain weaknesses in the form of cracks generated by thermal contraction. Thus, within a short time a large submerged gas bubble forms, causing the ice sheet overhead to bend and break. Thereafter, the vast majority of the gas from the blowout will escape to the atmosphere. Once the escaping gas is vented to the atmosphere, the oil from the blowout will begin to collect under and between ice floes near the blowout.

During the 2.5 days when the ice cover is in motion over the blowout, ice breakage is more problematical. If the ice is moving slowly and is heavily ridged, the gas will likely collect in large enough bubbles to break up the ice. When the ice speed is large and no large underside roughness exists, or large multiyear floes are passing over the blowout, the gas is likely to spread beneath the ice until it reaches a thermal crack or a lead containing thin ice. The width of the swath of oil and gas will depend upon the spacing of natural weaknesses and the speed at which the ice is moving.

The crude oil, at a temperature between 60 and $90^{\circ}C$, contains enough heat to melt between 9.5×10^3 and 1.4×10^4 m^3 of sea ice. Since surface currents outside the wave ring tend to flow inward toward the blowout, the oil and heat will tend to concentrate inside the wave ring. However, some warm oil or heated water will escape the circulation system inside the wave ring, possibly melting the ice cover thinner or reducing the ice growth rate. The bottom water entrained in the plume is likely to be so cold in these shallow areas that it contributes little to ice melting. During periods of ice motion the amount of ice melted will have little noticeable effect on the spread of the oil or the ice thickness along the blowout track. When the ice is stationary or nearly so, some of the ice within the wave ring will be melted. The heat from 2.5-day's oil flow will melt from 0.36 to 0.54 m thickness of ice over the 130-m-diameter wave ring.

In general, the oil undergoes very little physical or chemical change during the blowout. Evaporation is unimportant because so little oil is exposed to the atmosphere. Outside the blowout plume, there is no mixing energy to form emulsions. Dissolution and sedimentation occur, but probably in very insignificant amounts.

Spread of Oil Beneath the Ice

Assuming that the oil melts 4.8×10^3 m^3 of ice during the 2.5-day period when the ice is nearly stationary, then about 15 percent of the total oil released will replace this melted ice. Some of this oil will appear on the water surface where the ice has been broken up or melted. The spread of oil onto the upper surface of the ice will depend upon the depth to which oil can pool beneath the ice. In an opening through 1.5-m-thick ice with a density of 910 kg/m^3 floating in sea water with a density of 1020 kg/m^3, floating crude oil with a density of 890 kg/m^3 will have only 0.04 m more freeboard than the surrounding ice when the oil and ice have equal drafts. Air temperatures below the oil's pour point, ice roughness and snow on the ice surface will all tend to restrict the spread of oil on the upper ice surface. Significant spreading on the surface will occur only if the oil can pool to depths of several meters beneath the ice. Most of the remaining oil released during the period of no ice motion will spread beneath the ice. Of the 1.6×10^4 m^3 of oil released during these 2.5 days, 4.8×10^3 m^3 replaces melted ice and about 1.1×10^4 m^3 spreads beneath the ice.

The keels of ridges in the area might restrict the spread of oil beneath the ice and form deep pools of oil. It is unlikely that oil will form pools deeper than about 2-m behind ridge keels before flowing through gaps in the keel to the adjacent areas of flat ice. A 2-m-deep pool of oil beneath the ice will force some oil out onto the upper ice surface but the oil on the surface will amount to only a few percent of the total and will cover a relatively small area before being stopped by ridges or snow drifts. The 1.1×10^4 m^3 of oil will cover an area of 5.5×10^3 m^2 to a depth of 2 m.

On the other hand, if the area is not so heavily ridged, the oil could pool in the naturally occurring ice roughness to an average depth everywhere of about 0.05 m. No significant amount of oil would be forced onto the ice surface. The 1.1×10^4 m^3 of oil will then spread under about 0.22 km^2 of ice.

During the 2.5 days when the ice is in motion over the blowout, an area 130 m wide by 15 km long is swept by the blowout plume. The 1.6×10^4 m^3 of oil released during this time can cover this area (1.95 km^2) to an average depth of about 8 mm. This is less oil than the ice is capable of containing in the underside roughness. Because of the gas that can be trapped beneath a moving ice cover, the area over which the oil spreads will probably be larger, and the concentration of oil less.

During the 5-day period then, 50 percent of the oil (1.6×10^3 m^3) is spread beneath about 1.95 km^2 of ice while the ice is moving, and 35 percent of the oil (1.1×10^4 m^3) spreads beneath the ice during the period of no ice motion, covering as little as 5.55×10^3 m^2 and as much as 2.2×10^5 m^2 of ice. The remaining 15 percent (4.8×10^3 m^3) replaces melted ice over the blowout.

The currents over the inner shelf are generally too small to affect the size of the oil-contaminated area. The primary effect of currents will be to control the direction of the oil spread, not the extent of the spread.

Incorporation of Oil Into the Ice

Oil on the upper surface of the ice will be mixed with snow and possibly covered by new or blowing snow. If the oil has spread beneath flat ice, collecting in individual pools averaging 0.15 m in depth, it will be encapsulated by new ice growth below the pools. Approximately 0.1 m of new ice growth may be expected below the pools of oil before ice growth stops in May. If the oil has collected in very deep and continuous pools between confining ridge keels, ice growth may not occur beneath the oil.

Some new ridges are likely to be built of oiled ice between the beginning of the blowout and June. As much as 5 percent of the ice which passes over the blowout will be thin ice in refrozen leads. If all this ice becomes ridged, then a maximum of 5 percent of the oil might be incorporated into ridges.

Oil may also become incorporated into existing ridges. The ridges in the area are mostly of recent origin and are not completely consolidated. Oil will fill some of the voids in the ridge keels. The percentage of oil involved will be relatively small, but that oil may remain in the ridges through one or more melt seasons.

Transport of Oiled Ice

Between the blowout in early April and breakup in June, the ice can travel up to 60 km/month toward the west. Although the area of oiled ice will not increase during this period it is possible that individual floes contaminated with oil will be widely dispersed. As the pack ice loosens up in June, this dispersal of oiled floes will become greater. By July, there may be oiled ice floes anywhere between the blowout site and Cape Halkett, 180 km to the west.

Release of Oil From the Ice

In late February or early March, as the air temperature began to rise, brine trapped between the columnar ice crystals has begun to drain. By late April or early May, the brine channels will have become large enough that oil can travel up the channels and begin to appear on the ice surface. Periods of cold weather will stop the oil flow temporarily, but by late May, pools of oil will be collecting on the ice surface. Because of the lowered albedo of the oiled ice, melting of the ice surface also begins in late May. Oil already on the ice surface and mixed with snow may locally accelerate the appearance of oil pools and ice melting.

Not all the oil will surface until all the level ice over the oil slick has melted. The presence of oil on the ice surface will accelerate the local ice melting by about 2 weeks. By early to mid-July, all the undeformed ice which is contaminated by oil will have melted leaving an oil slick on the water surface.

Most of the oil trapped in ridged ice will not escape at this time. Brine drainage and release of trapped oil will occur, but at a much slower rate than in an undeformed ice sheet. Oil which does escape from a ridge will accelerate melting of the ridge, but the ridge may still last through the summer. By the end of the summer, most of the oiled ridges will be in the northern Chukchi Sea.

Fate of the Oil

As soon as oil begins to appear on the ice surface in May, weathering processes will begin. By the end of June, approximately 50 percent of the oil will have evaporated. Most of the remaining oil is in open water slicks among the remaining ice floes west of Cross Island. Due to the partly weathered state of the oil and the intact ice surrounding the oil-contaminated area, the oil slick, or slicks, which may cover several square kilometers of water, are still much smaller that would be a slick of unweathered oil released into open water conditions. Some water-in-oil emulsions will form where oil is floating on surface melt pools exposed to agitation by the winds. Other weathering processes will take place as the oil is released from the ice, but only insignificant amounts of oil will be involved. The low temperatures, the reduced wind action due to the remaining ice cover, and the thick, viscous oil layer on the water surface will act to inhibit dissolution, bacterial degradation, and dispersion.

The pack ice does not generally retreat until sometime after early July. By that time, most of the oil will have been blown onto island or mainland beaches to the south or southwest due to the prevailing wind direction (from the east or northeast about 60 percent of the time during June). Of course, the probability is still high that some of the oil will be blown offshore into the permanent pack ice.

The above scenario assumes that no cleanup of the oil takes place. If part of the oil is cleaned up following the blowout, the major change in the scenario would be a reduction in the amount of oil involved.

Oil Spill Scenario No. 10

On 31 March, just at the end of the drilling season, an underwater oil well blowout is assumed to occur under the fast ice in Stefansson Sound. The hypothetical blowout releases 4.5×10^6 barrels (7.15×10^5 m^3) of oil over a period of 90 days.

Scene

Stefansson Sound is located inside the barrier islands within the fast ice zone. At the time of the blowout, a continuous ice canopy about 1.5 m thick extending from the shore to the barrier islands covers the sound. Winds during the freezeup period and immediately after produced much small-scale relief such as rafted floes but, as the ice season progresses the primary under-ice relief is due to differential ice growth beneath variations in the snow cover. By the end of March, these undulations in the bottom surface of the ice provide an average containment volume of 4.8×10^4 m^3/km^2.

Water depths in the vicinity of the blowout are about 6 m. Wind-driven currents died out as soon as the ice cover formed and now the under-ice currents are driven by the tides and a thermohaline circulation. The tidal component is weak (less than 0.01 or 0.02 m/s) and oscillatory. The thermohaline currents produced by cold, salty water flowing offshore along the bottom are on the average small, but extremes of up to 0.11 m/s have been observed. It is postulated that an onshore current of up to 0.2 m/s must exist just beneath the ice to replace the water flowing offshore along the bottom, but this has not been observed. By the end of March, ice growth is slow and the thermohaline circulation much less important. In general, measured currents beneath the fast ice inside the barrier islands are small, about 0.02 to 0.03 m/s, and variable.

Water temperatures in the shallow sound are near freezing and the 90th percentile air temperature range for early April is -36 to -11°C. By the end of June, the air temperature range is -2 to +11°C.

Blowout

A ruptured casing and a fault in the bedrock allow the oil and gas to escape under the solid ice canopy some distance from the well head. The reservoir is assumed to be about 3000 m deep and the crude oil similar to a Prudhoe Bay crude (density about 890 kg/m^3 and pour point about $-9.5^{\circ}C$).

A total of 7.15×10^5 m^3 of crude oil escapes over a period of 90 days before control efforts successfully stop the flow. An estimated 1.07×10^8 m^3 of gas is also released. Flow rates during the 90-day blowout average 5.5 m^3/min of oil and 830 m^3/min of gas.

During the blowout, a plume of oil, gas bubbles, and entrained water rises to the surface. Soon after the blowout begins, gas trapped under the thin ice breaks up the ice over the plume, allowing all the gas released during the blowout to escape to the atmosphere.

The vertical currents in the plume flow radially outward at the surface then downward at some distance from the plume to complete a closed circulation system. The downward-flowing currents entrain some water from outside the circulation system and a weak, inward-flowing surface current is developed outside the plume region to replace this entrained water. A wave ring forms where the outward- and inward-flowing surface currents meet. For a 6-m water depth and a gas flow rate of 830 m^3/min, the diameter of this wave ring is calculated to be about 38 m.

The crude oil, at a temperature between 60 and $90^{\circ}C$ contains enough heat to melt between 2.1×10^5 and 3.2×10^5 m^3 of sea ice. Since surface currents outside the wave ring tend to flow inward toward the blowout, the oil and heat will tend to concentrate inside the wave ring. Some warm oil or heated water will escape the circulation system inside the wave ring, possibly melting the ice cover thinner or reducing the ice growth rate. The bottom water entrained in the plume is likely to be so cold in these shallow areas that it contributes little to ice melting.

It is likely that the 1.7×10^3 m^3 of ice lying within the wave ring will be melted soon after the blowout begins. As oil continues to be released during the 90-day blowout much of the heat from the oil is transferred directly to the atmosphere through the hole already melted in the ice. Some heat goes into melting the ice laterally about the melt hole and some is transferred to the water column to be eventually distributed to the ice further from the blowout. The heat distributed beneath the ice will reduce or halt growth of new ice during the course of the blowout. Lateral melting of ice about the central melt hole proceeds much slower than the melting of the original hole in the ice because of the much smaller surface area exposed to the oil.

In general, the oil undergoes very little physical or chemical change during the blowout. Evaporation is unimportant because so little oil is exposed to the atmosphere. Outside the blowout plume there is no mixing energy to form emulsions. Dissolution and sedimentation occur, but probably in very insignificant amounts.

Spread of Oil Beneath the Ice

Other than the relatively small amount of oil in the central melt hole, most of the oil will spread beneath the ice. Very little oil will flow onto the top surface of the ice through cracks in the ice or the melt hole. A 1.5-m-thick layer of oil with a density of 890 kg/m^3 will have only about 0.04 m more freeboard than a 1.5-m-thick ice sheet with a density of 910 kg/m^3 in sea water with a density of 1020 kg/m^3. Air temperatures below the oil's pour point, ice roughness, and snow on the ice will all tend to prevent the oil from spreading onto the ice surface, thus increasing the thickness of the oil pool enough that oil will begin flowing beneath the ice.

By the end of March, the 1.5-m-thick first-year fast ice has an average roughness amplitude of about 0.3 m. Ice with this amount of roughness has the potential of containing about 4.8×10^4 m^3 of oil per square kilometer. Thus, 7.15×10^5 m^3 of oil from the blowout spreads to cover only 15 km^2 of ice, or slightly less when the oil contained in the central melt hole is taken into account. The ice cover increases in thickness by about 0.1 m during April and May, when ice growth ceases. Since ice growth near the blowout is probably halted due to the warm oil and water circulating beneath the ice, the containment potential of the ice near the blowout is increased and the spread of oil reduced.

Toward the end of the blowout (mid-June) the ice begins to break up with areas of open water appearing near the blowout site. Newly released oil will pool in open leads and polynyas.

The currents in the nearshore area are generally too small to affect the size of the oil-contaminated area. Occasional brief currents of up to 0.2 m/s may occur. Currents of this magnitude will move an oil slick under smooth ice but not under natural sea ice with 0.3 m of relief and a skeletal layer of growing ice crystals. The primary effect of currents will be to control the direction of the oil spread. Over a period of 90 days, the effect of currents will tend to average out.

Incorporation of Oil Into the Ice

During the spring it takes approximately 10 days for an oil lens to be encapsulated by new ice growth. For a 90-day blowout, though, it is possible that a great deal, perhaps most of the oil, will not be frozen into the ice. Ice growth has slowed down by the time the blowout begins in April, and ceases altogether in May. Many of the pools of oil near the blowout are being continually replenished by fresh oil, overflowing into adjacent pools, and so on. While this oil is in motion it is unlikely that ice growth will occur beneath the oil. The hot oil from the blowout will also warm the water column slightly in the vicinity of the blowout. Isolated pools of oil will probably become frozen into the ice, but the majority of the oil will not.

In the absence of strong under-ice currents, this lack of incorporation will have little effect upon the spread of the oil. Sedimentation and dissolution of the oil will proceed at a faster rate but the long term effects of the spill will not be significantly different. The eventual release of the oil from the ice will not be greatly changed either.

Transport of Oiled Ice

No significant ice motion takes place in the fast ice zone between the blowout in late March-early April and about mid-June. At that time oil-contaminated ice will have broken up enough to be moved by the winds.

Release of Oil From the Ice

In late February or early March, as the air temperature began to rise, brine trapped between the columnar ice crystals began to drain. By late April or early May, the brine channels will have become large enough that oil will begin to appear on the ice surface. Periods of cold weather will stop the oil flow temporarily, but by late May pools of oil will be collecting on the ice surface. Because of the lowered albedo of the oiled ice, melting of the ice surface also begins in late May. The presence of oil on the ice surface will accelerate the local ice breakup by about 2 weeks. Thus, by mid-June, the oil-contaminated ice will have broken up enough that it can be moved by the wind. About the same time, rivers will begin flowing again, flooding the ice about the river mouths. By mid-June, shore polynyas will have been melted by the flowing rivers. The most likely ice motion will be toward the shore and the area of open water.

By early to mid-July, all the ice which is contaminated by oil will have melted. In 2 or 3 more weeks, all the uncontaminated ice will have melted leaving the oil slick on the water surface.

Fate of the Oil

As soon as oil begins to appear on the ice surface in May, weathering processes will begin. By the end of June, approximately 50 percent of the oil will have evaporated. Some water-in-oil emulsions will form where oil is floating on surface melt pools exposed to agitation by the winds. Other weathering processes will take place as the oil is released from the ice, but only insignificant amounts of oil will be involved. The low temperatures, the reduced wind action due to the remaining ice cover, and the thick, viscous oil layer on the water surface will act to inhibit dissolution, bacterial degradation, and dispersion. The silt carried out by the flowing rivers may increase the rate of sedimentation, though.

The pack ice does not generally retreat until sometime after early July. Grounded ridges seaward of the barrier islands may remain grounded until late summer, thus preventing the oil from being blown out to sea at least until later in the summer. By that time most of the oil will have been blown onto mainland beaches to the west or southwest due to the prevailing wind direction (from the east or northeast about 60 percent of the time during June). Of course, the probability is still high that some of the oil will be blown offshore onto island beaches or into the pack.

The above scenario assumes that no cleanup of the oil takes place. If part of the oil is cleaned up following the blowout, the major change in the scenario would be a reduction in the amount of oil involved.

Oil Spill Scenario No. 11

On 31 March, just at the end of the drilling season, an underwater oil well blowout is assumed to occur 5 km northeast of Narwhal Island in the stamukhi zone. The hypothetical blowout releases 4.5×10^6 barrels (7.15×10^5 m^3) of oil over a period of 90 days.

Scene

Narwhal Island lies about 20 km offshore of the Alaskan coast, just north of the Sagavanirktok River mouth. It is one of the barrier islands which protect the fast ice shoreward of the islands from interaction with the pack ice. The ice cover outside the barrier islands has been subject to much ridge building activity during the preceding fall and winter. By the end of March there are approximately 6 to 12 ridges/km in the area of the blowout. Many of these ridges are grounded, so no significant ice motions occur until the following summer. The ridges generally run parallel to the shore, but intersecting ridges tend to divide the area into large irregular areas of flat ice. On the average there are from 65 to 150 m of flat ice between ridges. The flat ice is mostly first-year ice about 1.5 m thick.

Water depths in the vicinity of the blowout are about 15 m. Wind-driven currents died out as soon as the ice cover formed, and now the under-ice currents are due to the tides and the mesoscale circulation. The tidal component is weak, less than 0.01 or 0.02 m/s, and oscillatory. The geostrophic component is also weak, 0.01 to 0.05 m/s, and generally toward the east or west, but with considerable variation. In general, measured currents beneath the ice just outside the barrier islands are small, about 0.02 to 0.03 m/s, and variable.

Water temperatures are near freezing and the 90th percentile air temperature range during early April is about -36 to -11°C. By the end of June, the air temperature range is about -2 to +11°C.

Blowout

A ruptured casing and a fault in the bedrock allow the oil and gas to escape under the solid ice canopy some distance from the well head. The reservoir is assumed to be about 3000 m deep and the crude oil similar to a Prudhoe Bay crude (density about 890 kg/m^3 and pour point about -9.5°C).

A total of 7.15×10^5 m^3 of crude oil escapes over a period of 90 days before control efforts successfully stop the flow. An estimated 1.07×10^8 m^3 of gas is also released. Flow rates during the 90-day blowout average 5.5 m^3/min of oil and 830 m^3/min of gas.

During the blowout, a plume of oil, gas bubbles, and entrained water rises to the surface. The vertical currents in the plume flow radially outward at the surface then downward at some distance from the plume to complete a closed circulation system. The downward-flowing currents entrain some water from outside the circulation system, and a weak, inward-flowing surface current is developed outside the plume region to replace this entrained water. A wave ring forms where the outward- and inward-flowing surface currents meet. For a 15-m water depth and a gas flow rate of 830 m^3/min, the diameter of this wave ring is calculated to be about 82 m.

The escaping gas and the turbulent blowout plume may not immediately break up the ice canopy overhead. But gas is escaping at the rate of 830 m^3/min and the surrounding ridges will be able to hold most of the gas within a few thousand square meters area. The ice will also be weakened by existing cracks generated by thermal contraction. Thus, within a short time a large submerged gas bubble forms, causing the ice sheet overhead to bend and break. Thereafter, the vast majority of the gas from the blowout will escape to the atmosphere. Once the escaping gas is vented to the atmosphere, the oil from the blowout will begin to collect under and between ice floes near the blowout.

The crude oil, at a temperature between 60 and 90°C, contains enough heat to melt between 2.15×10^5 and 3.22×10^5 m^3 of sea ice. Since surface currents outside the wave ring tend to flow inward toward the blowout, the oil and heat will tend to concentrate inside the wave ring. However, some warm oil or heated water will escape the circulation system inside the wave ring, possibly melting the ice cover thinner or reducing the ice growth rate. The bottom water entrained in the plume is likely to be so cold in these shallow areas that it contributes little to ice melting. Much of the ice within the wave ring will be melted by the warm oil and an area of open water will develop. Lateral melting will continue through the 90-day blowout but at a greatly reduced rate due to the smaller area of ice in contact with the oil and exposure of the oil to the atmosphere in the hole already melted.

In general, the oil undergoes very little physical or chemical change during the blowout. Evaporation is unimportant because so little surface area is exposed to the atmosphere. Outside the blowout plume, there is no mixing energy to form emulsions. Dissolution and sedimentation occur, but probably in very insignificant amounts.

Spread of Oil Beneath the Ice

The spread of oil onto the upper surface of the ice will depend upon the depth to which oil can pool beneath the ice. In an opening through 1.5-m-thick ice with a density of 910 kg/m^3 floating in sea water with a density of 1020 kg/m^3, floating crude oil with a density of 890 kg/m^3 will have only 0.04 m more freeboard than the surrounding ice when the oil and ice have equal drafts. Air temperatures below the oil's pour point, ice roughness and snow on the ice surface will all tend to restrict the spread of oil on the upper ice surface. Significant spreading on the surface will occur only if the oil can pool to depths of several meters beneath the ice.

The keels of ridges in the area might restrict the spread of oil beneath the ice and form deep pools of oil. It is unlikely that oil will form pools deeper than about 2 m behind ridge keels before flowing through gaps in the keels to the adjacent areas of flat ice. A 2-m-deep pool of oil beneath the ice will force some oil out onto the upper ice surface, but the oil on the surface will amount to only a few percent of the total and will cover a relatively small area before being stopped by ridges or snow drifts.

If the area is heavily ridged and the oil forms pools between the ridges to a depth of 2 m, the 7.15×10^5 m^3 of oil from the blowout will cover an area of 0.36 km^2. On the other hand, if the area is not so heavily ridged, the oil could pool in the naturally occurring ice roughness to an average depth everywhere of about 0.05 m. No significant amount of oil would be forced onto the ice surface. Then the 7.15×10^5 m^3 of oil will cover an area of about 14 km^2 to an average depth of 0.05 m. Thus, even the maximum area of possible oil contamination is relatively small. The difference between the minimum and maximum extent of oil spread (and thus the depth of the oil layer) can be extremely significant, though, when cleanup is considered.

The currents over the inner shelf are generally too small to affect the size of the oil-contaminated area. The primary effect of currents will be to control the direction of the oil spread, not the extent of the spread.

Incorporation of Oil Into the Ice

Oil on the upper surface of the ice will be mixed with snow and possibly covered by new or blowing snow. If the oil has spread beneath flat ice, collecting in individual pools averaging 0.15 m in depth, it will be encapsulated by new ice growth below the pools. Approximately 0.1 m of new ice growth may be expected below the pools of oil before ice growth stops in May. If the oil has collected in very deep and continuous pools between confining ridge keels, ice growth may not occur beneath the oil. The continual release of oil and motion of the oil as it spreads beneath the ice will also prevent new ice growth. It is likely that the majority of the oil will not be frozen into the ice. The oil will remain in place, though, due to the absence of ice motion or large currents.

New ridges are not likely to be built in the immediate vicinity of the blowout before spring breakup occurs. Grounded ridges will prevent ice motions except possibly in the event of a severe springtime storm.

Oil may still become incorporated into existing ridges. The ridges in the area are mostly first-year ridges and are not completely consolidated; thus, oil will fill some of the voids in the ridge keels. The percentage of oil involved will be relatively small, but that oil may remain in the ridges through one or more melt seasons.

Transport of Oiled Ice

Until breakup occurs in June, the ice over the blowout site will remain in place. Ridges which have become grounded in waters up to 20 m deep during the winter anchor the surrounding ice cover.

Release of Oil From the Ice

In late February or early March, as the air temperature began to rise, brine trapped between the columnar ice crystals began to drain. By late April or early May, the brine channels will have become large enough that oil can travel up the channels and begin to appear on the ice surface. Periods of cold weather will stop the oil flow temporarily, but by late May, pools of oil will be collecting on the ice surface. Because of the lowered albedo of the oiled ice, melting of the ice surface also begins in late May. Oil already on the ice surface and mixed with snow may locally accelerate the appearance of oil pools and ice melting.

Since most of the oil lies beneath 1.5 m of ice, not all the oil will surface until all the level ice over the oil slick has melted. The presence of oil on the ice surface will accelerate the local ice melting and breakup by about 2 weeks (mid-June), but grounded ridges in the area prevent any significant ice motion until mid-July.

By early to mid-July, all the undeformed ice which is contaminated by oil will have melted leaving an oil slick on the water surface. In 2 or 3 more weeks all the uncontaminated ice except for ridges will have melted.

Most of the oil trapped in ridged ice will not escape at this time. During the winter, the ridges have become consolidated masses of ice. Brine drainage and release of trapped oil will occur, but at a much slower rate than in an undeformed ice sheet. Oil which does escape from a ridge will accelerate melting of the ridge, but the ridge may still last through the summer. By the end of the summer, most of the oiled ridges will be in the northern Chukchi Sea. A few securely grounded ridges may remain in place through the summer.

Fate of the Oil

As soon as oil begins to appear on the ice surface in May, weathering processes will begin. By the end of June, approximately 50 percent of the oil will have evaporated. Most of the remaining oil is in open-water slicks among the remaining ice floes and grounded ridges seaward of Narwhal Island. Due to the partly weathered state of the oil and the intact ice surrounding the oil-contaminated area, the oil slick, or slicks, which may cover several square kilometers of water, are still much smaller than would be a slick of unweathered oil released into open-water conditions. Some water-in-oil emulsions will form where oil is floating on surface melt pools exposed to agitation by the winds. Other weathering processes will take place as the oil is released from the ice, but only insignificant amounts of oil will be involved. The low temperatures, the reduced wind action due to the remaining ice cover, and the thick, viscous oil layer on the water surface will act to inhibit dissolution, bacterial degradation, and dispersion.

The pack ice does not generally retreat until sometime after early July. Grounded ridges seaward of the blowout site may remain grounded until late summer, thus preventing the oil from being blown out to sea until later in the summer. Grounded ridges are not continuous along the coast, though, so some of the oil is likely to be blown offshore into the pack ice. Most of the oil will be blown onto island or mainland beaches to the west or southwest due to the prevailing wind direction (from the east or northeast about 60 percent of the time during June).

The above scenario assumes that no cleanup of the oil takes place. If part of the oil is cleaned up following the blowout, the major change in the scenario would be a reduction in the amount of oil involved.

Oil Spill Scenario No. 12

On 31 March, just at the end of the drilling season, an underwater oil well blowout is assumed to occur 20 km north of Cross Island in the pack ice zone. The hypothetical blowout releases 4.5×10^6 barrels (7.15×10^5 m^3) of oil over a period of 90 days.

Scene

Cross Island lies about 20 km offshore of the Alaskan coast, just north of the Sagavanirktok River mouth. The ice cover north of the island has been subject to much ridge building activity during the preceding fall and winter. By the end of March, there are approximately 6 to 12 ridges/km in the area of the blowout. The ridges generally run parallel to the shore but intersecting ridges tend to divide the area into large irregular areas of flat ice. On the average there is from 63 to 146 m of flat ice between ridges. The flat ice is mostly first-year ice about 1.55 m thick.

Ice motions in the nearshore fast ice zone during April and afterwards are generally toward the west and range from 30 to 90 km per month. These motions are not continuous but occur during periods of high winds. Typically, the ice is motionless or nearly so about half the time and it averages about 6 km/day of motion about half the time. The ice motion is generally toward the west, but some meandering motion is to be expected as well as occasional significant motions to the east. For the purpose of this scenario, it is arbitrarily assumed that during the 90-day blowout period (April through June) each consecutive 5-day period consists of 2.5 days of no significant ice motion followed by 2.5 days where the total ice motion averages 6 km/day and the net westward transport averages 4 km/day. Thus, after 90 days, the original ice over the blowout ends up 180 km west of the blowout site after traveling a total of 270 km.

Water depths in the vicinity of the blowout are about 30 m. Wind-driven currents died out as soon as the ice cover formed, and now the under-ice currents are due to the tides and the mesoscale circulation. The tidal component is weak, less than 0.01 or 0.02 m/s, and oscillatory. The geostrophic component is also weak, 0.01 to 0.05 m/s, and generally toward the east or west, but with considerable variation. In general, measured currents beneath the ice just outside the barrier islands are small, about 0.02 to 0.03 m/s, and variable.

Water temperatures are near freezing and the 90th percentile air temperature range is about -36 to $-11^{o}C$ in early April, warming up to -2 to $+11^{o}C$ by the end of June.

Blowout

A ruptured casing and a fault in the bedrock allow the oil and gas to escape under the solid ice canopy some distance from the well head. The reservoir is assumed to be about 3000 m deep and the crude oil similar to a Prudhoe Bay crude (density about 890 kg/m^3 and pour point about $-9.5^{o}C$).

A total of 7.15×10^5 m^3 of crude oil escapes over a period of 90 days before control efforts successfully stop the flow. An estimated 1.07×10^8 m^3 of gas is also released. Flow rates during the 90-day blowout average 5.5 m^3/min of oil and 830 m^3/min of gas.

During the blowout, a plume of oil, gas bubbles, and entrained water rises to the surface. The vertical currents in the plume flow radially outward at the surface then downward at some distance from the plume to complete a closed circulation system. The downward-flowing currents entrain some water from outside the circulation system, and a weak, inward-flowing surface current is developed outside the plume region to replace this entrained water. A wave ring forms where the outward- and inward-flowing surface currents meet. For a 30-m water depth and a gas flow rate of 830 m^3/min, the diameter of this wave ring is calculated to be about 140 m.

The escaping gas and the turbulent blowout plume may not immediately break up the ice canopy overhead. When the ice is motionless and gas is escaping at the rate of 830 m^3/min, the surrounding ridges will be able to hold a great deal of gas within a few thousand square meters near the blowout. The ice may already contain weaknesses in the form of cracks generated by thermal contraction. Thus, within a short time a large submerged gas bubble forms, causing the ice sheet overhead to bend and break. Thereafter, the vast majority of the gas from the blowout will escape to the atmosphere. Once the escaping gas is vented to the atmosphere, the oil from the blowout will begin to collect under and between ice floes near the blowout.

During the 2.5-day periods when the ice cover is in motion over the blowout, ice breakage is more problematical. If the ice is moving slowly and is heavily ridged, the gas will likely collect in large enough bubbles to break up the ice. When the ice speed is large and no large underside roughness exists, or when large multiyear floes are passing over the blowout, the gas is likely to spread beneath the ice until it reaches a thermal crack or a lead containing thin ice. The width of the swath of oil and gas will depend upon the spacing of natural weaknesses and the speed at which the ice is moving.

The crude oil, at a temperature between 60 and 90°C, contains enough heat to melt between 2.1×10^5 and 3.2×10^5 m^3 of sea ice. Since surface currents outside the wave ring tend to flow inward toward the blowout, the oil and heat will tend to concentrate inside the wave ring. However, some warm oil or heated water will escape the circulation system inside the wave ring, possibly melting the ice cover thinner or reducing the ice growth rate. The bottom water entrained in the plume is likely to be so cold in these shallow areas that it contributes little to ice melting. During periods of ice motion, the amount of ice melted will have little noticeable effect on the spread of the oil or the ice thickness along the blowout track. When the ice is stationary or nearly so, some of the ice within the wave ring will be melted. During 2.5 days, a layer of ice from 0.39 to 0.58 m thick can be melted over the area of the 140-m-diameter wave ring.

In general, the oil undergoes very little physical or chemical change during the blowout. Evaporation is unimportant because so little oil is exposed to the atmosphere. Outside the blowout plume, there is no mixing energy to form emulsions. Dissolution and sedimentation occur, but probably in very insignificant amounts.

Spread of Oil Beneath the Ice

Assuming that the oil melts 6.0×10^3 m^3 of ice during each 2.5-day period when the ice is nearly stationary, then about 15 percent of the total oil released will replace this melted ice. Some of this oil will appear on the water surface where the ice has been broken up or melted. The spread of oil onto the upper surface of the ice will depend upon the depth to which oil can pool beneath the ice. In an opening through 1.5-m-thick ice with a density of 910 kg/m^3 floating in sea water with a density of 1020 kg/m^3, floating crude oil with a density of 890 kg/m^3 will have only 0.04 m more freeboard than the surrounding ice when the oil and ice have equal drafts. Air temperatures below the oil's pour point, ice roughness and snow on the ice surface will all tend to restrict the spread of oil on the upper ice surface. Significant spreading on the surface will occur only if the oil can pool to depths of several meters beneath the ice. Most of the remaining oil released during the period of no ice motion will spread beneath the ice. Of the 2.0×10^4 m^3 of oil released during each of these 2.5-day periods, 6.0×10^3 m^3 replaces melted ice and about 1.4×10^4 m^3 spreads beneath the ice.

The keels of ridges in the area might restrict the spread of oil beneath the ice and form deep pools of oil. It is unlikely that oil will form pools deeper than about 2 m behind ridge keels before flowing through gaps in the keel to the adjacent areas of flat ice. A 2-m-deep pool of oil beneath the ice will force some oil out onto the upper ice surface but the oil on the surface will amount to only a few percent of the total and will cover a relatively small area before being stopped by ridges or snow drifts. The 1.4×10^4 m^3 of oil which spreads beneath the ice during a 2.5-day period will cover an area of 7.0×10^3 m^2 to a depth of 2 m. For the 45 days of no ice motion, a total of 0.13 km^2 of ice might contain a 2-m-deep layer of oil.

On the other hand, if the area is not so heavily ridged, the oil could pool in the naturally occurring ice roughness to an average depth everywhere of about 0.05 m. No significant amount of oil would be forced onto the ice surface. The 1.4×10^4 m^3 of oil will then spread under about 0.28 km^2 of ice. For the 45 days of no ice motion, about 5 km^2 of ice would contain the 2.5×10^5 m^3 of oil which spreads beneath the ice.

During the 2.5-day periods when the ice is in motion over the blowout, an area 140 m wide by 15 km long is swept by the blowout plume.

The 2.0×10^4 m^3 of oil released during this time can cover this area (2.1 km^2) to an average depth of about 10 mm. This is less oil than the ice is capable of containing in the underside roughness. Because of the gas that can be trapped beneath a moving ice cover, the area over which the oil spreads will probably be larger, and the concentration of oil less.

During the 90-day blowout, there will be 18 periods of 2.5 days each where the ice is nearly motionless. About 15 percent of the oil (1.1×10^5 m^3) will replace melted ice directly over the blowout. About 35 percent of the oil (2.5×10^5 m^3) will spread under the ice during these stationary periods, covering as little as 0.13 km^2 or as much as 5 km^2 of the ice. The remaining 50 percent of the oil is spread under about 38 km^2 of ice during the 18 periods of ice motion.

The currents over the inner shelf are generally too small to affect the size of the oil-contaminated area. The primary effect of currents will be to control the direction of the oil spread, not the extent of the spread.

Incorporation of Oil Into the Ice

Oil on the upper surface of the ice will be mixed with snow and possibly covered by new or blowing snow. If the oil has spread beneath flat ice, collecting in individual pools averaging 0.15 m in depth, it will be encapsulated by new ice growth below the pools. Approximately 0.1 m of new ice growth may be expected below the pools of oil before ice growth stops in May. If the oil has collected in very deep and continuous pools between confining ridge keels, ice growth may not occur beneath the oil. During late May and June, none of the oil released will be incorporated by new ice growth.

Some new ridges are likely to be built of oiled ice between the beginning of the blowout and June. As much as 5 percent of the ice which passes over the blowout will be thin ice in refrozen leads. If all this ice becomes ridged, then a maximum of 5 percent of the oil might be incorporated into ridges.

Oil may also become incorporated into existing ridges. The ridges in the area are mostly of recent origin and are not completely consolidated. Oil will fill some of the voids in the ridge keels. The percentage of oil involved will be relatively small, but that oil may remain in the ridges through one or more melt seasons.

Transport of Oiled Ice

Between the blowout in early April and breakup in June, the ice can travel up to 60 km/month toward the west. Although the area of oiled ice will not increase during this period, it is possible that individual floes contaminated with oil will be widely dispersed. As the pack ice loosens up in June, this dispersal of oiled floes will become greater. By July, there may be oiled ice floes anywhere between the blowout site and Cape Halkett, 180 km to the west.

Release of Oil From the Ice

In late February or early March, as the air temperature began to rise, brine trapped between the columnar ice crystals began to drain. By late April or early May, the brine channels will have become large enough that oil can travel up the channels and begin to appear on the ice surface. Periods of cold weather will stop the oil flow temporarily, but by late May, pools of oil will be collecting on the ice surface. Because of the lowered albedo of the oiled ice, melting of the ice surface also begins in late May. Oil already on the ice surface and mixed with snow may locally accelerate the appearance of oil pools and ice melting.

Not all the oil will surface until all the level ice over the oil slick has melted. The presence of oil on the ice surface will accelerate the local ice melting by about 2 weeks. By early to mid-July, all the undeformed ice which is contaminated by oil will have melted leaving an oil slick on the water surface.

Most of the oil trapped in ridged ice will not escape at this time. Brine drainage and release of trapped oil will occur, but at a much slower rate than in an undeformed ice sheet. Oil which does escape from a ridge will accelerate melting of the ridge, but the ridge may still last through the summer. By the end of the summer, most of the oiled ridges will be in the northern Chukchi Sea.

Fate of the Oil

As soon as oil begins to appear on the ice surface in May, weathering processes will begin. By the end of June, approximately 50 percent of the oil will have evaporated. Most of the remaining oil is in open-water slicks among the remaining ice floes and grounded ridges west of Cross Island. Due to the partly weathered state of the oil and the intact ice surrounding the oil-contaminated area, the oil slick, or slicks, which may cover several square kilometers of water, are still much smaller than would be a slick of unweathered oil released into open-water conditions. Some water-in-oil emulsions will form where oil is floating on surface melt pools exposed to agitation by the winds. Other weathering processes will take place as the oil is released from the ice, but only insignificant amounts of oil will be involved. The low temperatures, the reduced wind action due to the remaining ice cover, and the thick, viscous oil layer on the water surface will act to inhibit dissolution, bacterial degradation, and dispersion.

The pack ice does not generally retreat until sometime after early July. By that time, some of the oil will have been blown onto island or mainland beaches to the west or southwest due to the prevailing wind direction (from the east or northeast about 60 percent of the time during June). Of course, the probability is high that some of the oil will be blown offshore into the permanent pack ice.

The above scenario assumes that no cleanup of the oil takes place. If part of the oil is cleaned up following the blowout, the major change in the scenario would be a reduction in the amount of oil involved.

Flow Research Report No. 189

Harrison Bay Sea Ice Conditions Relating to Oil Spills

By

D. R. Thomas

Flow Research Company
A Division of Flow Industries, Inc.
21414 - 68th Avenue South
Kent, Washington 98031
(206) 872-8500

Flow Research Report No. 189
April 1981

Table of Contents

List of Figures

1. Introduction

During the next few years there will be many exploratory and possibly production oil wells drilled on the northern continental shelf of Alaska. Worldwide, about one in 3000 offshore wells drilled experiences some kind of blowout. Many of these are relatively harmless in terms of environmental damage. It has been estimated that the chance of a "serious" blowout incident is less than one in 100,000 wells drilled. These odds vary of course with the definition (and definer) of "serious." Irrespective of the exact probability, the possibility exists, and when a serious blowout such as Santa Barbara or IXTOC 1 occurs, the consequences are also serious.

In the near future, drilling in U.S. waters in the Beaufort Sea will proceed from natural or artificial (ice or gravel) islands in relatively shallow waters. While this procedure will reduce the probability of blowouts and possibly the environmental effects by providing a stable base for control efforts and spill containment, it is possible for a blowout to occur away from the drill hole. The 1969 blowout in Santa Barbara Channel occurred through faults and cracks in the rock as far as ~0.25 km from the drill site. Thus, it is certainly conceivable that a blowout could occur underwater away from an island drill platform.

Present regulations require that any offshore drilling in the Beaufort Sea be done in the period from November through March. The entire sea surface is covered by a floating ice sheet during that time, except for the occasional brief appearance of leads of open water. Thus, sea ice will have an important bearing on the behavior and fate of oil spilled by a blowout in the Beaufort Sea.

There has been little practical experience with oil spills in ice-covered waters. Several accidental surface spills have occurred in ice covered waters in subarctic regions, for example the Buzzards Bay, Massachusetts, spill in 1977 (Ruby et al., 1977). These spills have not been in arctic-type ice which will generally be thicker, more continuous, and increasing in thickness throughout the winter. The Canadian government sponsored an oil spill experiment at Balaena Bay, N.W.T., during the winter of 1974-75, as part of the Beaufort Sea Project. That experiment is probably the single most important source of information concerning the interaction of crude oil and sea ice. For practical reasons, logistic and environmental, there were aspects of oil-ice interactions not investigated in the Balaena Bay experimental spills. These include, among others, a moving ice cover, deformation of oiled ice, large ocean currents, and the process of spring breakup when large quantities of oil are present and not being cleaned up.

Research efforts have continued since completion of the Beaufort Sea Project. The Outer Continental Shelf Environmental Assessment Program (OCSEAP) has sponsored a great deal of ecological background research in Alaskan waters, as well as research in specific oil-ice interactions (e.g., the effect of currents on oil under ice, the migration of oil through brine channels) or site-specific descriptions of the ice cover (e.g., ice motions, ice morphology). The objective of the OCSEAP Alaskan program is to conduct environmental studies to provide a basis for making the decisions necessary to ensure protection of the environment during the search for and development of petroleum resources. One aspect of this endeavor is to attempt to predict the consequences of a "serious" polluting incident, such as a large oil well blowout. These predictions are an extremely important part of decision making, whether or not they are formally elucidated.

Of course, the prediction of a complex chain of events such as would follow an oil well blowout is impossible in a deterministic sense. Probabilistic predictions based upon historical data and previous experience are the only realistic results attainable. For some purposes, and at a time when data needed for predictions are lacking, it is preferable to make the worst conceivable case predictions.

As part of the process of predicting the effects of an oil well blowout, it is necessary to describe where an oil spill from a blowout would end up and when it would get there. The oil can be evaporated, dispersed into the water column, frozen into the ice and blown out to sea, moved beneath the ice from one location to another by currents, etc. In each case, the effects upon the environment and biological activity would be different.

The purpose of this report is to summarize relevant knowledge about sea ice conditions in the Harrison Bay, Alaska region. A previous report (Thomas, 1980) dealt with sea ice conditions in the vicinity of Prudhoe Bay. Harrison Bay is only 100 to 200 km west of Prudhoe Bay so it is to be expected that some similarity in ice conditions exists between the two areas. Differences do exist though, due primarily to the coastal configuration and to the absence of barrier islands in Harrison Bay. This report is limited to the geographical area of lease sale 71 near Harrison Bay. Generally, we restrict this report to factors which can be expected to play a major role in the sequence of events following an under-ice oil well blowout in the lease area.

We begin by discussing in Section 2 the geography, climate, and oceanography of the lease sale area. The relevant factors which are discussed include the coastal configuration and the locations of shoals which determine the development of ice zones, the winds which can move and deform the ice, the air temperature upon which ice freezeup, ice growth, and ice breakup depends, and ocean currents which may affect the direction and extent of oil spreading.

In Section 3 we review the characteristics of the sea ice in the lease sale area. The area is divided into zones (undeformed fast ice, deformed fast ice, and deformed and moving pack ice) based upon the morphological traits of the ice. The chronological development of each zone is followed. The ice characteristics which are important in connection with under-ice oil spills are ice freezeup, ice growth and decay, motion and deformation of the ice cover, and variations in ice draft and bottom topography.

And finally, in Section 4 we summarize the sequence of events following an under-ice blowout and review the important aspects of oil and sea ice interactions.

2. Geography, Climate, and Oceanography

2.1 Geography

Lease sale 71 is located on the inner continental shelf off the north central coast of Alaska. The lease area includes Harrison Bay and the waters immediately adjacent.

Between Thetis Island off the mouth of the Colville River and Cape Halkett, Harrison Bay is open to the Beaufort Sea with no intervening barrier islands. Numerous shoals lie just outside the bay though. During the winter and spring, grounded ice features can act as artificial barrier islands, stabilizing and protecting the fast ice. These grounded ice features may remain in place through the summer, offering protection against incursions of the pack ice into Harrison Bay.

Much of Harrison Bay is very shallow, less than 2 m deep and as a consequence, no multiyear ice will be found near shore except as a result of storm surges. The shallow inner bay will be essentially ice free during the summer with new ice forming in place each fall.

Outside the bay, the shelf slope is fairly uniform to the shelf break except for the shoal areas. During the summer, this area may or may not be ice free depending upon the winds and resulting pack ice motions. During the winter, large shearing or compressive forces are dissipated in this area when the pack ice is in motion relative to the shore and the fast ice. Many of the resulting ridges become grounded, moving the zone of relative motion, the shear zone, further offshore.

Several small streams drain into Harrison Bay but the Colville River is the dominant feature. In the spring, river runoff increases by orders of magnitude, causing early ice melting and breakup near the river mouths. As much as 200 to 300 km^2 of ice may be flooded by the Colville runoff in late May or early June. Large quantities of suspended particulate matter are discharged at this time. This sediment lowers the albedo of the ice, further enhancing melt.

2.2 Climate

Winds and air temperature are of crucial importance to the nearshore ice morphology in the Beaufort Sea. In the fall, development of the fast ice cover, ice motion and deformation, and location of the pack ice edge all depend upon atmospheric conditions. Throughout the winter, pack ice motions, and thus the development of the stamukhi zone, depend upon the wind. Melting and breakup of the fast ice in the spring is largely controlled by the number of accumulated thawing-degree days (TDD). During the open-water season, the nearshore currents are essentially wind driven.

2.2.1 Winds

The most complete source of surface wind data for the north coast of Alaska is the Climatic Atlas of the Outer Continental Shelf Waters and Coastal Regions of Alaska, Vol. III, Chukchi-Beaufort Sea (Brower et al., 1977).

In Figures 2.1, 2.2, and 2.3, we have summarized the wind data from the Climatic Atlas for Oliktok, Alaska, the station nearest Harrison Bay. Figure 2.1 shows the monthly cumulative distribution of wind speeds; the speeds are given in knots (one knot = 0.515 m/s). Figure 2.2 shows the monthly cumulative distribution of wind directions by octant. Since larger winds are more important in terms of ice motion and deformation, we show in Figure 2.3 the monthly cumulative distribution of direction for winds greater than 11 knots (6 m/s) in magnitude.

Winds for the offshore region of the Beaufort Sea may be computed from sea level pressure maps available from the National Center for Atmospheric Research for historical data (Jenne, 1975) or the National Weather Service analysis for current data. The accuracy of this data has been discussed by Leavitt (1979), and the resulting wind-driven ice drift has been presented by Thomas and Pritchard (1979).

2.2.2 Temperature

Atmospheric temperature statistics for the central Beaufort Sea coast are given in Figure 2.4. The data were taken from the Climatic Atlas (Brower et al., 1977) for the Lonely and Oliktok stations. Monthly median temperatures as well as the 5th and 95th percentiles are presented.

The temperature statistics may be compared with the dates of fast ice freezeup and breakup given by Barry (1979). The median air temperature is below -1.8° C, the freezing point of sea water, from about 21 September on. Barry found that new ice forms in the fast ice zone about 3 October. The 2-week difference is presumably the time it takes for the shallow, well-mixed

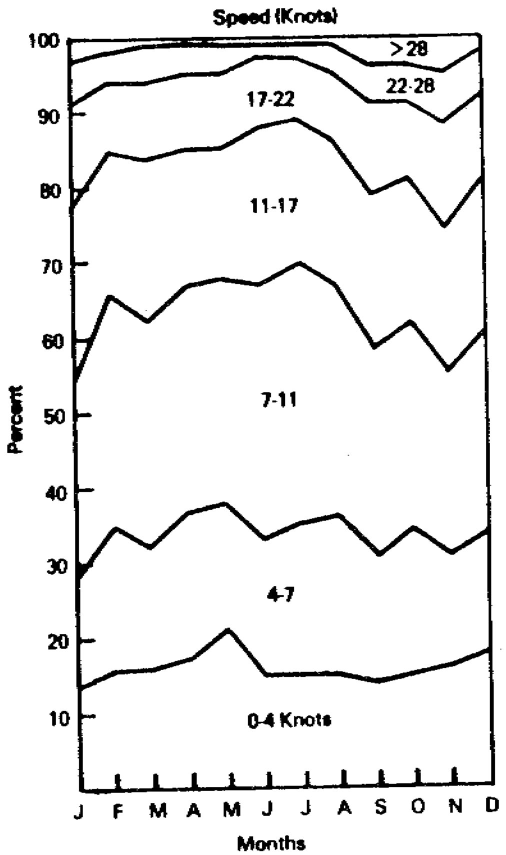

Figure 2.1. Cumulative Monthly Wind Speeds at Oliktok, Alaska. Wind speed intervals are given in knots (1 knot = 0.515 m/s). Data were taken from the Climatic Atlas (Brower et al., 1977).

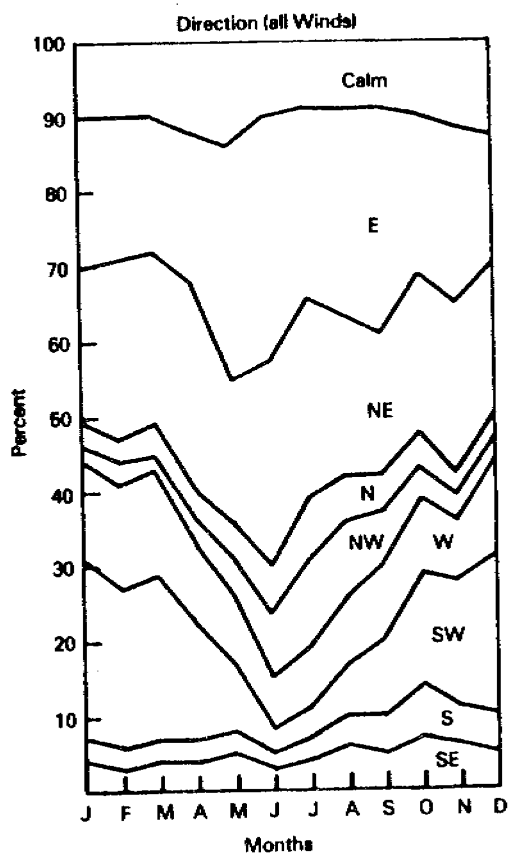

Figure 2.2. Cumulative Monthly Wind Directions at Oliktok, Alaska. Wind directions are given by octant. Data were taken from Climatic Atlas (Brower et al., 1977).

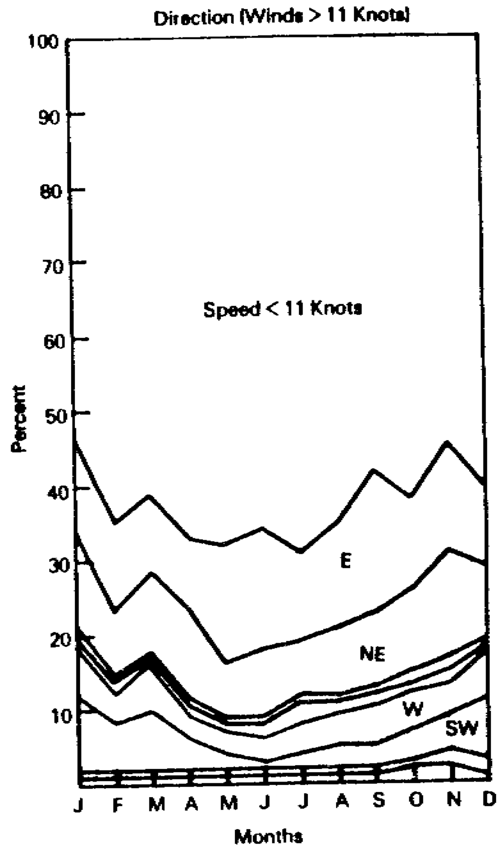

Figure 2.3. Cumulative Monthly Wind Directions for Wind Speeds Greater than 11 Knots (5.7 m/s) at Oliktok, Alaska. Wind directions are given by octant. Data were taken from the Climatic Atlas (Brower et al., 1977).

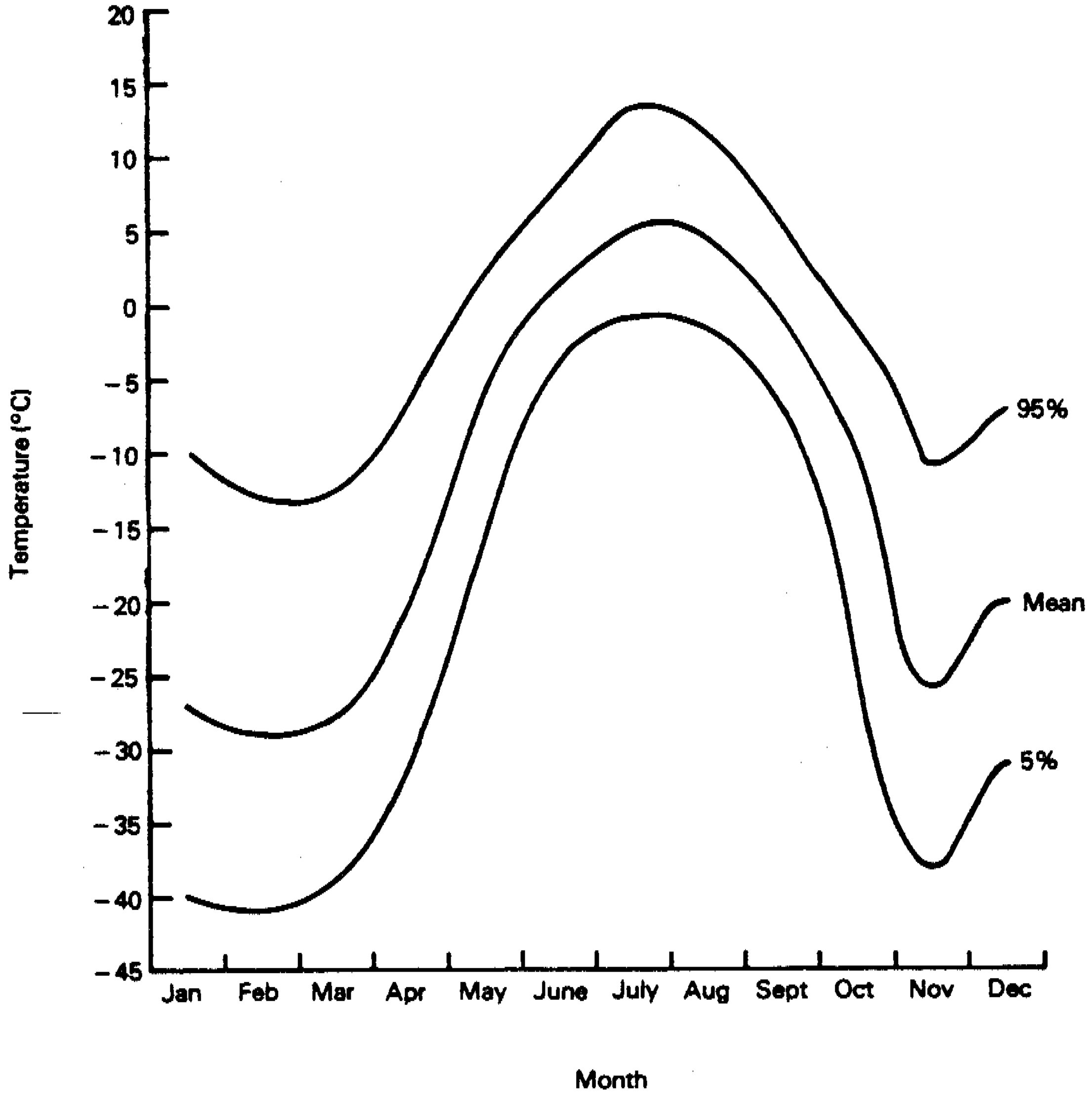

Figure 2.4. Monthly Air Temperature Statistics for Oliktok, Alaska. The mean, 5th percentile, and 95th percentile are plotted at mid-month and connected by a freehand curve. Data were taken from the Climatic Atlas (Brower et al., 1977).

waters near shore to be cooled to near-1.8°C. There is also a ±10 day uncertainty in the dates given by Barry.

Barry (1979) also reports the first melt pools forming on the fast ice about 10 June and the fast ice mostly melted by 1 August. Bilello (1980) found a roughly one-to-one correspondence between accumulated TDD above 0°C and the decrease in ice thickness in centimeters for several Canadian and Alaskan stations. From the median temperature curve, we see positive temperatures beginning about 10 June. By 1 August, there are roughly 135 accumulated TDD. Since the average ice thickness is assumed to be about 160 cm, the agreement is reasonably good. The difference is probably due to lateral melting of the ice once open water begins to appear (about the end of June).

2.3 Oceanography

On the inner shelf in summer, currents are wind driven following the bottom topography and dampening quickly when the wind stops. After a solid ice cover forms, the transfer of momentum from surface winds to the sea is greatly reduced. From October through June, then, under-ice currents are driven by some other source in the fast ice zone. On the average, the ice freezes to a thickness of up to 2 m during the winter and will freeze fast to the bottom in shallow areas. Where the ice freezes close to the bottom, the remaining water becomes extremely saline due to brine exclusion. This cold, dense water will flow offshore (downslope) to be replaced by thermohaline circulation.

Tidal amplitudes are small along the north coast of Alaska, ranging from 0.05 to 0.2 m. In summer, the associated currents are also small, less than 0.01 m/s. In winter, the ice may act to intensify tidal currents by limiting the cross section available for water to flow through (Barnes et al., 1979). Net transport over periods greater than 12 hours, however, will be zero. The ice cover may also intensify currents due to storm surges and currents associated with flooding of the ice in the spring when the rivers thaw.

Very little information has been published about the underice currents in Harrison Bay. Weeks and Gow (1980) report one current measurement beneath the fast ice in Harrison Bay. The measurement was of instantaneous velocity a few centimeters beneath the ice during the spring of 1978. The water velocity was

0.03 m/s toward the NW (325°). Just to the NW of Cape Halkett, Weeks and Gow measured instantaneous under ice currents of 0.06 m/s toward the NW (288°).

Outside Harrison Bay, but beneath the fast ice along the north coast of Alaska, instantaneous current measurements made by Weeks and Gow (1980) and Kovacs and Morey (1978) are small (0.01 to 0.12 m/s) and generally along shore.

Aagaard (1980) has reported time series of Lagrangian current measurements taken beneath the ice in the southern Beaufort Sea. Two current meters were located at 10 m below the surface in 25- and 35-m-deep water north of Narwhal Island during April 1976. He recorded currents of 0.05 m/s or less with variable direction. Larger currents were measured further offshore in much deeper water but those measurement were made 40 m or more beneath the ice and are not relevant to oil-ice interactions. These deep currents are important when considering the transportation of the ice, though.

Lagoon inlet channel currents were measured by Matthews (1980) in 1977-78. One current meter was placed 4.7 m deep in the lagoon inlet channel to the east of Egg Island in 5-m -deep water. Currents of 0.02 to 0.05 m/s were recorded through the first part of June 1977 until the ice was flooded by the Kuparuk River. At that time, currents rose to 0.2 m/s out of the lagoon and the salinity dropped dramatically. Current measurements made in May 1972 by Barnes et al. (1977) show tidal components of up to 0.2 m/s through the Egg Island channel with a much lower mean flow. A single measurement by Kovacs and Morey (1978) in the channel between Narwhal and Jeanette Islands shows a current of 0.11 m/s in May 1976 at 0.1 m under the ice. These inlet channel current measurements are probably typical of currents between some of the grounded ice features in Harrison Bay.

A number of measurements have been made within the lagoon system to the east of Harrison Bay. Just south of Narwhal Island under 0.1 m of ice, Kovacs and Morey (1978) made current measurements at five locations in shallow water. The currents averaged 0.04 m/s in May 1976. Weeks and Gow (1980) gives three measurements within the lagoon system averaging 0.02 m/s at 0.2 m under the ice in April 1978. Barnes et al. (1977) measured a current in shallow water north of the Egg Island Channel in spring 1972 of less than 0.02 m/s. Matthews (1981) has made continuous time-series measurements of currents at a site south of Narwhal Island in the middle of Stefansson Sound. Currents were measured at 1 and 2 m above the bottom in 5.6-m-deep water.

Average currents were less than 0.01 m/s, but extremes of up to 0.11 m/s were measured at both meters. The currents were uniformly offshore. For continuity, Matthews argues that a return current of up to 0.2 m/s onshore must flow near the surface and that this return flow is driven partly by salinity differences but primarily by tidal and surge pumping. No strong near surface flow has been observed but Matthews (1980) also reports that many of the under ice drifters released beneath the ice during the spring were found directly on-shore of the release points.

In summary, measured near-surface currents in the offshore continental shelf waters do not exceed about 0.1 m/s, though currents at greater depths may be higher. Currents in openings between barrier islands or grounded ice features may be twice as high. A tidal component of up to 0.2 m/s may be common, but this provides no net transport. Currents of 0.2 m/s may also be seen off the Colville River delta during flooding of the ice in June. Other mechanisms for producing large currents, such as storm surges, have not been observed during long time-series current measurements.

3. The Ice Environment

The sea ice in the lease areas off the north coast of Alaska cannot be described in any simple way. The character of the ice cover changes with time during the year, varies with location, is changed to violent episodic events, and can differ markedly from year to year. Ice thickness near shore, for example, varies from zero (open water) in the summer to about 2 m for first-year ice in the spring. Multiyear ice reaches an equilibrium thickness of about 3 m, and deformed ice may reach thicknesses of 20 to 40 m. Bottom roughness also varies greatly, from smooth, thin ice with only millimeter-scale roughness features to the many meters of relief beneath ridges and rubble fields.

To simplify the problem somewhat, we have divided the ice off the north coast of Alaska into zones based upon large-scale dynamic processes and the resulting ice morphology. These zones are the fast ice zone, the stamukhi zone, and the pack ice zone. Others have generally separated the Arctic into a pack ice zone and a seasonal ice zone and then divided the seasonal zone into the fast ice, etc. This division is useful when open water is being considered, but when the dynamics of ice motion is of interest, it is more useful to consider the ice cover in terms of the fast ice zone, the stamukhi zone, and the pack ice zone.

The fast ice zone is the nearshore area protected by coastal promontories, barrier islands or shoals and grounded ridge systems. This zone is usually ice free during the summer with new ice forming in place during the fall. The fast ice is relatively smooth and undeformed. In Harrison Bay, a second region of relatively undeformed and motionless first year ice forms outside the area of early winter ridge building activity. This ice is considered to be part of the fast ice zone although it developes later than the fast ice adjacent to shore.

Seaward of the fast ice zone is the stamukhi zone. This is a region of heavily deformed seasonal ice which forms throughout the winter in essentially the same area each year. The stamukhi zone is the past and present location of the shear zone, which is a region several hundred meters wide which marks the active boundary between the moving pack and the stationary fast ice. The location of the shear zone is determined by the geographical configuration of the coastline. Coastal promontories and barrier islands offer protection from the moving pack, which has an average motion to the west along the north Alaskan coast. Large shear ridges form along the outer edge of the protected fast ice. Some of these ridges become grounded and thus act like artificial barrier islands or coastal promontories. The shear zone must then occur seaward of these grounded ridges. As winter progresses, more ridges form and become grounded, moving the shear zone seaward and extending the region of deformed ice. This region of deformed ice, which was first called the stamukhi zone by Reimnitz et al. (1977a), may extend along the coast in a band 20 to 50 km wide. As ridges become grounded, large areas may become protected from incursions of pack ice so that smooth undeformed regions of fast ice may form inside the stamukhi zone. The stamukhi zone is sometimes considered part of the fast ice zone since grounded ridges immobilize it, but we consider it a separate zone due to the character of the ice relief and the processes which create the zone.

Outside the stamukhi zone is what we consider the pack ice zone. The pack ice zone can be further divided into a seasonal ice zone and a permanent pack or central Arctic zone. The seasonal zone begins seaward of the stamukhi zone and includes the region which was largely ice free during the most recent summer season. Although the lease areas will not extend beyond the seasonal zone, in some years the central Arctic pack is driven close to shore so that the following ice season the seasonal ice zone has the characteristics of the permanent pack; therefore, both types of pack ice must be considered. In general, the pack ice zone is characterized by large motions and the formation of leads and ridges between floes.

The three geographic ice zones, fast ice, stamukhi, and pack ice, are described fully in the following sections. The general characteristics of the ice in each zone, including seasonal variations, thickness distribution, deformations, ridging, and bottom roughness, are discussed. A discussion of the open-water season which is to some extent applicable to all three zones is presented first.

3.1 Open-Water Season

Normally, the southern Beaufort Sea is ice free for about 2.5 months of the year, from late July to early October. The seaward extent of open water along the Harrison Bay sector of the coast varies throughout the course of the season. In situ melting varies little from year to year in the nearshore region. The ice begins melting in mid-June, primarly near river mouths. By the end of July, the fast ice is essentially gone.

The extent of open water from this time on depends upon the location of the southern edge of the polar pack. The position of the pack ice edge can change due to episodic events such as storms and can also vary from year to year due to long-term flow patterns in the atmosphere. Stringer (1978) examined Landsat images and produced open-water maps for the years 1973 to 1977. By July open water extends from 10 to 30 km offshore in the Harrison Bay sector. The greatest year-to-year variation occurred to the west at the Colville River. A survey of historical data (Hunt and Naske, 1979) confirms this wide range of open-water extent. Historical open water extent at Harrison Bay during July varies from about 30 to 60 km. During August the open water is from 10 to 130 km wide at Harrison Bay, and during September from 30 to 105 km.

Ice edge statistics from the Climatic Atlas for the Chukchi-Beaufort Seas (Brower et al., 1977) indicate that the extreme distance from the coast near Harrison Bay to the ice edge (defined as an ice concentration of one-eighth or more) can be 400 km (late September). The mean distance taken from the atlas also peaks in September at about 100 km from shore.

In Figure 3.1 we present a plot of the mean and extreme distance from the shore near Cape Halkett and from the Colville River delta to the ice edge. The data were taken from the Climatic Atlas which in turn used aerial, ship, and satellite observations of the ice edge for the years 1954 to 1970. Numbers were estimated to the nearest 5 km from the maps. The ice edge was defined as the location of ice concentrations greater than one okta. Note that the extreme minimum extent of open water is zero.

While the extreme minimum extent of open water is zero, this does not mean that the fast ice does not melt and break up. Rogers (1978), in correlating accumulated TDD with fast ice breakup, records only 2 years between 1921 and 1976 when less than 250 TDD were accumulated. Some melting and breakup probably occurred even during those 2 years. The primary reason for a lack of open water along the coast is incursions of wind-driven pack ice.

Rogers (1978) has examined temperature data from 1921 and meteorological data from 1940 to the present. He has found correlations between air temperature, sea level pressure (SLP) distribution, and surface wind direction with northward pack ice retreat at Pt. Barrow. The trends in SLP and accumulated thawing-degree days (TDD) indicate a decline in favorable nearshore ice conditions. Due to topological effects, the open-water extent

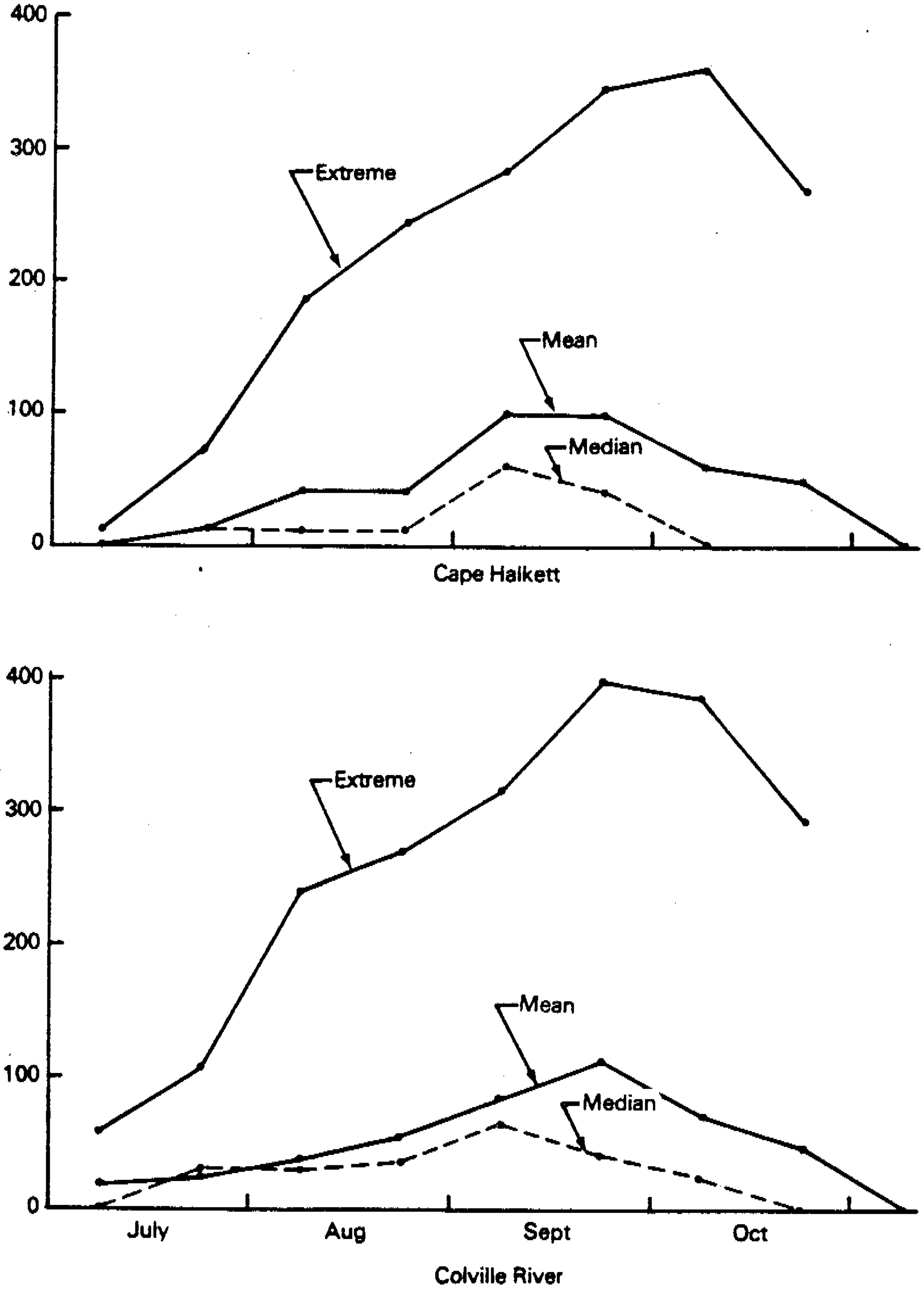

Figure 3.1. Monthly Mean, Median and Extreme Distance from Shore near Harrison Bay to the Ice Edge. Monthly Extreme Minimum Distance is Zero for all Months. Data were Taken from the Climatic Atlas (Brower et al., 1977).

in the Harrison Bay region does not correspond directly with that at Pt. Barrow, but the basic trend is the same.

In summary, the fast ice begins to melt in mid-June, and from late July to early October, the fast ice zone is generally ice free. The mean open-water extent is 100 km offshore in September, and the extreme distance can be more than 400 km. Large variations in the open-water extent are caused by incursions of pack ice driven shoreward by strong winds.

3.2 Fast Ice Zone

The fast ice zone is the area near shore that is usually ice free during the summer with new ice forming in place during the fall. The ice is relatively smooth, remaining motionless and protected from large deformations by barrier islands and grounded ridge systems.

3.2.1 Freezeup

Sometime in late September to mid-October new ice begins to grow in the fast ice zone. Sea ice can begin to grow in one of three different forms: columnar, frazil, or slush ice (Weeks, 1976; Martin, 1977). Columnar ice grows in still sea water. This ice is relatively smooth on the bottom, but the lower 10 to 40 mm consist of a porous and fragil skeletal layer. Frazil ice grows when a wind blows across sea water that is at its freezing point. Wind-generated waves stir and slightly supercool the water column so that ice crystals form below the surface. Upon reaching the surface they form a porous mass with a random crystal structure. The wind tends to pile this ice up creating thickness variations of several centimeters. When snow accompanies the wind, the third kind of ice, slush ice, forms. The snow is mixed with the sea water and is probably accompanied by frazil ice formation. Once a layer of ice solid enough to protect the sea from direct stirring by the wind has formed, columnar ice growth begins. As sea ice grows downward, the ice crystals form a series of plates of pure ice with layers of extruded brine between. As growth continues, bridging occurs laterally between the plates, trapping series of elongated brine pockets. As the ice season progresses, some of these brine pockets drain or become interconnected vertically and horizontally. It is not until about late April or May when air and ice temperatures warm up toward freezing that brine drainage results in top-to-bottom opening and enlarging of the drainage channels. The horizontal spacing of these open channels is about 0.1 m (Martin, 1977).

Barry (1978, 1979) studied satellite images for 5 years and arrived at the average date of new ice formation of 3 October, $\pm$ 7 to 10 days. The new ice begins to form first in the shallow waters near shore where salinity is lower and where the water can cool faster. By mid-October, the ice cover has usually become continuous (Barry, 1978, 1979), weather conditions permitting. This thin ice in unprotected areas is free to move when driven by modest winds and can easily be deformed.

3.2.2 Deformation

In regions sheltered by the barrier islands or grounded ridge systems remaining from previous seasons, it is possible for the fast ice to grow in place with little or no surface relief, depending upon the winds (and waves) during freezeup. Generally, though, some deformation will occur in this thin ice. The deformation may occur as pancake floes, rafting, or small pressure ridges. Most of the deformation will create relief of only a few centimeters.

The amount of deformation that occurs is dependent on the strength of the ice and the wind stress. An estimate of the isotropic compressive strength of a uniform sheet of thin ice (less than about 0.5 m thick) may be made based upon the ice model developed by AIDJEX. Using the AIDJEX model formulation, Rothrock (1979) estimated the compressive strength (p*) of ice of uniform thickness to be $0.17\ h^2 \times 10^5$ N/m where h is the ice thickness in meters. Pritchard (to appear, 1981), using different values of some of the parameters, calculates ice strength to be 2 or 3 times larger than that. Parmerter (1974) has modeled the rafting of thin ice finding a strength about one-half that based upon the ridging model, using nominal values of ice properties. Parmerter also calculated that the switch from rafting to ridging occurs when the ice is about 0.17 m in thickness.

Assuming that a strength of $0.17\ h^2 \times 10^5$ N/m is of the right order of magnitude for thin sea ice, what kinds of winds will cause deformation? The stress generated by a wind will depend upon the speed of the wind, the fetch of the wind, and the drag coefficient. The wind stress times the fetch, or the force that must be resisted by the strength of the ice, p*, may be written as

$$\tau^* = \ell \rho_a C_a U^2 \qquad (3.1)$$

where ℓ is the fetch, ρ_a is the air density, C_a is the atmospheric drag coefficient, and U is the wind speed. Using nominal values of $\rho_a = 1.4\ kg/m^3$ and $C_a = 9 \times 10^{-4}$ (Thomas and Pritchard, 1979), $\tau^* = 1.26\ \ell U^2 \times 10^{-3}$ N/m. Ice motion and deformation will occur whenever $\tau^* > p^*$, or when $\ell U^2 > 1.3\ h^2 \times 10^7\ m^3/s^2$.

In Figure 3.2 we show the critical values of wind speed, U, as a function of ice thickness, h, for several values of fetch, ℓ. The information in Figure 3.2 is not intended to be used as an accurate predictor of when ice deformation occurs because of complicated spatial variations in the stress field that depend on shoreline geometry and far-field sea ice stresses. It does illustrate, however, that for reasonable values of material properties, modest winds can produce deformation in very thin ice.

As the ice becomes thicker during the winter, it becomes strong enough to withstand the normal range of wind stress. Assuming that this region is protected from incursions of pack ice by barrier islands or grounded ridges, no significant deformation occurs. Measurements of motion in the fast ice zone during April and May 1976 and 1977 (Tucker et al., 1980) and from December 1976 through May 1977 (Agerton and Kreider, 1979) showed displacements of at most a few meters; these have been attributed to thermal expansion. Tidal cracks also form at the junction of floating ice and ice grounded in water depths less than the ice thickness. About 75 percent of the fast ice zone in Harrison Bay lies between the shore and the 2 m water depth (about the maximum thickness for first-year ice). Therefore, a majority of the ice in this zone will become grounded by late winter.

Storm surges may also occur during the ice season. Mid-winter surges with heights of up to 1.5 m have been reported (Henry and Heaps, 1976). Negative surges of 1.0 m have also occurred (Aagaard, 1978). These events would tend to fracture the ice cover but not to cause any significant deformation.

3.2.3 Ice Thickness

Measurements of the fast ice thickness have been made at several locations along the southern Beaufort Sea coast. Schell (1974) presents a composite of ice thickness data taken during the years 1970 to 1973 at Harrison Bay-Simpson Lagoon and at Elson Lagoon-Dease Inlet. New ice was observed to form around the first of October and to grow in thickness almost linearly through the next February. Growth rates were about 10 mm/day, decreasing somewhat during March

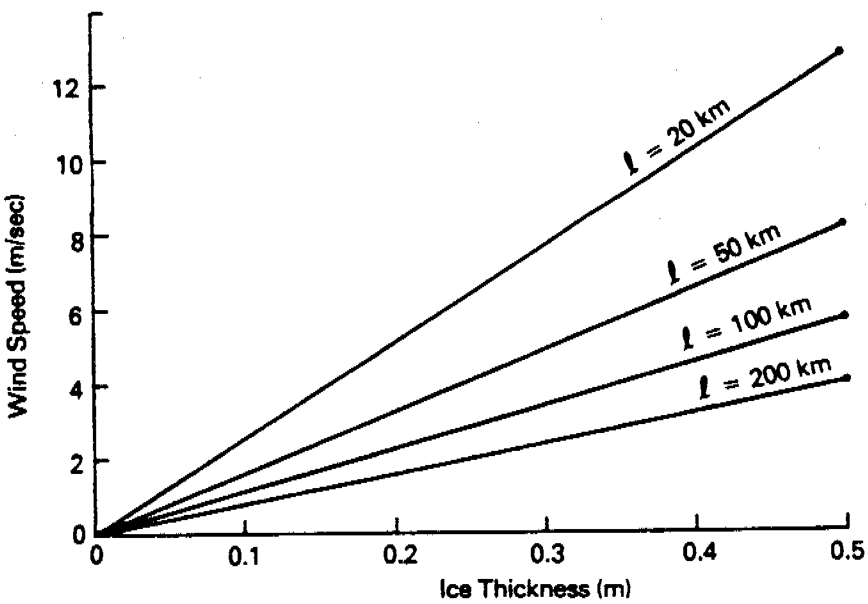

Figure 3.2. Wind Speed Needed to Cause Deformation in a Uniform Ice Sheet, as a Function of Ice Thickness and Wind Fetch.

and April and leveling off during May. The maximum mean thickness was about 1.8 m with a range of 1.45 to 2.25 m. Schell's data is reproduced in Figure 3.3.

NORCOR (1975) presents the results of ice thickness measurements at Balaena Bay and Cape Parry during the 1974-75 season. While these locations are about a thousand kilometers east of Harrison Bay, the latitude is about the same. A maximum mean thickness of 1.55 m was observed during May with a range of 1.35 to 1.75 m (approximately 24 percent of the mean). Data for Cape Parry only for the years 1970 to 1975 showed a median ice thickness in May of about 1.70 m with a range of 1.45 to 2.00 m (approximately 32 percent of the median).

Kovacs (1979) reports ice thickness measurements made in May 1978. At a site near Tigvariak Island, the mean thickness was about 1.56 m. This site had a heavy snow cover and could be expected to have thinner ice than areas with less snow. Kovacs (1977) reports average ice thickness measurements of 1.87 m near Prudhoe Bay in April 1976. The range of measurements was 1.70 to 2.01 m (approximately 17 percent of the mean).

Barnes et al. (1979) report on ice thickness measurements at three sites in Prudhoe Bay-Stefansson Sound taken in May 1978. Means at the three sites ranged from 1.34 to 1.57 m with ranges of 14 to 31 percent of the mean. Correlations between snow depth and ice thickness ranged from -0.5 to -0.7. Obviously, the thickness to which fast ice grows depends upon location, year, and snow cover. The actual mean thickness is not too important since the primary effect of thickness will be the time it takes for the ice to melt and break up in the spring.

Bilello (1980) looked at decay patterns of fast ice, primarily in the Canadian Archipelago. From a maximum thickness in May (1.55 to 2.30 m), the ice generally melts to zero thickness during the first 3 weeks of July. Decay at Kotzebue, the only Alaskan station studied, occurred in the later part of June. These dates correspond roughly with the date of 1 August given by Barry (1979). All these miscellaneous data are shown in Figure 3.4.

From the data described above it should be possible to give the range of mean ice thickness throughout the year in the fast ice zone. First, freezeup takes place about the first of October but probably varies a week or so in either direction. Growth rates are approximately linear at about 10 mm/day through the end of February. Maximum ice thickness is reached about mid-May

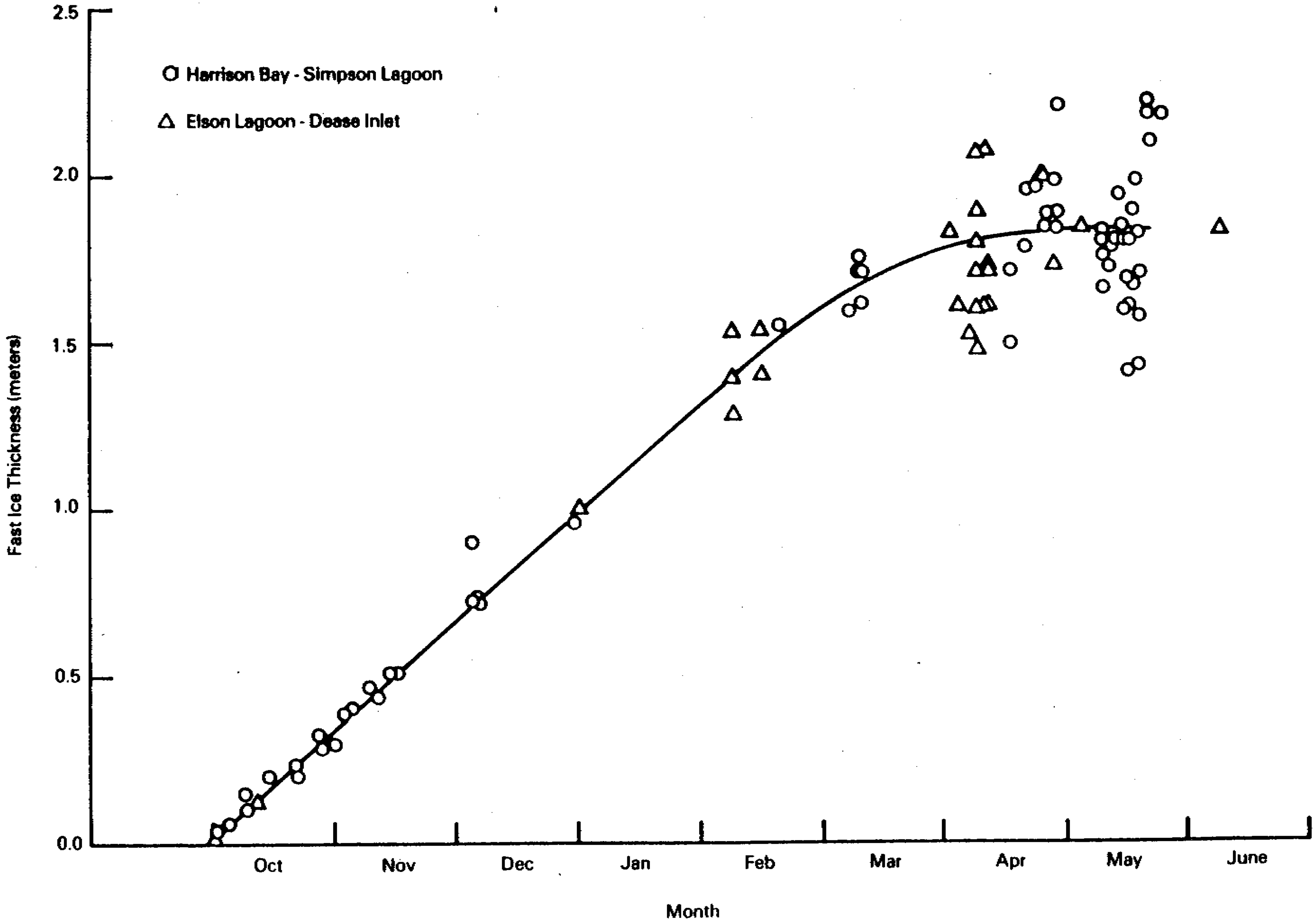

Figure 3.3. Fast Ice Thickness Data, North Coast of Alaska, 1970-73. (Figure 5 from Schell, 1974.)

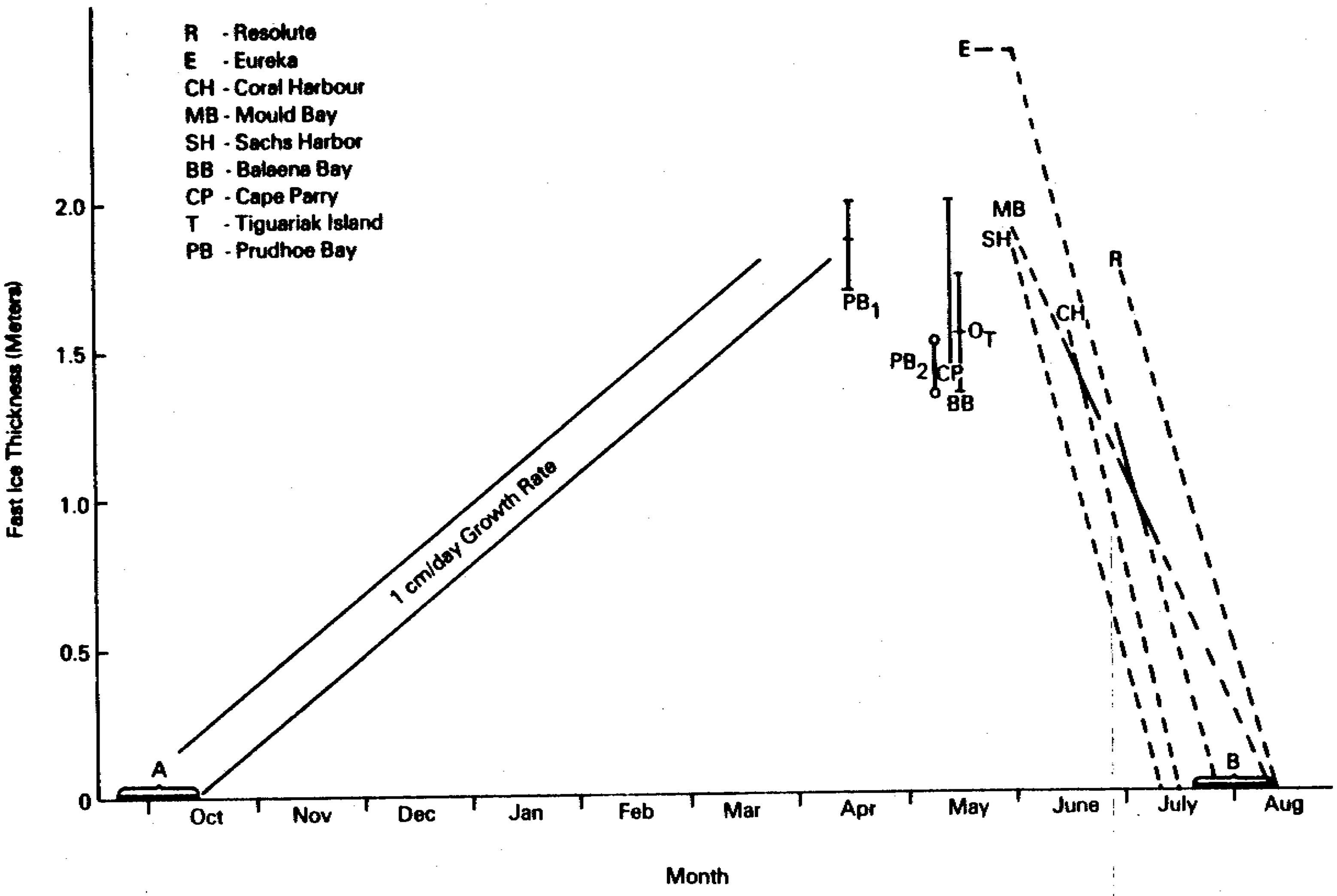

Figure 3.4. Composite Data for Arctic Fast Ice Growth, Decay, and Thickness Range. Intervals A and B indicate the approximate dates of freezeup and ice-free water in the fast ice zone along the north coast of Alaska. Solid lines represent ice growth of 1 cm/day beginning early and late in interval A. Dashed lines are typical fast ice decay rates at various Arctic stations (Bilello, 1980). Vertical bars are ranges of fast ice thickness measurements (NORCOP, 1975; Kovacs, 1977 and 1979; Barnes et al., 1979).

with melting starting around the first of June. By August, again plus or minus 1 week, most of the ice will have melted. The average ice thickness in May may vary between 1.35 and 1.85 m, depending upon location and weather (temperature and snowfall) that season. Figure 3.5 shows this range of mean ice thicknesses.

3.2.4 Bottom Roughness

The bottom roughness is a primary factor when oil containment is being considered, since oil released beneath the ice would immediately fill any under-ice voids. Bottom roughness is measured in terms of the variations of ice draft over a given area. The reports discussed in the previous section give ranges of ice thicknesses from 14 to 44 percent of the mean. Since these are thickness variations, the variations in draft must be somewhat less. Using the data presented in Barnes et al. (1979) for the Prudhoe Bay area in May, the variations in draft amount to 26, 32, and 40 cm for three sites, corresponding to 24, 17, and 26 percent of the mean ice thickness. NORCOR (1975) found the fast ice in Balaena Bay to have a maximum variation in thickness of 20 percent the ice thickness for ice greater than 0.5-m thick. This thickness variation is related to variations in snow cover on top of the ice (Barnes et al., 1979; Kovacs, 1979).

For new ice less than 0.5 m in thickness, other mechanisms act to cause bottom roughness, as discussed in Section 3.2.1, Freezeup. Thickness variations of thin ice have not been reported in the literature. For ice of 0.5 m and thicker, NORCOR (1975) reports that in addition to the large-scale roughness due to variation in the snow cover, a small-scale roughness with relief of a few centimeters and spacings of 0.1 m was present under the ice. This scale of variation was attributed to random variations in the ice growth. It seems reasonable to suppose that these random variations in thickness also occur under very thin ice.

3.2.5 Ice Decay and Breakup

In late May or early June, the decay of the fast ice in the Beaufort Sea begins. The first stage of the decay is the flooding of nearshore ice by the increasing river flow. Areas of several hundred square kilometers may be flooded in early June (Barry, 1979). The first openings in the fast ice zone appear near the river mouths. These shore polynyas spread laterally and

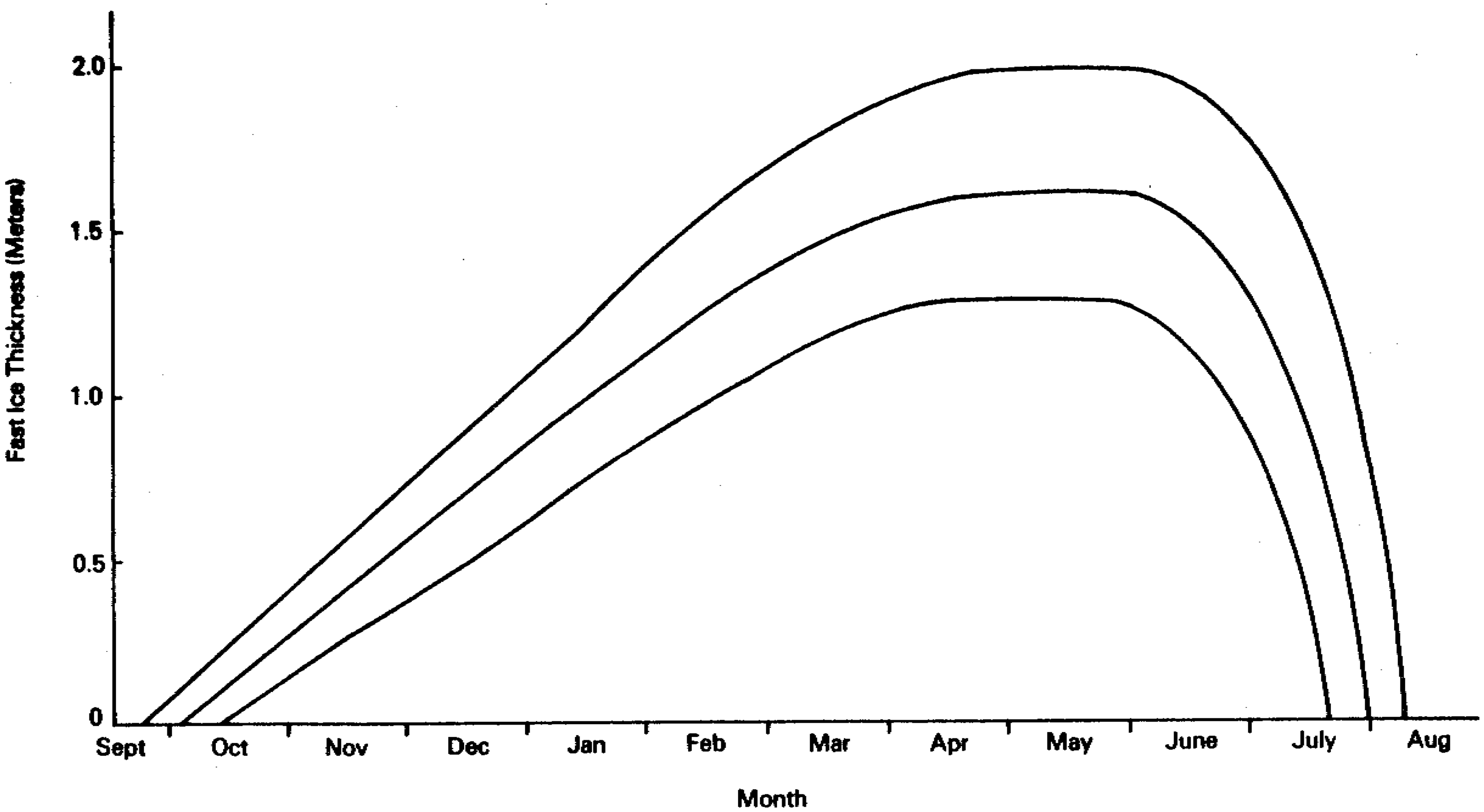

Figure 3.5. **Typical Fast Ice Mean Thickness and Approximate Range of Mean Thicknesses Throughout the Year for the North Coast of Alaska. These curves are derived from the data presented in Figures 3.3 and 3.4.**

seaward from mid-June through early July. Meanwhile, the ice sheet itself is melting from the surface. The first melt pools form on the ice surface about 10 June (Barry, 1979). By the end of June, the fast ice has thinned and weakened enough that wind and water stresses can cause movement and openings. The first ice motions are often toward the shore polynyas. Early in July, some of the surface melt-water ponds drain through cracks and thaw holes.

Seaward of the smooth fast ice zone, the stamukhi zone remains mostly fast during this time due to grounded ridges. Therefore, the extent of nearshore ice motion is limited by the stamukhi zone. The melting fast ice will almost certainly drift about a great deal within the limited area available. During the months of June and July, approximately 60 percent of the winds blow from the east or northeast. The ice drift is therefore mostly toward the west.

The nearshore area is usually ice free or nearly so by the first of August. The actual date by which an area is ice free will vary greatly due to the ice thickness, the temperature, and the movement of loose ice from one area to another by wind. The melting rate of the ice is almost linearly related to accumulated thawing-degree days, one centimeter of ice being melted for each TDD (Bilello, 1980).

3.3 Stamukhi Zone

Following Reimnitz et al. (1977a, 1977b) we use the term "stamukhi zone" for the recurring band of grounded ridges lying seaward of the fast ice zone. Since new ridges are being built and becoming grounded throughout the ice season, the dimension of the stamukhi zone is expanded with each ridge which becomes grounded. At times, we use the term "stamukhi zone" to mean the entire region where grounded ridges normally occur. Context will determine which of these meanings is implied.

3.3.1 Freezeup

Early in the fall during freezeup, most of the stamukhi zone is covered by thin new ice. Remnants of the previous winter's grounded ridge systems may have survived the summer. Some multiyear floes may be incorporated in the ice cover forming in the outer part of Harrison Bay depending upon the position of the pack ice at the time of freezeup. The amount of multiyear ice in the entire seasonal ice zone can range from near 0 to near 100 percent. The stamukhi zone, being relatively close to shore, probably would have low concentrations of multiyear ice. No significant amounts of multiyear ice will be found for several kilometers offshore inside Harrison Bay because of shallow water.

Since the ice is mostly thin during the fall in this area, deformation occurs easily with only moderate winds or pack ice pressure. During the early part of the ice season, this area will develop much as the fast ice zone does.

3.3.2 Deformation

By late November, the new ice has grown to a thickness (0.5 m or more) that can resist wind stresses generated within this area. The pack ice offshore can still be moved by wind of a sufficient magnitude acting over a much larger fetch. The motion of the pack ice off the north coast of Alaska is generally westward. When a component of onshore stress exists in the pack, along with an alongshore motion, a line of slippage occurs between the moving pack and the stationary fast ice. The location of this line of slippage depends upon the configuration of the coastline, coastal promontories tending to protect areas downstream (to the west). The barrier islands and surviving grounded ice features act as extensions of the coast. Shear ridges develop along this line of slippage. The actual shear ridge building seems to occur in a zone only a few hundred meters wide (Reimnitz et al., 1977a, 1977b) which is called the active shear zone.

As shear ridges are being built, some become grounded. This grounding initially occurs between the 10- and 20-m isobaths, depending upon the shape of the coast and the size of the ridges being built. When a ridge becomes grounded, it stabilizes the shoreward ice, so the active shear zone must move seaward. As the shear zone is continually moved seaward during the course of the winter, an ever-widening zone of deformed ice and grounded ridges is left behind. By late winter, this deformed ice zone, the stamukhi zone, can be more than 50 km wide off Harrison Bay. The stamukhi zone off Harrison Bay consists of two zones of deformed ice separated by an area of relatively undeformed ice. This configuration of the stamukhi zone and fast ice zone is well documented (Stringer, 1978) and appears to be an annual feature. According to Reimnitz et al. (1977), this separation of the stamukhi zone is best explained by the generally westward moving pack ice in the southern part of the Beaufort Sea interacting with the irregular shoreline geometry early in the ice season, and grounded ice features later in the season. During the fall and early winter when the ice is thin the line of slippage between the moving pack ice and the shore fast ice roughly follows the major coastline configuration. Ridges built during this time will become grounded in shallow waters. In Harrison Bay, the bottom contours generally follow the coastline, extending into the Bay. Just east of Harrison Bay, several shoals are located 25-30 km from the coast. When ridges become grounded on these shoals, the line of slippage will occur outside of these stamukhi, and extend across Harrison Bay to the shoals off shore of Cape Halkett. Ridges forming along this shear line may still become grounded in the relatively shallow (less than 20-m deep) waters outside Harrison Bay. The area between this shearline and the early season grounded ridges which conformed more closely to the coast line, develops throughout the remainder of the season as floating fast ice.

The stamukhi zone shoreward of the active shear zone exhibits little significant motion throughout the winter. Tucker et al. (1980) and Weeks et al. (1977) report measured motions in the fast ice of only a few meters which they attribute to thermal expansion of the ice. In the stamukhi zone, motions were larger but still on the order of hundreds of meters during the months of April and May. The stations furthest seaward were in pack ice with motions slightly over 1 km observed during April and May 1977 and motions of about 7 km during April and May 1976. These motions were predominately offshore/onshore with little shearing taking place. The ice generally returned to near its original position after moving offshore then onshore, which implies that leads must have opened and closed. Thin ice forming in these newly opened leads must have been deformed into pressure ridges. Thus, even during times when the pack ice is relatively motionless and the shear zone inactive, deformation still occurs seaward of grounded ridge systems.

3.3.3 Extent of Stamukhi Zone

The extent of the stamukhi zone varies with the time of year and geographical position. There is annual variation also, although the larger grounded ridge systems tend to occur in the same places each year (Stringer, 1978; Barry, 1979). In early winter, ridges become grounded in water 8 to 15 m deep, but by late winter they may become grounded in waters 20 m or more deep. Outside Harrison Bay the stamukhi zone may be 50 km or more wide. This includes the band of relatively undeformed ice just outside Harrison Bay though. Off Cross Island, the stamukhi zone is well defined and is about

20 km wide at the end of winter. Figure 3.6 (from Reimnitz et al., 1977a) gives a general picture of the stamukhi zone from Harrison Bay to Prudhoe Bay. The heavy black arrows represent pack ice motion.

3.3.4 Amount of Deformed Ice

Estimating the amount of deformed ice in the stamukhi zone is extremely difficult. From observations and photographs, one knows that in places 100 percent of the ice cover consists of highly deformed ice, but areas of flat, undeformed ice may also exist. Typical values are difficult to estimate for several reasons. One reason is that new ridges are being built throughout the winter. Other reasons are the spatial variability and yearly variations in ridge density.

Tucker et al. (1979) have reported on ridge densities over the continental shelves of the Beaufort and Chukchi Seas. Laser profilometer data were collected during February, April, and December 1976 and March 1978 at several locations along the coast including Cross Island and Lonely. Ridge densities were averaged over 20-km segments of the track perpendicular to the shore. A ridge was defined as ice more than 0.9 m higher than the surrounding ice.

The data for the Cross Island track and the Lonely track are given in Figures 3.7a and 3.7b, respectively. Note that three different ice seasons are represented in Figure 3.7: the winters of 1975-76, 1976-77, and 1977-78. Due to probable annual variations in ice motion and ridge building, we can assume that the data shown in Figure 3.7 does not give a progression of ridge densities from December through April. In general, the density of ridges is greatest in the first or second 20-km segment out from Cross Island, then decreases over the next 40 to 80 km. The pack ice in the central Beaufort Sea had a ridge density of about 2.5 ridges per kilometer in February 1976 (represented by the AIDJEX data point in Figure 3.7). The largest ridge density shown in Figure 3.7 is the 12 ridges per kilometer in March 1978 for the 20-km segment just north of Cross Island. At Lonely the largest ridge density of 8.25 ridges per kilometer occurs 60 to 80 km offshore. The first 20-km segment offshore has a low ridge density but this segment includes the fast ice zone where presumably deformation is limited to the early winter period.

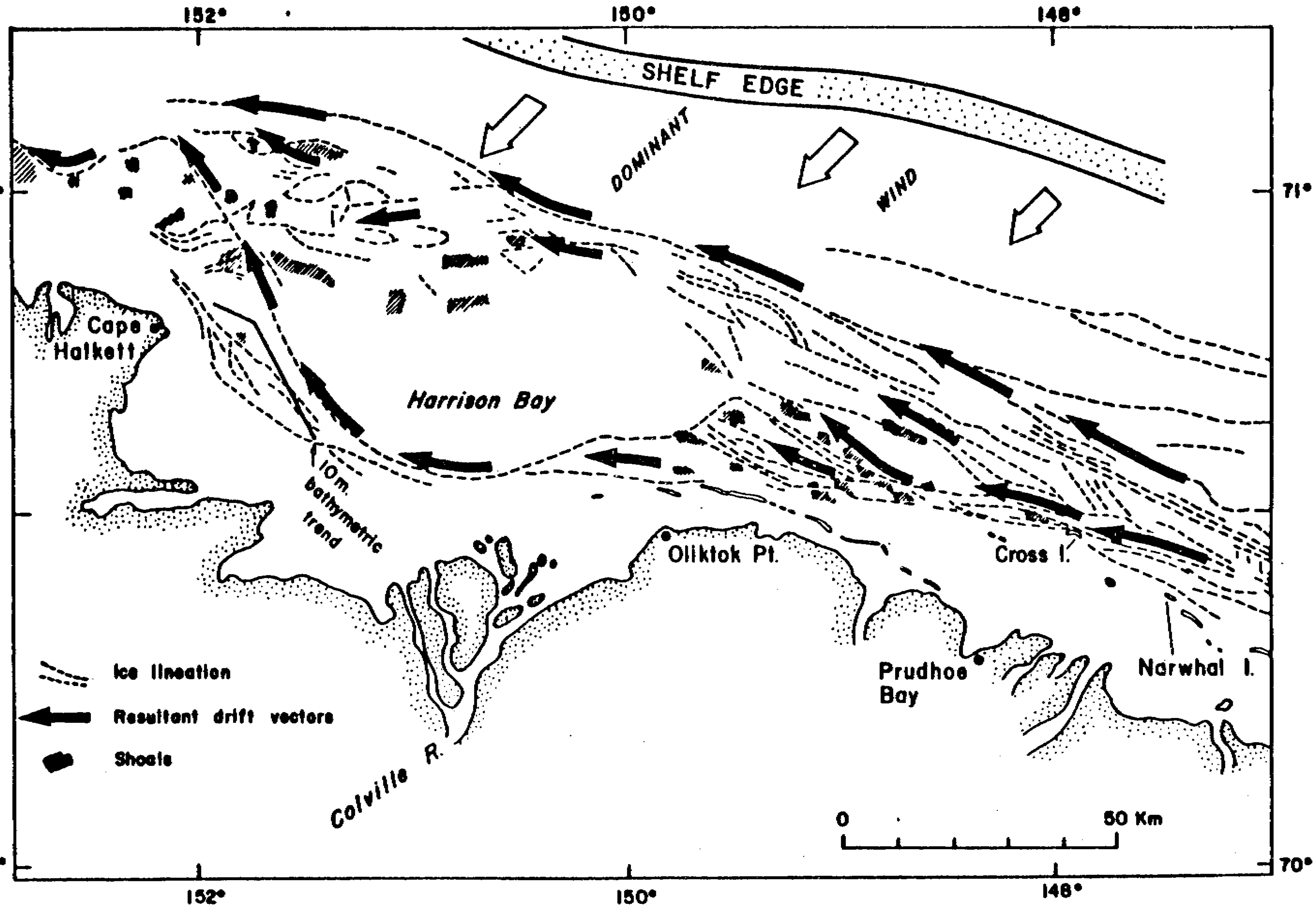

Figure 3.6. Generalized View of the Stamukhi Zone between Harrison Bay and Prudhoe Bay. (Figure 10 from Reimnitz et al., 1977a.) Predominant pack ice motions and winds are indicated. Major linear ice features (ridges and linear hummock fields) were traced from Landsat images.

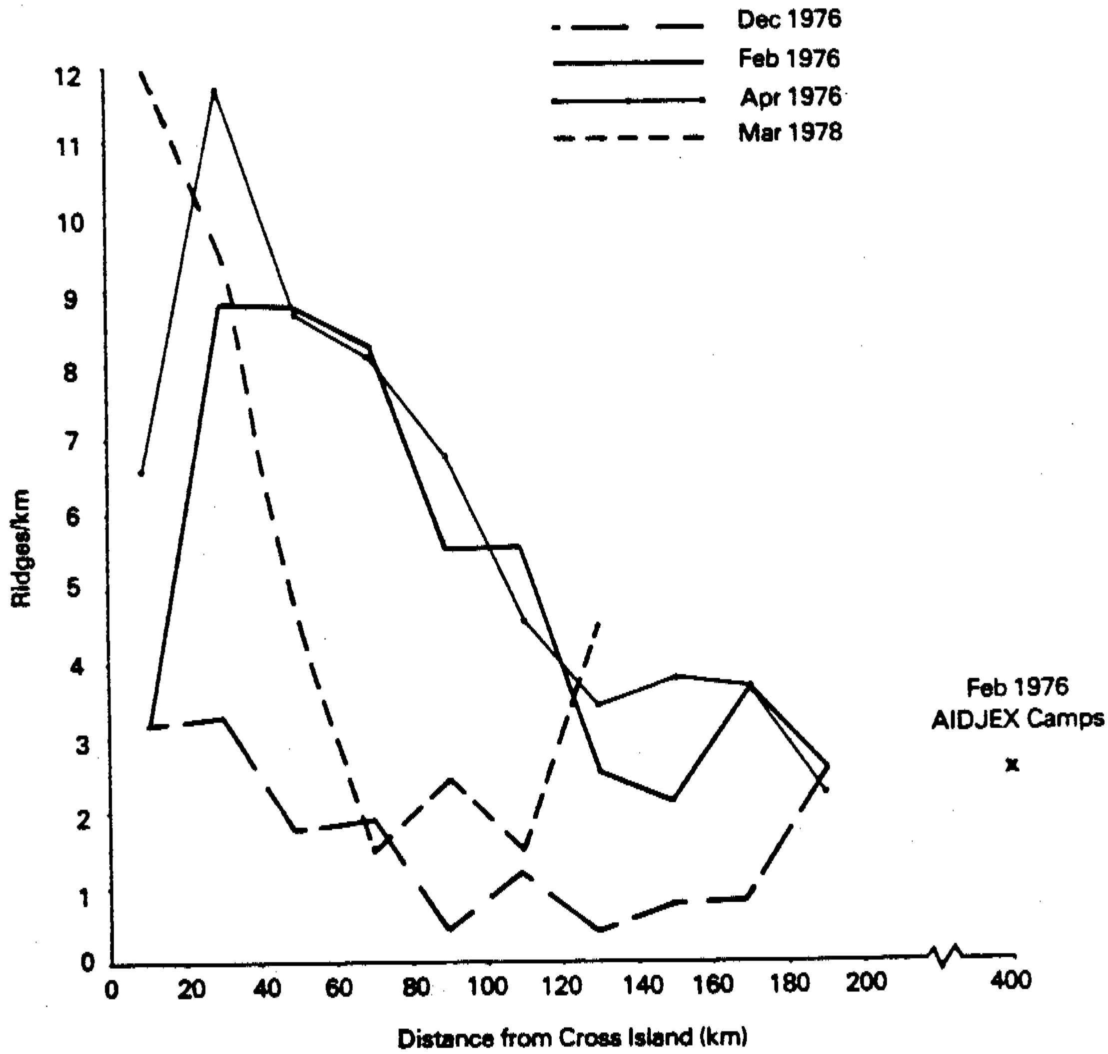

Figure 3.7a Ridge Densities Offshore from Cross Island. Values are averages for 20 km segments of laser profiles extending north of the island. Data taken from Tucker et al., (1979).

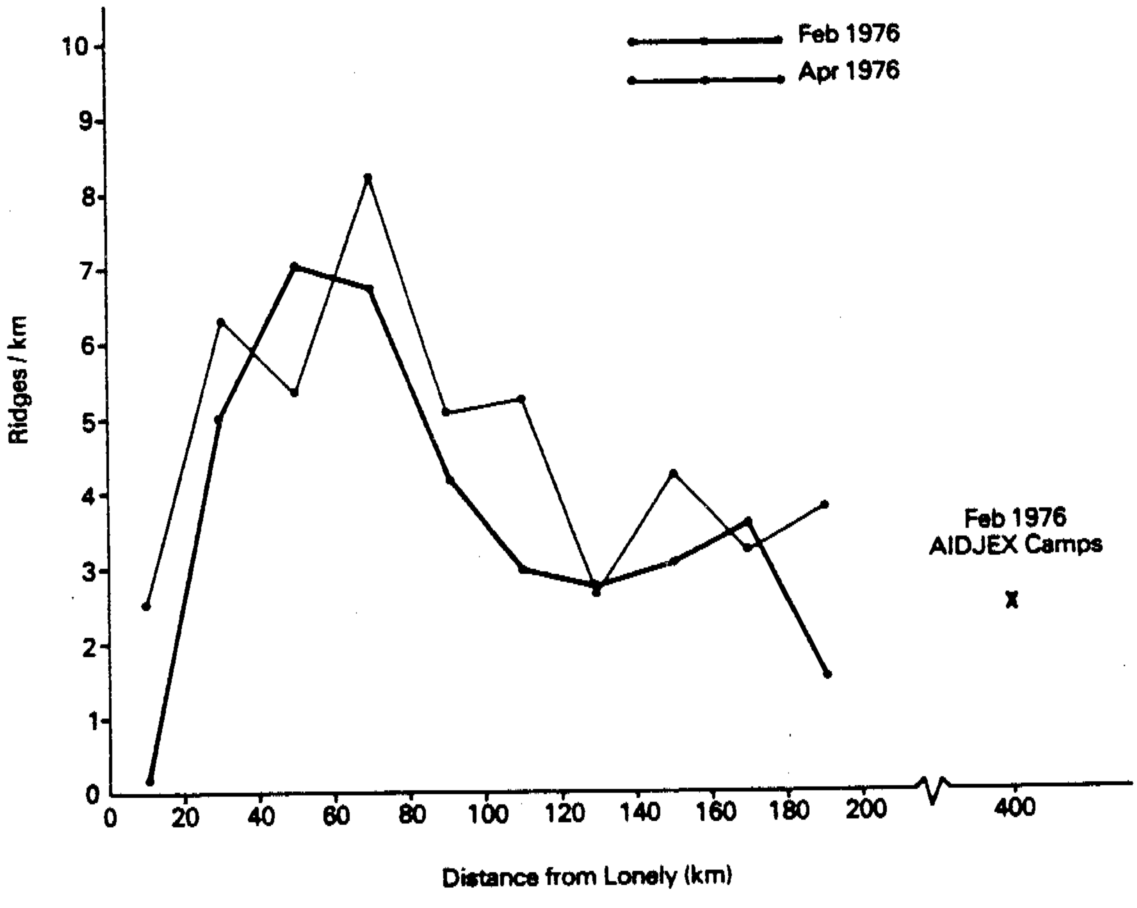

Figure 3.7b **Ridge Densities Offshore from Lonely. Values are averages for 20 km segments of laser profiles extending north from the coast. Data taken from Tucker et al., (1979).**

From the motions observed near Narwhal Island by Weeks et al. (1977) and Tucker et al. (1980), it is likely that many of the ridges built in the stamukhi zone seaward of any grounded ice features are pressure ridges rather than shear ridges. During a storm with offshore winds, the pack ice will move offshore, opening leads between the fast ice and the pack. Leads are also opened in the pack due to differences in motion throughout the pack, but the largest difference in motion usually occurs between the stationary fast ice and the pack. During most of the year, thin ice begins to form immediately on these open leads. Then, when onshore winds blow, the pack closes up the leads and, with or without a shearing type of motion, one or more new ridges are built.

During the early months of 1976, an AIDJEX buoy was located about 30 km offshore of Cross Island (Thorndike and Cheung, 1977). From 1 January to 21 April 1976, the net motion of this buoy was only 9.6 km. The net onshore motion was 6 km. The radial position error of this type of buoy is generally about 1 km (Martin and Gillespie, 1978). Thus, the onshore motion of this buoy was between 4 and 8 km during the first 3-2/3 months of 1976. This onshore motion must have created some new ridges between the buoy and the shore. If any thin ice existed in the 30 km offshore from Cross Island during that period, it would have been the first ice ridged. Since the net motion was onshore, thicker ice must also have been built into ridges. As a rough estimate, assume that the ridges produced by the 4- to 8-km onshore motion were built from ice 0.5 m thick. Then, between 8,000 and 16,000 m^2 of ice (all areas are for a profile in the north-south direction) was built into ridges between the buoy and Cross Island during the 3-2/3 months. This equals a monthly rate of 2180 to 4360 m^2/month of deformed ice produced.

To determine the volume of ice built into a ridge, we must define a ridge size and shape. Many pressure ridges have a roughly triangular profile above and below the ice surface. We assume this to be the typical shape of ridges built in the stamukhi zone from first-year ice. The average slope of the above-water sail of first-year pressure ridges is 24°, and the slope of the subsurface ridge keel is 33° (Weeks et al., 1971). The depth of the keel is about 4 times the sail height (Kovacs and Mellor, 1974). A keel depth of 3.6 times the sail height satisfies hydrostatic equilibrium for the above angles. The area of the above-water portion of a ridge profile is $H^2/\tan(24^{\circ})$, where H is the height of the sail. The submerged portion of the ridge has an area of 16 $H^2/\tan(33^o)$. Thus, the area of a typical ridge profile is roughly 27 H^2. The average height of ridge sails in the stamukhi zone is about 1.5 m (Tucker et al., 1979). About 10 percent of a newly built ridge volume consist of voids between irregularly shaped ice blocks, (Rigby and Hanson, 1976), therefore the area of ice in a typical ridge profile is about 54 m^2. Thus, between 40 and 80 new ridges are added to the width of the stamukhi zone each month.

Information on the length of ridges is sparse. Hibler and Ackley (1974), looking at ridge sails in terms of possible vehicle crossing points, found the majority of ridge segments to be less than about 1 km in length. Many ridges are longer than this of course, especially newly built shear ridges.

In the stamukhi zone and the near shore pack ice zone, where ridge densities are high, there will be a great many intersecting ridges. New ridges may tend to be oriented parallel to the coast but deformation occurs in all direction and floes containing older ridges may be rotated, so that generally, any area of ice will be bounded by intersecting ridges.

3.4 Pack Ice Zone

The pack ice zone is considered to be the area seaward of the maximum extent of deformed ice in the stamukhi zone. The ice in this area is generally more free to move and deform under wind and current stresses. It is this motion or possible motion that distinguishes this zone from the others in the context of oil spill pollution pathways.

The pack ice zone can be further divided into a seasonal or offshore zone and a permanent pack or central Arctic zone. The seasonal pack ice zone is considered to begin seaward of the active shear zone and includes only the ice that is free to move as pack ice. The lease areas offshore of the north coast of Alaska do not extend beyond the seasonal pack ice zone. The central Arctic permanent pack ice zone is seaward of the seasonal zone and is covered with pack ice year round.

In some seasons the central Arctic pack is driven close to shore during the summer so that the following ice season the ice in the seasonal ice zone has the characteristics of the permanent pack. We must therefore examine the characteristics of both types of pack. Normally, the ice in the seasonal zone is mostly first-year ice while the Arctic pack has a high proportion of ice that has survived at least one melt season. Multiyear ice is thicker, less saline, less porous, and stronger than first-year ice.

3.4.1 Ice Thickness

Thorndike et al. (1975) modeled 2 years of ice thickness distribution for the central Arctic zone, using a measured initial thickness distribution (Swithinbank, 1972) and strain rates derived from drifting stations. The modeled climatological mean thickness for central Arctic pack ice varied from 2.8 to 3.2 m in late summer/early fall to about 3.8 to 4.2 m for winter/spring. Using the same model, and starting with open water in August, a maximum thickness of 1.7+ m is reached in April/May.

Wadhams and Horne (1978) present the results of submarine sonar ice profiles in the central Beaufort Sea during April 1976. Mean drafts over 50-km sections ranged from 2 to 3.8 m, with an overall mean of 3.07 m. The most probable draft (mode) for level ice was 2.7 to 2.8 m. The overall mean thickness was thus about 3.45 m, and the level ice mode thickness was about 3.1 m.

Taking into account measurement errors, seasonal variations in growth rates, and concentrations of multiyear ice it is reasonable to accept the convention that first-year ice grows to a thickness of about 2 m in the pack ice zone while multiyear ice will average about 3 m (level ice only) (Weeks, 1976).

3.4.2 Ice Type and Concentration

Ramseier et al. (1975) compiled maps of first-year and multiyear ice concentrations over the Beaufort Sea for the years 1972 to 1975. The maps were compiled from NIMBUS 5 satellite passive microwave imagery. Early in September, the seasonal pack ice zone (out to about 200 km from shore) contains 50 to 100 percent open water, and the central Beaufort Sea (permanent pack ice zone) contains 0 to 25 percent open water. Early in October, more year-to-year variation is evident. In 1974, no open water existed for about 100 km offshore, with 0 to 25 percent open 100 km offshore, with 0 to 25 percent open water in the central Beaufort Sea. In 1975, the seasonal pack ice zone still contained 25 to 100 percent open water out to about 200 km from shore.

By December, open water has frozen into first-year ice. In December 1972 and 1973, 45 to 65 percent of the ice within approximately 200 km of shore was first-year ice, the remainder being multiyear ice. The central Beaufort Sea contained 0 to 45 percent first-year ice. In 1979, the central Beaufort Sea only had 0 to 15 percent first-year ice while the seasonal ice zone had 0 to 45 percent first-year ice. Large-scale ice motions during the summer and fall have a significant effect on the amount of multiyear ice in the seasonal pack ice zone.

Typically, the seasonal pack ice zone seems to contain about half first-year and half multiyear ice but with a great deal of annual variation. The central Beaufort Sea seems to have from over half to 100 percent multiyear ice. Weeks (1976) gives a summary of ice types identified by U. S. Navy Birdseye ice reconnaissance flights. The seasonal ice zone contained 46 percent multiyear ice and 53 percent first-year ice (with approximately 1 percent open water). The central Arctic Basin contained 81 percent multiyear ice, 18 percent first-year ice, and approximately 1 percent open water. These were wintertime mean values.

The amount of open water in the winter pack ice was given by Weeks (1976) as about 1 percent. Wadhams and Horne (1978) report the amount of thin ice (0 to 0.5 m draft) observed by the U.S.S. GURNARD in April 1976 to be 0.9 percent overall, varying from 0.2 to 3.5 percent over different sections of the Beaufort Sea. For ice with draft less than 1 m, the overall mean was 3.4 percent. This thin ice is distributed in refrozen leads and polynyas. Narrow leads less than 50 m in width were found to occur at the spacing of 4.6 per kilometer. Leads from 50 to 500 m in width were spaced at about 0.1 per kilometer. A great deal of variation was observed to exist along the submarine track, but the variation did not seem to be related to position off-shore. Thus, one need only travel a little over 200 m on the average across ice 2- or 3-m thick before finding some ice only 1-m or less thick. No mean lead width is given by Wadhams and Horne, but it is probably closer to zero than 50 m since the frequency of leads decreases sharply with width.

Weeks et al. (1977) examined side-looking airborne radar (SLAR) images taken on flights north of Alaska in late September 1975. New ice had begun to form between the multiyear floes in the seasonal ice zone. They found the majority of these floes to be roughly circular in shape and between 100 and 700 m in diameter with floe size being distributed approximately as a negative exponential. Figure 3.8, reproduced from Weeks et al. (1977), shows the floe size distribution.

In the fall and early winter, the ice cover in the seasonal pack ice zone will typically consist of about 50 percent multiyear floes from 100 to 200 m

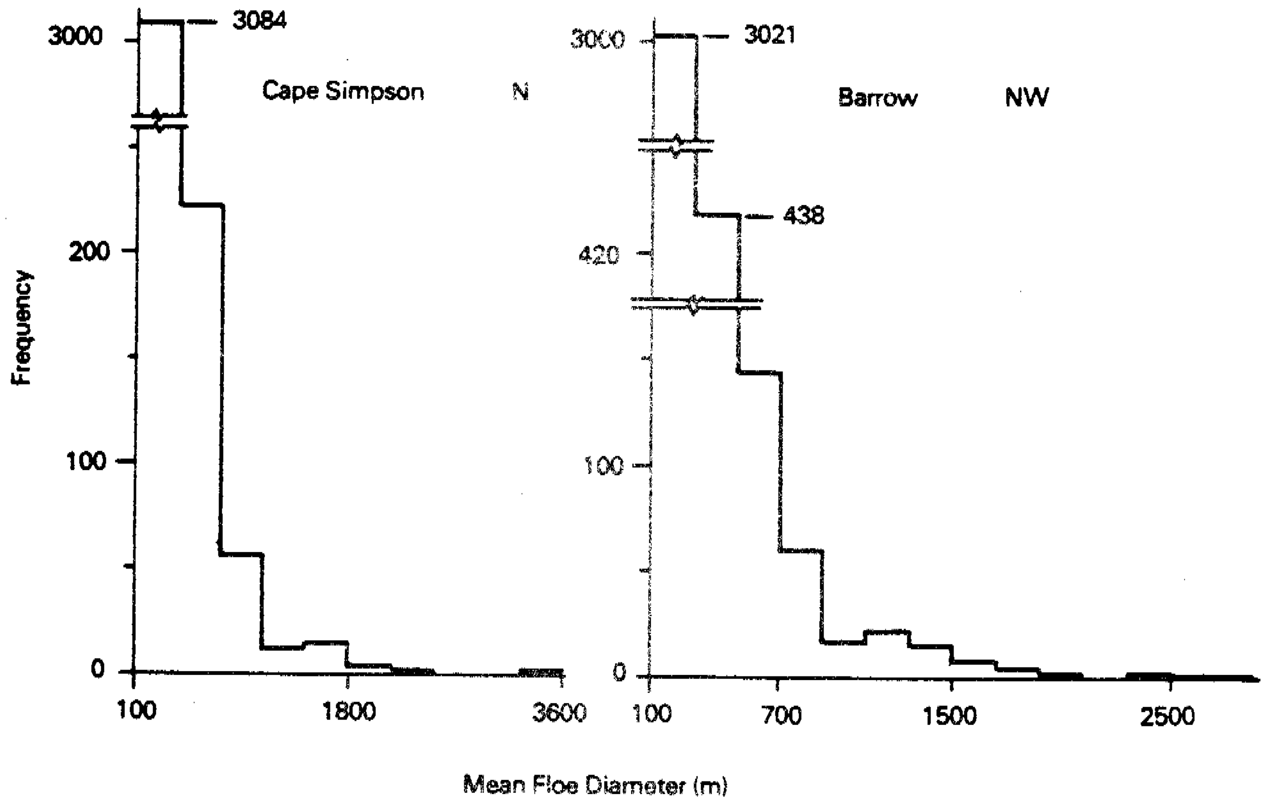

Figure 3.8. Histograms of Floe Size Distribution for Two Areas in the Beaufort Sea During September 1975. (Figure 7 from Weeks et al., 1980.)

in diameter and 50 percent much thinner ice between the old floes. Later in the winter and in the spring, the difference in draft between multiyear and first-year ice will be much less. New leads, and thus new areas of thin ice, will be continually created during the winter. At any time, from 1 to 5 percent of the area within the pack is open water or very thin ice. Much of this thin ice existing after freezeup or created during the winter ultimately gets broken up and piled into rubble fields and pressure ridges.

3.4.3 Ridges

Measurements of the number of ridges in the pack ice zone show considerable regional and temporal variation. Therefore, it is only possible to make a rough approximation of the number of ridges in the seasonal and permanent pack zones during various times of the year.

Weeks et al. (1980) report a ridge density of 6.61 ridges per kilometer for the region 50 to 100 km offshore of Barter Island (laser profile, February 1976). Wadhams and Horne (1978) report a keel density of 14.8 keels per kilometer for the region approximately 60 to 110 km offshore of Barter Island (U.S.S. GURNARD sonar profile, April 1976). If each ridge observed above the ice surface is associated with a keel beneath the surface, why is there such a large difference between the number of surface ridges in February and the number of keels just 2 months later? There are probably several reasons for this. First, it is likely that the definitions of ridges and keels did not include the same ice structures. Second, there may have been more ridges built during those 2 months. While AIDJEX buoys in the area at that time showed only small net motions, there was considerable back-and-forth motion occurring (Thorndike and Cheung, 1977; Tucker et al., 1980) which probably caused more ridges to be built. And third, there might be some variation due to the exact area sampled.

In the next two 50-km sections between 110 and 210 km offshore of Barter Island, Wadhams and Horne (1978) reports keel densities of 10.3 and 8.1 keels per kilometer while Weeks et al. (1980) report 4.3 and 3.8 ridges per kilometer. The ridge densities between 50 and 100 km offshore varied from 2.8 per kilometer at Barrow to 7.56 per kilometer at Cross Island (Weeks et al., 1980). Weeks (1976) gives confirmation of the higher numbers in giving summaries of U.S. Navy Birdseye ridge data of 16 to 22 ridges per kilometer off the north coast of Alaska during the summer. It seems reasonable to accept the submarine count of about 14.8 keels (ridges) per kilometer as typical in the seasonal pack ice zone.

For the central Beaufort Sea area, Wadhams and Horne (1978) reports an average keel density of 6.7 per kilometer. If the ice in this area is assumed to be mostly multiyear ice, we can estimate the ridge/keel density at freezeup in the seasonal pack ice zone. Right at freezeup, before thin ice has had a chance to become deformed, the ridge/keel density will be 6.7 times the concentration of multiyear ice. Assuming a 50 percent multiyear ice cover at the time of freezeup (October), the ridge/keel density would be 4 per kilometer. Then, 14.8 minus 3.4 or 11.4 new ridges/keels per kilometer must be built by the next April. This amounts to an average rate of 1.3 ridges per kilometer per month during the fall and winter. The rate is probably much higher during the fall when more thin ice is present. Furthermore, there is probably such a region-to-region and year-to-year variation in ridging intensity that all the above numbers can be considered as no more than very rough approximations. Wadhams (1975) reports many fewer ridges in April 1975 from the Mackenzie Delta to the central Beaufort Sea. Nearshore ridge counts were only 1 or 2 per kilometer while in the central Beaufort Sea the density was 2 to 3 ridges per kilometer. Some ridge/keel density measurements for the area near Cross Island are given in Figure 3.7.

3.4.4 Ice Motion

The pack ice motion has a long-term westward trend. Over periods of a few days, the motion may be to the east, but eventually the westward trend dominates. During the winter there are often periods of days or weeks when no significant pack ice motion occurs. This happens when the pack is very consolidated and the winds are small or have blown from the north or west for long periods. On the other hand, for most of the summer and occassionally during the winter when the pack is unconsolidated, the ice has little or no internal resistance to the wind and water forces and moves about freely. This condition, known as free drift, represents the maximum extreme of possible ice motion. In between these extremes of no motion and free drift, ice motion will depend upon the atmospheric and oceanic driving forces, the sea surface tilt, the Coriolis effect, and internal stresses transmitted through the ice. This last term is the difficult one to model for long periods of time since small errors in velocity will affect the distribution of ice and thus the ice strength which in turn affects future velocities.

Thomas and Pritchard (1979) bypassed this difficulty by computing the extremes of possible pack ice motion. Wind data for the past 25 years were used to compute monthly free drift ice trajectories. Monthly means and variations were then computed. During the summer when the pack is usually open, these monthly average trajectories represent the most likely ice motions. During the winter when the ice is usually not in a free drift condition, the results represent a most likely maximum motion. Note that while an individual monthly trajectory during a light ice year may be longer than the maximum represented by mean free drift, it usually will not be.

The mean pack ice motion, or limit to motion depending upon the season, is generally to the northwest at between 0.67 and 3.67 km/day. Ocean currents were not included when dree drift trajectories were computed. Near the shore along the north coast of Alaska, the currents are generally small and variable to the east or west. Further offshore around the shelf break, currents are larger but they still reverse directions. Beyond the shelf, the southern edge of the Beaufort Gyre circulation contributes to the westward motion. During the winter, observed motions (Thomas and Pritchard, 1979) were generally to the west, although in February 1976 the motions were consistently to the east. Observed monthly motions throughout the Beaufort Sea were generally less than or equal to the mean free drift maximum.

Daily ice motions are more variable than monthly motions. While the westward trend persists from month to month over many years, daily motions exhibit a great deal of meandering and back-and-forth motion in all directions. Average daily ice speeds are therefore higher than average monthly ice speeds.

The variations in speed of the nearshore pack ice have not been adequately reported. Thorndike and Colony (1980) have described the ice motion of a station in the central Beaufort Sea, and Tucker et al. (1980) have described the motion of nearshore pack ice, but for only a short period of time. Examination of these two sources shows that there is a seasonal difference in ice motion (less motion during winter and spring) and that pack ice motion probably decreases toward the pack ice edge (at least during winter).

In Figure 3.9 we show a histogram of the speed of one of the AIDJEX data buoys during the winter of 1975-76. This buoy (number R61) was located approximately 50 to 60 km offshore near Prudhoe Bay. During January to mid-May, the monthly histograms appeared very similar, so the data were

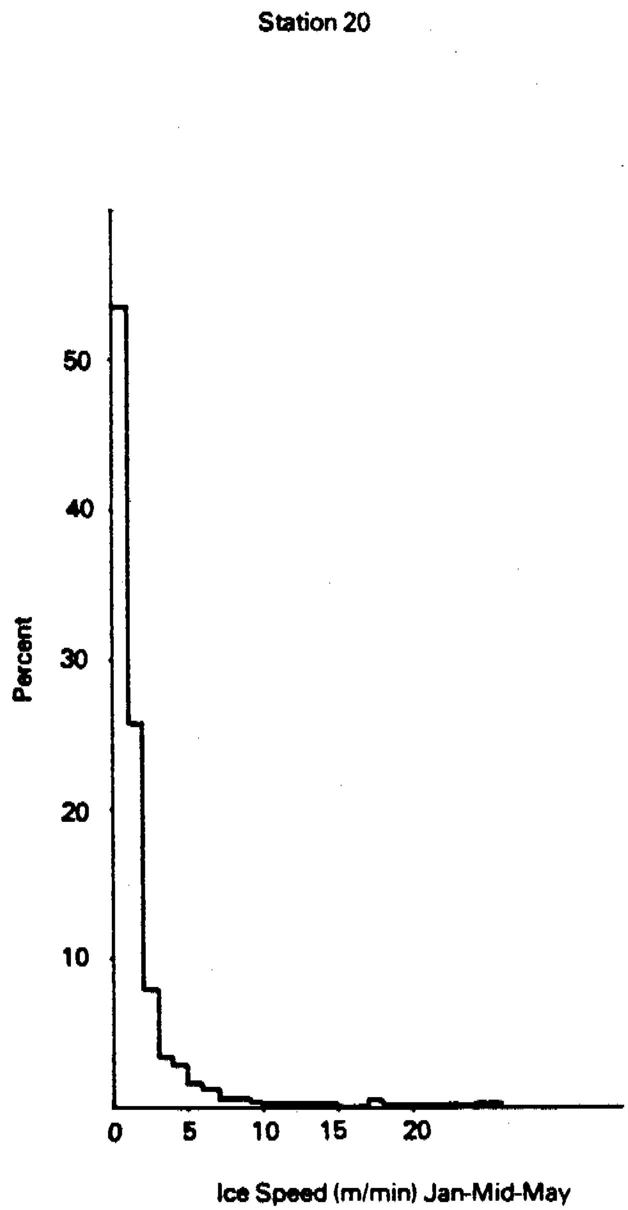

Figure 3.9. Histograms of Ice Speed as Determined from the Motion of a Satellite-Tracked Buoy Located about 40 km North of Flaxman Island. Data taken from Thorndike and Cheung (1977) for AIDJEX Station 20 from January 1976 through mid-May 1976.

combined into a winter ice speed histogram. During that winter, at least, the pack ice nearest shore was most likely to be moving at speeds between 0 and 1 m/min. The mean speed was about 2 m/min.

Lacking enough data to see the seasonal variations of nearshore pack ice motion, we have examined the seasonal variation of the motion of two manned camps in the central Beaufort Sea. Figure 3.10 shows histograms of ice speeds for these two camps throughout the year. Monthly histograms were made first and then the similar consecutive months were lumped together. During the summer months, July through September, the ice is almost constantly in motion. During freezeup in October, the pack is still in constant motion but at somewhat slower speeds than in the summer. The fall-early winter (November through January) speeds have decreased sharply with about half being less than 2 m/min. The winter months (February through April) look much like the nearshore motion with over half the speeds being less than 1 m/min. During May and June, speeds begin to increase again as new ice growth stops and the pack begins to loosen up.

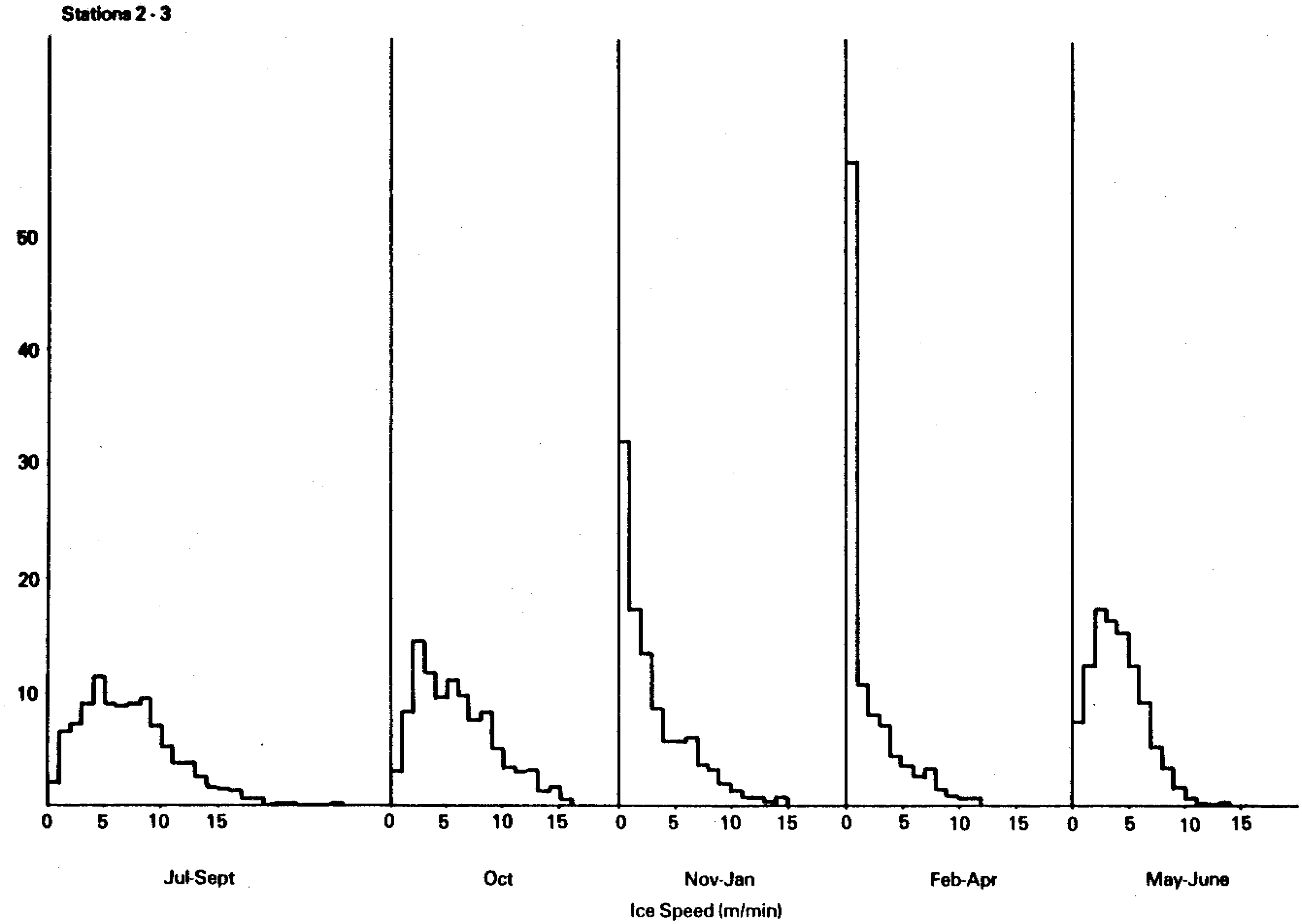

Figure 3.10. **Histograms of Ice Speed for Two Manned Camps in the Central Beaufort Sea During 1975 and 1976. Months with similiar distributions of ice speeds are pooled. Data taken from Thorndike and Cheung (1977) for AIDJEX Stations 2 and 3 from**

4. Summary of Oil and Sea Ice Interaction

In a previous report we have described the interaction of crude oil from a well blowout and the sea ice cover (Thomas, 1980). That report dealt with the region near Prudhoe Bay specifically but the sections on oil and sea ice interactions apply to any area such as Harrison Bay with similar ice morphology and developmental history. Therefore, in this report we merely summarize the sequence of events following an under-ice blowout and point out the effects an ice cover will have upon the spread and transport of spilled oil.

The events following an under-ice blowout may usefully be divided into five more or less independent and sequential phases. The phases are: (1) the initial phase, (2) the spreading phase, (3) the incorporation phase, (4) the transportation phase, and (5) the release phase. Depending upon the season, location, and duration of the blowout, several of these phases may occur simultaneously or may not occur at all, but generally a particle of oil can be followed through each phase in turn.

The initial phase of an under-ice blowout consists of the release of oil and gas from the sea floor, the rise of the oil and gas to the surface, and the initial interaction of the oil and gas with the existing ice cover. The buoyant gas and oil entrain large amounts of water while rising to the surface. This plume and the resulting surface wave ring are only marginally important to the eventual fate of the oil. The turbulence at the surface may play some part in breaking up the ice over the blowout, especially when the ice cover is moving. A much more important factor, though, is the buoyancy of the gas from the blowout. Under a stationary ice cover, this gas is almost certain to cause breakage of the ice which allows the gas to escape to the atmosphere. Under a moving ice cover, especially for thicker multiyear ice, it is not certain that the gas trapped beneath the ice will cause the ice to break. Large amounts of gas trapped beneath the ice can have a significant effect on the spread of oil under the ice. It is believed, though, that only a limited quantity of gas can be trapped under sea ice due to the presence of naturally occurring thermal cracks in the ice. These cracks provide escape routes for the gas or at least weaken the ice so that trapped gases can break the ice and then escape. From theoretical studies and casual observations, these thermal cracks in the ice occur frequently enough that only a small percentage of any gas from a blowout will be trapped under the ice. Because of the possible importance of cracks to the escape of gas, especially for thicker multiyear ice, quantitative data on the development and spacing of thermal cracks in the different ice zones at different times of the year is desirable.

During the initial phase of a blowout under stationary ice, the heat of the oil and possibly heat from bottom water circulated by the blowout plume can also be instrumental in producing an ice-free area directly over the blowout. A large quantity of oil will replace the melted ice, although this may be a fairly small percentage of the total oil released. This melt hole could, however, act as a reservoir from which oil could be pumped.

It is unlikely that much oil will be deposited on the ice surface during a winter blowout. The oil will tend to overflow onto the ice wherever an opening occurs, but low air temperature and snow on top of the ice will act to restrict the horizontal spread.

A spreading phase follows the initial phase of the blowout. This phase involves the relative motion of and concentration of oil beneath the ice layer. Factors which are particularly important during the spreading phase are the bottom roughness of the ice, ocean currents, existing ridge keels, motion of the ice cover, and increasing ice thickness. The roughness of the underside of the ice generally provides an upper limit to the size of the under-ice oil slick, except under very smooth, new ice. For very smooth ice, the size of the slick is determined by the equilibrium thickness of oil under ice, which is many orders of magnitude greater than slick thickness on open water.

For blowouts lasting more than a few days, the spread of oil beneath the ice may be significantly restricted by the increasing thickness of the ice outside the immediate blowout vicinity. For very large blowouts, and in the absence of ice motions or large under-ice currents, this mechanism would tend to collect the oil in a single, relatively small but deep pool. The implications for cleanup are obvious. Further thought and work should be devoted to this topic.

Under-ice currents can be a major factor in the spread and transport of oil spilled under sea ice. In the Harrison Bay lease sale area, however, steady currents are generally too small during the ice season to affect oil spread. Tidal currents beneath the ice and between grounded ridges may be an exception but are probably not significant in terms of oil spreading since the tidal currents are oscillatory.

Ridge keels also can affect the direction of oil spreading. In the stamukhi zone, ridges may be frequent enough to control the size of the under-ice slick in the absence of large currents.

Motion of the ice cover may also control the size of the slick. While much of the gas is likely to escape through existing cracks in the ice, the ice motion may allow some gas to be trapped. The amount of gas that can be trapped depends upon ice speed and thermal crack spacing. Because of the importance of gas release, especially in thicker, moving pack ice, the existence and spacing of cracks in the ice should be confirmed by field studies.

An incorporation phase will follow the spreading phase. Oil spilled under sea ice during the winter will generally become encapsulated within the ice. This oil is protected from weathering processes until the ice begins to warm in the spring, releasing the oil. This is probably the most important aspect of under-ice oil spills in the Arctic. It means that spills which occur from sometime in October through the following May will in effect occur at the beginning of the ice breakup period in the late spring. Oil is thus released into a limited amount of open water at a time critical to all levels of biological activity. This delay, however, does allow time for cleanup efforts between the actual and effective release of the oil.

Oil spilled outside the grounded ridges which delineate the protected fast ice zone has an indeterminate but relatively high chance of being incorporated into a ridge. Due to ice motions relative to a fixed boundary, a large amount of ridge building occurs in this area during periods of pack ice motion. Significant percentages of large oil spills occurring in this area at certain times of the year will be incorporated into ridges. This conclusion was made on the basis of a limited amount of data concerning ridge counts. Data on ridge densities need to be collected throughout the ice season in order to accurately describe the development of the stamukhi zone and predict the amount of oil from spills occurring at different times that will be incorporated into ridges. Data over many ice seasons are necessary in order to assess the uncertainty of predictions.

The whole problem of oil after it is incorporated in ridges is largely conjectural at this time. The amount of oil which can be held inside a ridge and how long it will remain in the ridge are important questions when considering the possibility of a blowout in the stamukhi zone. No data exists concerning the interaction of crude oil and pressure or shear ridges in Arctic sea ice. Field or laboratory experiments will be necessary in order to begin answering these questions.

During the transportation phase, oil which is trapped by bottom roughness or which is frozen into the ice is moved about with the ice cover. In the fast ice zone, transport does not occur except early in the ice season when the ice is thin and weak or late in the ice season as the ice breaks up and begins to move. Even during those times, the amount of ice motion is small, less than a few kilometers.

It is in the pack ice zone that significant transportation of the oil by the ice takes place. The pack moves generally to the west with much short--term meandering. It is likely that some of the oil will be spread over a large area in low concentrations. Differential motions of individual floes within the pack after the blowout will tend to further separate oiled areas of ice.

In the spring, all the oil except possibly that trapped within ridges will begin to be released from the ice. This release phase takes place by two routes: surfacing of the oil through brine drainage channels and melting of the ice cover. By mid to late July, most of the oil-contaminated ice will have melted, leaving partially weathered oil on the water surface. Open-water areas and shorelines to the west, possibly as far as the Chukchi Sea, may be contaminated with oil during the summer. During the period when the oil is being released and the ice is melting and breaking up, the motion of the oil already released on the water is largely unknown. The concentration of the ice cover and the motion of the ice undoubtedly influence the motion of the oil, but further work is needed to determine the extent of the influence.

Cleanup of any large under-ice oil spill will be extremely difficult in the spring. This is because oil will surface slowly in many separate melt pools over a large area for a long period of time. As soon as the oil surfaces, it begins to weather, making it difficult to burn. The continuous release and weathering of the oil makes it necessary to burn each melt pool containing surfaced oil several times. The surfaced oil also accelerates the deterioration of the ice cover, decreasing the time interval when the ice is safe for surface work. A spill covering several square kilometers will surface in many thousands of separate pools. In the pack ice, these pools are likely to be separated and spread over many kilometers. Even in the fast ice, the logistics of burning or cleaning up many thousands of pools of oil will become prohibitive.

Cleaning the oil from the water surface as the ice melts will also be difficult. Conventional open-water cleanup methods will be difficult to use until the ice concentration is low, which may be too late for preventing widespread dispersion of the oil. For small spills or remnants of large spills, both burning and open-water cleanup methods could be practical.

A much safer cleanup strategy would involve pumping the oil from beneath the ice during the winter or early spring. Logistically, this would be extremely difficult, unless the oil was pooled in large concentrations beneath the ice. This is unlikely to occur naturally, except perhaps in the fast ice zone where ice growth can outpace oil accumulation or in heavily ridged areas of the stamukhi zone. However, in the fast ice zone, an effective preventive measure would be to create under-ice reservoirs by artificially redistributing snow in areas where blowouts might occur. In the pack ice, this procedure would be impractical due to ice motions.

References

Aagaard, K., and contributors (1978) "Physical Oceanography and Meteorology," Environmental Assessment of the Alaskan Continental Shelf, Interim Synthesis: Beaufort/Chukchi, NOAA/OSCEAP, Boulder, Colorado, pp. 56-100.

Aagaard, K. (1980) "Current Measurements in Possible Dispersal Regions of the Beaufort Sea," To appear in: Environmental Assessment of the Alaskan Continental Shelf, Annual Reports, NOAA/OSCEAP, Boulder, Colorado.

Agerton, D. J., and J. R. Kreider (1979) "Correlation of Storms and Major Ice Movements in the Nearshore Alaskan Beaufort Sea," Proceedings Port and Ocean Engineering Under Arctic Conditions, Trondheim, Norway, Vol. 1., pp. 177-190.

Barnes, P. W., E. Reimnitz, and G. Smith (1977) Some Coastal Oceanographic Observations Beaufort Sea, Alaska, U. S. Geol. Survey Open-File Report 7 -477, Menlo Park, California.

Barnes, P., E. Reimnitz, L. Toimil, and H. Hill (1979) Fast Ice Thickness and Snow Depth in Relation to Oil Entrapment Potential, Prudhoe Bay, Alaska, U.S. Geol. Survey Open-File Report 79-539, Menlo Park, California.

Barry, R. G. (1978) "Study of Climatic Effects on Fast Ice Extent and Its Seasonal Decay Along the Beaufort-Chukchi Coasts," Environmental Assessment of the Alaskan Continental Shelf, Annual Reports, NOAA/OSCEAP, Boulder, Colorado. Vol. IX. Transport, pp. 604-719.

Barry, R. G. (1979) "Study of Climatic Effects on Fast Ice Extent and its Seasonal Decay Along the Beaufort-Chukchi Coasts," Environmental Assessment of the Alaskan Continental Shelf, Final Reports, NOAA/OCSEAP, Boulder, Colorado. Vol. 2. Physical Science Studies, pp. 272-375.

Bilello, M. A. (1980) "Decay Patterns of Fast Sea Ice in Canada and Alaska," Sea Ice Processes and Models, Ed. R. S. Pritchard, University of Washington Press, Seattle, Washington, pp. 313-326.

Brower, W. A., H. F. Diaz, A. S. Prechtel, H. W. Searby, and J. L. Wise (1977) Climatic Atlas of the Outer Continental Shelf Waters and Coastal Regions of Alaska, Vol. III, Chukchi-Beaufort Sea. Arctic Environmental Information and Data Center, U. of Alaska, Anchorage, Alaska.

Hibler, W. D. III, and S. F. Ackley (1974) "A Sea Ice Terrain Model and Its Application to Surface Vehicle Trafficability," AIDJEX Bulletin No. 25, University of Washington, Seattle. pp. 107-126.

Hunt, W. R., and G. M. Naske (1979) "A Baseline Study of Historic Ice Conditions in the Beaufort Sea, Chukchi Sea and Bering Strait," Environmental Assessment of the Alaskan Continental Shelf, Final Reports, NOAA/OCSEAP, Boulder, Colorado. Vol. 1. Physical Science Series, pp. 122-534.

Jenne, R. L. (1975) Data Sets for Meteorological Research, National Center for Atmospheric Research Technical Note NCAR-TN/IA-III, Boulder, Colorado.

Kovacs, A. (1977) "Sea Ice Thickness Profiling and Under-Ice Oil Entrapment," Proceedings 1977 Offshore Technology Conference, Houston, Texas. Vol. III, pp. 547 554.

Kovacs, A. (1979) "Oil Pooling Under Sea Ice," Environmental Assessment of the Alaskan Continental Shelf, Annual Reports, Vol. VIII, Transport, pp. 310-353.

Kovacs, A., and M. Mellor (1974) "Sea Ice Morphology and Ice as a Geologic Agent in the Southern Beaufort Sea," The Coast and Shelf of the Beaufort Sea, Eds. C. Reed and E. Slater, Arctic Institute of North America, Arlington, Virginia, pp. 113-162.

Kovacs, A., and R. M. Morey (1978) "Radar Anisotropy of Sea Ice Due to Preferred Azimuthal Orientation of the Horizontal C Axes of Ice Crystals," J. Geophys. Res., Vol. 83, No. C12, pp. 6037-6046.

Leavitt, E. (1979) "Comparison between Geostrophic Winds Derived from the Standard Pressure Measurement Network and the AIDJEX Network," Environmental Assessment of the Alaskan Continental Shelf, Annual Reports, NOAA/OCSEAP, Boulder, Colorado. Vol. VIII. Transport, pp. 46 56.

Martin, P. and C. R. Gillespie (1978) "Artic Odyssey - Five Years of Data Buoys in AIDJEX," AIDJEX Bulletin No. 40, June, University of Washington, Seattle, pp. 7-14.

Martin, S. (1977) The Seasonal Variation of Oil Entrainment in First Year Sea Ice: A Comparison of NORCOR/OCS Observations, Dept. of Oceanography, Spec. Report #71, University of Washington, March.

Matthews, J. B. (1980) "Observations of Surface and Bottom Drifter Movements in the Beaufort Sea Near Prudhoe Bay, Alaska," Submitted to J. Geophys. Res.

Matthews, J. B. (1981) "Observations of Under-Ice Circulation in a Shallow Lagoon in the Alaskan Beaufort Sea," Ocean Management, Vol. 6, pp. 223-234.

NORCOR Engineering and Research, Ltd. (1975) The Interaction of Crude Oil with Arctic Sea Ice, Beaufort Sea Technical Report #27, Beaufort Sea Project, Dept. of the Environment, Victoria, B.C.

Parmerter, R. (1974) "A Mechanical Model of Rafting," AIDJEX Bulletin No. 23, University of Washington, Seattle, pp. 97-116.

Pritchard, R. S. (1981) "Mechanical Behavior of Pack Ice," To appear in Mechanical Behaviour of Structural Media, Ed. A. P. S. Selvadurai, Elsevier, Amsterdam.

Ramseier, R. O., M. R. Vant, L. D. Arsenault, L. Gray, R. B. Gray, and W. J. Chudobiak (1975) Distribution of Sea Ice Thickness in the Beaufort Sea, Beaufort Sea Technical Report No. 30, Beaufort Sea Project, Dept. of the Environment, Victoria, B.C.

Reimnitz, E., L. J. Toimil, and P. Barnes (1977a) "Arctic Continental Shelf Processes and Morphology Related to Sea Ice Zonation, Beaufort Sea, Alaska," AIDJEX Bulletin No. 36, University of Washington, Seattle, pp. 15-64.

Reimnitz, E., L. J. Toimil and P. W. Barnes (1977b) "Stamuhhi Zone Processes: Implications for Developing the Arctic Offshore," Proceedings 1977 Offshore Technology Conference, Houston, Texas. Vol. III, pp. 513 518.

Rigby, F. A. and A. Hanson (1976) "Evolution of a Large Arctic Pressure Ridge," AIDJEX Bulletin No. 34, December, University of Washington, Seattle, pp. 43-72.

Rogers, J. C. (1978) "Meteorological Factors Affecting Interannual Variability of Summertime Ice Extent in the Beaufort Sea," Monthly Weather Review, Vol. 106, No. 6, June.

Rothrock, D. A. (1979) "Modeling Sea-Ice Features and Processes," J. of Glaciology, Vol. 24, No. 90, pp. 359-375.

Ruby, C. H., L. G. Ward, I. A. Fischer, and P. J. Brown (1977) "Buzzards Bay Oil Spill-An Arctic Analogue." Proceedings Fourth International Conference on Port and Ocean Engineering Under Arctic Conditions, St. John's, Newfoundland, pp. 844-855.

Schell, D. M. (1974) "Seasonal Variations in the Nutrient Chemistry and Conservative Constituents in Coastal Alaskan Beaufort Sea Waters, "Environmental Studies of an Arctic Estuarine System, Institute of Marine Science, University of Alaska, Fairbanks.

Stringer, W. J. (1978) Morphology of Beaufort, Chukchi and Bering Seas Nearshore Ice Conditions by Means of Satellite and Aerial Remote Sensing, Geophysical Institute, U. of Alaska, Fairbanks.

Swithinbank, C. (1972) "Arctic Pack Ice from Below," Sea Ice: Proceedings of an International Conference, Reykjavic, Iceland, Ed. T. Karlsson, National Research Council, Reykjavic, pp. 246-254.

Thomas, D. R., and R. S. Pritchard (1979) "Beaufort and Chukchi Sea Ice Motion; Part I. Pack Ice Trajectories," Environmental Assessment of the Alaskan Continental Shelf, Annual Reports, NOAA/OCSEAP, Boulder, Colorado. Vol. VIII, Transport, pp. 361-469.

Thomas, D. R. (1980) Behavior of Oil Spills Under Sea Ice - Prudhoe Bay. Flow Research Report No. 175. Flow Research Company, Kent, Washington.

Thorndike, A. S., and J. Y. Cheung (1977) "AIDJEX Measurements of Sea Ice Motion, 11 Apr 1975 to 14 May 1976," AIDJEX Bulletin No. 35, January, University of Washington, Seattle.

Thorndike, A. S., and R. Colony (1980) "Large-scale Ice Motion in the Beaufort Sea during AIDJEX, April 1975-April 1976," Sea Ice Processes and Models, Ed. R. S. Pritchard, University of Washington Press, Seattle, Washington, pp. 249-260.

Thorndike, A. S., D. A. Rothrock, G. A. Maykut, and R. Colony (1975) "The Thickness Distribution of Sea Ice," J. Geophys. Res., Vol. 80, No. 33, November, pp. 4501-4513.

Tucker, W. B., W. F. Weeks, and M. Frank (1979) Sea Ice Ridging Over the Alaskan Continental Shelf, CRREL Report 79-8, Hanover, New Hampshire.

Tucker, W. B., W. F. Weeks, A. Kovacs, and A. J. Gow (1980) "Nearshore Ice Motion at Prudhoe Bay, Alaska," Sea Ice Processes and Models, Ed. R. S. Pritchard, University of Washington Press, Seattle, Washington, pp. 261-272.

Wadhams, P. (1975) Sea Ice Morphology in the Beaufort Sea, Beaufort Sea Technical Report No. 36, Beaufort Sea Project, Dept. of the Environment, Victoria, B.C.

Wadhams, P. and R. Horne (1978) An Analysis of Ice Profiles Obtained by Submarine Sonar in the AIDJEX Area of the Beaufort Sea, Scott Polar Research Institute Technical Report 78 1, Cambridge.

Weeks, W. (1976) "Sea Ice Conditions in the Arctic," AIDJEX Bulletin No. 34, University of Washington, Seattle, pp. 173-206.

Weeks, W. F., and A. J. Gow (1980) "Crystal Alignment in the Fast Ice of Arctic, Alaska," J. Geophys. Res., Vol. 85, No. C2, pp. 1137 1146.

Weeks, W. F., A. Kovacs, and W. D. Hibler III (1971) "Pressure Ridge Characteristics in the Arctic Coastal Environment," Proceedings 1st International Conference on Port and Ocean Engineering under Arctic Conditions, Trondheim, Norway, Vol. I, pp. 152-183.

Weeks, W. F., A. Kovacs, S. J. Mock, W. B. Tucker, W. D. Hibler III, and A. J. Gow (1977) "Studies of the Movement of Coastal Sea Ice Near Prudhoe Bay, Alaska, U.S.A.," J. Glaciology, Vol. 19, No. 81, pp. 533 546.

Weeks, W. F., W. B. Tucker III, M. Frank, and S. Fungcharoen (1980) "Characterization of the Surface Roughness and Floe Geometry of Sea Ice Over the Continental Shelves of the Beaufort and Chukchi Seas," Sea Ice Processes and Models, Ed. R. S. Pritchard, University of Washington Press, Seattle, Washington, pp. 300-312.

DT/113R

ANNUAL REPORT

North Aleutian Shelf Transport Experiment

Edward T. Baker

Pacific Marine Environmental Laboratory
Environmental Research Laboratories, NOAA
7600 Sand Point Way, N.E.
Seattle, WA 98115

Contract No: R7120897
Research Unit: 594
Period: 28 April 1980 to 1 April 1981
Number of Pages: 61

I. SUMMARY

During the present reporting period, the NASTE project was organized and two field programs (August - September, 1980, and January - February, 1981) in the southeastern Bering Sea were carried out. Only data and results from the first cruise will be discussed in this report since information is not yet available from the second cruise.

Data from both the North Aleutian Shelf (NAS) area and the St. George Basin (SGB) area showed a close relationship between SPM distributions and hydrographic properties such as temperature and salinity. SPM landward of the 50 m isobath (the coastal domain) was generally well mixed throughout the water column. SPM profiles seaward of the 50 m isobath always consisted of surface and near bottom concentration maxima separated by a uniform, low concentration zone. Frontal regions were characterized by relatively low values of SPM concentration in the near bottom layer. Particle size distributions indicated that surface and near bottom SPM populations were distinct seaward of the coastal domain. Estimates of the vertical eddy diffusion coefficient made from the SPM profiles show that the bottom layer is a zone of energenic turbulent mixing capped by a thinner layer of much lower eddy diffusivity.

II. OBJECTIVES

The general objective of this research unit is to measure the distribution, transport and physical characteristics of suspended particulate matter (SPM) in various regions of the southeastern Bering Sea.

Specific objectives include:

1. Conduct detailed measurements of the distribution and composition of SPM along the North Aleutian Shelf.
2. Obtain direct information of SPM flux through simultaneous and continuous current meter/transmissometer measurements and sediment trap deployments at four locations on the North Aleutian Shelf.
3. Characterize the SPM at several locations along and across the coastal front in terms of particle size distribution, organic matter content, and x-ray mineralogy. SPM measurements will be compared to similar measurements from surficial bottom sediments collected at the same stations.
4. Conduct measurements of SPM distributions and particulate size distribution in St. George Basin for comparison to other physical and chemical oceanographic studies.
5. Examine the possibilities of using specific particulate fractions as transport tracers analogous to the models proposed for methane.

III. STUDY AREA

The study area comprises most of the southeastern portion of the Bering Sea Shelf. Particular emphasis is placed on the area immediately north of the Alaskan Penninsula and on the waters overlying St. George Basin, approximately between the 100 and 200 m isobaths. Stations used in this report are shown in Fig. 1 of the first report in Section IV.

IV. PRESENT STATUS

A. A report prepared for the St. George Basin Synthesis Meeting, April 28-30, 1981.

B. A paper prepared to accompany an abstract presented at the 1980 Fall National American Geophysical Meeting (Pearson, C.A., Baker, E.T. and Schumacher, J.D., 1980. CTD and SPM observations during reestablishment of a structural front: Bristol Bay, Alaska. E O S 61: 1002).

DISTRIBUTIONS OF SUSPENDED PARTICULATE MATTER IN THE SOUTHEAST BERING SEA: August-September, 1980

1. INTRODUCTION

Although OCSEAP and PROBES investigators have nurtured a large body of literature describing the distribution of hydrographic properties and dissolved nutrients in Bristol Bay, there is only scattered information on the relationship of the distribution of suspended particulate matter (SPM) to the hydrographic structure in this area. This report summarizes results from the first of three cruises designed, in part, to describe the distributions and physical characteristics of SPM in Bristol Bay, with specific reference to St. George Basin and the North Aleutian Shelf area.

2. METHODS

Continuous profiles of light attenuation were recorded at all stations within the study area (Fig. 1) by means of a 0.25 m path length transmissometer interfaced to a Plessey CTD. Values of light attenuation can be translated into absolute concentration data by comparison with water samples filtered through 0.45 μm pore size membrane filters (Fig. 2). The intercept value for such a regression is close to the attenuation value for clear water at 660 nm (the wavelength of the transmissometer light source) (Jerlov, 1976), implying that the transmissometer signal is due to particle, not dissolved organic matter, attenuation.

Size characteristics of the SPM were measured with a model ZBI Coulter

Counter using 50 and 200 μm apertures to yield a diameter range of ∿ 1.2 to 80 μm.

3. NORTH ALEUTIAN SHELF

The NAS study area comprises a narrow zone ∿ 70 km wide stretching along the Alaska Peninsula from Unimak Island to Ugashik Bay. This region encompasses the transition zone between the well mixed coastal and stratified mid-shelf domains on the Bering Sea Shelf as described by Kinder and Schumacher (1981). One of the goals of this project was to ascertain the effect of this zone (the inner front) on the distribution and transport of SPM.

3.1. Surface Water

A plot of surface salinity from the NAS region for mid-August, 1980 (Fig. 3), shows a strong source of freshwater from the northeast (presumably the Kvichak and other smaller rivers), a minor source of freshwater from Heredeen Bay, and a characteristic curvature of the salinity contours from orthogonal to the coast seaward of the 50 m isobath to parallel on the landward side. Also present was an isolated patch of low salinity water in the center of the region.

A plot of surface attenuation values shows much the same pattern (Fig. 4). Concentrations are highest in the northeast corner and decrease both seaward and to the southwest. The patch of low salinity water seen in Fig. 3 is expressed as high attenuation in Fig. 4. The principal distinction between the two maps is that attenuation remains high (though variable) all along the coast inside the 50 m isobath, approximately the zone occupied by the well mixed coastal domain.

3.2. Bottom Water

A plot of the bottom water salinity (Fig. 5) is very similar to that of the surface salinity (Fig. 3). Principal differences include: weakened freshwater source to the northeast, the 31.4 and 31.6 $^{o}/oo$ contours displaced landward along the coast, and a greater influence of high salinity water to the southwest. Through most of the region the salinity gradient is greatest in the region of the inner front, along the 50 m isobath.

A bottom water map of attenuation (Fig. 6), however, is substantially different than its surface water counterpart (Fig. 4). Although the bottom pattern is more complicated than that of the surface, certain important trends are definable. As in the surface, the highest concentrations are found along the coast inside the 50 m isobath and are similar to the surface values. CTD profiles indicate this area is generally well mixed with respect to temperature, salinity and SPM. Unlike the surface plot, however, there appears to be a consistent zone of minimum attenuation values centered at or just seaward of the 50 m isobath. The absolute values of these minimums decrease to the southwest along with the general regional decrease in that direction.

3.3. Cross-Sections

The frontal region suggested by the areal data can be seen more clearly on salinity and attenuation cross-sections of the area (Fig. 7) which extend from near Cape Newenham south to Herendeen Bay (Fig. 1). The salinity cross-section shows cross-shelf change from the coastal domain at PL24, through the stratified mid-shelf domain (Y1 through ∿ NA 42) and across the inner front and into the well mixed coastal domain (NA 45 and 46). The attenuation cross-section shows analogous changes, being also well mixed in the coastal domain and strongly stratified (surface and bottom maximums centered around a mid-depth minimum) in the mid-shelf domain. The near bottom minimum seen in the vicinity or just landward of the inner front appeared to be a consistent feature in the NAS area during this survey period.

3.4. Particle Size Distributions

Another method of illustrating the stratification differences in SPM between the coastal and mid-shelf domains is to use the particle size distributions (PSD) from surface and bottom waters of each region. PSD spectra at Station NA 46 (Fig. 8) are nearly identically shaped, with the volume concentrations in the bottom sample increasing for larger particle diameters with respect to the surface sample. These curves suggest that the particle source is principally from bottom sediment resuspension, and that the probability of a particle being turbulently mixed throughout the water column decreases with increasing size. PSD spectra from NA 42 show a quite different situation (Fig. 9). The PSD in the surface water shows a low level of particulate volume at all sizes excpet for a dominant peak between 20 and 30 μm, presumably phytoplankton. Near bottom SPM shows a broad peak extending from ∿ 5 to > 50 μm. Clearly there is little direct transfer of particles between the surface and bottom layers in the mid-shelf domain.

4. ST. GEORGE BASIN

4.1. Cross-Shelf Transect

A cross-shelf transect of the southeastern Bering Sea (Fig. 1) reveals the hydrographic structure described by Coachman et al. (1980) in salinity (Fig. 10), temperature (Fig. 11) and SPM (Fig. 12). Typical near bottom variations in the horizontal salinity gradients were found during the August cruise, with the bottom mixed layer about 50 m thick in the outer domain and 25 m thick in the mid-shelf domain. Near bottom temperatures of < 4°C characterized both the outer domain and the mid-shelf domain (Fig. 11). Surface water in the mid-shelf domain was likewise characterized by cold water - in this case < 8°C. An additional pool of cold water was observed just seaward of the shelf break.

The light attenuation contour pattern (Fig. 12) was similar to that of temperature and clearly is also related to the hydrographic structure in some way. The bottom mixed layer across the shelf is characterized by a strong bottom nepheloid layer (BNL) with maximum concentrations at the center of the outer and mid-shelf domains. The outer, middle and inner front regions all have bottom attenuation values of < 1 m^{-1}, the only areas on the shelf to have such low SPM levels in the bottom water.

Immediately above the BNL is a broad area of uniformly low SPM levels (< 0.8 m^{-1}) generally bracketing the center of the pycnocline. The wind mixed layer is also mixed with respect to SPM, but maximum values vary greatly across the shelf. The highest values in August were always associated with the coldest surface water (compare Figs. 11 and 12). No distinct surface expression of the middle front was present in the SPM data.

The coastal domain was marked by a change from layered to uniformly varying vertical SPM profiles as was seen along the NAS area (Fig. 7). Turbulent wind and tidal mixing throughout the water column eliminated the mid-depth minimum seen seaward of the 50 m isobath.

A more detailed illustration of the relationship between SPM concentration and density at various points along this transect is given in Fig. 13. Because particulate matter is negatively buoyant its concentration profile in the bottom half of the water column is similar to that of density but is displaced downwards. A near bottom low gradient layer of high SPM concentration is capped by one or more layers of high SPM gradient. Surface water gradients are controlled by the depth of the wind mixed layer, with an increased concentration of particles (presumably phytoplankton) found just above the pyconcline. High surface values in the mid-shelf domain appear to result from a hightened phytoplankton growth due to a shallowing of the wind mixed layer (see Section 4.2). In the coastal domain SPM decreases monotonically from bottom to surface, suggesting that bottom resuspension is the primary particle source.

4.2. Particle Size Distributions

As was done for the NAS area, PSD's can be utilized to characterize the kinds of particles in each layer of the St. George Basin transect and to provide evidence of origin of these particles. Surface, mid-depth and bottom water PSD's from various locations along the SGB transect show features similar to that of the NAS sample.

Surface samples from the outer domain (Fig. 14), middle front (Fig. 15) and mid-shelf domain (Fig. 16) show a consistently peaked spectra strongly suggestive of phytoplankton cell dominated distributions. Modal sizes are typically 4-5 μm, 8-10 μm and 30-50 μm. A consistent mininum is present at ∿ 20 μm. Samples centered in the mid-depth minimum zone at each station (compare depths with Fig. 13 profiles) are uniformly low and featureless with no indications that the modal particle sizes seen in the surface water are abundant below the surface layer.

Samples from 5 m above bottom are distinct from either surface or mid-depth samples. PSD's reveal a broad uni-modal population centered around 6 μm and with sporadic increases in the > 30 μm region. Total volume at the middle front station (PL 8, 143.5 x 10^4 μm^3 ml^{-1}) was less than at either the outer domain station (PL 6, 169.3 x 10^4 μm^3 ml^{-1}) or the middle domain station (PL 14, 258.2 x 10^4 μm^3 ml^{-1}), in good agreement with the light transmission trends (Fig. 12).

In the coastal domain (Fig. 17) PSD's are identical in both the surface and near bottom layers and show a distinct shift to a coarser mode at ∿ 30 μm. The shift in the near bottom mode is presumably a result of both increased turbulent energy in the coastal domain and a shoreward trend to coarser mean bottom sediment grain sizes (Sharma, 1979).

It is clear from the foregoing data that SPM trends across the inner front in Bristol Bay were similar in both the NAS area and along the SGB transect line. The coastal domain is characterized by uniform or monotonically changing vertical SPM profiles and similar PSD's throughout the water column, both features resulting from a well mixed water column where the primary particle source is bottom resuspension. The mid-shelf domain is characterized by a strongly layered SPM profile and PSD's which indicate distinct sources for the surface and near bottom SPM. Relatively few particles appear to leave the surface layer by simple individual sinking; particles may be biogically or physically agglomerated in the surface waters and thus be transported rapidly to the seafloor in relatively large, rare particles not sampled by the water bottles. Sediment trap samples from the mid-shelf domain to be recovered in June, 1981, may address this transport mode.

4.3. Vertical Eddy Diffusion Coefficients

According to Coachman et al. (1980), vertical diffusivity varies by as much as two orders of magnitude between the frontal and non-frontal regions since vertical transport is thought to be enhanced in the fronts. Some indications of this variability should be present in the SPM data. Coefficients of vertical eddy diffusion for particles can be estimated from the attenuation profiles using a sediment mass continuity equation:

$$\frac{\partial c}{\partial t} + \bar{u}\,\frac{\partial c}{\partial x} + \bar{v}\,\frac{\partial c}{\partial y} + (\bar{w} - w_s)\,\frac{\partial c}{\partial z} = \frac{\partial}{\partial y}\left(K_y\,\frac{\partial c}{\partial y}\right) + \frac{\partial}{\partial z}\left(K_z\,\frac{\partial c}{\partial z}\right)$$

where C is the SPM concentration in mass/unit volume, $\bar{u}$, $\bar{v}$, and $\bar{w}$ is the advective flow in the horizontal and vertical directions, w_s is the SPM settling velocity, and K_y and K_z are the horizontal and vertical eddy diffusion coefficients. This equation can be simplified by assuming a steady state situation ($\partial c/\partial t = 0$), and $\partial c/\partial y$ and $\partial c/\partial x$ negligible compared to $\partial c/\partial z$; thus

$$0 = \frac{\partial}{\partial z}\left[K_z\,\frac{\partial}{\partial z} + (\bar{w} - w_s)C\right]$$

and

$$\frac{C_z}{Ca} = \exp\left[-\int_a^z \frac{(\bar{w} - w_s)}{K_z}\,dz\right]$$

where C_z is the concentration level of SPM at some level z above a reference level Ca. Levels of approximately constant K_z are assumed wherever a semi-log plot of C vs. depth yields a straight line, and K_z in these intervals may be evaluated by the expression:

$$K_z = \frac{(\overline{w} - w_s)(z-a)}{\ln(C_z/Ca)}$$

Fig. 78 illustrates C vs. depth plots for several profiles in various hydrographic regions along the St. George Basin transect. Note that in this figure values of total light attenuation have been uniformly reduced by the clear water attenuation of 0.4 m^{-1} in order to plot only the curvature due to the particle population. These plots illustrate that the near bottom layers can be partioned into one or more layers of approximately uniform K_z. Station PL 6 was visited twice (August 29 and September 3) and showed little change, justifying the steady state assumption.

K_z can be accurately estimated for each interval only if the term $\overline{w} - w_s$ (the sum of vertical advection and particle settling velocity) is known. The settling velocity can be estimated from the Stokes equation:

$$w_s = \frac{2g}{9}\frac{(\rho s - \rho)r^2}{r}$$

if the particles are assumed to be spherical and their radius (r) and net density ($\rho s - \rho$) is known. The PSD's yield limits on the size range at various depths, but the in-situ density of the particles is unknown at present. Furthermore, since w_s for most particles is likely to be in the range of 10^{-2} to 10^{-4} cm sec^{-1} (Table 1), the vertical advection term is likely to be an important factor. J. Schumacher (personal communication) has suggested that the vertical advection term in Bristol Bay, particularly in frontal areas, may be on the order of 10^{-3} cm sec^{-1}.

For comparative purposes, then, Table 1 gives values of $K_z/(\bar{w} - w_s)$ for each interval. Values of K_z are also calculated for some reasonable values of $(\bar{w} - w_s)$. Certain trends are clear from this data. Turbulent mixing is always highest in the tidally mixed bottom layer. Above this layer, values of K_z decrease either abruptly or by means of a transition layer into a layer of low K_z which ends in the uniform concentrations of the mid-depth minimum (where it is present). Seaward of the inner front, the highest values of K_z in the bottom layer were found at PL 14, although the assumption of steady state cannot be guaranteed there. As expected, the lowest K_z values were found above the bottom layer in the mid-shelf domain. However, contrary to expections based on the frontal model (Coachman et al., 1980), values of K_z, at PL 9, in the middle front, were not higher than at PL 6, the outer domain. This result could be modified if values for $\bar{w}$ and $(\rho s - \rho)$ were significantly different for the frontal and non-frontal regions.

Values of K_z in the inner front and coastal domain show no evidence of a diffusive cap seen in the more seaward stations. Steady state assumptions are also likely to be tenuous in this region. A sharp increase in the near particle size at these stations (Figs. 14 - 17) also dictates a large increase in w_s and thus a larger value of K_z for a concentration gradient similar to the more seaward stations.

REFERENCES

COACHMAN L.K., KINDER T.H., SCHUMACHER J.D. and TRIPP R.B. (1980) Frontal systems of the southeastern Bering Sea Shelf. In *Stratified Flow, 2nd Int. Assoc. Hydraulic Res. Symposium, Trodheim,* June, 1980 (eds T. Carstens and T. McClinians) TAPIR Publishers, Norway, 917-933.

JERLOV N.G. (1976) *Marine Optics*. Elsevier, Amsterdam, 231 pp.

KINDER T.H. and SCHUMACHER J.D. (1981) Circulation over the continental shelf of the southeastern Bering Sea. In *The Eastern Bering Sea Shelf: Oceanography and Resources*. (eds D.W. Hood and J.A. Calder) NOAA Office of Marine Pollution Assessment, 53-75.

SHARMA G.D. (1979) *The Alaska Shelf*. Springer-Verlag, New York, 498 pp.

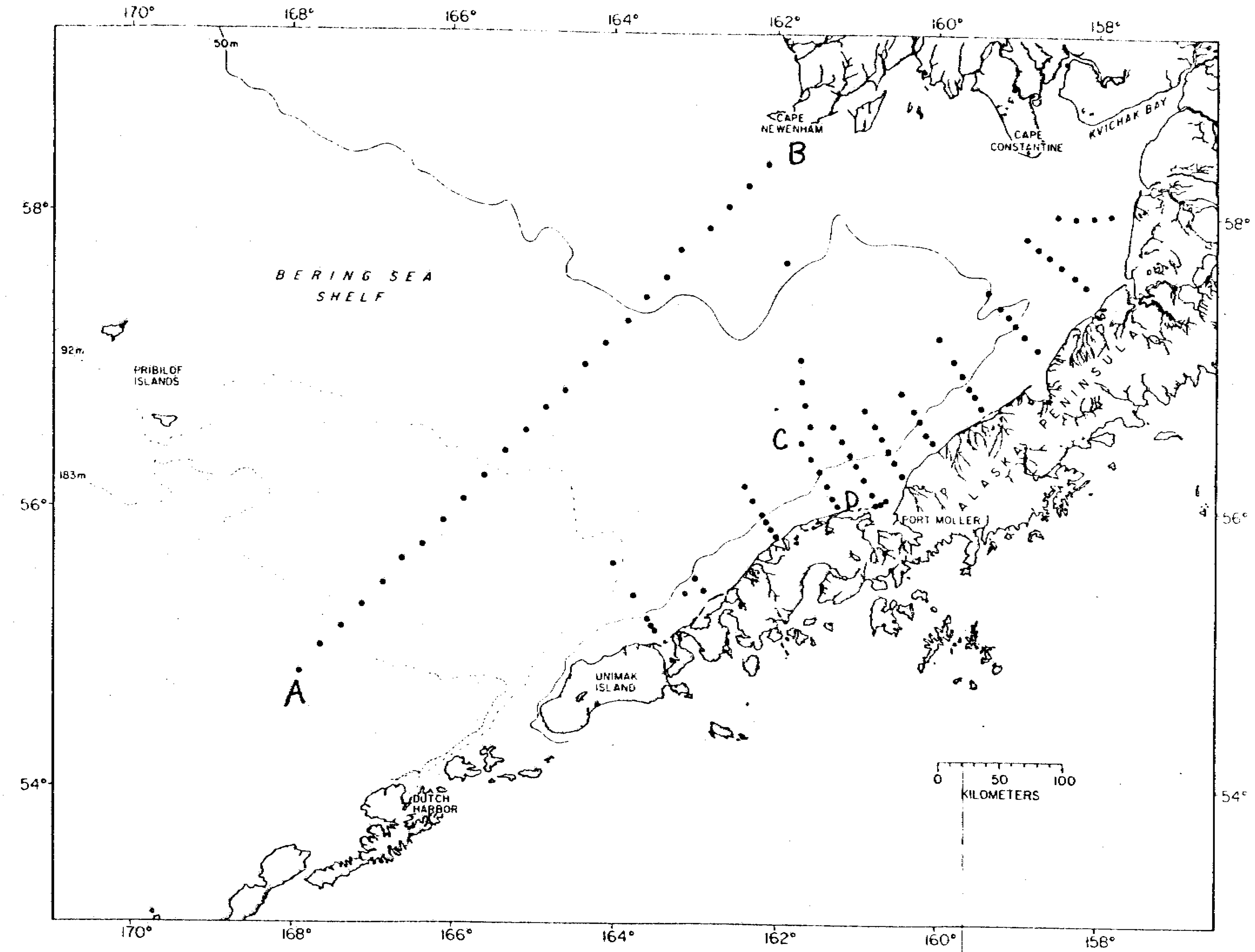

Figure 1. The southeastern Bering Sea Shelf area and station locations discussed in this report.

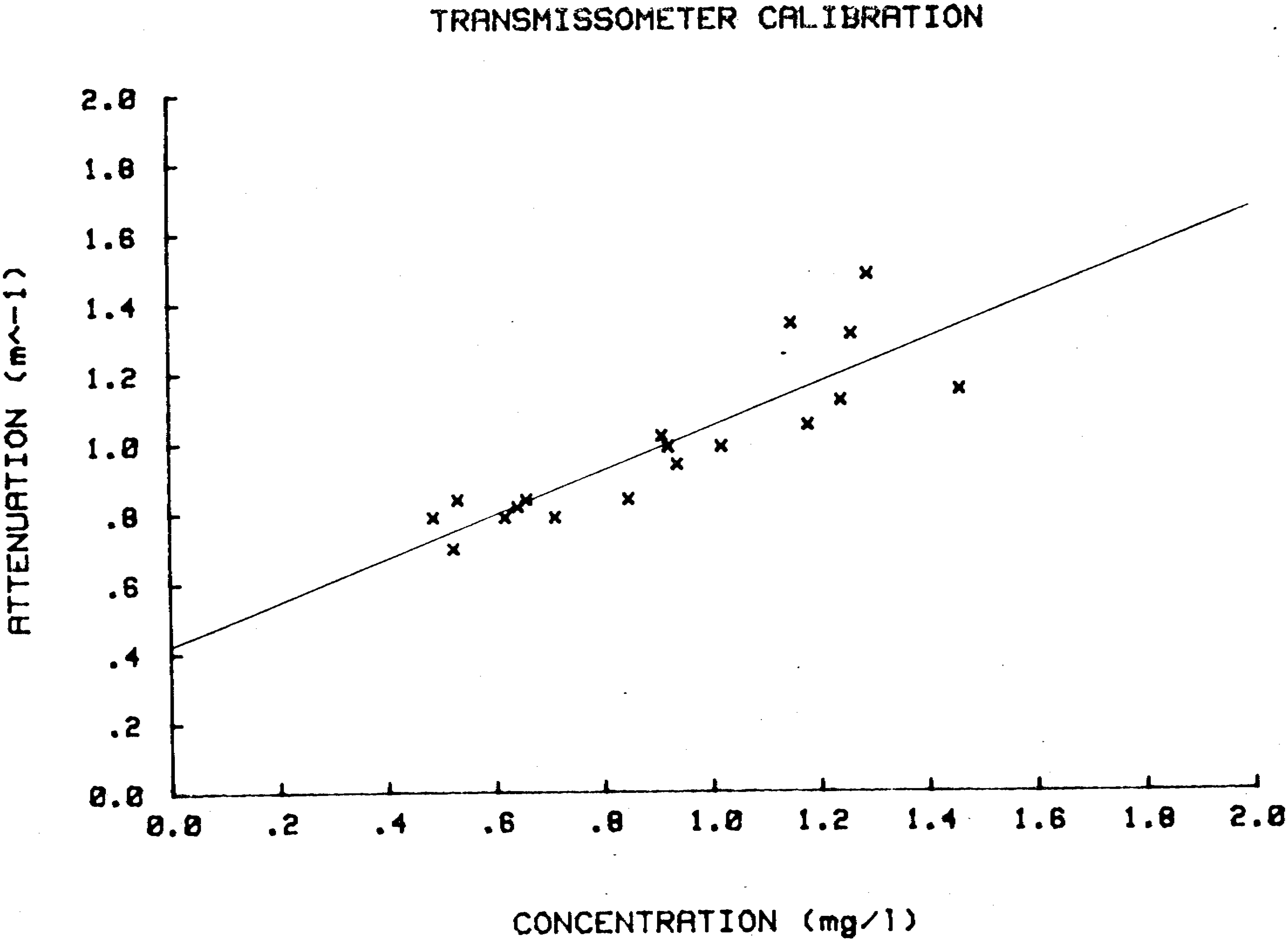

Figure 2. Scatter plot of light attenuation vs. measured SPM concentration for some representative stations. The intercept value is close to the attenuation value to be expected from clear

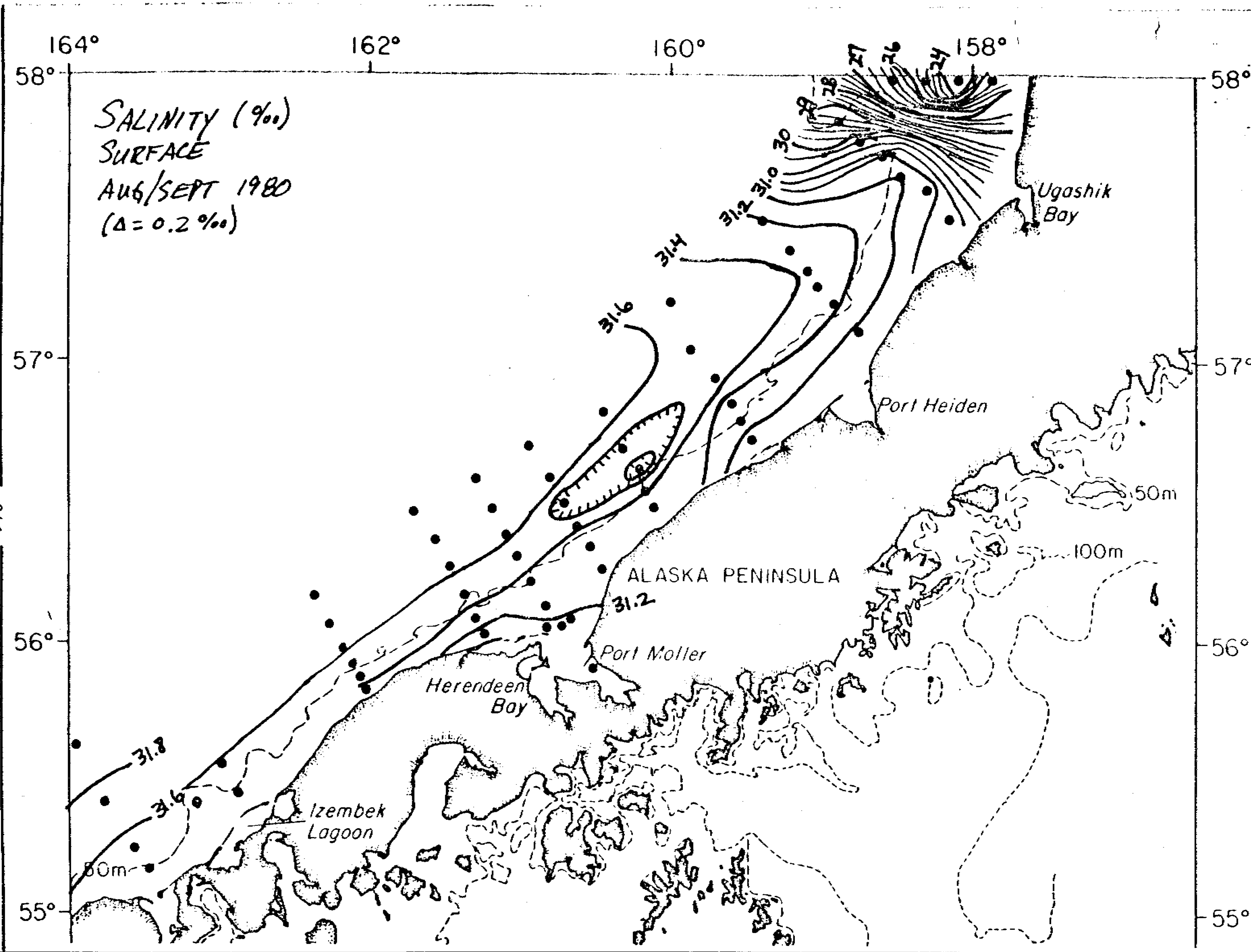

164°
162°
160°
158°
58°
57°
56°
55°
SALINITY (‰)
SURFACE
AUG/SEPT 1980
(Δ = 0.2 ‰)
27
26
24
28
29
30
31.0
31.2
31.4
31.6
31.8
31.2
31.6
Ugashik
Bay
Port Heiden
50m
100m
ALASKA PENINSULA
Port Moller
Herendeen
Bay
Izembek
Lagoon
50m

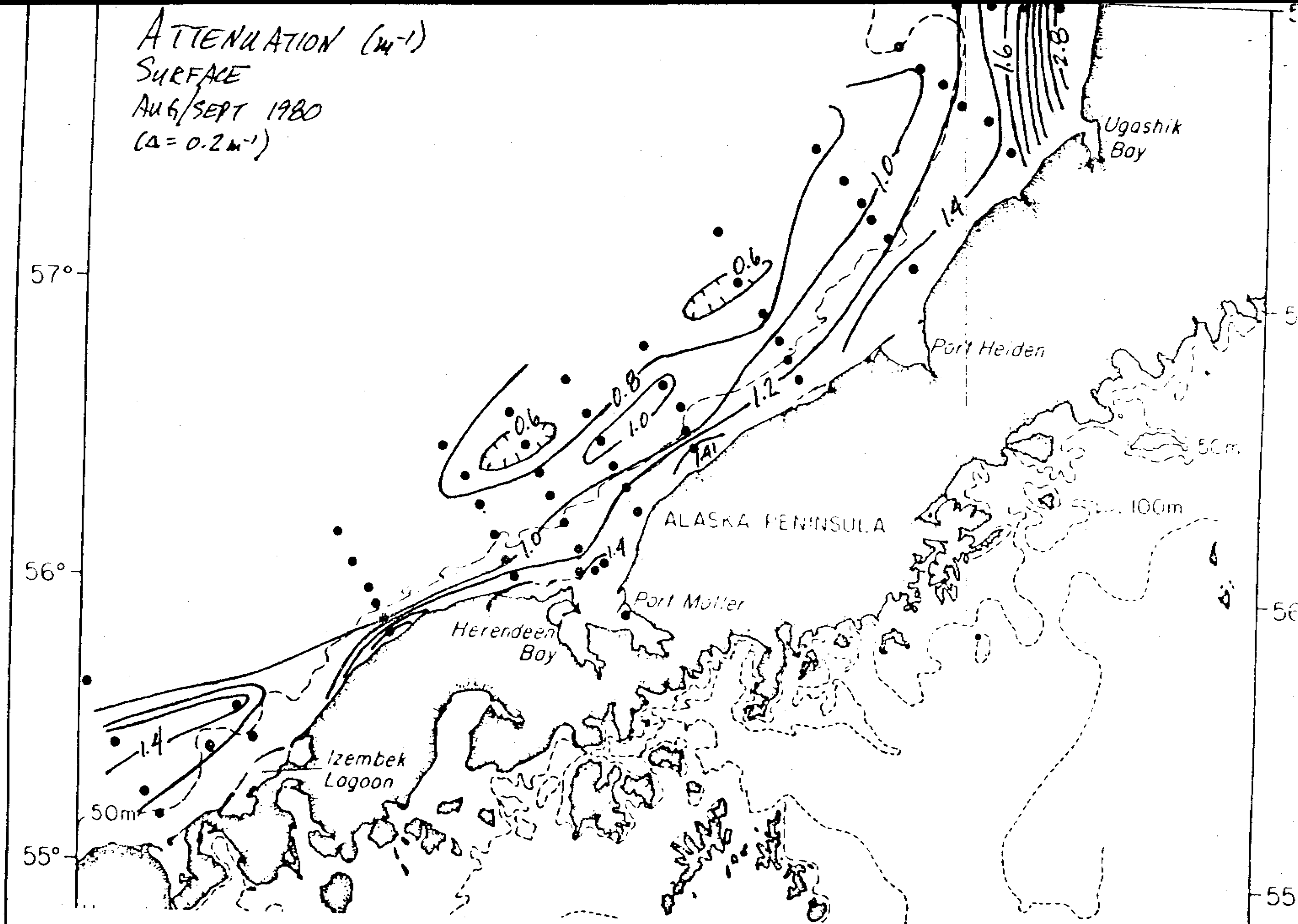

Figure 4. Surface attenuation for NAS stations acquired simultaneously with salinity.

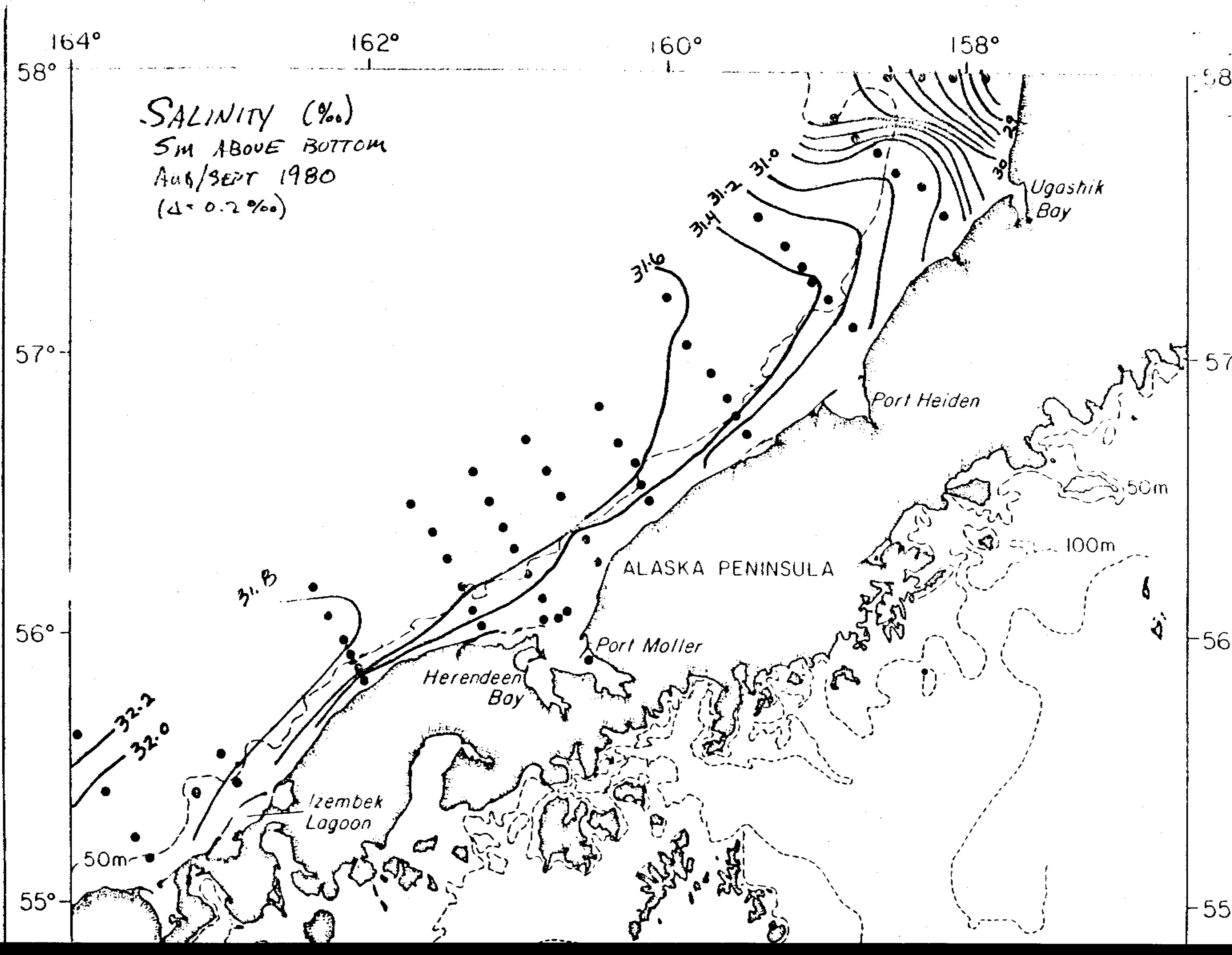
SALINITY (‰)
5M ABOVE BOTTOM
AUG/SEPT 1980
(Δ = 0.2 ‰)
164°
162°
160°
158°
58°
57°
56°
55°
31.0
31.2
31.4
31.6
31.8
32.2
32.0
30
29
Ugashik Bay
Port Heiden
ALASKA PENINSULA
Port Moller
Herendeen Bay
Izembek Lagoon
50m
100m

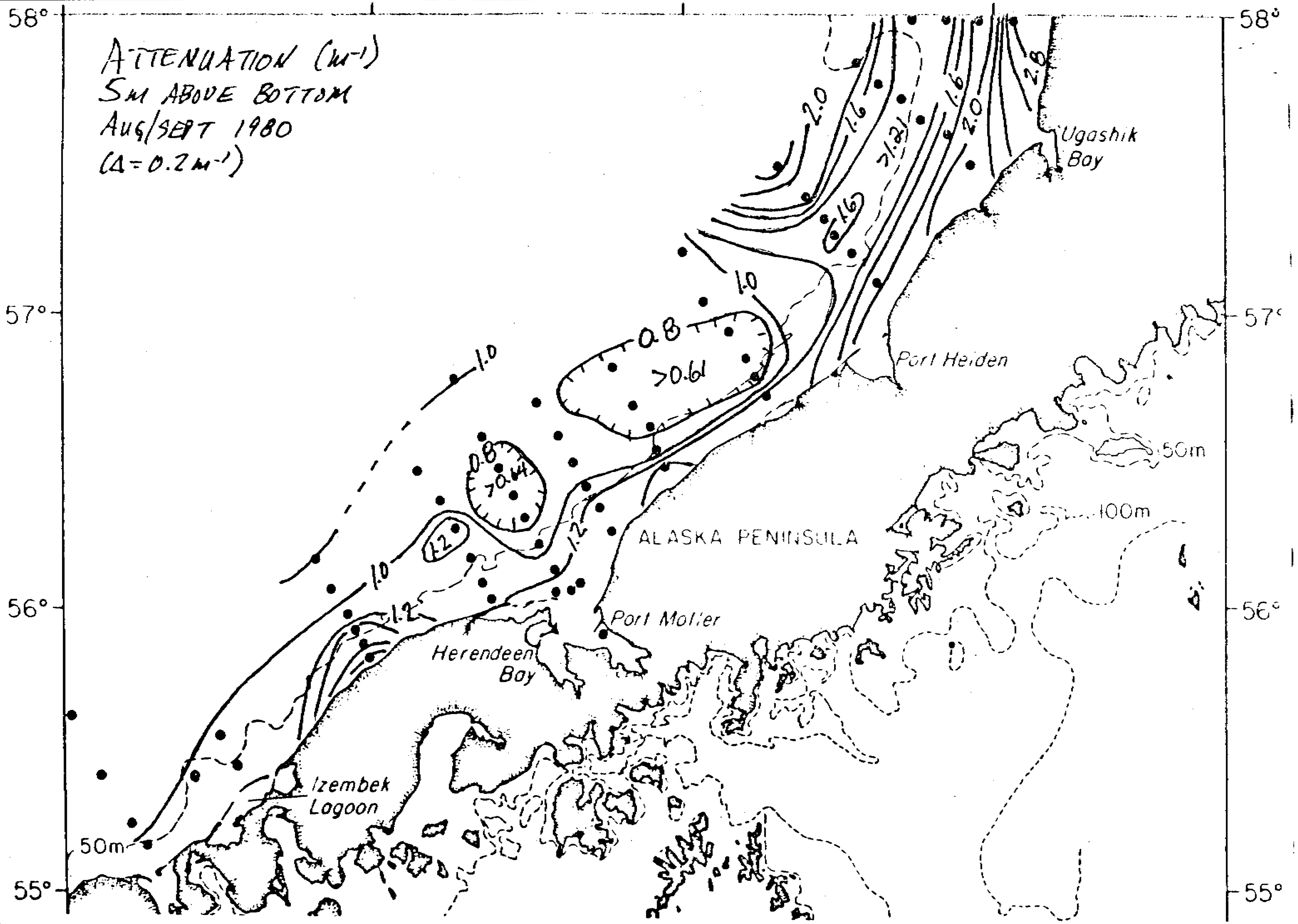

Figure 6. Attenuation 5 m above bottom for NAS stations. Note regional minimum zone at or just seaward of 50 m isobath.

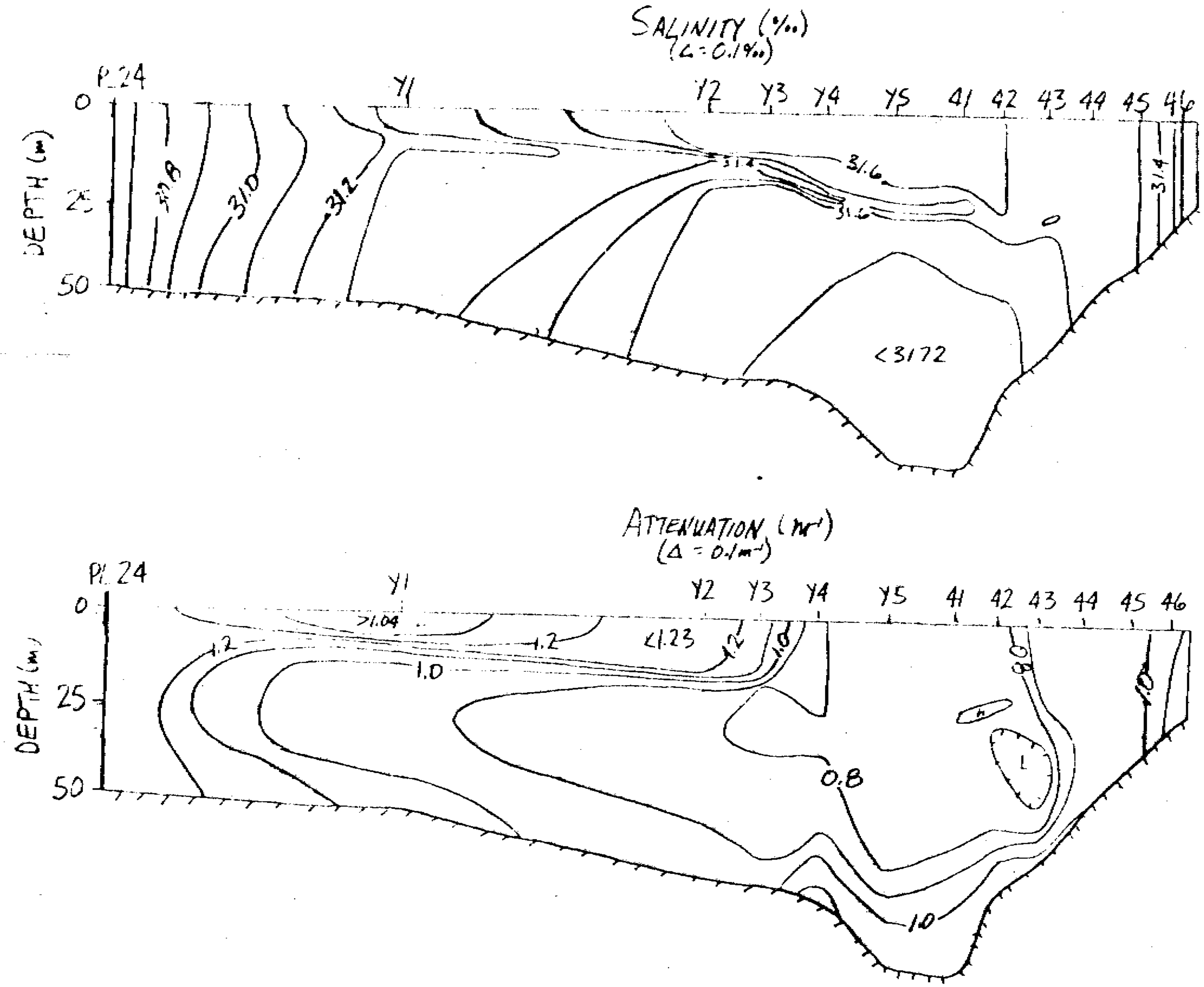

Figure 7. Salinity (top) and attenuation (bottom) cross-sections along line B-C-D in Fig. 1. The thin salinity minimum at stations Y2-NA41 may be an artifact of temperature effects as the CTD passes through the thermocline. Note minimums in bottom attenuation surrounding the mid-shelf maximum region at stations Y4 to NA43. A similar pattern can be seen on the SGB cross-section (Fig. 12).

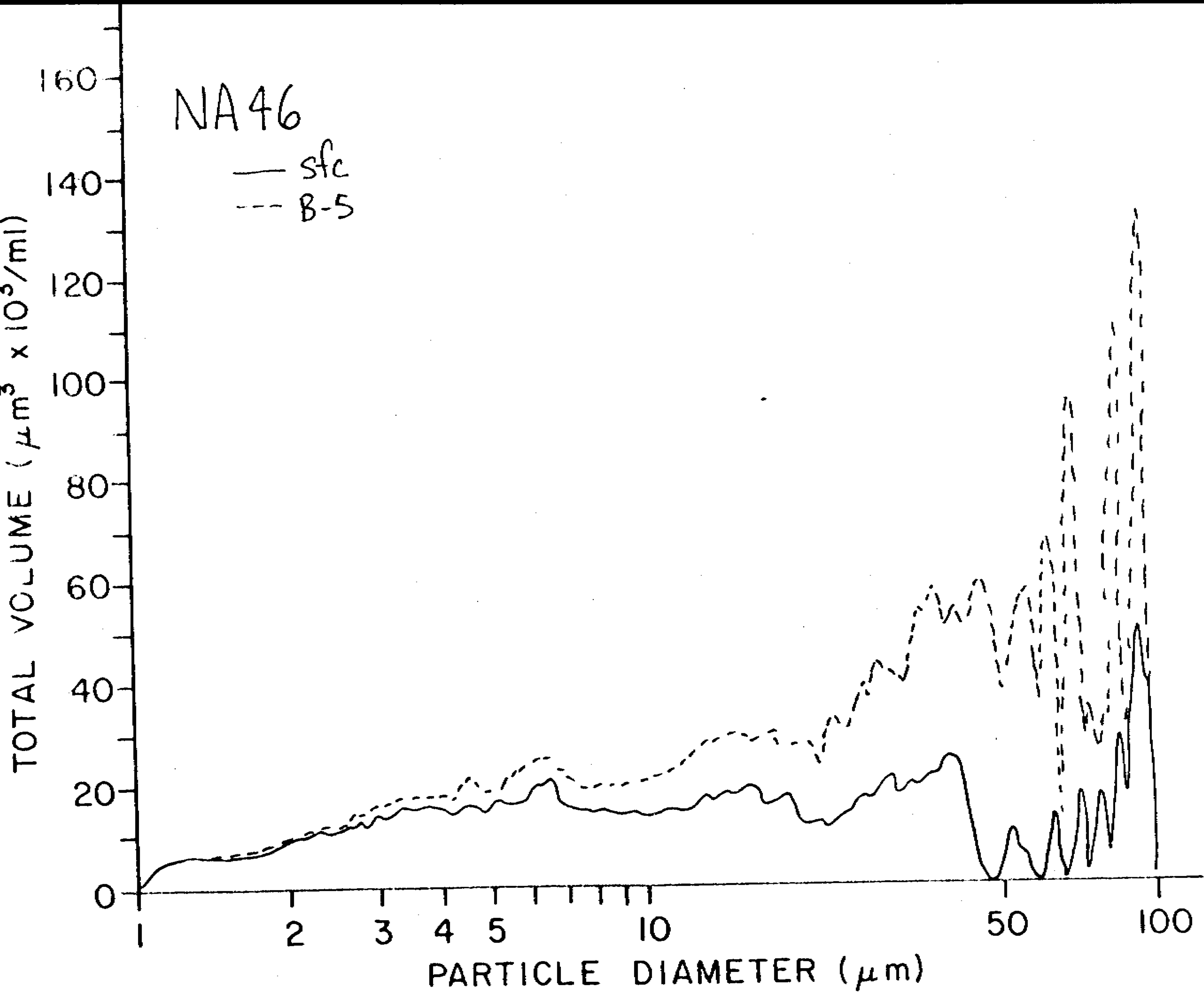

Figure 8. Particle size distributions for surface and near bottom samples at NA46.

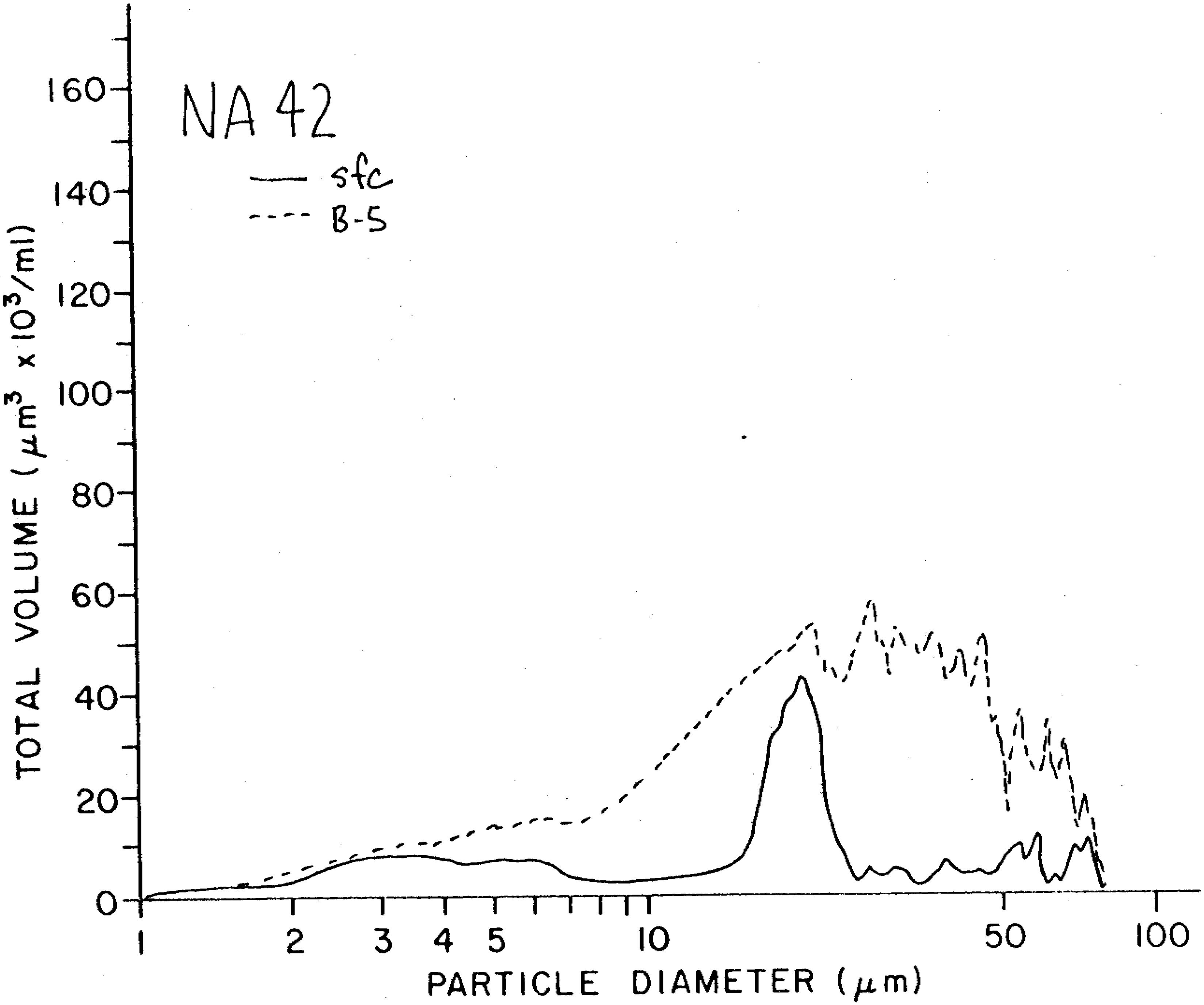

Figure 9. Particle size distributions for surface and near bottom samples from NA42.

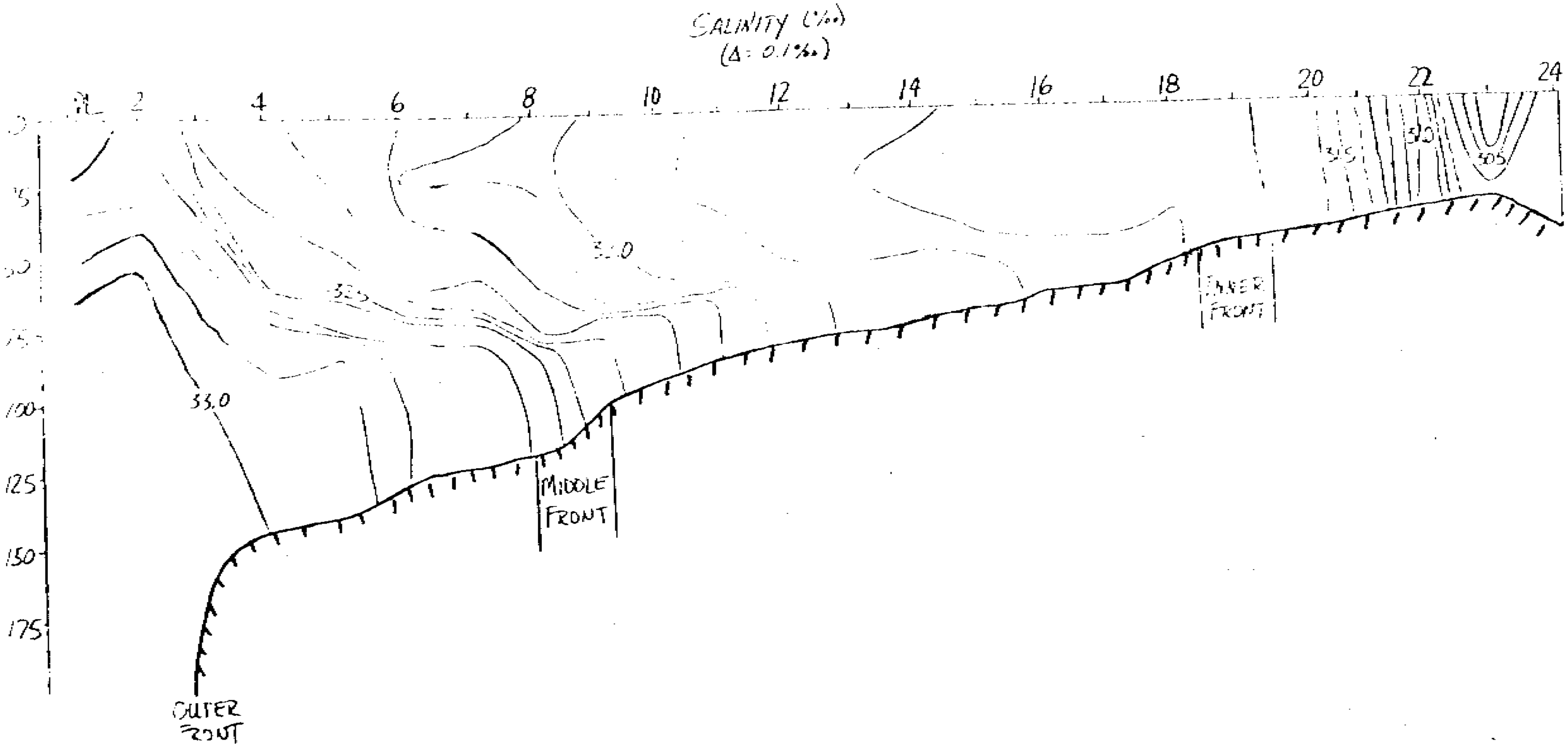

Figure 10. Salinity cross-section for 24 stations along line A-B in Fig. 1. Position of the fronts were estimated from criteria described in Kinder and Schumacher (1981) and other sources.

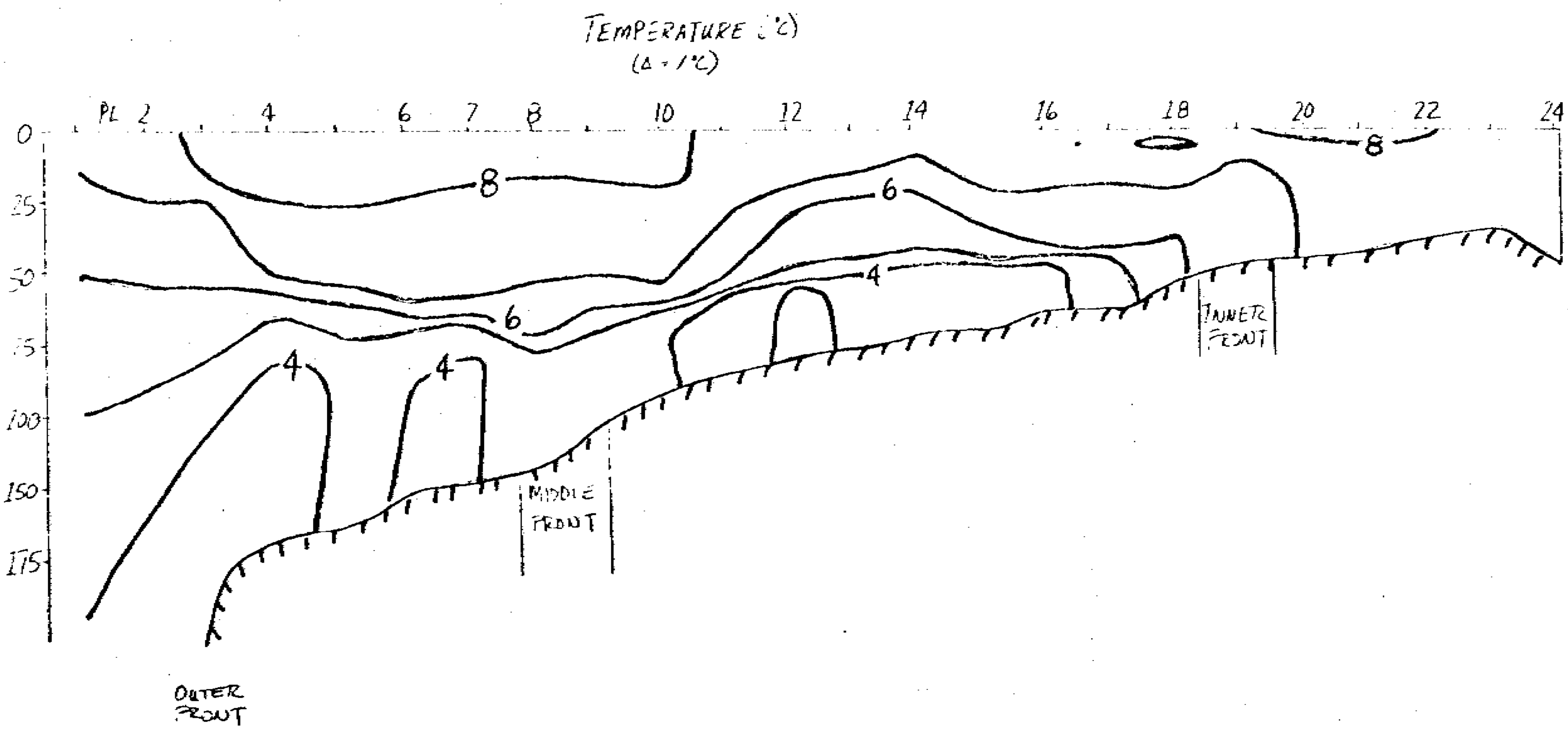

Figure 11. Temperature cross-section for 24 stations along line A-B in Fig. 1. Cold water pools were present on the bottom in the mid-shelf and outer domains, and in the surface water of the mid-shelf domain and just seaward of the shelf break.

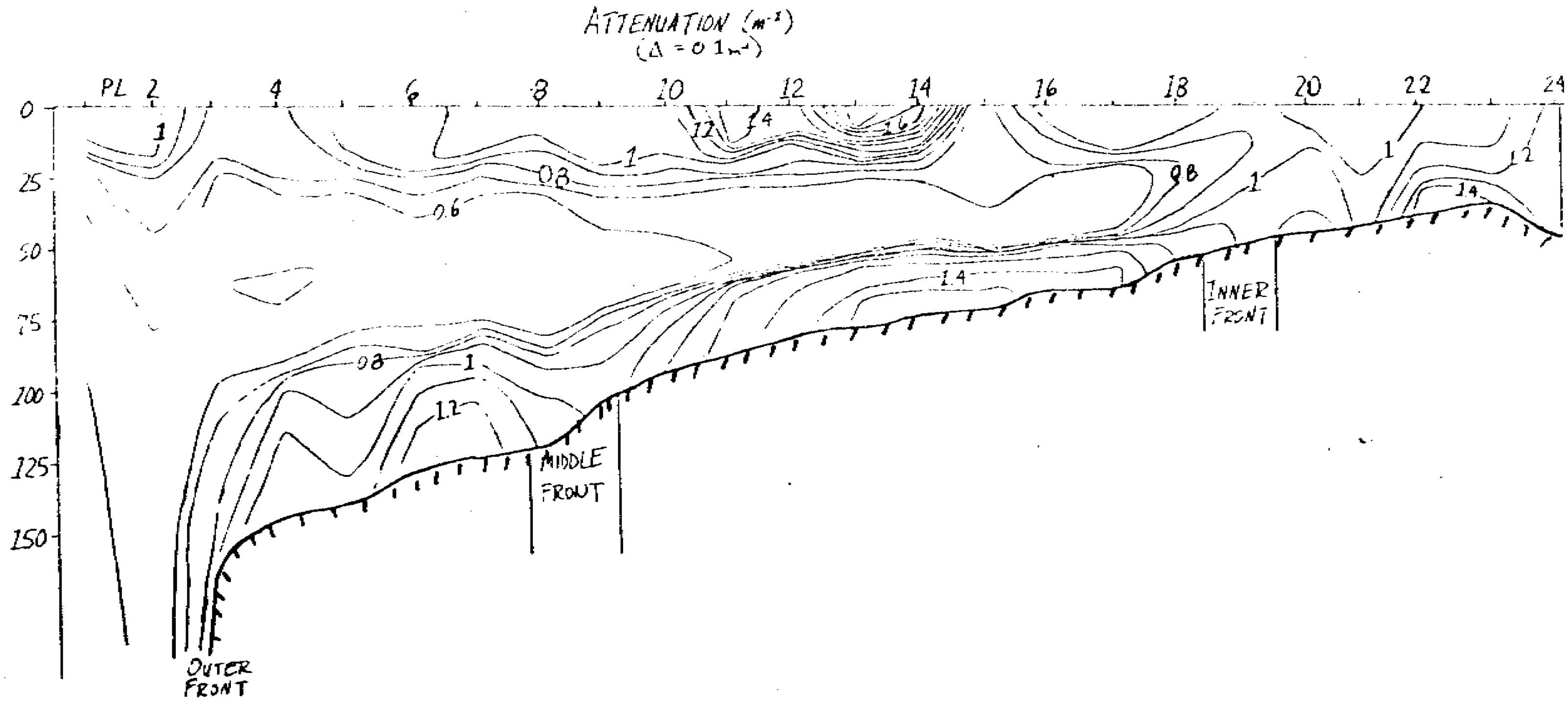

Figure 12. Attenuation cross-section for 24 stations along line A-B in Fig. 1. Note similarity to temperature contour pattern. Attenuation minimums were found in bottom water near the frontal zones.

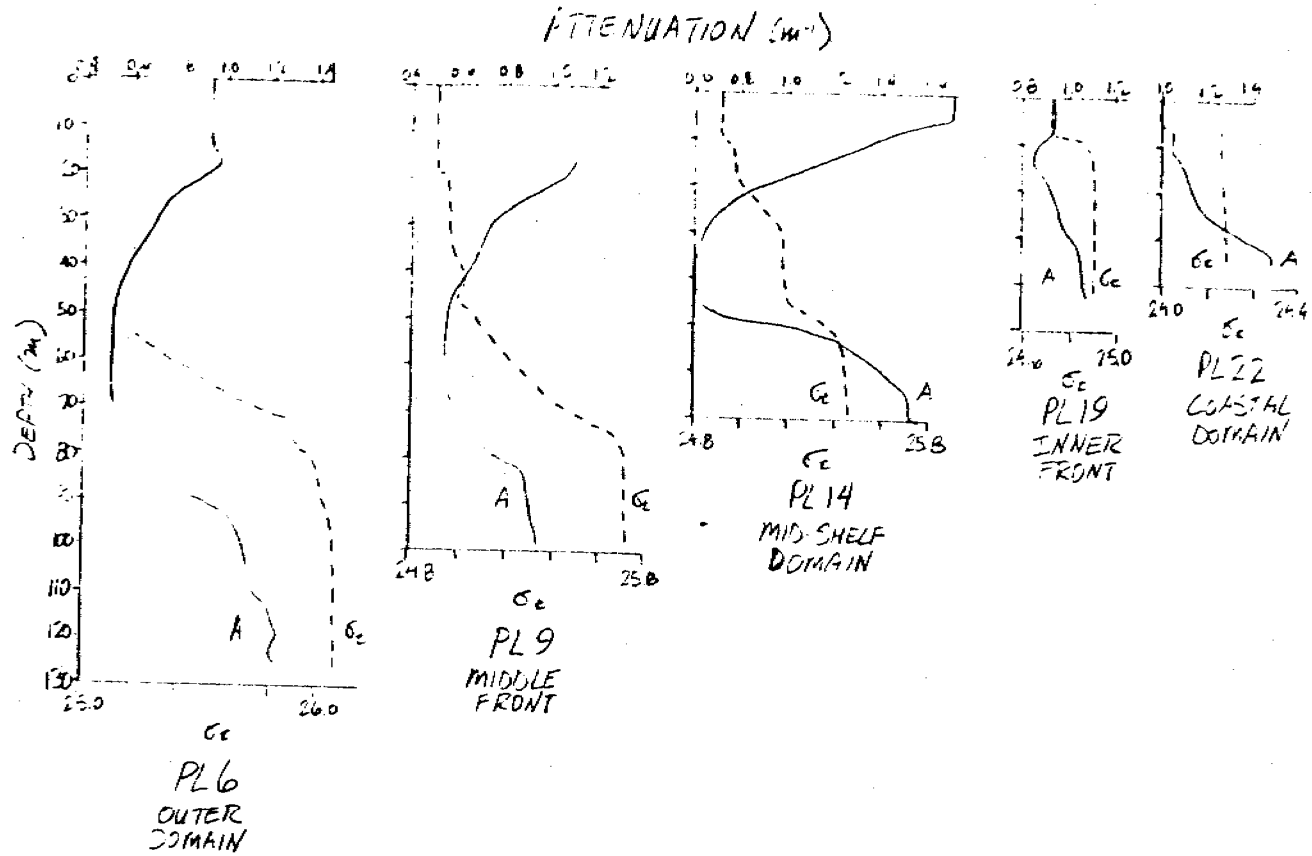

Figure 13. Attenuation and density (σ_t) profiles for five representative stations along the SGB transect.

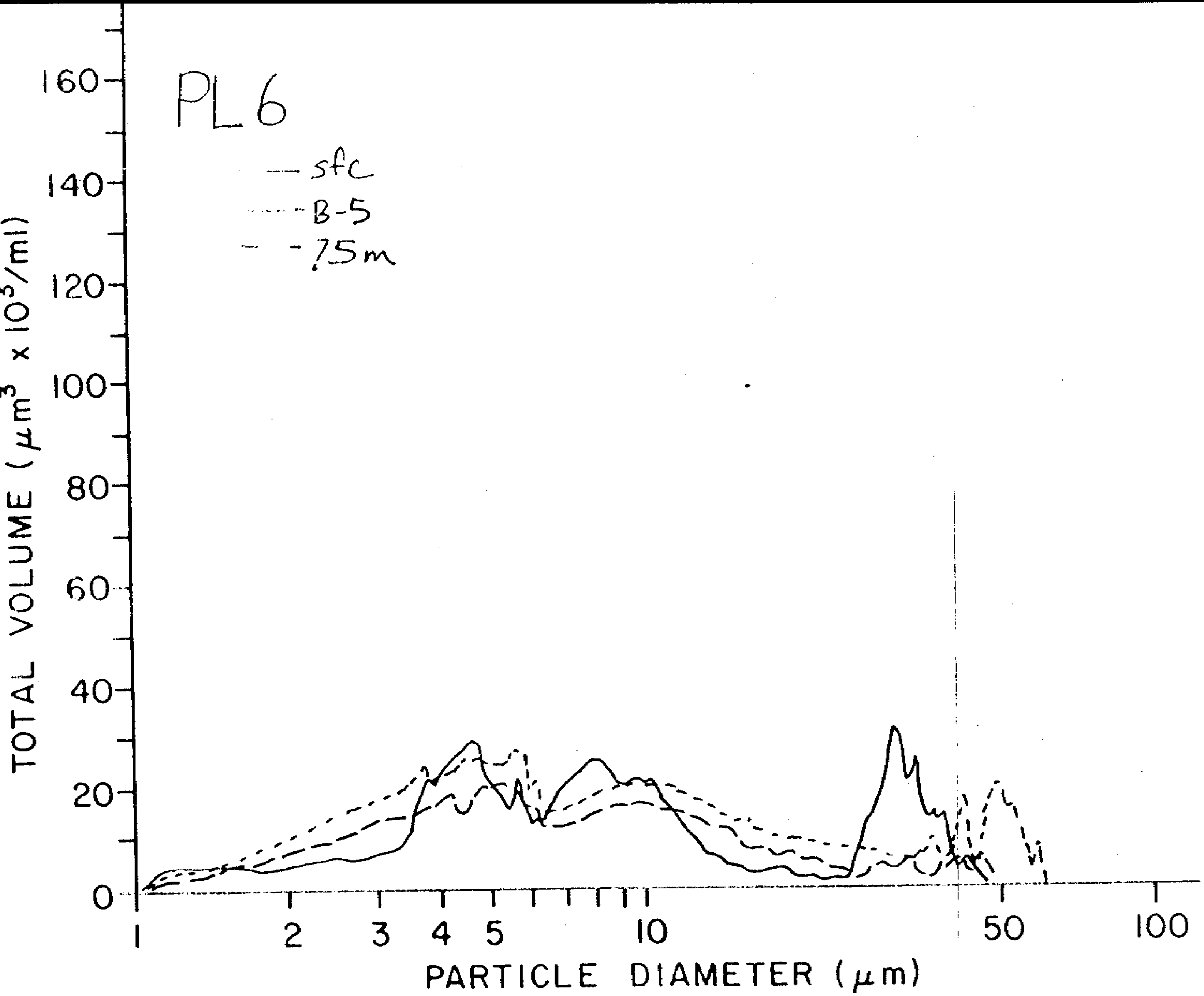

Figure 14. Particle size distributions form three depths at PL6 (outer domain).

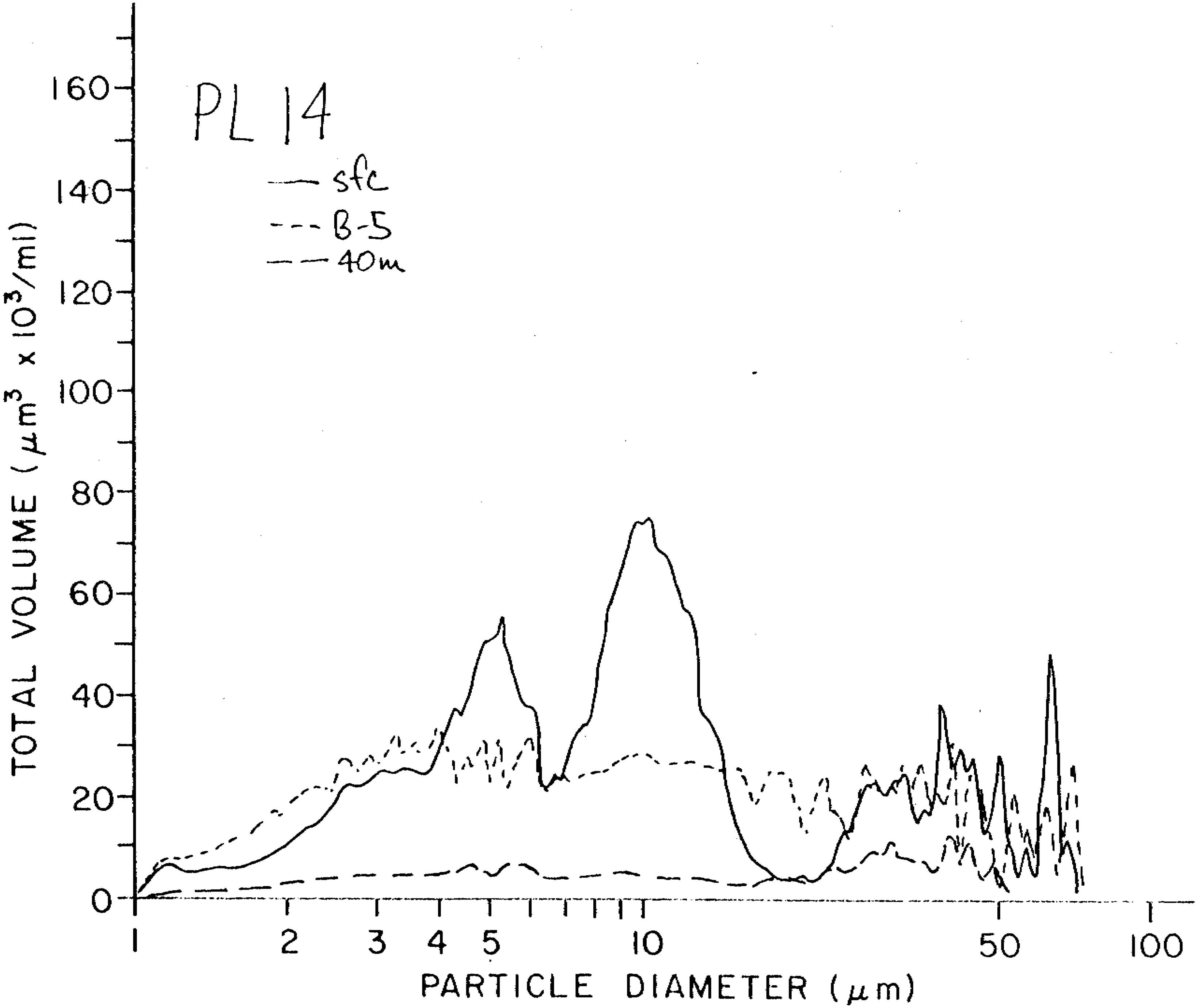

Figure 16. Particle size distributions from three depths at PL14 (mid-shelf domain).

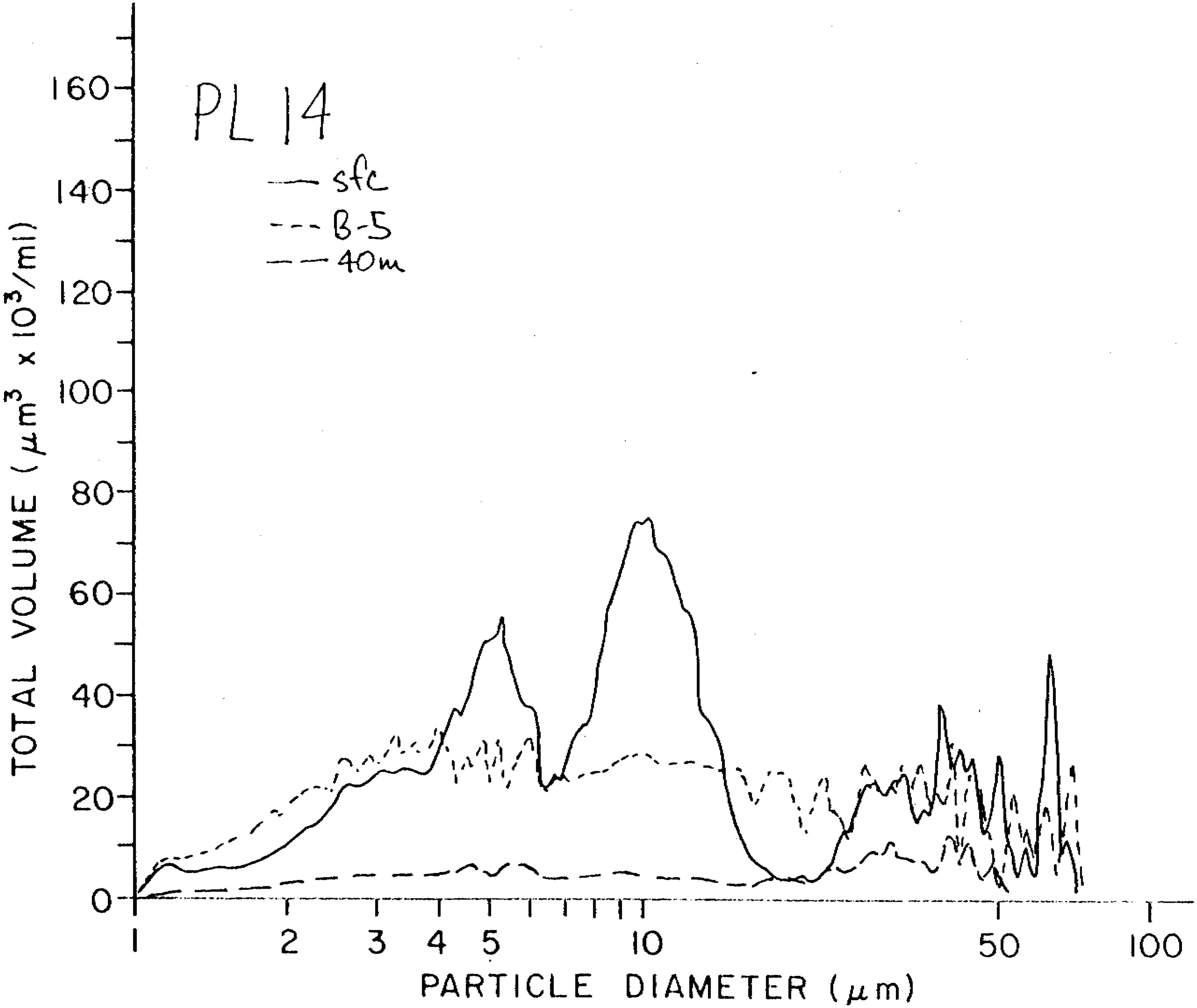

Figure 16. Particle size distributions from three depths at PL14 (mid-shelf domain).

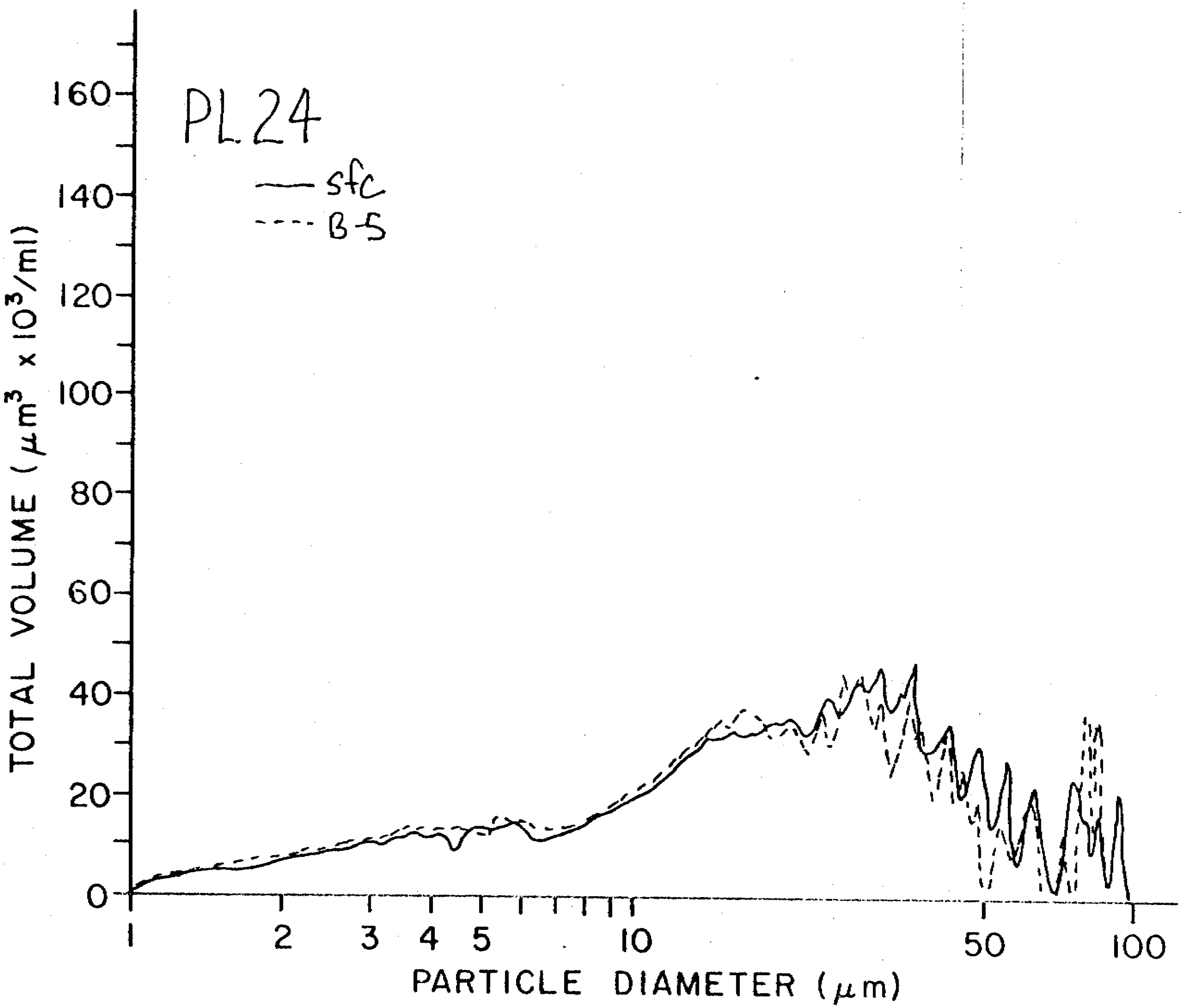

PL 24
sfc
B-5
TOTAL VOLUME (μm^3 x 10^3/ml)
160
140
120
100
80
60
40
20
0
1
2
3
4
5
10
50
100
PARTICLE DIAMETER (μm)

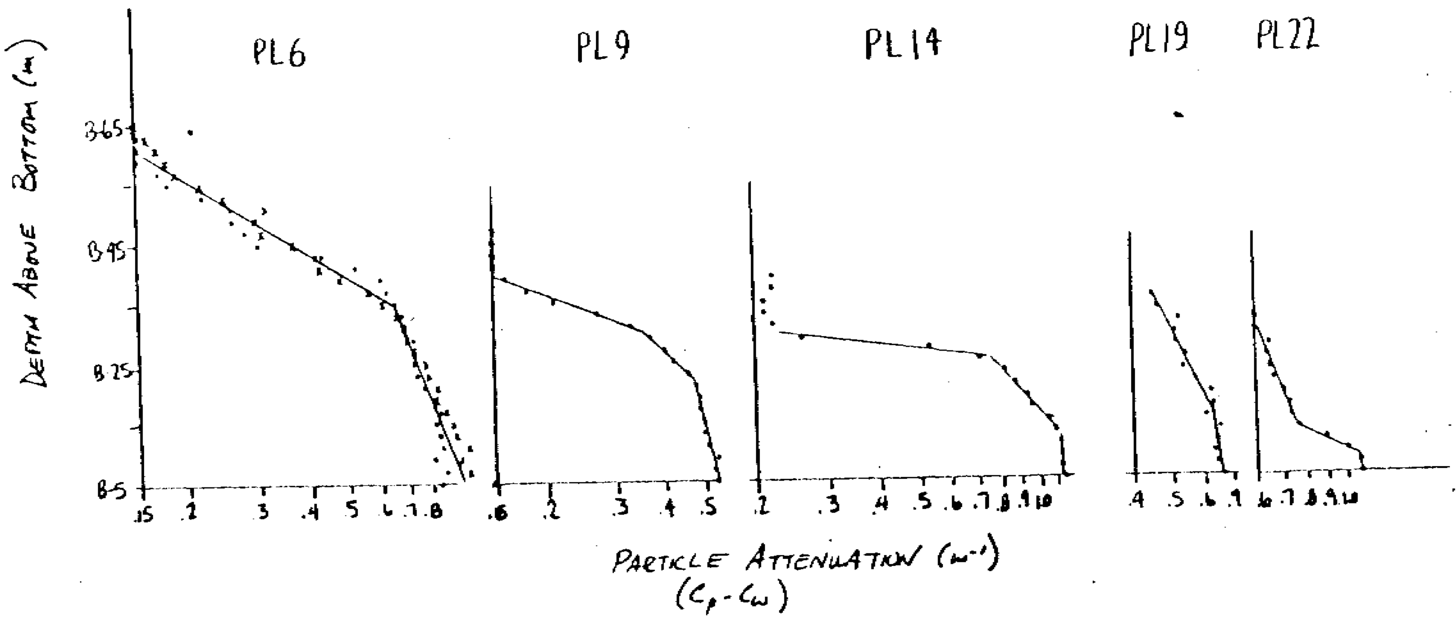

Figure 18. Semi-log plots of particle attenuation vs. distance above the bottom. Attenuation due to the water itself has been removed from these curves. PL6 was sampled twice, on August 29 (•) and September 3 (x). Straight lines have been fitted by eye for depth intervals where the slope (and presumably the eddy diffusion coefficient) is constant. K_z values for these intervals are given in Table 1.

TABLE I

Calculation of vertical eddy diffusion coefficients (K_z) from SPM profiles

$$\frac{K_z}{(\bar{w} - w_s)} = \frac{z - a}{\ln(Cz/Ca)} \quad \text{where} \quad w_s = \frac{2\, g r^2 (\rho s - \rho)}{9\,\eta}$$

STA	z	a	ln(Cz/Ca)	$K_z/(\bar{w} - w_s)$	K_z (cm^2/sec)			
	(m above bottom)				$\bar{w} = 0$, r = 5 μm, $(\rho s - \rho) = 1.5$	$\bar{w} = 0$, r = 5 μm, $(\rho s - \rho) = 0.15$	$\bar{w} = 10^{-3}$, r = 5 μm, $(\rho s - \rho) = 1.5$	$\bar{w} = 10^{-3}$, r = 5 μm, $(\rho s - \rho) = 0.15$
PL-6	35	5	-0.38	- 7905	14.8	1.5	6.9	0.7
	60	35	-1.47	- 1700	3.2	0.3	1.5	0.2
PL-9	22	5	-0.12	-14433	27.0	2.7	12.6	1.3
	32	22	-0.44	- 2287	4.3	0.4	2.0	0.2
	40	32	-0.73	- 1102	2.1	0.2	1.0	0.1
PL-14	12	5	-0.01	-74549	139.4	13.0	64.9	6.5
	24	12	-0.31	- 3912	7.3	0.7	3.4	0.3
	31	24	-1.18	- 594	1.1	0.1	0.5	0.1
PL-19	17	5	-0.05	-25795	48.2 (193.5)*	4.8 (19.4)*	22.4 (167.7)*	2.2 (16.8)*
	35	17	-0.34	- 5350	10.0 (40.1)*	1.0 (4.0)*	4.6 (34.8)*	0.5 (3.5)*
PL-22	14	8	-.35	- 1707	3.2 (12.8)*	0.3 (1.3)*	1.5 (11.1)*	0.2 (1.1)*
	31	14	-0.24	- 7191	13.4 (53.9)*	1.3 (5.4)*	6.3 (46.7)*	0.6 (4.7)*

* Calculated for r = 10 μm.

Hydrographic, Suspended Particulate Matter, Wind and Current Observation During Reestablishment of a Structual Front: Bristol Bay, Alaska

by

C. A. Pearson

E. Baker

and

J.D. Schumacher

all at Pacific Marine Environmental Laboratory

3711 15th Ave. NE

Seattle, Washington 98105

prepared
for
Fall 1980 AGU

ABSTRACT

In summer a structural front located in the vicinity of the 50m isobath separates a well-mixed coastal domain from the two-layered middle shelf domain of the southeastern Bering Sea. This system was perturbed in mid-August by a strong storm (winds in excess of 30m sec^{-1}) which vertically mixed temperature, salinity and suspended particulate matter (SPM) throughout the water column. Using CTD and SPM data collected 1, 7, and 14 days after the storm, we document the subsequent reestablishment of frontal and domain characteristics. Prior to the second occupation of stations, a period of moderate (5 to 10 ms^{-1}) northeasterly winds appeared to drive an offshore Ekman flux, resulting in stratification across the entire study area with an SPM minimum at or near the maximum density gradient. By the third observational series, increasingly strong tides had reestablished the well-mixed coastal domain. These observations illustrate that distributions of both conservative and nonconservation properties of the water column are similarly governed by the balance between tidal stirring and buoyancy flux.

INTRODUCTION

The Bering Sea is the northernmost mediterranean sea of the North Pacific (Sayles, et al, 1979). The northeastern one-half of the sea is underlaid by a flat and shallow shelf (figure 1). The southeastern portion of this shelf supports one of the world's richest fisheries resource and potentially large quantities of petroleum. In order to make knowledgeable decisions regarding fate and impact of petroleum development, the Outer Continental Shelf Environmental Assessment Program (OCSEAP) had funded extensive field experiments since 1975 to describe the regional oceanography, and to understand important transport processes.

Physical oceanographic results from OCSEAP and Processes and Resources of the Bering Sea shelf (PROBES) e.g., Coachman and Charnell, 1977, 1979; Coachman, Kinder, Schumacher and Tripp, 1980; Kinder and Coachman, 1978; Kinder, Schumacher and Hansen, 1980; Kinder and Schumacher, 1981a and 1981b; Pearson, Mofjeld and Tripp, 1981; Reed, 1978; Schumacher, Kinder, Pashinski and Charnell, 1979 are summarized below in terms of features germane to the present study. During periods of positive bouyancy flux at the surface (ice melt and insolation), three distinct hydropraphic domains exist. These domains are separated by regions of enhanced horizontal temperature and salinity gradients - fronts - which are located in the vicinity of the 50 and 100m isobaths. A typical summer hydrographic cross-section (figure 2) clearly shows these features and the relation between vertical structure, depths, and domains. Herein we will focus on the mixed coastal and two-layered middle shelf domains located adjacent to the Alaska Peninsula. We note that there are no major sources of fresh water along the peninsula, and the amount of ice cover along the Peninsula is highly variable year to year.

The most common forcing mechanisms for coastal circulation are tides and winds, however, recent studies (Beardsley and Winant, 1980; Csanady, 1978) suggest that interactions between oceanic circulation and the shelf may also be important. For the southeastern Bering Sea shelf, Kinder and Schumacher (1981b) have summarized current data (figure 3) and note that tides dominate the horizontal kinetic energy (HKE). Tides are thought to be responsible for the cross-shelf flux of salt required to maintain the observed mean salt balance; over most of this shelf, tidal diffusion appears to be the dominant transport mechanism (Coachman <u>et al</u>, 1980). There is little or no evidence that weakly organized oceanic circulation (the Bering Slope Current) results in advection on the shelf proper (Kinder, Schumacher and Hansen, 1980). Further, the vast size of this shelf makes it unlikely that any oceanic/outer shelf eddies could propogate into the middle shelf or coastal domains. In these latter areas tides account for ≧90% of the HKE and current spectra indicate only a small fraction (≦10%) of the HKE lies in the periods (2 to 10 days) associated with meteorlogical forcing (Kinder and Schumacher, 1981b). While winds may not be important over long time scales (0 months), they provide (via wind stress and wave generation) energy to typically generate a 20 to 30-m mixed upper layer and aperiodic eastward travelling storms can result in significant pulses of advection and vertical mixing. During August, however, winds are generally weak, 40% of wind speeds are ≦5 m/sec with monthly vector mean winds ≦2.5 m/sec toward the northeast (Brower, et al, 1977).

The purpose of this preliminary note is to present hydrographic, suspended particular matter, (SPM) wind and current data collected along the Alaska Peninsula (figure 4) during a 14-day period in August 1980. These data show that a storm significantly altered mean hydrographic conditions, stirring middle shelf domain waters throughout the water column and thus had a profound impact on vertical transport. Further, Ekman fluxes (coastal divergence and convergence) appear to play an important role in reestablishment of stratification and together with enhanced tidal mixing (using the mean of the speed cubed as a measure of mixing energy) resulted in a return to mean conditions within 14 days.

DATA ACQUISITION AND PROCESSING

Hydrographic data were collected using Plessey model 9040 system with model 8400 data logger. This system sampled five times per second for values of temperature, conductivity, and pressure. Data were recorded only during the down-cast using a lowering rate of 30 m/min. Nansen bottle samples were taken at most stations to provide temperature and salinity calibration. The correction factors for these data were S = -0.04 g kg^{-1} and T = -0.01°C.

Data from monotonically increasing depth were "despiked" to eliminate excessive values and were averaged over 1-m intervals to produce temperature and salinity values from which density was computed.

Seven Neil Brown vector averaging acoustic current meters (ACM) were suspended beneath a surface float, at depths of 5, 10, 15, 20, 29, 39, and 50 meters, in water depth of 65 meters. Here we present results from the 5 and 39 meter depths. The ACM's emit continuous high frequency acoustic signals which are phase advanced or delayed as they travel with or against the current. The relative phase is converted to a voltage which is directly proportional to the water velocity. Currents are measured along two right angle horizontal paths. At a pre-determined interval, in this case one minute, the component velocities are averaged and recorded. Ten minute segments of the original one minute sample interval data were averaged. These data were then low-pass filtered (half amplitude at a period of 2.9 hours) and a second order polynomial was used to interpolate to whole hours. A Munk-Cartwright response tide analysis was then performed on the data, and a predicted tide series was subtracted from the original series. Finally, a 25 hour running mean was applied to the detided series, and the meaned series was resampled at a six hour interval.

Winds were recorded at 1 hour intervals onboard the NOAA ship SURVEYOR. The wind sensor is located about 20 m above the sea surface. During the first five days, the ship was operating within about 75 km of mooring TP3. After this time, the ship operated from inner Bristol Bay to the Pribilof Islands.

SPM measurements, given in terms of light attenuation coefficient, were made with a continuously recording 0.25 m beam transmissometer inter-faced to the CTD. The light source was a light emitting diode with a wavelength of 660 μm. This wavelength eliminates attenuation problems due to dissolved humic acids. Accuracy and stability are sufficient to provide data with an error less than 0.5% of true light attenuation.

RESULTS

Hydrography and Light Attenuation The line of CTD stations normal to the peninsula (figure 4) was occupied on 19, 24 and 31 August 1980. Temperature, salinity, sigma-t and light attenuation sections are shown in figures 5, 6 and 7. The time to run a complete line was about six hours. About one day prior to running the first section, the remanents of typhoon Marge passed eastward through the study area. This storm resulted in winds up to 30 ms^{-1} and 6 to 8 m waves. The turbulence associated with this storm mixed the water column at least 45 km seaward of the coast (figure 5). Suspended particulate matter was also well mixed within 10 km of the shore and seaward of station 45 isopleths exhibited weak monotonically increasing vertical gradients.

During the second occupation of this section (figure 6), the entire shelf region was thermally stratified, with surface minus bottom temperature difference (ΔT) from 0.6 to 2.7°C. Colder bottom waters intruded onshore, with a displacement of the 8.5°C-isotherm of about 10 km. A similar change of mixed to stratified structure was observed in isohalines with the strongest stratification (ΔS=0.13 g kg^{-1}) over the normally mixed coastal domain. Again, the data suggested an onshore flux, e.g. at station 42 bottom salinity increased by 0.05 gkg^{-1}, while upper layer salinities decreased. Light attenuation values indicated a 50% reduction in nearshore concentration of SPM, while over the middle shelf domain ($z \geqq 50$ m) a subsurface minimum layer was established.

Hydrographic conditions observed on 31 August (figure 7) showed a return to more typical stratification distributions (c.f. figure 2); middle shelf waters were stratified with $\Delta\sigma_t \geqq 0.43$ and coastal domain waters were vertically well mixed. We note that stratification was now stronger than that observed on May 31 (inset, figure 4) by about a factor of three. SPM profiles also indicated mixed conditions in the coastal domain and a minimum layer was clearly established near or below the pycnocline.

Winds and Currents Alongshore (v positive 60°T, see figure 4) winds are shown in Figure 8. The passage of the storm resulted in maximum alongshore wind speeds of about 25 ms^{-1}. About 3.5 days after the storm's peak speeds, a period of relatively steady alongshore winds existed for about 3 days with a mean speed of -5.5 ms^{-1}. We note that with the exception of the storm winds and those on 24 August, onshore wind speeds (not shown) were only about 1 ms^{-1}.

Currents at 5 and 39 m below the surface are shown in the next two panels of figure 8, where the alongshore axis is the same as for the wind and the onshore axis is u positive 150°T. Near-surface currents reversed from onshore to offshore concomittant with the wind reversal and this initial offshore pulse lasted for about 3 days. While near surface currents were offshore those at 39 m were onshore for the same time period. The visual correlation between wind and near-surface current did not extend to currents at 39 m depth. The along-shore current appeared to be similar at the two depths.

In the bottom panel of figure 8 we present 25-hr average $\overline{s^3}$ values. The flux of turbulent energy generated at the sea floor, E_t, was estimated by assuming that the mean rate of work of tidal currents against bottom stress ($\tau=\rho_o C_o u|u|$) is $\overline{\tau \cdot u}$ where u is the mean flow velocity near the bottom (Fearnhead, 1975). Here we have used hourly values of current speed from the 39 m depth current record, and have not included either a drag coefficient or density (including these parameters yields dimensions of tidal power but $\overline{s^3}$ gives a relative measure of this quantity). By the third occupation of the CTD section, tidal mixing power had increased by about a factor of three.

DISCUSSION AND SUMMARY

The destruction and subsequent reestablishment of typical summer middle shelf and coastal domain hydrographic features was related to winds and tides. The initial vertical mixing of the water column resulted from a combination of wind-wave and current shear turbulence which destroyed vertical structure at least 40 km, or twice the usual distance, from the shore. Longshore winds then reversed and generated an offshore Ekman flux in the near surface waters and a continuity preserving onshore flux at depth. The offshore flux brought warmer less saline surface water offshore, while the onshore flux at depth provided colder more saline waters; these resulted in stratification across the entire study area. As tidal mixing power increased, coastal domain waters became vertically mixed and middle shelf domain waters returned to a two-layered configuration.

Near-surface current spectra (not shown) indicated that of the total fluctuating horizontal kinetic energy ($KE_c'=\frac{1}{2}[u'^2+v'^2]^{\frac{1}{2}}$) per unit mass, subtidal energy was 16 $cm^2\ s^{-2}$ or about 4%. This is consistent with previous studies (Kinder and Schumacher, 1981b). We note that 50% of the subtidal HKE was contained in the 2 to 5 day period bands. The wind spectrum contained little energy (1.3 $m^2\ s^{-2}$ or about 10% of the total KE_ω') at tidal or higher frequencies, however, 25% of the KE_ω' was contained in 2 to 5 day periods with the remainder at periods ≧7 days.

The visual correlation between longshore winds and onshore currents, suggesting Ekman dynamics, was substantiated by a linear correlation coefficient between the two low-pass filtered time-series of r=0.83 at 0 lag. In frequency, the maximum coherence between hourly wind and current components was at a period of 2.9 days with a coherence squared of 0.995 or about 99% of the variance. A second maximum occurred at 4.8 days with a coherence squared of

0.91 (for both estimates the 95% level of significance was 0.78). Onshore currents and alongshelf winds were correlated to a lesser extent at lower depths, with correlations decreasing (0.57, 0.53, and 0.42) and lags increasing (0, 6 and 60 hours) at 10, 15 and 29 m respectively. The current record from 39m depth had a negative correlation ($r = -0.68$ at 48 hours) with alongshore winds. These results suggest that longshore winds generated off/onshore Ekman fluxes in an upper layer with, at times (e.g. 21 to 24 August), a compensating flow lower in the water column. During this particular event, coastal divergence would result in a barotropic pressure gradient toward shore. If this were geostrophically balanced, then an alongshore current (in this reference frame a negative value) would be generated. The observations indicated such flow during both 21 to 24 August and 30 August to 1 September wind events.

An emperical estimate of 5 m onshore current response to alongshore wind was 10^{-2} to 1, or a 10 ms^{-1} wind generated a 10 cm s^{-1} current. Theoretically, we can employ the shallow sea model developed by Csanady (1980) which assumes a semi-infinite ocean bounded by a straight coastline, constant water depth $H=h+h'$, where h is a slightly less dense upper layer and the wind begins at time $t=0$, exerting a stress $\tau_0=\rho F$ at the water surface, directed parallel to the coast, constant in space and in time $t>0$ but $t<$ inertial period. Non-linear accelerations and frictional stress are neglected (thus the upper limit on t). The full solution contains some inertial oscillations and an aperiodic part describing a "coastal jet" structure near shore and Ekman drift offshore. Csandy's results indicate two fields germane to our study area; near shore, or within one internal radius of deformation and intermediate, or that shelf region lying between the internal and surface or barotropic radius of deformation. Carefully selecting a time period when stratification holds over the coastal domain (23 August) and wind stress was quasi-steady at ~1.4 dyne c^{-2} for about 12 hours, we solve the following equations:

I. Near-shore ($x \leqq 6$ km):

$$v = \frac{Ft}{h}$$

$$v' = 0 \tag{1}$$

II. Intermediate field (200 km$\geqq x \geqq$6 km)

$$u = \frac{F}{f(h+h')}\frac{h'}{h}$$

$$u' = \frac{-F}{f(h+h')} \tag{2}$$

$$v = \frac{Ft}{h+h'} = v' \tag{3}$$

where:

$$F = \tau/\rho = -1.4\ c^2s^{-2}$$

$$h' = 4\text{x}10^3c$$

$$h = 2\text{x}10^3c$$

$$t = 4.3 \times 10^4\ s$$

$$f = 10^{-4}s$$

the prime indicates lower layer and v is alongshore and u is onshore as previously defined. Using the observed values, the following values were calculated:

TABLE 1

Comparison between Csanady's model and observations on the north Aleutian shelf

	Model	Observed	
near-shore	$v = -30.0\ cs^{-1}$	*	
intermediate-field	$u = -5.0\ cs^{-1}$	$-10.0\ cs^{-1}$	
	$u' = +2.5\ cs^{-1}$	$2.5\ cs^{-1}$	
	$v=v' = -10.0\ cs^{-1}$	$-\ 5.0\ cs^{-1}$	(upper layer)
		- 2.5 cs-1	(lower layer)

* Current meters presently in the water may allow a comparison with near-shore model velocity.

The agreement between model and observed values was good, considering that winds were not steady state, the model yields an integrated upper and lower layer velocity rather than a measurement at one specific depth, and that the "bottom layer" observed currents were obtained 25 m above the seafloor.

In summary, preliminary analysis of wind, current, hydrographic and SPM data suggest the following:

1) Storms radically alter mean hydrographic domains. The enhanced turbulence vertically mixed middle shelf water and increased SPM concentrations. These two factors could dominate vertical transport of oil, resulting in greater concentrations on the bottom in a shorter time than detrital rain.

2) Although tides dominate HKE, in the vicinity of coastal boundaries Ekman fluxes are important to transport and water mass distributions.

3) The effectiveness of tidal mixing power was evident between 24 and 31 August. During this period, tidally generated turbulence reduced vertical stratification from 0.20 and 0.31 sigma-t units to zero.

4) It appears that the dynamics of coastal flow may adhere to physics in Csanady's (1980) model. Bottom pressure, current and wind measurements presently underway will help elucidate alongshore and cross-shelf pressure and velocity fields, provide improved wind measurements, and allow further comparisons with models of coastal dynamics.

ACKNOWLEDGEMENTS

We thank all those who assisted in data collection, processing, manuscript preparation and lent moral support, in particular: the compliment of the NOAA SHIP SURVEYOR, Dave Pashinski, Lynn Long, Dave Katchel, Joy Golly, Gini May, Phyllis Hutchens and Glenn Cannon. This study was supported in part by the Bureau of Land Management through an interagency agreement with the National Oceanic and Atmospheric Administration, under which a multi-year program responding to needs of petroleum development of the Alaskan continental shelf is managed by the Outer Continental Shelf Environmental Assessment Program (OCSEAP) office, Juneau.

REFERENCES

Beardsley, R.C. and C.D. Winant, 1979. Mean circulation in the mid-Atlantic bight. JPO, 9(3): G12-619.

Brower, W.A., H.F. Diaz, A.S. Prechtel, H. Searby and J.L. Wise, 1977. Climatic atlas of the outer continental shelf waters and coastal regions of Alaska. Vol II NOAA/OCSEAP. Final Report (RU 347): 443 pp.

Coachman, L.K. and R.L. Charnell, 1977. Finestructure in outer Bristol Bay, Alaska. Deep-Sea Res., 24(10): 809-889.

Coachman, L.K. and R.L. Charnell, 1979. Lateral water mass interactions-a case study, Bristol Bay, Alaska. JPO, 9(2): 278-287.

Coachman, L.K., T.H. Kinder, J.D. Schumacher and R.B. Tripp, 1980. Frontal systems of the southeastern Bering Sea shelf. In Stratified Flow, 2nd Int. Assoc. Hydraulic Res. Symposium, Trondheim, June 1980, T. Carstens and T. McChmans Eds., TAPIR Publishers, Norway.

Csanady, G.T., 1978. The arrested topographic wave. JPO 8(1): 47-62.

Csanady, G.T., 1980. The coastal jet conceptual model in the dynamics of shallow seas. In the Sea, Vol 6: 117-144.

Fearhead, P.G. On the formation of fronts by tidal mixing around the British Isles. Deep-Sea Res., 22(5): 311-322.

Kinder, T.H. and L.K. Coachman, 1978. The front overlaying the continental slope of the eastern Bering Sea. J. Gophy. Res. 83: 4551-4550.

Kinder, T.H., J.D. Schumacher and D.V. Hansen, 1980. Observation of a baroclinic eddy: an example of mesoscale variability in the Bering Sea. JPO, 10(8): 1228-1245.

Kinder, T.H. and J.D. Schumacher, 1981a. Hydrographic structure over the continental shelf of the southeastern Bering Sea. In The Bering Sea: Oceanography and Resources, D. W. Hood, Editor, in press.

Kinder, T.H. and J.D. Schumacher, 1981b. Circulation over the continental shelf of the southeastern Bering Sea. In the Bering Sea: Oceanography and Resources, D. W. Hood, Editor, in press.

Pearson, C.A., H. Mofjeld and R.B. Tripp, 1981. Tides of the eastern Bering Sea shelf. In The Bering Sea: Oceanography and Resources, D. W. Hood, Editor in press.

Reed, R.K., 1978. Heat budget in the eastern Bering Sea. J. Geophys. Res. 83: 5613-5619.

Sayles, M.A., K. Aagard and L.K. Coachman, 1979. Oceanographic Atlas of the Bering Sea basin. Univ. Washington Press, Seattle: 158 pp.

Schumacher, J.D., T.H. Kinder, D.J. Pashinski and R.L. Charnell, 1979. A structural front over the continental shelf of the eastern Bering Sea. JPO, 9(1): 79-87.

Wu, J., 1969. Windstress and surface roughness at the air-sea interface. J. Geophys. Res., 74(2): 444-445.

Wynant, C.D., 1980. Coastal circulation and wind-induced currents. In Annual Reviews of Fluid Mechanics, Vol 12: 271-302.

FIGURE LEGENDS

Figure 1. The Bering Sea. The line extending from Bristol Bay (off Cape Costantine) to the shelf break indicates location of hydrographic features on figure 2. Depths are in meters.

Figure 2. Hydrographic characteristics of southeast Bering Sea shelf waters during typical summer conditions.

Figure 3. Spatial configurations of hydrographic domains. Also shown are net current vectors (from Kinder and Schumacher, 1981b).

Figure 4. North Aleutian Shelf study area, showing location of hydrographic data section (NA41 to NA46) and mooring TP3. Also shown are CTD data from 31 May 1980 and axes used for current and wind data.

Figure 5. Hyrographic and light attenuation sections from 19 August 1980. Note the location of the 8.5°C isotherm.

Figure 6. Hydrographic and light attenuation sections from 24 August 1980. Contour intervals are 0.5°C, 0.25 gm kg^{-1}, 0.25 σ_t units and 0.2 m^{-1} for light attenuation. Magnitude of upper minus lowest 1m average parameter is presented under a given station as a Δ. Note, lowest 1m average salinity at station 42 was 31.71 gm kg^{-1}.

Figure 7. Hydrographic and light attenuation sections from 31 August 1980.

Figure 8. a) Alongshore windspeed, b) onshore current at 5 and 39m, c) alongshore current at 5 and 39m and d) 25-hr. average tidal mixing parameter $\overline{s^3}$ from the 39m depth current record.

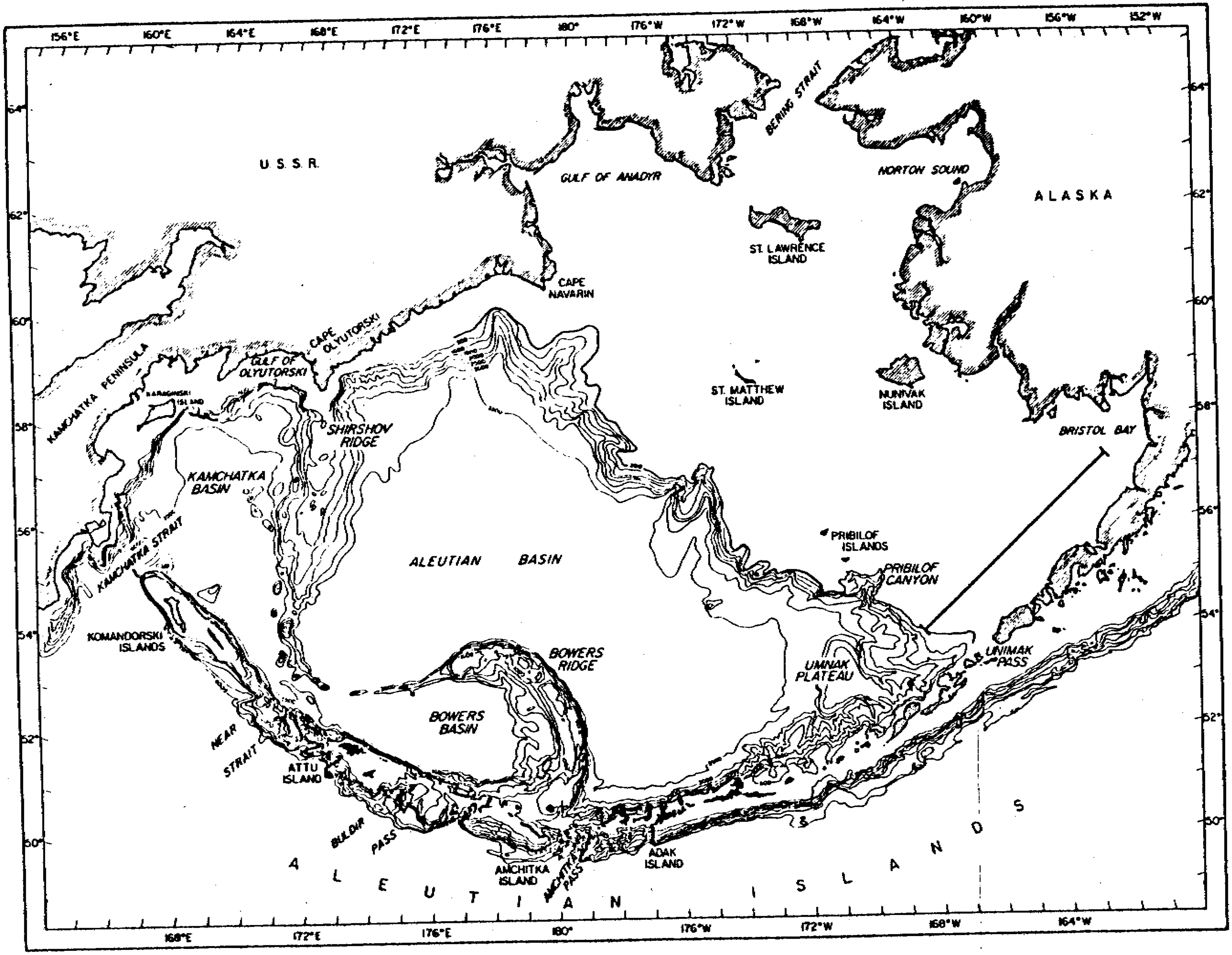
U.S.S.R.
ALASKA
GULF OF ANADYR
BERING STRAIT
NORTON SOUND
ST. LAWRENCE ISLAND
CAPE NAVARIN
CAPE OLYUTORSKI
GULF OF OLYUTORSKI
KAMCHATKA PENINSULA
KARAGINSKI ISLAND
SHIRSHOV RIDGE
KAMCHATKA BASIN
KAMCHATKA STRAIT
ST. MATTHEW ISLAND
NUNIVAK ISLAND
BRISTOL BAY
PRIBILOF ISLANDS
PRIBILOF CANYON
ALEUTIAN BASIN
KOMANDORSKI ISLANDS
BOWERS RIDGE
BOWERS BASIN
UMNAK PLATEAU
UNIMAK PASS
NEAR STRAIT
ATTU ISLAND
BULDIR PASS
AMCHITKA ISLAND
AMCHITKA PASS
ADAK ISLAND
ALEUTIAN ISLANDS
156°E
160°E
164°E
168°E
172°E
176°E
180°
176°W
172°W
168°W
164°W
160°W
156°W
152°W
64°
62°
60°
58°
56°
54°
52°
50°

FIGURE 1

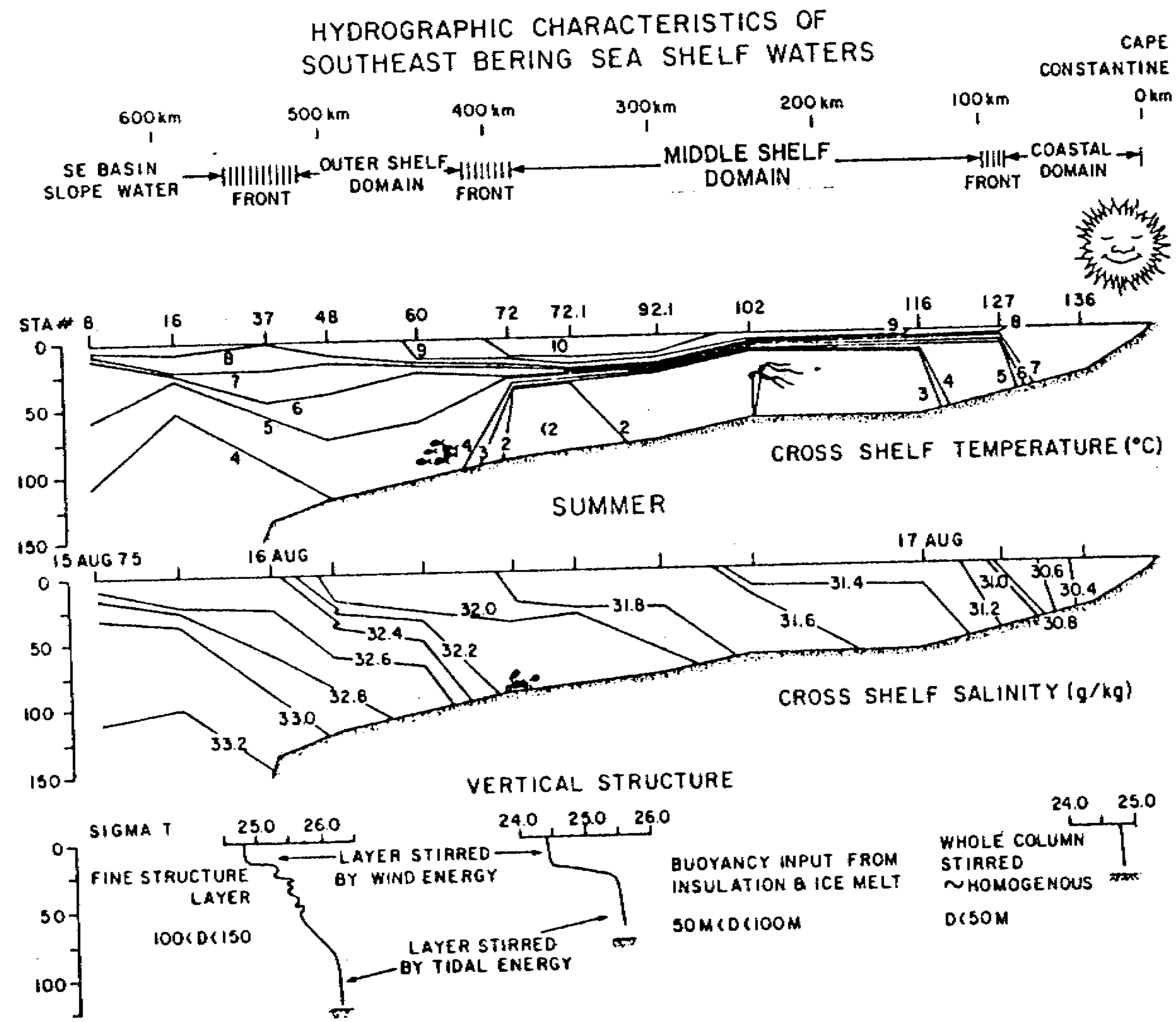
HYDROGRAPHIC CHARACTERISTICS OF
SOUTHEAST BERING SEA SHELF WATERS
CAPE
CONSTANTINE
600km
500km
400km
300km
200km
100km
0km
SE BASIN
SLOPE WATER
FRONT
OUTER SHELF
DOMAIN
FRONT
MIDDLE SHELF
DOMAIN
FRONT
COASTAL
DOMAIN
STA# 8
16
37
48
60
72
72.1
92.1
102
116
127
136
CROSS SHELF TEMPERATURE (°C)
SUMMER
15 AUG 75
16 AUG
17 AUG
32.0
31.8
31.4
31.6
32.4
32.6
32.2
32.8
33.0
33.2
31.0
30.6
30.4
31.2
30.8
CROSS SHELF SALINITY (g/kg)
VERTICAL STRUCTURE
SIGMA T
25.0
26.0
24.0
FINE STRUCTURE
LAYER
100<D<150
LAYER STIRRED
BY WIND ENERGY
LAYER STIRRED
BY TIDAL ENERGY
BUOYANCY INPUT FROM
INSULATION & ICE MELT
50M<D<100M
WHOLE COLUMN
STIRRED
~HOMOGENOUS
D<50M

FIGURE 2.

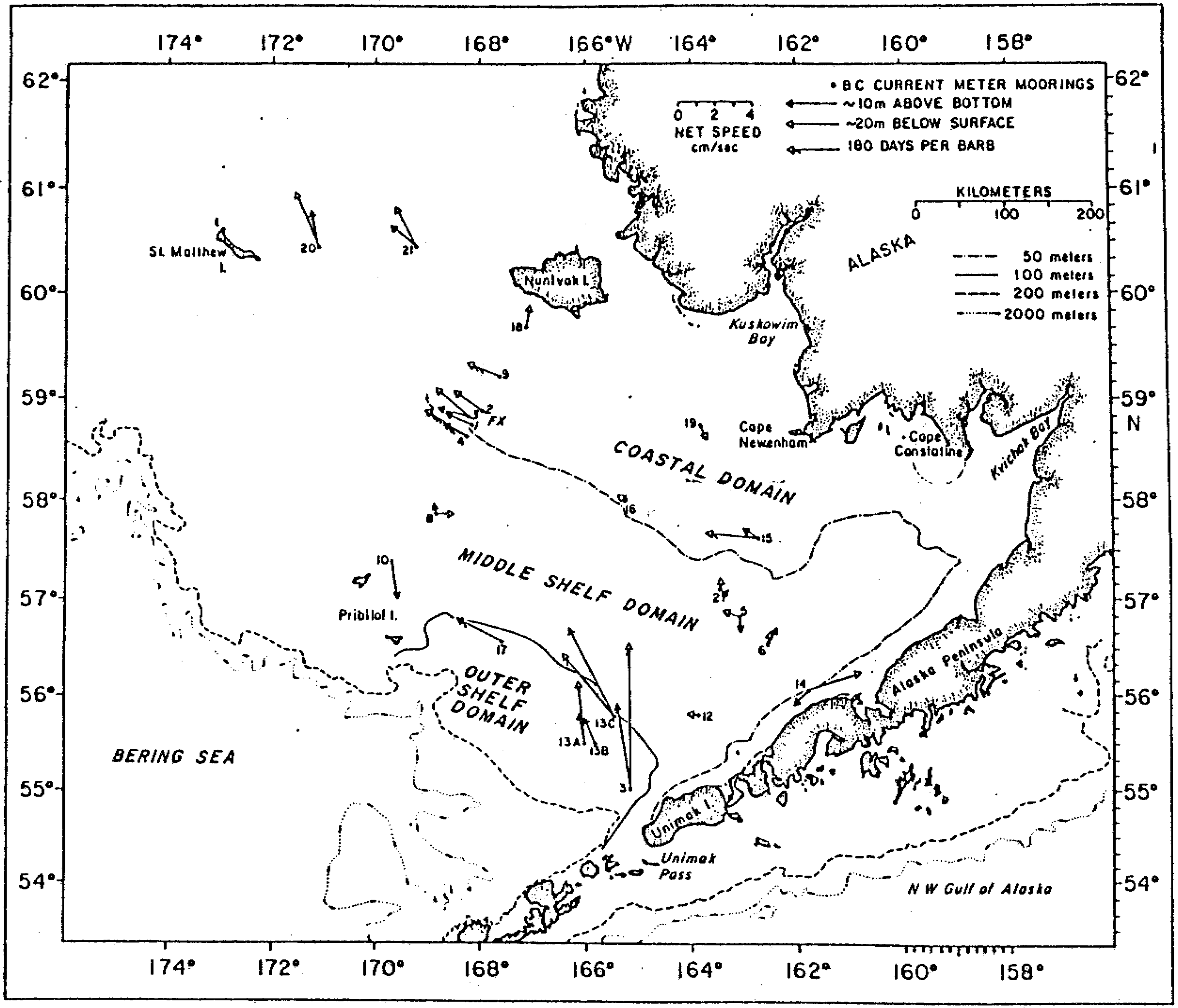

174°
172°
170°
168°
166°W
164°
162°
160°
158°
62°
61°
60°
59°
58°
57°
56°
55°
54°
N
• BC CURRENT METER MOORINGS
~10m ABOVE BOTTOM
~20m BELOW SURFACE
180 DAYS PER BARB
0 2 4
NET SPEED
cm/sec
KILOMETERS
0 100 200
50 meters
100 meters
200 meters
2000 meters
ALASKA
St. Matthew I.
Nunivak I.
Kuskowim Bay
Cape Newenham
Cape Constatine
Kvichak Bay
COASTAL DOMAIN
MIDDLE SHELF DOMAIN
OUTER SHELF DOMAIN
Pribilof I.
Alaska Peninsula
Unimak I.
Unimak Pass
BERING SEA
N W Gulf of Alaska
FX
20
21
18
9
2
4
19
16
8
15
10
17
6
14
12
13A
13B
13C
3
174°
172°
170°
168°
166°
164°
162°
160°
158°

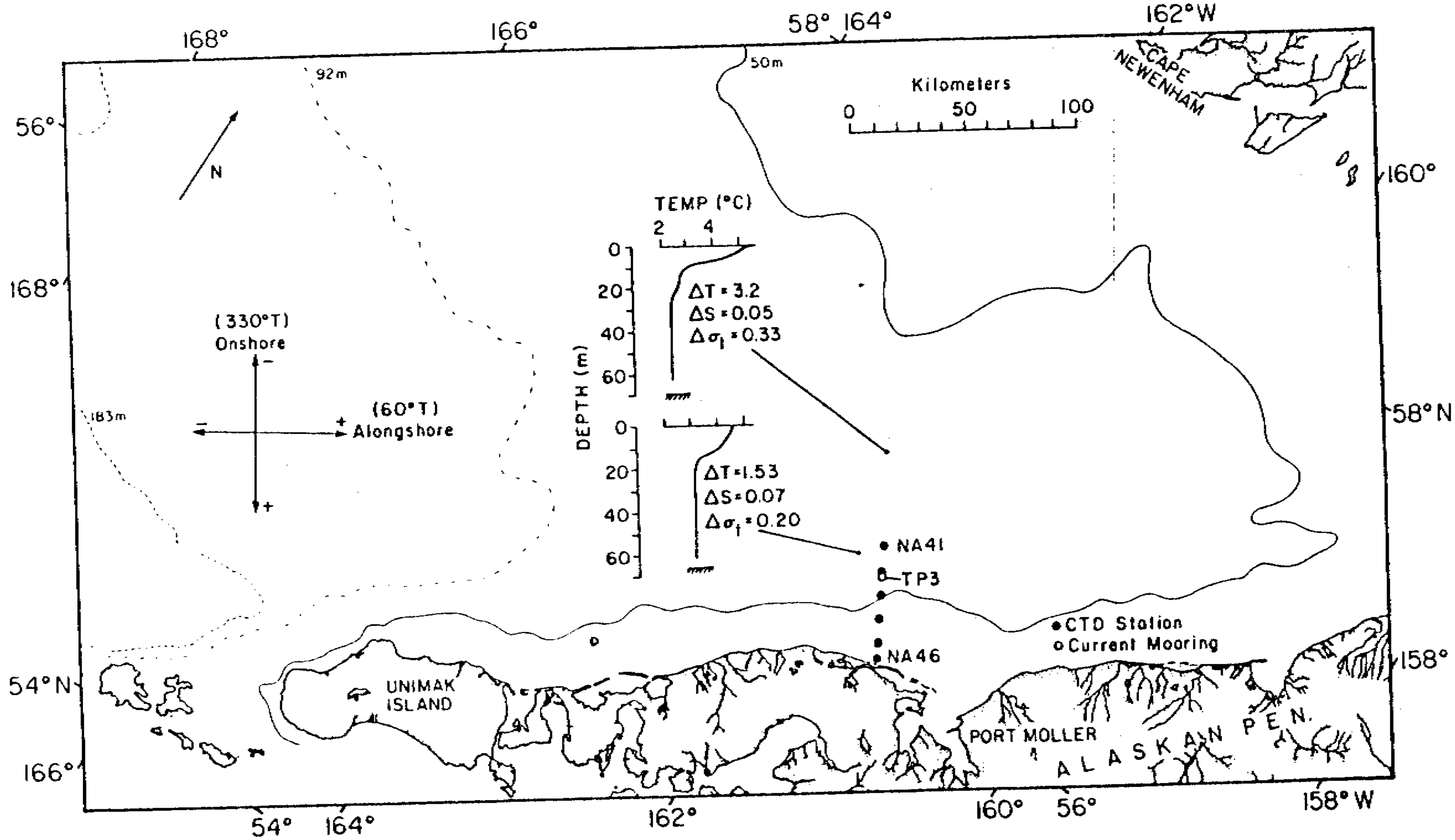

168°
166°
58° 164°
162°W
CAPE NEWENHAM
Kilometers
0 50 100
56°
160°
N
92m
50m
TEMP (°C)
2 4
DEPTH (m)
0
20
40
60
ΔT = 3.2
ΔS = 0.05
Δσt = 0.33
ΔT = 1.53
ΔS = 0.07
Δσt = 0.20
168°
(330°T)
Onshore
(60°T)
Alongshore
183m
58°N
NA41
TP3
NA46
• CTD Station
o Current Mooring
158°
54°N
UNIMAK ISLAND
PORT MOLLER
ALASKAN PEN.
166°
54° 164°
162°
160° 56°
158°W

FIGURE 4.

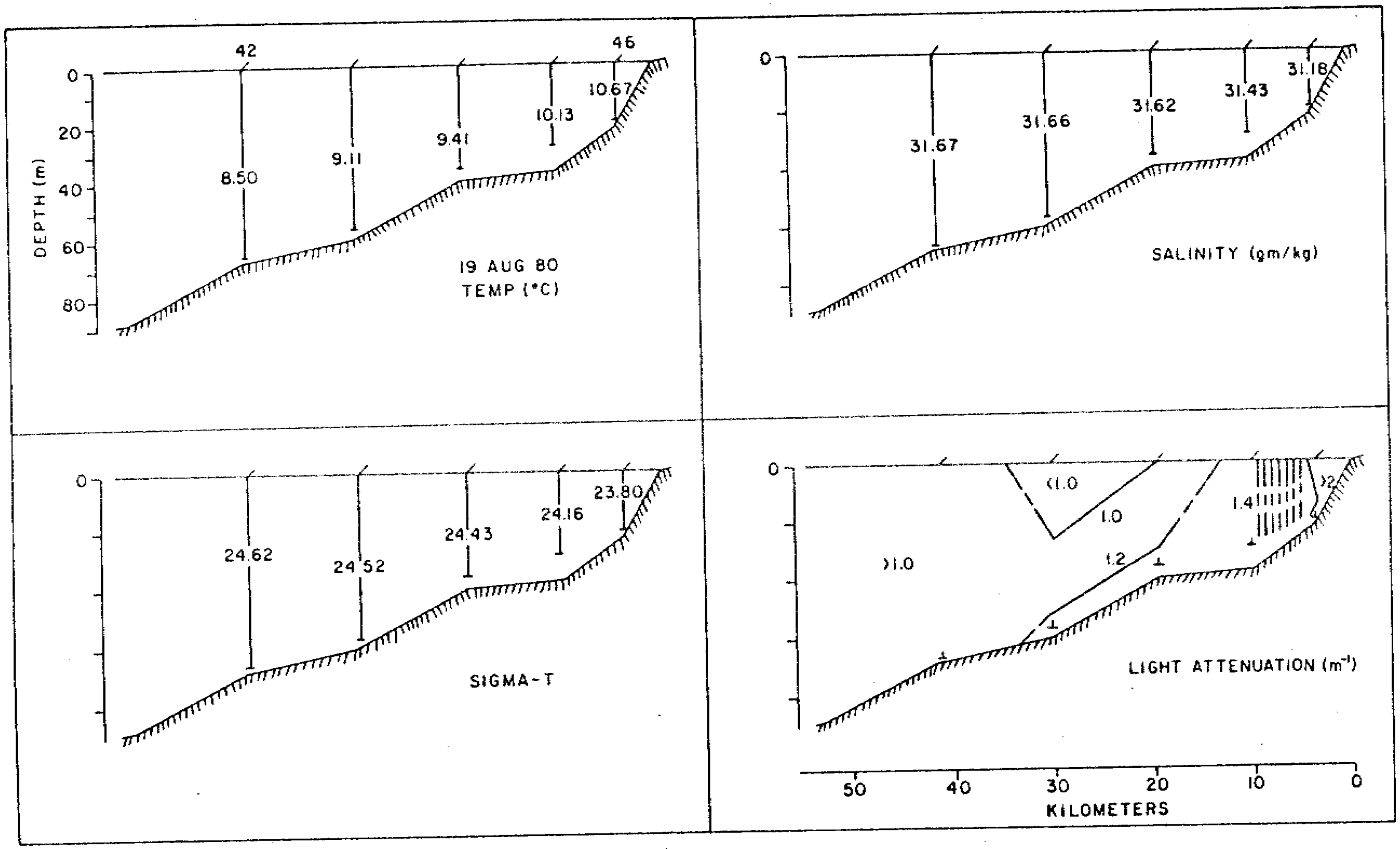

DEPTH (m)
0
20
40
60
80
42
46
8.50
9.11
9.41
10.13
10.67
19 AUG 80
TEMP (°C)
31.67
31.66
31.62
31.43
31.18
SALINITY (gm/kg)
24.62
24.52
24.43
24.16
23.80
SIGMA-T
(1.0
1.0
1.2
1.4
)2
)1.0
LIGHT ATTENUATION (m⁻¹)
50
40
30
20
10
0
KILOMETERS

FIGURE 5.

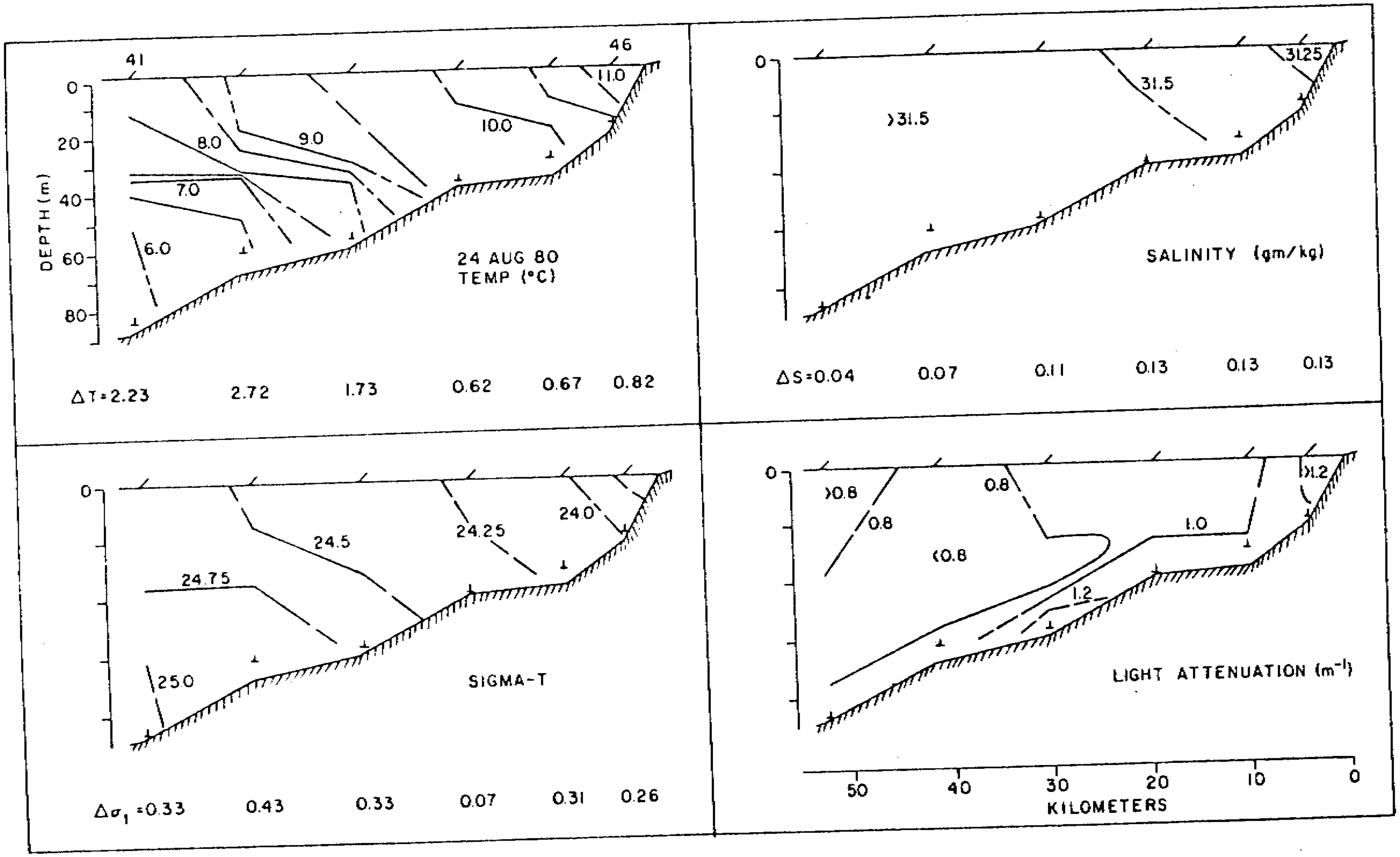

41
46
11.0
10.0
9.0
8.0
7.0
6.0
DEPTH (m)
0
20
40
60
80
24 AUG 80
TEMP (°C)
ΔT=2.23
2.72
1.73
0.62
0.67
0.82
31.25
31.5
>31.5
SALINITY (gm/kg)
ΔS=0.04
0.07
0.11
0.13
0.13
0.13
24.0
24.25
24.5
24.75
25.0
SIGMA-T
Δσ1=0.33
0.43
0.33
0.07
0.31
0.26
>0.8
0.8
0.8
<0.8
1.0
>1.2
1.2
LIGHT ATTENUATION (m⁻¹)
50
40
30
20
10
0
KILOMETERS

FIGURE 6.

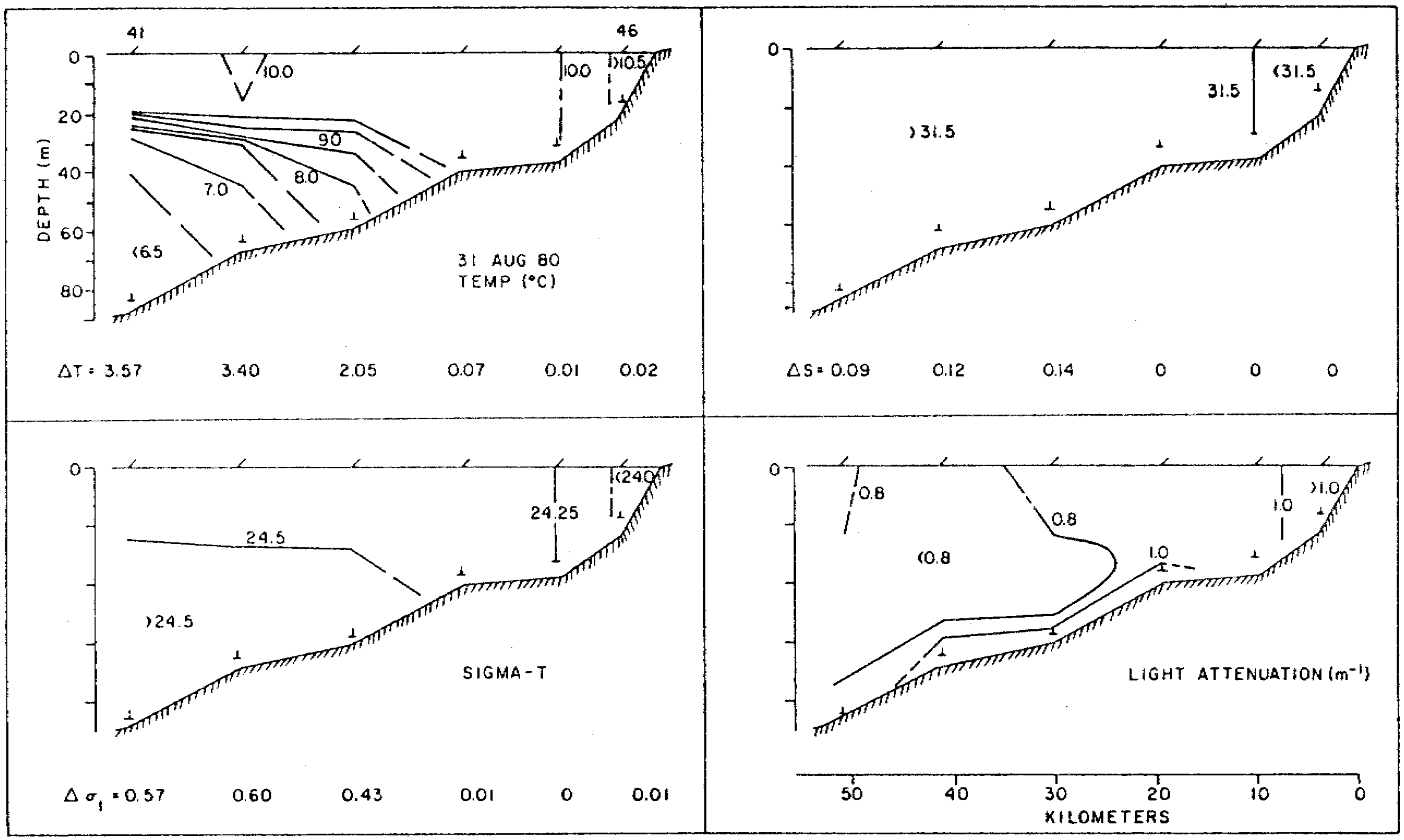

41
46
DEPTH (m)
0
20
40
60
80
10.0
10.0
)10.5
9.0
8.0
7.0
(6.5
31 AUG 80
TEMP (°C)
ΔT = 3.57
3.40
2.05
0.07
0.01
0.02
(31.5
31.5
)31.5
ΔS = 0.09
0.12
0.14
0
0
0
(24.0
24.25
24.5
)24.5
SIGMA-T
Δσt = 0.57
0.60
0.43
0.01
0
0.01
0.8
0.8
(0.8
1.0
1.0
)1.0
LIGHT ATTENUATION (m⁻¹)
50
40
30
20
10
0
KILOMETERS

FIGURE 7.

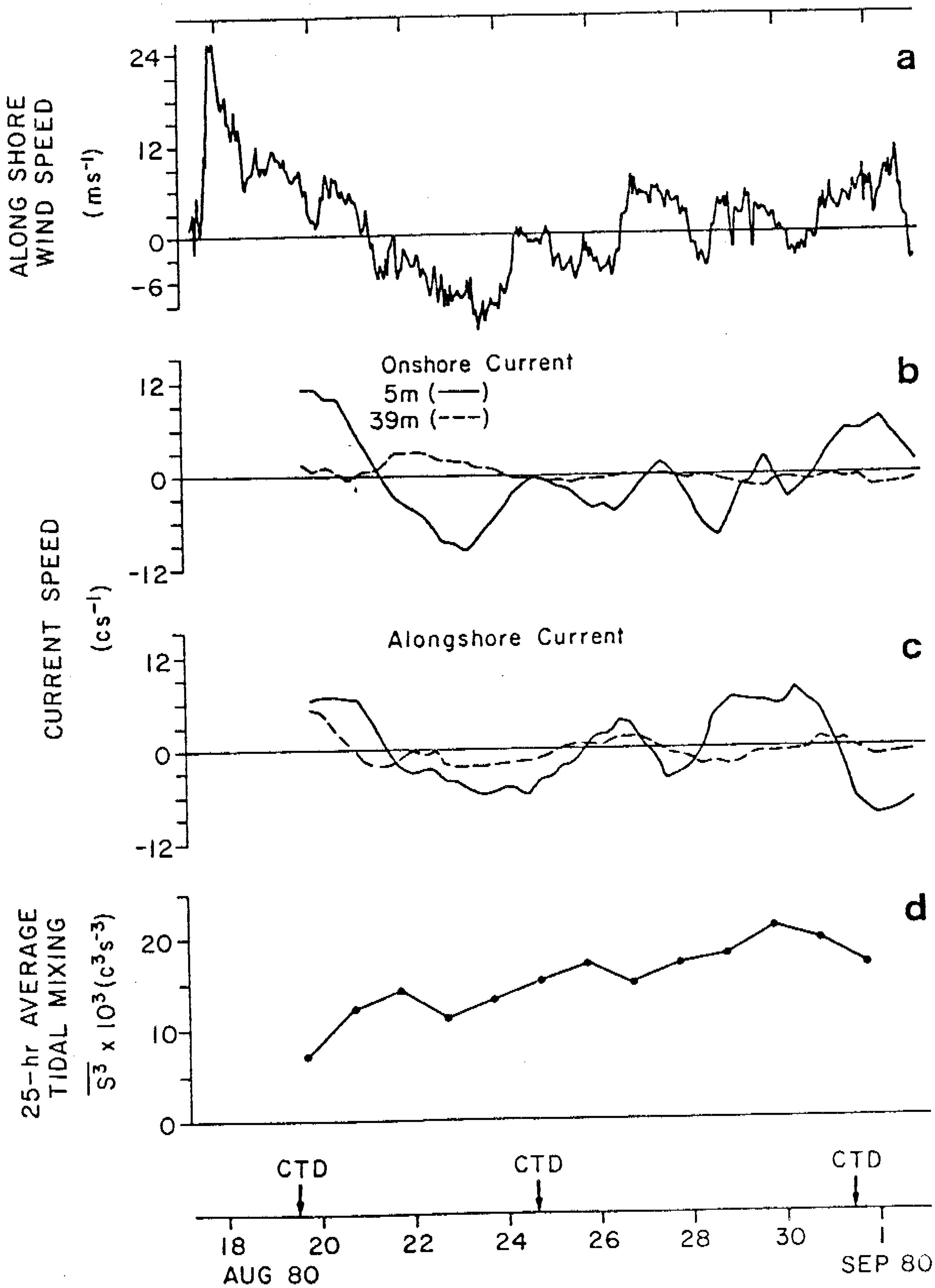

a
24
12
0
-6
ALONG SHORE WIND SPEED
(ms-1)
b
Onshore Current
5m (——)
39m (---)
12
0
-12
CURRENT SPEED
(cs-1)
c
Alongshore Current
12
0
-12
d
25-hr AVERAGE TIDAL MIXING
S3 x 103(c3s-3)
20
10
0
CTD
CTD
CTD
18
20
22
24
26
28
30
1
AUG 80
SEP 80

FIGURE 8.

V. COOPERATION

All aspects of this study are being closely coordinated with R.U.'s 549, 153 and 595. Current meter data from Schumacher and Pearson (R.U. 549) will be used to calculate SPM fluxes. Data on percent organic matter in particular samples will be provided to Griffiths and Morita (R.U. 595) for comparison with bacterial data. Distribution of SPM will be compared to the methane distributions measured by Cline (R.U. 153).

VI. NEEDS FOR FURTHER STUDY

In order to obtain more accurate estimates of the vertical eddy diffusion coefficients (K_z), detailed knowledge of the settling velocities of the SPM must be made. At present, only relative variations in K_z in different hydrographic regimes can be made. We plan to make initial measurements of SPM settling velocities at several stations during the spring NASTE cruise.

Particle size distribution spectra show that surface and bottom SPM maxima seaward of the coastal domain consist of different particle populations. At present, the flux of SPM from the surface layer to the bottom is unknown. This measurement is vitally important for estimating the transport of oil-laden particles both horizontally and vertically in case of an oil spill or pipe rupture. Initial data will be available from four sediment traps in the NASTE area to be recovered in June. Further sediment trap deployments should be considered, particularly in the St. George Basin area, to examine the variations in SPM flux between frontal and non-frontal zones. Such a study would also complement investigations of benthic ecology in this region.

The variation of SPM concentration in the near bottom layer across the southern Bering Sea suggests substantial differences in the probability of sediment resuspension in different hydrographic areas. At present, it is not clear why minimum SPM values apparently occur at or near the frontal zones. Variable resuspension across this area would have important implications for the redistribution of any spilt oil reaching the sea floor. The relationship between resuspension and hydrographic domain deserves further study.

VII. CONCLUSIONS

Almost all aspects of the study of the dynamics of SPM in the southeastern Bering Sea have been successful to date. We have shown a clear correlation between the various frontal structures in this area and the distribution of SPM. Data on the horizontal flux of SPM in the NAS area will be analyzed as soon as the current meter data are processed. The only failure involved a prototype model of the PMEL Sequentially Sampling Sediment Trap which failed to operate after deployment in August. These traps have since been debugged and we expect to later collect four successfully operating traps now in the midst of a January to June deployment.

Annual Report

Contract #30-5-022-68
Report Period 1 June, 1980 to
31 March, 1981

Number of Pages: 56

RU #595

Microbial Processes as Related to Transport in the North Aleutian Shelf and St. George Lease Areas

SUBMITTED BY

Robert P. Griffiths
Co-Principal Investigator
Assistant Professor-Senior Research
Department of Microbiology
Oregon State University
Corvallis, OR 97331

Richard Y. Morita
Co-Principal Investigator
Professor of Microbiology
and Oceanography
Department of Microbiology
Oregon State University
Corvallis, OR 97331

TABLE OF CONTENTS

Page No

I. Summary of Objectives, Conclusions, and Implications with Respect to OCS Oil and Gas Development.

A. Objectives

Our main objective during this project is to provide data on the sources and sinks of methane which are associated with microbial processes. This will enable the chemists in the North Aleutian Shelf Transport Study to more accurately assess the transport processes which are found in the perspective lease areas of the North Aleutian Shelf and St. Georges Basin. This information is required so that the most likely routes for crude oil transport can be determined.

B. Conclusions and Implications

1. The data presented in this report do not provide information about the transport processes in the North Aleutian Shelf and St. George Basin lease areas. As the data is analyzed it is given to Dr. Cline for integration into his transport model. The transport data resulting from the integration of these two data sets will be reported by him in RU #153 reports. The resulting transport model will be required to predict vertical and horizontal oil transport rates in the two lease areas being studied.

2. During the first two NASTE cruises, we have also accumulated data on the relative microbial activity in both the waters and sediments in this region. From these data and methanogenesis data, there are several implications which can be made relative to the biological processes in these two lease areas and the potential impact of crude oil on these processes. Port Moller is evidently an area which acts as a carbon trap. This is evident from the large

quantities of methane that is being produced in the heads of the two major arms of this embayment. The other major bays along the Aleutian Peninsula may act in much the same way. Although the relative significance of the transport of organic carbon through the detrital food chain in these embayments is not known, it could provide an important local food source for the organisms present in these areas. As we have shown in our Kasitsna Bay studies, crude oil could interfere with this process if allowed to become incorporated into the sediments of these bays.

We have conducted a study of relative microbial activity in the waters along the North Aleutian Shelf (NAS). These data suggest that there is a biologically active water layer at the water-sediment interface. Although carbon analyses of these waters have not as yet been completed, it is presumed that this water layer contains particles which have a high organic carbon content. It is known that crude oil tends to accumulate with the flocculant layer at the water-sediment interface. At this time it is not known how the presence of crude oil in this zone might effect the dynamics of the detrital food chain, but this is a region where there could be a considerable environmental impact because of the close proximity of the potentially toxic crude oil and the biologically active portion of the water column.

The most likely area of long-term perturbation following an oil spill appears, however, to be in the St. George Basin lease area. One of the major conclusions of the PROBES study is that the detrital food chain is apparently a very important factor in nutrient transfer in the region. The data on relative microbial activity and nitrogen fixation in the sediments of this region are still in the preliminary stages of analysis and are not given in this report. The raw data strongly suggests that there is a region of high biological activity in the sediments located along the PROBES line from station PL8 to PL14 and to the north of this line. If large quantities of crude oil were to become incorporated into these sediments, this would undoubtedly result in reduced productivity in the region.

II. Introduction

A. General Nature and Scope of Study

This study was designed to determine transport processes in the North Aleutian Shelf and St. George Basin lease areas. This study included observations on the physical, chemical, and biological factors which were relevant to the problem of predicting the horizontal and vertical transport of crude oil in the event of a spill. This information is essential for predicting the potential impact of crude oil production and transport in these two lease areas. There were two microbiological components of this study; the biodegradation rates of petroleum hydrocarbons conducted by Dr. Atlas and the biological sources and sinks of methane in the study area which was the objective of our study.

B. Specific Objectives

1. To measure _in situ_ rates of methane production in these two lease areas with particular emphasis on the main methane source areas that have been identified by the chemists. The major emphasis of this study is to measure methane production rates in marine sediments; however, rates in the water column were also to be considered.

2. To measure rates of methane oxidation in the waters that were being studied by the chemists. Both the uptake rates at one methane concentration and uptake kinetics were to be determined.

3. To determine the major sources and sinks of methane in these two lease areas.

C. Relevance to Problems of Petroleum Development

Without a comprehensive model for oil transport within the lease areas, there is no way that the link between potential spill sites and the most sensitive impact areas can be established. The purpose of this study is to provide that link.

III. Current State of Knowledge

To our knowledge, the only data on the *in situ* rates of methane oxidation and methanogenesis that has been collected in these two lease areas is that which we have presented in this report.

IV. Study Area

Figures 1 and 2 show the station locations where samples were collected during the first NASTE cruise conducted in August-September, 1980. Figures 3 and 4 show the station locations where samples were collected during the second NASTE cruise conducted in January-February, 1981.

V. Methods and Materials

A. August-September NASTE cruise

1. Sample Collection

With the exception of the sediment samples taken by hand near the cannery pier at Port Moller and the samples taken with a small grab sampler from a small boat in Port Moller, all sediment samples were collected using a Smith-MacIntyre grab sampler. Subsamples of the sediments collected with this grab were taken with plastic core

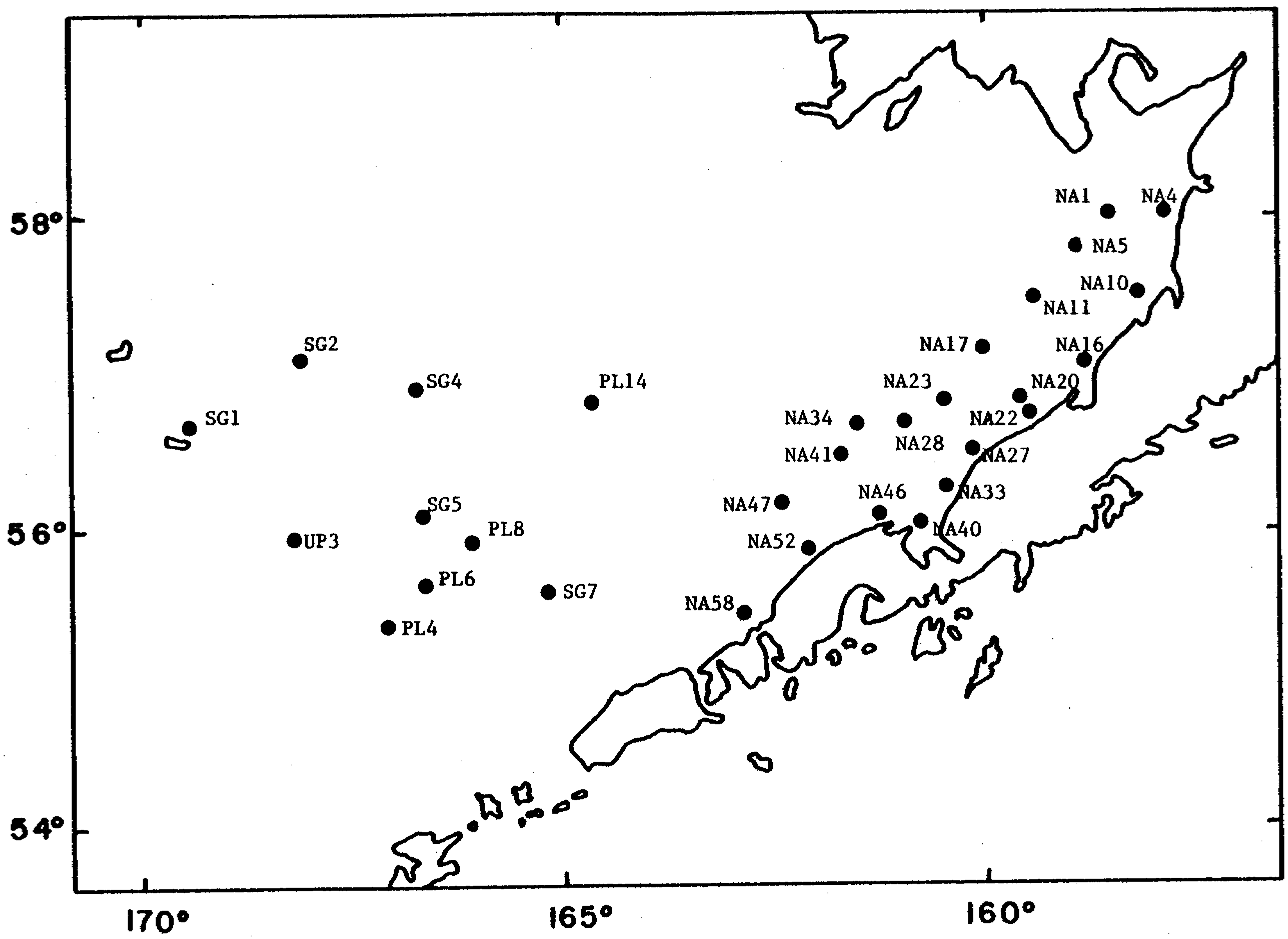

Figure 1. Positions and station designations for locations sampled during the August, 1980 North Aleutian Shelf Transport Study cruise.

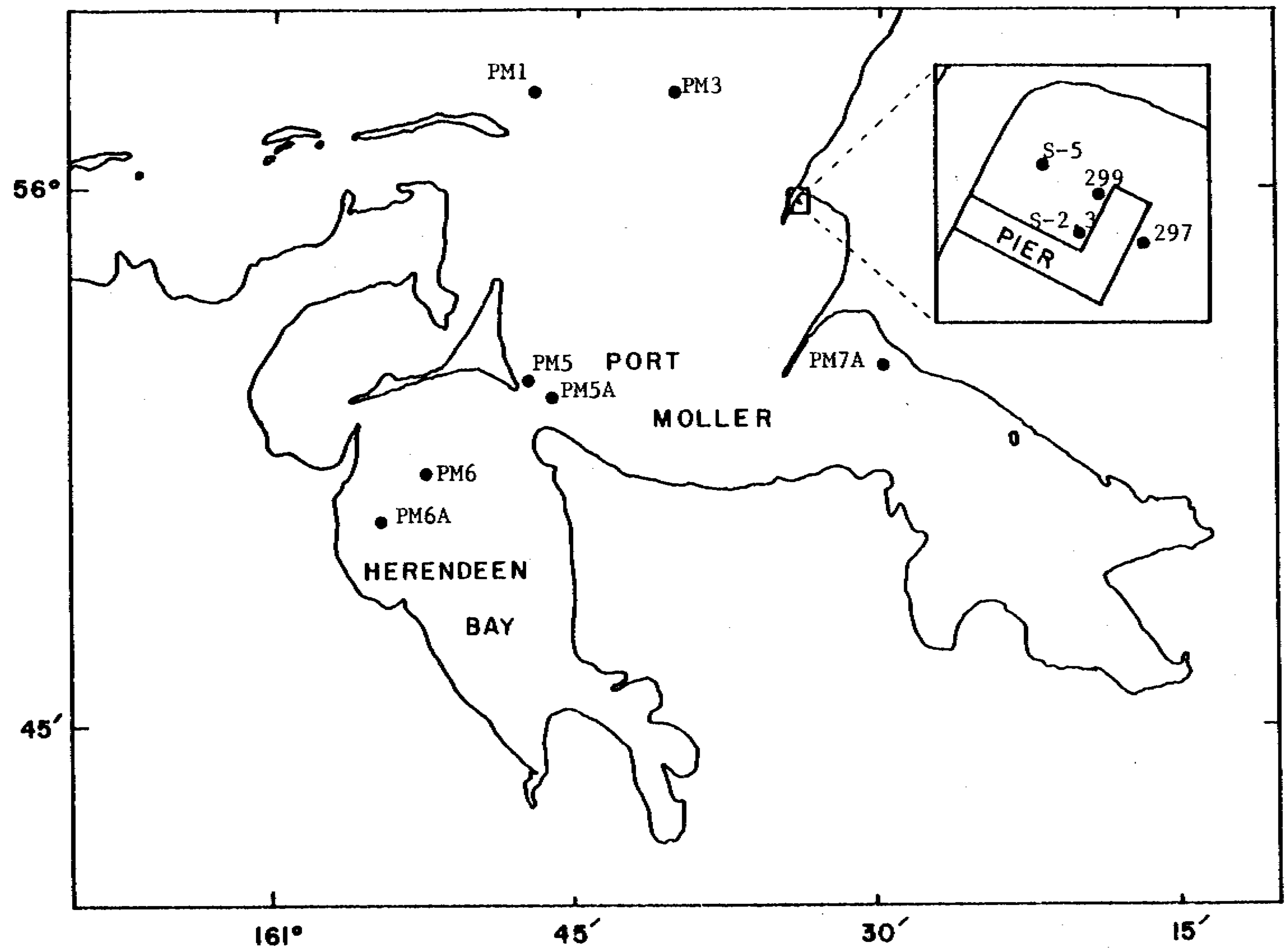

Figure 2. Positions and station designations for locations sampled in Port Moller during the August, 1980 North Aleutian Shelf Transport Study.

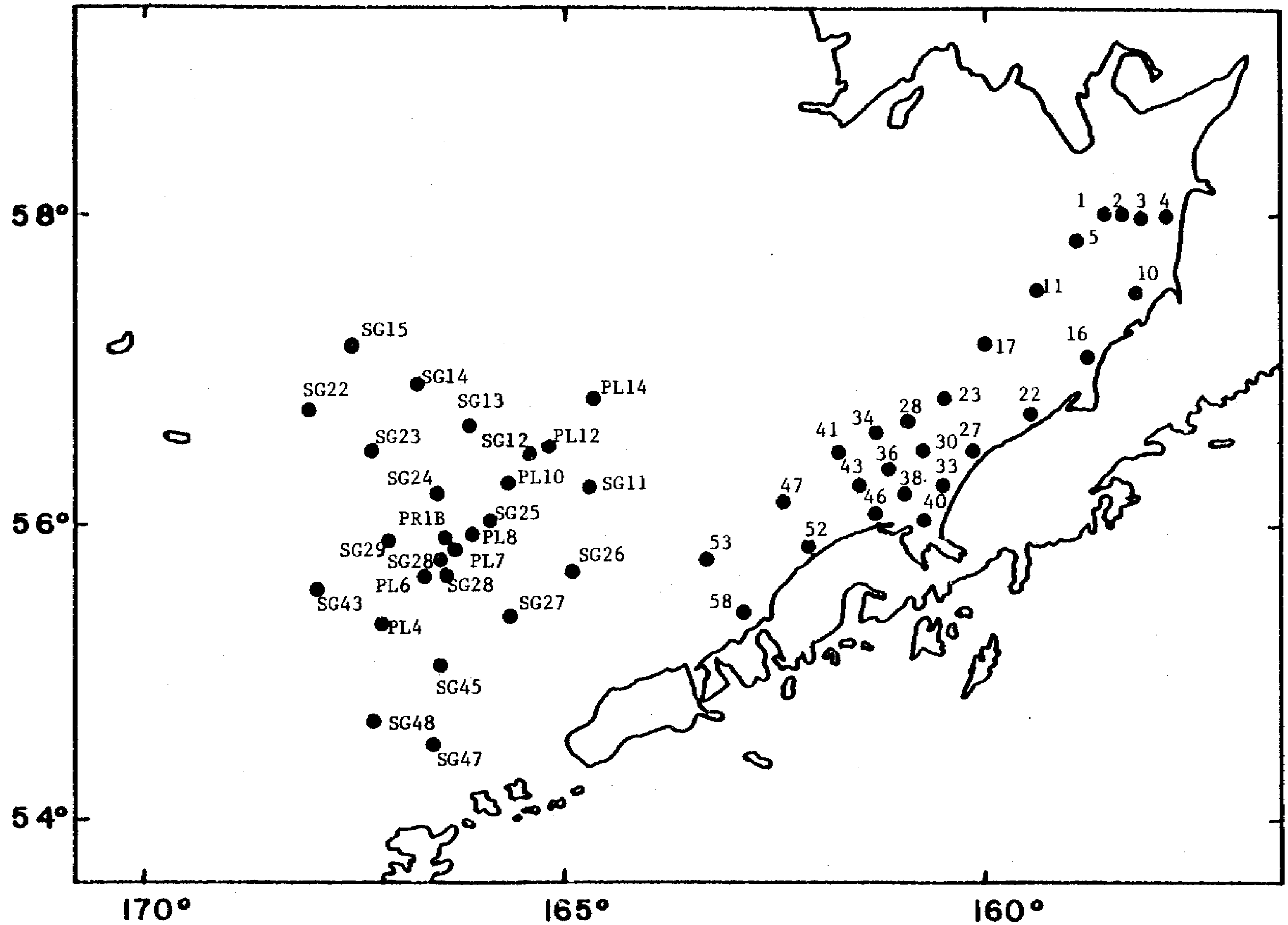

Figure 3. Positions and station designations for locations sampled during January, 1981 North Aleutian Shelf Transport Study (excluding Port Moller stations). Stations without letter designators are "NA" stations.

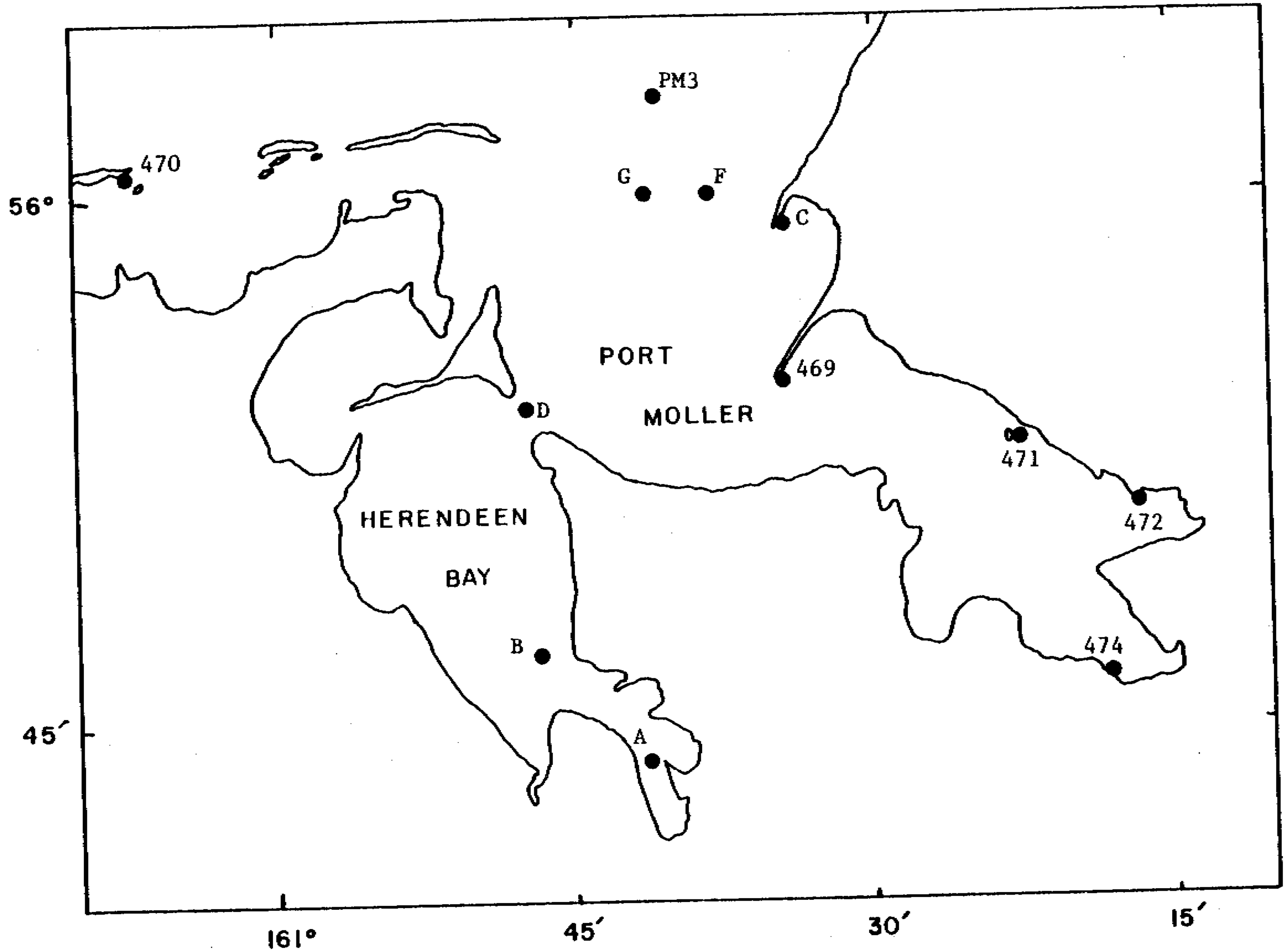

Figure 4. Positions and station designations for locations sampled in Port Moller during the January 1981 cruise.

liners measuring 6 cm in diameter and 25 cm in length. The core liner was slowly pushed into the grab sample. The core liner was then removed slowly and sealed at each end with a #12 rubber stopper. The sediments taken in this way measured ca. 10 cm in length.

All water samples were collected using a Niskin "butterfly" sampler fitted with a sterile plastic bag. The bottom water samples were taken with 10 cm of the water-sediment interface by using a specially modified inverted Niskin "butterfly" sampler mounted on the Smith-MacIntyre grab.

2. Assay for Methanogenesis

After the cores were taken, they were placed in an anaerobic glove bag in which the head space over the cores, all glassware and the glove bag used in the experiment were purged with oxygen-free nitrogen. After these items were sufficiently purged with oxygen-free nitrogen, the glove bag was purged with the same and then sealed.

a. Assay using [2-^{14}C] acetic acid (Method 1)

After the subcores were taken, they were placed into glass roll tubes measuring 1.6 x 6.0 cm which have a volume of 8 ml when stoppered with special 00 butyl rubber stoppers (A. H. Thomas Co., Philadelphia, PA). Before the roll tubes were placed into the glove bag, the labeled substrate was added to them. In most experiments, duplicate subsamples at each of four substrate concentrations was used. The substrate used was (2-^{14}C) acetic acid, sodium salt, from Amersham with a specific activity of 59 mCi/mmole. The substrate was prepared by diluting the material received from Amersham with distilled water to give a solution containing 1.04 μCi/ml. This was filter sterilized through a 0.45 μm Millipore membrane filter and dispensed into sterile 2 ml ampules which were then sealed and frozen. These were kept frozen until just prior to their use. In the concentration series, 0.025, 0.05, 0.10, and 0.20 ml were used. No attempt was made to keep these solutions anaerobic prior to use because it was assumed that after these small volumes were gassed vigorously with oxygen-free nitrogen while in the roll tubes, very little oxygen would remain in solution.

Before and after the sediment was added to the roll tubes, the tubes were purged with O_2 free N_2. At this point one of two techniques was used. In some cases, two sets of tubes from the same sediment sample were treated using both approaches. In the first approach, nothing else was added. The tubes were mixed with a vortex mixer for 15 seconds. The tubes were then incubated at the *in situ* temperature ± 1°C and analyzed for labeled methane as described below. In the second procedure, we removed 2 ml of gas with a syringe and replaced this with 2 ml of cysteine water. The cysteine water was made up of 3% NaCl, 0.05% cysteine-HCl, 0.0001% resazurin at pH 7.0. Any overpressure remaining in the tubes was removed by the syringe. When the cysteine water was used, controls were also run using the cysteine water containing 0.1% w/v sodium azide. In our preliminary experiments, we found that azide solution was very effective in stopping methanogenesis.

After an incubation time of 1 to 14 days, the tubes were assayed for the presence of ^{14}C methane using a Packard model 894 gas proportional counter. One ml of head space was withdrawn from each sample with a one ml gas-tight syringe and injected into a model 5734 Hewlett Packard gas chromatograph. A helium carrier gas was used at a flow rate of 60 ml per min. The gas chromatograph was fitted with 6 meter x 1/8 inch stainless steel column packed with Porapak R. (80/100 mesh). The temperatures used were; injection port 150°C, detector 300°C, oven ambient with the oven open. These conditions permitted a 3 minute separation between the labeled CO_2 and methane peaks as detected by the gas proportional counter. The signal from the gas proportional counter was analyzed and calibrated on a Hewlett Packard model 3380 integrator.

Labeled bicarbonate and methane of known specific activities and concentrations were used to calibrate the gas proportional counter. By counting the radio activity of methane at varying concentrations, we determined that the limit of detection for one ml of gas was between 200 and 400 DPM (1.5-3.0 pmole). We also determined that the response of the instrument was linear between 200 and 1000 DPM.

Although most of the samples were analyzed within the first two days incubation, some were allowed to incubate for periods up to 14 days.

b. Assay using gas chromatography (Method 2)

Using a 3 ml plastic disposable syringe with the end of the barrel removed, a total of 6 subcores were taken by holding the plunger steady while the barrel was slowly pushed into the sediment. Six subcores containing 3 ml each were taken from the bottom half of the core. Of the 6 subsamples taken, 3 were used as controls and 3 were the active samples. The cores were treated in the same way as that described in method 1 except no labeled acetate was added. In samples where both techniques were used, the same methanogenes rate was observed.

Two techniques were used to prepare the sediments for the assay. In the first technique, there was nothing added to the sediment and in the second, 2 ml of headspace was removed and 2 ml of cysteine water was added using a syringe. In the first technique, the sediments were poisoned with 1 ml of acetylene and in the second technique, the sediments were poisoned with 0.1 w/v sodium azide.

After the roll tubes had been incubated in the dark for varying lengths of time (up to 14 days), they were assayed for methane concentrations between 4 to 6 times during the course of an experiment. During the assay itself, 0.3 ml of the headspace was removed using a 0.5 ml gas-tight syringe.

The concentration of methane in all tubes was determined by gas chromatography. The instrument used was a Hewlett Packard model 5734A gas chromatograph fitted with a dual flame ionization detector. The resulting detector output was analyzed using a Hewlett Packard model 3380 recording integrator. The column used was a 2 meter x 1/8 inch stainless steel column filled with Porapak R. A helium carrier gas with a flow rate of 40 cc/min was used. The following temperatures were used in the GC: injection port 150°C, oven 50°C, and detector 300°C.

The integrator was calibrated using a gas standard of 100 ppm methane in nitrogen prior to each set of determinations.

c. Water samples

Methanogenesis was measured in water samples using two techniques. In the first technique, 1 liter of water was filtered through a 0.45 μm

Millipore membrane filter (47 mm in diameter) to trap the particulate fraction. The membranes were then placed into a roll tube which had been purged with oxygen-free nitrogen as described previously. When the roll tubes were removed from the glove bag, 2 ml of cysteine water was added. Three filters per sample were observed for methane production. The amount of labeled acetate solution added to each tube was 0.2 ml.

The second method used to measure methanogenesis in water samples was to add 55 ml of seawater to a 60 ml serum bottle. These samples were removed from a Niskin sterile water sample bag using a 50 syringe which had been flushed with oxygen-free nitrogen and sealed with a rubber stopper on the end of the syringe needle. Care was taken to prevent gas from entering the sample bag before and during taking the samples. Before the water sample was placed into the serum bottle, the bottle was purged with gas in the glove bag and then the sample was transferred under an anaerobic atmosphere. After the samples had been incubated, the head space was analyzed for labeled methane as described previously.

3. Methane Oxidation Assay

Water samples were taken with a Niskin sterile bag water sampler. After sample collection, the water samples were placed in 500 ml glass bottles and shaken. A 50 ml plastic syringe fitted with a cannula was used to transfer the water sample from the larger glass bottle into the serum bottles. When methane oxidation rates in sediments were assayed, fifty ml of a 1:10 dilution of sediment in sterile seawater was added to a 60 ml serum bottle and sealed with a serum bottle stopper.

Six subsamples were used in each methane oxidation rate determination (duplicate at each of three methane concentrations). The ^{14}C-methane used in this study was especially prepared by Amersham with a specific activity of 58 μCi/μmole. The final methane concentration was 1 μCi/ml in the gas that was added to the serum bottles. Three volumes of the gas mixture (^{14}C-methane in nitrogen) were used (0.25, 0.5 and 1.0 ml). This will result in a final concentration of 0.29, 0.58, and 1.16 μl of methane/liter of seawater respectively. This is within the natural methane concentration range normally encountered in the study area (0.2-2.5 μl/liter).

In some cases methane oxidation rates were measured using one concentration of labeled methane (0.58 μl/liter). In these samples, triplicate subsamples were assayed. Before the labeled methane was added to the serum bottle, an equal volume of head space was removed so that there was no net pressure change when the methane is injected with the syringe. One set of control subsamples was run with every third sample processed. Methane oxidation was stopped in the controls by adding 1.0 ml acetylene to the head space.

Once the methane was added, the samples were incubated in the dark on a rotary shaker at the in situ temperature ± 1°C. The incubation period was 48 hours. At the end of the incubation period, the reaction was terminated by adding 1.0 ml of 10 N NaOH with a syringe through the stopper. The serum bottle was then shaken for 1 hr at room temperature to permit the labeled CO_2 to be absorbed into solution. The rubber stopper was then removed and the sample transferred to a 125 ml serum bottle using a 50 ml syringe fitted with a cannula. This procedure removed the labeled methane while the labeled CO_2 remained in solution. The serum bottle was then stoppered with a serum bottle stopper fitted with a plastic bucket containing a flutted strip of filter paper. Two ml of 10 N H_2SO_4 was then added to the sample to release the labeled CO_2. The sample was then shaken for 1 hr at room temperature to release the labeled CO_2 which was then trapped on 0.2 ml of β-phenethylamine which was placed in the filter paper using a 1 ml syringe. The CO_2 trapping procedure and the assay for radioactivity in the cell fraction is essentially the same as that which we have used in the past (Griffiths et al., 1978).

After the CO_2 was trapped, the sample was filtered through a 0.45 nm membrane filter which trapped the cells so that the amount of label incorporated into cell material could be determined. These filters were then dried and assayed using a liquid scintillation counter.

4. Microbial Activity Determinations

The procedure used in these studies involved adding a U-^{14}C compound to identical subsamples which were contained in 50 ml serum bottles. After addition of subsamples, the 50 ml serum bottles that were used for reaction vessels were sealed with rubber serum bottle caps fitted with plastic rod and cup assemblies (Kontes Glass Co., Vineland, N.J.: K-882320) containing 25 x 50 mm strips of fluted Whatman #1 chromatography paper. The samples were incubated in the dark within 1.0°C of the in situ temperature. After the incubation period, the bottles were injected through the septum with 0.2 ml of 5N H_2SO_4 in order to stop the reaction and release the $^{14}CO_2$. After the addition of the acid, 0.15 ml of the CO_2 absorbent, β-phenethylamine was injected onto the filter paper.

The bottles were then shaken on a rotary shaker at 200 rpm for at least 45 minutes at room temperature to facilitate the absorption of CO_2. The filter papers containing the $^{14}CO_2$ were removed from the cup assemblies and added to scintillation vials containing 10 ml of toluene based scintillation fluor (Omifluor, New England Nuclear).

The subsamples were filtered through a 0.45 μm membrane filter (Millipore). The trapped cells on the filter were washed with three 10 ml portions of seawater at 0-3°C. The filters were dried and then added to Filmware scintillation bags containing 2 ml of the above mentioned fluor. The vials were counted in a Beckman model LS-100 C liquid scintillation counter located in our laboratory at Oregon State University.

In the sediment samples, a 10.0 ml subsample was diluted 1,000 times (v/v) with a 32 o/oo (w/v) solution of sterile artificial seawater. Ten ml subsamples of the sediment slurry were dried and weighed to determine the dry weights. These dry weights were used to calculate the observed uptake rates in terms of grams dry weight of sediment.

U-^{14}C L-glutamic acid with a specific activity of 285 mCi/mmole (Amersham-Searle) was used in all water samples at a final concentration of 5.4 μg/liter. Glutamic acid with a lower specific activity (10 mCi/mmole) was used in all sediment samples. U-^{14}C D-glucose with a specific activity of 291 mCi/mmole (Amersham-Searle) was used in all water and sediment samples. The final concentration used was 3.8 μg/liter.

Triplicate subsamples were analyzed for each sample and the results reported in Figures 5 to 11 are the means of the observed values. The channels ratio method for determining counting efficiencies was used. The observed CPM was converted to DPM before the mean value was calculated. The percent respiration was calculated by dividing the amount of labeled carbon taken up by the cells (both cell and CO_2 radioactivity) and multiplying this ratio by 100.

B. January-February, 1981 NASTE Cruise

1. Methanogenesis Assay

During this cruise, no radioactive tracer exeriments were conducted. Methane production rates generated from sediment subcores were estimated by assaying the headspace in roll tubes or by assaying the water column over an intact core. In the latter case, the methane was stripped from the water and collected in a liquid nitrogen cold trap before assaying on a gas chromatograph. The water analyses were conducted by Mr. Chuck Katz of PMEL. In the roll tube experiments, 2 controls and 4 methane-producing subsamples were assayed for each sediment analyzed. In these experiments, no cysteine water was used. Methanogenesis in the controls was terminated by the addition of 1 ml 37% buffered formaldehyde. All other procedures were the same as that described for the previous cruise. The headspace of the roll tubes was assayed for methane after 1,3,5,7, and 9 days incubation.

When we returned to Oregon State University after the cruise, the methane data was analyzed by three different methods. In all methods, the amount of methane in the headspace removed during the course of the experiment was accounted for in the calculations.

The first approach used was to subtract the mean methane concentration found in the two controls from the methane concentration observed in the headspace after 7 days incubation. The rate was the mean of those values divided by 7. By knowing the volume of the headspace, the volume of sediment and the incubation time, the amount of methane produced per ml of sediment per day was calculated.

The second approach was to assume that it took one day to allow the sediment to come to equilibrium. This assumption was based on the observation that methane production rate observed during the first day was generally greater than that observed from the first day to the seventh day of incubation. This increase in apparent methane production was undoubtedly due to the establishment of a new equilibrium between methane in the sediment and methane in the headspace. The mean of the control methane concentration was subtracted from the concentration observed in sediments that had been incubated 1 and 7 days. The concentration of methane observed after 1 day incubation was then subtracted from the concentration observed after 7 days for each of the 4 subsamples. The net mean production was calculated using an incubation period of 6 days. The third method consisted of running a linear regression on the observed methane concentrations for all 4 methane-producing subsamples at all times that the methane concentrations were determined up through 7 days. In essentially all cases, the rate observed between 7 and 9 days incubation was greater than observed during any other time period. The 9 day values were therefore not used in any of the above calculations.

In this last method, the methanogenesis rate was the slope of the best fitting line through all points. Surprisingly, the rates calculated using all three approaches produced very similar results. Of the three methods used, we feel that the last one mentioned is the most valid statistically and therefore it was the one that was adapted to estimate methanogenesis rates reported for both cruises. The methanogenesis rates and the observed correlation coefficients measured using this method are given in Table 1.

Table 1. Methane production rates in ml x m^{-2} x day^{-1} and the corresponding correlation coefficients observed in sediments collected during the January NASTE cruise.

Station	Methane Production	Correlation Coefficient	Station #	Methane Production	Correlation Coefficient
NA40	0.07	0.3	PL6	0.12	0.7
NA46	0	0.6	PL8	0.24	0.5
SG11	0.04	0.5	PL10	0.03	0.6
SG12	0.10	0.3	PL12	0.03	0.4
PL7	0.02	0.2	PL14	0.08	0.6
SG28	0	0.7	SG13	0.22	0.8
NA52	0.02	0.4	SG14	0.08	0.7
PR1B	0	0.5	SG15	0.06	0.7
PR1B	0.07	0.4	SG22	0.18	0.7
NA16	0.02	0.5	SG23	0.04	0.5
PM3	0.17	0.7	SG24	0.12	0.7
297	0.77	0.9	SG25	0.10	0.8
A	49	0.5	SG26	0.04	0.5
B	1.7	0.8	SG27	0.07	0.6
NA40	0.07	0.8	SG45	0	0.5
NA46	0.06	0.4	SG28	0.04	0.7
PL4	0.21	0.6	SG29	0.01	0.2
			SG48	0.02	0.2
			SG47	0	0.4

The production rate units that are the most useful for the chemists is the amount of methane produced per m^2 per day. This conversion was made by assuming that the active depth for net methane production was 10 cm. In most cases, subcores were made of the sample core from the surface down to a depth of 5 cm. In some samples, two sets of cores were taken one from the top and the other from the bottom of the core. These subcores were taken parallel to the length of the original core. Since most cores were 10 cm in length, subcores taken from both the top and bottom represented the total length of the core. When both top and bottom cores were taken at a given location, the mean value for rates observed in both cores are used to estimate rates for the total core. Where only top subcores were taken, the rates estimated for the total core is double the 5 cm estimate.

During the first NASTE cruise, two methods of determining methanogenesis rates were used; radioactive tracer and GC analysis of the headspace (methods 1 and 2). During the second cruise, a third method was employed along with method 2. In this method, four identical cores were taken using the Pamatmat multiple coring device. This sampler produced four undistrubed cores with each cast. The corers are made out of a plastic material that is impervious to O_2 and have an inside diameter of 5.7 cm.

When the sampler was brought on board after a sample had been taken, the cores were removed from the sampler and stoppered at each end with number 12 rubber stoppers. The cores were taken into the laboratory where the water overlaying the core was removed and replaced with surface water which contained a low concentration of methane (ca. 225 μl/liter). The core tubes were resealed and placed into an incubation chamber designed to hold the core tubes vertically. The incubator was plumbed into the ship's seawater system to maintain a constant flow of fresh seawater, thus keeping the cores within 0.5 C of the surface water temperature. The water level within the incubator was kept at a constant level so that the entire core was submerged in the water.

After the cores had incubated for 1 day, the water from one core was removed and assayed. This methane concentration was considered the time 0 control although determinations of the methane in the surface water used to cover the cores was also determined. The core water samples in the remaining three cores were assayed after 4, 6, and 8 days. From these observations, a rate of methanogenesis was generated using the observed concentrations, the core length and the total water volume over the core. These calculations were made by Mr. Katz of PMEL. In the cases where there were only three good cores available from sampling, water samples were assayed after 1, 4 and 8 days incubation.

The method used to assay methane oxidation was the same during both cruises.

VI. Results

A. Methane Oxidation

1. North Aleutian Shelf

During the August cruise, we measured rates of methane oxidation in 93 water and 5 sediment samples. In the water samples, relative methane oxidation rates were measured in all samples analyzed and the kinetics of methane oxidation were measured in 61 samples. Along the North Aleutian Shelf, the methane oxidation rates were generally higher in the samples collected inshore than those collected offshore (Figs. 5 and 6). In the surface water samples, the mean rate was 1.2 nl x liter^{-1} x day^{-1} for the offshore samples and the mean rate in the inshore samples was 1.7 nl x liter^{-1} x day^{-1}; however, this difference was not statistically significant. In the bottom samples, the difference was greater with the mean values for offshore and inshore samples being 1.6 and 3.3 nl x liter^{-1} x day^{-1} respectively. The level of significance for this difference was $p = 0.005$.

These statistical analyses were conducted on the methane oxidation rates reported in figures 5 to 8. During the January cruise, the same trend was observed. In surface waters, the mean rates for offshore and inshore samples were 0.3 and 0.6 nl x liter^{-1} x day^{-1} respectively (Figs. 7 and 8). In the bottom waters, the mean values were 0.6 and 2.0 respectively for offshore and inshore waters. The significance of these differences were $p = 0.002$ and 0.09 respectively.

During both cruises, the methane oxidation rates in the bottom waters were generally greater than that observed at the surface at the same location (Figs. 5-8). During the August cruise, the mean rates observed in surface and bottom waters were 1.5 and 2.2 nl x liter^{-1} x day^{-1} respectively. During the January cruise, the mean methane oxidation rates in the surface and bottom waters were 0.4 and 1.2 nl x liter^{-1} x day^{-1} respectively. The significance of these differences between surface and bottom waters for the August and January cruises was $p = 0.02$ and 0.05 respectively.

In the surface waters analyzed during both cruises, there was a plume of high activity in the area around Port Moller (the enclosed areas in Figs. 5 and 7). This same pattern was observed in the bottom

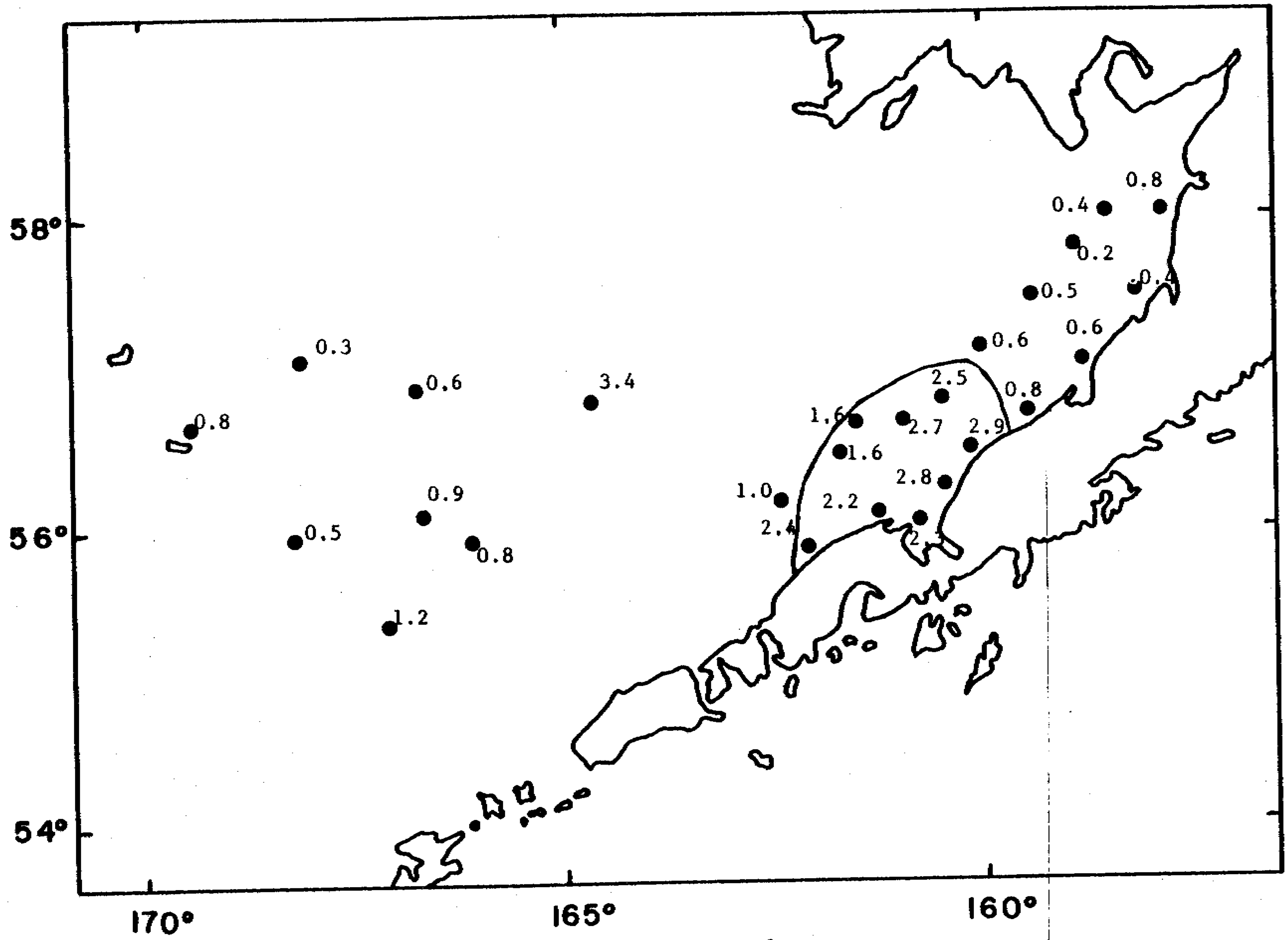

Figure 5. Methane oxidation rates in nl x liter^{-1} x d^{-1} observed in surface water samples from the August 1980 cruise.

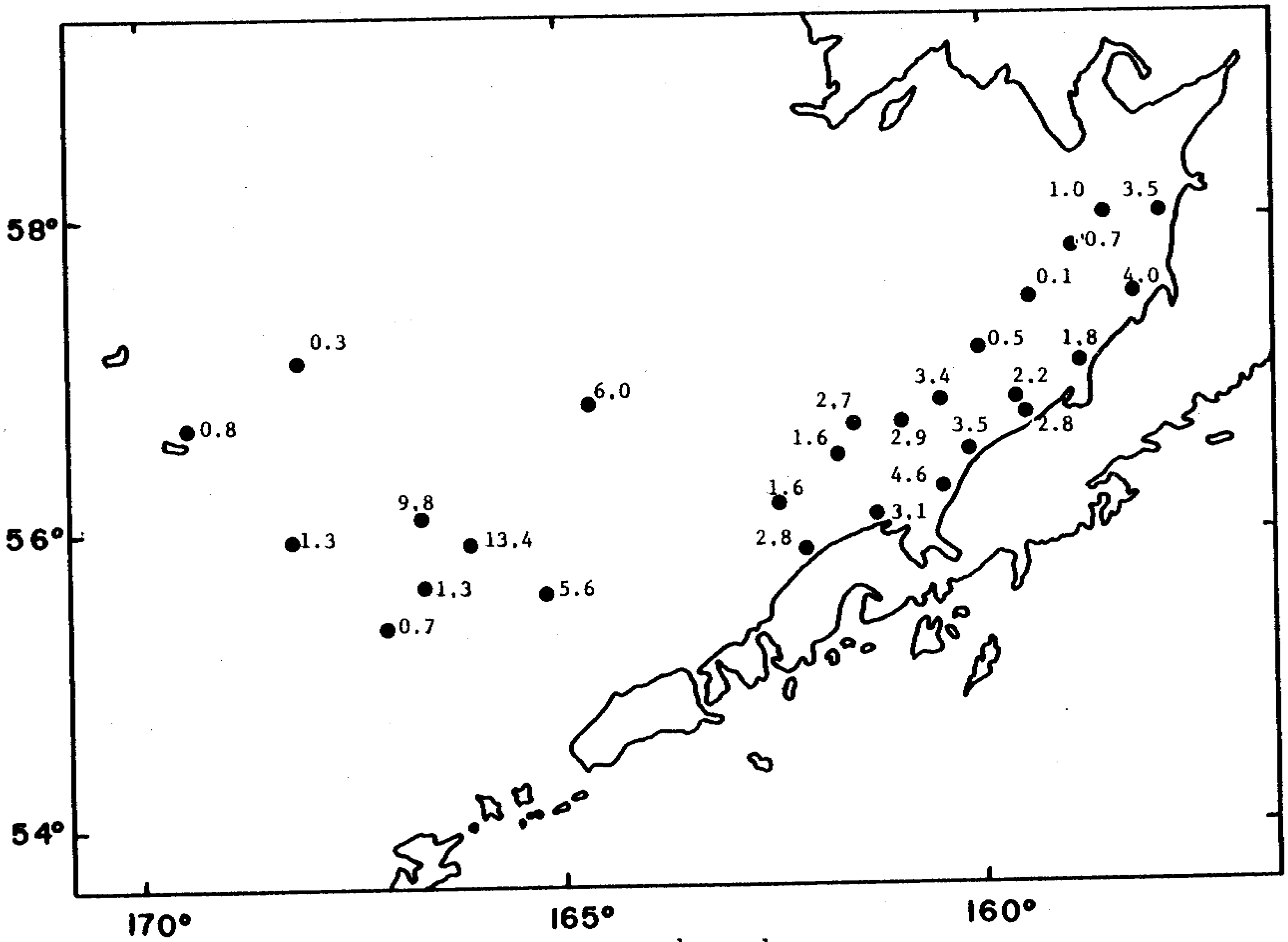

Figure 6. Methane oxidation rates in nl x liter^{-1} x d^{-1} observed in bottom water samples from the August 1980 cruise.

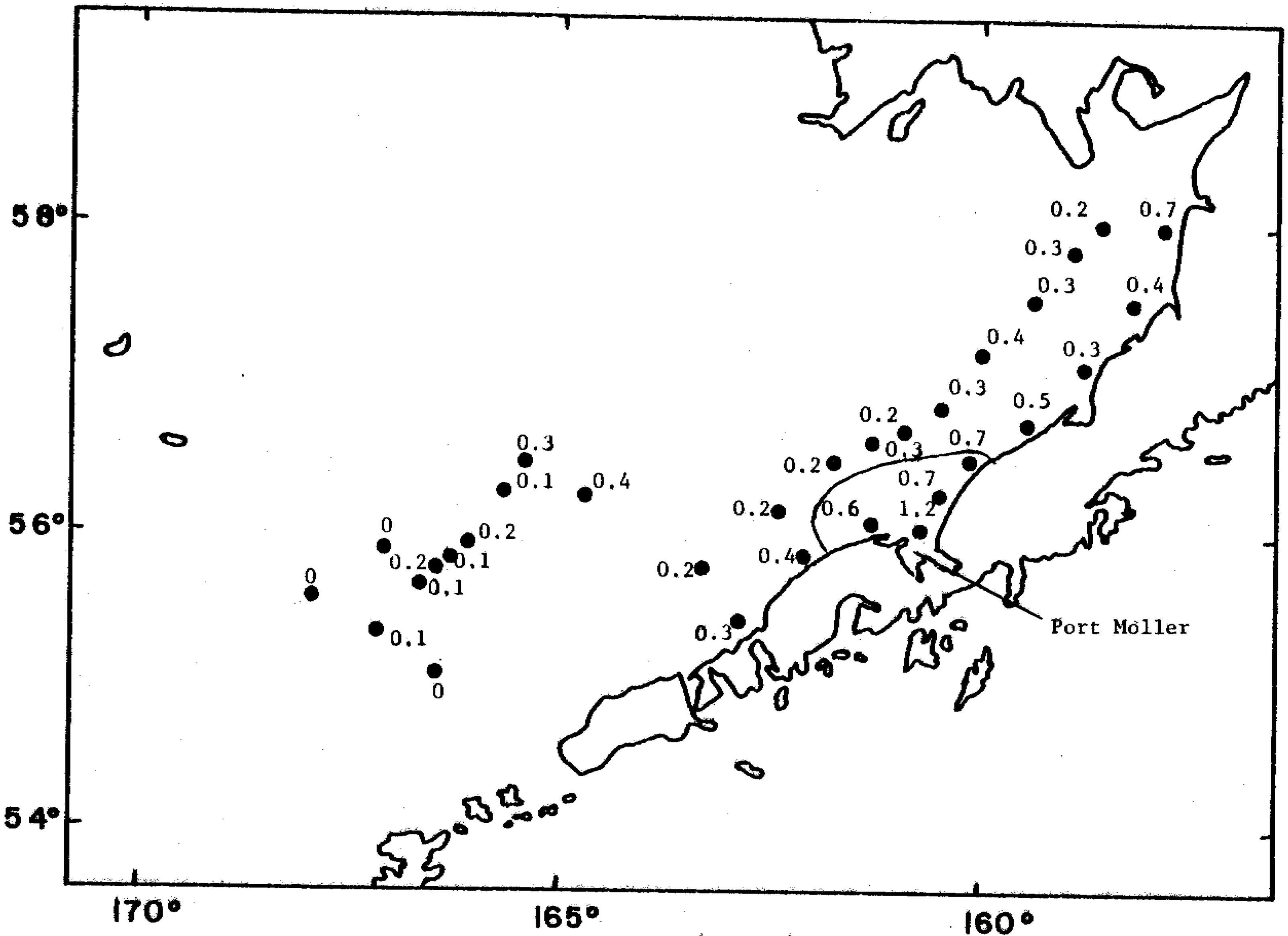

Figure 7. Methane oxidation rates in nl x liter^{-1} x d^{-1} observed in surface water samples from the January, 1981 cruise.

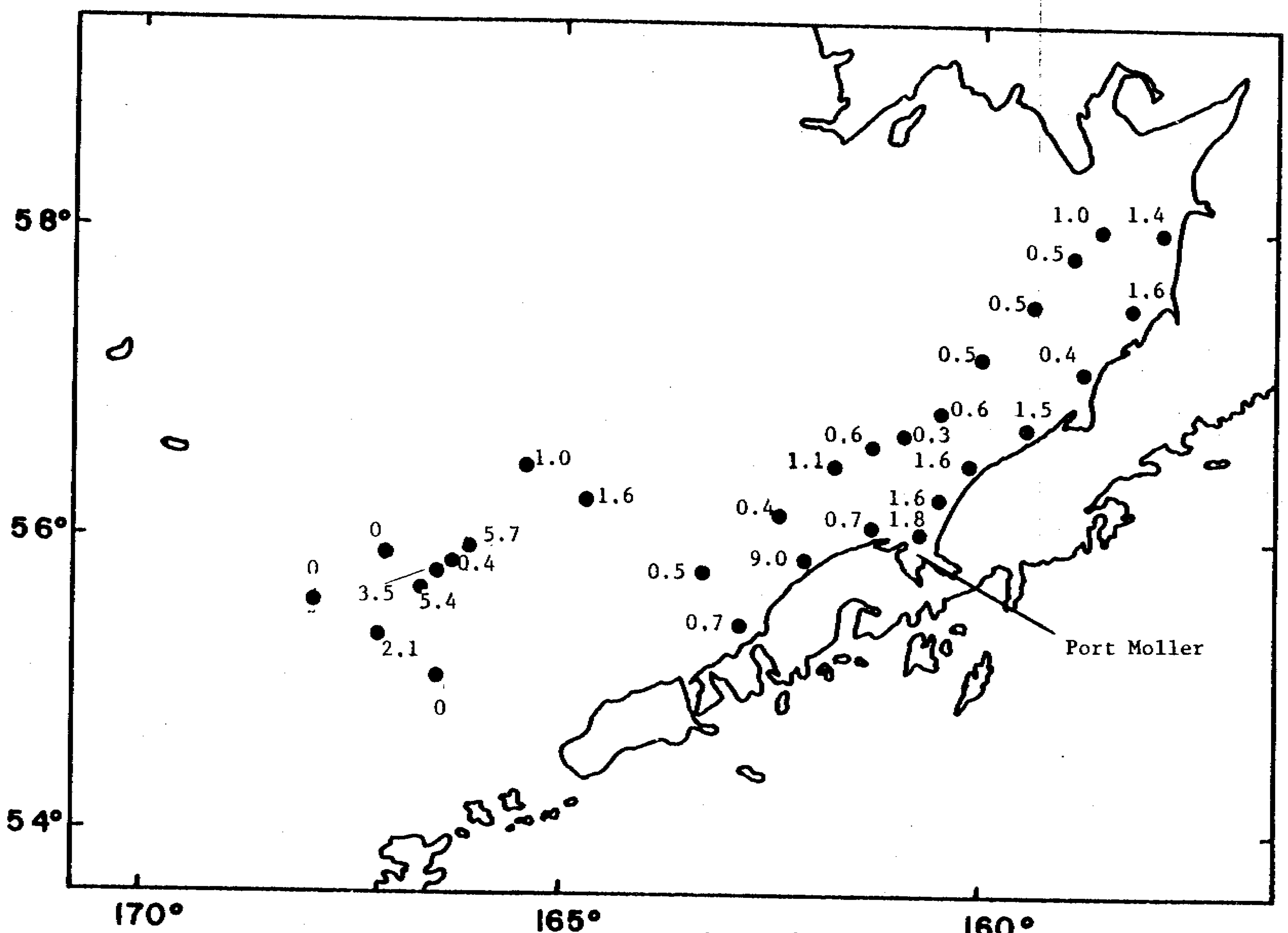

Figure 8. Methane oxidation rates in nl x liter^{-1} x d^{-1} observed in bottom water samples from the January, 1981 cruise.

waters (Figs. 6 and 8) but high rates were also observed along the coast in the inshore stations to the east of Port Moller.

2. Port Moller

During the August cruise, we were able to take samples only near the mouth of Port Moller. The methane oxidation rates observed were generally higher than the mean methane oxidation rate observed in the North Aleutian Shelf samples but they were not high relative to those found in the stations near Port Moller (Fig. 9). During the January cruise, we were able to sample more intensively in Port Moller. The methane oxidation rates observed there were much greater than those observed at any other location (Figs. 10 and 11). The highest rates were observed at the head of Port Moller and Herendeen Bay. The rates observed in the samples collected near the mouth were lower than the rates observed in samples collected in the same general area during the previous cruise.

3. St. George Basin

In the St. George Basin (SGB), we observed the same trend that was seen in the North Aleutian Shelf region. The methane oxidation rates in the bottom waters were higher than those observed in surface waters. During the August cruise the mean methane oxidation rates in the surface and bottom waters were 1.1 and 4.4 nl x liter^{-1} x day^{-1} respectively. During the January cruise, the rates for surface and bottom waters were 0.1 and 2.0 nl x liter^{-1} x day^{-1} respectively. The significance of these differences was $p = 0.07$ and 0.001 respectively.

There was not a consistent pattern to the geographical distribution of methane oxidation rates in the surface water samples collected

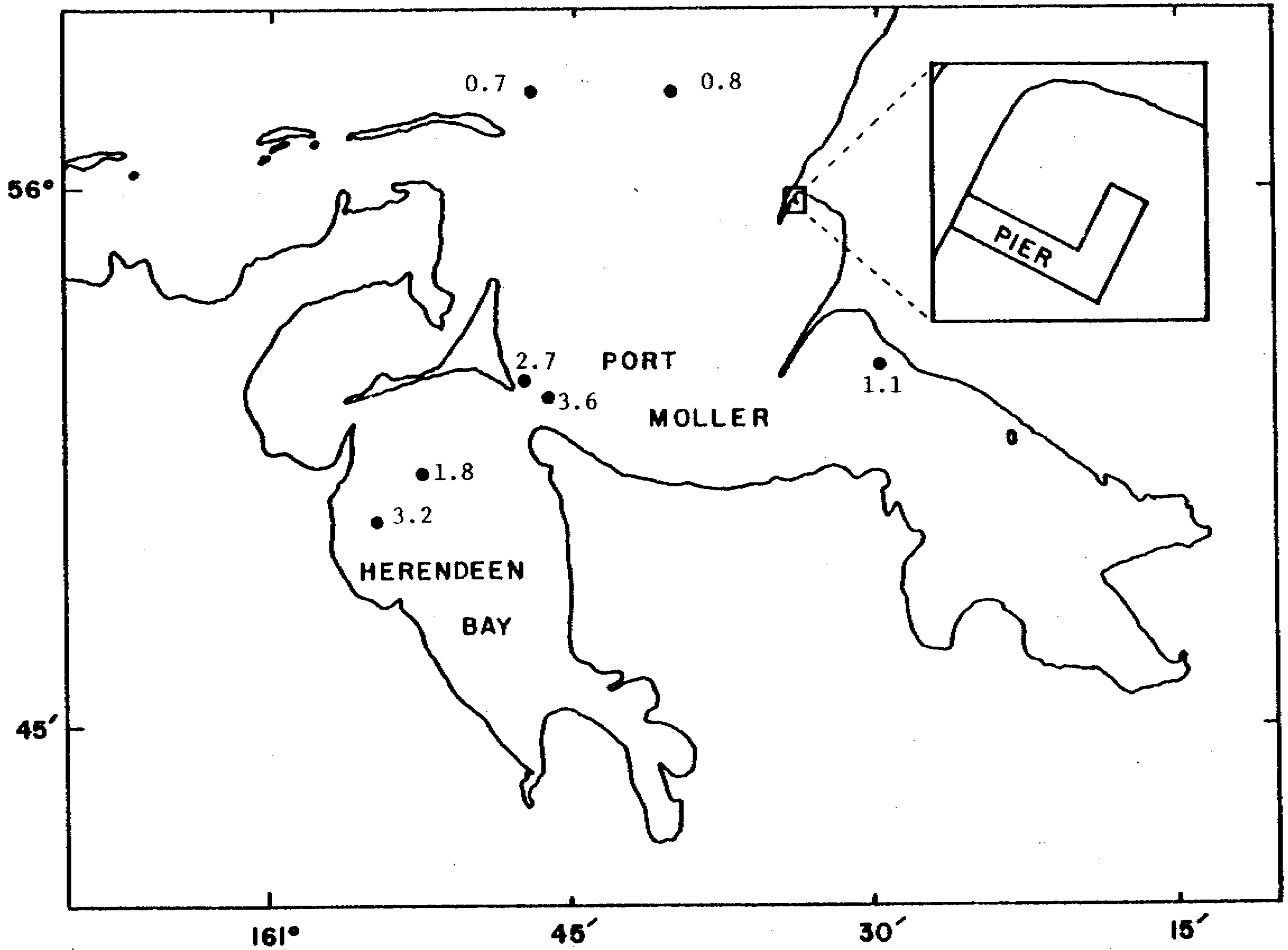

Figure 9. Methane oxidation rates in nl x liter^{-1} x d^{-1} for water samples collected in Port Moller during the August, 1981 cruise.

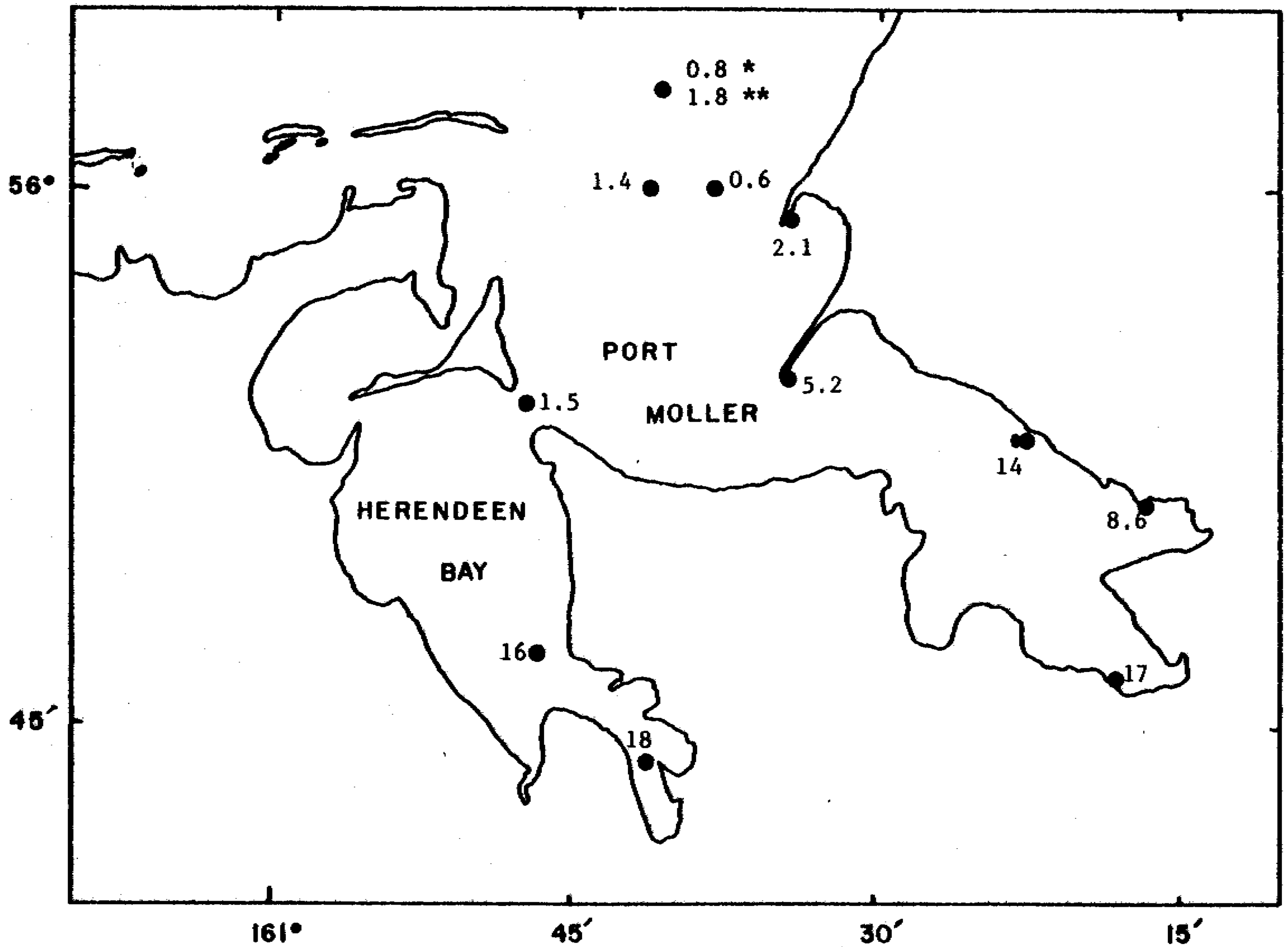

Figure 10. Methane oxidation rates in nliters x liter^{-1} x d^{-1} for surface waters in Port Moller during the January, 1981 cruise. * Denotes rate at high slack water; ** rate at low slack water.

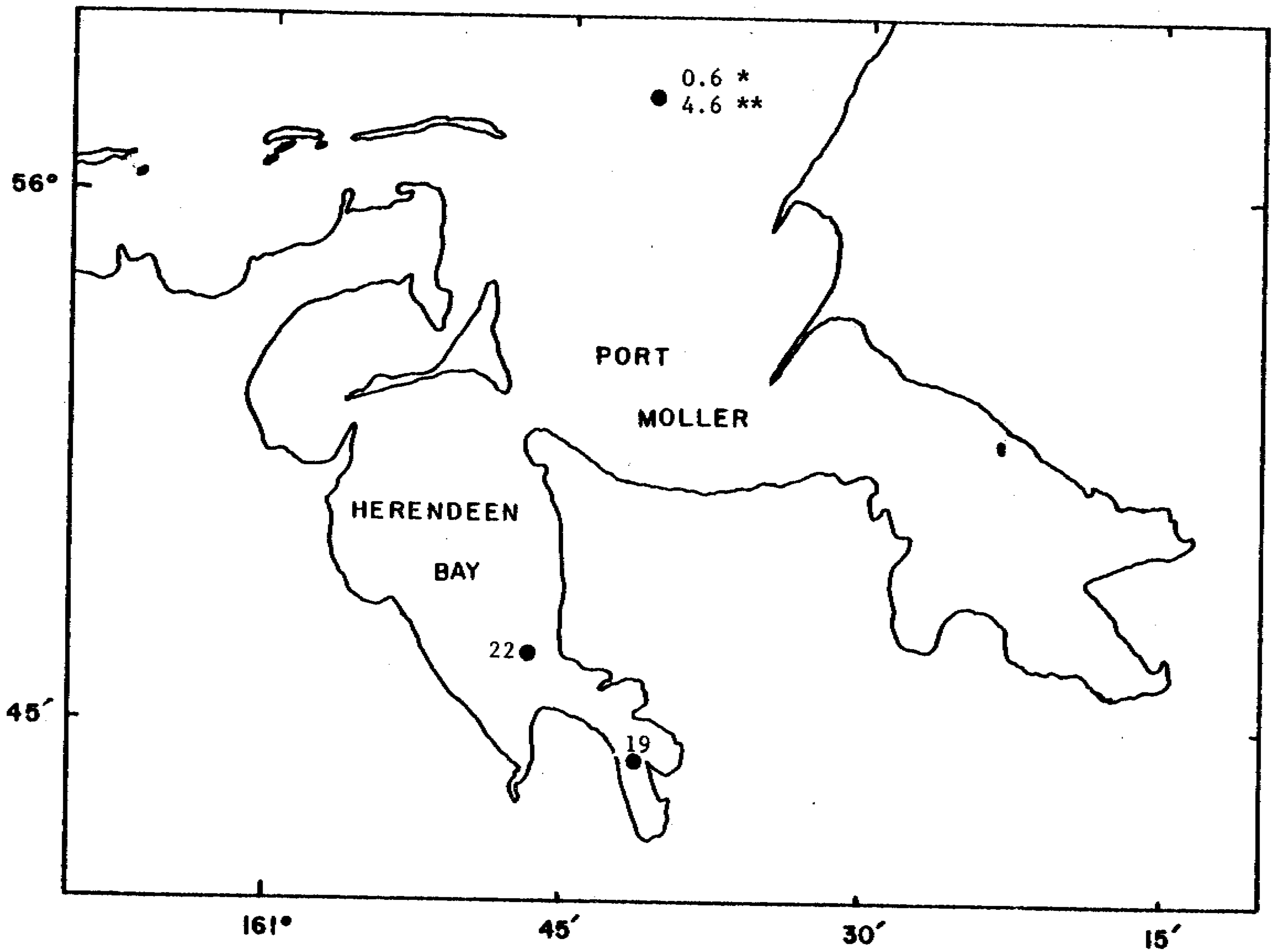

Figure 11. Methane oxidation rates in nliters x liter^{-1} x d^{-1} for bottom waters in Port Moller during the January, 1981 cruise. * Denotes rate at high tide, ** rate at low tide.

during either cruise in SGB but elevated methane oxidation rates were observed in the bottom water samples collected in the vicinity of stations PL 6-8 during both cruises.

4. Seasonal differences

When the methane oxidation rates observed in water samples collected from the same areas are compared seasonally, there were many differences noted. The mean methane oxidation rate in bottom water samples collected along the North Aleutian Shelf dropped from 2.2 nl x liter^{-1} x day^{-1} in August to 1.3 in January (a 41% reduction). When the surface water samples from the same area are compared seasonally, there was a 73% reduction. In the St. George Basin, the seasonal difference was even more dramatic. The methane oxidation rate dropped 55% in the bottom waters and 91% in the surface waters.

5. Methane oxidation rates in sediments

During the August cruise, methane oxidation rates were measured in 5 sediment samples collected from stations SG7, NA5A, and the Port Moller cannery pier. If these rates are compared to the rates observed in the overlaying waters on an equal volume basis, the rates were generally 10 times greater.

B. Methanogenesis

1. Methanogenesis in water

Methanogenesis rates were measured in 10 water samples during the August cruise. Even with incubation times of up to 14 days, no detectable methane production was observed. The lower limit of detection in this system was 0.25 nl x liter^{-1} x day^{-1}. The samples were collected from the following stations: NA4A, NA22, NA40, SG7, UP3, PM3, PL4, PL6, PL14 and the pier at Port Moller.

2. Methanogenesis in sediments.

During the August cruise, methane production rates were measured in 11 sediments using method number 2 (gas chromatographic analysis of headspace). The results of these measurements are shown in Figs. 12 and 13. The highest methane production rates were observed in the St. George Basin at stations PL8 and PL14. High rates were also observed in the sediments near the Port Moller cannery pier. During the second NASTE cruise, methanogenesis rates were measured in 35 sediments (Figs. 14 and 15). In Herendeen Bay we were able to collect samples in an area that we were not able to sample during the previous cruise. At the head of this bay, we observed methane production rates much greater than that observed anywhere else during either cruise. The mean production rate for all other samples analyzed was 0.15 ml x m^{-2} x day^{-1}. The rate observed in the sediment collected at the head of Herendeen Bay (49 ml x m^{-2} x day^{-1}) was over 300 times that rate. High methanogenesis rates were also observed in the other sediment collected in this bay and in the sediment collected at the cannery pier. The rates observed in the other sediments analyzed from the North Aleutian Shelf were very close to the detection limits of the technique used (ca. 0.01 ml x m^2 x day^{-1}). In the St. George Basin, there were three areas where the methanogenesis rates were 0.1 ml x m^{-2} x day^{-1} or greater (enclosed areas in Fig. 14). The highest rate observed was that in the sediment collected at station PL8 (0.24 ml x m^{-2} x day^{-1}).

There were 7 stations where methane production rates were measured in sediments collected during both cruises (Table 2).

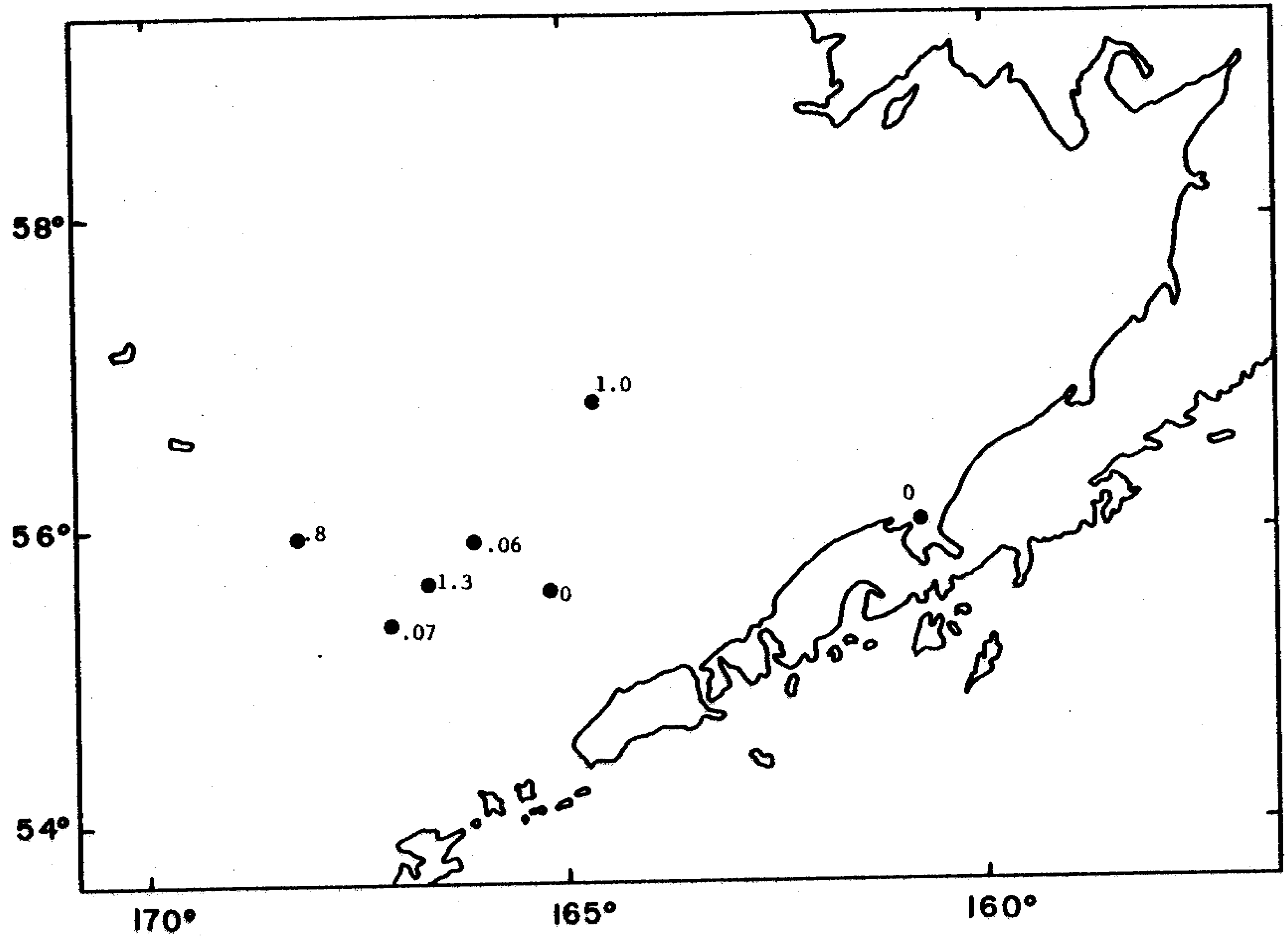

Figure 12. Methane production rates in mls x m^{-2} x day^{-1} for top 10 cm from August 1980 cruise.

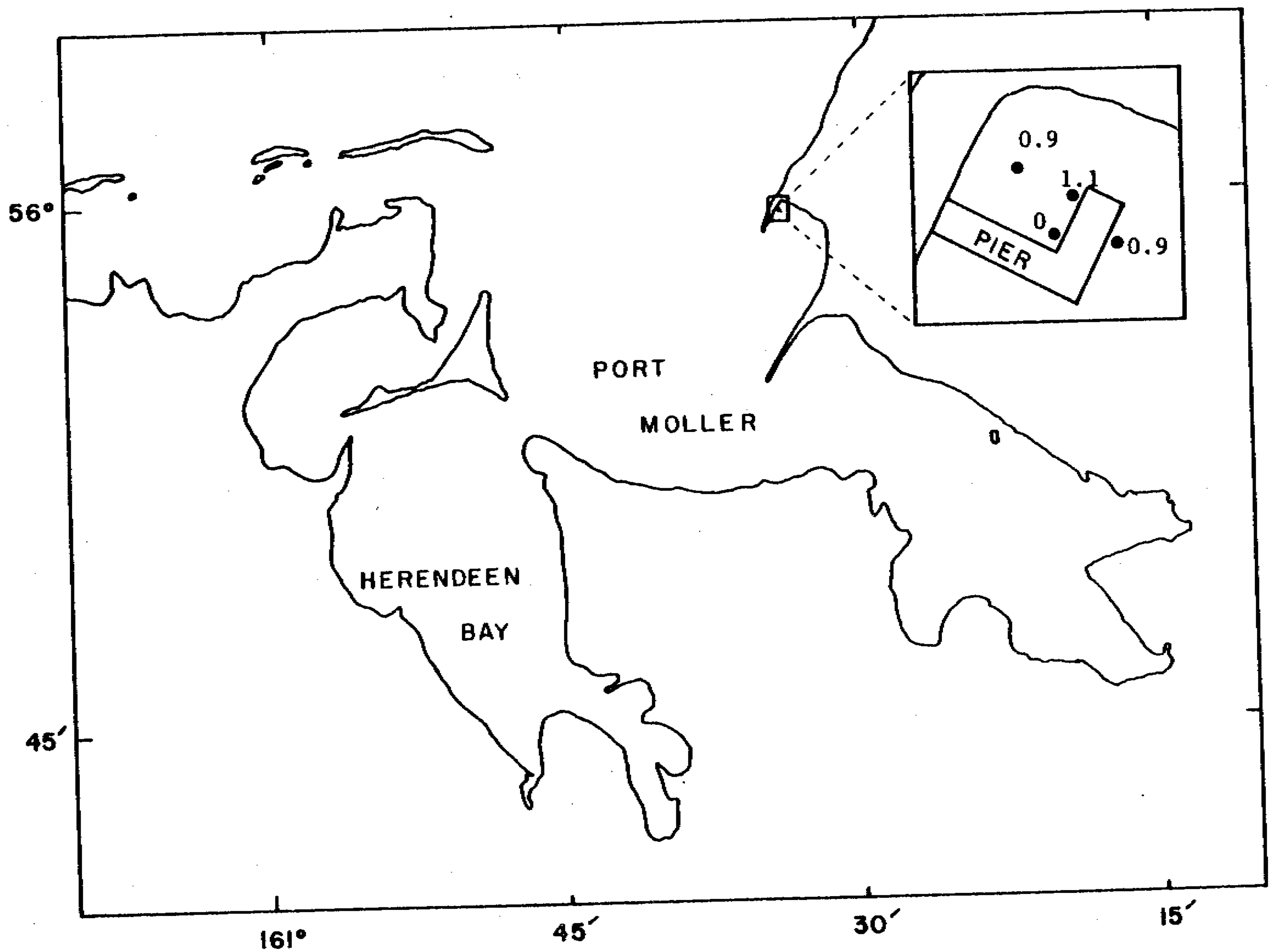

Figure 13. Methane production rates in mls x m^{-2} x day^{-1} for top 10 cm in Port Moller from August 1980 cruise.

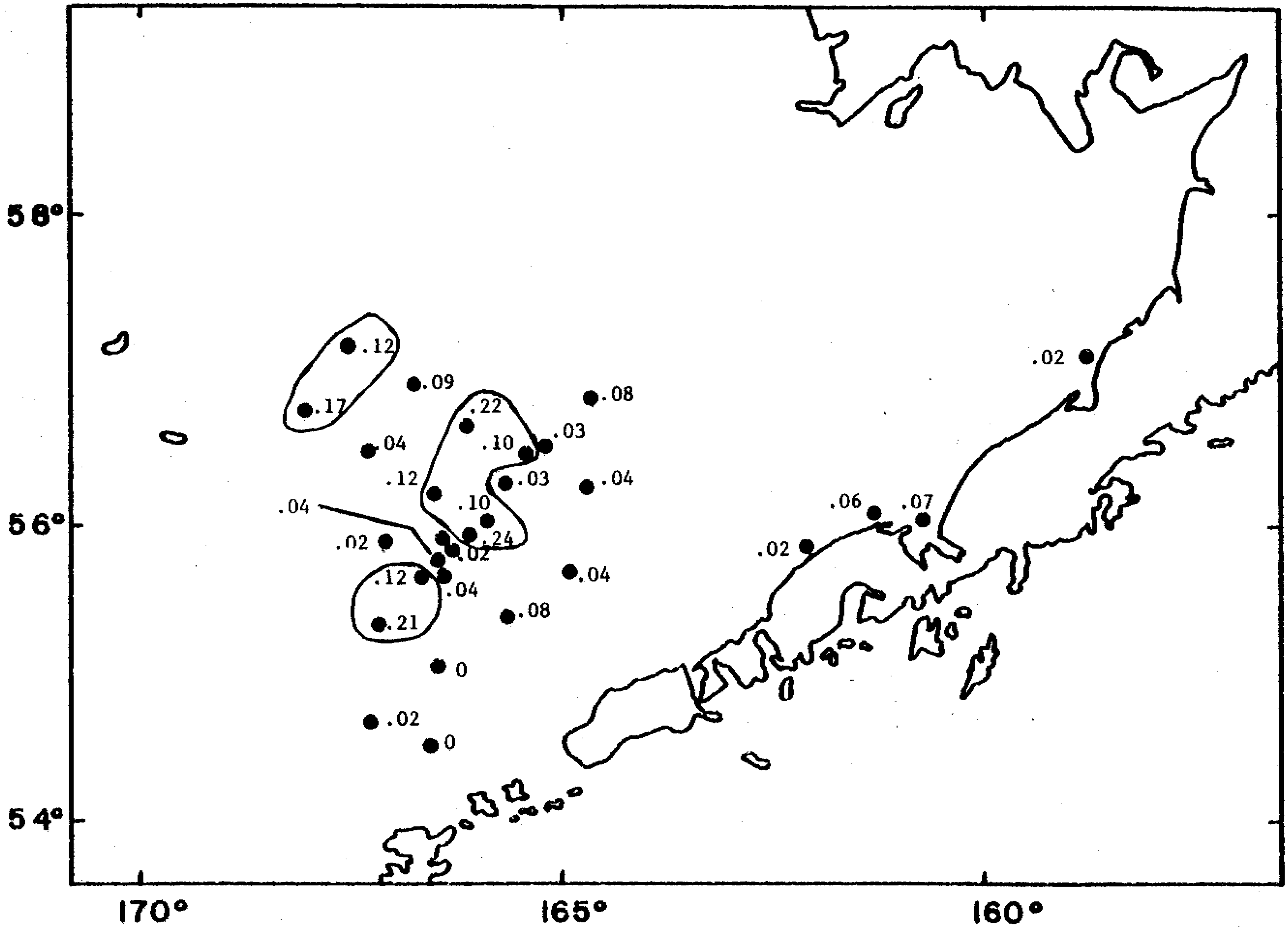

Figure 14. Methane production rates in mls x m^{-2} x day^{-1} observed in top 10 cm of sediment from January, 1981 cruise (excluding Port Moller).

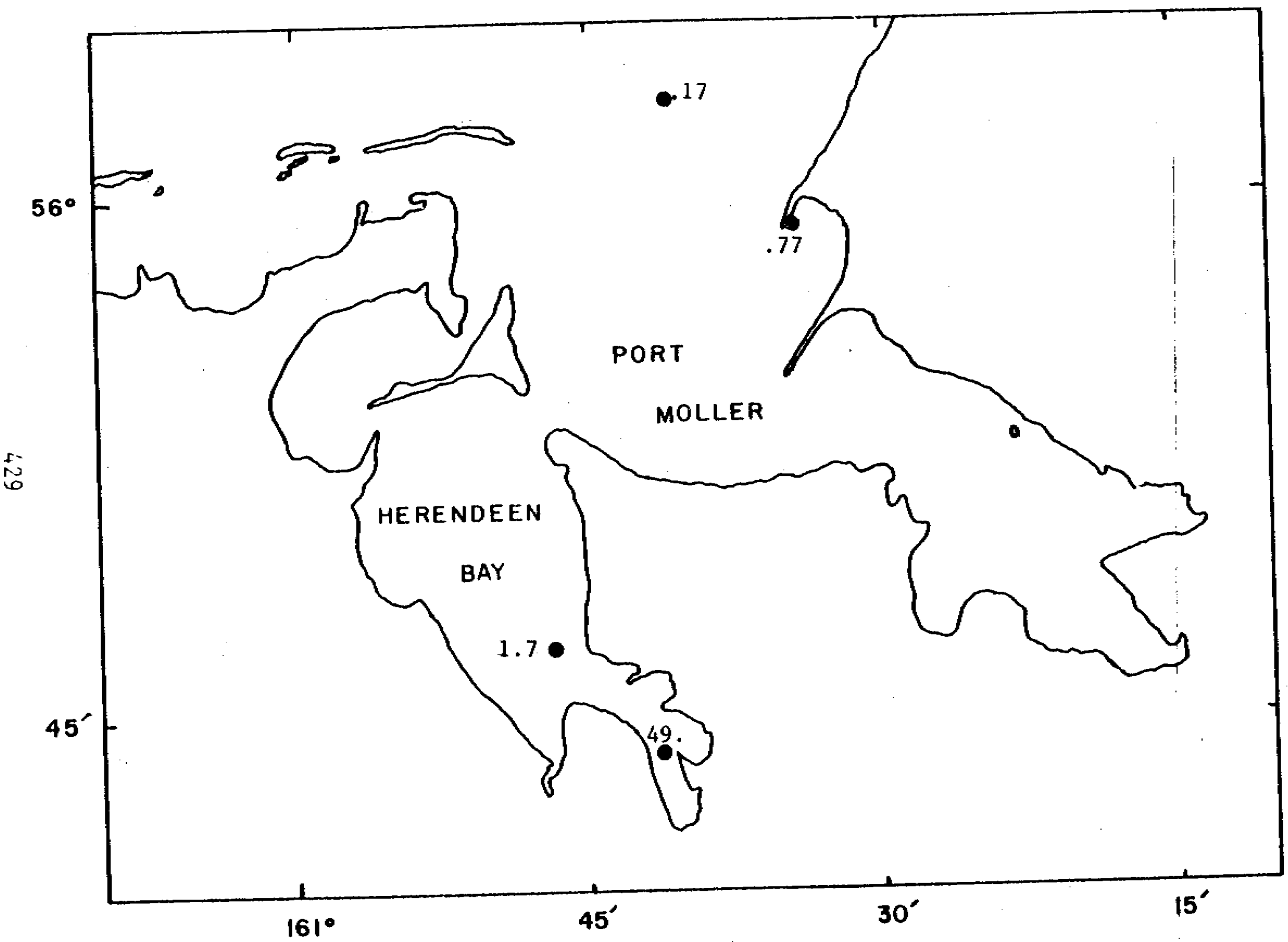

Figure 15. Methane production rates in mls x m^{-2} x day^{-1} observed in top 10 cm of sediment during January 1981 cruise.

Table 2. Methane production rates in 7 sediment samples collected at the same locations during both cruises. The units are ml x m^{-2} x day^{-1}. These values were calculated assuming an active methane production depth of 10 cm.

Location	August	January
PL14	1.0	0.8
PL8	0.6	1.0
PL6	1.3	1.2
PL4	0.4	2.1
SG7/SG26	0	0.04
NA40	0	0.07
Cannery Pier	1.1	0.8
Mean (all samples)	0.6	0.9

With the exception of the sediments collected at station PL4, there is good agreement between the rates observed during the two cruises. This shows that this technique produces methanogenesis rates which are reproducible from one sampling period to the next. The observed rates can thus be considered internally consistant. When a linear regression analysis is performed on these data, the correlation coefficient was high when the PL4 data are omitted from the analysis ($r = 0.9$; $r^2 = 0.8$; $p = 0.01$). The difference in the mean values observed between the two sets of data is not statistically significant.

During the January cruise, the cores were taken with a Pamatmat multiple coring device (method #3). Cores were taken at four locations along the PROBES line (PL stations). The rates observed using this method were approximately 2 orders of magnitude lower than those observed at the same location as measured using method #2 (Table 3).

Table 3. Comparison of methane production rates as measured using methods #2 and #3. The units used in both sets of data is µl x m^{-2} x day^{-1}

Location	Method #2	Method #3
PL6	120	0
PL8	240	0.15
PL10	30	0.14
PL12	30	0.16

During the August cruise, methane production rates were measured in 19 sediment samples using method #1 (radioactive tracers). No methane production was observed in any of the samples tested even though we know that some of these sediments were producing methane as determined by method #2.

C. Relative microbial activity

During both cruises, we measured relative microbial activity in water samples using ^{14}C labeled glutamic acid. The trends observed in relative microbial activity paralleled those observed in the methane oxidation data (Figs. 16-21). In the North Aleutian Shelf area, the level of microbial activity in the offshore waters was lower than that observed in the waters collected from inshore locations. During the August cruise, the mean uptake rate in the inshore waters and offshore waters were 7.7 and 4.0 ng x liter^{-1} x hr^{-1} respectively in the surface waters and 81 and 10 ng x liter^{-1} x hr^{-1} respectively in the bottom waters. The level of significance for these differences was $p = 0.07$ in the surface waters and $p = 0.12$ in the bottom waters. In January, the same trend was noted. The mean uptake rates in the inshore and offshore waters were 10 and 1.5 ng x liter^{-1} x hr^{-1} respectively for surface waters and 42 and 7.4 respectively for the bottom waters. The level of significance for these differences was $p = 0.01$ in the surface waters and $p = 0.11$ in the bottom waters.

There was also a pattern in the microbial activity in the bottom vs. the activity in the surface water samples. During the August cruise, the mean uptake rates in bottom and surface samples

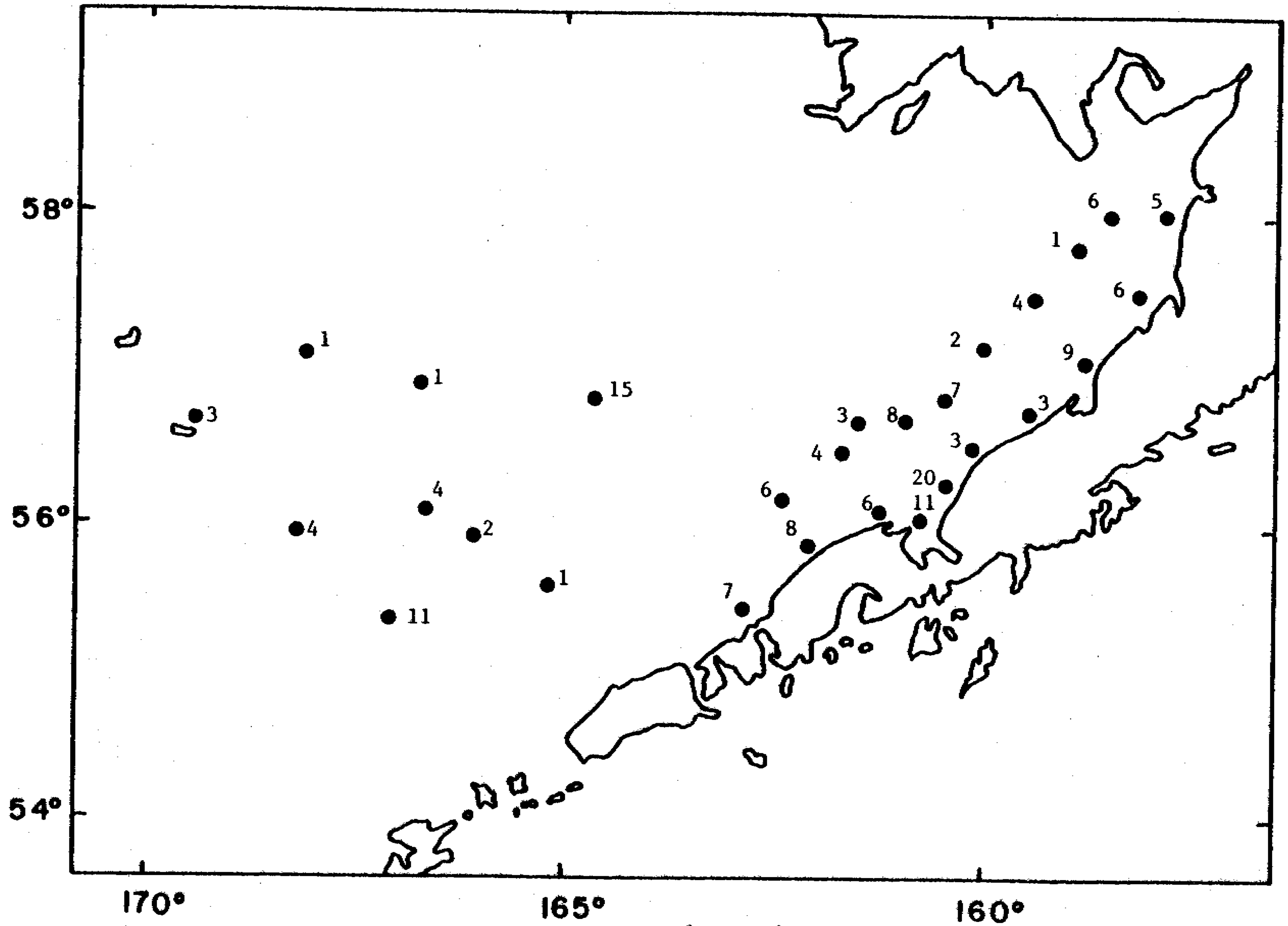

Figure 16. Glutamate uptake rates in ng x liter^{-1} x hr^{-1} in surface water samples observed during the August, 1980 cruise.

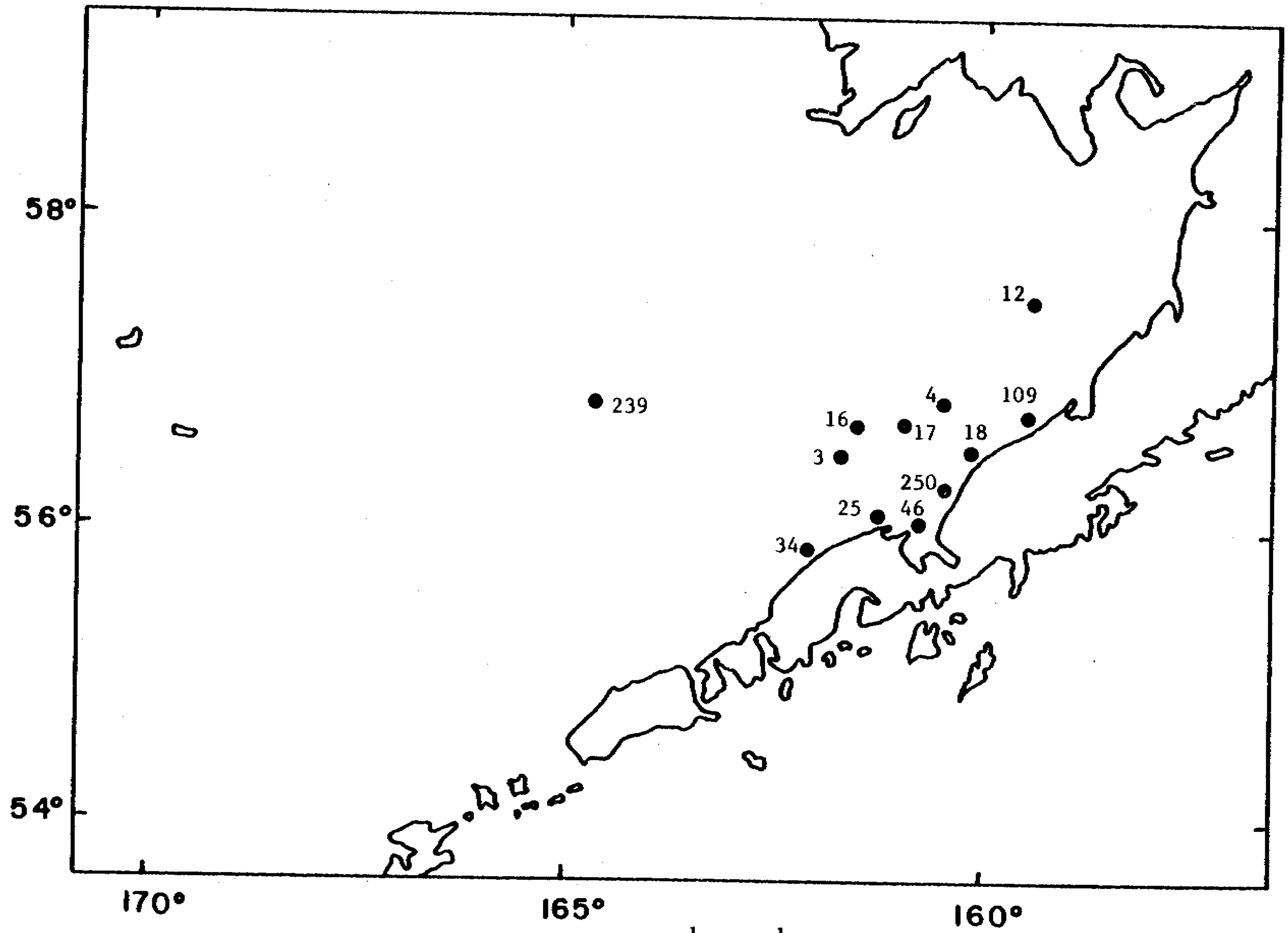

Figure 17. Glutamate uptake rates in ng x liter^{-1} x hr^{-1} in bottom water samples observed during the August, 1980 cruise.

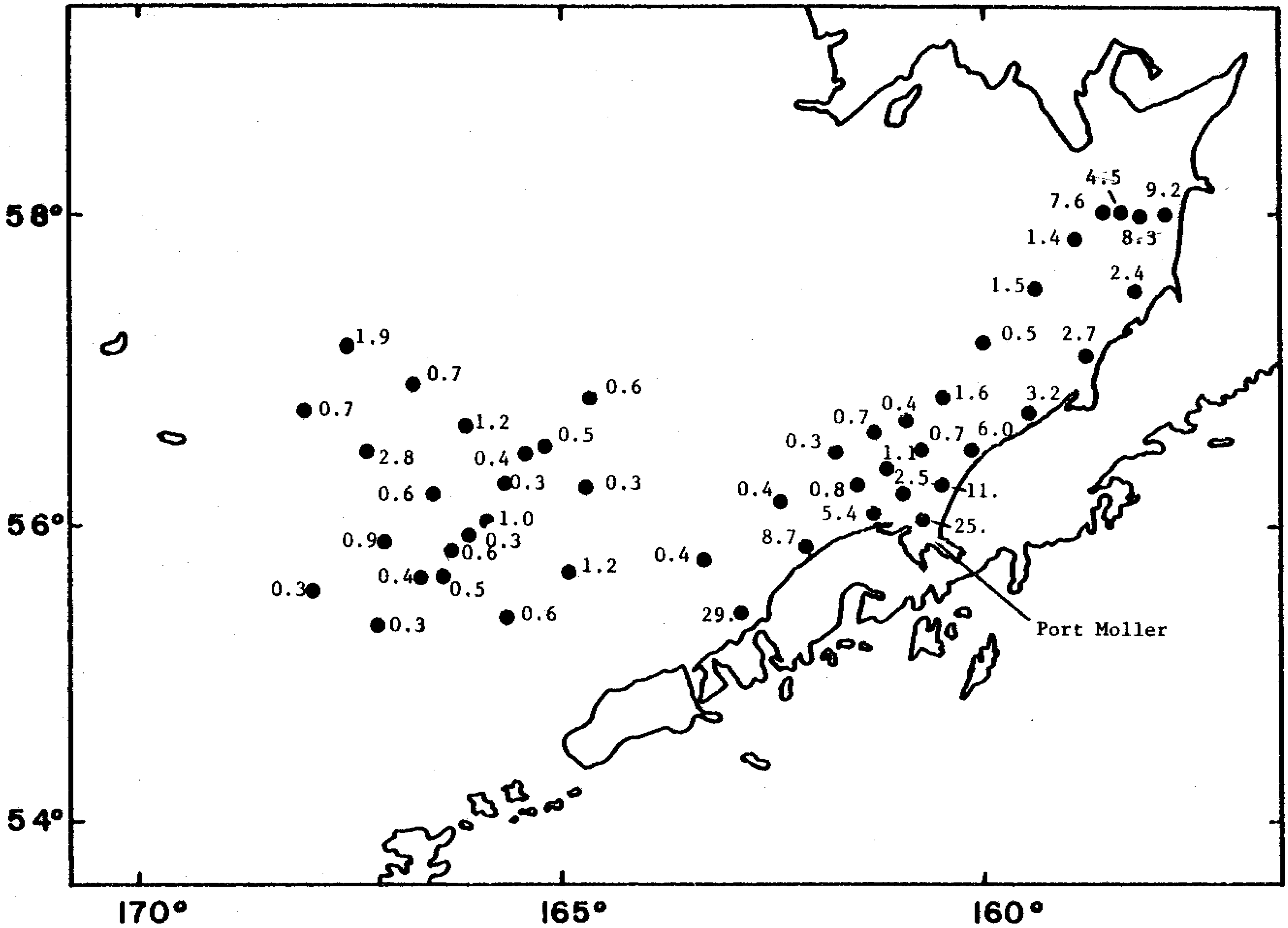

Figure 18. Glutamate uptake rates in ngrams x liter^{-1} x hr^{-1} from surface water samples from the January, 1981 cruise.

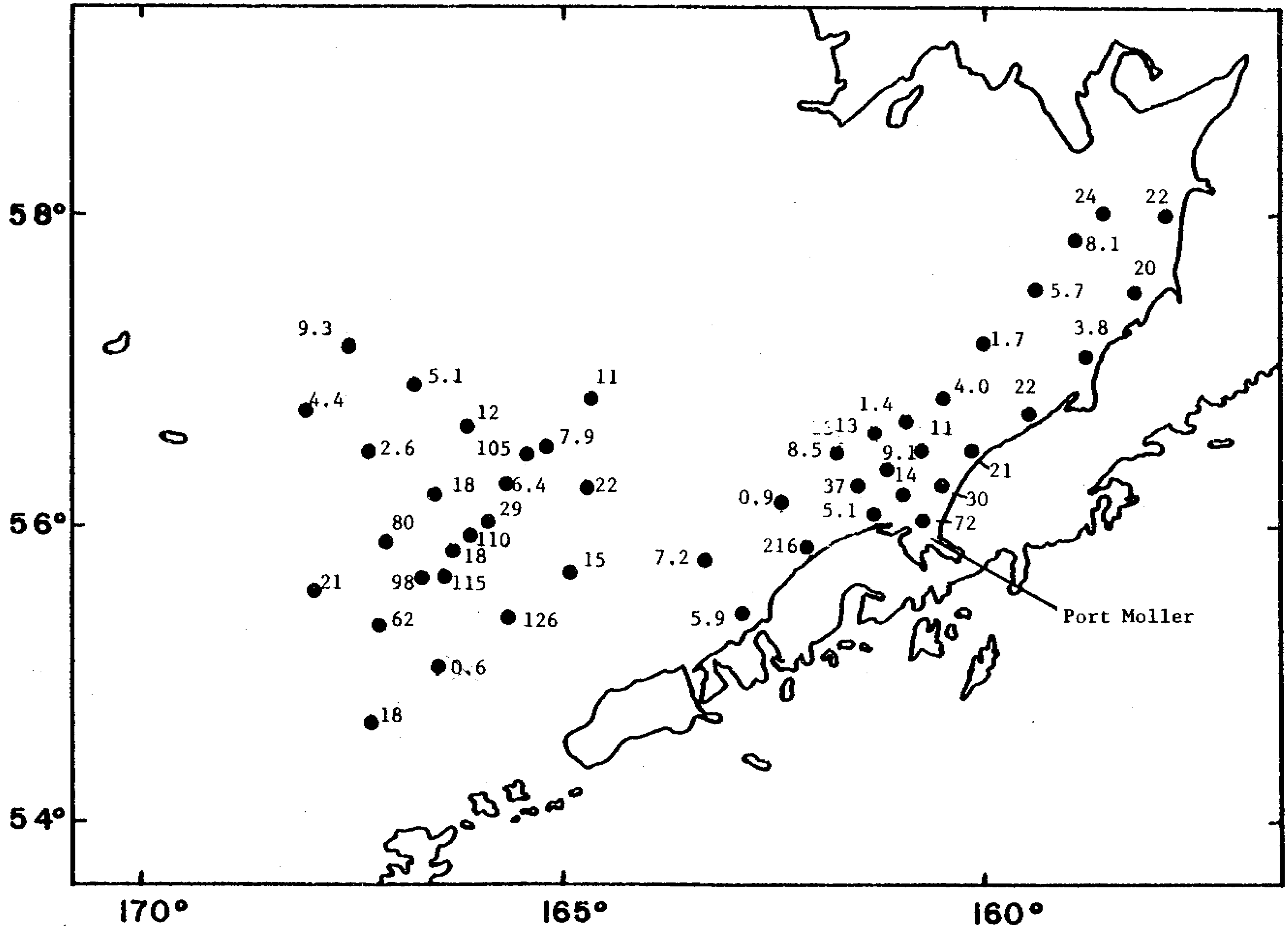

Figure 19. Glutamate uptake rates in ngrams x liter^{-1} x hr^{-1} from bottom water samples from the January, 1981 cruise.

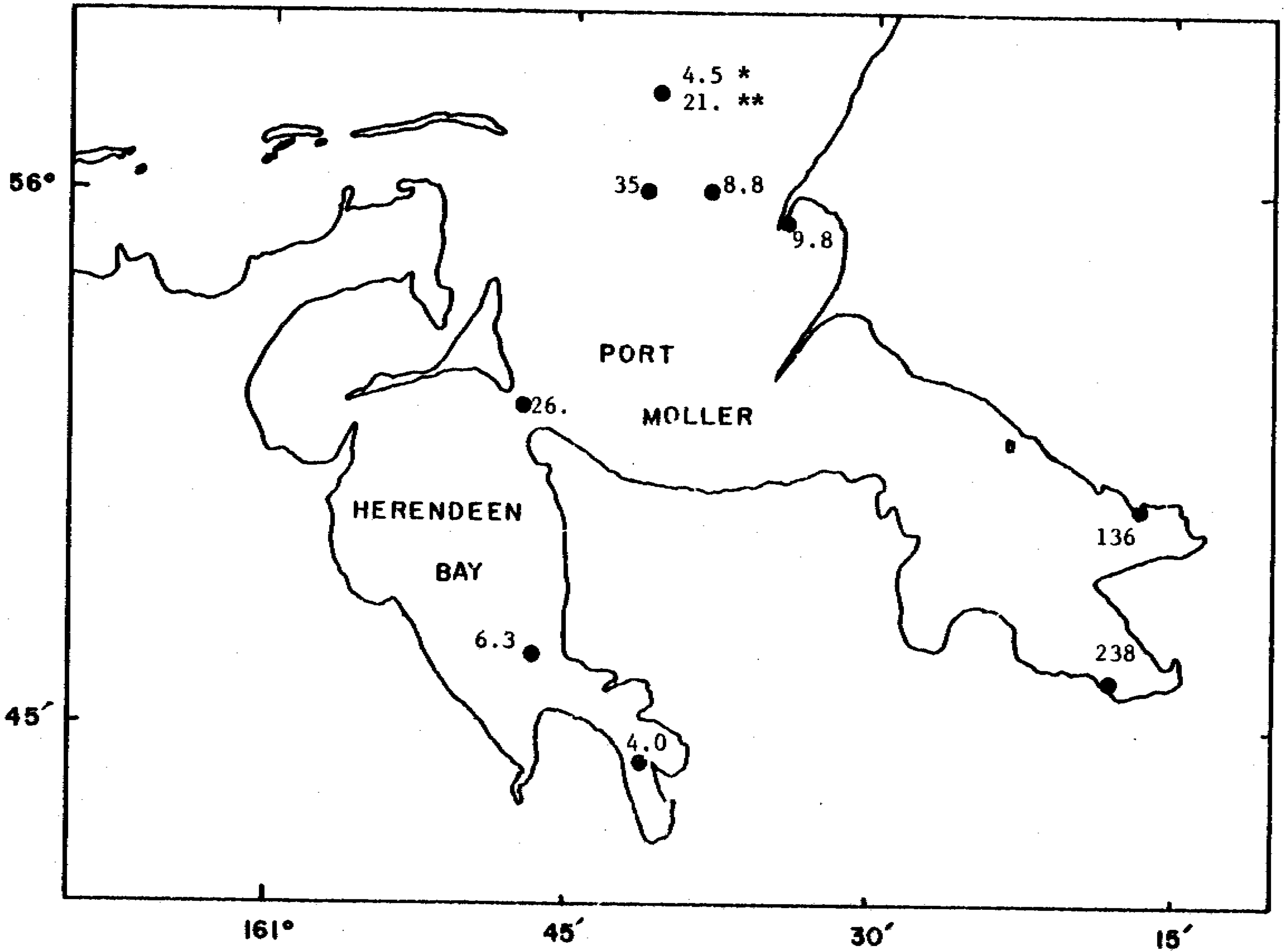

Figure 20. Glutamate uptake rates in ngrams x liter^{-1} x hr^{-1} from surface waters in Port Moller during the January, 1981 cruise. * Denotes rate at high tide, ** rate at low tide.

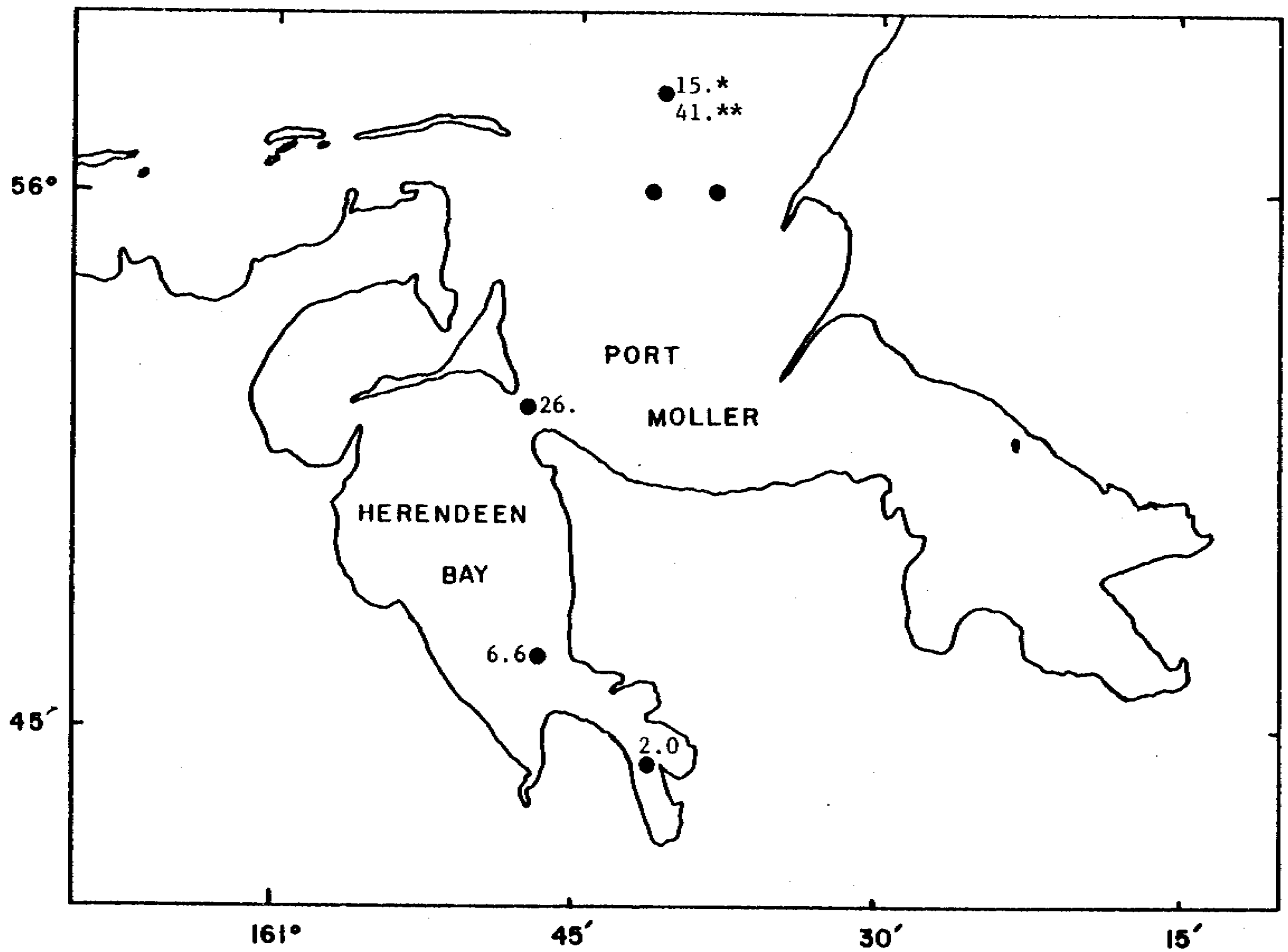

Figure 21. Glutamate uptake rates in ngrams x liter^{-1} x hr^{-1} from bottom waters in Port Moller during the January, 1981 cruise. * Denotes rate at high tide, ** rate at low tide.

that were collected at the same locations were compared. The mean rates for surface and bottom waters were 8 and 65 ng x $liter^{-1}$ x hr^{-1} ($p = 0.04$). During the January cruise, the comparable rates were 3 and 29 ng x $liter^{-1}$ x hr^{-1} ($p = 0.0002$).

As was the case in the methane oxidation data, the rates were higher in waters collected during the August cruise than those observed during the January cruise. In January, the mean surface water rate decreased by 63% and the bottom water rate decreased by 55%.

The microbial activities observed in Port Moller and Herendeen Bay were essentially the same as the rates observed in the waters just offshore from Port Moller (Figs. 20 and 21). The highest rates measured in this area were observed in the waters collected at the head of Port Moller.

VII. Discussion

A. Methane Oxidation

The main reason for determining the methane oxidation rates was to provide the chemists with the data they required to estimate biological methane sinks in these two lease areas. At this point, the chemists are still studying the results of our studies to determine if methane oxidation by microorganisms is a significant factor relative to the other terms in their transport model. The initial analyses have indicated that in the North Aleutian Shelf area, methane oxidation is not a significant term when analyzing transport processes in the area near Port Moller; however, it does appear to be an important factor when estimating these processes to the east of Port Moller where the concentrations of methane are lower. The methane oxidation rates also appear to be an important term in analyzing transport processes in the St. George Basin where the rate of advection is lower than that found in the North Aleutian Shelf area.

The methane oxidation data collected during both NASTE cruises is the first such data collected in marine environment using ^{14}C labeled methane. The resulting data appears to be internally consistent and it followed patterns which were reproducible during both cruises. Our conclusion is that this method has allowed us to determine rates which reflect the _in situ_ rates of methane oxidation when interpreted in light of the known methane concentrations.

Essentially all samples studied showed first order kinetics. When linear regression analyses were conducted on the observed uptake rates at various concentrations in a given water sample, the r value was 0.95 or greater in most cases. From these analyses, equations were generated which can be used by the chemists to calculate actual _in situ_ methane oxidation rates from known methane concentrations.

Before we initiated the actual field observations, it was assumed that the methane oxidation rates should show a high correlation with methane concentrations. When one compares the distribution of methane throughout the study area, the areas where high concentrations of methane have been observed are also the areas where we observed the highest rates of methane oxidation. The highest methane concentrations observed during either cruise was observed in the heads of Port Moller and Herendeen Bay in the samples collected during the January cruise (see Dr. Cline's annual report). We observed high rates of methane oxidation in this same area (Fig. 10). In the North Aleutian

Shelf area, the highest methane concentrations were observed near Port Moller and along the coast to the east of Port Moller with the highest concentrations in the nearshore stations. Again, this parallels the pattern observed in methane oxidation rates.

During the January cruise, we conducted a time study of methane oxidation rates over one tide cycle. We observed a much higher methane oxidation rate in the water that was coming out of Port Moller on an outgoing tide than in water that was flooding into this embayment (Figs. 10 and 11). This same trend was observed in the methane concentrations (higher concentrations on the ebbing tide [Mr. Chuck Katz, personnel communication]).

In St. George Basin, the highest methane concentrations were found in the bottom waters. The surface water methane concentrations were generally lower. The highest methane concentrations were observed in the vicinity of station PL6 and SG28. This is similar to the pattern of methane oxidation rates found in this region. We found relatively low methane oxidation rates in the surface waters during both cruises (Figs. 5 and 7). The methane oxidation rates were consistantly higher in the bottom waters with the highest rates observed near the area where the highest methane concentrations were observed (Figs. 6 and 8). When these data are compared seasonally, there is also good agreement. The methane concentration in the bottom waters of the St. George Basin was reduced approximately 50% in January relative to the higher values observed in August. The same trend was also observed in methane oxidation rates. On a large scale, these two sets of data appear to be in good agreement.

To check the validity of this correlation, we conducted a statistical analysis of linear regression between these two variables and found that when the data were compared on a sample by sample basis, there was essentially no correlation. The correlation coefficient (r) between methane oxidation rates and methane concentration was 0.14 for the August data and 0.70 for the January data. After the last cruise in this series, we will conduct a more exhaustive statistical analysis on all of the data but at this point, there does not appear to be a strong linear relationship between these two variables. This suggests to us that once a set of methane concentration data has been collected in a given area, one cannot predict methane oxidation rates from the methane concentrations present. Thus, actual observations must be made in each water sample in which methane oxidation rates must be determined.

During these cruises, we also conducted experiments to determine relative microbial activity in most water samples collected. These measurements were made using ^{14}C labeled glutamic acid. When a linear regression analysis was conducted on this data set and the methane oxidation data, the correlations were higher than that observed with methane concentrations. In the August data set, $r = 0.6$ ($p = 0.00005$) and in the January data set $r = 0.9$ ($p = 5 \times 10^{-10}$). Thus, the degree to which the variation in methane oxidation rates can be accounted for by variations in glutamate uptake rates is 36% and 81% for the August and January cruises respectively.

When the microbial activity data is analyzed in light of the patterns observed in the methane oxidation data, clear correlations are apparent. This is true of geographical and seasonal trends in both lease areas. Both data sets showed lower rates in surface than in the bottom waters and both sets of data showed similar trends relative to tidal fluxes at the mouth of Port Moller (station PM3 data in January).

Upon close inspection, there are some areas in which these two data sets do not match up. In the water samples taken in Herendeen Bay, the methane oxidation rates were some of the highest observed anywhere (Figs. 10 and 11) yet the microbial activity measured in the same samples was not unusually high for the Port Moller area (Figs. 20 and 21). The reduction in methane oxidation rates in surface waters in January was 91% as contrasted with a reduction of 63% in microbial activity in the same waters. With these few exceptions the correlation seems very tight between methane oxidation and microbial activity.

At the present time, we have no direct evidence which explains this correlation. The method used to determine microbial activity (glutamate uptake), measures the activity of heterotrophic bacteria (those bacteria that obtain both energy and carbon from organic sources). The bacteria that are oxidizing methane are evidently chemoautotrophic organisms that obtain energy from methane but do not utilize the carbon. During our experiments, we measured both the incorporation of methane into cells and the respiration of methane to CO_2. With the exception of samples collected in Port Moller, the percent of label (from the methane) that became associated with cell material was less than 5% and in most cases was less than 2% of the total methane taken up by the cells. Since these organisms obtain their carbon from CO_2, it is likely that the small amount of label that became associated with the cells did not result from the direct incorporation of methane carbon into cell material but the incorporation of CO_2 that originated from the labeled methane. This observation supports the hypothesis that the methane oxidizing bacteria in the study area are indeed chemoautotrophs. This is in contrast with the results of a study conducted by Panganiban et al. (1979) in which methane oxidation in lake water samples was observed. They reported that under aerobic conditions, 30 to 60% of the methane carbon became associated with cell material. In these waters the methane oxidizing bacteria appear to function as heterotrophs rather than as chemoautotrophs.

In a study of methane oxidation in a pure culture, Patel et al. (1978) showed that Methylobacterium organophilum was capable of oxidizing a broad spectrum of organic substrates including organic acids. It is therefore possible to have changes in methane oxidizing activity in response to changes in a number of organic molecules. In addition, the apparent methane oxidation rates could be altered by competitive inhibition by substrates other than methane that might be present in the sample being tested.

The simplest explanation for the correlation between methane oxidation and glutamate uptake rates is that the concentration and/or activities of the methane oxidizers is proportional to the general heterotrophic microbial population which is reflected in the uptake of glutamate.

B. Methanogenesis

The main reason for the methanogenesis study was to provide the chemists with the methane source term for their transport model. From the concentration of methane observed in the water column, the chemists can predict the approximate input of methane into the water column that would be required to maintain the observed gradient. Although the data is still in the preliminary analytical stages, it appears that the rates of methane production in the sediments of Port Moller and the St. George Basin are very close to the estimated input of methane into the water column from the sediments in those areas.

In the North Aleutian Shelf area, the major source of methane appears to be Port Moller. During the August cruise, high rates of methane production were observed near the cannery pier at Port Moller which suggested that at least some of the methane being produced in Port Moller originated from this source. The methane production was undoubtedly the result of the high organic content of the effluent from the fish packing operation located there.

During the January cruise, we were able to obtain sediment samples from the head of Herendeen Bay. The methane production rate in one of the sediments was much greater than that observed anywhere else. The very high methane concentrations observed in the head waters of Port Moller and Herendeen Bay also suggests that these areas may be the main source of methane for the NAS area. The extensive sampling that is planned for the next NASTE cruise will provide us more detailed information about the exact contribution of these highly productive areas in Port Moller. Analyses of sediments found outside of Port Moller showed that very little, if any, methane input originating from outside Port Moller.

In the St. George Basin lease area, elevated methane production rates were observed in the three areas shown in Fig. 14. The largest area was to the north of the location where the highest methane concentrations in the water column were observed. Elevated methane production rates were also observed in the sediments collected from stations PL4 and PL6 which are both close to SG28, the station where the highest methane concentrations were observed during the January cruise. Although the average methane production rate observed in the St. George Basin was within a factor of 2 of being the rate required to sustain the methane concentration observed in the water column, it is not known at this time if the location of the major methane production from the sediments can account for the distribution patterns in the water column. This will not be known until the data is further analyzed by the chemists.

When the methane production rates measured using method #2 (GC analysis of the headspace) were compared to those measured using method #3 (GC analysis of water over intact cores), there was a large difference in the observed rates. The reason for this discrepancy is not known. There are several factors that might account for this difference. Since the core tubes were incubated for up to one week, there is a possibility that some of the methane that had been produced was lost by diffusion through the core tube, the stoppers, or through small gas bubbles trapped within the water over the cores.

There is some evidence that this might have occurred; however, it is unlikely that this would account for the large difference observed in these two data sets. It is also possible that methane was being produced at the rate indicated by method 2 but that methane oxidation was removing the methane at approximately the same rate thus resulting in a very low net methane production rate from the sediments. The methane oxidation rates observed in sediments suggests that this is not the case. It is also possible that the sample manipulation required under method 2 caused erroneously high values to be observed. This seems unlikely since this should have had the opposite effect.

The best way of determining which rate is correct (that measured by method 2 or 3) is to determine the methane gradient in the interstitial waters in St. George Basin sediments. These measurements will be made during the May NASTE cruise.

VIII. Conclusions

The methane oxidation and methanogenesis data that we have collected in the St. George Basin and North Aleutian Shelf lease areas during the NASTE cruises have been useful in determining the biological sources and sinks of methane in these areas. The implications of these observations relative to the problem of transport processes in these lease areas is still being analyzed by the chemists at PMEL. The conclusions that can be drawn from these data at this point in the analysis will be discussed in Dr. Cline's annual report for RU #153.

IX. Needs for Further Study

A. The recent Bering Sea synthesis meetings conducted by NOAA have shown that very little information is available concerning the microbiology of the Bering Sea (Eastern Bering Sea Shelf: Oceanography and Resources - in press). During the same series of meetings, it was shown that the St. Georges Basin is one of the most productive and important fisheries in Alaska. In a recent article by Iverson et al. (1979), it was concluded that in the very productive middle shelf region of the St. Georges Basin, most of the food available to higher trophic levels was routed through the detrital food chain. If significant quantities of crude oil became incorporated into the sediments of this region as a result of crude oil production and transport, it is quite likely that this fishery will be impacted.

During the Bering Sea Ecological Processes Workshop held in July 1980, it was recommended that one of the objectives of future studies in the southern Bering Sea should be to determine the answer to the question "is the growth of benthic crab food a direct function of detrital flux, and if so, what is the rate of conversion of detrital material to benthic food?" This is an objective that cannot be fulfilled without knowledge of the microbial component of that food chain since it forms the basis for it.

We strongly recommend that a study of microbial function, as it relates to nutrient recycling, be conducted in the St. Georges Basin. At this time, the importance of the detrital food chain in this region can only be estimated by indirect means. A study of this nature would provide more direct evidence for this relationship, if it exists. It is also quite likely that microbial processes provide much of the inorganic nutrients required for the high rates of primary productivity in the region. The presence of high concentrations of inorganic nutrients in the photic zone is caused by wind driven currents that mix the upper portion of the water column with the nutrient rich bottom layers. Since there is very low advective flow in this region, it is quite likely that most inorganic nutrients found in these deeper waters have been generated locally by microbial mineralization in the sediments. This is also needs to be documented.

Our effects studies have shown that crude oil interferes with both the detrital food chain and mineralization processes. Although these effects have been documented elsewhere (Beaufort Sea and Cook Inlet), these effects need to be documented for this region as well. This study could be conducted by collecting sediments from the St. Georges Basin near the end of a cruise and transporting them to Oregon State University for analysis. Once the sediments were taken to OSU, a time series experiment could be conducted using various concentrations of crude oil. By measuring key variables for periods up to one month, we would be able to document long-term effects in these sediments.

X. Acknowledgements

We would like to thank Drs. Herbert Curl, Jr. and James Schumacher for their assistance as chief scientists during the NASTE cruises. In addition, we would like to thank Penny Amy, Bill Broich, Bruce Caldwell, and Lois Killewich for their technical assistance during these investigations. We would also like to thank the personnel from PMEL and the crew of the Surveyor for their help during this investigation.

XI. Literature Cited

Griffiths, R. P., S. S. Hayasaka, T. M. McNamara, and R. Y. Morita. 1978. Relative microbial activity and bacterial concentrations in water and sediment samples taken in the Beaufort Sea. Can. J. Microbiol. 24: 1217-1226.

Iverson, R. L., L. K. Coachman, R. T. Cooney, T. S. English, J. J. Goering, G. T. Hunt, Jr., M. C. Macauley, C. P. McRoy, W. S. Reeburg, and T. E. Whitledge. 1979. pp. 437-466. In R. J. Livingston (ed.) Ecological Processes in Coastal and Marine Systems. Plenum Publishing Corp.

Panganiban, A. T., Jr., T. E. Patt, W. Hart, and R. S. Hanson. 1979. Oxidation of methane in the absence of oxygen in lake water samples. Appl. Environ. Microbiol. 37:303-309.

Patel, R. N., C. T. Hou, and A. Felix. 1978. Microbial oxidation of methane and methanol: isolation of methane-utilizing bacteria and characterization of a facultative methane-utilizing isolate. J. Bacterial. 136:353-358.

SAI/NW-81-595-08

FIRST ANNUAL REPORT

Research Unit #600
Reporting Period: 1 May 1980
31 May 1981

Number of Pages: 43

COASTAL OCEANOGRAPHY OF THE NORTHEAST GULF OF ALASKA

31 May 1981

R.D. Muench
P.R. Temple
J.T. Gunn

Science Applications, Inc.
13400B Northrup Way #36
Bellevue, Washington 98005
(206) 747-7152

TABLE OF CONTENTS

LIST OF FIGURES

LIST OF FIGURES (continued)

LIST OF FIGURES (continued)

LIST OF TABLES

I. SUMMARY OF OBJECTIVES, CONCLUSIONS AND IMPLICATIONS WITH RESPECT TO OCS OIL AND GAS DEVELOPMENT

The general objectives of this program are to determine the nature of advective and diffusive processes in the near-coastal region in the northeast Gulf of Alaska and to relate these processes to potential pollution problems due to OCS petroleum development. At the time of preparation of this report, field data from the program are not yet completely processed and analyzed. It is possible, however, to present the following preliminary conclusions.

- Circulation in the coastal band (from the coastline to about 10 km offshore) was bimodal and along-shore in the autumn (October-November 1980) period. Flow was along-shore to the southeast about 40 percent of the time and along-shore to the northwest about 60 percent of the time.

- Occurrence of a strong wind-driven longshore current event during the autumn field program suggested that such events, which can have currents of 50 cm/sec or greater to the northwest, may be common during the winter period of intense storm activity.

- Longshore water movement in the surf zone (littoral current) was highly dependent upon the wavefield incident upon the shoreline. In autumn, water moved to the northwest in response to southeast swell generated by winter storm activity. The following spring (March-April) the wave activity was less, and the longshore currents were bimodal. Seabed drifter studies indicated that bottom water movement in and just outside the surf zone was shoreward.

- Temperature/salinity analyses indicated that local freshwater input along the coastline was mostly constrained to a narrow (less than about 10 km) coastal band which occupied the upper 10-20 m of the water column.

- The generally well-defined northwestward flow observed farther seaward off Yakutat by previous programs was not in evidence at the near-shore locations from which observations were obtained in autumn 1980. Some of the current records showed a great deal of fluctuating activity due, probably, to the complex regional bottom topography.

With respect to pollutants, our preliminary results suggest that flushing from the near-shore region by longshore flow may be ineffective due to small mean flows. During a wind-driven flow event, such flushing would be more likely. Pollutants deposited in and just seaward of the surf zone would move somewhat along-shore in response to littoral currents, the direction of motion depending upon the wavefield at the time of the spill. Pollutants entrained into bottom sediments near the surf zone would, if suspended by wave action, probably be transported onto the beach as were the seabed drifters. Additional analyses of our data will further clarify the relations between circulation, local winds, and freshwater input.

II. INTRODUCTION

A. General Nature and Scope of Study

The general objective of this work unit is to relate oceanic advective and diffusive processes to potential pollution problems due to OCS petroleum development. This is being accomplished through field activities including moored current measurements and water mass analysis using temperature and salinity observations. The region being considered includes the northeast Gulf of Alaska (NEGOA) continental shelf east from about the longitude of Yakutat, Alaska to Cross Sound and extends to the continental shelf break some 100 km offshore (Figure 1).

B. Specific Objectives

1. Estimate the mean baroclinic circulation pattern in the NEGOA area during the two extreme field seasons using dynamic topographies derived from the temperature and salinity data.
2. Obtain temperature and salinity (hence derived density) data to serve as input to the Galt diagnostic model.
3. Obtain mid-shelf and near-shore (less than 10 km) current data from taut-wire moorings for estimation of structure, intensity, and seasonal variability of the near-shore currents with particular emphasis upon the near-shore baroclinic current driven by coastal freshwater input.
4. Estimate near-shore currents and lateral dispersion rates using ship-deployed radar-tracked drogued buoys.
5. Estimate longshore wave-induced transport (littoral transport) in the surf zone using aerially-deployed seabed drifters and engineering equations coupled with observed wave parameters.
6. Construct a time history of the local wind field during the field experiments using winds observed along the coast, FNWC-computed geostrophic winds, and inspection of surface atmospheric pressure charts.
7. Compare observed temperature, salinity, density, and current fields with those observed in the past to establish a context for the results in terms of whether or not any unusual conditions were present during the field study.
8. Compare extent of the freshwater plumes from Yakutat Bay and other local sources with the observed near-shore circulation, temperature and salinity fields.
9. Compare observed currents with the baroclinic field to estimate the relative importance of baroclinic driving forces.
10. Apply conventional wisdom, obtained from the open scientific literature, on shelf dynamic processes to data in order to increase general scientific understanding of shelf processes.

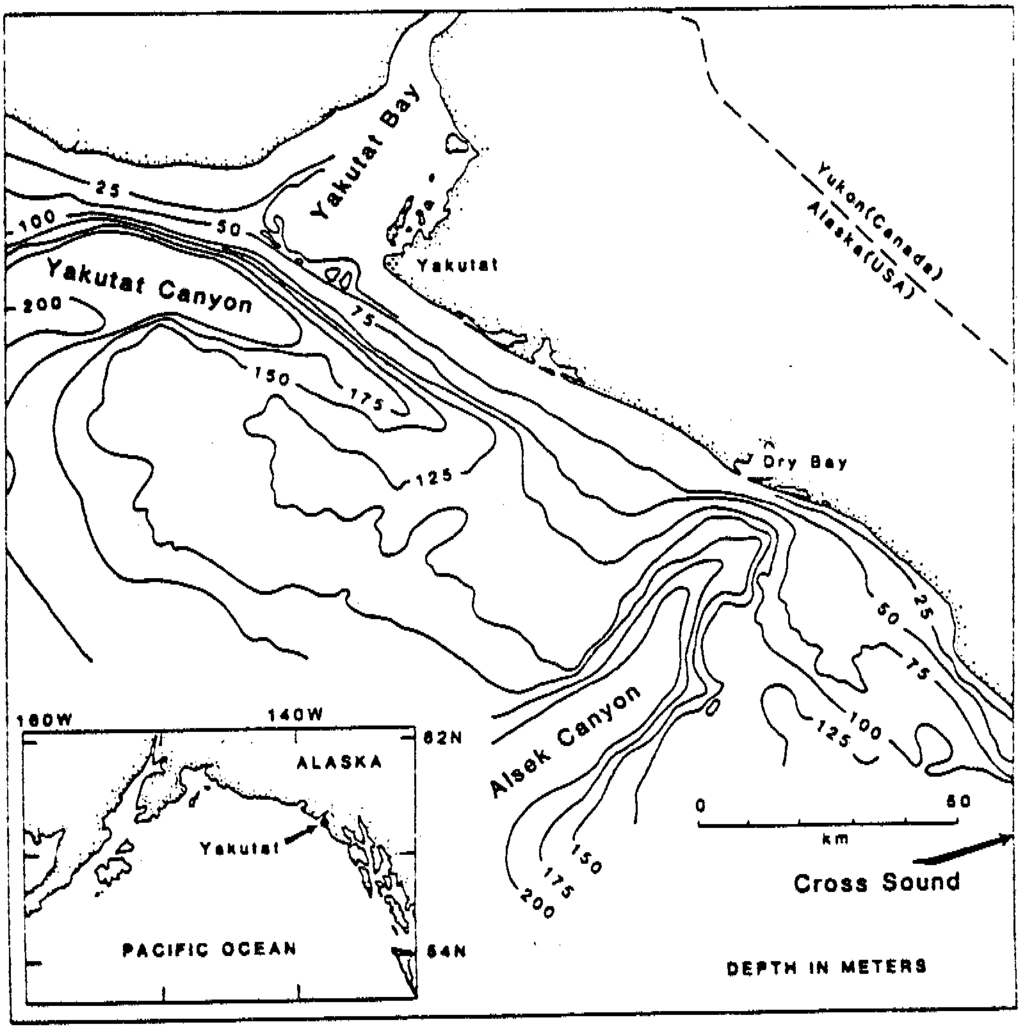

Figure 1. Geographical location of the study region in the northeast Gulf of Alaska.

11. Estimate anticipated trajectories of surface and near-surface pollutants under varying seasonal and climatological conditions, using available measurements from the mid-shelf, near-shore and surf zones.

C. Relevance to Problems of Petroleum Development

Two distinct environmental problems can accompany petroleum development in a marine region: catastrophic spills and chronic or long-term leakage. This research unit addresses both of these problems. The eventual effect of a catastrophic spill depends upon where the spilled oil goes, i.e. its trajectory, how long it takes to get there, and how much diffusion of oil occurs along the trajectory. This study will provide estimates of the fields of water motion which exert primary control over such trajectories and over diffusion processes along the trajectories. Oil introduced into the environment via long-term or chronic leakage is more likely to be dispersed throughout the water column and, possibly, scavenged by suspended particulate matter. The problem then becomes one of understanding net transport of suspended matter, a process related to advective and diffusive fields within the water column. Understanding of these processes requires an analysis of the velocity field and its driving mechanisms; this study addresses these latter points.

III. CURRENT STATE OF KNOWLEDGE

Prior to this study, little work had been accomplished within 50 km of the coast in the Yakutat-Cross Sound region. A synthesis of past work (Muench et al., 1979) indicates that the mesoscale offshore circulation and some limited aspects of shelf circulation to the northwest of Icy Bay have been investigated. The general flow in the offshelf Alaska Current is to the northwest, and a permanent anticyclonic eddy is located well off Icy Bay (Royer et al., 1979). The only near-shore observations of flow for this region occurred when one of the drogues used in the above study came within five miles of the coast to the west of Icy Bay (Royer et al., 1979); this drogue substantiated that flow was, at the time, northwesterly.

Studies of smaller length scales have been conducted in a region which had Icy Bay as the eastern boundary (Hayes, 1978; Hayes and Schumacher, 1976). These experiments began at least five miles seaward from the coast and continued out across the shelf break, and results demonstrated a broad diffuse westward flow roughly aligned with the isobaths. However, since 20 meters was the shallowest depth for a moored current meter, flow of the surface currents could only be inferred. This type of inference has the additional complication that seasonal variables such as fresh water runoff and wind may drastically alter the vertical water column structure (Royer, 1977). For instance, in the spring (about May) there is a minimum stratification while a maximum stratification is caused in the fall (about October) by the accumulation of fresh water runoff (Royer, 1979). This change in vertical density would be expected to induce changes in the surface currents, particularly near shore.

Field observations, carried out through the present study, of the near-shore (inside 10 km) Yakutat-Cross Sound region will yield new information in an area not previously studied. Sections VI-VIII of this report present preliminary conclusions of this work and update the above summary.

IV. STUDY AREA

The area addressed by this study lies on the northeast Gulf of Alaska continental shelf between Yakutat and Cross Sound (Figure 1). Emphasis is upon the near-shore region within about 10 km of the shoreline, though CTD station coverage extends to the shelf break.

The continental shelf in the study region has complex topography. It is cut by Yakutat Canyon, which extends northwest then seaward off Yakutat, and by the Alsek Canyon off Dry Bay (Figure 1); both of these canyons have maximum axial depths exceeding about 200 m, in distinction to the 125 m depths of the surrounding continental shelf region. The bottom slope is much steeper near the heads of these canyons than elsewhere on the shelf. Overall width of the shelf is about 100 km.

Regional meteorology is dominated by the interaction between the Aleutian atmospheric low pressure system and the North Pacific High. During winter, the Aleutian Low dominates, resulting in frequent storms and southeasterly winds. In summer the winds are weak and variable. Drainage winds, which can achieve high (but undocumented for this region) speeds, flow seaward from Yakutat Bay and Dry Bay during winter.

There are several ungauged rivers and small streams along the shoreline in the study area. Though the exact freshwater input is unknown, knowledge of the regional precipitation patterns suggests that there are two freshwater input peaks: one in autumn with the onset of winter storms and before it is cold enough so that precipitation falls mainly as snow, and a second in later spring with the onset of snow melting in the mountainous coastal regions.

V. SOURCES, METHODS AND RATIONALE OF DATA COLLECTION

Instrumentation, field and processing methods are identical in most cases to those used in previous OCSEAP investigations. These methods are documented in Annual Reports from OCSEAP Research Unit 138, in Muench and Schumacher (1979; 1980), and in numerous publications which have resulted from these studies. Where deviations from these methods are considered significant, they are discussed within the context of the appropriate program sub-study.

VI. RESULTS

A. Littoral Current Observations Using Sea Bed Drifters

Introduction

Two deployments of sea bed drifters were made on 23-30 October and 21-24 March 1981. For each experiment, three groups of 50 drifters each were launched from a light plane in the near-shore surf zone on a line perpendicular to the coast. The innermost group was deployed just shoreward of the breaking waves, the next group in the breaking waves, and the final group about 150 m beyond group 2. Each bundle of drifters was bound using a salt block such that the bundle would be released in approximately three hours. For three days following the launch, the coast was searched by plane for stranded drifters. Since pickup required landings on the beach, only one pickup could be made per day during the daylight low tide.

The area of deployment and recovery is shown in Figure 2. The drifters were released just northwest of the mouth of the Akwe River and generally drifted to the northwest along the scale shown on the figure. The distribution of the mean longshore speeds for each of the three recoveries is shown in Figures 3 through 5 for the fall and Figures 6 through 8 for the spring. The results from the two experiments were quite different; the higher speeds occurring during the fall were probably the result of storm conditions the first day of the fall deployment which were not present in the spring. The data from each experiment are discussed in detail below.

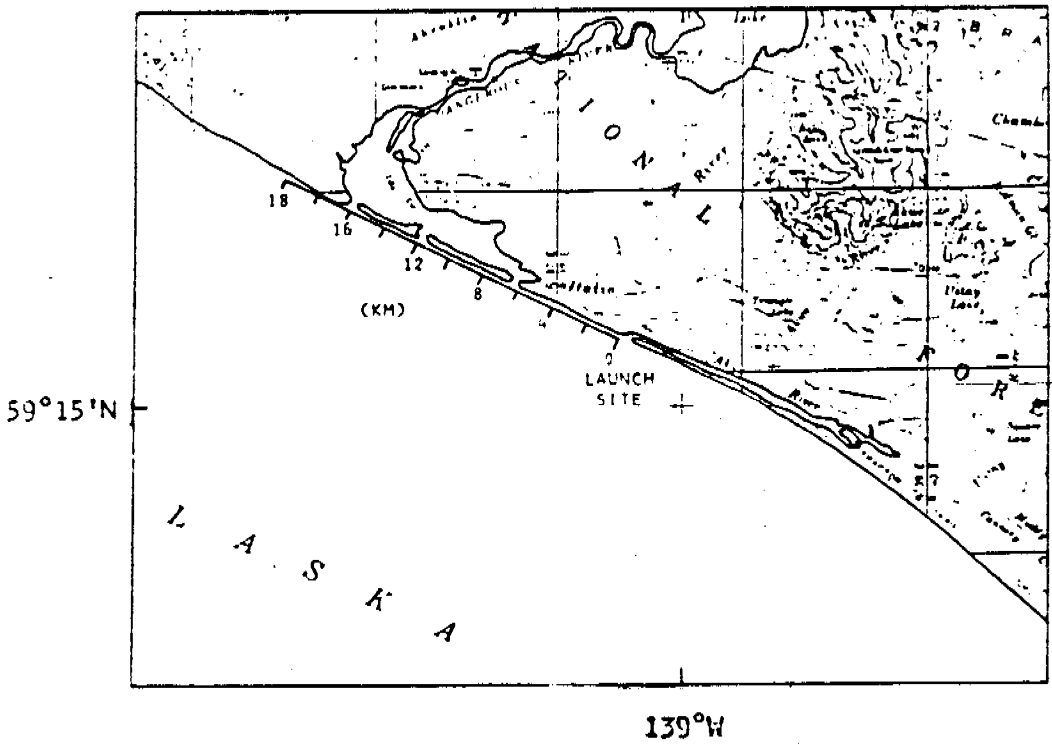

Figure 2. Launch site and recovery area for seabed drifters (distance in kilometers). See text for discussion of offshore distance of launchings.

The Fall Experiment

The three groups of drifters will be discussed in order from near-shore to off-shore. The recoveries from group 1F occurred generally on the first day close to the launch site, resulting from mean longshore speeds to the northwest from 0 to 3 cm/sec (Figure 3). Two drifters from this group were recovered on the second day and reflected similar speeds. None of the drifters were recovered on the third search day.

The recoveries from group 2F showed a distinct bimodal distribution of mean speeds for the first day (Figure 4). The lower speed peak ranged from 2-30 cm/sec with a weighted mean value of 15 cm/sec. The higher peak showed speeds ranging from 23-34 cm/sec with a mean value of 29 cm/sec. The second day of recoveries for this group showed two-day mean speeds to be similar to the lower speed peak seen on the first day of recoveries, with speeds to the northwest ranging from 2-16 cm/sec with a weighted mean of 12 cm/sec. Again, no drifters were recovered on the third day.

The outermost group, 3F, had a recovery pattern similar to group 2F (Figure 5). The first day of recoveries displayed a velocity peak at 18 cm/sec with some drifters having speeds up to 35 cm/sec. On the second day the two-day average speed was 12 cm/sec with values ranging from 8-16 cm/sec. No drifters were recovered the third day.

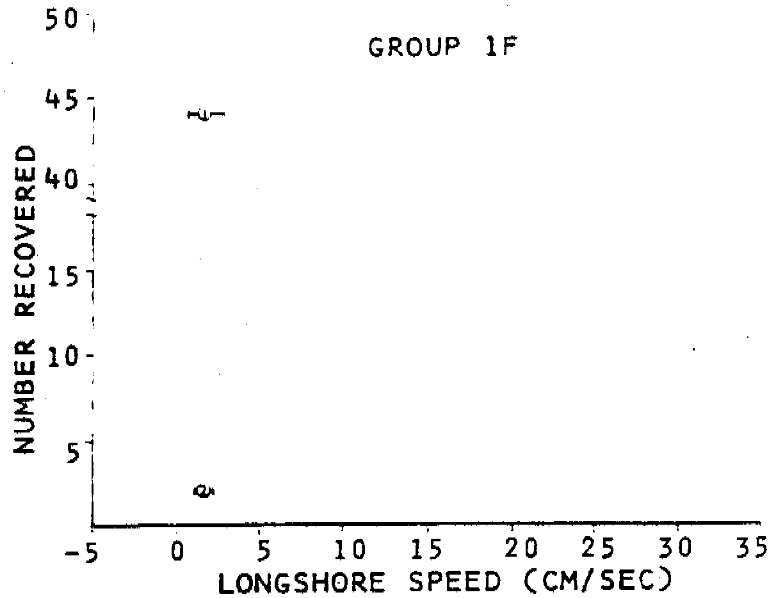

Figure 3. Histogram of longshore speed, group 1, fall (positive is northwestward). Circles are mean speed for a particular group of drifters where height above horizontal axis reflects number in group. Number inside circle indicates number of days speed is averaged over (day of recovery). Error bars take into consideration uncertainty of position, time of release, and time of stranding (generally the largest contributor).

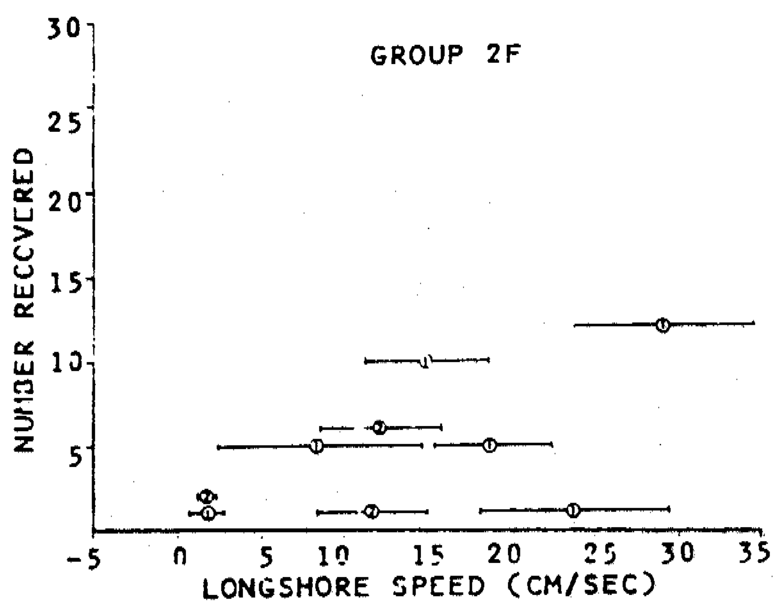

Figure 4. Histogram of longshore speed, group 2, fall (positive is northwestward). Circles are mean speed for a particular group of drifters, where height above horizontal axis reflects number in group. Number inside circle indicates number of days speed is averaged over (day of recovery). Error bars take into consideration uncertainty of position, time of release, and time of stranding (generally the largest contributor).

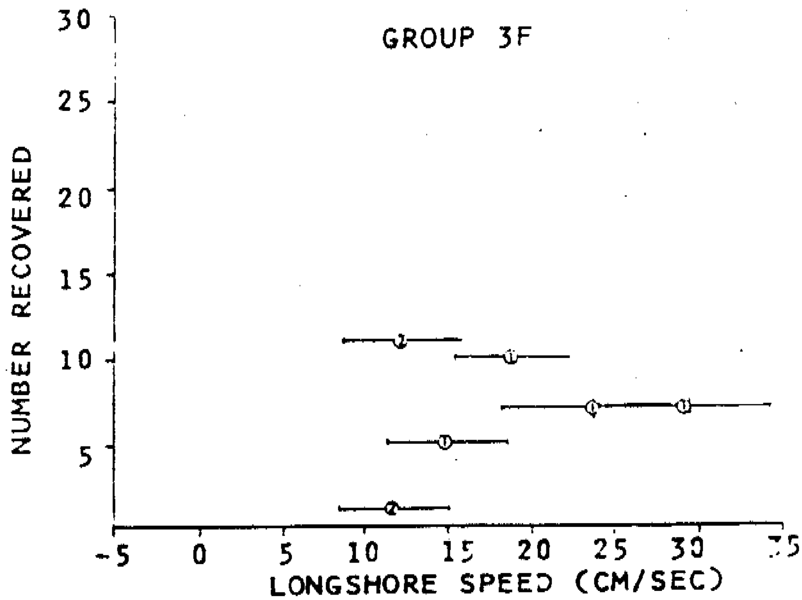

Figure 5. Histogram of longshore speed, group 3, fall (positive is northwestward). Circles are mean speed for a particular group of drifters, where height above horizontal axis reflects number in group. Number inside circle indicates number of days speed is averaged over (day of recovery). Error bars take into consideration uncertainty of position, time of release, and time of stranding (generally the largest contributor).

The similar recovery patterns for groups 2F and 3F suggest that some drifters from these groups were subjected to higher current speeds on the first day. The remaining drifters showed similar speeds for the two day period.

The Spring Experiment

The spring experiment showed quite a different recovery pattern than did the fall experiment, probably as a consequence of the lack of a strong storm event during the measurement period.

Results from group 1S (Figure 6), the inshore position, showed a slight southeast flow for the first day recoveries, gradually changing to a moderate northwest flow. The drifters showed a range of speeds on the first day from -4 to 2.5 cm/sec with a weighted mean of -2.5 cm/sec (negative values imply flow to the southwest). By the second day the flow was to the northwest, with a two-day average speed of 1 cm/sec to the northwest and a range of 0-4 cm/sec. By the third day the northwestward flow was well established with one recovery reflecting a speed of 9 cm/sec.

The results from group 2S (Figure 7) also reflected this reversal of flow from the southeast to the northwest. The first day recoveries showed a southeast flow with a weighted average of -2 cm/sec and a range from -3.5 to 1 cm/sec. On the second day the two-day average speed was 1 cm/sec with a range from 0-5 cm/sec. The three-day average speeds ranged from 5-11 cm/sec with a mean of 8 cm/sec.

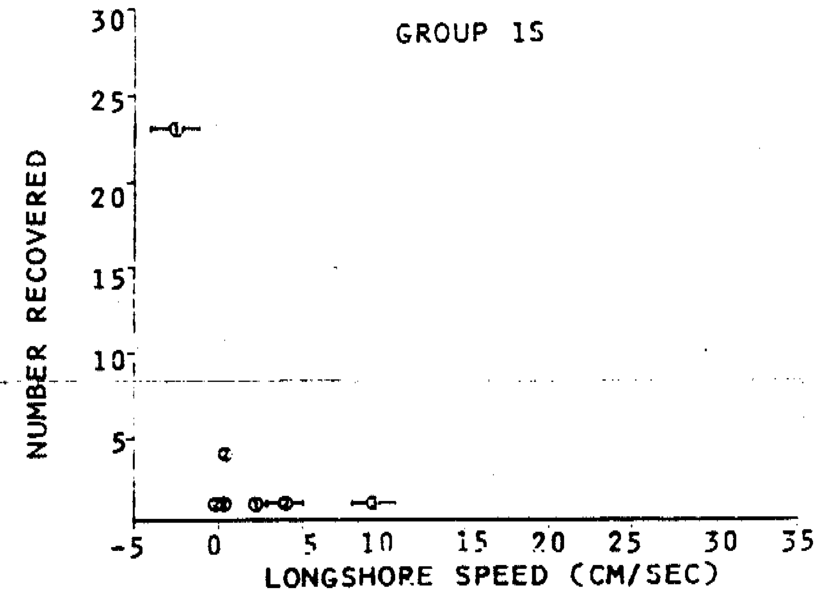

Figure 6. Histogram of longshore speed, group 1, spring (positive is northwestward). Circles are mean speed for a particular group of drifters, where height above horizontal axis reflects number in group. Number inside circle indicates number of days speed is averaged over (day of recovery). Error bars take into consideration uncertainty of position, time of release, and time of stranding (generally the largest contributor).

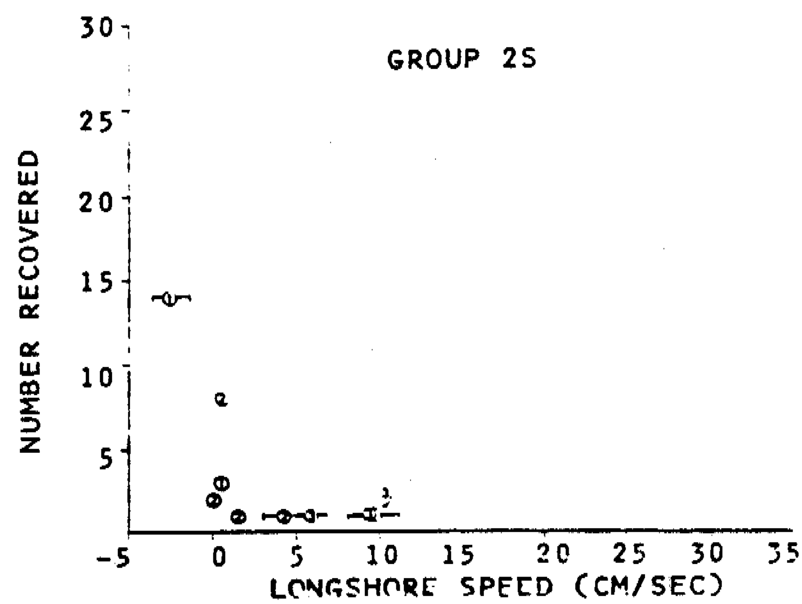

Figure 7. Histogram of longshore speed, group 2, spring (positive is northwestward). Circles are mean speed for a particular group of drifters, where height above horizontal axis reflects number in group. Number inside circle indicates number of days speed is averaged over (day of recovery). Error bars take into consideration uncertainty of position, time of release, and time of stranding (generally the largest contributor).

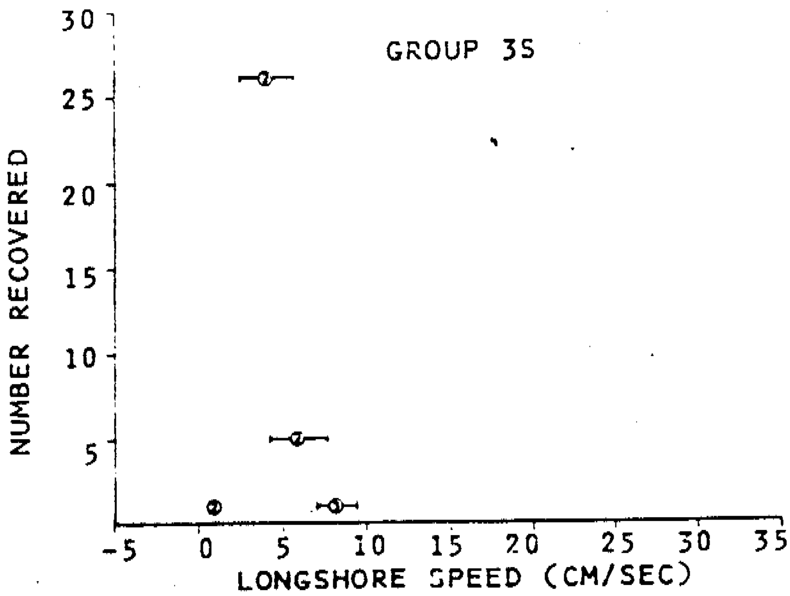

Figure 8. Histogram of longshore speed, group 3, spring (positive is northwestward). Circles are mean speed for a particular group of drifters, where height above horizontal axis reflects number in group. Number inside circle indicates number of days speed is averaged over (day of recovery). Error bars take into consideration uncertainty of position, time of release, and time of stranding (generally the largest contributor).

Groups 1S and 2S thus show similar patterns in the reversal from a southeast to a northwest flow. The third group (3S) which was farthest offshore did not show this pattern but its results are consistent with the other groups (Figure 8). There were no recoveries of this group the first day, so the flow for that period is integrated into the two-day average values. Those showed a large number of recoveries centered around a mean of 4 cm/sec, slightly higher than the two-day mean values from the other groups. On the third day one drifter was recovered, reflecting a three-day average flow of 8 cm/sec; this is not significantly different from the two-day mean speed considering the uncertainty in the measurements.

To summarize the spring data, the two inshore groups of recovered drifters show a reversal in the current direction from southeast to northwest and then a gradual increase in speed. While this reversal is not seen in the offshore group, results in the latter are consistent with this pattern.

B. Current and Wind Observations

The current and wind observation program was designed to investigate the near-coastal circulation and the interaction between this circulation and local winds. Current observations were carried out both through deployment of moored, recording current meters and using near-surface, drogued drifting buoys equipped with radar reflectors which could be tracked from the vessel. Wind observations were carried out using recording meteorological stations deployed at two locations on the beach during each of the field experiments. These methods are elaborated upon in the following discussions.

Recording Current Meter Observations

Recording current meters were deployed in taut-wire mooring configurations during autumn (October-November) 1980 and late winter (March-April) 1981. A single mooring was, additionally, left deployed throughout the entire October-March period. Results presented here are those from only the autumn series of moorings, because at this writing both the late winter and over-winter data are still undergoing preliminary processing.

Geographical locations of the autumn current meter moorings are indicated on Figure 9. These moorings were of a taut-wire configuration as described in Muench and Schumacher (1980). Information on mooring location, dates, current meter placement upon each mooring, and observed currents is presented in Table 1. The

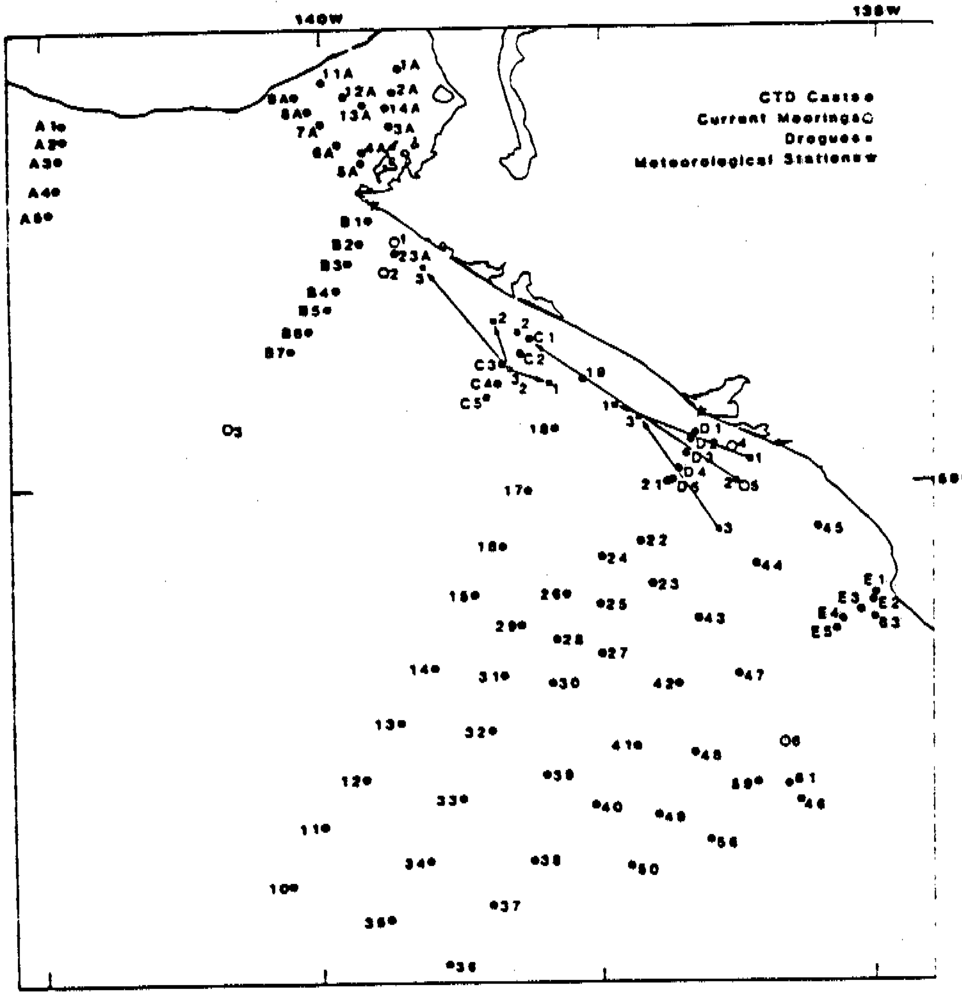

Figure 9. Geographical locations of CTD stations, recording current moorings, radar-tracked drogue tracks (schematic only) and meteorological stations during the October-November 1980 field program in the northeast Gulf of Alaska coastal region.

Table 1

SUMMARY OF INFORMATION CONCERNING DEPLOYMENT OF, AND INFORMATION OBTAINED FROM, CURRENT METER MOORINGS UTILIZED IN THE OCTOBER-NOVEMBER 1980 FIELD PROGRAM IN THE NORTHEAST GULF OF ALASKA

MOORING ID	LATITUDE N	LONGITUDE W	DEPLOYMENT DATE/HR	RECORD LENGTH (DAYS)	BOTTOM DEPTH (M)	METER DEPTH (M)	MEAN SPEED (CM/SEC)	SPEED ST.DEV.	MEAN DIR.(°T)	DIR. ST.DEV
1[1]	59°27.2'	139°44.1'	10-23-81/1909	10	57	26	18	13	217	94
2[2]	59°24.1'	139°46.4'	10-23-81/2033	10	139	40	21	9	211	100
"	"	"	"	"	"	125	13	7	225	100
3[2,3]	59°06.8'	140°20.3'	10-24-81/0030	10	132	37	--	--	--	--
4[1]	59°04.5'	138°31.1'	10-22-81/1048	11	75	38	16	13	188	101
5[2]	59°00.0'	138°28.5'	10-22-81/1159	11	65	15	36	12	157	101

[1]Vector-averaging current meter.

[2]Aanderaa RCM-4 current meter.

[3]Temperature and salinity records only were obtained.

near-shore moorings (1 and 4) utilized vector-averaging current meters recording at 7.5-minute intervals, while moorings farther offshore (2,3 and 5) utilized Aanderaa RCM-4 current meters recording at 5-minute intervals. Mooring 6 (Figure 9) was the over-winter mooring from which results are not yet available.

The data recovered from moorings 1-5 are presented in Figures 10-16. Since both current meters on mooring 3 malfunctioned, yielding only temperature and salinity records from the 37-m deep meter, the discussion will focus upon observations at moorings 1, 2, 4 and 5. This discussion is augmented, in addition, by Appendix 1 which summarizes a presentation at the Spring 1981 AGU meeting in Baltimore, Maryland.

Each of the current time-series records presented has been passed through a one-hour lowpass filter to remove high-frequency noise. High-frequency noise removed by this filter appeared to be appreciable only at the upper current meter at mooring 5; because of irregular bathymetry in the vicinity, this mooring was deployed so that the meter was only 15 m below the surface rather than the design depth of 20 m. Consequently the record was probably affected to some degree by wave-induced rotor pumping and vane motion.

The two moorings nearest the coast (1 and 4; Figures 10 and 11) showed the flow strongly constrained to parallel the shoreline, i.e. along-shore current speed was large compared to the cross-shelf speed. Flow direction was bimodal, being directed either to the northwest or to the southeast, with roughly a 60-40 split between directions. This bimodality was illustrated graphically by the current direction histogram for mooring 1, chosen as representative for both moorings 1 and 4 (Figure 12). This is in contrast to previously accepted conceptualizations of the coastal circulation in this region, which have perpetrated the

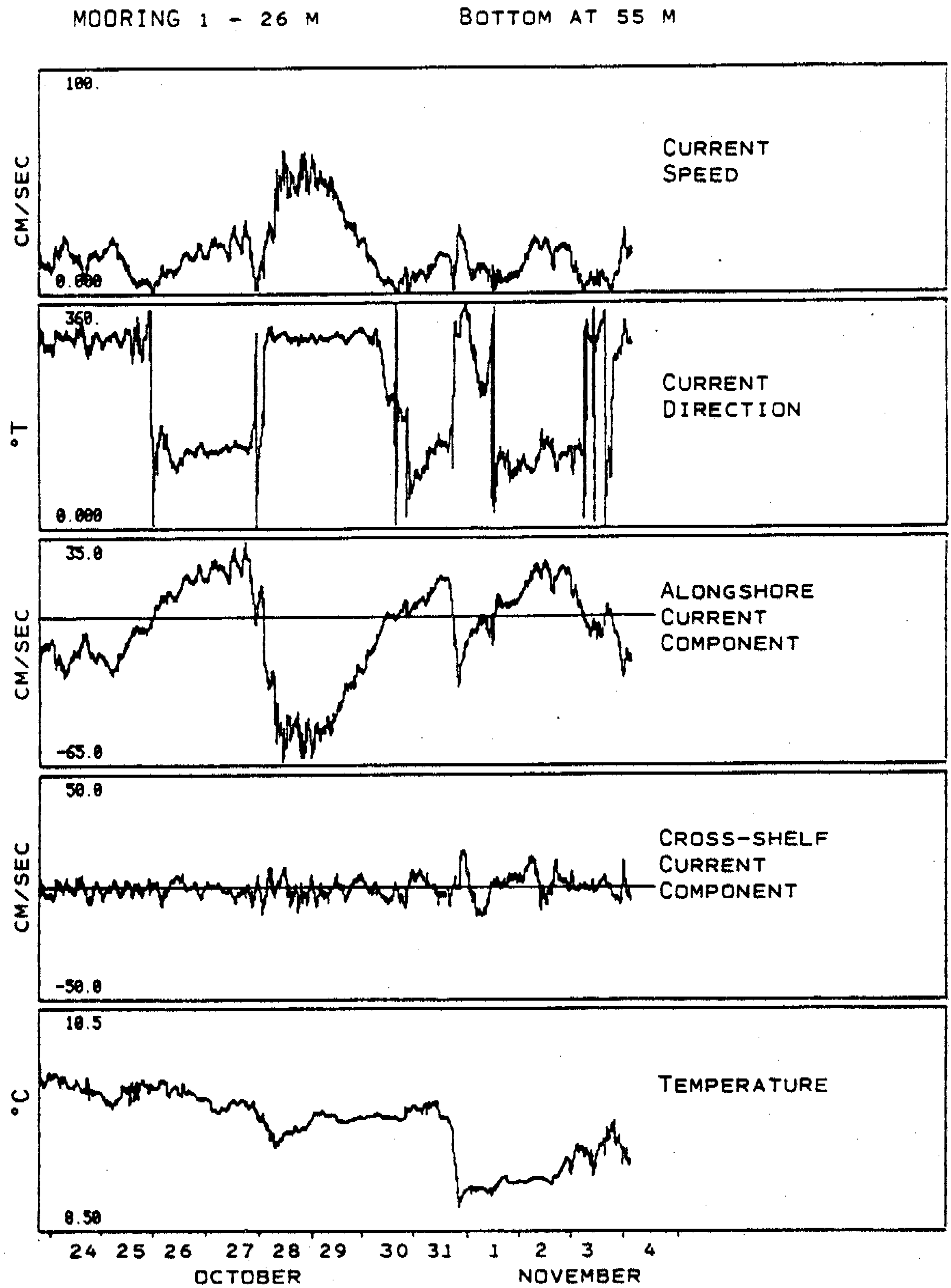

Figure 10. Time-series plot of one-hour lowpass filtered current and temperature data from the 26-m deep current meter at mooring 1, 23 October-4 November 1980. Mooring location is shown on Figure 9.

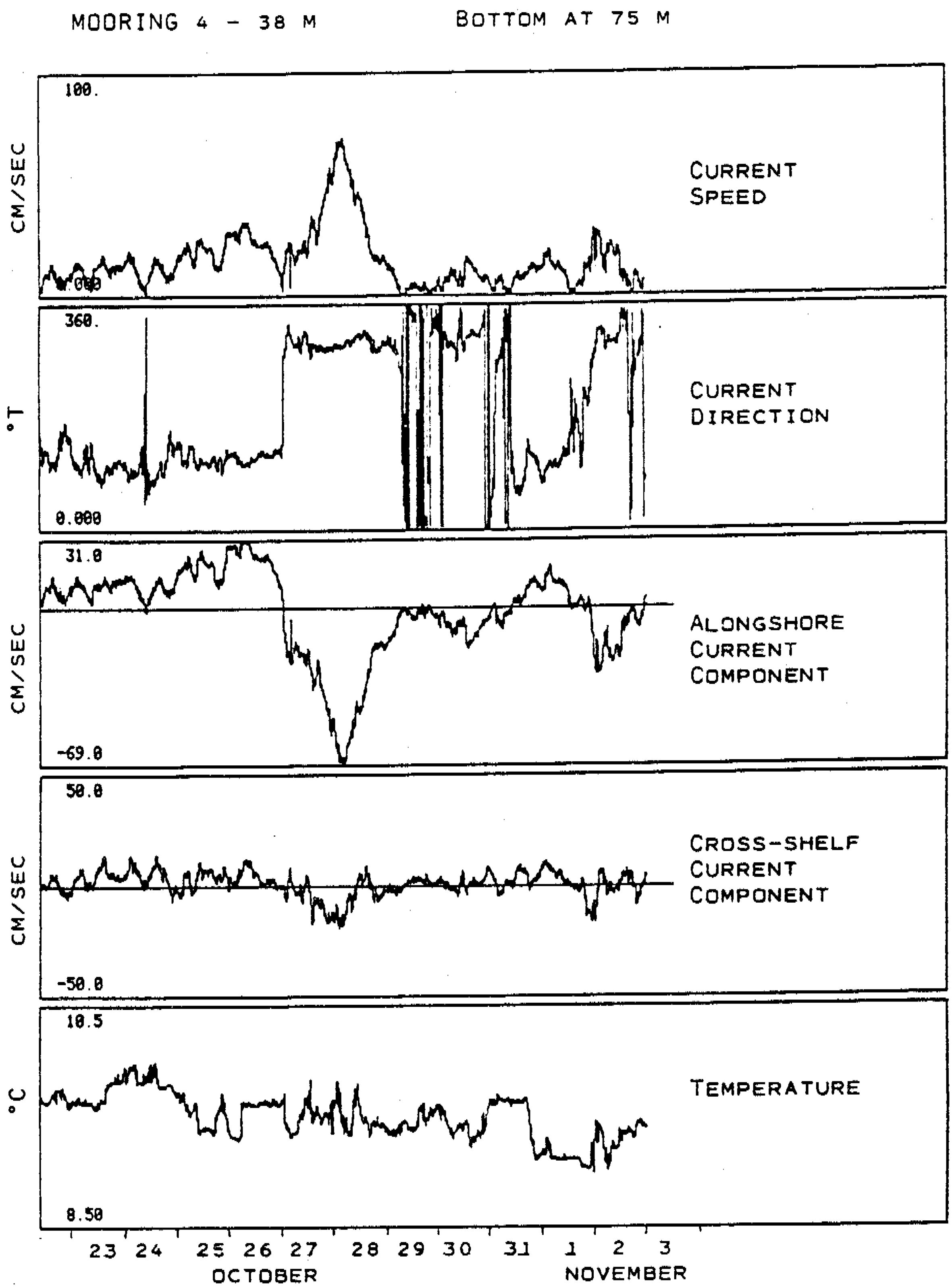

Figure 11. Time-series plot of one-hour lowpass filtered current and temperature data from the 38-m deep current meter at mooring 4, 22 October-3 November 1980. Mooring location is shown on Figure 9.

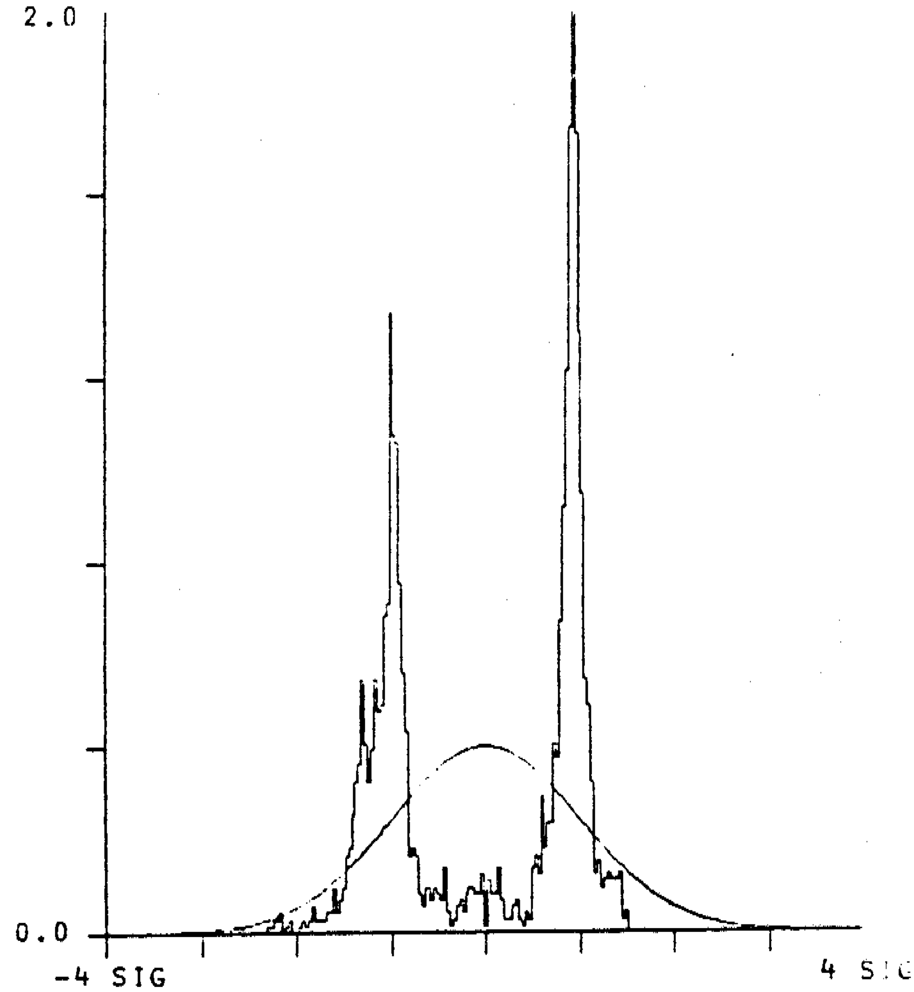

Figure 12. Normalized distribution of current direction at mooring 1 computed from the time-series record shown on Figure 10, showing the strongly bimodal nature. The left-hand peak corresponds to the southeast along-shore direction, and the right-hand peak corresponds to the northwest along-shore direction. The smooth curve illustrates a hypothetical Gaussian distribution for comparison purposes.

belief that flow is generally to the northwest in concert with the regional flow in the Alaska Current along the shelf break. The strong (60-70 cm/sec) northwesterly flow event which occurred on 27 October is discussed in more detail in Appendix 1. Current speeds showed a generally high variance (Table 1). Tidal currents were small relative to the lower frequency flow, as shown by visual inspection of the time-series plots. No attempt was made to compute spectral estimates of current energy contained in the different frequencies; the relatively short (10-day) record lengths precluded such estimates for lower-than-tidal frequency components, which can typically have time scales of several days in this region (cf. Hayes, 1978; Hayes and Schumacher, 1976).

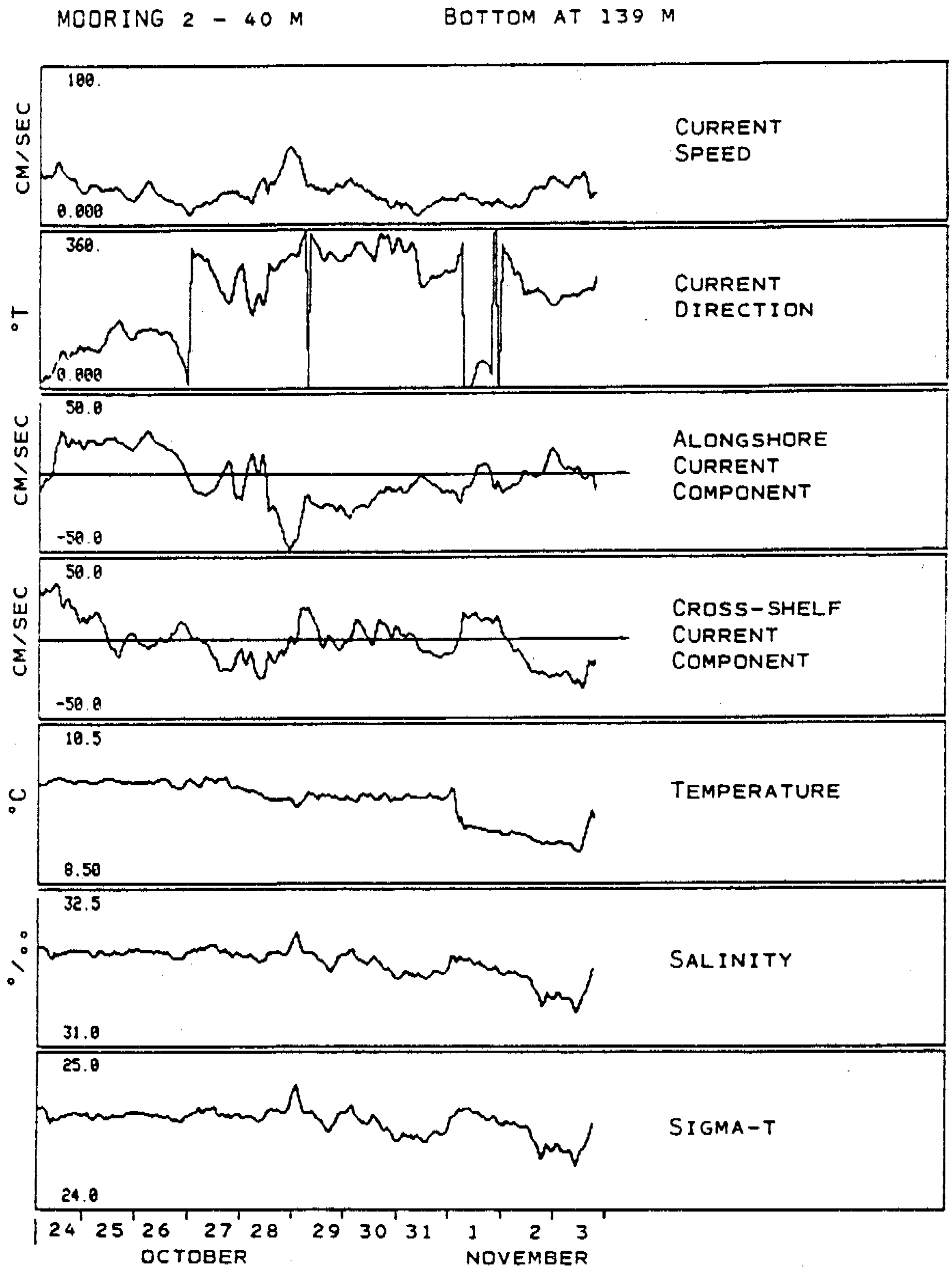

Figure 13. Time-series plot of one-hour lowpass filtered current, temperature, salinity and derived density (sigma-t) data from the 40-m deep current meter at mooring 2, 24 October-3 November 1980. Mooring location is shown in Figure 9.

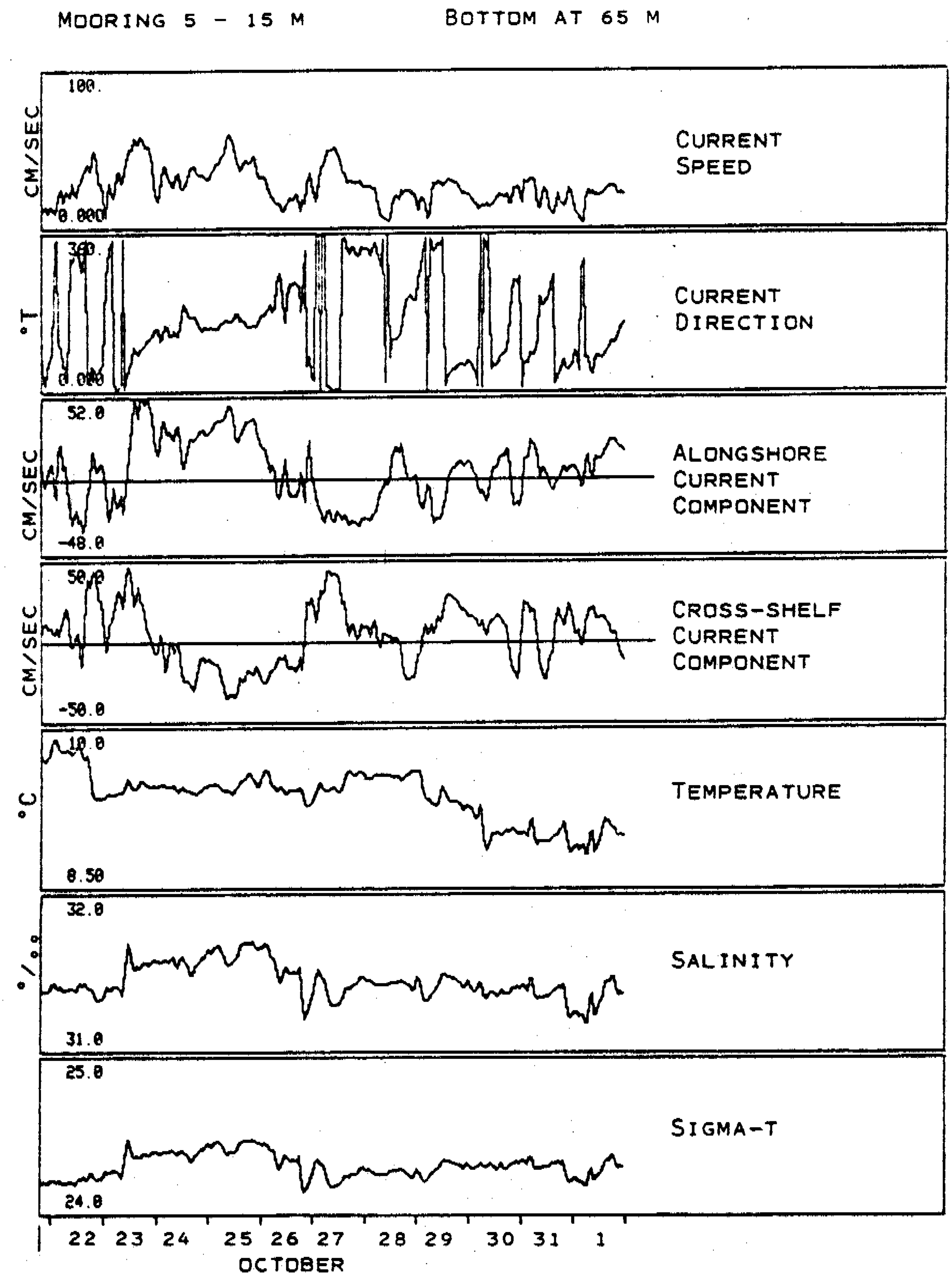

Figure 14. Time-series plot of one-hour lowpass filtered current, temperature, salinity and derived density (sigma-t) data from the 15-m deep current meter at mooring 5, 21 October-1 November 1980. Mooring location is shown on Figure 9.

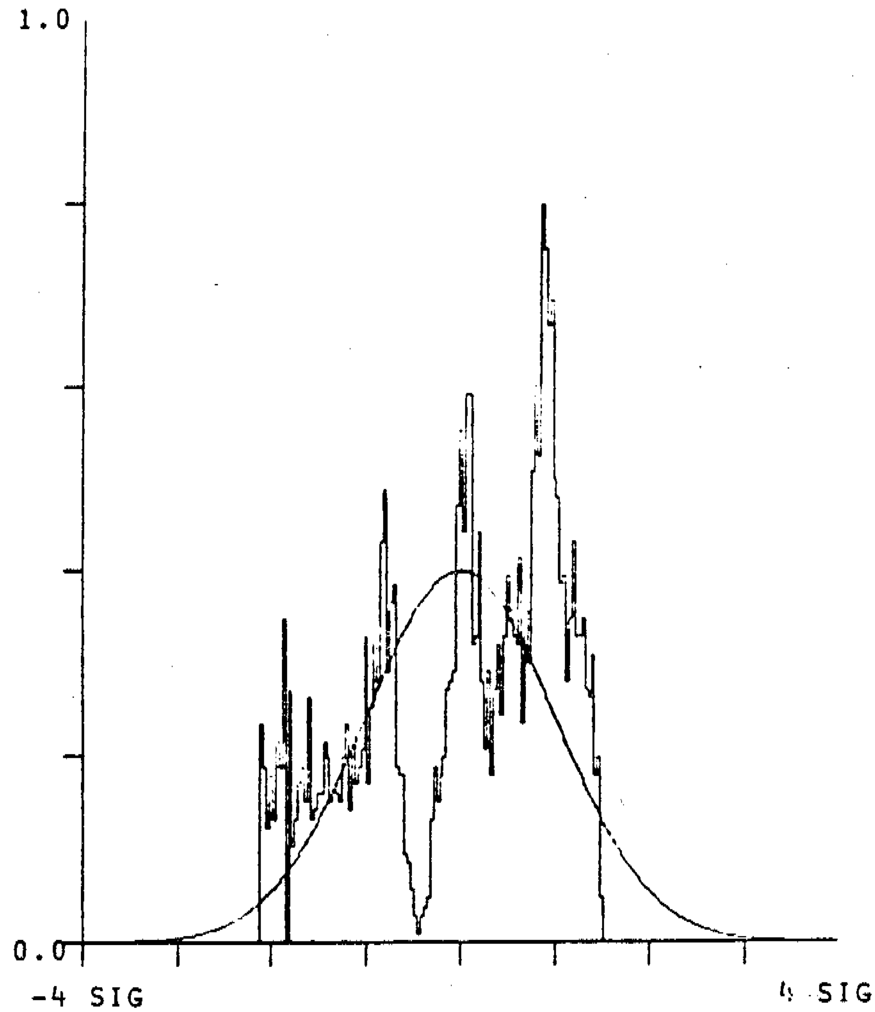

Figure 15. Normalized distribution of current direction at 40-m at mooring 2 computed from the time-series record shown on Figure 13, showing the weakly bimodal nature. The left-hand peak corresponds to a southeasterly flow direction, and the right-hand peak corresponds to a northwesterly flow. The smooth curve illustrates a hypothetical Gaussian distribution for comparison purposes.

The near-surface meters at moorings 2 and 5 showed less topographic control than nearer the coastline, as there was a larger cross-shelf current component at the former stations (Figures 13 and 14). Current speeds and direction were highly variable, and peak observed speeds were lower (only as great as about 50 cm/sec during the northwestward pulse of 27 October) than at the nearer-shore moorings. As for the near-shore moorings, the along-shore flow appeared to be roughly bimodal. The mean currents computed from moorings 1, 2, 4 and 5 (Table 1) indicate that the variability (as standard deviation) was large enough for speed and direction over the sample period so that little significance can be attached to the means.

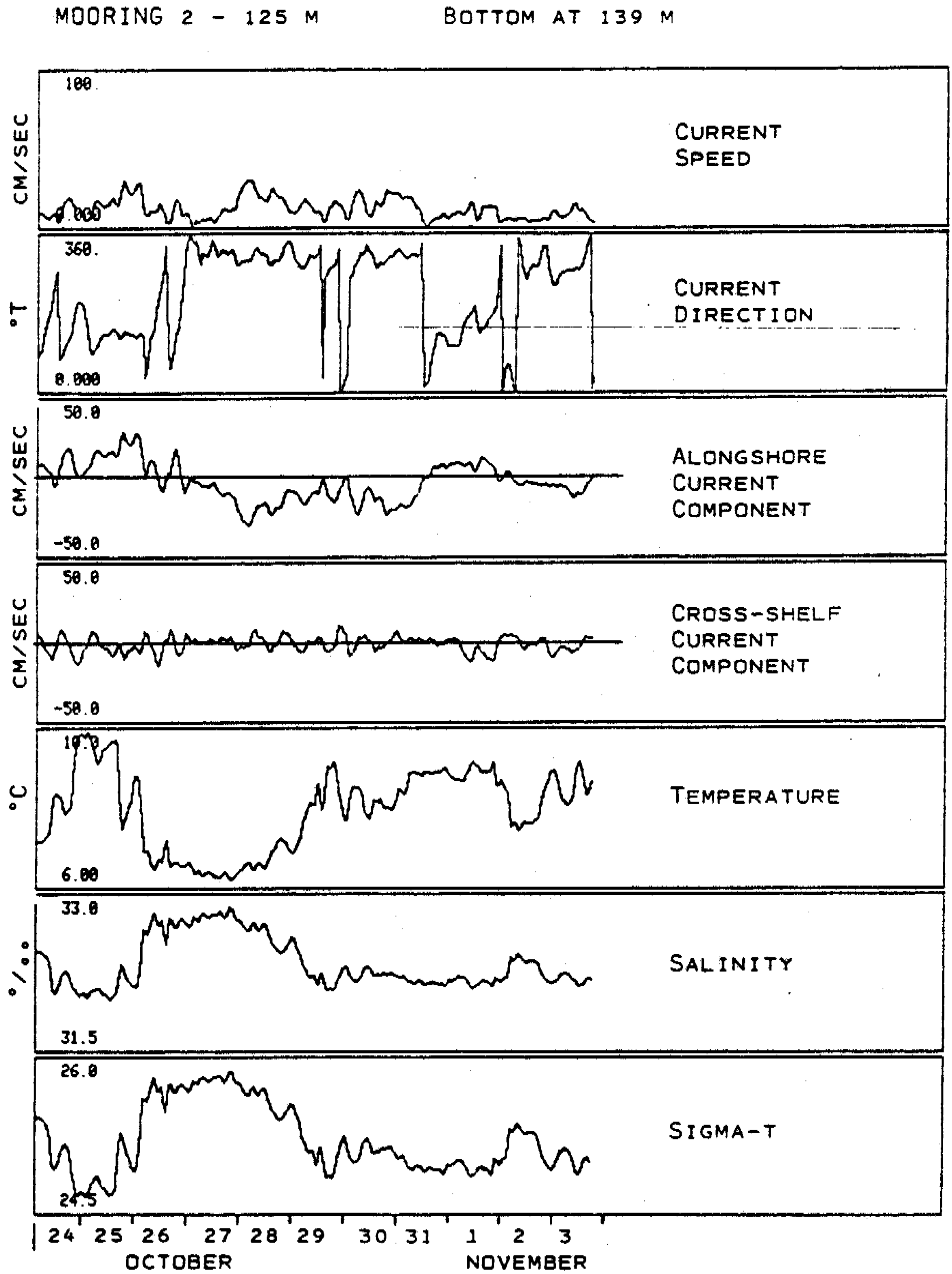

Figure 16. Time-series plot of one-hour lowpass filtered current, temperature, salinity and derived density (sigma-t) data from the 125-m deep current meter at mooring 2, 24 October-3 November 1980. Mooring location is shown on Figure 9.

The deeper current record at mooring 2 (Figure 16) indicates that speeds were lower by about a factor of two at depth than near the surface at that mooring. Current direction was more nearly aligned in an along-shore direction, reflecting a greater near-bottom topographic control.

The time-series of temperature (at moorings 1 and 4) and temperature and salinity (at moorings 2, 3 and 5) showed considerable variability in these parameters during the observation period. These records are discussed below within the context of the observed regional temperature and salinity distribution.

Radar-Tracked, Surface Drogue Buoy Observations

In order to obtain near-surface flow trajectories to supplement the recorded current moorings discussed above, window-shade type drogues were attached to surface floats which were equipped with radar transponders and deployed from 26-30 October 1981 in the near-coastal portion of the study region. The drogues were adjusted so that they would follow water motion at a depth of approximately 20 m. Times of deployment and recovery, and drogue tracks are shown on Figures 17-20; the larger-scale drogue deployment pattern in shown on Figure 9.

The drogue tracks reflect the highly time-varying circulation indicated by the recorded current records. Drogue #1 actually was deployed twice. During the first deployment (Figure 17) it had significant southeast movement. On the second deployment farther to the southeast (Figure 18) it showed northwest flow which was a response to the strong northwesterly current pulse which is evident on Figures 10, 11, 13 and 14 and is discussed in Appendix 1. Drogues 2 and 3 (Figures 19 and 20) moved northwest in response to this same flow event. The shoreward motion of drogue #2 (Figure 19), even more pronounced for #3 (Figure 20), probably reflected the response of water circulation to topographic control. Streamlines would tend to parallel bottom contours which delineate the head of Alsek Canyon. Drogue speeds were of similar magnitude to those observed with the current moorings.

Wind Observations

Recording meteorological stations were deployed on the beach at the locations indicated on Figure 9 during both autumn (October-November) 1980 and late winter (March-April) 1981. These periods of deployment coincided with current mooring deployment periods. The meteorological stations used were Aanderaa recording units equipped with wind speed and direction and temperature sensors. Data from these stations will be eventually supplemented with wind data obtained from the vessel, with winds observed by the NWS station at Yakutat airport, and geostrophic winds computed by FNWC in Monterey, California. At this time we present the wind data only for the autumn deployment as the remainder of the data is still being processed.

The autumn 1980 wind data are presented as wind speed, along-shelf and cross-shelf components for the stations at Dry Bay and Ocean Cape (Figures 21-22). The scalar total and cross-shelf speed at Dry Bay showed a great deal of fluctuation. The along-shore speed, in contrast, showed relatively small values except for three pronounced high-speed (about 20 m/sec) events which occurred on about 17 October, 27-28 October and 4 November. The wind speed at Ocean Cape had smaller fluctuations than at Dry Bay, both in the along-shore and cross-shelf directions

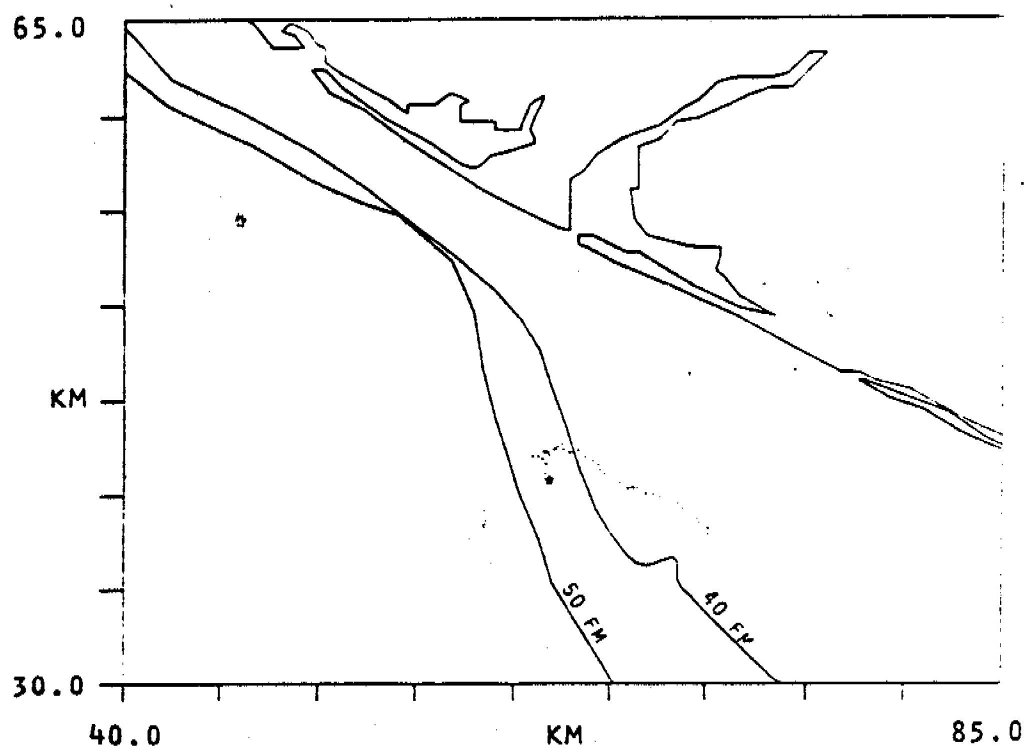

Figure 17. Track of radar-tracked drogue #1 from 0030Z, 26 October 1980 to 0130Z, 27 October 1980. Tick marks indicate half-hour intervals, and star (*) indicates deployment location. Deployment location relative to overall study area is indicated on Figure 9.

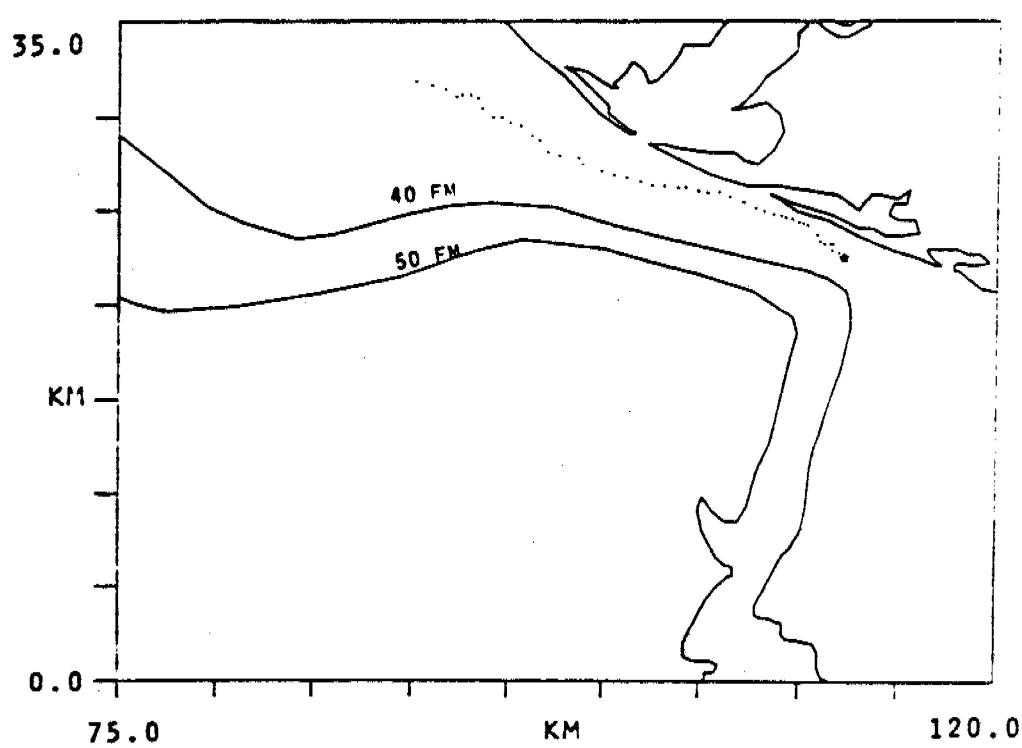

Figure 18. Track of radar-tracked drogue #1 from 1800Z, 29 October 1980 to 1800Z, 30 October 1980. Tick marks indicate half-hour intervals, and star (*) indicates deployment location. Deployment location relative to overall study area is indicated on Figure 9.

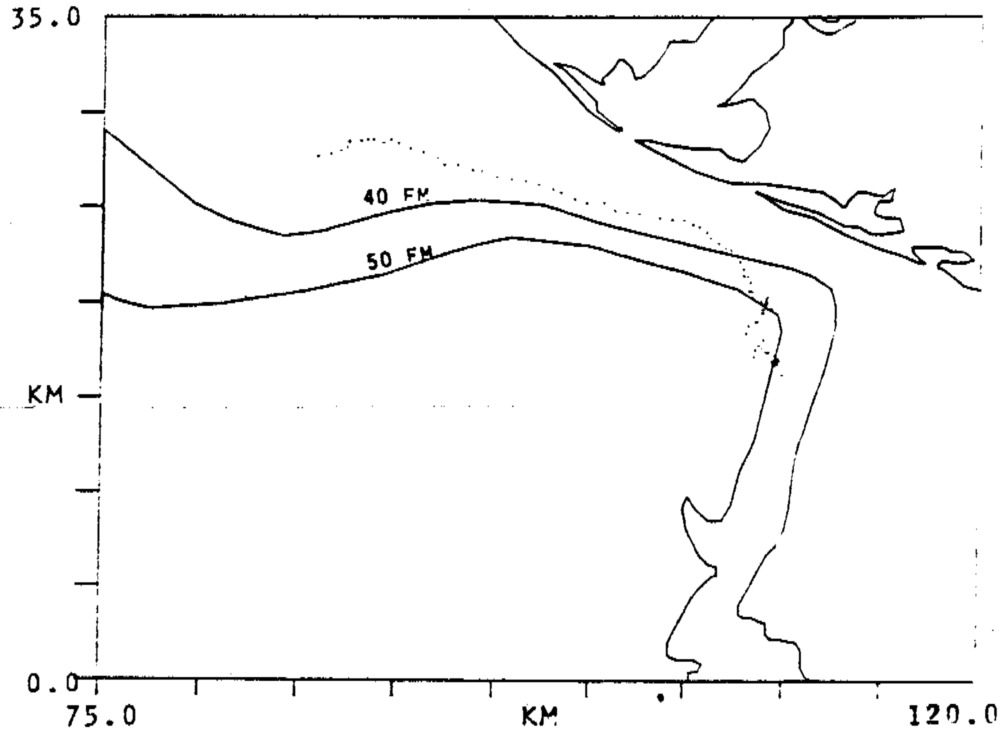

Figure 19. Track of radar-tracked drogue #2 from 0230Z, 29 October 1980 to 1800Z, 30 October 1980. Tick marks indicate half-hour intervals, and star (*) indicates deployment location. Deployment location relative to overall study area is indicated on Figure 9.

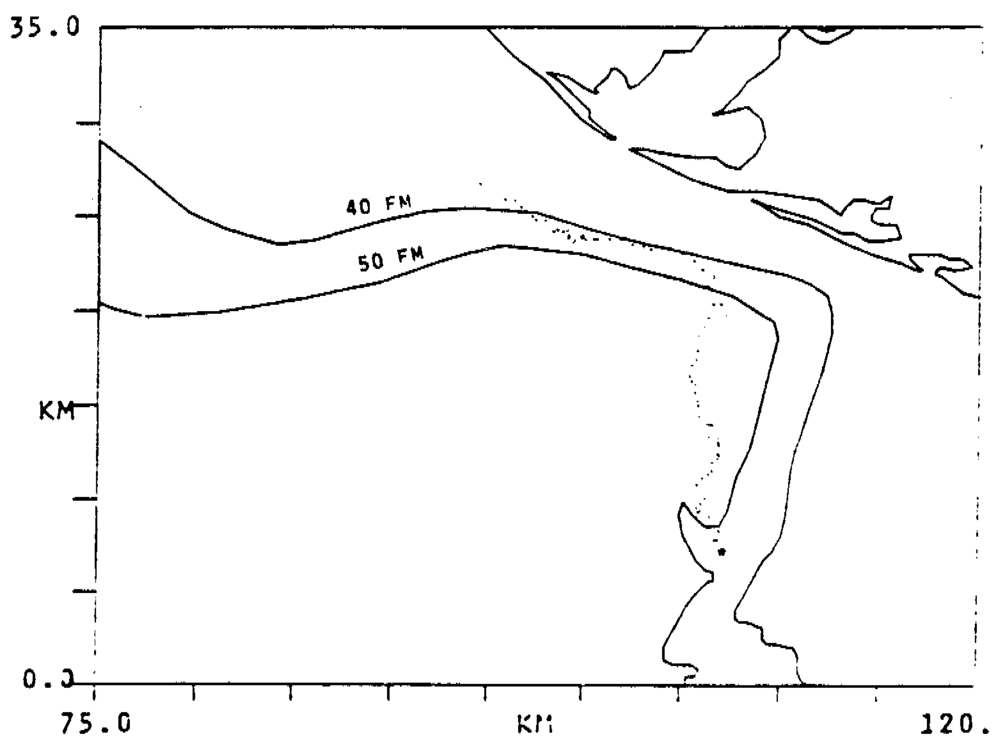

Figure 20. Track of radar-tracked drogue #3 from 0230Z, 29 October 1980, to 1800Z, 30 October 1980. Tick marks indicate half-hour intervals, and star (*) indicates deployment location. Deployment location relative to overall study area is indicated on Figure 9.

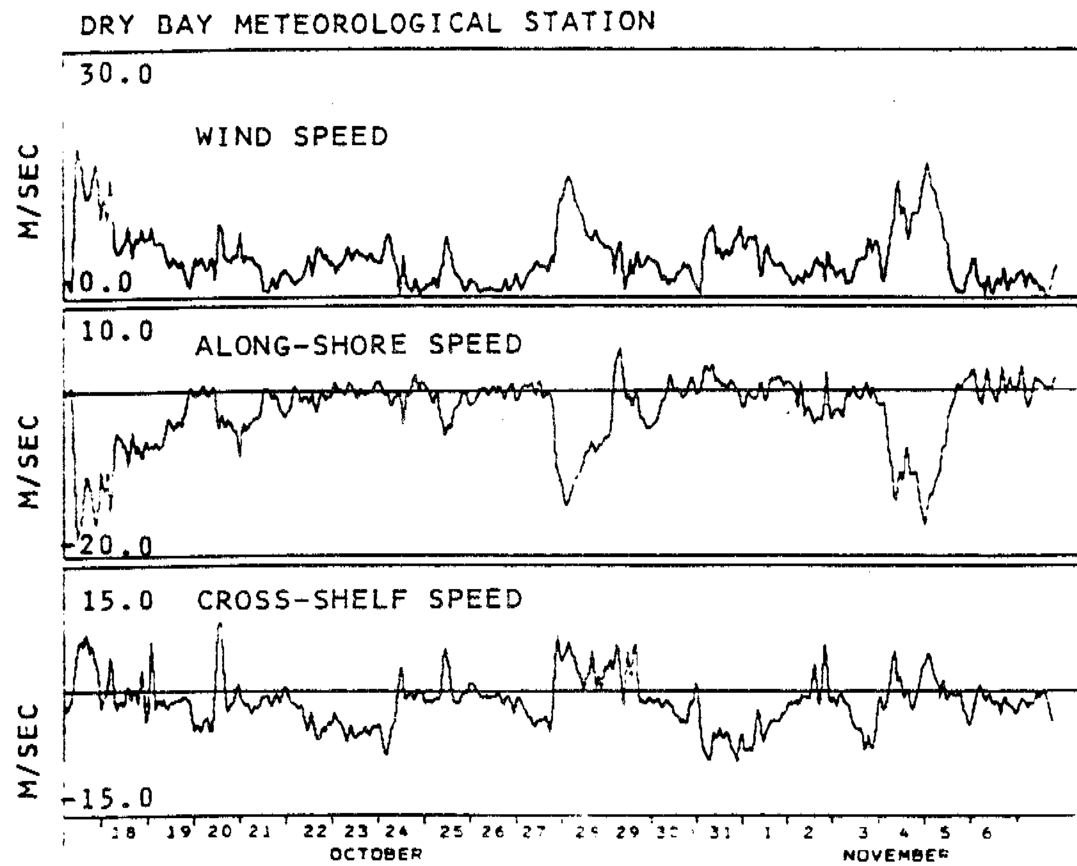

Figure 21. Time-series plot of one-hour lowpass filtered wind speed, along-shore and cross-shelf components at the Dry Bay meteorological station, 17 October-7 November 1980. Station location is shown on Figure 9.

except for the same wind events as observed at Dry Bay; those on 28 October and 4 November (the Ocean Cape record did not start early enough to have recorded the 17 October pulse which was observed at Dry Bay). As at Dry Bay, the wind pulses were primarily along-shore to the northwest, though there was also a pronounced (7-8 m/sec) on-shore component present during each such event. Since the 4 November wind events occurred after the current moorings (except for mooring 6) had been recovered, we are concerned here primarily with the 27-28 October wind pulse. The relations between this pulse and the observed near-coastal currents are summarily discussed in Appendix 1.

C. Temperature and Salinity Observations

As for the current and wind observations presented above, temperature and salinity observations were carried out in the study area during both autumn (October-November) 1980 and late winter (March-April) 1981. Since the temperature and salinity data from the latter cruise are currently in the final stages of processing, only the results from the autumn 1980 observation program will be presented here.

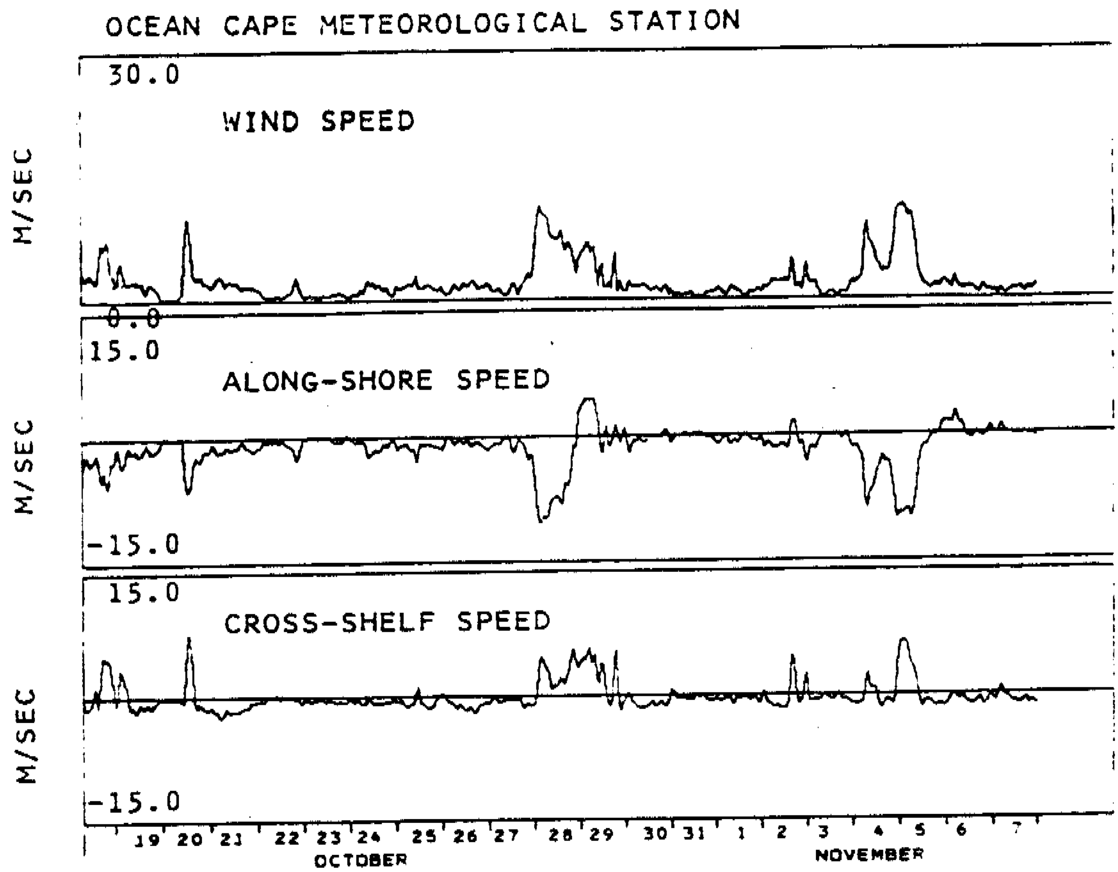

Figure 22. Time-series plot of one-hour lowpass filtered wind speed, along-shore and cross-shelf components at the Ocean Cape meteorological station, 18 October-7 November 1980. Station location is shown on Figure 9.

Temperature and salinity were measured as a function of depth during 23 October-4 November 1980. A Plessey (since changed to Grundy) Model 9040 CTD (conductivity/temperature/depth) unit was used to obtain these observations. Locations of the stations for these observations are shown on Figure 9. On about every third cast, a calibration sample was obtained to ensure proper functioning of the CTD. During calibration casts, temperature was obtained by means of a deep-sea reversing thermometer and salinity was measured on board the vessel using an inductive laboratory salinometer.

The horizontal distributions of salinity at depths of 5 m and 100 m are indicated on Figures 23 and 24, respectively. Horizontal variations in the vertical temperature, salinity and density structure are illustrated by the near-shore, mid-shelf, and off-shore vertical profiles, chosen as representative of regional conditions, shown in Figures 25-27.

The prominent feature of the near-surface salinity distribution (Figure 23) is the low-salinity (30.0-31.5 $^{o}/oo$) band parallelling and adjacent to the coastline. This band reflects the presence, along the coast, of accumulated low salinity water due to admixture of freshwater land runoff. Its proximity to the

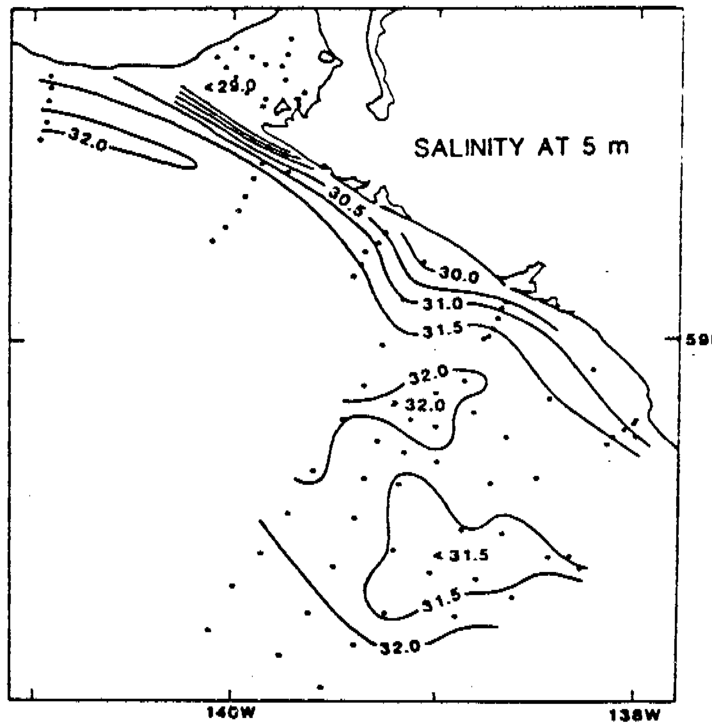

Figure 23. Horizontal distribution of salinity at 5 m depth, 23 October-4 November 1980. The distribution within Yakutat Bay is not shown because the contours there are too closely packed for adequate resolution on this horizontal scale.

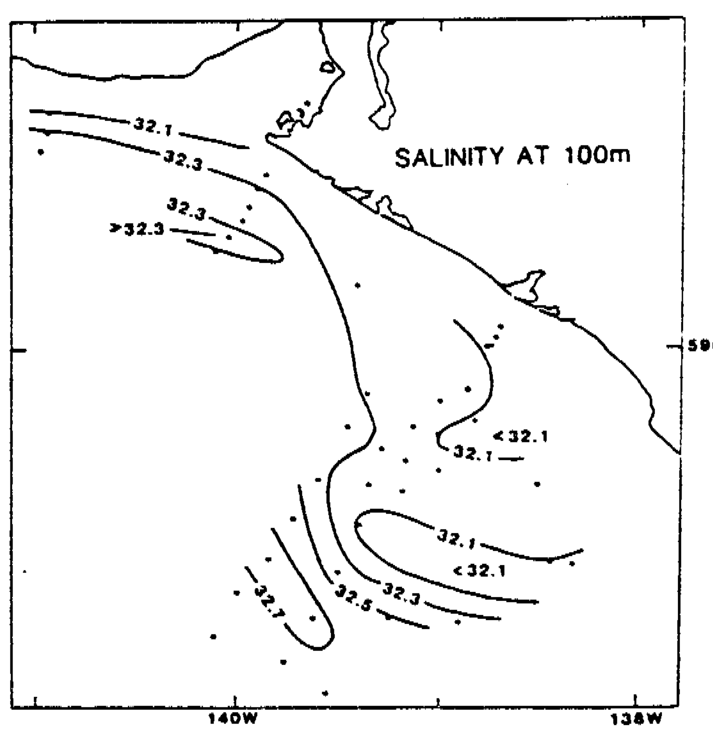

Figure 24. Horizontal distribution of salinity at 100 m depth, 23 October-4 November 1980.

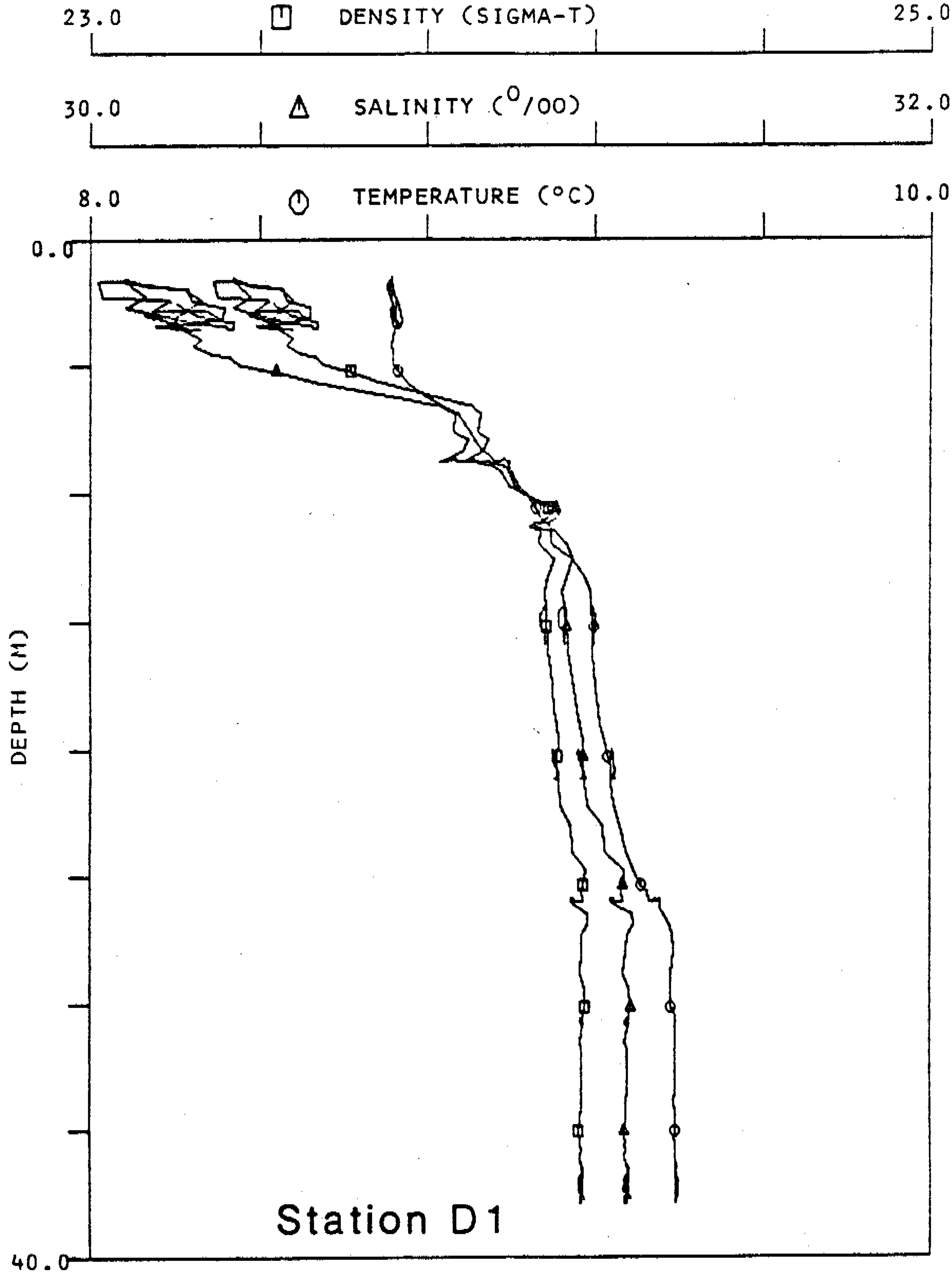

Figure 25. Vertical profile of temperature, salinity and density at near-shore CTD station D1. Station location is shown on Figure 9.

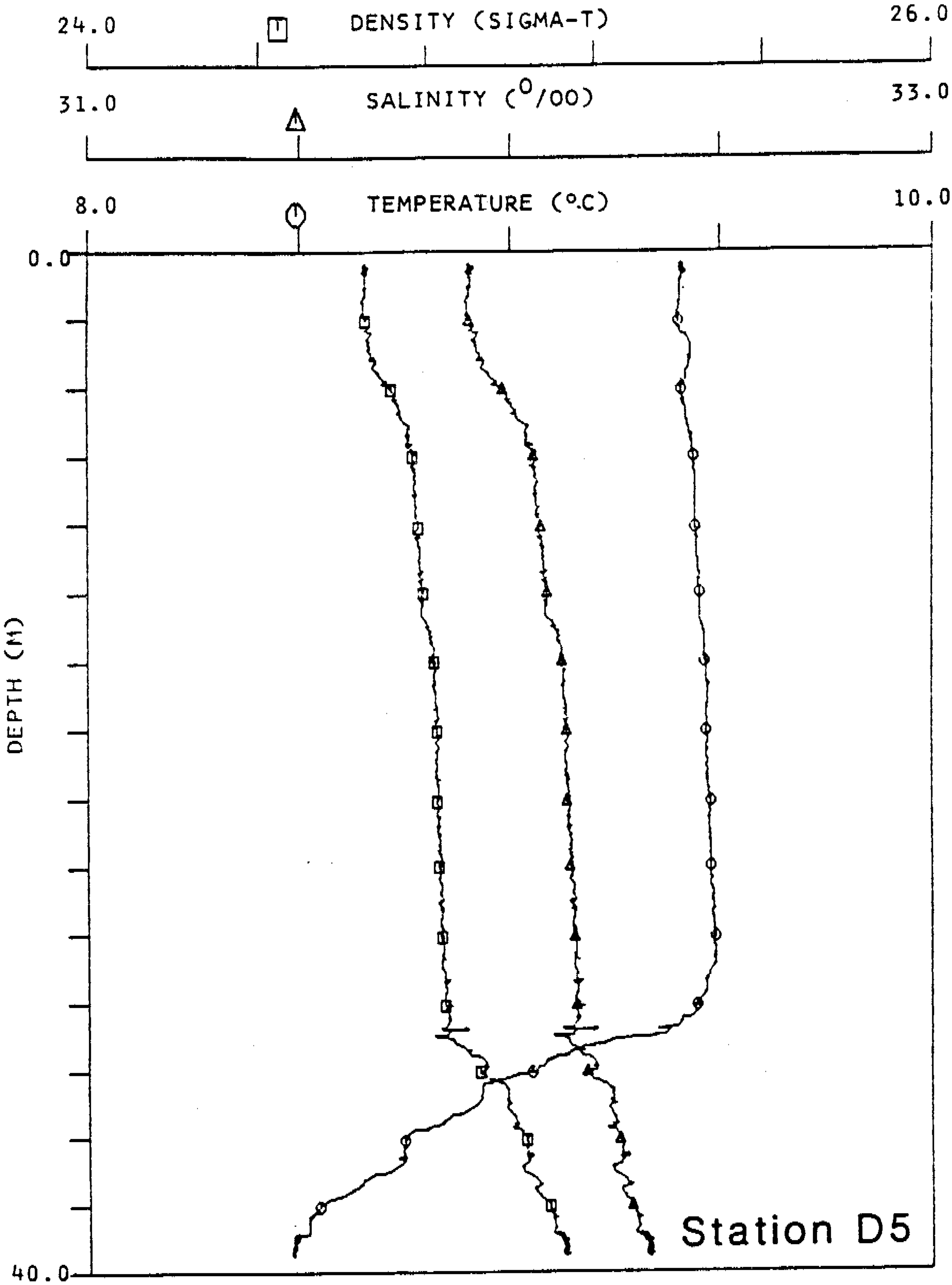

Figure 26. Vertical profile of temperature, salinity and density at CTD station D5 partway across the continental shelf. Station location is shown on Figure 9.

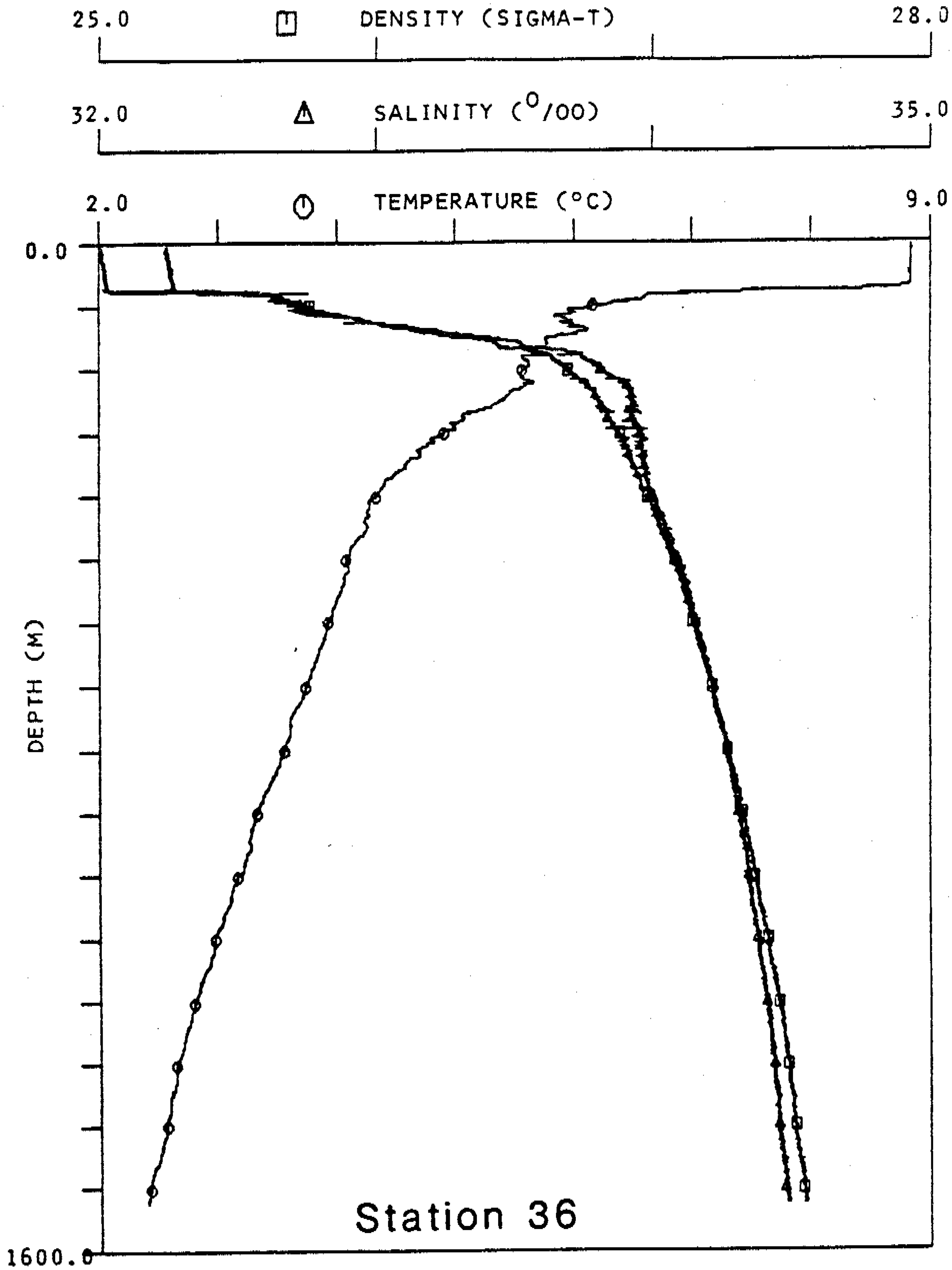

Figure 27. Vertical profile of temperature, salinity and density at CTD station 36 seaward of the continental shelf break. Station location is shown on Figure 9.

coast reflects the tendency, as discussed above, of near-shore currents to parallel the coastline. Spatial distribution of this low-salinity coastal band of water is further illustrated and discussed in Appendix 1. Farther offshore, a poorly-defined region of less saline (less than 31.5 $^{o}/oo$) water may represent the remnant of low-salinity outflow of southeast Alaskan coastal water from Cross Sound. Well offshore, near-surface salinities are about 32.0 $^{o}/oo$ and show little variability compared to near-shore.

The 100-m deep salinity distribution (Figure 24) shows far less variability than near the surface. There was no evidence of the low-salinity coastal band at 100 m (see also the vertical distributions illustrated in Appendix 1). Slightly lower salinities in the eastern than in the western parts of the study area -- < 32.1 as compared to > 32.3 $^{o}/oo$ -- suggest some deep admixture there of waters from southeast Alaska which may have entered the region via Cross Sound.

The horizontal distributions presented in Figures 23 and 24 should be viewed with some caution. Each of the current moorings where salinity was recorded (Figures 13, 14 and 16) indicated rapid fluctuations in salinity during the period over which the CTD observations were carried out. At 5 m depth, relatively small vertical fluctuations would have led to large salinity variations because of the large vertical gradients present at those shallow depths. This is particularly true of the near-shore stations, as represented by the profiles shown on Figure 25 where the strong near-surface salinity gradient extended through 5 m depth. Farther offshore, a second region of high vertical gradients in salinity (as well as in temperature and density) occurred at 120-130 m (Figure 26). Vertical motion, in conjunction with this gradient, may have led to the time variations observed at 125 m depth at mooring 2 (Figure 16). Finally, a vertical temperature, salinity and density profile obtained beyond the shelf break (Figure 27) clearly indicates the vertical gradients in the 100-200 m depth range. Both the mid-shelf and the shelf break stations (Figures 26 and 27) indicate that the water above about 100 m was well-mixed relative both to water below that depth and closer to shore.

VII. DISCUSSION

To date, the program to study coastal oceanography in the northeast Gulf of Alaska has analyzed primarily the current, temperature, salinity and wind data obtained from the study area from 23 October-4 November 1980. At that time, maximum freshwater was present in the continental shelf waters due to admixture of continental runoff derived from the autumn precipitation peak. At the same time, the first severe storms of the winter season were impacting the region. These environmental variables provided a working framework within which to examine specific problems.

Farther west, terrestrial freshwater runoff is quite large in autumn and results in generation of an appreciable baroclinic coastal current system -- the Kenai Current (Schumacher and Reed, 1980). This current is characterized by a consistently westward near-coastal flow with maximum speeds through October and November, with speeds being lower at other times of the year. Our autumn 1980 results from the northeast Gulf of Alaska coastal region suggest that there is no consistent coastal westward flow there comparable with the Kenai Current. While there are few reliable estimates of local freshwater input, it seems likely, based upon known river input, that it is considerably less in the northeast than in the northern-northwestern Gulf of Alaska. The Copper River, the Bering Glacier Stream and the rivers entering upper Yakutat Bay all input to the coastal current observed farther west, whereas there are no major rivers east of Yakutat. Consequently, the observed low-salinity water occupies a relatively shallow, narrow coastal band and does not appear to have large westward flows associated with it. In fact, observations of currents indicate that near-coastal flow during the study period was along-shore and bimodal, with nearly as great a flow toward the southeast as toward the northwest. The current observations obtained from moorings within 10 km of shore indicated a variability in flow which was large enough to preclude meaningful computations of mean flow. Nearer shore (within 5 km) the flow was almost entirely along-shore, with little onshore-offshore component, and was bimodal in direction. Farther offshore (about 10 km) the flow was still weakly bimodal in a southeast-northwest direction but also had appreciable onshore-offshore components. The large variability in flow was revealed both by time-series observations obtained using recording current meters and through observations obtained using radar-tracked, drogued surface buoys.

The near-shore (within 10 km) current moorings indicated a major flow event consequent to passage of a strong storm through the region on 27-28 October 1980. This event led to northwesterly along-shore flows of 60-70 cm/sec reversing the southeasterly flow which prevailed for much of the current observation period. Two other such storm events were observed on the wind records obtained, but current observations were not obtained simultaneously with the other two wind events. Occurrence of three such wind events over the observation period for winds suggests a storm event time scale of 5-6 days. consistent with similar scales postulated for weather patterns farther west (Muench and Schumacher, 1980).

While conclusions concerning the mechanism for generation of the coastal current events are hypothetical at this time, the dynamics of shelf waves suggest that along-shore wind stress is relatively efficient at generating along-shore travelling, right-bounded shelf waves having associated currents similar to those observed (LeBlond and Mysak, 1978). As discussed in more detail in Appendix 1, the observed current pulse had the proper characteristics to be consistent with such a travelling, wind-generated disturbance. Given that this generation mechanism for the current pulses is physically valid, and given the frequency of storm-related winds in the study region, it seems reasonable that such current "pulses" would occur in the coastal region with time scales of 5-6 days through the stormy winter period. The degree to which these currents are constrained to the near-shore region awaits analysis of the current data from mooring 6 (cf. Figure 9), which was farther offshore than the mooring data which has been analyzed to date. If the above conceptualization is valid, we would expect the related currents to drop off with distance from the coastline. This is borne out, to some extent, in that the observed pulse-related currents decrease somewhat between the moorings 5 km offshore (1 and 4) and those 10 km offshore (2 and 5).

The effects of a relatively complex local bathymetry are apparent in the current records. All records show a tendency toward along-isobath flow, with the tendency strongest near the coastline (moorings 1 and 4) and near the bottom (at mooring 5). The radar-tracked drogues indicated, moreover, a pronounced tendency to follow isobaths around the head of Alsek Canyon. The extreme variability of currents, in both speed and direction, at mooring 5 may have been due in part to interaction with the steep bathymetry near the head of Alsek Canyon. Ongoing work is further addressing the possible nature of such interaction.

A near-shore study using seabed drifters was designed primarily to determine the wave-induced longshore (littoral) currents within the surf zone. This study revealed currents as high as 30 cm/sec, with a large variability in speed, and direction of the currents being dependent upon wave height and direction. This problem is undergoing continuing analyses. Generally, the wave field associated with southerly winds drove a northwesterly along-shore littoral flow, and vice versa. No attempt is made to compare littoral drift with the current observed farther off-shore, because different mechanisms are responsible and we would not expect to find a good comparison.

It seems probable that freshwater admixed into seawater within the southeastern Alaskan archipelago influences the observed water properties in the northeast Gulf of Alaska. Low-salinity water observed well off-shore may have reflected input of such water via Cross Sound; however, there was no indication that this water was entrained into the near-coastal flow. Additional temperature-salinity analyses of subsurface waters during autumn 1980 and late winter 1981 will be used to address this problem in greater detail.

VIII. CONCLUSIONS

The following conclusions can be stated based upon research results to date. These should be regarded at this time as preliminary because the field data are not yet completely processed. Except for #5, they reflect conditions observed in October-November 1980.

1. The lowered salinity due to local freshwater input from terrestrial sources was confined to a coastal band less than about 15 km wide and 10-20 m deep. This was in general a far smaller effect than observed farther west along the Gulf of Alaska coast by previous researchers, probably because freshwater input to the northeast Gulf of Alaska is smaller than farther west.

2. Currents measured using recording current meters on taut-wire moorings were dominated by non-tidal flow. Record lengths were 10-11 days. Non-tidal currents within 10 km of the coastline were observed to be primarily along-shore and bimodal in direction. About 60 percent of the time they were to the northwest and about 40 percent to the southeast. At about 5 km from shore, on- and off-shore components were negligible. At about 10 km from shore they were larger than near-shore but still smaller than the along-shore components.

3. The local coastal current response to a vigorous cyclonic storm was strong (60-70 cm/sec) currents to the northwest for a period of 1-2 days. This response appeared, in the single documented case, to propagate to the northwest along the coastline as a travelling wave.

4. The shelf bathymetry, particularly near the head of Alsek Canyon, exerted control over the local currents. Drogued drifter trajectories were observed to roughly parallel the isobaths near the head of Alsek Canyon, leading to a strong shoreward flow component in that region.

5. The longshore (littoral) currents inside, in and just outside the surf zone were dependent upon the height and angle of incidence of incoming swell. During autumn 1980 these currents were generally to the northwest at 15-30 cm/sec in response to swell from the south. In spring 1981 the directions were variable, with littoral currents either to the southeast or the northwest depending upon swell conditions. Movement of near-bottom water in the surf zone was onshore, as shown by the relatively high recovery rate from the beach of seabed drifters released in the surf zone.

IX. NEEDS FOR FURTHER STUDY

A primary need is for information from the continental shelf region off the Southeast Alaska Archipelago, southeast of our study area. A combined review and synthesis of existing literature and data would contribute greatly toward our understanding of this region, which acts as a primary source for the waters in our present study area. Of particular interest is the possibility, mentioned in this report, that winter-cooled southeast Alaskan coastal water acts as a source for the subsurface waters off Yakutat.

A second need is for additional time and funding to allow further analyses of data which were acquired from the study region during the two field efforts in 1980-81. These efforts were extremely successful and resulted in a large quantity of data which are highly pertinent to OCSEAP needs. Additional funds would allow more in-depth analyses than will be possible within the present constraints and, consequently, enhanced understanding of the natural system.

X. SUMMARY OF APRIL-JUNE QUARTER; SHIP OR LABORATORY ACTIVITIES

Ship activities carried out during March-April 1981 were summarized in the 31 March Quarterly Report for this Research Unit (RU 600). No additional such activities are planned for this Research Unit.

XI. AUXILIARY MATERIAL

A. References Used (Bibliography)

Hayes, S.P. 1978: Variability of current and bottom pressure across the continental shelf in the northeast Gulf of Alaska. J. Phys. Oceanog. 9, 88-103.

Hayes, S.P. and J.D. Schumacher 1976: Description of wind, current and bottom pressure variations on the continental shelf in the northeast Gulf of Alaska from February to May 1975. J. Geophys. Res. 81, 6411-6419.

LeBlond, P.H. and L.A. Mysak 1978: Waves in the Ocean. Elsevier, New York, 602 pp.

Muench, R.D. and J.D. Schumacher 1979: Some observations of physical oceanographic conditions on the northeast Gulf of Alaska continental shelf. NOAA Tech. Memo. ERL PMEL-17, 84 pp.

Muench, R.D. and J.D. Schumacher 1980: Physical oceanographic and meteorological conditions in the northwest Gulf of Alaska. NOAA Tech. Memo. ERL PMEL-22, 147 pp.

Royer, T.C. 1977: Hydrographic data report, northeast Gulf of Alaska, July 1975-June 1976. Univ. of Alaska, Fairbanks (unpub. manuscript).

Royer, T.C. 1979: On the effect of precipitation and runoff on coastal circulation in the Gulf of Alaska. J. Phys. Oceanog. 9, 555-563.

Royer, T.C., D.V. Hansen and D.J. Pashinski 1979: Coastal flow in the northern Gulf of Alaska as observed by dynamic topography and satellite-tracked drogued drift buoys. J. Phys. Oceanog. 9, 785-801.

Schumacher, J.D. and R.K. Reed 1980: Coastal flow in the northwest Gulf of Alaska: the Kenai Current. J. Geophys. Res. 85, 6680-6688.

B. Papers in Preparation or Print

Gunn, J.T. and R.D. Muench: Observations of near-bottom littoral currents using seabed drifters* (in preparation for submission to Geophys. Res. Letters).

Muench, R.D., P.R. Temple and L.E. Hachmeister: A coastally trapped, propagating current event in the northeast Gulf of Alaska* (in preparation for submission to J. Phys. Oceanog.).

C. Oral Presentations

Temple, P.R. and R.D. Muench 1981: A propagating wind-related coastal current event in the northeast Gulf of Alaska. EOS 62 (302)(abstract of talk presented at Spring AGU meeting; see Appendix I).

Muench, R.D.: Oceanographic conditions in the northeast Gulf of Alaska (seminar in preparation for presentation at Institute of Ocean Sciences, Patricia Bay, Canada, 14 July 1981).

*Tentative titles.

Appendix 1. Summary of presentation made at Spring 1981 AGU meeting by P.R. Temple.

A PROPAGATING WIND-RELATED COASTAL CURRENT EVENT IN THE NORTHEAST GULF OF ALASKA

by

P.R. Temple
R.D. Muench

Abstract

Coastal circulation in the northeastern Gulf of Alaska was monitored using moored current meters, radar-tracked buoys, and supplementary CTD measurements. Preliminary results indicate that large autumnal freshwater inputs had created a definite two-layered near-shore water column; the internal radius of deformation was about 7 km. Current observations obtained from moorings 3.5 km offshore during an 11-day period showed a bimodal along-shore preference (northwest or southeast) reaching peak velocities of over 50 cm/sec. Current meter records and buoy observations portrayed currents in direct response to wind forcing and relaxation of the system following cessation of the wind event. In one instance, variation in along-shore wind stress resulted in a current pulse that propagated along-shore to the northwest at a speed of about 75 cm/sec. The magnitude and direction of wind forcing appear important in the generation of coastal current events.

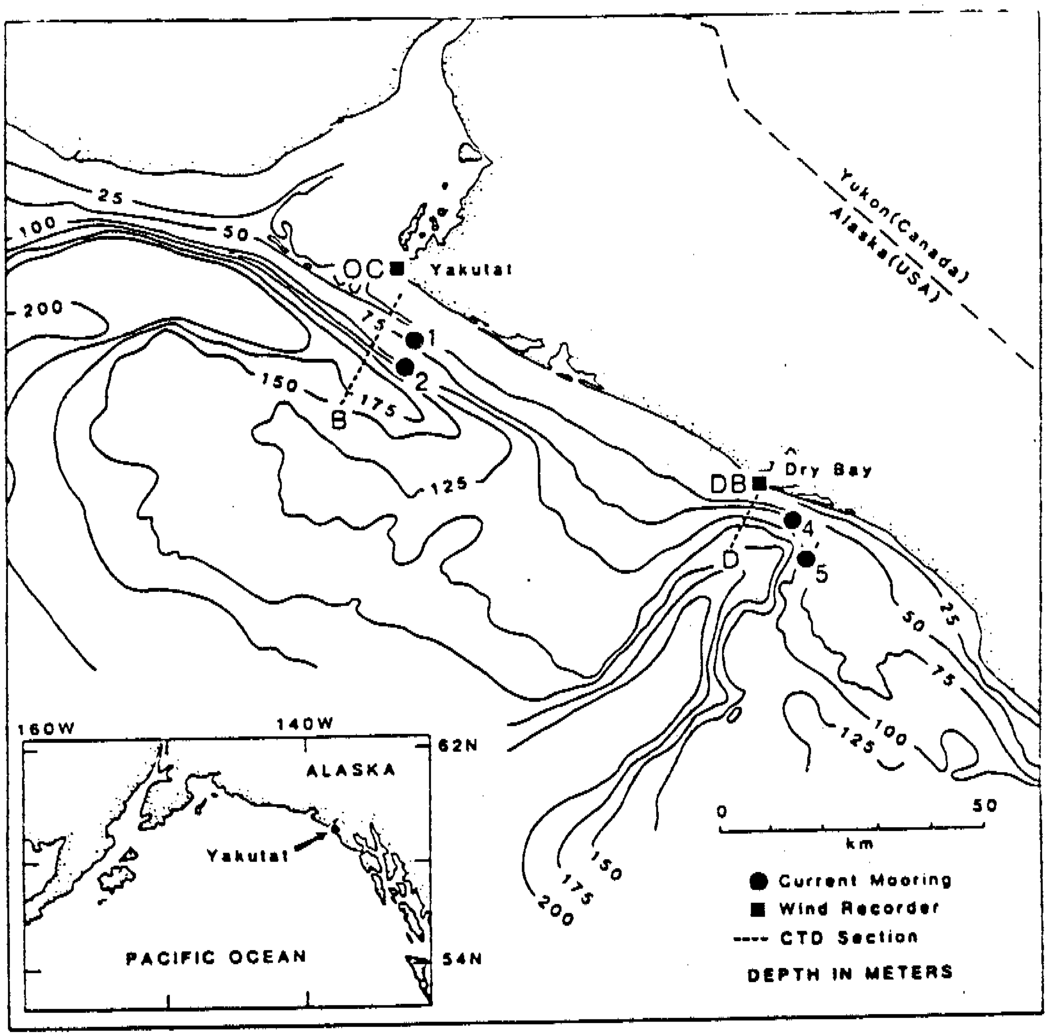

Figure 1-1.* Geographical location of the study region in the northeast Gulf of Alaska, showing positions of the wind recorders, current meters and CTD sections used in the analysis. Current meter moorings 1 and 4 are 3.9 and 3.1 km, respectively, from the coastline and are well within the computed 6 km internal Rossby radius of deformation. Moorings 2 and 5 are 9.8 and 9.4 km, respectively, from the coastline. Pertinent topographic features are the relatively straight, uniform bottom contours inshore of about the 50-m contour and the complex topography broken by transverse submarine valleys seaward of that contour.

*Figures shown here were used as slides in the presentation.

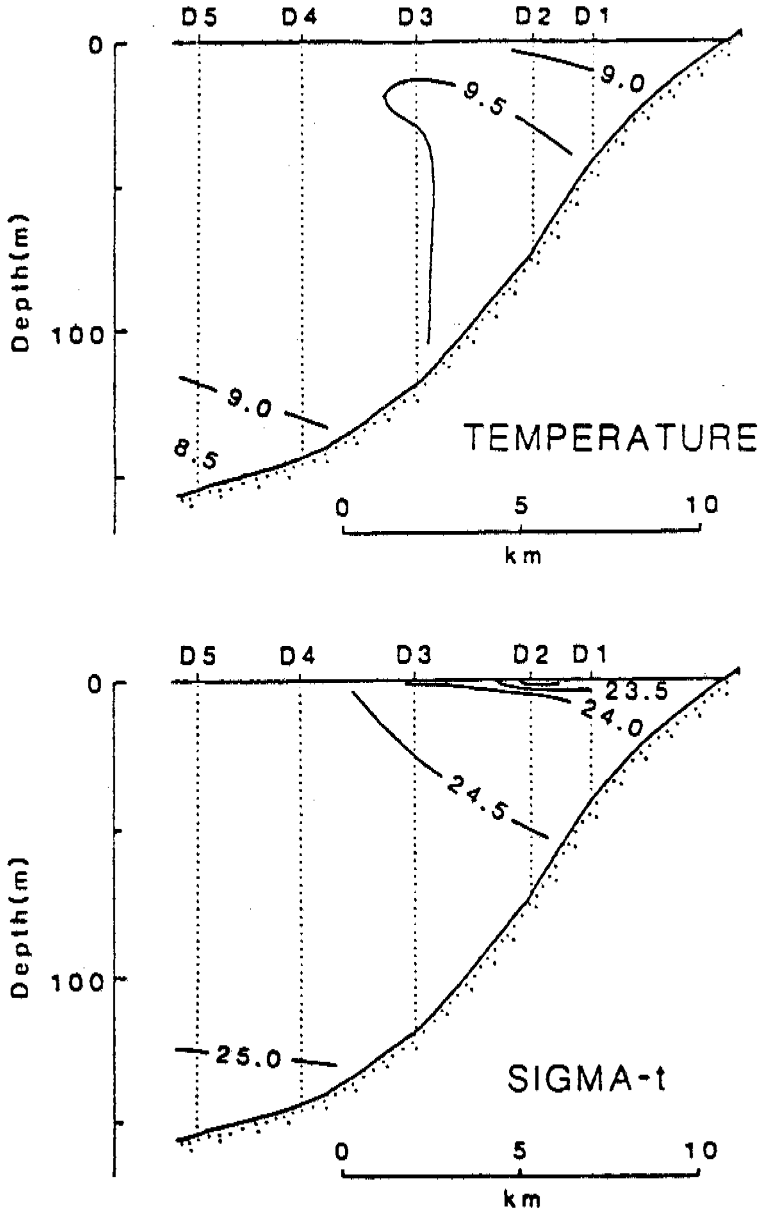

Figure 1-2. Vertical distribution of temperature (top) and density as sigma-t (bottom) along CTD transect D. Note the narrow shallow wedge of low-density water at stations D1 and D2 which reflects coastal input of freshwater. This band is roughly the same width (6 km) as the computed internal radius of deformation. The isopycnal slopes suggest a weak baroclinic flow to the northwest throughout the section.

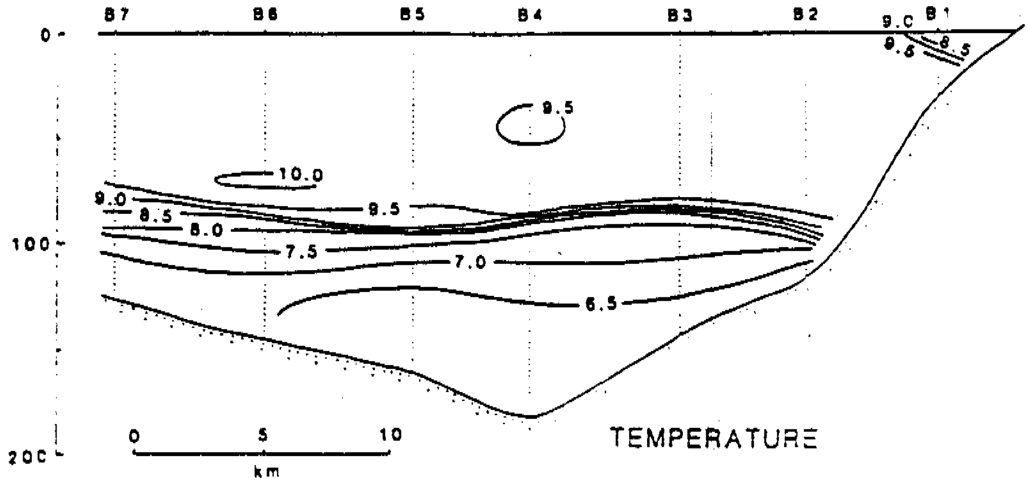

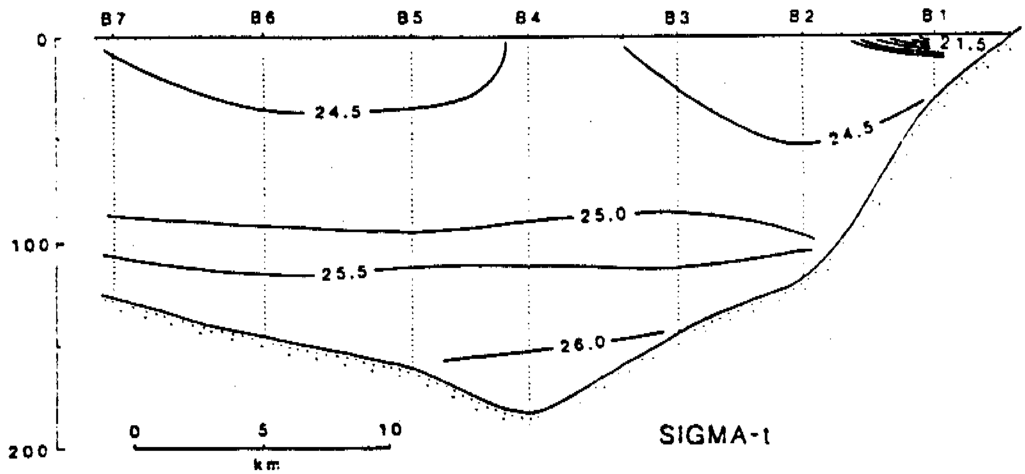

Figure 1-3. Vertical distribution of temperature (top) and density as sigma-t (bottom) along CTD transect B. The coastal wedge of low-density water was the same here as at section D (Figure 1-2). This section also reveals the relatively weak thermocline/pycnocline at about 100 m depth. Water above this depth was uniform in temperature and density relative to that in the thermocline, except for the coastal wedge. This section intersects the head of the submarine valley which transects the shelf off Yakutat (cf. Figure 1-1).

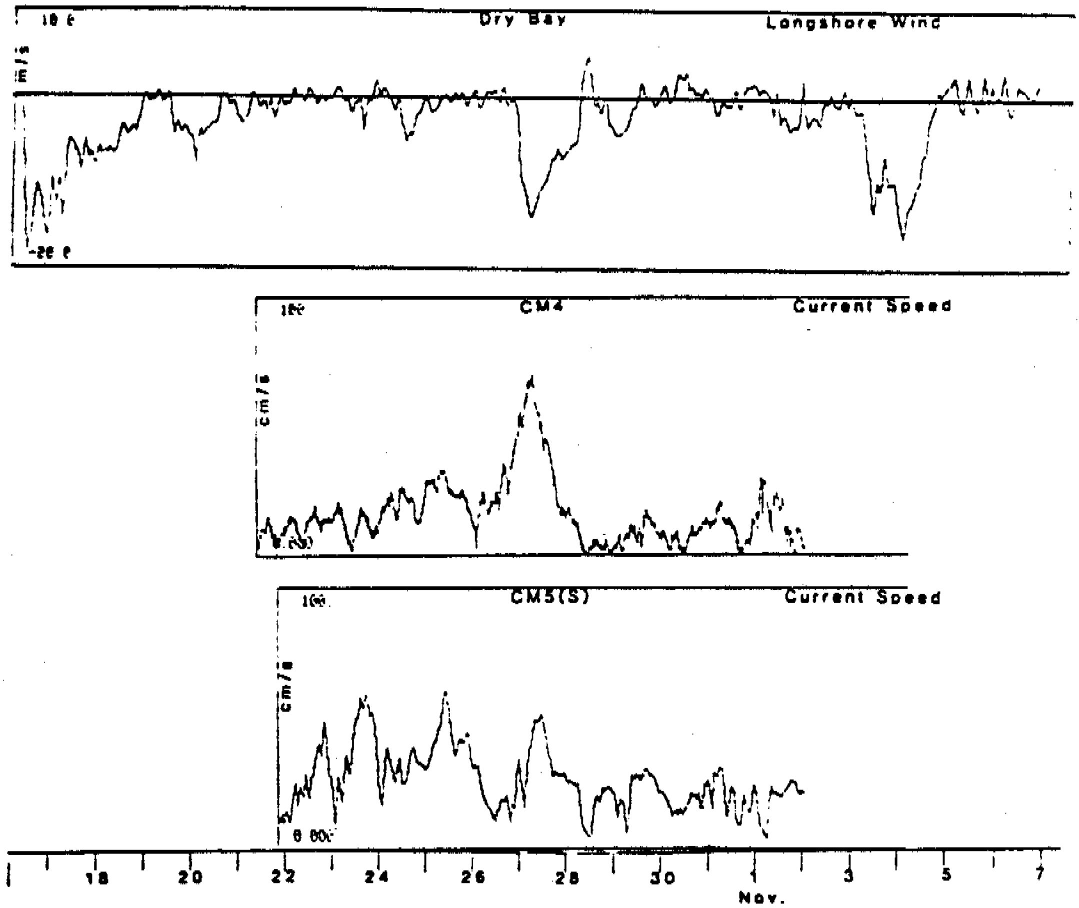

Figure 1-4. Comparison of the longshore wind and current speeds obtained off Dry Bay at moorings 4 and 5 (Figure 1-1) showing the coincident wind and current pulses which occurred on 27 October 1980. The wind pulse was southeasterly (directed towards the northwest); the current pulse was to the northwest. Note that the current pulse at mooring 5 (lower record) was smaller in magnitude and occurred slightly later than at closer-to-shore mooring 4 (middle record), and that the pulse at mooring 4 coincided closely in time with the wind pulse observed at Dry Bay.

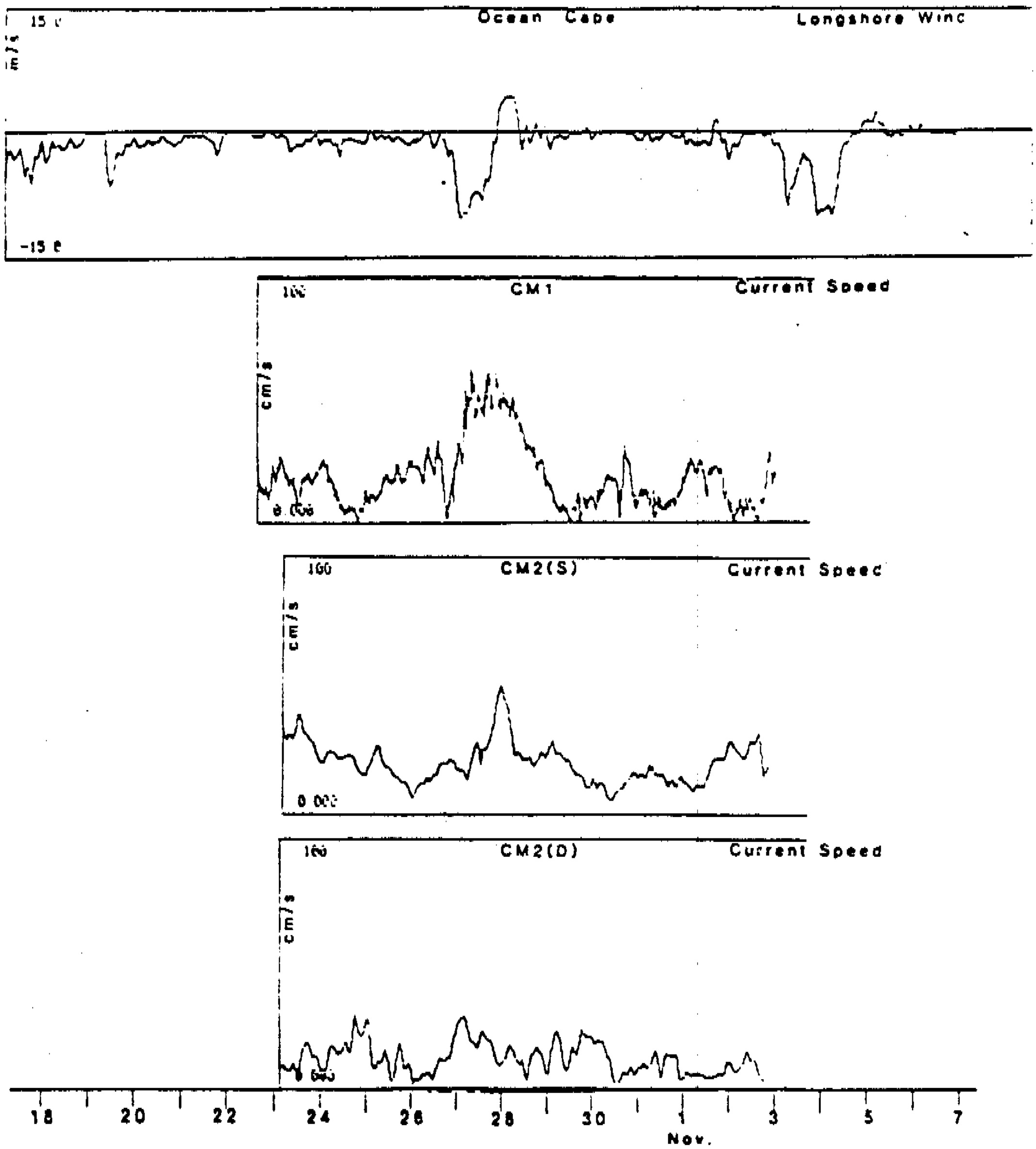

Figure 1-5. Comparison of the longshore wind and current time series obtained off Ocean Cape at moorings 1 and 2 (Figure 1-1). Note that, in distinction to the coincident wind and current pulses off Dry Bay, the nearshore current pulse off Ocean Cape (mooring 1) lagged the wind pulse by about 18 hours. As off Dry Bay, the offshore current record (2) revealed that the wind-associated current pulse offshore lagged the near-shore and was smaller in magnitude than the near-shore. The deeper record (bottom) at the offshore location showed no detectable trace of the current pulse.

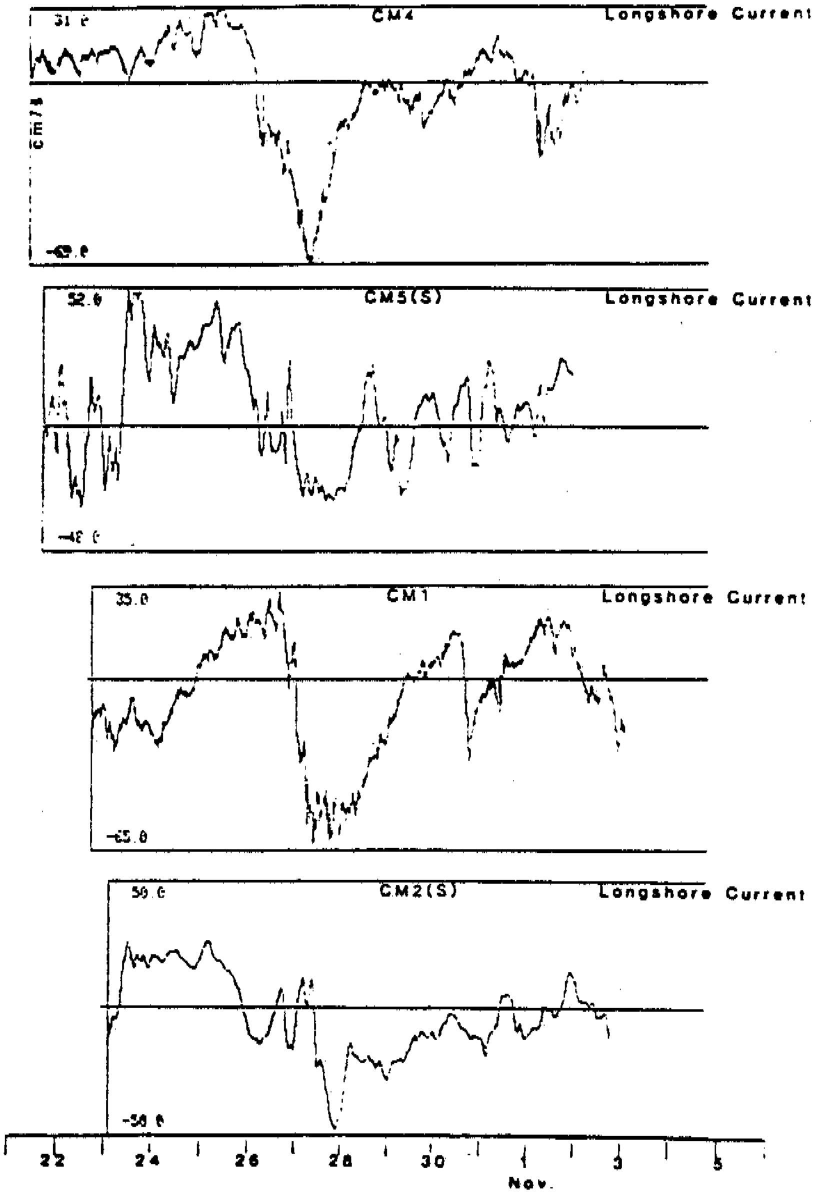

Figure 1-6. Comparison of the longshore components of currents at moorings 4, 5, 1 and 2, showing continuity of the wind-driven pulse between the moorings. Note the pronounced time lag between appearance of the pulse at mooring 4 and at mooring 1, which suggests northwestward propagation of the pulse along the coastline at speeds of about 100 cm/sec. The pulses offshore lagged the pulses near-shore and were lower in magnitude.

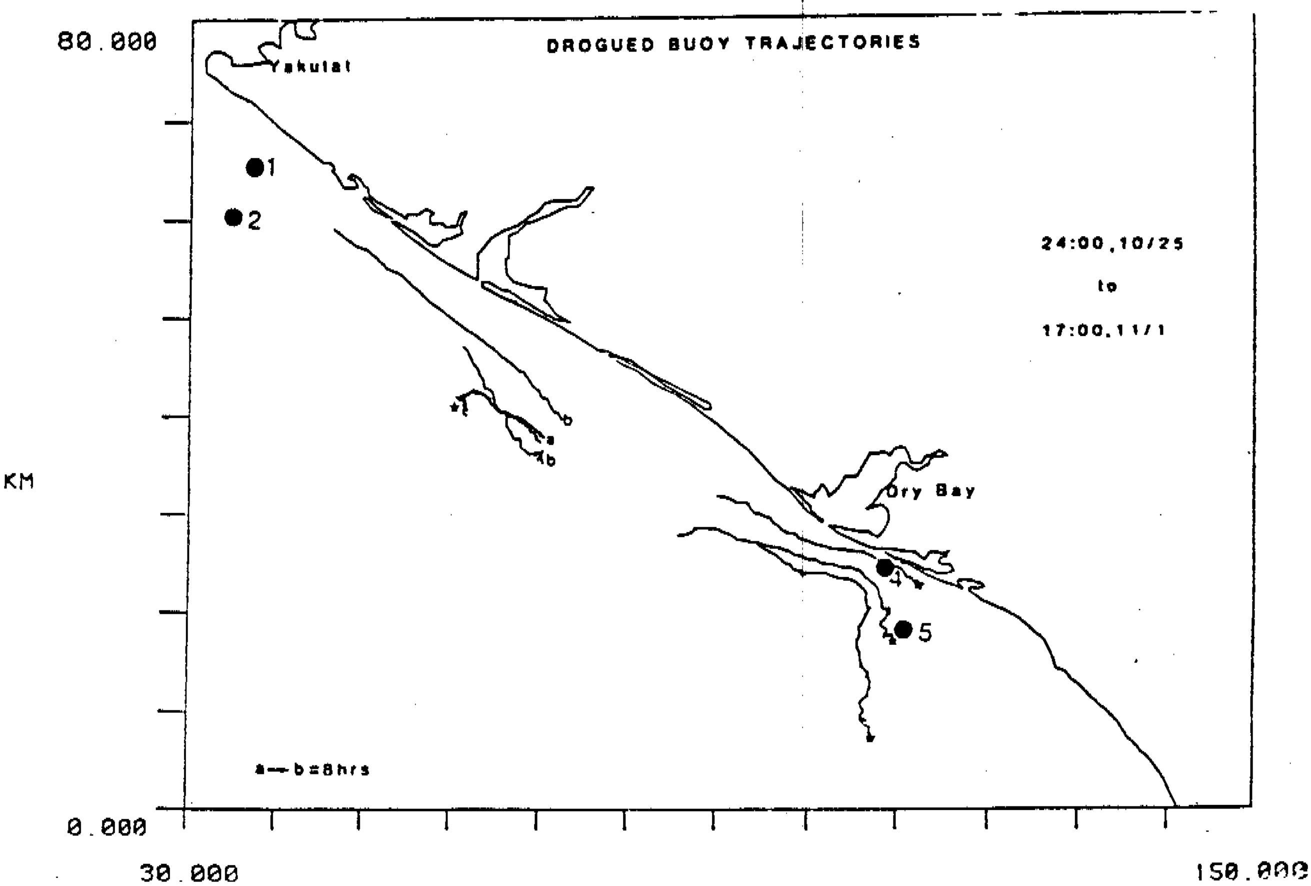

Figure 1-7. Trajectories of surface-drogued radar-tracked buoys deployed during the wind-driven current pulse. These documented that the near-surface current speeds were of the same order as those observed deeper with the current meters. In addition, the shoreward curving of the trajectories off Dry Bay demonstrates the influence of the submarine valley there upon local currents which tend to parallel isobaths. The letters a and b indicate location of the first deployment of the drogues. The stars indicate the locations of deployment during a second period of tracking.

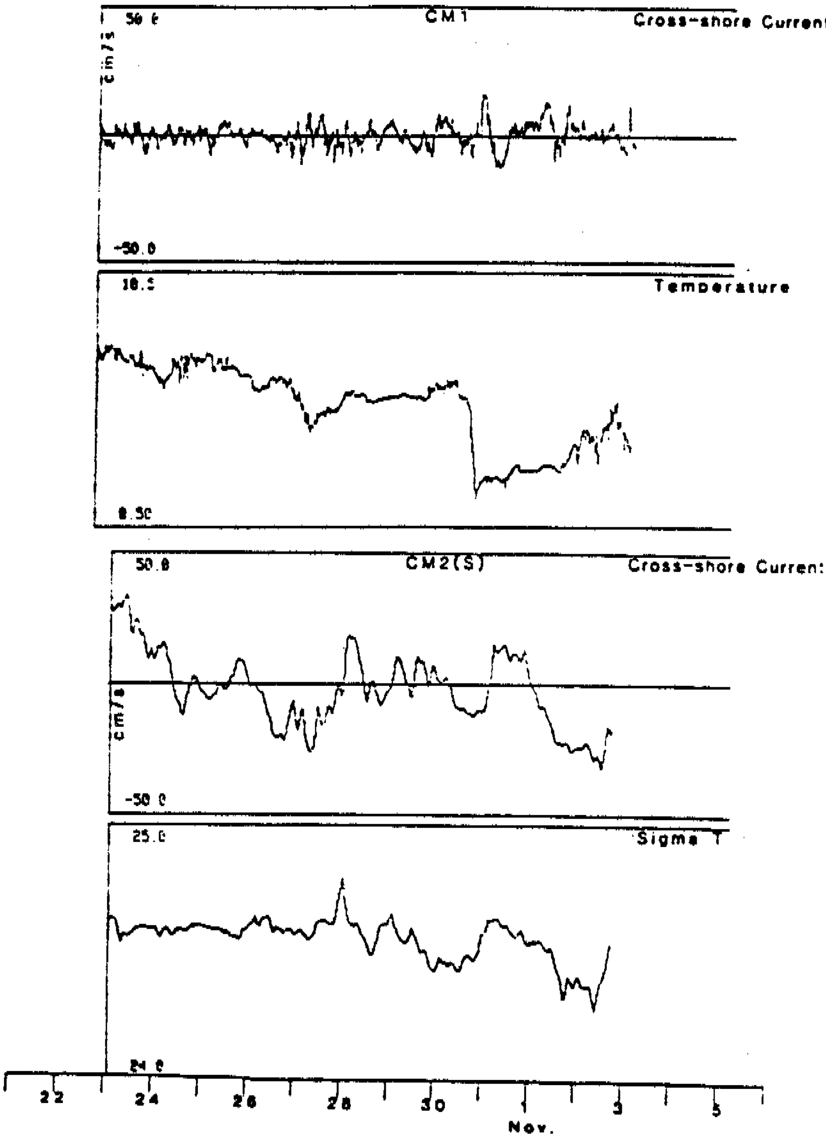

Figure 1-8. Comparison of cross-shore current components at near-shore mooring 1 and offshore mooring 2, showing the lack of motion normal to the coastline at the near-shore mooring. Mooring 1 was shoreward of the computed internal radius of deformation, whereas mooring 2 was outside this radius.

VELOCITY PULSE CHARACTERISTICS
TIME LAG, CM4 TO CM1:
WIND - 6 ± 2 HRS.
CURRENT PULSE - 22 ±2 HRS.
PROPAGATION SPEED: ~100 CM/SEC OR 87 KM/DAY
FREQUENCY: 0.4 CPD

Figure 1-10. This table summarizes the observed characteristics of the wind-associated current speed pulse which was evident on the current records for 27-28 October 1980. The pulse characteristics are consistent with those which would be expected for a slowly-propagating, right-bounded coastal Kelvin wave moving to the northwest. Continued investigation of the regional density field and the density time changes at each mooring will aid in determining the validity of this hypothesis, and further intercomparison between the wind and current fields may indicate whether the pulse was locally wind-generated or had propagated into the region from the southeast.

U.S. Department of Commerce
National Oceanic & Atmospheric Administration
Office of Marine Pollution Assessment
Alaska Office, RD/MPF24
P.O. Box 1808
Juneau, Alaska 99802

POSTAGE AND FEES PAID
U.S. DEPARTMENT OF COMMERCE
COM-210

U.S.MAIL

OFFICIAL BUSINESS
PENALTY FOR PRIVATE USE, $300